Univerza
v Ljubljani
Fakulteta
za gradbeništvo
in geodezijo

Doktorand/ka
GABRIJELA STAREŠINIČ

POTRESNI ODZIV VODORAVNIH BETONSKIH FASADNIH SISTEMOV ARMIRANOBETONSKIH MONTAŽNIH STAVB

Doktorska disertacija

SEISMIC RESPONSE OF HORIZONTAL CONCRETE FACADE SYSTEMS IN REINFORCED CONCRETE PREFABRICATED BUILDINGS

Doctoral dissertation

Ljubljana, avgust 2021

Univerza
v Ljubljani
Fakulteta
za gradbeništvo
in geodezijo

Mentorica: prof. dr. Tatjana Isaković, UL FGG.

Somentor: doc. dr. Matija Gams, UL FGG.

Poročevalci za oceno doktorske disertacije:

- prof. dr. Matjaž Dolšek, UL FGG,
- izr. prof. dr. Sebastjan Bratina, UL FGG,
- prof. dr. Roberta Apostolska, Univerza sveti Ciril in Metodij, IZIIS, Skopje, Severna Makedonija.

POPRAVKI/ERRATA

Stran z napako/ Page	**Vrstica z napako/ Line**	**Namesto/ Error**	**Naj bo/ Correction**

BIBLIOGRAFSKO – DOKUMENTACIJSKA STRAN IN IZVLEČEK

UDK: **624.012.3:624.042.7:692.23(043)**
Avtor: **Gabrijela Starešinič**
Mentor: **prof. dr. Tatjana Isaković**
Somentor: **doc. dr. Matija Gams**
Naslov: **Potresni odziv vodoravnih betonskih fasadnih sistemov armiranobetonskih montažnih stavb**
Tip dokumenta: **Doktorska disertacija**
Obseg in oprema: **289 str., 27 pregl., 231 sl., 51 en., 7 pril.**
Ključne besede: **armiranobetonske montažne stavbe, vodoravni fasadni system, stiki, mehanizem odziva, numerično modeliranje, parametrična študija, potresni odziv**

Izvleček

Raziskan je bil potresni odziv AB-montažnih stavb z betonskimi vodoravnimi fasadnimi sistemi, ki se pogosto uporabljajo v srednji Evropi. Analitične in numerične študije, ki so predstavljene v doktorski nalogi, so bile podprte z obsežnimi dinamičnimi preizkusi. Številni testi so bili uspešno simulirani z na novo definiranimi numeričnimi modeli.

Osnovni mehanizem odziva fasadnih stikov je sestavljen iz treh značilnih faz: faza drsenja, pri kateri se aktivira majhno trenje, stik s panelom, ki povzroči skokovito porast togosti stika, in krhka porušitev. Ugotovljeno je bilo, da so zgornji stiki najšibkejši člen pritrdilnega sistema. S preizkusi na potresni mizi in parametrično študijo je bil ugotovljen mehanizem odziva celotnega montažnega sistema z vodoravnimi paneli in analiziran vpliv panelov na odziv glavne montažne konstrukcije. Ugotovili smo, da lahko obremenitev in kapaciteto sistema stikov izrazimo s pomikom stebra na ravni panela. V okviru parametrične študije je bil analiziran vpliv različnih parametrov na potresni odziv panelov in konstrukcije. Pokazali smo, da je odziv vodoravnega fasadnega sistema odvisen predvsem od začetnega položaja stikov.

Vodoravni fasadni sistemi imajo v splošnem majhen vpliv na odziv glavne montažne konstrukcije. Vpliv je opazen le ob zelo vitkih konstrukcijah z majhno maso povprečnega stebra. V nalogi je ovrednoten trenutni projektantski pristop, s katerim lahko razmeroma dobro ocenimo odziv glavne montažne konstrukcije. Podan je sorazmerno preprost postopek za približno oceno obremenitev fasadnega sistema. V zadnjem delu disertacije sta bili narejeni numerična analiza in presoja pridrževalcev.

BIBLIOGRAPHIC – DOCUMENTALISTIC INFORMATION AND ABSTRACT

UDC:	**624.012.3:624.042.7:692.23(043)**
Author:	**Gabrijela Starešinič**
Supervisor:	**Prof. Tatjana Isaković, Ph. D.**
Co-supervisor:	**Assist. Prof. Matija Gams, Ph. D.**
Title:	**Seismic response of horizontal concrete facade systems in reinforced concrete prefabricated buildings**
Document type:	**Doctoral Dissertation**
Notes:	**289 p., 27 tab., 231 fig, 51 eq., 7 ann.**
Keywords:	**reinforced concrete precast buildings, horizontal façade system, connections, response mechanism, numerical modelling, parametric study, seismic response**

Abstract

The seismic performance of prefabricated, reinforced concrete (RC) structures with horizontal concrete façade systems typically used across Central Europe was investigated. Extensive static and dynamic experiments supported analytical and numerical research presented in the dissertation. Many tests were successfully simulated by newly defined numerical models.

A basic in-plane response mechanism of the fastening system consists of three distinct stages: sliding with limited friction, contact with the panel causing an increase in stiffness of the connection and brittle failure. The top connections are the weakest components of the fastening system. Experimental observations during the shake table tests and extensive parametric study showed that the column drift along the single panel could measure capacity and demand on the fastening system.

Various important parameters and their influence on the seismic response were analysed. The initial position of cladding connections significantly influences the responses and the drift capacity of the system. Thus, a proposal was made in the dissertation to improve the façade system based on providing more space for connections to slide.

The influence of the façade system on the response of the main structure is small. It can be noticed only for very slender structures with small tributary mass. The response of the main precast structure could be reasonably well estimated with a current design approach. A relatively simple procedure for estimating the approximate demand on the façade system is given. At the end of the thesis, a numerical analysis and evaluation of a restrainer system were performed.

ZAHVALA

Zahvaljujem se prof. dr. Mateju Fischingerju za izkazano zaupanje in priložnost, da se preizkusim v znanstveno raziskovalnem delu. Posebna zahvala velja mentorici prof. dr. Tatjani Isaković, ki mi je s svojim znanjem, izkušnjami in vztrajnostjo nudila izredno strokovno podporo. Iskrena hvala somentorju doc. dr. Matiji Gamsu za vsak nasvet, usmerjanje in potrpežljivost.

Hvala fantom iz III/7, ki so me sprejeli v svojo skupnost. Vseh ne morem tukaj našteti, pa vendar ste nekateri odigrali pomembno vlogo. Blaž, brez tvoje pomoči bi bili začetki veliko bolj zahtevni. Anže, Mirko in Jure, zahvaljujem se vam za vse nasvete, razlage in debate ob kavi ali računalniku.

Sara, Nina in Katarina, hvala za iskreno razumevanje in spodbudne besede. Teja in Anita, hvala za družbo, ko sem to potrebovala.

Za vso podporo hvala staršem in Katji. Hvala tudi starim staršem, ker so bili vedno veseli mojih dosežkov.

Za vsak pogovor iskrena hvala dr. Zalki Drglin.

Marko, hvala, ker verjameš vame. In Julija, tebi hvala za brezpogojno ljubezen.

CONTENTS

LIST OF FIGURES

LIST OF TABLES

KAZALO SLIK

KAZALO PREGLEDNIC

1 INTRODUCTION

Reinforced concrete (RC) precast structures are among the most common structural systems used for industrial and commercial purposes in Europe. The predominant type of such systems consists of an assemblage of cantilever columns tied together by beams and surrounded with peripheral cladding panels.

The behaviour of reinforced precast structures during past earthquakes was very diverse. Several site inspections showed various responses, ranging from undamaged structures to complete collapses (Fajfar et al., 1978; Tzenov et al., 1978; Fajfar et al., 1981; Arslan et al., 2006; Toniolo & Colombo, 2012; Bournas et al., 2013; Liberatore et al., 2013). Even though such a structural system has been used for decades, its seismic response was poorly understood. The poor knowledge about the seismic response of RC precast structures has resulted in rigorous code requirements and a very conservative design approach for this structural type (Toniolo, 2012a). In the first draft of Eurocode 8, the precast structures were put at a disadvantage compared to the monolithic RC structures, triggering very intensive research activity all over Europe.

In the past two and a half decades, comprehensive systematic studies of RC precast buildings were performed within several EU research projects, combining the efforts of industry and different academic institutions (Biondini & Toniolo, 2004; Ferrara et al., 2004; Biondini et al., 2008; Biondini & Toniolo, 2009; Toniolo, 2012b; Zoubek et al., 2013; Fischinger et al., 2014; Isaković et al., 2014b; Zoubek et al., 2016a; Negro & Lamperti Tornaghi, 2017; Toniolo & Dal Lago, 2017; Psycharis et al., 2018; Yüksel et al., 2018). Many important observations about the seismic response of RC precast buildings have been obtained.

Despite the extensiveness of large European projects and some parallel studies (Belleri et al., 2016; Belleri et al., 2018; Del Monte et al., 2019), the complex seismic response of the concrete façade systems has still been poorly understood. Precast concrete buildings are structures made of separate prefabricated elements joined together at the construction site. The response of such systems under seismic load depends very much on details in the connections. Possible interaction between the main precast structure and the cladding panels has been the subject of discussion for many years, and different expert opinions have been expressed regarding this issue. It was not possible to fully determine the role of panel fastenings and their realistic boundary conditions without a more complex study of the whole-system response.

To find the answers to these questions, the research project *Seismic resilience and strengthening of precast industrial buildings with concrete claddings*, funded by the Slovenian Research Agency, has been launched. One of the main parts of this project was devoted to full-scale shake table experiments of an RC building with cladding panels. The results of these experiments were used for the research performed within the present doctoral dissertation. The façade system investigated in the dissertation is one of the most common systems used in Central Europe.

1.1 Motivation and objectives

Precast industrial buildings house a large share of the European industrial activity. Because of their rapid construction, open space and low cost, they are becoming a more and more popular structural system all over Europe. In Europe alone, approximately 50 million square meters of precast buildings are built every year (Fischinger et al., 2014), demonstrating the importance of this structural type.

RC precast structures have been used for industrial purposes and large shopping centres with tens of thousands of visitors per day. For reference, one of the largest shopping centres in Slovenia has 21 million visitors per year (BTC, 2014). Damage or collapse of RC precast buildings could cause human casualties and considerable direct and indirect economic losses due to production disruption, as was observed during the past earthquakes in Northern Italy (Bournas et al., 2013; Magliulo et al., 2014; Savoia et al., 2017).

The estimated economic losses are enormous. Magliulo et al. (2014) report that the direct financial loss after the two Emilia earthquakes amounted to about 1 billion euros, while the induced or indirect financial loss due to production interruption amounted to about 5 billion euros. Some sources report even higher numbers – according to CATDAT report (Daniell and Vervaeck, 2012), the final loss estimate for direct economic losses by the Italian government for the series of earthquakes in the Emilia-Romagna region was something above 12 billion euros.

Several EU research projects that included extensive studies of RC precast buildings were carried out by partners from industry and academic institutions to avoid such consequences. The last joint EU project, SAFECLADDING (2015), was devoted to the connections of the façade cladding panels to the main structural system of industrial buildings to improve the related design practice.

Before the SAFECLADDING (Fischinger et al., 2014; Zoubek et al., 2016a; Negro & Lamperti Tornaghi, 2017; Toniolo & Dal Lago, 2017; Psycharis et al., 2018; Yüksel et al., 2018) and some parallel studies (Belleri et al., 2016; Belleri et al., 2018; Del Monte et al., 2019) were conducted, the knowledge about the seismic response of cladding panels was very poor, and even the

fundamental mechanisms of seismic response were not known. The design practice was inadequate because the response of façade panels and their fastenings in the more critical horizontal direction parallel to the plane of the panels was not considered (Toniolo & Colombo, 2012; Bournas et al., 2013; Fischinger et al., 2014; Magliulo et al., 2014; Belleri et al., 2016). The inadequate design has been confirmed in the recent earthquakes in Northern Italy, where the failure of the fastening system was one of the reasons for the collapse of cladding panels. As reported by Toniolo & Colombo (2012), collapses of cladding panels during the L'Aquila earthquake affected around 15% of existing buildings.

The comprehensive experimental (Negro & Lamperti Tornaghi, 2017; Toniolo & Dal Lago, 2017) and analytical studies performed within the aforementioned European project considerably improved the knowledge about the seismic response of the cladding panel fastening systems. The part of the research carried out at the University of Ljubljana – UL (Fischinger et al., 2014) was devoted to the fastening systems of vertical (Zoubek et al., 2016a) and horizontal cladding panels that are widely used in Central Europe. Although many important observations about the seismic response of investigated cladding panels have been obtained, the research could not fully reveal and explain all aspects of this complex response.

Many of the analytical and numerical studies considering different types of cladding connections performed within SAFECLADDING and other national projects were based on monotonic and cyclic tests of single connections (Belleri et al., 2016; Zoubek et al., 2016; Psycharis et al., 2018; Yüksel et al., 2018; Del Monte et al., 2019) as well as cyclic and pseudo-dynamic tests on full-scale structures (Negro & Lamperti Tornaghi, 2017; Toniolo & Dal Lago, 2017). The research considered the response of single components as well as different innovative system solutions. However, many aspects of the behaviour of the complex cladding system remained unexplained.

To develop a better insight into earthquake performance of the complete precast structural system, full-scale shaking table tests were performed on a structure with realistic boundary conditions, including the main precast structure, cladding panels and connections. The research was done within the Slovenian national project *Seismic resilience and strengthening of precast industrial buildings with concrete claddings* in cooperation with the Institute of Earthquake Engineering and Engineering Seismology – IZIIS in Skopje, Republic of North Macedonia. Experiments presented in the dissertation were one of the first shaking table tests performed on an RC precast structure with non-structural cladding panels. The main objective of the shaking table tests was an analysis of the seismic system response of the precast building with RC cladding panels under realistic boundary conditions. Within these experiments, different parameters such as the orientation of the cladding panels, the type of fastenings and the configuration of the specimen (symmetric and

asymmetric) were varied. The doctoral thesis includes shaking table tests performed on the structure with horizontal panels.

The shaking table tests and subsequent analytical and numerical studies were carried out to study the behaviour of the complete system under dynamic seismic excitation, to evaluate the possible interaction between the main precast structure and cladding panels, and identify limitations, if any, for the structural type.

To be able to set up these highly complex tests, studies of single components performed within SAFECLADDING (Isaković et al., 2013; Zoubek, 2015) were complemented with additional cyclic and dynamic tests. The main aim of the single component tests was to obtain as much data as possible about basic seismic response mechanisms and the capacity of connections before the experiment on the shaking table. The part of the research campaign concerning the connections of horizontal panels is included in this thesis.

The analytical studies augmented the experimental studies performed on single components to define a numerical model that can describe the behaviour of the fastening system under cyclic and dynamic loading. Formulated numerical models were then also used for the design of shaking table tests. Different possibilities for the mathematical modelling of investigated fastening systems were considered within the thesis. The numerical model was validated by single component tests as well as full-scale shake table experiments.

Experimental research was followed by an extensive parametric study, with the main aim of defining parameters that influence the response of horizontal concrete facade systems in RC prefabricated buildings. One of the goals was to determine the influence, if any, of horizontal façade systems on the overall structure's response and the possible level of interaction between horizontal panels and the main precast structure. Within the parametric analysis included in this thesis, the verified numerical model was applied to real RC precast structures. Several parameters were studied to analyse their influence on the structural response of RC precast buildings: different structural configurations, construction imperfections, the interaction of adjacent panels and the connection of bottom panels to the foundation. The conclusions and findings drawn from the experiments were reconsidered. Finally, a proposal for improvement of the horizontal cladding connections is presented.

In the design practice of precast industrial buildings with concrete façade systems, the interaction between the panels and the main structural system of RC buildings is typically neglected. The cladding panels are often considered only as masses added to the main structure. However, the latest strong earthquakes in Northern Italy (Toniolo & Colombo, 2012; Bournas et al., 2013) put this

assumption under question. For this reason, a design approach that neglects the interaction between panels and the main structural system of RC buildings was also thoroughly assessed.

A possible solution for improving the safety of existing buildings could be so-called restrainers (Zoubek, 2015; Zoubek et al., 2016b) that would protect the cladding panels from falling in the case of the failure of the fastenings during strong earthquakes. In this dissertation, an analytical estimation of seismic demand on restrainers used to protect horizontal panels is given.

1.2 The organisation of the dissertation

The dissertation begins with a brief introduction, the motivation and objectives of the thesis presented in Chapter 1. The objectives are then thoroughly covered in the following chapters.

Chapter 2 contains the state-of-the-art review of the research done in the field of RC precast structures. Observations after past earthquakes are summarised. Previous research done within the extensive European projects and some parallel studies emphasise the façade systems. The typology of the prefabricated industrial buildings is described to wrap up the overview of the examined precast system.

In Chapter 3, single cladding connections typically used for attaching horizontal cladding panels to the main precast structure in Central Europe are experimentally investigated. The response mechanisms of the top and bottom components and the complete fastening system are defined. The individual response parameters are discussed, and failure criterion is identified.

Full-scale shake table tests on the realistic precast building were performed within the UL research project *Seismic resilience and strengthening of precast industrial buildings with concrete claddings*. The experimental results of those tests were used for a detailed analysis and discussion of the seismic response of the complete structural system with horizontal façade panels, which is presented in Chapter 4.

In Chapter 5, the numerical models of the investigated fastenings are defined and described. The proposed numerical models are validated using single component tests (Chapter 3) and full-scale shaking table experiments (Chapter 4). A thorough analysis and discussion of the response parameters are provided.

The main part of the thesis is an extensive parametric study of the seismic response of RC precast buildings with horizontal concrete façade systems, which is presented in Chapter 6. The main goals of this study were to identify which parameters have considerable influence on the response of horizontal façade systems in one-storey industrial buildings, to determine the level of interaction

between the horizontal panels and the main precast structure, and to determine the influence, if any, of the horizontal façade systems on the overall system response. A wide array of one-storey RC precast buildings was included in this study. Various important parameters influencing their response were analysed: different structural configuration, construction imperfections, the interaction of adjacent panels and the connection of bottom panels to the foundation.

In the current design practice in Slovenia, the interaction between the panels and the main structural system of RC buildings is typically neglected. The influence of panels on the overall seismic response is taken into account only by adding their mass to the mass of the main structural system. In Chapter 6, this approach is thoroughly assessed.

A proposal for improving cladding connections for horizontal façade panels is presented in the final part of Chapter 6.

Protection from falling panels in the case of failure of their fastenings can be provided with seismic restrainers. An analytical and numerical analysis of the seismic demand on the restrainers used to protect horizontal cladding panels is presented in Chapter 7. The existing analytical procedure for estimation of the maximum impact forces that could act on the restrainers is evaluated for the case of horizontal panels.

Finally, in Chapter 8, all conclusions of the presented work are summarised. An extended abstract of the thesis has been written in the Slovenian language. It can be found in Chapter 9.

2 STATE OF THE ART

This chapter contains a literature survey. First, the observations after the past strong earthquakes demonstrate the diverse behaviour of the precast structures. Lack of knowledge about the response of RC prefabricated buildings subjected to seismic loading has triggered the intensive research conducted in the last 30 years. In this chapter, a state-of-the-art review of the research done within several European projects and some parallel studies are presented with the emphasis on RC façade systems. The overview is concluded with the description of common typology and different solutions for the RC prefabricated industrial buildings used in Central Europe.

2.1 Observations after past earthquakes

Many valuable data about the dynamic behaviour of a certain structural system can be gained from observations after the earthquakes. There have been several earthquakes in Europe that gave insight into the response of RC precast structures. From one strong earthquake to another, the field inspections and reports showed different responses, from good behaviour on the one hand, to total disasters on the other.

For instance, the 1976 Friuli earthquake in Italy pointed out the relatively good behaviour of prefabricated buildings (Fajfar et al., 1978; EERI, 1976). However, the frequency of the ground motion was relatively high, while the predominant structural periods of relatively flexible RC precast structures are usually around one second or even above (Kramar, 2008). According to EERI (1976), most damage after the Friuli earthquake could be attributed to the collapse of the roof system due to the lack of connections between the beams and columns, relying only on friction.

Satisfying behaviour of precast structures, in general, was also observed during the 1979 Montenegro earthquake (Fajfar et al., 1981), apart from some collapses in Port of Bar. In contrast, there have been catastrophic collapses of prefabricated structures observed after the 1988 Spitak Earthquake in Armenia that created distrust of precast construction in general. Fischinger et al. (2014) have pointed out that the large panel precast structures performed well (see Figure 2.1). Therefore, any generalised conclusions about the good or bad performance of precast structures should not be drawn. However, during the Spitac earthquake, the industry suffered long-term business interruptions because many industrial facilities either collapsed entirely or were severely damaged (EERI, 1989).

Figure 2.1: Large panel precast structure standing among the rubble of the precast frames that caused a tragedy during the Spitak 1988 earthquake (Fischinger et al., 2014)
Slika 2.1: Visoka montažna panelna zgradba stoji praktično nepoškodovana poleg ruševin AB montažne okvirne konstrukcije, ki so bile med drugim vzrok za tragedijo med potresom leta 1988 v Armenskem mestu Spitak (Fischinger et al., 2014)

Damage of precast buildings was reported after the 1977 Vrancea earthquake in Romania (Tzenov et al., 1978) and during earthquakes in Turkey, that is, the 1998 Ceyhan, 1999 Kocaeli and 1999 Düzce earthquakes (Saatcioglu et al., 2001; EEFIT, 2003; Arslan et al., 2006; Dogan et al., 2010). Three common types of structural damage were observed: flexural hinges at the base of columns, axial movement of the roof girders, leading to pounding at columns or unseating of the girders, and failure of the roof girders in an out-of-plane direction (Dogan et al., 2010). The probable reason for a considerable number of collapses and substantial damage after these earthquakes might also be the strong low-frequency content of the ground motions.

More recently, the 2009 L'Aquila earthquake in Italy demonstrated that the behaviour of the main precast structures, that is, the columns and roof elements, was, in general, good. The majority of the damage observed during this event can be attributed to the failure of non-structural parts, explicitly to the failure of heavy cladding panels (Toniolo & Colombo, 2012). Failures occurred with different types of connections and buildings concerning both vertical and horizontal panels. These observations confirmed the reliability of the design of the structures according to seismic provisions and, at the same time, pointed out the inadequate design of fastening systems for cladding panels. Fastening systems often have not even been analysed for the effect of seismic loading because the main response mechanisms were not known.

In 2012, a series of earthquakes hit the Emilia Romagna region in Northern Italy, causing much damage, followed by many field inspections (Bournas et al., 2013; Liberatore et al., 2013; Magliulo et al., 2014; Savoia et al., 2017). This industrial region with intense economic activity was only classified as seismic since the year 2003, meaning that most of the structures were not designed for seismic loading (Daniell and Vervaeck, 2012). However, some of the newly designed buildings have also suffered substantial damage, which could be, as in the case of Turkish earthquakes, related to the relatively strong energy content of the second shock in the low-frequency range.

Most industrial buildings in the affected area were designed for gravity loads only, with the lack of adequately designed connections between precast elements (Bournas et al., 2013). For this reason, many roof failures due to unseating of the main beams from the columns have been reported. Approximately 75% (Bournas et al., 2013) of precast industrial buildings designed without seismic provisions in the area of the Emilia earthquake suffered damage and detachment of the wall cladding panels. Bournas et al. (2013) even claim that the number of cladding connection failures was not significantly reduced in the newly designed buildings. Examples of the collapses in the Emilia Romagna earthquake are shown in Figure 2.2.

Many authors (Toniolo & Colombo, 2012; Bournas et al., 2013; Belleri et al., 2015; Savoia et al., 2017) thought that the main reason for the failure of panels was insufficient displacement capacity of the cladding-to-structure connections in the direction parallel to the panel plane, which led to the overturning of façade panels. Namely, the cladding fastening systems were often not designed according to seismic provisions. Only the forces acting in the direction perpendicular to the panel plane, calculated based on the panel mass, were considered (CEN, 2004).

(a)  (b) 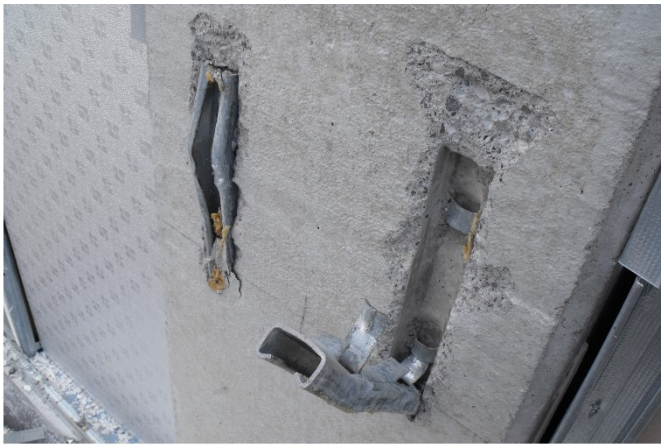

Figure 2.2: (a) Failure of the horizontal RC cladding panels and (b) the damaged cladding connections during the earthquake in Emilia Romagna

Slika 2.2: (a) Porušitev horizontalnih armiranobetonskih panelov in (b) poškodovani fasadni stiki med potresom v Emiliji-Romanji

The L'Aquila Earthquake provided evidence of displacements up to ± 150 mm at the top of some buildings (Toniolo & Colombo, 2012). This could have a relevant impact on the cladding-to-structure connections, which must accommodate large displacements in a longitudinal, that is, in-plane, direction.

Leading causes for the damage and collapses of precast buildings observed during the past earthquakes can be summarised as:

- *Failure of the columns:* Inadequate confinement and detailing of the hoops led to buckling of the longitudinal bars and substantial damage to precast columns.
- *Unseating roof elements:* Connections between beams and columns in older buildings designed without seismic provisions relied only on friction. Mechanical connections between the columns and the roof girders were not included in the design.
- *Failure of the peripheral cladding panels:* Because the cladding connections were designed only for out-of-plane forces, the insufficient deformation capacity of the fastening systems in the longitudinal direction parallel to the panel plane led to the failure of panels. Mostly in older buildings, failure of the panels occurred also due to the failure of the main structural system.

The first two of the listed reasons for damage in precast structures were more evident during the earthquakes that occurred in the past. Formerly even the main precast structure, that is, columns and roof elements, was not designed according to seismic provisions. As the code provisions are improving, the behaviour of the newly designed precast structures on their own was relatively good during the recent earthquakes (e.g. L'Aquila earthquake), and the issue related to the inappropriate seismic response of the façade system was more exposed.

2.2 Past research and projects

In the past, major research activity considering the seismic response of RC buildings dealt with monolithic structures rather than with RC precast buildings. As mentioned in the Introduction, the lack of knowledge about the behaviour of precast structures has resulted in strict code requirements and a too-conservative approach for the design of this structural type. In the first draft of Eurocode 8, very low behaviour factors were defined for the design of precast structures, which put them at a disadvantage compared to the cast-in-situ RC structures.

On the initiative of the industrial sector, comprehensive systematic studies of RC precast buildings were performed within several EU research projects combining the efforts of industry and different

academic institutions. As a result, knowledge about the dynamic behaviour of prefabricated structures has improved, and the competitiveness of precast building stock was enhanced.

An excellent overview of the European research of seismic behaviour of precast structures done from the mid-nineties until 2015 was made by Toniolo (2012) and Fischinger et al. (2014). This section summarises the most relevant information and complements it with recent findings.

The first draft edition of the Eurocode 8 in 1994 with a considerably conservative approach to seismic design of precast structures was the main trigger. Soon after that, the Italian association of the prefabrication industry ASSOBETON has supported a series of cyclic and pseudo-dynamic tests on precast columns in pocket foundations (Saisi & Toniolo, 1998). The test campaign confirmed the good behaviour of the precast columns, but there was still no experimental evidence about the response of the complete precast structural system.

The European project ECOLEADER - *European Consortium of Laboratories of Earthquake Dynamic Experimental Research* has provided the experimental comparison between the precast and cast-in-place one-storey frame structure (Biondini & Toniolo, 2004; Ferrara et al., 2004; Biondini & Toniolo, 2009). Both prototypes were designed for the same base shear resistance and had the same fundamental period. Experimental results have demonstrated the same seismic capacity and quite similar behaviour of the two tested systems.

The next project, PRECAST - *Seismic Behaviour of Precast Concrete Structures with respect to Eurocode 8,* was supported by ten partners from Slovenia, Italy, Portugal, Greece and China. Within the project, pseudo-dynamic and cyclic tests of a full-scale one-storey precast structure were performed at ELSA, the European Laboratory for Structural Assessment in Ispra, Italy (Biondini et al., 2008). The tested structure had a realistic roof that proved to behave like a rigid diaphragm. Research also pointed out the significant effect that the connections between precast elements and cladding panels might have on the behaviour of the complete structure. In the case of the tested structure, the cladding panels changed the response significantly. This response, however, depends on the type of cladding connections used because different types of connections may provide different levels of interaction between the panels and the main structure (see Section 2.3).

As explained by Fischinger et al. (2014), the tested precast structure had large overstrength. Yielding of the columns was not observed until the last pseudo-dynamic test with a maximum ground acceleration of 0.525 g. Substantial top displacements of 40 cm or 8% drift were achieved, where the yield drift was over 2%. These large drifts match the response of precast RC buildings during the Emilia-Romagna earthquake. Ercolino et al. (2016) reported the large yielding rotations of precast columns at around 2% drift, which was also confirmed with subsequent nonlinear dynamic analyses.

Experimental research performed within the PRECAST project provided valuable data about the seismic response of RC precast structures, which was subsequently used in extensive numerical and analytical studies (Biondini & Toniolo, 2009; Kramar et al., 2010). In the past, numerical modelling of precast structures has been extensively studied at the University of Ljubljana (Kramar, 2008; Zoubek, 2015; Babič, 2017). An inelastic numerical model for columns was modified to accurately estimate the seismic response of slender columns typical of prefabricated industrial buildings (Fischinger et al., 2008). Such columns have high shear span ratios (height to width of column) of more than 10, low axial compressive load ratios (less than 0.16), high deformability and large deformation capacity (over 2% yield drift and around 8% ultimate drift).

The recommended model for columns (Fischinger et al., 2008) assumed a yield chord rotation (i.e. yield drift) to be the sum of theoretically determined flexural deformations as proposed by Fardis & Biskins (2003) and the empirically calibrated contributions of shear and bond-slip. The numerical model was validated by full-scale cyclic and pseudo-dynamic tests of a one-storey precast structure (Toniolo, 2007). The whole building was modelled as an equivalent cantilever column using the lumped plasticity beam-column element model with a zero-length plastic hinge at its base. The hysteretic moment–rotation response was described with two different models: the modified Takeda hysteretic model (Takeda et al., 1970) and the modified Ibarra hysteretic model (Ibarra et al., 2005) calibrated by Haselton (2006). Both were able to adequately describe the response observed within the tests. Verified models were further used in systematic seismic risk studies of realistic one-storey industrial buildings used in practice (Kramar et al., 2010).

Many experimental and numerical studies of the different types of connections, most commonly used in the European design practice of precast buildings, have been done within the European project SAFECAST - *Performance of Innovative Mechanical Connections in Precast Building Structures under Seismic Conditions*. Four classes of the connections were investigated: floor to floor, floor to beam, beam to column, and column to foundation (Toniolo, 2012b).

The most extensive and essential series of pseudo-dynamic tests of a full-scale, three-storey precast building were performed at the ELSA Laboratory of Ispra (Negro et al., 2013). Also, many tests on sub-assemblies of structural elements connected with joints have been done in other European laboratories. The main interest of the research team at the University of Ljubljana was the study of the beam-to-column dowel connections (Zoubek et al., 2013; Zoubek et al., 2014; Zoubek et al., 2015). The dowel-type connections are the most frequently used beam-to-column connections in Central European precast industrial buildings. Complete information about the failure mechanisms of dowel connections was obtained using numerical models calibrated by the set of experiments reported in Zoubek et al. (2013). The proposed procedure for calculating the resistance of a dowel

connection for different reinforcement layouts (Zoubek et al., 2015) is included in the recently composed draft of the Eurocode 8 standards.

The last joint EU project, SAFECLADDING - *Improved Fastening Systems of Cladding Wall Panels of Precast Buildings in Seismic Zones,* was devoted to the connections of façade cladding panels to the main structural system of industrial buildings. The goals of the project were identification of basic response mechanisms of different cladding connection types, improvement and definition of the design procedures and a proposal for the improvements of the connections (SAFECLADDING, 2015). Comprehensive experimental (Negro & Lamperti Tornaghi, 2017; Toniolo & Dal Lago, 2017) and analytical studies performed within the aforementioned European project considerably improved the knowledge about the seismic response of the cladding panel fastening systems.

Within the SAFECLADDING project, cyclic and pseudo-dynamic tests on full-scale structures were performed (Negro & Lamperti Tornaghi, 2017; Toniolo & Dal Lago, 2017), as well as many monotonic and cyclic tests of single connections (Zoubek et al., 2016a; Psycharis et al., 2018; Yüksel et al., 2018). The behaviour mechanisms of different connection types were defined, and proposed numerical models were used in many subsequent analytical and numerical studies. Three different basic concepts (presented in the following Section 2.3) were assessed and considered within the studies.

Part of the research, performed at the UL (Isaković et al., 2013; Fischinger et al., 2014; Isaković et al., 2014b), was devoted to the fastenings systems of vertical and horizontal cladding panels that are widely used in the existing practice in Central Europe. The behaviour of hammer-head strap connections that are typical cladding connections for vertical panels was explained and studied in detail by Zoubek et al. (2016a). A design procedure was also recommended, and reliable macro models for simulation of hysteretic response were proposed.

Recent projects significantly raised the awareness of many problems with the existing design and construction practice. One of the SAFECAST project outcomes was a manual, *Design Guidelines for Connections of Precast Structures under Seismic Actions* (Negro & Toniolo, 2012), which became an ISO standard ISO 20987:2019. The SAFECLADDING project resulted in the new design guidelines for precast structures with cladding panels (Colombo et al., 2016b) and wall panel connections (Colombo et al., 2016a).

Similar research campaigns were performed on national levels, mostly in Slovenia and Italy, in parallel with the mentioned European projects. The in-plane and the out-of-plane seismic response of the connections used to fasten the horizontal cladding panels was experimentally and analytically studied by Belleri et al. (2016; 2018). The isostatic types (described in Section 2.3) of connections

for vertical and horizontal panels were extensively investigated by Del Monte et al. (2019). They successfully modified the cladding connections to improve their displacement capacity.

Despite the extensiveness of the projects presented above, past research mainly focused on investigating the response of single components based on the monotonic and cyclic experiments. Many important observations about the seismic response of cladding panels typical for Central Europe have been obtained at the UL within the SAFECLADDING project. Many experiments have been done, and valuable data were obtained (Isaković et al., 2013; Isaković et al., 2014b; Zoubek et al., 2016a). Results of these studies have also been used within the STREST project (Esposito et al., 2020) to derive fragility functions of industrial precast building classes and perform seismic risk analyses (Babič & Dolšek, 2016). However, this research could not completely reveal and explain all the aspects of this complex response. The behaviour of the cladding systems under the dynamic loading was insufficiently studied. It was not possible to fully determine the role of panel fastenings and their realistic boundary conditions without a more complex study of the whole-system response. Research continued within the UL research project *Seismic resilience and strengthening of precast industrial buildings with concrete claddings*, funded by the Slovenian Research Agency (CLADDINGS, 2016) to find answers to these questions.

One of the main phases of this project was devoted to the full-scale shake table experiments of an RC building with cladding panels. Different parameters within these experiments were varied, including the orientation of cladding panels, the type of cladding-to-structure connections and the configuration of the specimen (symmetric and asymmetric).

To be able to set up these tests, additional cyclic and dynamic tests of the single components were performed to obtain as much data as possible about their basic seismic response mechanisms and their capacity. Experimental observations and results of the shake table tests with vertical panels are presented in Isaković et al. (2018), while the research on horizontal panels is the topic of this doctoral dissertation. The experimental studies were proceeded by the related analytical studies and numerical analysis.

2.3 The typology of the most common precast industrial buildings

According to the structural typology, a precast building can be classified into panel structures, column structures or mixed structures. One-storey and multi-storey buildings can be distinguished by the number of storeys. A more detailed description and classification of the precast structures can be found in the literature (e.g. Isaković et al., 2012c; Magliulo et al., 2014; Savoia et al., 2017). This section describes one-storey column structures because they are most common in Europe and

have been studied within the scope of the dissertation. The emphasis is made on the precast structures with horizontal RC façade systems.

The typical RC precast industrial building in Central Europe consists of an *assemblage of cantilever columns* tied together by roof girders in a shorter transverse direction, as shown in Figure 2.3. Commonly precast concrete slabs are laid on the roof beams, and the roof is supposed to act as a diaphragm, enabling the equal distribution of forces to all columns. The connections between columns and beams are typically pinned. The common Central European practice for a beam-to-column connection is the dowel-type connection, shown in Figure 2.4. However, in older industrial buildings, designed before the implementation of seismic codes, the beams have been simply laid at the top of columns. There were no dowels, and those connections have relied only on friction between the elements.

The relatively slender cantilever columns are characterised by high shear–span ratios and low axial compressive loading. Distance between columns is from 6 to 12.5 m in the longitudinal direction and can reach up to 30 m in the transverse direction. They form a square or rectangular shape, are usually single or double span (although multi-span buildings can also be found) in the transverse direction and with several bays in the longitudinal direction. The storey height ranges from 5 to 10 m. The columns are typically built into pocket foundations that provide moment resistance.

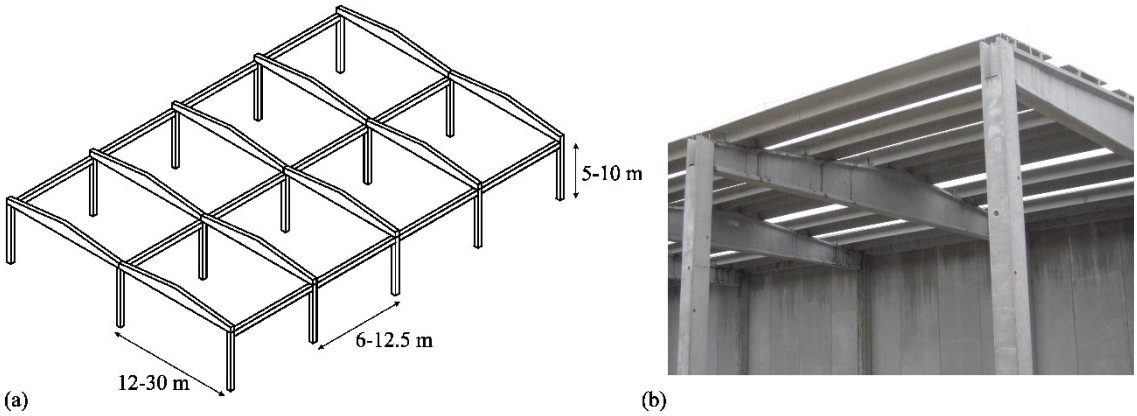

Figure 2.3: RC precast structure: (a) scheme of the structural system of the one-storey building and (b) the structure under construction

Slika 2.3: AB montažna hala: (a) shematski prikaz konstrukcijskega sistema enoetažnih hal in (b) montažna hala v izgradnji

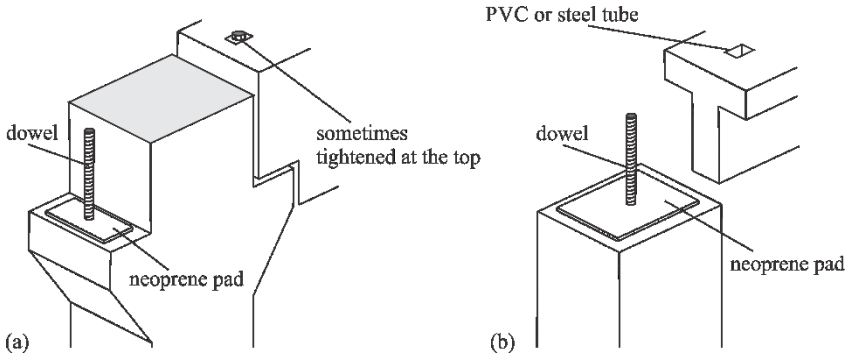

Figure 2.4: Beam-to-column dowel connection: (a) the connection constructed on the corbel and (b) the connection constructed at the top of the column (Zoubek, 2015)
Slika 2.4: Moznični stik med stebrom in nosilcem: (a) stik izveden na kratki konzoli ter (b) stik izveden na vrhu stebra (Zoubek, 2015)

The fundamental period of vibration of a typical one-storey RC precast industrial building is around one second and higher. As an example, the values calculated following a benchmark design study among Italy, Slovenia, Turkey and Greece range between 0.8 and 1.4 s (Bournas et al., 2013).

The main structure of an RC precast building is closed with infills or surrounded by prefabricated *façade panels*. RC or aluminium composite panels can be used. Usually, the panels are attached externally to the main structure; however, there are also solutions when they are inserted between columns.

RC façade panels are manufactured in different dimensions, with or without a thermal insulation layer between two concrete layers (Figure 2.5 a). Concrete panels with a thickness of 20 cm are often used for warehouses with no need for temperature control. Otherwise, the thermal insulation layer with a thickness of 10 and 15 cm is used for panels with a total thickness of 26 or 30 cm, respectively.

Two configurations of cladding panels are defined according to their geometry. The vertical panels have a height larger than their width, and horizontal panels have a width larger than their height. The horizontal façade panels are supposed to overcome the distance between adjacent columns with their width (from 6 to 12.5 m). Their height depends on the design of the building and may also vary along with the height of columns. Panels of height from 1.2 to 2.5 m can be found in Slovenian practice. Special transportation is required for the larger panels.

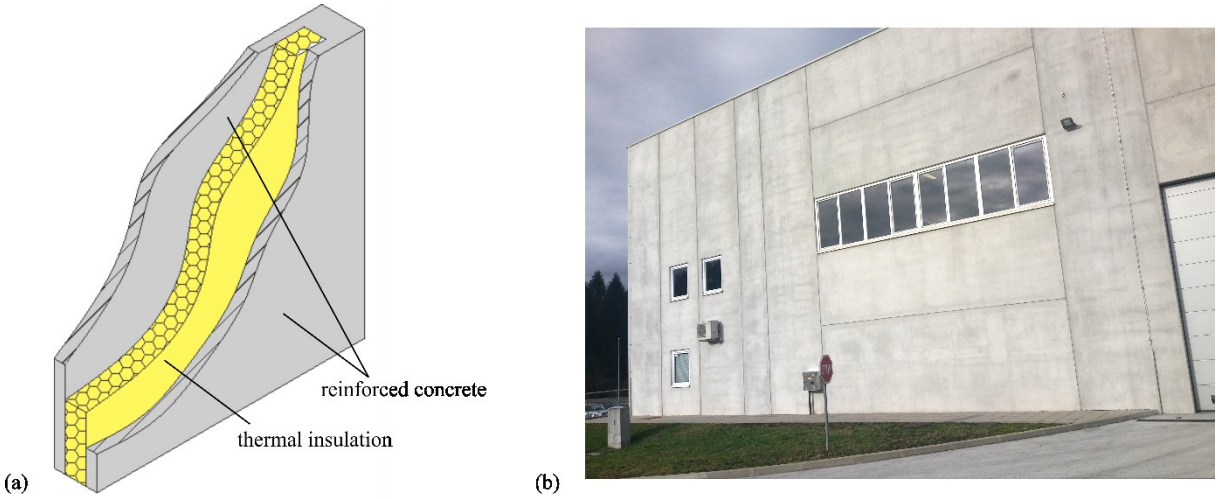

Figure 2.5: RC façade panels: (a) typical precast façade panel scheme with thermal insulation between the concrete layers and (b) a building with vertical and horizontal panels
Slika 2.5: AB fasadni paneli: (a) sheamtski prikaz fasadnega panela s toplotno izolacijo med zunanjo in notranjo AB plastjo in (b) objekt z vertikalnimi in horizontalnimi paneli

The type of cladding-to-structure *fastening system* mainly depends on the type of panels, that is, their orientation. Vertical panels are usually attached to beams, whereas horizontal panels are attached to columns of the main precast structure. Mixed solutions that include both vertical and horizontal panels are also used in European practice, as shown in Figure 2.5 (b).

A wide variety of the connections between façade panels and structural elements can be found in construction practice. Several producers provide different solutions based on steel connectors, such as channel bars, fasteners, angles and brackets, etc. (Magliulo et al., 2014). A comprehensive catalogue of existing cladding fastening systems used in Slovenia, Italy, Turkey and Greece was made within the SAFECLADDING project (Isaković et al., 2012a). Cladding connections that are being studied within this dissertation are typically used to attach the horizontal panels in RC industrial buildings in Central Europe. The considered fastening system consists of two main parts: a pair of top-bolted connections that provide the horizontal stability of the panel and a pair of bottom cantilever connections that support the panel weight. A detailed description and figures of the investigated fastening system are provided in Section 3.1.

Different types of cladding connections may provide different levels of interaction between the panels and the main structure. Three different basic concepts were assessed and considered within the studies (see also Negro & Lamperti Tornaghi, 2017; Toniolo & Dal Lago, 2017).

The integrated solution assumes that the connections provide full integration of the cladding panels into the main structural system (e.g. Psycharis et al., 2018). The main structure and panels are

restrained, and the displacements are coupled between the connecting parts. In such a system, the panel stiffness has an important influence on the overall response of a precast structure.

The isostatic solution assumes that the panels are isolated from the main precast structure, and the effect of the panel stiffness on the seismic response of the main structural system is small. The fastenings allow relative displacements between the panels and the main structural system by keeping the panels as non-structural elements (e.g. Dal Lago & Lamperti Tornaghi, 2018; Del Monte et al., 2019).

The arrangements of isostatic connection systems for vertical panels can be classified into: (a) the pendulum solution with a central hinged connection at the bottom of the panel and a central connection at the top (Figure 2.6 a), (b) the cantilever solution with fixed supports at the base of the panel and one or two sliding connections at the top (Figure 2.6 b), and (c) the rocking solution with two bottom bearings allowing uplifts of the panel, so to have the rocking behaviour at large displacements (Figure 2.6 c). The connections at the top of the panel should allow the vertical displacements for all three solutions to account for the thermal expansion (Toniolo & Dal Lago, 2017).

For the isostatic arrangement of horizontal panels, it is possible to use the so-called hanging solution, with two bearing brackets and two sliding joints at the top and bottom of the panel, respectively (Figure 2.7 a, b). In contrast, the seated solution (Figure 2.7 c, d) employs two bearing brackets at the bottom and two sliding joints at the top of the panel (Toniolo & Dal Lago, 2017). Within the present dissertation, only the seated isostatic type of connection for horizontal panels is considered.

The dissipative solution is in between the two approaches. In this solution, the fastening system of cladding panels or the connections placed between adjacent panels is used as an important source of energy dissipation (e.g. Dal Lago et al., 2017a; Dal Lago et al., 2018; Yüksel et al., 2018).

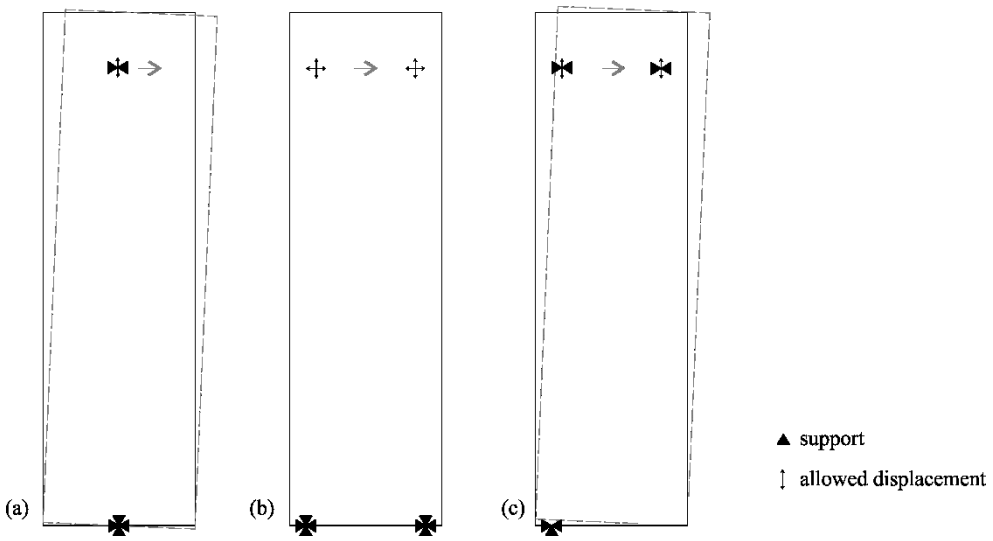

Figure 2.6: Isostatic arrangements of the connections for vertical panels: (a) pendulum solution, (b) cantilever solution and (c) rocking solution (Toniolo & Dal Lago, 2017)

Slika 2.6: Izostatične razporeditve stikov za vertikalne panele: (a) rešitev po principu nihala, (b) rešitev po principu konzole in (c) rešitev, ki dovoljuje rotiranje panelov okrog spodnjih robov

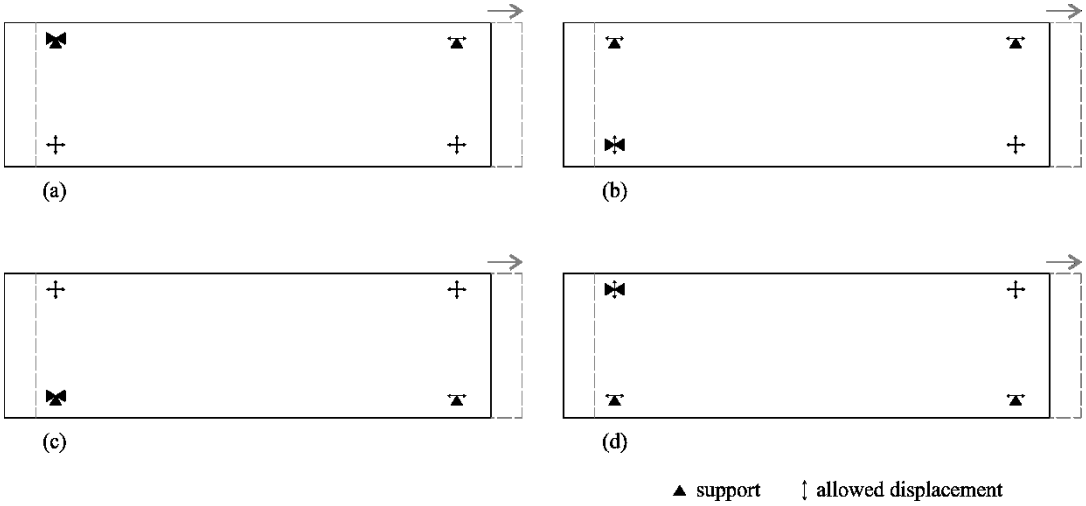

Figure 2.7: Isostatic arrangements of the connections for horizontal panels: (a, b) hanging solution and (c, d) seated solution (Toniolo & Dal Lago, 2017)

Slika 2.7: Izostatične razporeditve stikov za horizontalne panele: (a) obešen panel, v navpični smeri podprt z zgornjimi stiki in (b) posajen panel, v navpični smeri podprt s spodnjimi stiki

Many variations can be observed among connections between the panels and the foundation beam in European construction. Different solutions can provide total restraint of displacements or allow for the rocking of panels. The common Slovenian practice is shown in Figure 2.8 (a). The lowest panel is often attached to the foundation with steel anchors hammered into the façade panel and mounted into pre-drilled holes in the foundation beam. After assembly, the connection is grouted by mortar. However, some connections of the bottom panels to the foundation are made without

mechanical connections. In those cases, the panels and foundation are often joined together using slots and ribs.

Adjacent panels are typically connected by slots and ribs, as shown in Figure 2.8 (b). Horizontal and vertical joints between the panels are afterwards filled with the silicone strips. The primary role of the sealant is to provide waterproofing. It is also used to cover irregular slots and improve the appearance of the building. The sealant with a width-to-depth ratio of 2:1 is usually placed at both (external and internal) sides of the panels. The minimal silicone width depends on the joint length, from 20 mm for 6 m long panels to 35 mm for 10 m long panels. Dal Lago and other researchers (Dal Lago, 2015; Dal Lago et al., 2017b; Negro & Lamperti Tornaghi, 2017) have performed several experiments on concrete blocks, sub-assemblies, and full-scale structures with cladding panels sealed with silicone. They have provided some recommendations for considering the effect of silicone in the modelling and design of precast structures with RC panels.

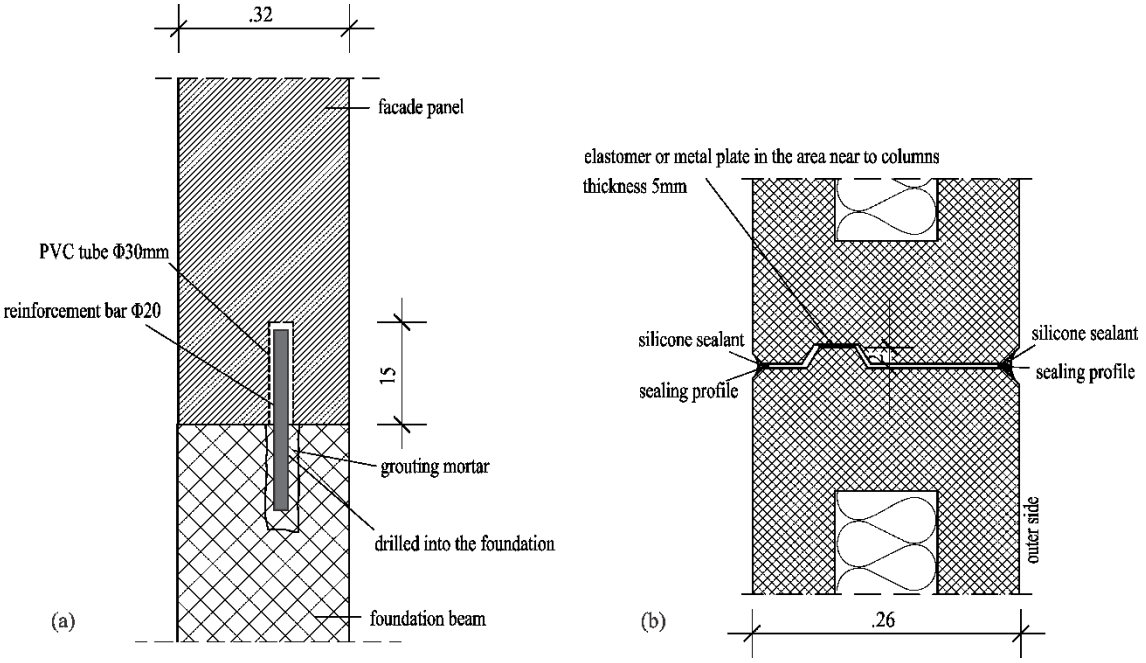

Figure 2.8: Cladding connections: (a) a connection between the cladding panel and the foundation beam and (b) a connection between adjacent cladding panels (Bužinel, 2019)

Slika 2.8: Fasadni stiki: (a) stik fasadnega panela s temeljem in (b) stik med sosednjimi fasadnimi paneli (Bužinel, 2019)

3 EXPERIMENTAL INVESTIGATION OF THE CLADDING CONNECTIONS

Although many important observations about the seismic response of cladding panels typically used in Central Europe have been obtained within the SAFECLADDING project (Fischinger et al., 2014; B. Zoubek et al., 2016; Toniolo & Dal Lago, 2017), this research could not completely reveal and explain all the aspects of this complex response. To obtain better insight into the earthquake performance of the complete precast structural system, the research project *Seismic resilience and strengthening of precast industrial buildings with concrete claddings*, funded by the Slovenian Research Agency, was launched (CLADDINGS, 2016). One of the main parts of this project was devoted to full-scale shake table experiments of an RC building with cladding panels.

Additional cyclic and dynamic tests of single components were performed to prepare for the complex shaking table tests. The main aim of the single component tests was to obtain as much data as possible about the basic seismic response mechanisms of the connections and their capacity before the experiment on the shaking table.

This chapter presents an experimental investigation of the cyclic and dynamic response of the typical fastening system for horizontal cladding panels in RC precast industrial buildings in Central Europe. The system consists of two main parts: a pair of top bolted connections that provide the horizontal stability of the panel and a pair of bottom cantilever connections that support the weight of the panel.

Two series of experiments were performed: (1) cyclic and dynamic tests of the top connections and (2) cyclic and dynamic tests of the complete fastening system (top bolted and bottom cantilever connections). A part of the cyclic tests of the top connections was performed within the European SAFECLADDING project and are included in the doctoral dissertation of Zoubek (2015). Those tests provided only part of the information about the response mechanism of the top connections. The response of the connections under dynamic loading was still completely unknown, and information about the response of the bottom connections was also needed.

In this chapter, cyclic tests of the top connections are augmented with the dynamic tests of the top connections and with the cyclic and dynamic tests of the complete fastening system. In the following paragraphs, the investigated fastening system and test setup are presented. The test results and observations are analysed. Typical response mechanisms of the components and the complete fastening system are presented, and the main response parameters are discussed.

3.1 Description of the tested cladding connections

The fastening system investigated within the presented research campaign is one of the most common systems used in Central Europe to attach horizontal cladding panels to the columns of RC precast structures. It consists of bolted connection for attaching the top part of the panel to the columns and a cantilever connection for supporting the panel in the vertical direction (Figure 3.1).

A This configuration that employs two bearing brackets at the bottom and two sliding joints at the top of the panel is a typical representative of the *seated solution* arrangement of isostatic panels. In contrast, it is also possible to use the *hanging solution* for horizontal panels with two bearing brackets and two sliding joints at the top and bottom of the panel, respectively (Toniolo & Dal Lago, 2017, see also Figure 2.7).

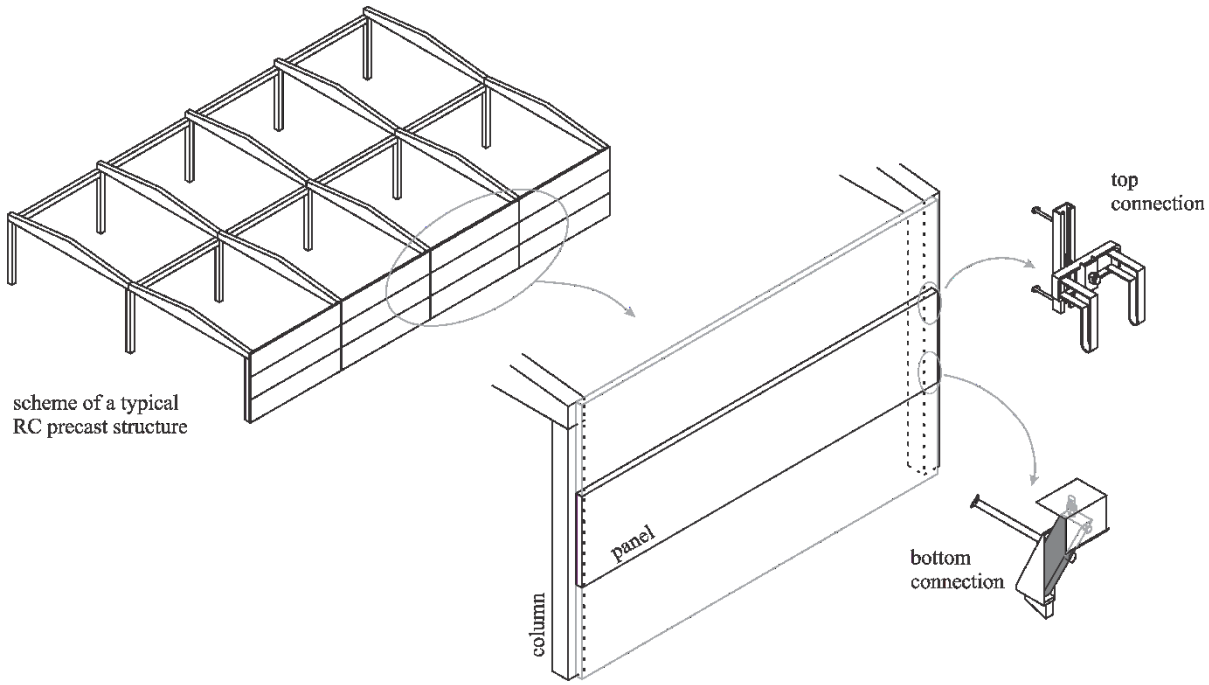

Figure 3.1: Scheme of a typical RC precast structure with horizontal panels
Slika 3.1: Shematski prikaz značilne armiranobetonske montažne hale s horizontalnimi paneli

The top connection is intended to provide out-of-plane stability of the panel (for this reason, it is also known as a tie-back connection). It consists of a vertical steel channel built into the column and a special box-shaped element cast in the panel, shown in Figure 3.2. These two elements are connected using a special hammer-head bolt set inside the channel (cast in the column) and firmly secured to the steel box element (cast in the panel) on the other side.

Bolts HS 40/22 M16 are typically used to attach panels to the column. The tightening torque prescribed by the producer is 65 Nm. Two quasi-static cyclic tests of the top connections were performed with cold-formed channels HTA 40/23, while the stronger hot-rolled channels HTA

40/22 were used (Figure 3.3 b, c) in all the other tests. All the components of the tested top bolted connections (Figure 3.3 a) were made from S275JR steel, except the bolts that had grade class 8.8.

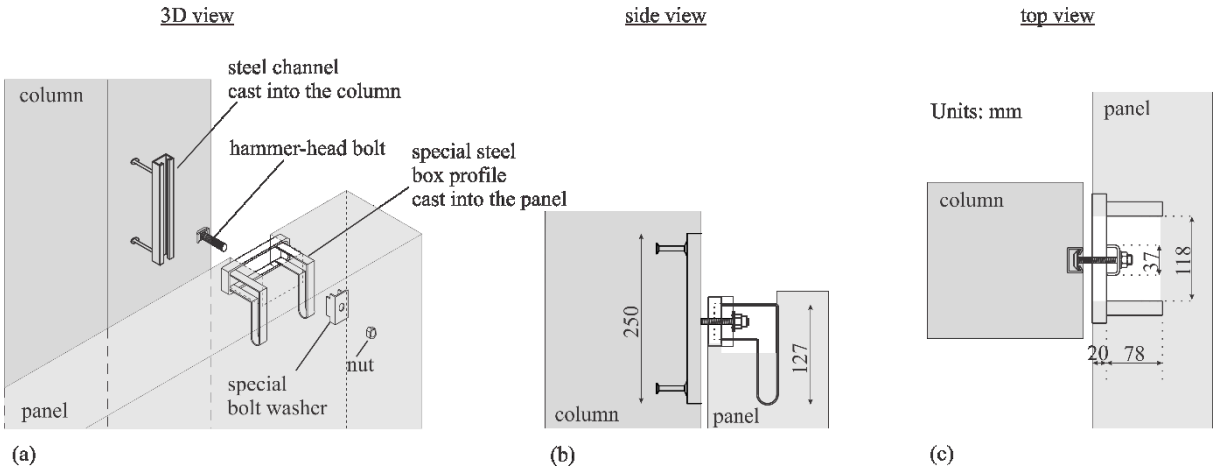

Figure 3.2: The assembly of the top bolted connection: (a) 3D view, (b) side view and (c) top view

Slika 3.2: Sestava zgornjega vijačenega stika: (a) 3D pogled, (b) stranski pogled in (c) pogled od zgoraj

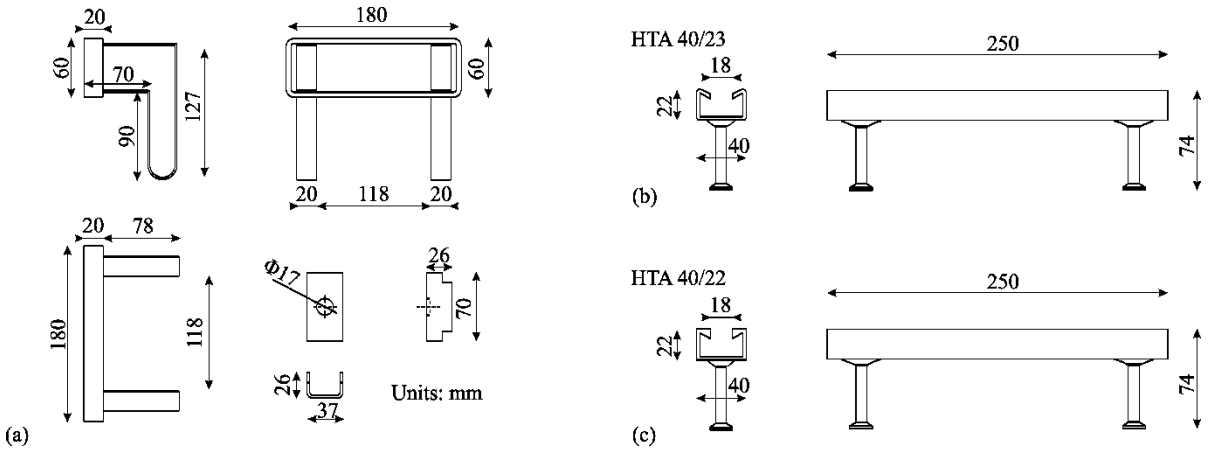

Figure 3.3: Geometrical details of the top bolted connection: (a) components of the connection, (b) cold-formed channels HTA 40/23 and (c) hot-rolled channels HTA 40/22

Slika 3.3: Geometrija zgornjega vijačenega stika: (a) komponente stika, (b) hladno oblikovani kanali HTA 40/23, ter (c) vroče valjani kanali HTA 40/22

The bottom component of the fastening system is a bearing cantilever connection (Figure 3.4 and Figure 3.5) placed at the bottom corners of the panel. The primary role of the bottom connection is to support the weight of the panel. It consists of a special steel box inserted in the column before casting, a steel bracket, and a steel plate cast into the panel.

During mounting of the panels, a cantilever steel bracket is placed in the steel box in the column and anchored to it using a skewed bolt. The tightening torque prescribed by the producer for this type of connection is 180 Nm. After that, the panel is simply laid on this steel cantilever element. Figure 3.4 shows that the panel is supported by the steel studs fastened to the top of the cantilever

brackets. These studs are used to regulate the level of the panel to account for tolerances. Finally, the panel is secured at the top with hammer-head bolts.

Steel brackets are available from the several producers that declare carrying capacities (in the vertical direction) of 50, 60, 80 or 120 kN. Typically, the steel box (cast into the column) and steel plate (cast into the panel) are made from S235JR steel, while the steel bracket is made from S355J0 steel. In the experiments, the steel cantilever bracket with a carrying capacity of 80 kN was used. All the tested connections are from the company Halfen (HALFEN, 2016) and can be found in their product catalogues.

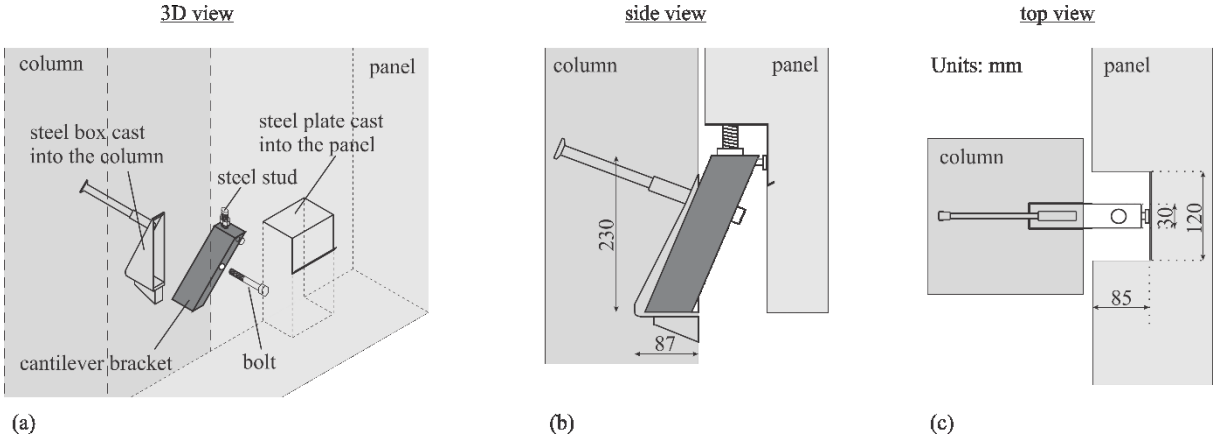

Figure 3.4: The assembly of the bottom cantilever connection: (a) 3D view, (b) side view and (c) top view

Slika 3.4: Sestava spodnjega konzolnega stika: (a) 3D pogled, (b) stranski pogled, ter (c) pogled od zgoraj

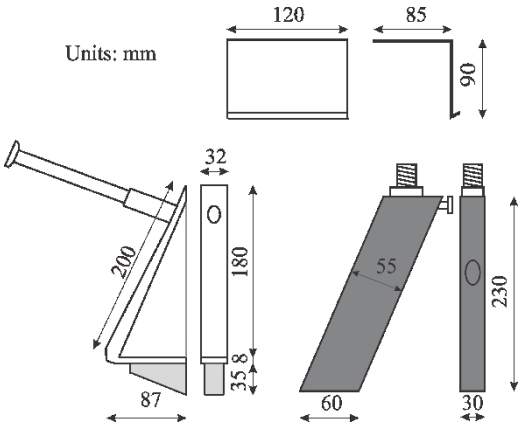

Figure 3.5: Geometrical details of components of the bottom cantilever connection

Slika 3.5: Geometrija komponent spodnjega konzolnega stika

3.2 Description of the experiments on the cladding connections

The tests on cladding connections for horizontal panels were performed in two series with the main aim of obtaining as much data as possible about the basic response mechanism of each of the components. First, the top bolted connections were tested cyclically and dynamically. For this series

of tests, the special steel rollers were utilised to provide vertical stability without compromising the horizontal resistance, as presented in the following paragraphs.

Because bottom cantilever connections are used mainly to support the weight of the panels, it was not possible to test only this component of the fastening system and at the same time ensure horizontal stability of the panel. Therefore, the second series of tests was performed on the complete fastening system consisting of top and bottom connections. Because the response of the top connections was known, it was possible to extract the response of the bottom connections from the tests performed on the complete fastening system.

The experiments on the cladding connections were performed at the laboratory of the Faculty of Civil and Geodetic Engineering, University of Ljubljana and at the Slovenian National Building and Civil Engineering Institute.

3.2.1 Description of the tested specimens and the test setup

Two series of experiments were performed:

(1) tests of the top connections, and

(2) tests of the complete fastening system consisting of top and bottom connections.

The general setup of the experiments is illustrated in Figure 3.6 and Figure 3.7. The inverted T-shaped beam was fixed to the laboratory floor. The panel was placed in parallel to the beam and connected to it using the fastening system. In the tests of top connections (Figure 3.6 a, b, c), the bottom of the panel was mounted on specially designed rollers that allowed for the friction-free movement of the panel parallel to the foundation beam. In the complete fastening system test (Figure 3.6 d, e, f), the bottom of the panel was supported by the cantilevers.

An actuator was connected to the panel, as illustrated in Figure 3.6 (c, f). The connections were tested in the horizontal direction parallel to the plane of panels.

To perform as many experiments as possible, the foundation block was designed to be used for two series of tests at each side. The top connections were tested in pairs. The inner top connections were used for one set of tests, and the outer two connections were used for the other set of tests (Figure 3.6 b). The distance between the connections was 45 cm in the case of the inner two connections and 135 cm in the outer two. The same approach was used to test the complete fastening system, consisting of two top and two bottom connections (Figure 3.6 e).

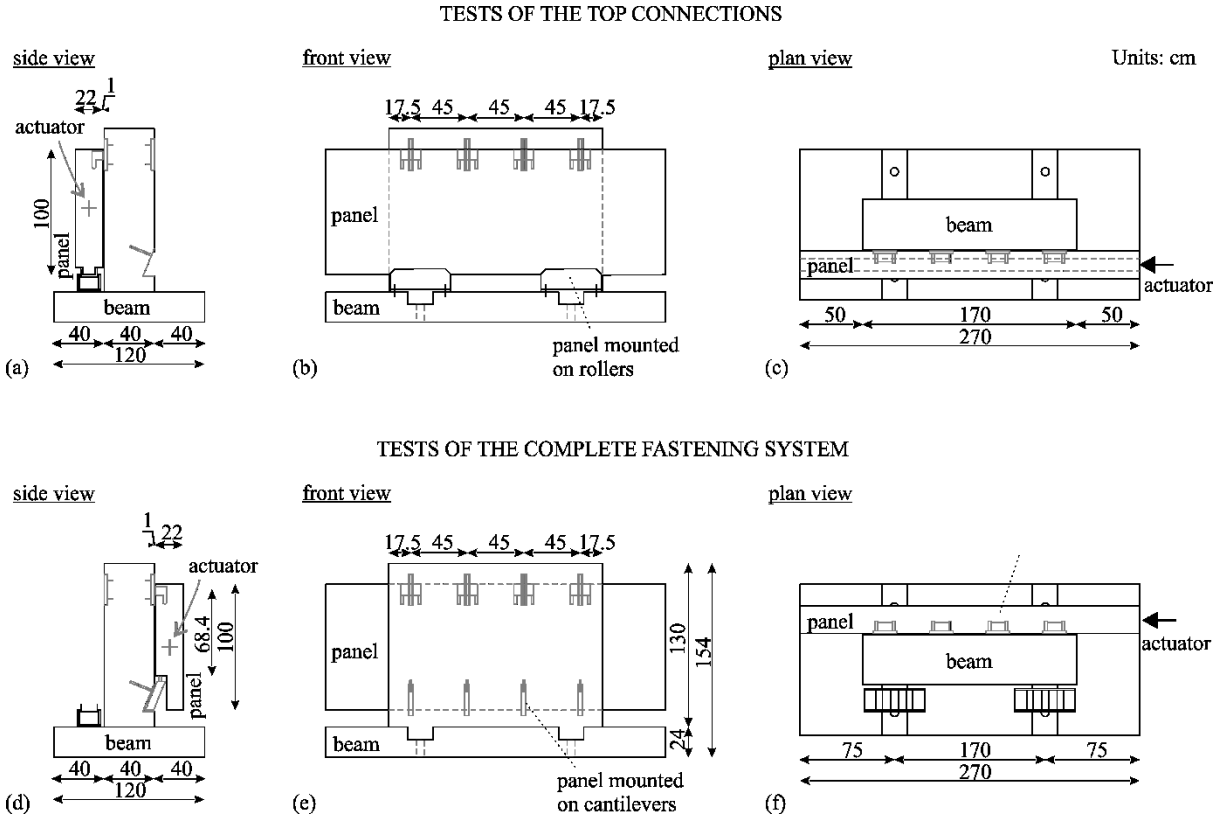

Figure 3.6: The general arrangement of the experimental setup: (a) side view of the specimen with the top connections, (b) front view of the specimen with the top connections, (c) plan view of the specimen with the top connections, (d) side view of the specimen with the complete fastening system, (e) front view of the specimen with the complete fastening system and (f) plan view of the specimen with the complete fastening system

Slika 3.6: Konfiguracija eksperimenta na fasadnih stikih: (a) stranski ris preizkušanca z zgornjimi stiki, (b) naris preizkušanca z zgornjimi stiki, (c) tloris preizkušanca z zgornjimi stiki, (d) stranski ris preizkušanca z zgornjimi in spodnjimi stiki, (e) naris preizkušanca z zgornjimi in spodnjimi stiki, ter (f) tloris preizkušanca z zgornjimi in spodnjimi stiki

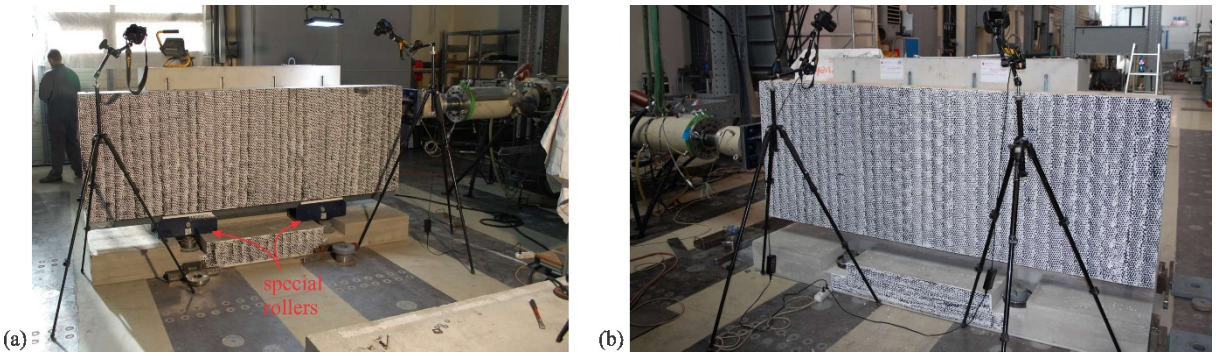

Figure 3.7: The experimental setup during testing (a) the top connections and (b) the complete fastening system

Slika 3.7: Postavitev preizkušanca med testiranjem (a) zgornjih stikov in (b) celotnega sistema stikov

3.2.2 Summary of the performed experiments and the loading protocol

The specimens were subjected to quasi-static cyclic or dynamic loading. In total, ten sets of experiments were performed. They are summarised in Table 3.1 and Table 3.2. Two quasi-static cyclic tests were performed on the top connections (denoted with *'Tc'*) and two quasi-static cyclic tests on the complete fastening system (*'Cc'*). Four and two dynamic tests were performed on the top connections (*'Td'*) and the complete fastening system (*'Cd'*), respectively.

The loading protocol for the *quasi-static cyclic tests* is presented in Figure 3.8. It is based on FEMA 461 guidelines (ATC, 2007) and features two full cycles per displacement amplitude and a gradual increase in the displacement amplitude (Isaković et al., 2013). The displacement amplitude a_{i+1} of the step $i+1$ is given by Equation 3.1. After the first two steps at 1.92 mm, the displacement amplitude was increased to 78.4 mm. The detailed testing schedule for quasi-static cyclic tests is provided in Table 3.3.

$$a_{i+1} = 1.4\, a_i \tag{3.1}$$

Table 3.1: Summary of the quasi-static cyclic experiments
Preglednica 3.1: Povzetek kvazi-statičnih cikličnih eksperimentov

Test	Type of the connections	Load type	Number of different amplitudes	Max amplitude [cm]
Tc1	Top connections	quasi-static cyclic	11	5.6
Tc2	Top connections	quasi-static cyclic	12	7.8
Cc1	Complete fastening system	quasi-static cyclic	12	7.8
Cc2	Complete fastening system	quasi-static cyclic	12	7.8

Table 3.2: Summary of the dynamic experiments
Preglednica 3.2: Povzetek dinamičnih eksperimentov

Test	Type of the connections	Load type	Number of runs	Max displacement [cm]	Max velocity [m/s]
Td1	Top connections	dynamic	5	8.2	0.10
Td2	Top connections	dynamic	3	11.0	0.13
Td3	Top connections	dynamic	3	11.0	0.13
Td4	Top connections	dynamic	3	11.0	0.13
Cd1	Complete fastening system	dynamic	5	5.9	0.07
Cd2	Complete fastening system	dynamic	5	5.9	0.07

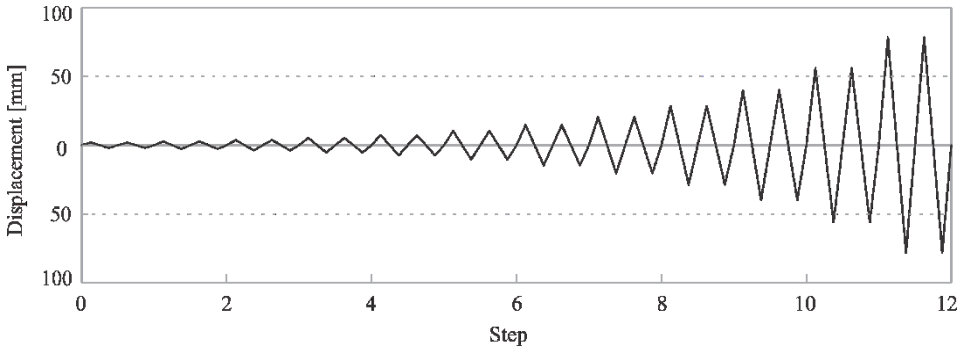

Figure 3.8: Displacement protocol for quasi-static cyclic tests

Slika 3.8: Protokol cikličnega obteževanja

The loading protocol for the *dynamic tests* was determined based on the estimated displacements and velocities in the connections of an actual building and considering the capacity of the hydraulic system. The actuator with a capacity of 250 kN (with a ±200 mm stroke) was used during the quasi-static tests. However, when performing dynamic tests, the capacity of the actuator is managed by the capacity of the hydraulic system, and the maximum force capacity is co-dependent on the applied velocities. This means that smaller forces can be reached at higher velocities.

To estimate the range of displacements and velocities, the response-history analysis of a structure planned to be tested on the shaking table was considered. The modified accelerogram corresponding to the acceleration spectrum matching the Eurocode acceleration design spectrum for soil type B (CEN, 2004) was used in the analysis. The Petrovac N-S (north-south) accelerogram registered during the Montenegro 1979 earthquake was used as the starting point to define the modified excitation. The dynamic analysis used 2% damping. The applied displacement response history was defined, considering these analytical studies and the capacity of the actuator used in the tests.

Each test consisted of several test runs with different intensities, as listed in Table 3.4. The displacement amplitude (and consequently also the velocities) gradually increased up to the failure of connections or the capacity of the actuator. The applied dynamic load (displacements and velocities) that corresponds to the scale factor 1.0 (see Table 3.4) is shown in Figure 3.9.

When the top connections were tested, the bolts were retightened to 65 Nm before each test run. In the complete fastening system tests, the bolts were tightened to 65 Nm only before the first run.

Besides tests on the connections, two dynamic tests without fastenings were performed (denoted with *'Nd'*) to evaluate the effectiveness of the special rollers at the bottom of the panel used in tests of the top connections. The complete testing schedule for dynamic tests is provided in Table 3.4.

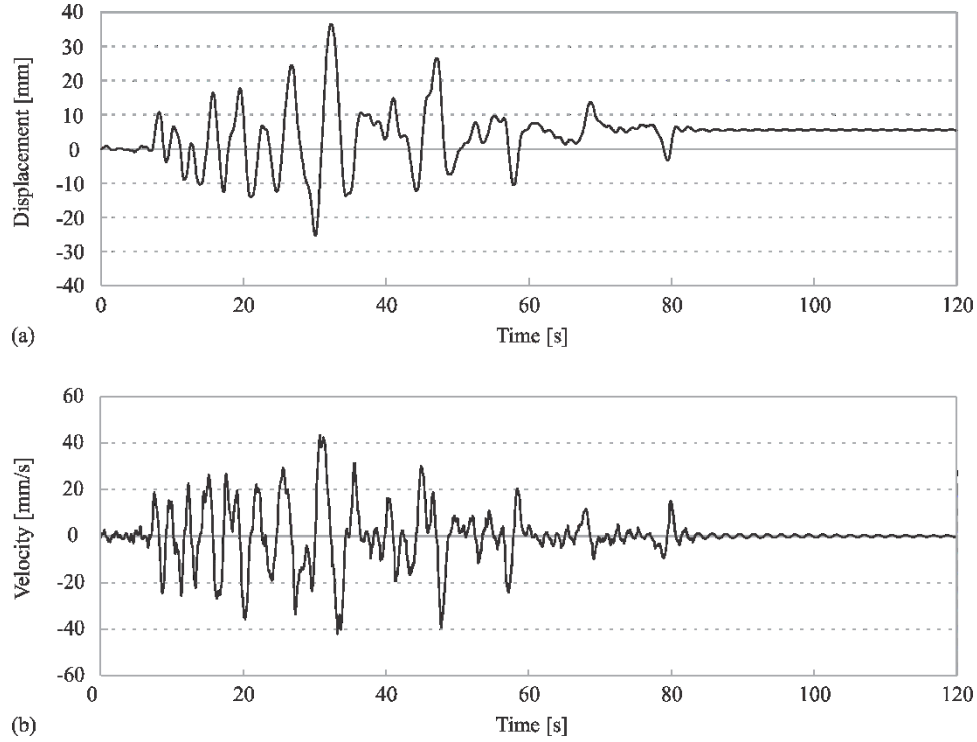

Figure 3.9: Testing protocol for dynamic tests: (a) displacement response history and (b) velocity response history

Slika 3.9: Protokol dinamičnega obteževanja: (a) časovni odziv pomikov in (b) časovni odziv hitrosti

Table 3.3: Complete testing schedule for the quasi-static cyclic tests

Preglednica 3.3: Celoten program kvazi-statičnih cikličnih preizkusov

Test	Type of the connections	Channel type	Position of the connections	Tightening torque [Nm]	Load type	Number of cycles	Number of different amplitudes	Applied displacement amplitudes [mm]
Tc1	Top connections	cold-formed	outer	65	cyclic	22	11	1.92 / 2.72 / 3.8 / 5.3 / 7.4 / 10.4 / 14.6 / 20.4 / 28.6 / 40 / 56
Tc2	Top connections	cold-formed	inner	65	cyclic	23	12	1.92 / 2.72 / 3.8 / 5.3 / 7.4 / 10.4 / 14.6 / 20.4 / 28.6 / 40 / 56 / 78.4
Cc1	Complete fastening system	hot-rolled	outer	65	cyclic	24	12	1.92 / 2.72 / 3.8 / 5.3 / 7.4 / 10.4 / 14.6 / 20.4 / 28.6 / 40 / 56 / 78.4
Cc2	Complete fastening system	hot-rolled	inner	65	cyclic	24	12	1.92 / 2.72 / 3.8 / 5.3 / 7.4 / 10.4 / 14.6 / 20.4 / 28.6 / 40 / 56 / 78.4

Table 3.4: Complete testing schedule for the dynamic tests

Preglednica 3.4: Celoten program dinamičnih preizkusov

Test	Type of the connections	Channel type	Position of the connections	Tightening torque [Nm]	Load type	Number of runs	Scale factor for test run	Max displacement for test run [cm]	Max velocity for test run [m/s]
Td1	Top connections	hot-rolled	outer	65	dynamic	5	0.5 / 1.0 / 1.5 / 2.0 / 2.5	1.8 / 3.7 / 5.5 / 7.3 / 8.2	0.02 / 0.04 / 0.06 / 0.09 / 0.10
Td2	Top connections	hot-rolled	inner	65	dynamic	3	1.0 / 2.0 / 3.0	3.7 / 7.3 / 11.0	0.04 / 0.09 / 0.13
Td3	Top connections	hot-rolled	outer	65	dynamic	3	1.0 / 2.0 / 3.0	3.7 / 7.3 / 11.0	0.04 / 0.09 / 0.13
Td4	Top connections	hot-rolled	inner	65	dynamic	3	1.0 / 2.0 / 3.0	3.7 / 7.3 / 11.0	0.04 / 0.09 / 0.13
Cd1	Complete fastening system	hot-rolled	inner	65	dynamic	5	1.0 /1.1 / 1.2 / 1.5 / 1.6	3.7 / 4.0 / 4.4 / 5.5 / 5.9	0.04 / 0.05 / 0.05 / 0.06 / 0.07
Cd2	Complete fastening system	hot-rolled	outer	65	dynamic	5	1.0 /1.2 / 1.4 / 1.5 / 1.6	3.7 / 4.4 / 5.1 / 5.5 / 5.9	0.04 / 0.05 / 0.06 / 0.06 / 0.07
Nd1	No connections	/	/	/	dynamic	1		3.7	
Nd2	No connections	/	/	/	dynamic	1		3.7	

3.3 Results and observations of the experiments

The test results are presented in the form of force–displacement hysteretic responses. The rigid foundation beam was fixed to the laboratory floor, and the displacements were imposed only on the panel. In this way, the imposed displacements were, at the same time, the relative displacements between the panel and the beam. Thus, the imposed displacements correspond to the displacements of each connection, and the recorded force in the actuator presents the sum of forces in tested connections. Equality of the displacements was additionally confirmed with the optical deformation measuring system GOM Aramis 5M (ZAG, 2019) that was also used. The main reason for using the optical system was to control the panel movements in the vertical direction, which were found to be negligibly small.

In the following paragraphs, the seismic response mechanism of the fastening system and characteristic response points are identified based on the typical hysteretic responses and observations during the experiments.

3.3.1 Test results of the top connections

The hysteretic responses observed during the cyclic and dynamic tests of top connections are presented in Figures 5.11 and 5.12, respectively. Each plot shows the results of all test runs performed within the addressed test. In figures representing hysteretic responses, the maximum friction forces (R_{fr}) and gaps in the connections (d_{gap}) are marked. An overview of the experimental results is presented in Table 3.5.

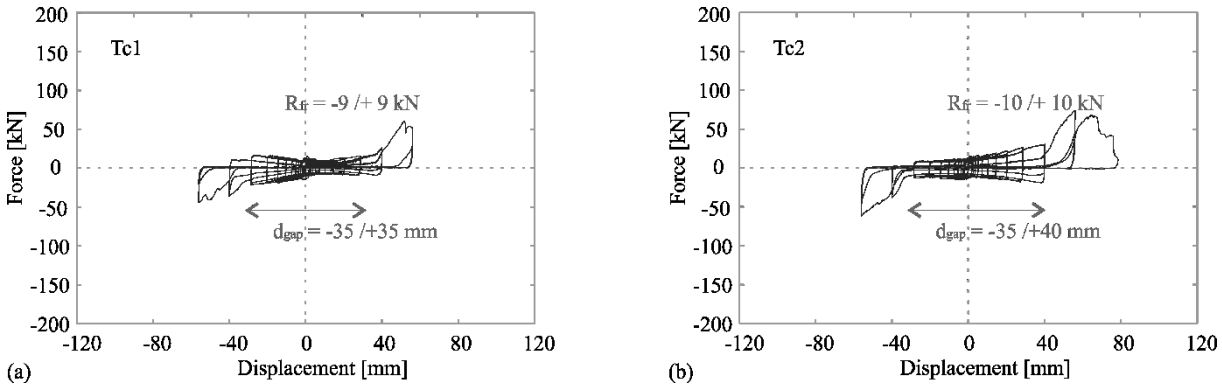

Figure 3.10: Hysteretic responses of the top connections during the quasi-static cyclic tests: (a) test *Tc1* and (b) test *Tc2*

Slika 3.10: Histerezni odziv zgornjih stikov med kvazi-statičnimi cikličnimi testi: (a) test *Tc1* and (b) test *Tc2*

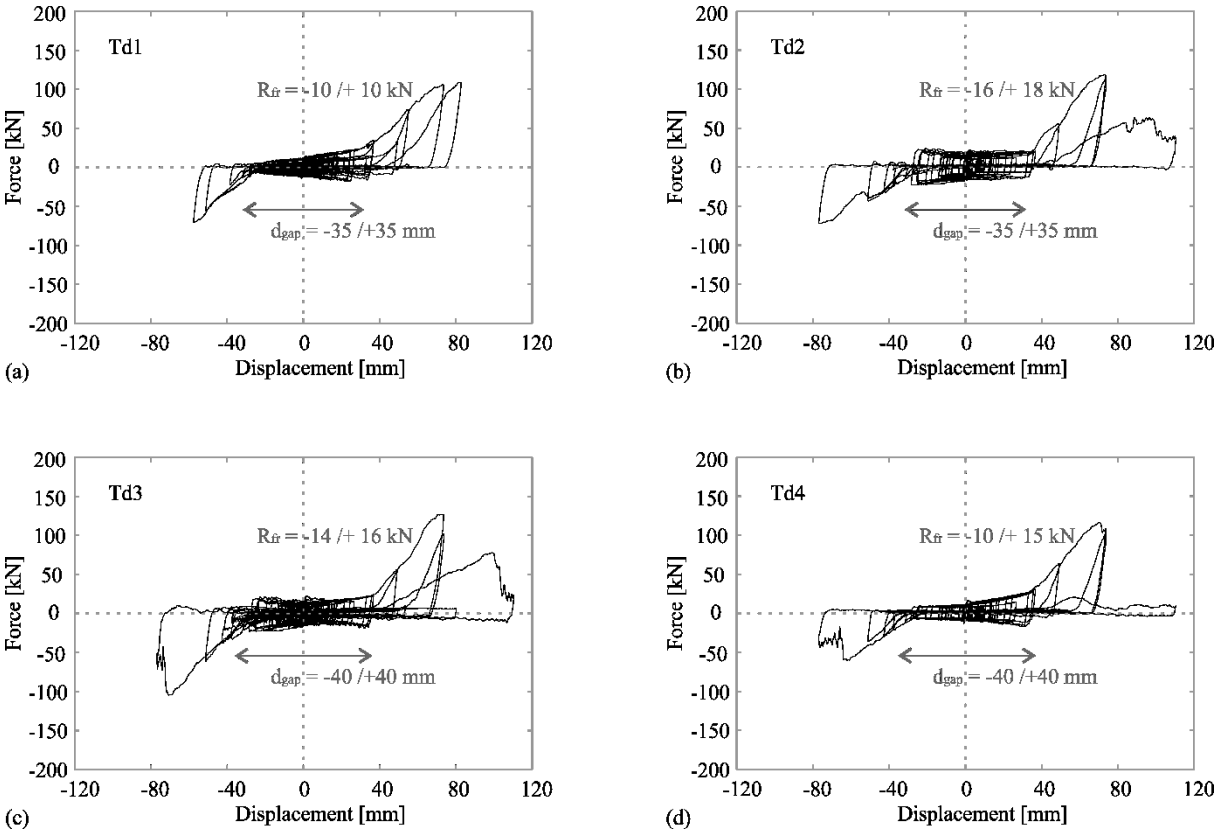

Figure 3.11: Hysteretic responses of the top connections during the dynamic tests for all performed test intensities: (a) test *Td1*, (b) test *Td2*, (c) test *Td3* and (d) test *Td4*

Slika 3.11: Histerezni odziv zgornjih stikov med dinamičnimi testi, prikazan za vse intenzitete: (a) test *Td1*, (b) test *Td2*, (c) test *Td3* and (d) test *Td4*

Table 3.5: Overview of the test results of the top connections

Preglednica 3.5: Povzetek rezultatov testov na zgornjih stikih

Test	R_{fr} [kN]	d_{gap} [mm]	R_{max} [kN]	d_u [mm]
Tc1	−9 / +9	−35 / +35	−44 / +60	−56 / +56
Tc2	−10 / +10	−35 / +40	−61 / +74	−56 / +56
Td1	−10 / +12	−35 / +35	−70 / +107	−58 / +83
Td2	−16 / +18	−35 / +35	−72 / +119	−77 / +73
Td3	−14 / +16	−45 / +35	−105 / +127	−71 / +73
Td4	−10 / +15	−35 / +35	−60 / +116	−64 / +74

3.3.2 Response mechanism of the top bolted connections

The response of the top bolted connections consists of three main stages, as presented in Figure 3.12 and marked with dots in typical hysteretic response shown in Figure 3.13:

(1) In the first phase (between dots 1 and 2), the bolt slides along the steel box profile cast in the panel (see Figure 3.12 and Figure 3.13). A limited friction force of about 10–16 kN (corresponding to the pair of connections) is activated at this stage. Its amount depends on the tightening moment applied to the bolt and the coefficient of friction between the special steel washer and the steel box profile cast in the panel (see Figure 3.12). The sliding phase is accompanied by a small increase in forces due to untightening of the bolt.

(2) The second stage (between dots 2 and 3) starts when the bolt washer reaches the edge of the steel box (see Figure 3.12 b), corresponding to a bolt slip of d_{gap} = 3–4 cm when the connections are centrally mounted. At this stage, the bolt is subjected to bending. Consequently, the lateral stiffness of the connection increases considerably (Figure 3.13 between dots 2 and 3). Plastic deformations of the bolt and the channel cast in the column gradually increase.

(3) At the last stage, the failure of the connection is reached (dot 3 in Figure 3.13). The connection typically fails due to the considerable plastic deformations of the channel and the bolt being pulled out (Figures 3.12 and 3.13, Stage 3).

The quasi-static cyclic tests were performed using cold-formed channels, whereas stronger, hot-rolled channels were used for dynamic tests. For this reason, the failure of the connections during quasi-static tests occurred at a somewhat smaller displacement and approximately two times smaller maximum forces at the failure. However, the response and failure mechanisms were the same in both cases. The results match Zoubek's (2015) observations, who considered only the quasi-static cyclic tests of the top bolted connections.

Failure was achieved in five out of six tests. Only sample *Td3* did not fail, but the channels and the bolts were severely deformed, and a decrease in the force resistance was observed. As mentioned, failure occurred due to the failure of the channel that led to the pull-out of the bolt. The shear failure of the bolt was only observed in one case (test *Td4*). However, in the same test, the other bolt was pulled out of the channel, and the hysteresis was not different from the other tests.

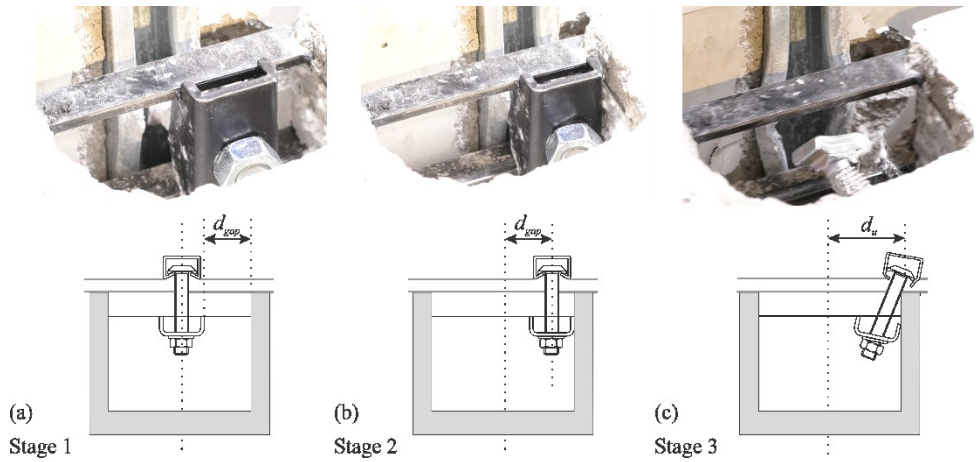

Figure 3.12: Response mechanism of the top bolted connections: (a) initial position, (b) the special bolt washer reaches the edge of the steel box profile cast in the panel and (c) failure due to the plastic deformations of the channel and the bolt being pulled out

Slika 3.12: Mehanizem odziva zgornjega vijačenega stika: (a) začetna lega, (b) podložka vijaka doseže rob jeklenega profila v panelu, in (c) porušitev stika zaradi plastičnih deformacij kanala in izpuljenja vijaka

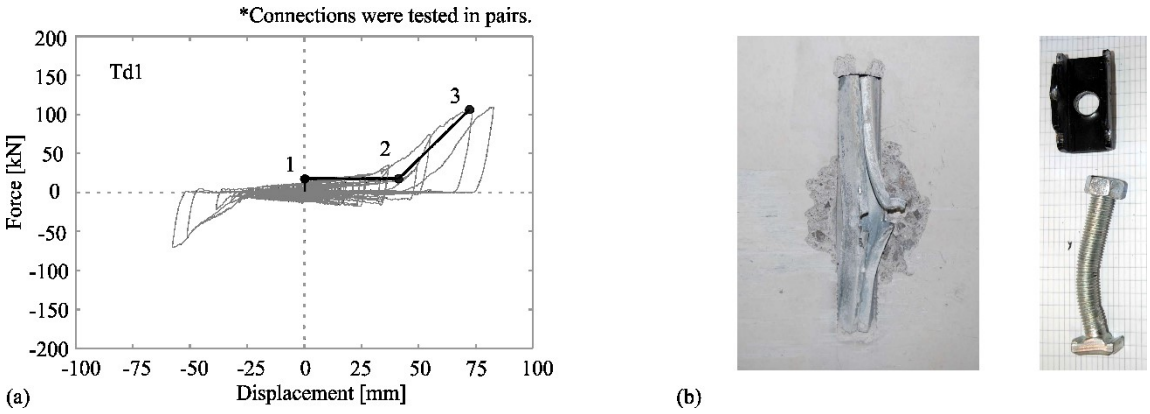

Figure 3.13: Test of the top bolted connections: (a) typical hysteretic response of the top connections, (b) failure of the channel and deformed bolt

Slika 3.13: Preizkus zgornjih vijačenih stikov: (a) značilen histerezni odziv zgornjih stikov, (b) porušitev kanala in deformiran vijak

3.3.3 Test results of the complete fastening system

Results of the cyclic and dynamic tests of the complete fastening system are presented in Figures 5.13 and 5.14, respectively. The hysteretic responses that correspond to all the test intensities are shown on each plot. As for the case of the top connections, the initial gaps (d_{gap}) and maximum friction forces (R_{fr}) are marked for each test. An overview of the test results of the complete fastening system is presented in Table 3.6.

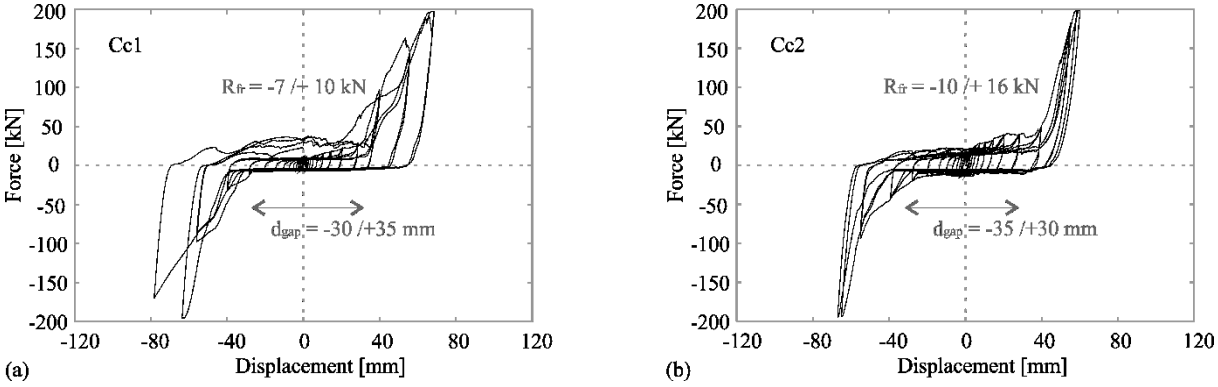

Figure 3.14: Hysteretic responses of the complete fastening system during the quasi-static cyclic tests: (a) test *Cc1* and (b) test *Cc2*

Slika 3.14: Histerezni odziv sistema stikov med kvazi-statičnimi cikličnimi testi: (a) test *Cc1* and (b) test *Cc2*

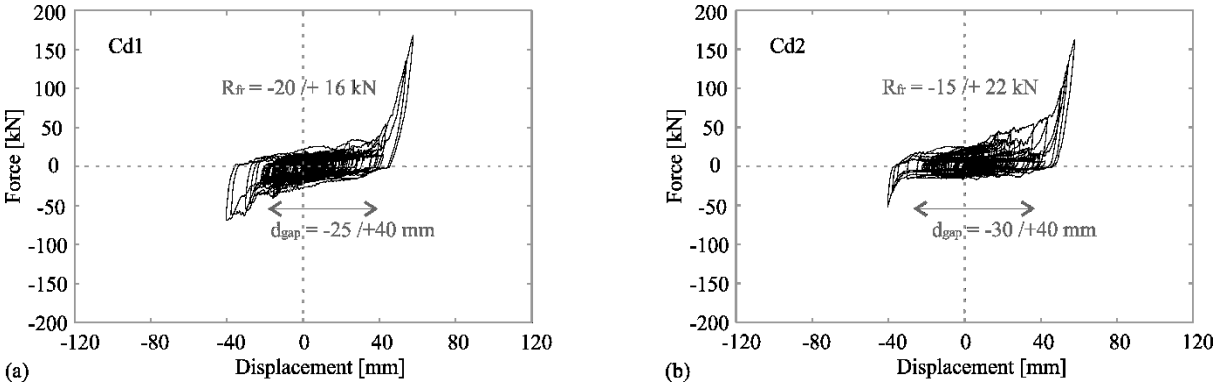

Figure 3.15: Hysteretic responses of the complete fastening system connections during the dynamic tests: (a) test *Cd1* and (b) test *Cd2*

Slika 3.15: Histerezni odziv sistema stikov med dinamičnimi testi: (a) test *Cd1* and (b) test *Cd2*

Table 3.6: Overview of the test results of the complete fastening system

Preglednica 3.6: Povzetek rezultatov testov na celotnem sistemu stikov

Test	R_{fr} [kN]	$d_{gap,top}$ [mm]	$d_{gap,bottom}$ [mm]	R_{max} [kN]	d_u [mm]
Cc1	−7 / +10	−30 / +35	−40 / +45	−194 / +197	−65 / +69
Cc2	−10 / +16	−35 / +30	−45 / +45	−194 / +199	−68 / +61
Cd1	−20 / +16	−25 / +40	−40 / +45	−69 / +167	−41 / +59
Cd2	−15 / +22	−40 / +40	−30 / +45	−52 / +162	−40 / +59

3.3.4 Response mechanism of the complete fastening system

The *response mechanism of the top connections*, observed within the experiments of the complete fastening system, was the same as described in Section 3.3.2.

The *response mechanism of the bottom cantilever connections* also consisted of three main stages, presented in Figure 3.16:

(1) Initially, the friction force was activated (Figure 3.16 a), followed by the sliding of the panel. The friction was considerably smaller than in the top connections.

(2) When the available gap in the connection was exhausted (Figure 3.16 b), the stiffness of the connection increased considerably due to the bending of the cantilever bracket.

(3) Due to the large stiffness and the strength of the cantilever bracket, the response of the connections was predominantly elastic. At the end of the tests (which were mostly terminated because the total capacity of the hydraulic system was approaching), limited plastic deformations of the steel cantilever were observed (see Figure 3.16 c).

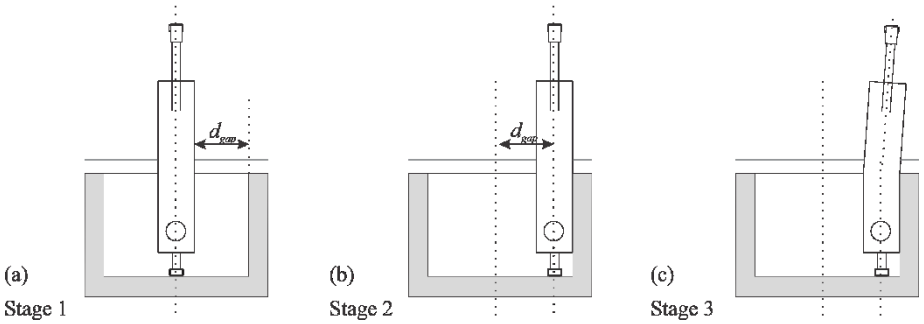

Figure 3.16: Behaviour mechanism of the bottom bearing cantilever connection: (a) initial position, (b) the cantilever bracket reaches the edge of the opening, and (c) minor deformations in the connection at the end of the test

Slika 3.16: Mehanizem odziva spodnjega konzolnega stika: (a) začetna lega, (b) jeklena konzola doseže rob odprtine v panelu, in (c) na koncu testa je kozola le minimalno deformirana

The response mechanism of the top and bottom connections was, in general, similar. Thus *the response of the complete fastening system* can also be characterised by three main stages (see the typical hysteretic response, presented in Figure 3.17 a):

(1) The friction force, which activated in the top and bottom connections at the beginning of the tests, was approximately 20 kN. It was mainly activated at the top connections (amounting to about 16 kN, see also Section 3.3.2 for more details).

(2) When the gaps in the top and bottom connections were depleted at a displacement of around 4 cm (note that the gaps in the top and bottom connections were quite similar), the stiffness was considerably increased due to the activated bending stiffness of the bolts and the channels of the top connections and the bending stiffness of the cantilever brackets in the bottom connections. The comparison between the response of the complete fastening system and that of the top connections confirmed that the increase in the stiffness of the whole

fastening system was considerably higher, mainly due to the activated bending stiffness of the cantilever bracket at the bottom connection.

(3) Due to the depleted capacity of the actuator, the tests were terminated before the connections failed. At that moment, however, the top connections were considerably damaged, and the channels and bolts at the top were substantially and irreversibly deformed (see Figure 3.17 b). In some cases, the concrete around the top connections was also damaged (see Figure 3.17 c). The failure of the top connections was likely to occur at a relatively small increase in the displacement demand. Because the damage to the bottom cantilever was minor at the same time (see Figure 3.17 b), it can be concluded that the failure of the whole fastening system would occur due to the failure of the top connection. This failure (as explained in Section 3.3.2) typically occurs due to the considerable plastic deformations of the channel and the bolt being pulled out.

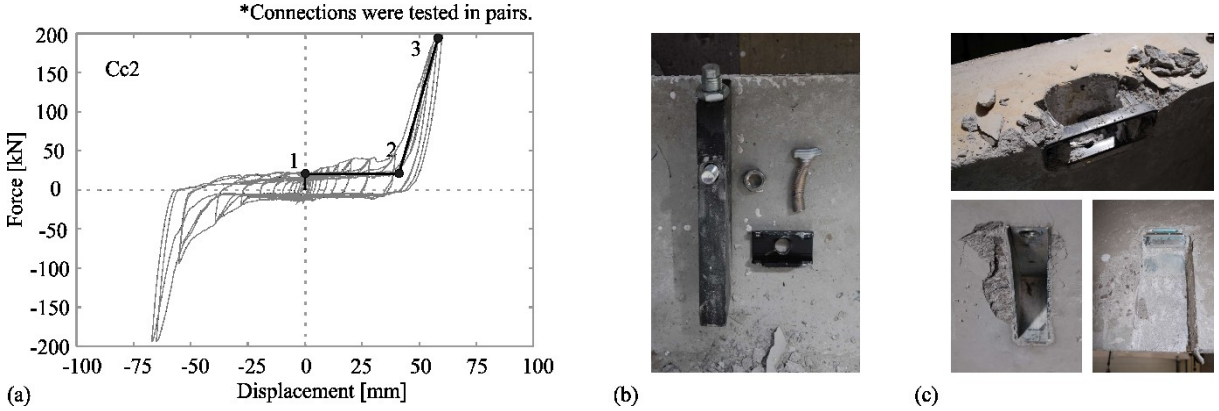

Figure 3.17: Test of the complete fastening system: (a) typical hysteretic response of the complete fastening system, (b) damaged connection parts after the test and (c) damaged concrete around the connections after the test

Slika 3.17: Test celotnega sistema fasadnih stikov: (a) značilen histerezni odziv sistema stikov, (b) poškodovani deli stika, in (c) poškodovan beton v okolici stika

3.3.5 Analysis and discussion of the response parameters

In the following paragraphs, the seismic response mechanisms of the tested connections (described in Sections 3.3.2 and 3.3.4) are elaborated in detail. First, the response envelopes of the cladding connections are defined. The main response parameters discussed include the size of the gap in the connections, displacement capacity of the fastening system, the stiffness of connections, the friction force between the elements and the maximum force. Further, the effect of the load type, the influence of the type of channels and the position of the connections are analysed.

At the end of this section, a short discussion about the repeatability of experiments is provided. The effectiveness of the rollers used during the tests of top connections is also discussed.

Response envelopes of the connections

To better illustrate the observations in Sections 3.3.2 and 3.3.4, the response of the top connections and the whole fastening system are compared in Figure 3.18. Both plots also show the corresponding envelope of the response (bold black line). In this particular case, the gaps at the top and the bottom connections were depleted approximately at the same time. Note, however, that this is not the rule, and it depends on the construction tolerances (the bolt and the cantilever bracket may not be positioned centrally).

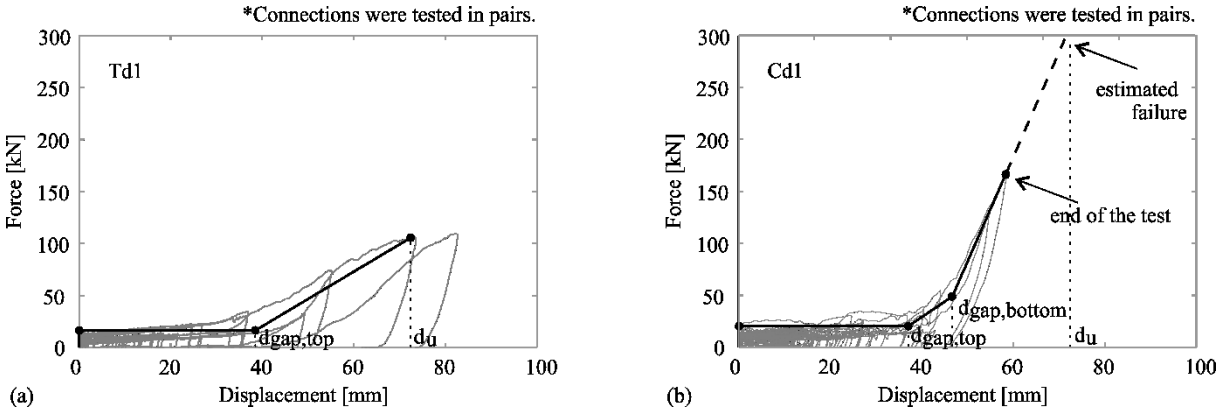

Figure 3.18: Response envelopes of the connections: (a) top connections and (b) complete fastening system
Slika 3.18: Ovojnice odziva stikov: (a) zgornji stik in (b) celoten sistem stikov

The top connections came first into contact with the panel at displacement $d_{gap,top}$. The stiffness of the fastening system was increased due to the increased stiffness of the top connections (see Figure 3.18 a and b). When the displacement demand was increased to $d_{gap,bottom}$, the stiffness of the complete fastening system increased the second time (see Figure 3.18 b) due to the activated bending stiffness of the bottom connection. Both top and bottom connections were in contact with the panel.

The test was terminated before the failure of the fastening system (due to the limitations of the actuator capacity). However, as explained and documented in Section 3.3.4, the top connections were subjected to considerable plastic deformations and were near their collapse. Taking into account the capacity of the top connections d_u observed in the tests (described in Section 3.3.2) and considering the almost elastic response of the bottom connections, the capacity of the fastening system was estimated as shown in Figure 3.18 (b) with a hatched line.

In the presented tests, the panels were attached to a rigid beam. In real precast structures, the panels are fastened to deformable columns. Due to the columns' rotations and bending, the relative displacements between panels and columns (i.e. slips) at the level of top and bottom connections are different and can occur in opposite directions (see also the response of the façade system during the shake table tests in Chapter 4). Note, however, that this does not affect basic response mechanisms of type of failure of the connections because the response of the panels remains predominantly translational even when columns are subjected to large rotations (bending).

The washer within the top connection is pinned by the bolt (see Figure 3.2). Thus, it does not notably rotate despite the considerable rotations of the columns. It can slide over the steel box profile in a similar manner as was observed in the presented tests. Consequently, the panels do not rotate (see also Chapter 4).

At the bottom connections, panels only lean on the steel stud. Thus, the rotations of the columns and the panels are different. It can be concluded that the bending of columns does not lead to rotations of panels, and the response of panels is predominantly translational.

Gap in the connections

In the tests, the bolt and the cantilever bracket were positioned approximately in the centre of the available space (see Figures 3.2 and 3.4). In that case, the size of the top and bottom connection gap was approximately the same—about 4 cm. This is half of the width of the available space in the panel (118 mm and 120 mm for the top and bottom connection, respectively) reduced by half of the thickness of the bolt or the cantilever bracket (37 mm and 30 mm, respectively):

$$d_{gap,top} = \frac{118}{2}\ mm - \frac{37}{2}\ mm = 40.5\ mm \tag{3.2}$$

$$d_{gap,bottom} = \frac{120}{2}\ mm - \frac{30}{2}\ mm = 45\ mm \tag{3.3}$$

Note, however, that the size of the gap is appreciably influenced by construction tolerances. During construction in real buildings, the position of the connections can be very eccentric. Because this can appreciably influence the response of the panel, both central and extreme positions are considered in analyses presented in Chapter 6.

Displacement capacity

According to the tests, the displacement capacity of the top connection was around 7.5 cm (relative displacements between the panel and the main structure). This can be considered as the displacement capacity of the complete connection assembly because the top connections are the weakest component (please see the discussion about the failure in Section 3.3.4).

The displacement capacity addressed above corresponds to the gap size of 4 cm (top connection). When the gap size is smaller (as discussed in previous paragraphs), the displacement capacity will be reduced to:

$$d_u = min\ d_{gap,top} + 3.5\ cm \tag{3.4}$$

Therefore, the displacement capacity of the fastening system can be expressed as a sum of the sliding displacement ($min\ d_{gap,top}$) and displacement after the contact with the panel, that is, plastic displacement (3.5 cm). Note that the response of the fastening system after the contact of the top connection with the panel is badly conditioned in terms of displacements. After the contact, the stiffness of the connection significantly increases, and there is a large increase of forces for a small displacement increment.

Friction force

The friction activated in the connection influences the interaction between the panel and the columns of the main building. The greater the friction force, the stronger is the interaction between the panel and the columns. Generally, the friction forces activated in the analysed connections are relatively small compared to the forces in the main precast structure (i.e. columns) during the seismic excitation.

During the experiments, the maximum friction force of $R_{fr,top}$ = 8 kN was observed at the top connections (note that the connections were tested in pairs, and the value 8 kN corresponds to one connection). The friction force in the top connection can be estimated based on the friction coefficient $c_{fr,top}$ and the tightening force in the bolt F_b (Zoubek, 2015):

$$R_{fr} = c_{fr,top}\ F_b \tag{3.5}$$

$$F_b = \frac{T_b}{c_0\ D_b} \tag{3.6}$$

where T_b is the tightening torque in the bolt, c_0 is the friction coefficient in the threaded bolt, which is equal to 0.2 (Zoubek, 2015), and D_b is the nominal diameter of the bolt. For the investigated

connections, the friction coefficient $c_{fr,top}$ = 0.4 is recommended. It was obtained based on the ratio between the measured friction forces ($R_{fr,top}$ = 8 kN) and the tightening force (F_b = 20 kN, corresponding to the tightening torque T_b = 65 Nm). The proposed value is in quite good agreement with the friction coefficients reported by Del Monte et al. (2019). They have evaluated the values of the static friction coefficient at about 0.45 and dynamic ones in the range of 0.32–0.35, according to the tests on similar connection types.

The typical friction force at the bottom connection $R_{fr,bottom}$ was estimated by subtracting the friction force of the top connections from that observed during the dynamic tests of the complete fastening system. The total friction force of the complete fastening system was 20 kN. The frictional resistance of the two top connections was 16 kN. Thus, the friction in the bottom connections was 4 kN in total or 2 kN per one connection. It was four times smaller than that in the top connections. Note, however, that the friction in the top connection strongly depends on the tightening torque in the bolt. When the torque is small, the friction of the top connection can also be reduced to about 2 kN (see the recommended values in Section 5.2.1).

When the top connections were tested, the bolts were retightened to 65 Nm before each test run. However, in the final test runs of the top connections, retightening was blocked by an irreversibly deformed bolt. In the complete fastening system tests, the bolts were tightened to 65 Nm only before the first run.

The friction activated in the fastening system was gradually reduced after several cycles due to the bolt loosening at the top connections. This reduction was somewhat more pronounced within the dynamic tests (see Figure 3.19). The measured friction forces are listed in Table 5.3.

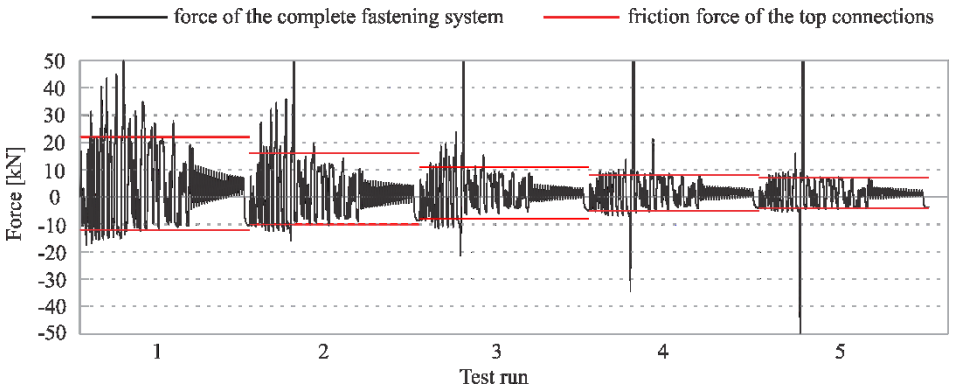

Figure 3.19: Gradual reduction of the friction force in top connections due to the loosening of the bolt during the test *Cd2* (friction force of 2 kN was taken into account for each bottom connection)

Slika 3.19: Zmanjševanje sile trenja v zgornjem stiku zaradi rahljanja vijaka med testom *Cd2* (upoštevana sila trenja v vsakem spodnjem stiku je 2 kN)

Table 3.7: Friction forces in the top connections

Preglednica 3.7: Sila trenja v zgornjih stikih

Test	$R_{fr,top}$ [kN]	Test	$R_{fr,top}$ [kN]
Tc1	5	*Cc1*	5
Tc2	5	*Cc2*	6
Td1	5 - 5 - 5 - 3 - 0	*Cd1*	8 - 6 - 4 - 3 - 2
Td2	8 - 6 - 0	*Cd2*	8 - 5 - 3 - 1 - 1
Td3	8 - 8 - 3		
Td4	8 - 5 - 2		

* Note that for dynamic tests, the friction force is gradually reduced in each test run.

Maximum force

Maximum forces reached during the tests were influenced by the type of the tested connections. During the dynamic tests of top connections, maximum forces of about 58 kN per one connection were recorded. In contrast, during the quasi-static cyclic tests, maximum forces at failure were almost two times smaller, around 34 kN per connection. The reason lies in the different channel types used to test top connections. The quasi-static cyclic tests were performed using cold-formed channels, whereas stronger, hot-rolled channels were used for the dynamic tests.

The shear force capacity of the tested connections, declared by the producer, is shown in Table 3.8. According to the experimental observations (see Section 3.3.2), two failure types were considered for the calculation of shear resistance (see Figure 3.20): (a) shear failure of the screw and (b) local flexure of the channel lip. Characteristic values without safety factors were used (Halfen, 2010) to calculate the resistance.

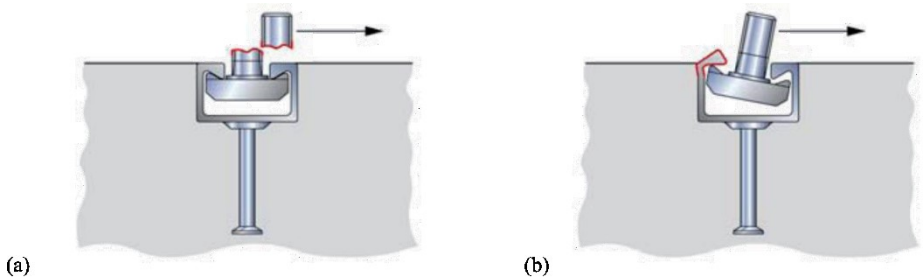

Figure 3.20: Failure types considered for the calculation of shear resistance: (a) shear failure of the screw and (b) local flexure of the channel lip (Halfen, 2010)

Slika 3.20: Porušni mehanizmi upoštevani pri računu odpornosti stikov na strig: (a) strižna porušitev vijaka in (b) lokalni upogib kanala (Halfen, 2010)

Table 3.8: Shear resistance of the top connections
Preglednica 3.8: Strižna nosilnost zgornjih stikov

Failure type	V_{Rd} [kN]
Shear failure of the screw	62.8
Local flexure of the channel lip (cold-formed channels)	20
Local flexure of the channel lip (hot-rolled channels)	26

* Note that the resistance is calculated, taking into account only one connection.

According to Halfen (2010), the critical failure type is local flexure of the channel lip, which was also observed in most of the performed tests. The maximum forces observed during the tests of top connections were much higher than shear resistance considering local flexure of channel lips. As mentioned, the shear failure of the bolt was observed in one of the tests. Table 3.8 shows that the characteristic shear resistance of the bolt is close to the demand force. However, in the same test, the other bolt was pulled out of the channel.

Note that after the contact of the connection with the panel, the force significantly increases, and characteristic shear resistance is reached soon after the gap in the connection is depleted. Evidently, these connections were not designed to sustain high forces that may occur during seismic excitation.

Higher maximum forces reached during the tests of the complete fastening system were due to the activation of lateral stiffness of the bottom connections. Forces up to 200 kN were recorded, which may significantly influence the response of the main precast structure. This issue is further investigated within the parametric study in Chapter 6.

Comparison of top and bottom connections responses

The analysis showed that the responses of the top and bottom connections under dynamic loading have somewhat different characteristics. The top connection appears to exhibit typical Coulomb friction behaviour, whereas variable friction was observed at the bottom connection.

Commonly, the friction force is physically explained by the Coulomb friction behaviour as the product of normal force on the surface and the coefficient of friction that is generally acknowledged to be constant. However, the friction force is not necessarily independent of sliding speed, and the friction coefficient may also vary according to the relative speed of motion (Rabinowicz, 1956; Kragelskii, 1965). The panels were subjected to dynamic loading in the presented tests (as well as

in real buildings subjected to seismic excitations). Thus, the friction was considerably affected by the velocity of the connections' excitations.

The friction also depends on the surface treatment (e.g. cleanliness, lubrication) and the wear of the material during the movement. During the tests, the galvanised steel plates at the bottom connections have shown signs of substantial material wear (Figure 3.21). Note that there is a difference in the material used at the top and bottom connections.

To demonstrate the difference in the top and bottom connection friction behaviours, the typical hysteretic response relationships (force–displacement and force–velocity) are shown for both connections in Figure 3.22. A rough estimate of the response of the bottom connection was obtained by subtracting the response of the top connection from the response of the complete fastening system in two initial test runs with identical loading protocols and the same tightening torque.

The force–displacement relationship typically observed in top connections can be represented by the elastic-perfectly plastic response typical for Coulomb friction (Figure 3.22 a). The registered force–displacement relationship for the bottom connection is better described by the viscous friction (Figure 3.22 b). The shape of force–velocity relationship (*'S'* shape) of the top connection is typical for Coulomb friction (Figure 3.22 c), whereas this relationship has a shape that is typical for viscous friction at the bottom connections (Figure 3.22 d).

Figure 3.21: The significant material wear at the bottom connections observed during the experiments
Slika 3.21: Znatna obraba materiala pri spodnjih stikih

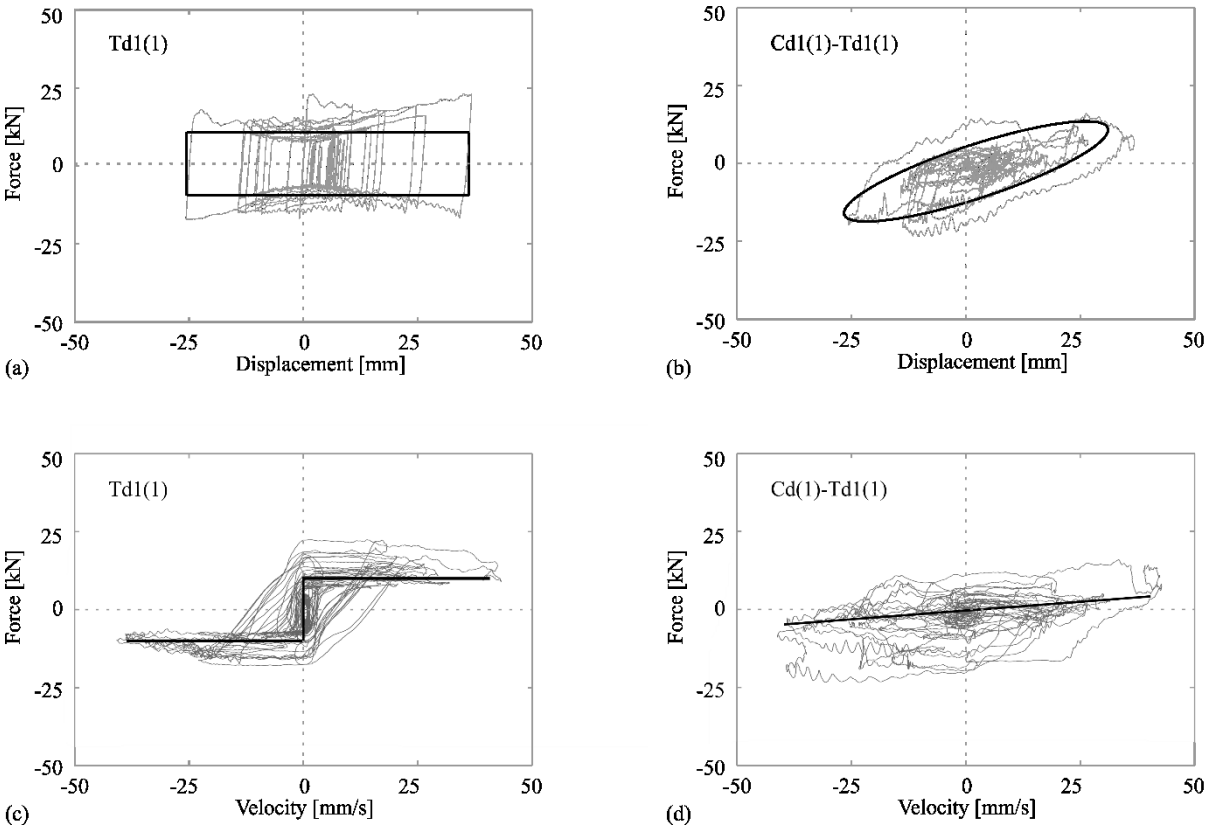

Figure 3.22: Hysteretic responses (grey) and idealised envelopes (black): (a) top connections: forces versus displacements, (b) bottom connections: forces versus displacements (c) top connections: forces versus velocities and (d) bottom connections: forces versus velocities

Slika 3.22: Histerezni odzivi (siva) in idealizirane ovojnice (črna): (a) zgornji stiki sila-pomik, (b) spodnji stiki sila-pomik, (c) zgornji stiki sila-hitrost, ter (d) spodnji stiki sila-hitrost

Stiffness

In general, the initial stiffness of the top and bottom connections is very large until the full friction is activated. After the friction is activated and the panel is sliding along the column, the stiffness is almost 0 as long as the gap is not depleted. Then the stiffness abruptly increases due to the activated bending stiffness of the bolt at the top connection and bending stiffness of the cantilever at the bottom connections. After the contact with the panel, larger stiffness of the bottom than of the top connections was observed (see estimated values in Section 5.2.1).

Type of loading

Hysteretic responses observed during the quasi-static cyclic and dynamic tests are compared in Figure 3.23. As explained in Section 3.3.2, the quasi-static cyclic and dynamic tests of the top connections were performed using two different types of channels. For this reason, the failure of

the connections in the quasi-static tests occurred at a somewhat smaller displacement than in the dynamic tests when stronger channels were used. The maximum force at failure was considerably smaller in the tests with weaker, cold-formed channels.

The asymmetric response of the connections observed during the dynamic tests (Figure 5.14) is due to higher displacement demand in a positive direction (see loading protocol in Figure 3.9 a).

Variable friction in the bottom connections was observed during the dynamic tests, as discussed in previous paragraphs. The reduction of the friction force due to the untightening of the bolt at the top was somewhat more pronounced in the dynamic tests. However, none of these observations had an important influence on the overall response. As shown in Figure 3.23, no significant differences between the cyclic and dynamic tests were observed in terms of either type of failure or response mechanism.

Due to the limitations of the actuator, only limited impact forces were observed. The effect of impacts is more carefully investigated within the full-scale tests and parametric study (see Chapters 4 and 6).

Type of the channels

The type of channel is one of the important parameters that influence the force and displacement capacity of the top connection. Responses of the tests performed with different channel types are compared in Figures 3.23 (a) and (b).

The quasi-static cyclic tests were performed using cold-formed channels (marked with red in Figures 3.23 a, b), whereas stronger, hot-rolled channels were used for dynamic tests (marked with black in Figures 3.23 a, b). The force capacity of the top bolted connection was approximately two times larger when the stronger, hot-rolled channels were used.

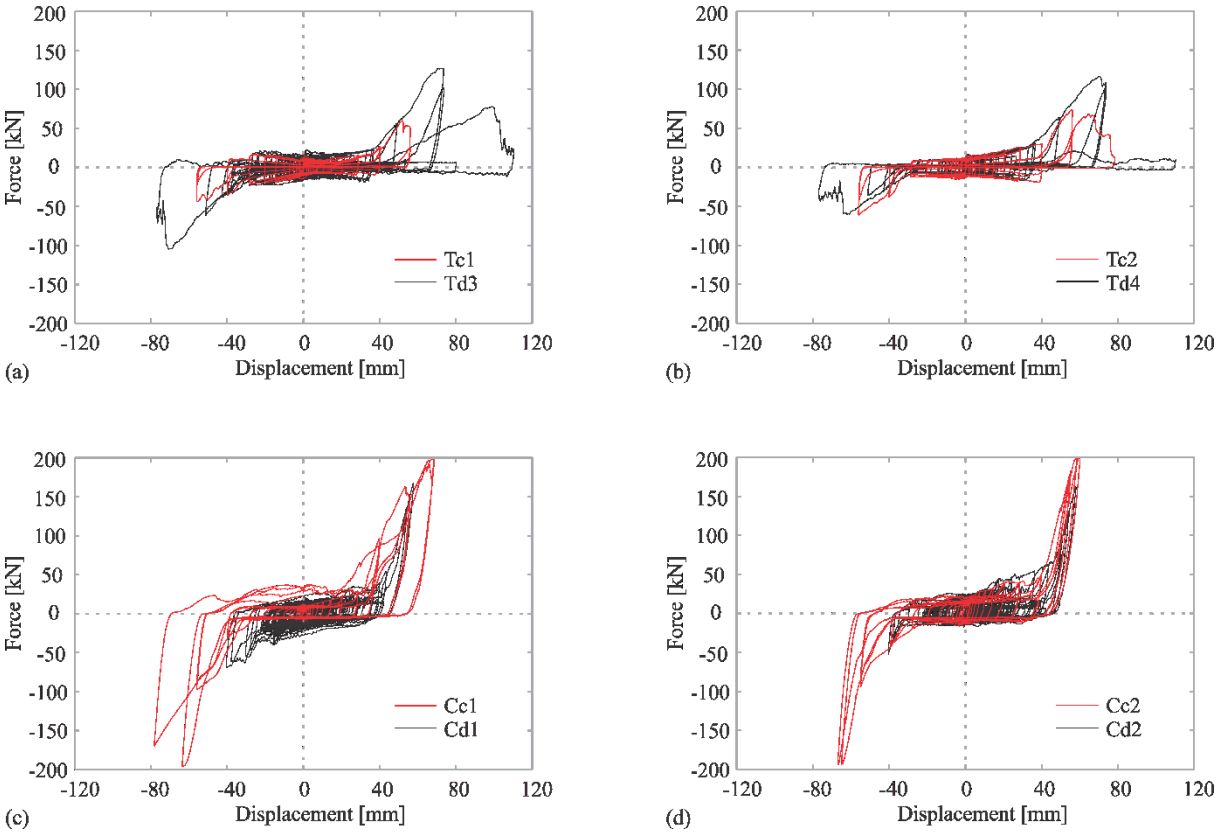

Figure 3.23: Comparison of the cyclic and dynamic tests: (a) *Tc1* vs *Td3*, (b) *Tc2* vs *Td4*, (c) *Cc1* vs *Cd1* and (d) *Cc2* vs *Cd2*

Slika 3.23: Primerjava cikličnih in dinamičnih eksperimentov: (a) *Tc1* in *Td3*, (b) *Tc2* in *Td4*, (c) *Cc1* in *Cd1*, ter (d) *Cc2* in *Cd2*

Position of the connections

To perform as many experiments as possible, the foundation block was designed to be used for two series of tests on each side (see setup description in Section 4.1.1). In each test, the inner or the outer two connections were used. The possible influence of the position of the tested connections, that is, the distance between them, is examined. The results of the comparative tests presented in Figure 3.24 show no important difference in the response of the inner or outer two connection pairs.

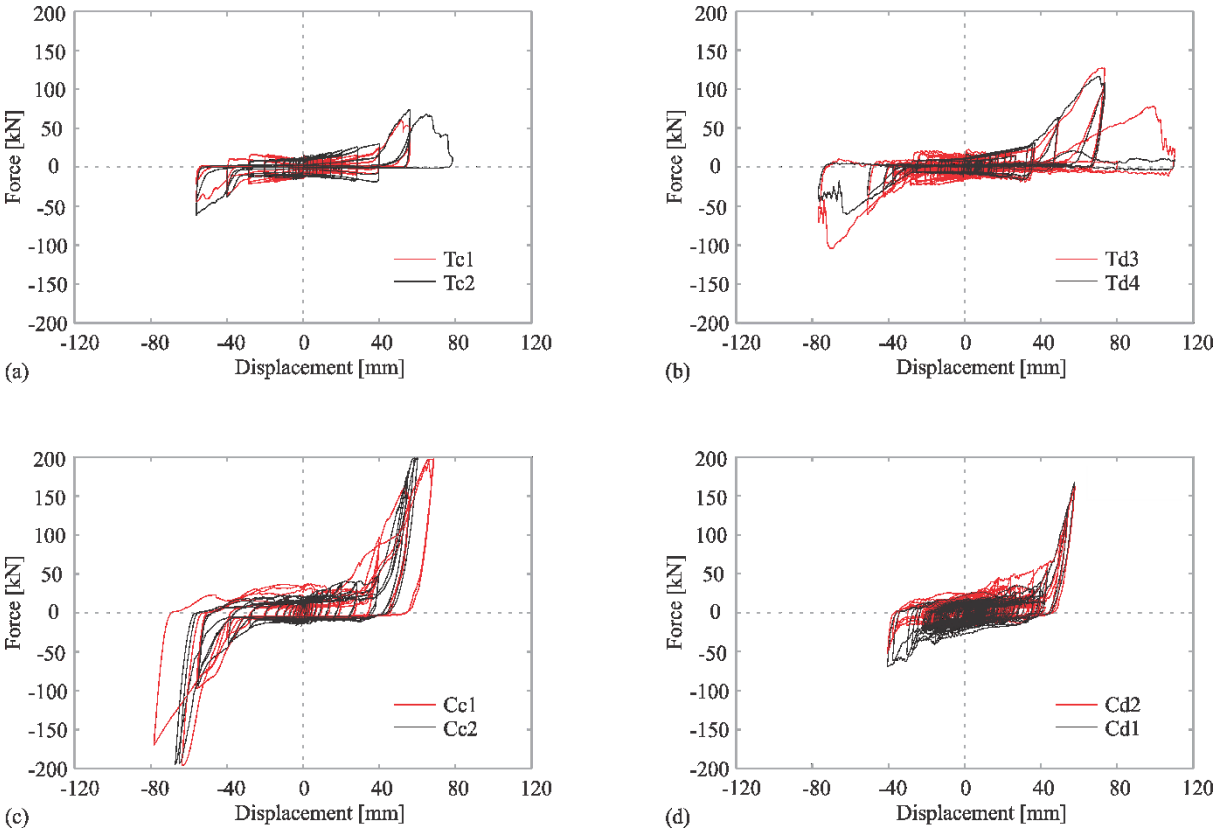

Figure 3.24: Comparison of the inner (black) and outer (red) position of the connections for test pairs: (a) *Tc1* vs *Tc2*, (b) *Td3* vs *Td4*, (c) *Cc1* vs *Cc2* and (d) *Cd1* and *Cd2*

Slika 3.24: Primerjava notranje (črna) in zunanje (rdeča) pozicije stikov za pare testov: (a) *Tc1* vs *Tc2*, (b) *Td3* vs *Td4*, (c) *Cc1* vs *Cc2* and (d) *Cd1* and *Cd2*

Repeatability of the experiments

Repeatability stands for the closeness of the agreement between the independent results obtained with the same method on identical test material and under the same conditions of measurements (IUPAC, 1997). The measure of repeatability is the standard deviation.

Results repeatability should be checked. However, it is sometimes difficult to provide a large number of tests performed under the same conditions, especially in large-scale experiments when the costs are high. Sometimes even one single experiment can be of utmost importance for the research industry, especially when the subject is investigated for the first time.

In the case of the presented experiments, only two test runs were performed under identical conditions. Therefore, it was not possible to evaluate the standard deviation. For this reason, the repeatability of the results was examined by comparing the hysteresis of the matching test runs (see Table 3.4). Hysteretic responses for the four matching pairs are shown in Figure 3.25. The comparative pairs were chosen to fulfil the equality conditions for the type of the tested connections,

the position of the connections, the load intensity (in Figure 3.25, the consecutive number of the test run is written in brackets) and the history of loading. The agreement between the results is very good, which confirms the repeatability of the tests.

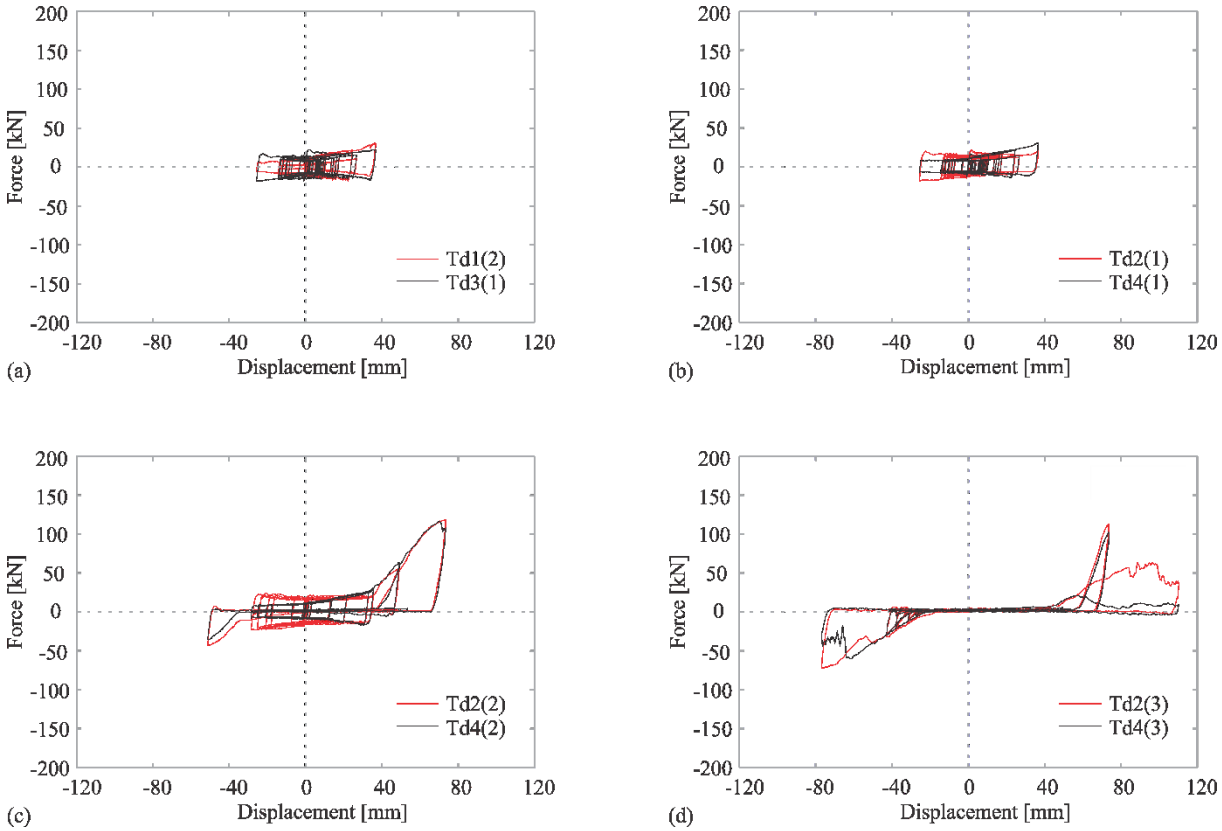

Figure 3.25: Validation of the repeatability of the experiments by comparing the hysteretic responses of the tests runs performed under the same test conditions (the consecutive number of the test run is written in brackets): (a) *Td1(2)* vs *Td3(1)*, (b) *Td2(1)* vs *Td4(1)*, (c) *Td2(2)* vs *Td4(2)* and (d) *Td2(3)* vs *Td4(3)*

Slika 3.25: Potrditev ponovljivosti testov s primerjavo preizkusov izvedenih pri istih pogojih (zaporedni test znotraj enega seta testov na istih stikih je zapisan v oklepajih): (a) *Td1(2)* in *Td3(1)*, (b) *Td2(1)* in *Td4(1)*, (c) *Td2(2)* in *Td4(2)*, ter (d) *Td2(3)* in *Td4(3*

Inertial forces and effectiveness of the rollers

Special steel rollers used in the tests of the top connections were intended to reduce the amount of friction to a minimum and, at the same time, allow the panel to slide parallel to the foundation beam. The results of the two tests performed without connections are presented in Figure 5.2. The inertial forces of the panel are plotted next to them. They were calculated as the product of the mass and the acceleration of the panel (Equation 3.7). Accelerations were obtained as the second derivative of the displacement protocol (record filtering was also applied).

$$F = m\,a \tag{3.7}$$

Figure 5.2 (a) shows that the forces measured in the actuator correspond to the inertial forces of the panel, which confirms the effectiveness of the roller bearings. The recorded friction (test in Figure 5.2 b) and inertial forces are relatively small compared to the forces activated in the connections (see test results in Figures 5.11-5.14) and can be disregarded.

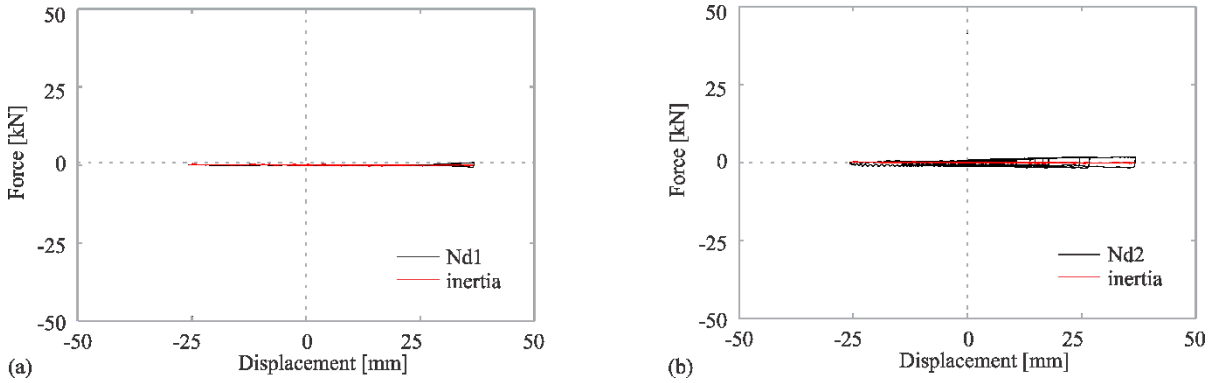

Figure 3.26: Force in the actuator during the tests without connections (black) and the inertial forces of the panel (red): (a) test *Nd1* and (b) test *Nd2*

Slika 3.26: Rezultati preizkusov v brez montiranih fasadnih stikov (črna) in vztrajnostne sile panela (rdeča): (a) preizkus *Nd1* in (b) preizkus *Nd2*

3.4 Summary and conclusions of the chapter

This chapter presents experimental studies of the fastening system typically used in Central Europe to attach horizontal cladding panels to the columns of RC precast buildings. This system consists of two main parts: a pair of top bolted connections that provide the horizontal stability of the panel and a pair of bottom cantilever connections that support the weight of the panel. This fastening system behaves as a seated isostatic connection system, which is supposed to provide unhindered horizontal relative displacement between the panel and the main structure of the building at the upper side of the panels.

Two sets of experiments were performed: (1) cyclic and dynamic tests of the top connections and (2) cyclic and dynamic tests of the complete fastening system (top bolted and bottom cantilever connections), with the main purpose of obtaining information about their capacity and basic seismic response mechanisms.

The typical response mechanism of the fastening system consists of three distinct stages: sliding with limited friction, contact with the panel causing an increase in the stiffness of the connection and failure. The capacity of the fastening system should be expressed in terms of displacement rather than strength because the system capacity is limited by the displacement capacity of the top

connection. The displacement capacity depends on the construction tolerances and the initial size of the gaps.

Experimental results showed that the deformation capacity is about 3.5 cm larger than the initial gap size of the top connection. However, after the connection contacts the panel, the stiffness of the connection significantly increases, and for small displacement increment, there is a significant increase in connection forces. Within the sliding phase, the fastening system behaves like an isostatic connection system that enables relative displacement between the panel and the structure. After the contact, there is an increase of forces and practically brittle failure of the connection occurs. For this reason, it is recommended that the displacement capacity of the connection be limited to the gap size.

The initial gap size depends on the construction tolerances. When a component is moved towards the edge of the hole in the panel, the interaction between the panel and the columns in one direction could be activated at a smaller displacement demand. Because it can considerably influence the response and because it is not known in advance, two extreme cases should be considered: centrally mounted connections, where the gap size in both directions is the same, and eccentrically positioned bolts and cantilever brackets. These cases are further investigated within the parametric study in Chapter 6.

The analysis showed that the responses of the top and bottom connections under dynamic loading have somewhat different characteristics. The top connection appears to exhibit typical Coulomb friction behaviour, whereas the response of the bottom connection is rather viscoelastic. Otherwise, no substantial differences between the cyclic and dynamic tests were observed.

In the presented tests, the panels were attached to a rigid beam. In real precast structures, the panels are fastened to deformable columns. Although column rotations do not impose notable rotations of panels and connections, they cause different relative displacements between columns and panels at the top and bottom connections. These displacements can occur in opposite directions (see Chapter 4). However, this does not affect the observed basic response mechanisms or the hysteretic response of the connections because the response is independent of the direction of relative displacements.

The experimental investigation presented in this section was of utmost importance for understanding the seismic response of the existing RC façade systems in precast industrial buildings. At the time of the experiments, the behaviour of the complete fastening system was completely unknown. However, the study of impacts in the connections and their possible influence on the response of the main structural system was limited by a single component test. For this reason, the experimental analysis was expanded by the more complex full-scale shake table tests (Chapter 4).

4 EXPERIMENTAL INVESTIGATION OF AN RC PRECAST BUILDING WITH HORIZONTAL CONCRETE CLADDING PANELS

The full-scale shake table tests of the realistic precast building were performed within the Slovenian national project *Seismic resilience and strengthening of precast industrial buildings with concrete claddings* (Zoubek et al., 2017). The shake table tests were not performed as part of the thesis but were only used to analyse the seismic response of the complete precast system with horizontal façade systems presented in this chapter.

Previous research mainly focused on investigating the response of single components, and many aspects of the complex cladding systems behaviour remained unexplained. Full-scale shaking table tests performed on a structure with realistic boundary conditions, including the main precast structure, cladding panels and connections, gave an insight into the earthquake performance of the complete precast structural system. Experiments were performed within the UL research project in cooperation with the Institute of Earthquake Engineering and Engineering Seismology – IZIIS in Skopje, Republic of North Macedonia.

The main objective of the shaking table tests was an analysis of the seismic response of the complete structural system with RC cladding panels under realistic boundary conditions. Parameters such as the orientation of panels, the type of cladding-to-structure connections and the specimen configuration (symmetric and asymmetric) were varied within these experiments.

This chapter presents an analysis of the full-scale dynamic shaking table tests performed on an RC precast structure with non-structural horizontal cladding panels. The tested fastening system used for attaching the horizontal cladding panels to the columns of the main structure is the system most commonly used in Central Europe. It consists of top bolted connections that provide the out-of-plane stability of the panel and bottom cantilever connections that support the panels' weight. A detailed description of the cladding connections and single component tests is provided in Chapter 3.

In the following sections, the experimental setup of shaking table tests is presented first. Then, the experimental results are presented and discussed. The horizontal cladding panel behaviour mechanism is explained in detail. The main response parameters are identified, and the precast system earthquake performance is evaluated.

4.1 Description of the shake table test

The specimen for testing on the shaking table was designed so that the relative displacements between the panels and the main structure (i.e. displacements of the fastening system) were realistic. Realistic dynamic properties and dimensions of the main structure and panels were preserved. The tests were performed in full scale because it was complicated to reduce the scale of cladding connections. Other important conditions during the design process were the limitations of the shaking table system, especially the limitation on the overturning moment (see Section 4.1.2).

4.1.1 Description of the full-scale specimen

The geometry of the tested structure is shown in Figures 4.1-4.3. The specimen consisted of four columns, a roof slab and horizontal panels. The columns were 4.5 m tall, slender cantilevers that were cast together with foundations. The dimensions of the column cross section were 0.3 m × 0.3 m, and the longitudinal reinforcement consisted of 8 Φ16 mm bars. Square and diamond stirrups Φ8 mm / 5 cm were provided in critical regions at the bottom 75 cm and top 195 cm of the columns (where the panels were mounted). In the middle part of the columns, the distance between the stirrups was 10 cm. Each foundation with the dimensions 1 m × 1 m × 0.5 m was fixed to the shaking table with four Φ38 anchors.

A 0.36-cm-thick solid slab was anchored centrally on each column by the Φ25 mechanical dowels. Between the columns and the slab, 1 cm thick neoprene pads were placed to allow for the relative rotations in the connections. The slab dimensions were 4.3 m × 2.3 m, and it was reinforced by Q785 mesh at the top and bottom. The mass of one column was 1 t, and the mass of the slab was 9.1 t, which provided a realistic fundamental period of vibration of the structure around 0.85 s.

Horizontal panels with a mass of 2.6 t each were attached to the main structure at the top of columns with two top and two bottom connections per panel, as shown in Figure 4..1 (b, c). The typical fastening system used in Central Europe for attaching the horizontal panels was used. A detailed description of the tested fastening system with all the dimensions can be found in Section 3.1. The initial position of the connections is important, and the gaps in the connections were different in different connections (please see Table 4.6 and Figure 4.20 in Section 4.2.5).

The 0.15 m thick panels had dimensions 4.5 m × 1.5 m (length × height) and were reinforced by Q335 mesh on both sides. In all elements, concrete class C 40/50 and reinforcement steel B500B was used.

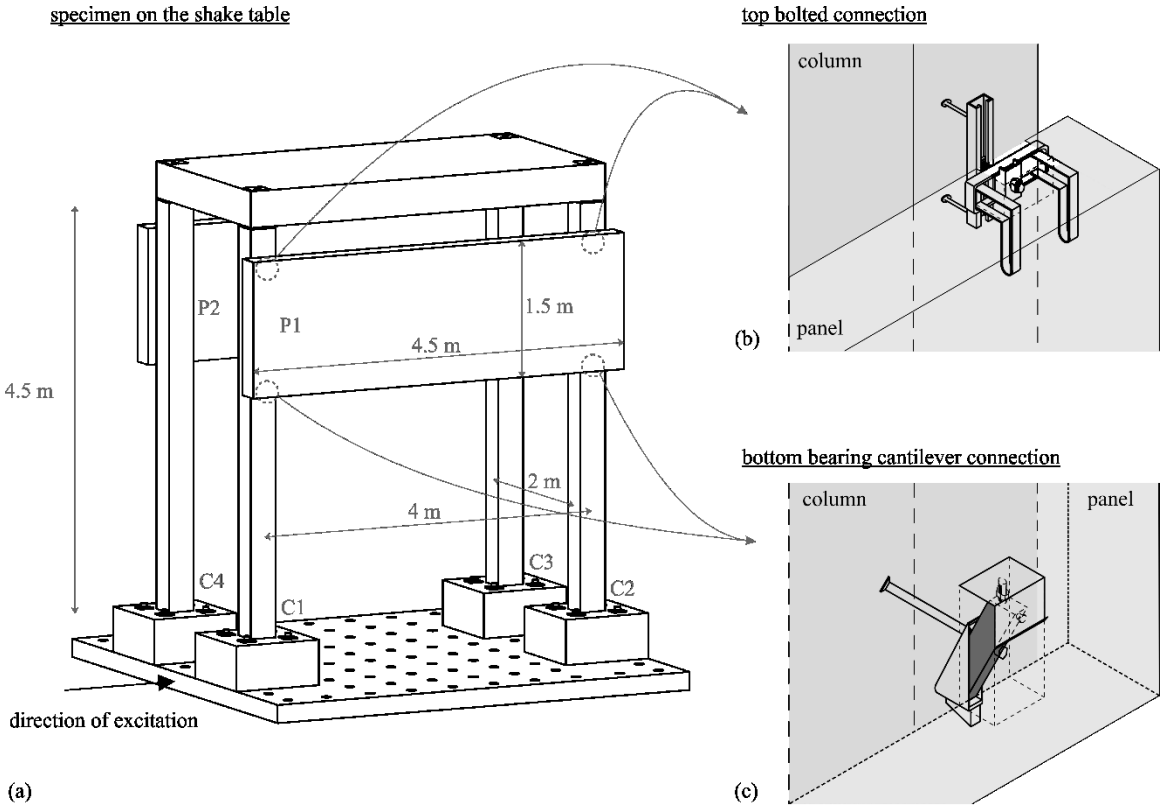

Figure 4.1: Tested specimen: (a) geometry in 3D view, (b) top cladding connection and (c) bottom cladding connection

Slika 4.1: Preizkušanec: (a) geometrija v 3D pogledu, (b) zgornji fasadni stik in (c) spodnji fasadni stik

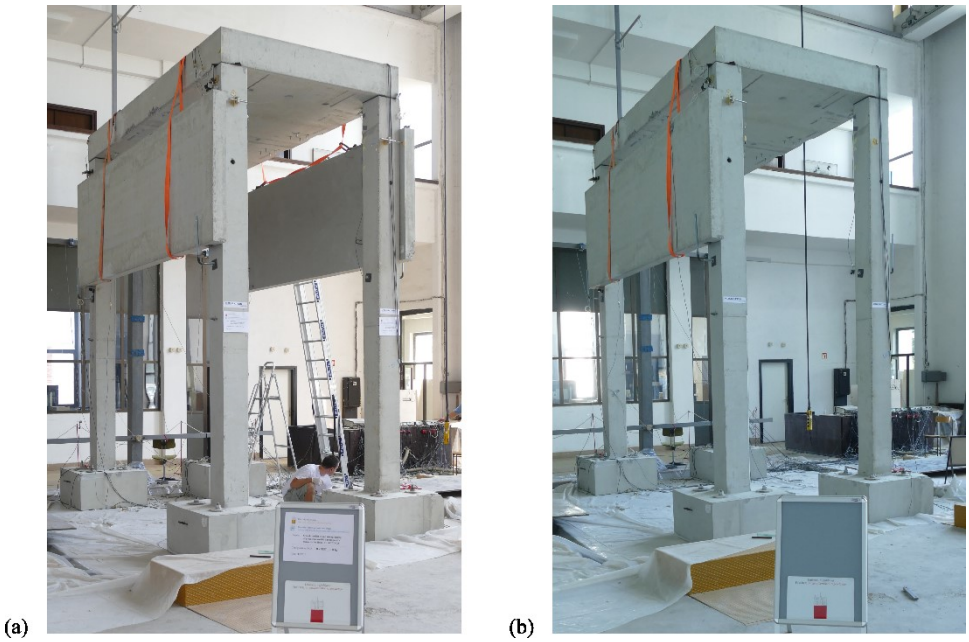

Figure 4.2: The full-scale specimen: (a) symmetric configuration and (b) asymmetric configuration

Slika 4.2: Preizkušanec v naravni velikosti: (a) simetrična konfiguracija in (b) asimetrična konfiguracija

Two different specimen configurations were tested: a symmetric configuration with panels mounted on opposite sides of the structure (Figure 4.2 a) and an asymmetric configuration with only one panel attached to the main precast structure (Figure 4.2 b). The asymmetric configuration was chosen with the main aim to induce the vibrations of the structure also in transverse direction and to have both horizontal components (in-plane and out-of-plane). The basic properties of the tested specimen are summarised in Table 4.1. The high shear span ratio (15) and low axial load ratio (1.04%) are typical for slender RC precast columns.

The same main structure has been used to test vertically oriented panels (Isaković et al., 2018; Menichini & Isaković, 2018) and a specimen with horizontally oriented panels. Altogether, 19 tests of the specimen with vertical panels and seven tests of the specimen with horizontal panels were performed on the same main structure.

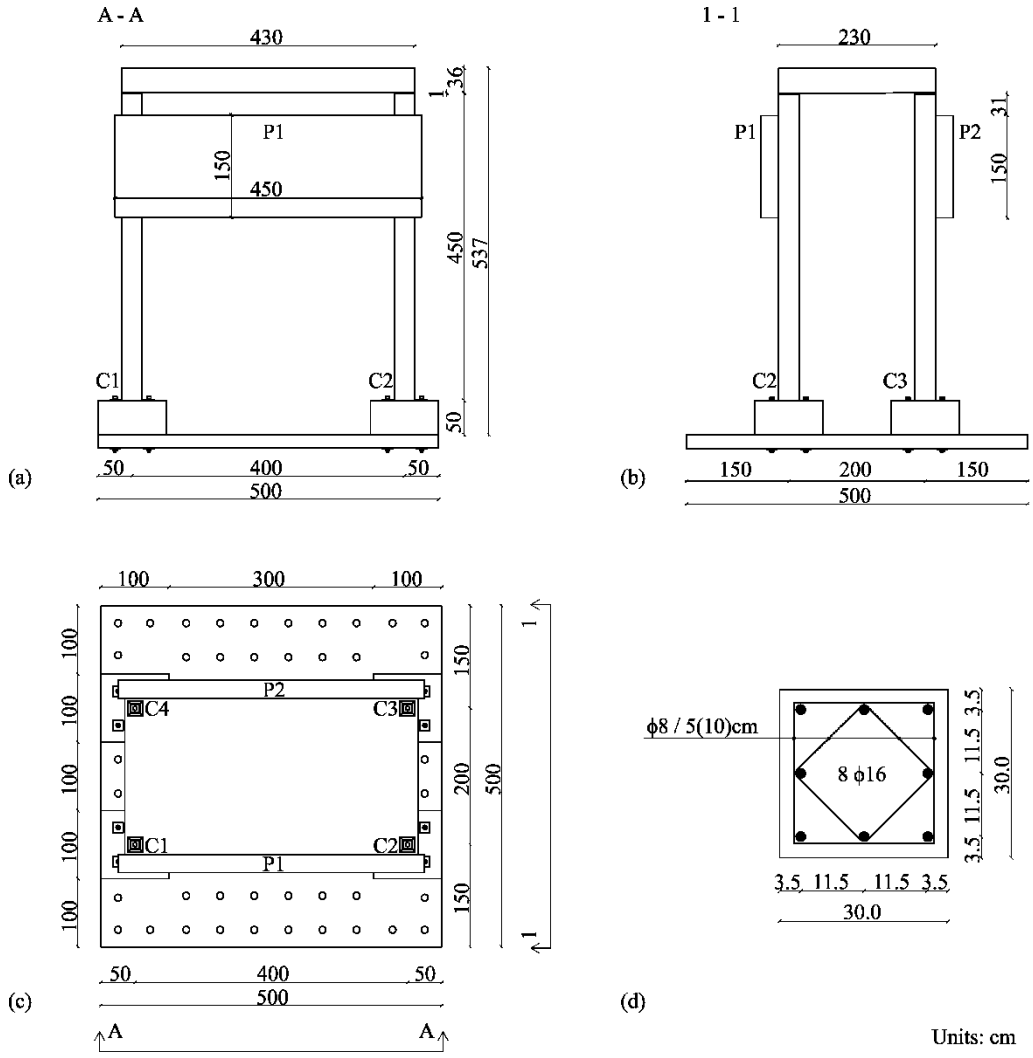

Figure 4.3: Tested specimen with two panels: (a-c) geometry of the specimen and (d) column cross section
Slika 4.3: Preizkušanec z dvema paneloma: (a-c) geometrija preizkušanca in (d) prečni prerez stebra

Table 4.1: Specimen properties

Preglednica 4.1: Glavne karakteristike preizkušanca

Columns	Value
Height above foundations	4.5 m
Dimensions of column cross section b_c / h_c	0.30 m / 0.30 m
Shear span L_s	4.5 m
Shear span ratio L_s / h_c	15
Mass of the column* m_{col} / 2	0.5 t
Axial load N	45 kN
Axial load ratio $v = N / A_g f_c'$	1.04%
Mean compressive strength of concrete f_c'	48 MPa
Slab	
Dimensions of the slab l / w / t	4.3 m / 2.3 m / 0.36 m
Mass of the slab m_s	9.1 t
Panels	
Dimensions of the panels l / h / t	4.5 m / 1.5 m / 0.15 m
Mass of one panel m_p	2.6 t
Position of the top connections (measured from the bottom of the columns)	4.2 m
Position of the bottom connections (measured from the bottom of the columns)	2.7 m

Note: *only ½ mass of the column was considered at the top of the column

4.1.2 Shake table properties

The earthquake simulation system installed in the Dynamic Testing Laboratory of the IZIIS institute in Skopje provides the possibility of exciting simultaneous earthquake motion in one horizontal and vertical direction (IZIIS, 2016). The shaking table at IZIIS is a prestressed RC slab with the dimensions 5.0 m × 5.0 m. In the horizontal direction, the table is controlled by two hydraulic actuators at a distance of 3.5 m and a total force capacity of 850 kN. The maximum mass of a specimen is 40 t, and the maximum height is 6.0 m. However, when testing tall and slender structures, the horizontal accelerations of the structure might initiate the rocking of the table. The limit on the overturning moment is 460 kNm and must be considered in the design of specimens.

4.1.3 Testing program

The accelerogram Petrovac N-S, registered during the Montenegro 1979 earthquake, was used to define earthquake excitation. The accelerogram was modified to match the Eurocode 8 spectrum for soil type B. In addition, filtering and baseline correction were applied to avoid residual

displacements. The modified accelerations were scaled to the intensity of 1.0 g. The displacement and velocity time histories are presented in Figure 4.4 (a, c, e). The corresponding response spectra at 2% damping are shown in Figure 4.4 (b, d, f) next to the time histories.

The summary of all performed tests is provided in Table 4.2. Each test consisted of a series of dynamic test runs with different intensities. The same precast structure was used for all the tests, and the peak ground acceleration (PGA) was scaled from 0.1 g to 0.4 g with 0.1 g steps. First, the symmetric specimen with two horizontal panels was tested. In the next phase, one panel was removed, and three test runs with the PGA intensities 0.1 g, 0.2 g and 0.3 g were performed on the asymmetric specimen. In all tests, the direction of loading was in the horizontal direction parallel to the panel plane (see Figure 4.). There was no excitation in the vertical direction.

Table 4.2: Summary of the performed shaking table tests
Preglednica 4.2: Povzetek testov na potresni mizi

Panel configuration	Number of test runs	PGA intensities
Symmetric	4	0.1 g / 0.2 g / 0.3 g / 0.4 g
Asymmetric	3	0.1 g / 0.2 g / 0.3 g

4.1.4 Instrumentation

The response of the tested structure was monitored by a high-speed multi-channel data acquisition system and sensors consisting of accelerometers (ACC), displacement transducers (LVDT), linear potentiometers (LP) and strain gauges (SG). They were used to measure: (a) accelerations of the main structure and panels, (b) relative displacements between the precast elements, (c) absolute displacements of the slab and panels and (d) strain in the reinforcement. The shake table system automatically measures displacements and accelerations in all three directions.

Positions and directions of LVDTs for the symmetric configuration are presented in Figure 4.5 (a). They were used to measure relative displacements between precast elements. Relative displacements between the columns and panels, which are of primary interest, were recorded at the cladding connection positions. Relative displacements between the foundations and table were also monitored, as were the relative displacements between the columns and slab.

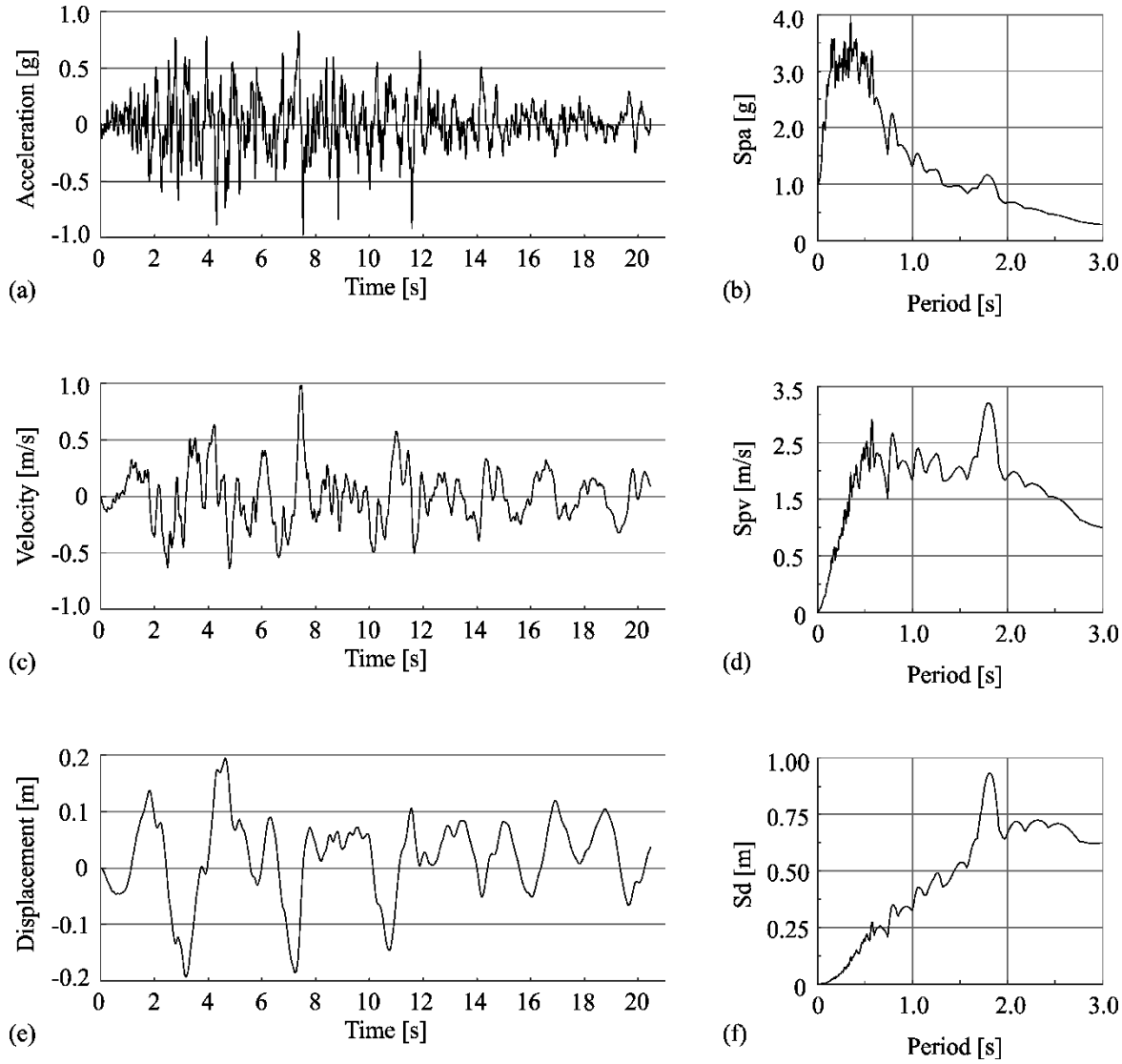

Figure 4.4: The applied loading protocol and relevant response spectra of the applied accelerogram at 2% damping: (a) acceleration time history, (b) pseudo-acceleration spectrum, (c) velocity time history, (d) pseudo-velocity spectrum, (e) displacement time history and (f) displacement spectrum

Slika 4.4: Uporabljen protokol obtežbe in pripadajoči spektri odziva pri 2 % dušenju: (a) časovni potek pospeškov, (b) spekter pseudopospeškov, (c) časovni potek hitrosti, (d) spekter pseudohitrosti, (e) časovni potek pomikov in (f) spekter pomikov

The positions and directions of ACCs and LPs are presented in Figure 4.5 (b). Absolute accelerations were measured in all three directions at the top of the slab and top and bottom corners of each panel. Horizontal accelerations in the direction of seismic excitation were recorded at the foundation level. Three LPs were mounted at the slab and the top of both panels to measure the absolute displacements in the loading direction.

Several strain gauges were used to record deformations of the reinforcement at the bottom of two columns. Strain gauges were also installed in two connections between the columns and the slab to record and control the deformations of dowels. The response of the structure was recorded by three

cameras that were mounted at each side of the structure and at the top. Additionally, three GoPro cameras were used to record the response of the connections, as shown in Figure 4.6.

In the asymmetric configuration, the instrumentation was similar; only the panel P2 and corresponding measuring devices have been removed.

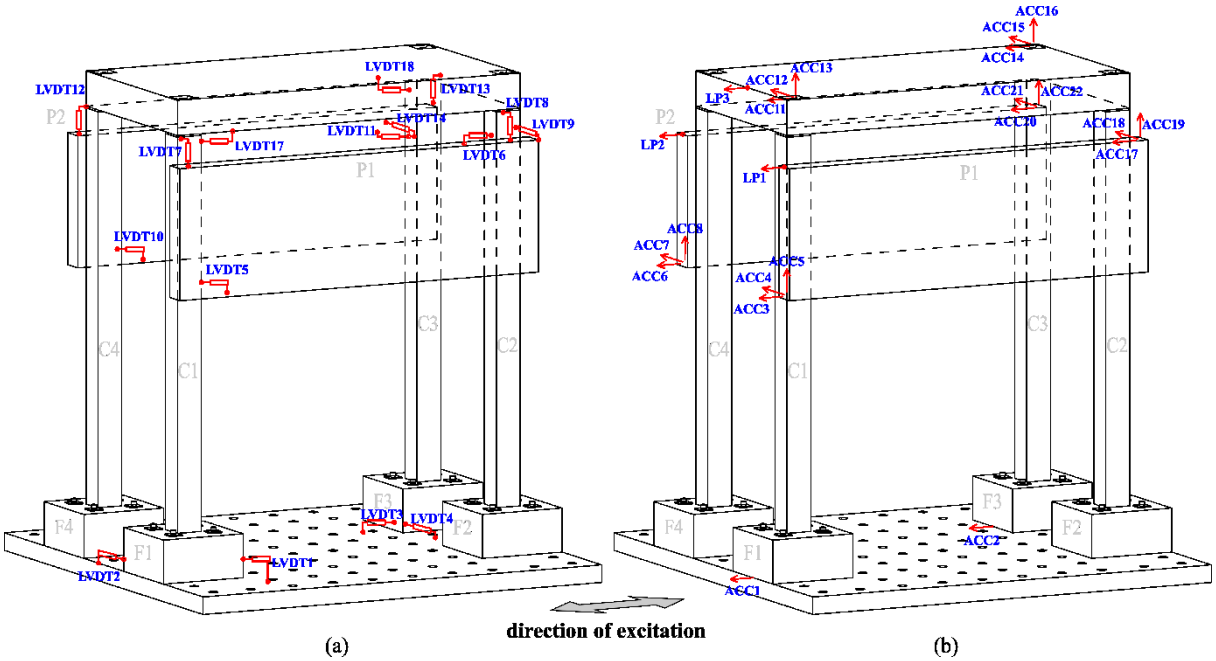

Figure 4.5: Instrumentation of the specimen: (a) displacement transducers, (b) accelerometers and linear potentiometers

Slika 4.5: Instrumentacija preizkušanca: (a) induktivni merilci pomikov, (b) akcelerometri in linearni potenciometri

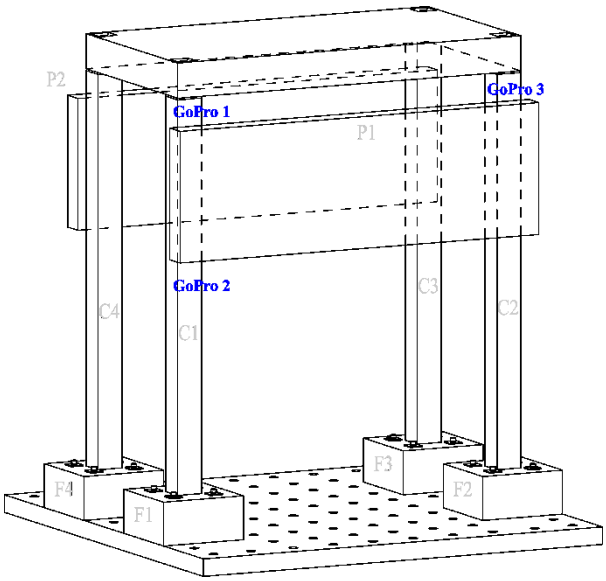

Figure 4.6: Positions of GoPro cameras used to record the response of the connections

Slika 4.6: Pozicije GoPro kamer za zajem odziva stikov

4.2 Results and observations of the experiments

The main experimental observations are presented in the following paragraphs. For brevity, the observations are validated by the results of one or two representative response histories. However, the conclusions apply to all the performed test runs (i.e. other intensities or panel configuration).

4.2.1 Summary of response history parameters

Maximum response parameters in the horizontal direction parallel to the panel plane for both specimen configurations are summarised in Table 4.3.

Table 4.3: The maximum displacements and accelerations in the horizontal direction parallel to the panel plane

Preglednica 4.3: Maksimalni pomiki in pospeški v vzdolžni smeri

Symmetric specimen	PGA 0.1 g	PGA 0.2 g	PGA 0.3 g	PGA 0.4 g
Displacement of the main structure [mm]	18	38	55	95
Displacement of the panel P1 [mm]	14	28	42	63
Displacement of the panel P2 [mm]	14	29	51	62
Acceleration of the slab [g]	0.16	0.31	0.50	0.86
Acceleration of the panel P1 [g]	0.13	0.37	0.54	1.06
Acceleration of the panel P2 [g]	0.14	0.31	0.59	1.32
Asymmetric specimen	PGA 0.1 g	PGA 0.2 g	PGA 0.3 g	
Displacement of the main structure [mm]	21	44	86	
Displacement of the panel P1 [mm]	18	33	55	
Acceleration of the slab [g]	0.19	0.41	0.71	
Acceleration of the panel P1 [g]	0.16	0.57	0.96	

4.2.2 Response of the panels and the main structure

The main properties of the global response of horizontal panels are presented in Figures 4.7-4.10. The response mechanism is schematically presented in Figure 4.7, whereas displacement response histories are shown in Figures 4.8-4.10. The key observation is that the panels, in general, followed the displacements of the columns (there were negligibly small uplifts or rotations), but there were slips in the connections (either at the top or at the bottom). The term *slip* designates the relative displacements (d_{slip}) of the panel with respect to columns.

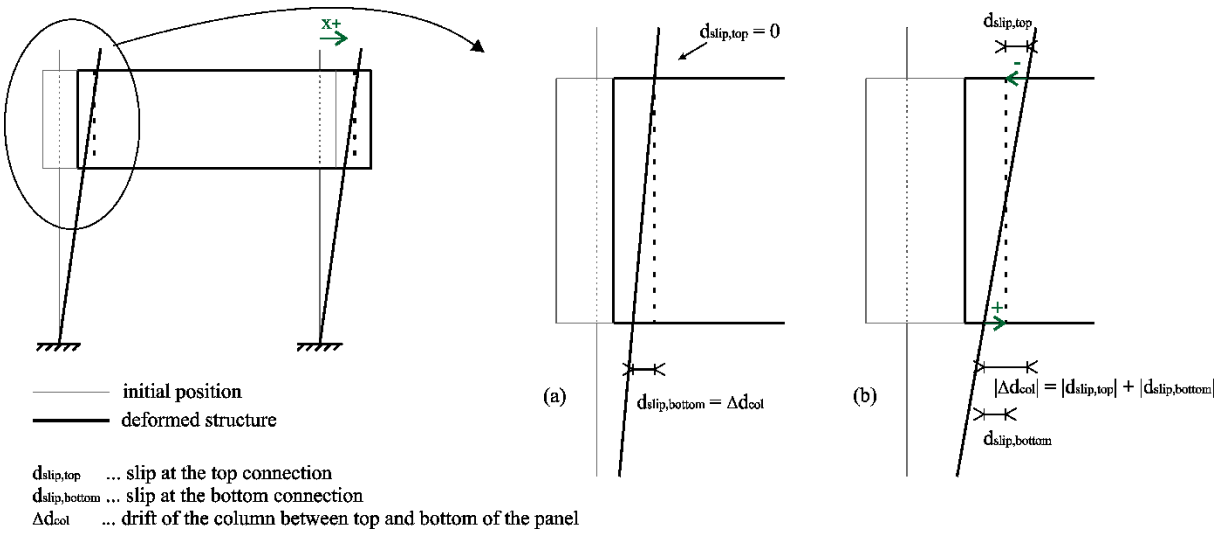

Figure 4.7: Behaviour mechanism of the horizontal cladding panel at (a) low load intensity and (b) high load intensity

Slika 4.7: Mehanizem obnašanja vodoravnih fasadnih panelov pri (a) nizki intenziteti obtežbe in (b) visoki intenziteti obtežbe

At the low excitation intensities (PGA 0.1 g), relative displacements between the top of the panel and the columns were not observed (see Figure 4.8 a). Panels were pinned to the columns at the level of the top connections and slid over the bottom connection. The slip at bottom connections was practically the same as the drift of the columns between the top and bottom edge of the panel (see Figure 4.7 a and Figure 4.8 b). This confirmed that the bottom connection acted basically as a sliding support. Note that in Figure 4.8 (b), the slip ($d_{slip,bottom}$) was measured, and the drift of columns (Δd_{col}) was calculated from known displacements of the column.

At the higher excitation intensities, panels slid at both top and bottom connections (Figure 4.9 a). Note that the relative displacements at the top and the bottom of the panel were in the opposite direction, which is different from the tests on components (Section 3.3). The response of the connections during the shake table tests and the component tests is compared in Section 4.2.4. A graph in Figure 4.9 (b) confirms that the column drift is the sum of the slip at the bottom and the slip at the top of the panel (Figure 4.7 b).

Figure 4.10 (a) shows that the amplitudes of displacements of the main structure and the panels are quite similar (the plot is for displacements at the top of the panel). The difference is only due to the slip in the top connections (Figure 4.10 b).

It is also evident from Figure 4.10 (a) that the main structure (MS) and both panels (P1 and P2) moved with the same period of vibration. The panels followed the movement of the main precast structure (see also discussion in Section 4.2.3).

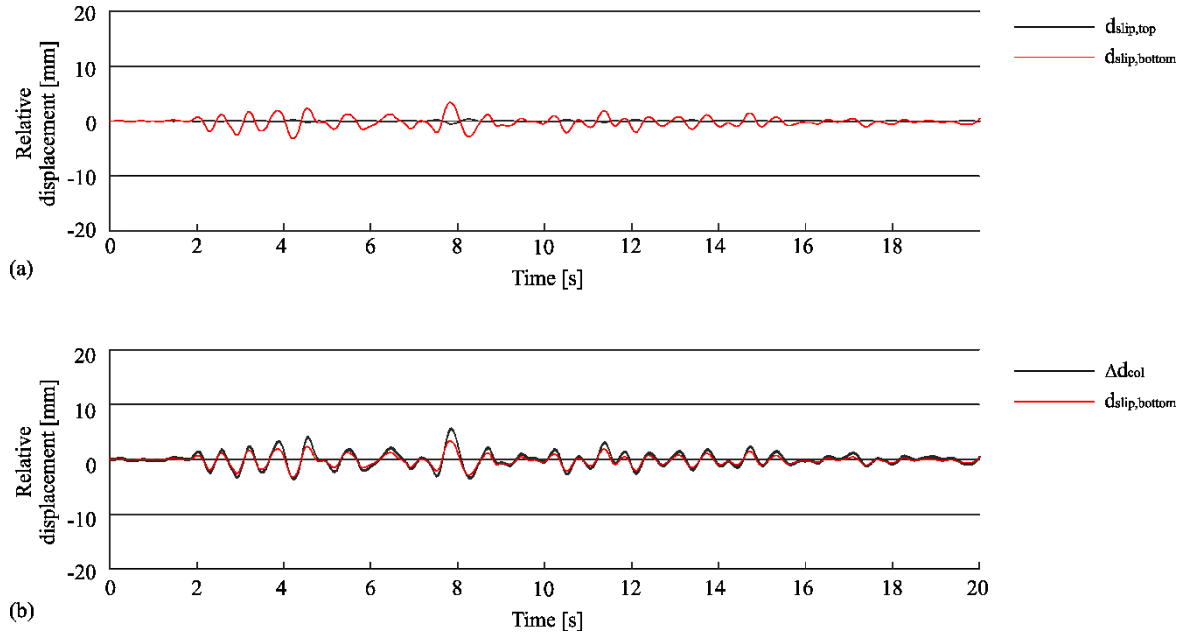

Figure 4.8: Panel P2 at PGA 0.1 g: (a) slip at the top (black) and bottom (red) connections and (b) comparison of the drift of the column between the top and bottom edge of the panel (black) and the measured slip (red) at the bottom connection

Slika 4.8: Panel P2 pri PGA 0.1 g: (a) zdrs v zgornjem (črna) in spodnjem (rdeča) stiku in (b) primerjava zamika stebra med zgornjim in spodnjim robom panela (črna) in izmerjenega zdrsa (rdeča) v spodnjem stiku

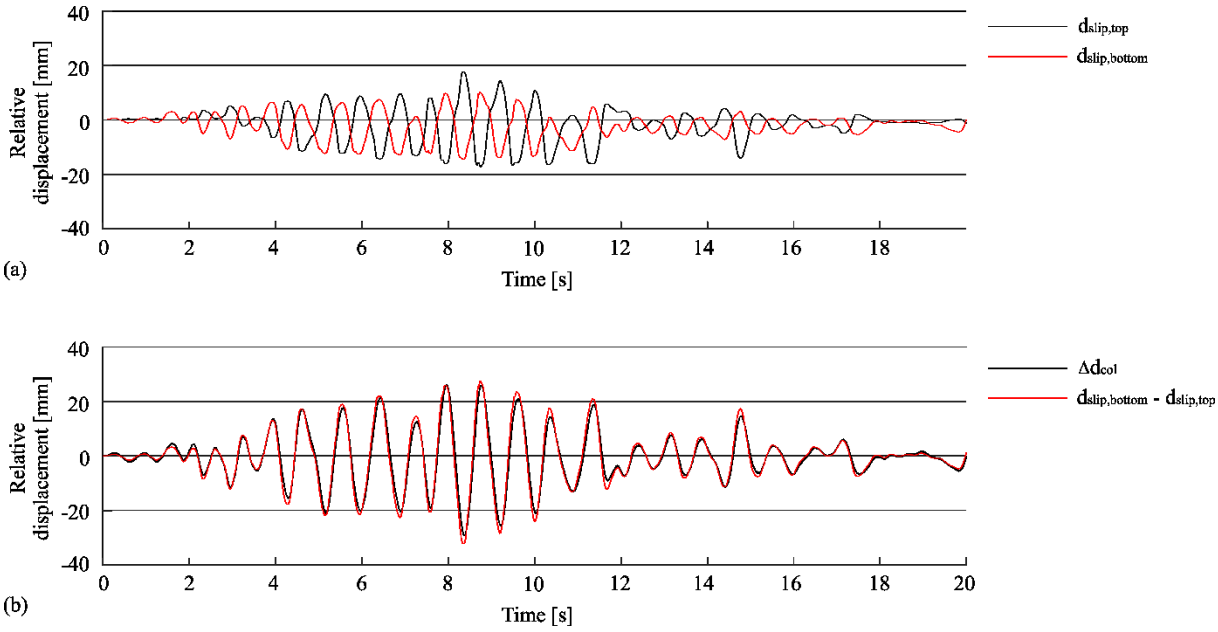

Figure 4.9: Panel P2 at PGA 0.4 g: (a) slip at the top (black) and bottom (red) connections and (b) comparison of the drift of the column (black) and the sum of the slips at the level of top and bottom connections (red)

Slika 4.9: Panel P2 pri PGA 0.4 g: (a) zdrs v zgornjem (črna) in spodnjem (rdeča) stiku in (b) primerjava celotnega zamika stebra (črne) in vsote zdrsov v zgornjem in spodnjem stiku (rdeča)

At higher excitation intensities, impacts between panels and columns were observed (see also Section 4.2.5). However, no failure of panels nor failure of the fastening devices occurred.

The responses of panels P1 and P2 were slightly different (see max response parameters in Table 4.3 and response histories in Figure 4.10). The main reason is that the initial positions of the connections were different. Consequently, the different connection gaps were depleted at different times or directions of seismic excitation, contributing to a different response. The initial position of the connections and impacts with the panel are discussed in Section 4.2.5.

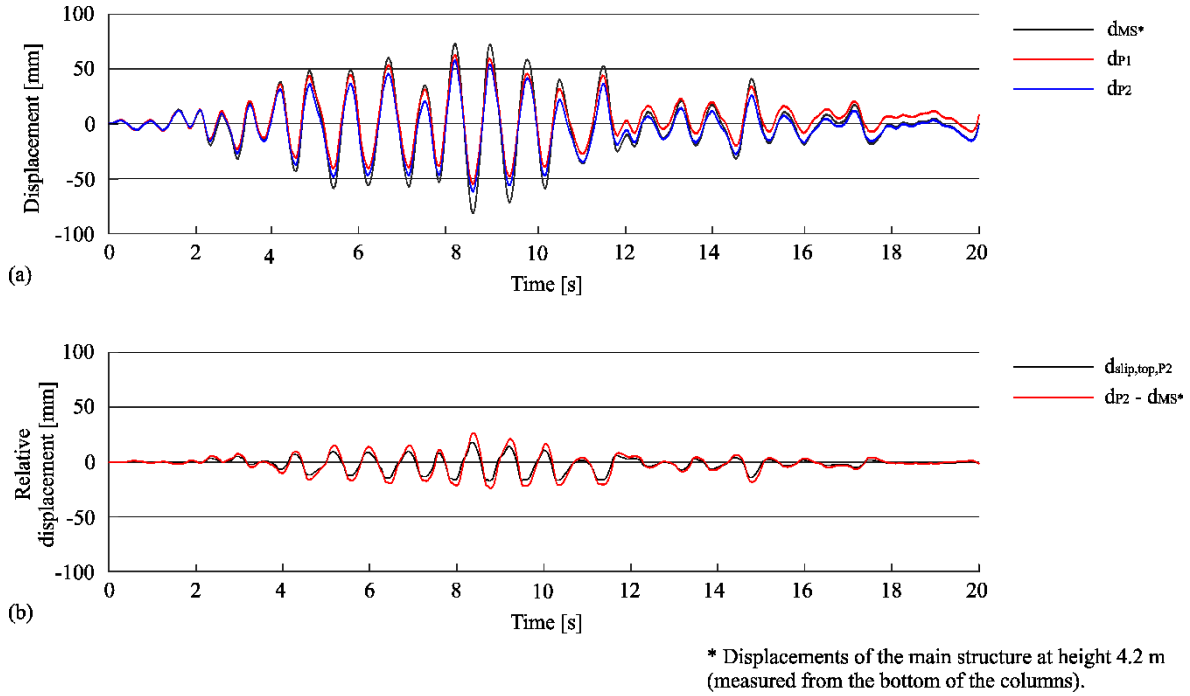

Figure 4.10: Displacement response histories of a specimen at PGA 0.4 g: (a) displacements of the main structure, panel P1 and panel P2 for the symmetric specimen and (b) slip in the top connections of panel P2
Slika 4.10: Pomiki preizkušanca pri PGA 0.4 g: (a) pomiki glavne konstrukcije, panela P1 in panela P2 in (b) zdrs v zgornjem stiku panela P2

Yielding of the reinforcement was registered only at the test of the symmetric configuration at PGA intensity 0.4 g. The maximum measured strain in the reinforcement was 3.00‰, which is just above the analytically estimated yield point of 2.88‰ considering the mean values of material properties. The columns were also close to the yield limit during the test of asymmetric configuration at PGA intensity 0.3 g when the measured strain in the reinforcement was 2.78‰. However, the response of the columns was essentially elastic.

4.2.3 Global response parameters of the specimen

Figure 4.11 shows the acceleration–slab displacement (AD) relationships for both symmetric (black) and asymmetric (red) specimen configurations and all test intensities. The linear

approximation obtained by linear basic fitting of AD relationships in MATLAB software is plotted (dashed lines in Figure 4.11) next to the experimental results.

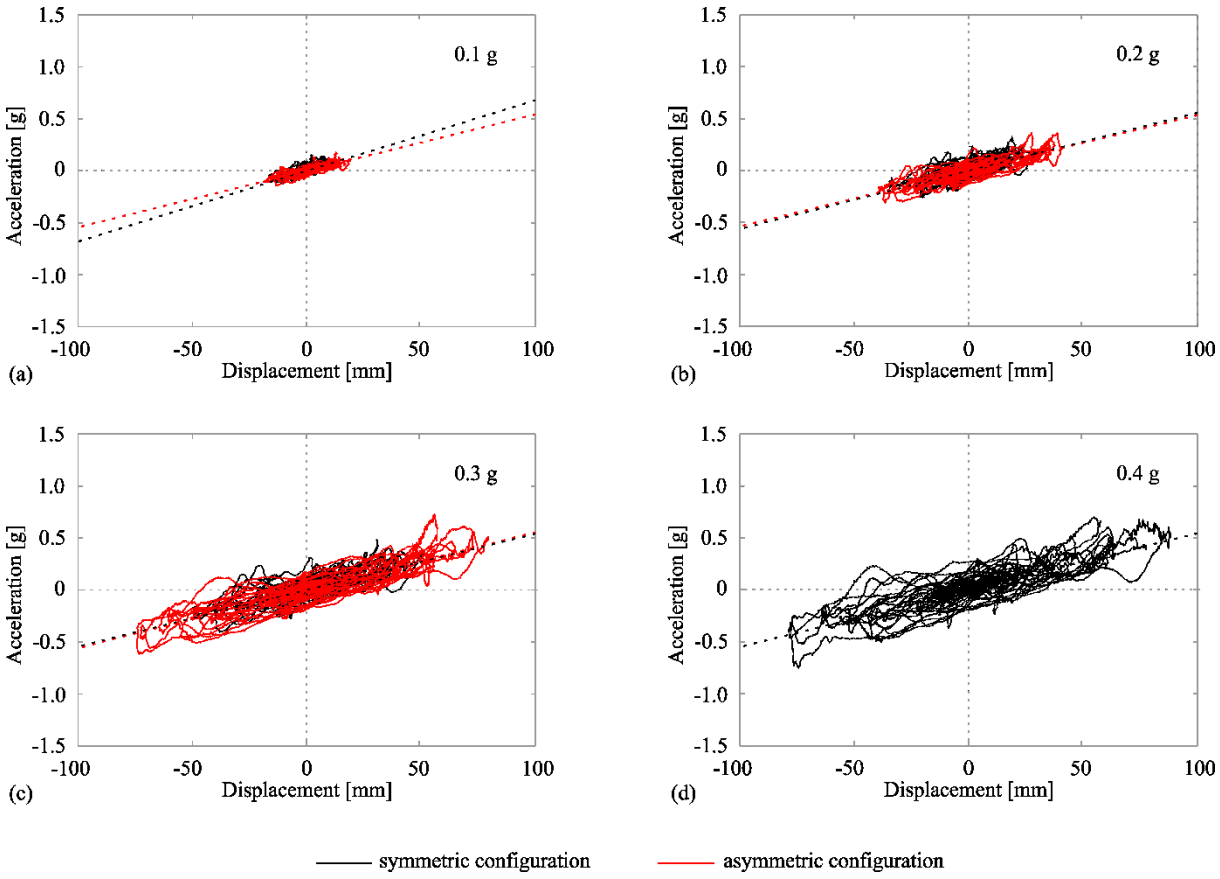

Figure 4.11: Acceleration–displacement response relationships for different PGA intensities: (a) 0.1 g, (b) 0.2 g, (c) 0.3 g and (d) 0.4 g
Slika 4.11: Odnos pospešek – pomik za različne intenzitete testov: (a) 0.1 g, (b) 0.2 g, (c) 0.3 g and (d) 0.4 g

The AD relationships and basic formulas for the single degree-of-freedom (SDOF) system (Equations 4.1-4.3) were used to experimentally estimate the period of vibration of the tested structure. Values are listed in Table 4.4 and are similar for most of the tests.

$$F = m \cdot a \tag{4.1}$$

$$k = \frac{F}{d} \tag{4.2}$$

$$T = 2\pi\sqrt{\frac{m}{k}} \quad \rightarrow \quad T = 2\pi\sqrt{\frac{d}{a}} \tag{4.3}$$

The period of vibration was also estimated analytically, considering the elastic response of the columns. The stiffness of four cantilever columns was taken into account, assuming 25% of the gross cross section because before the tests of structure with horizontal panels, the same main

structure was used to perform 19 tests of the structure with vertical panels. The fundamental period of the main structure during the tests of vertical panels was around 0.7 s, corresponding to 30% of the column gross-section. Because of the many previous tests, the reduction of the cross-section properties was somewhat larger for the tests of horizontal panels.

The match of numerical models and shake table tests in Chapter 5 confirms that the reduction of cross-section properties was appropriate. To achieve an even better match of experimental and numerical response histories, cross-section properties corresponding to 23% of the gross cross section were taken to analyse the asymmetric configuration of horizontal panels (Chapter 5).

It was assumed that the mass of the main structure and the mass of the panels were concentrated at the top of the columns. The analytically estimated period of vibration is 0.91 s for the symmetric specimen and 0.87 s for the asymmetric one (Table 4.4).

Table 4.4: Period of vibration of the tested specimen
Preglednica 4.4: Nihajni čas preizkušanca

Specimen configuration	PGA [g]	The period of vibration [s] (experimental estimation)	The period of vibration [s] (analytical estimation)
Symmetric	0.1	0.76	0.91
Symmetric	0.2	0.84	
Symmetric	0.3	0.85	
Symmetric	0.4	0.85	
Asymmetric	0.1	0.85	0.87
Asymmetric	0.2	0.86	
Asymmetric	0.3	0.85	

The period of vibration is also clearly visible at the displacement and acceleration response histories shown in Figures 4.12 and 4.13. As marked, the period is similar for all the intensities and both configurations.

As shown in Figures 4.10 (a) and 4.14 and already mentioned, the main structure (MS) and both panels (P1 and P2) moved with the same period of vibration. However, the panels also had their own period of vibration around 0.03 s. This can be observed in the displacement response histories shown in Figure 4.14.

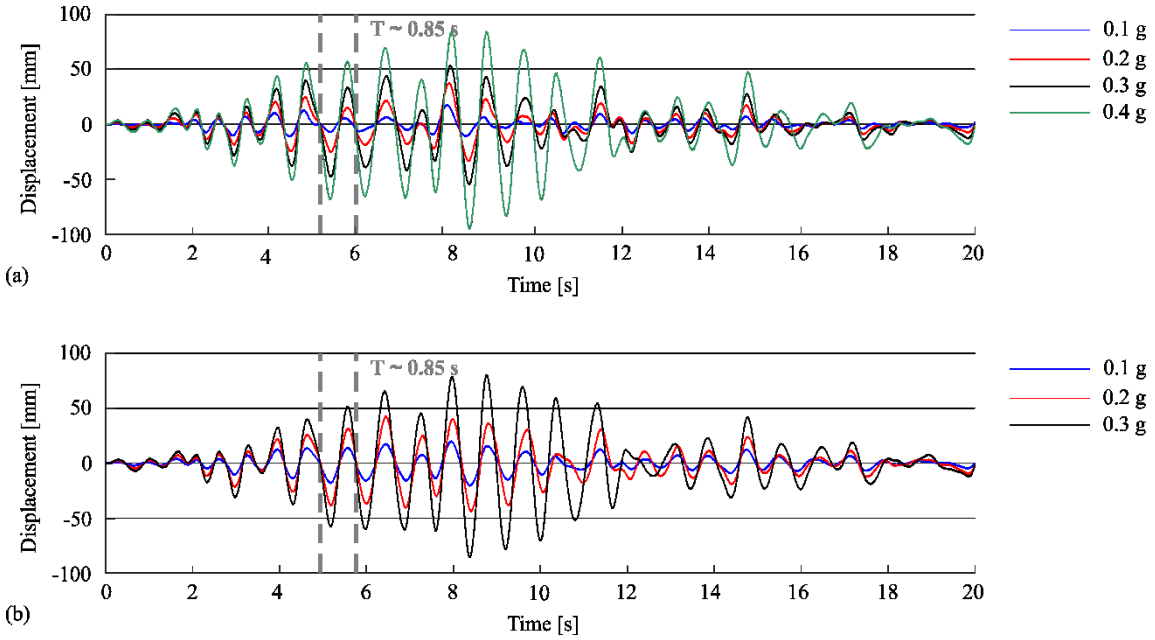

Figure 4.12: Displacements response histories of the main structure, measured at the top of the slab: (a) symmetric and (b) asymmetric specimen

Slika 4.12: Pomiki glavne konstrukcije izmerjeni na vrhu plošče: (a) simetrični in (b) asimetrični preizkušanec

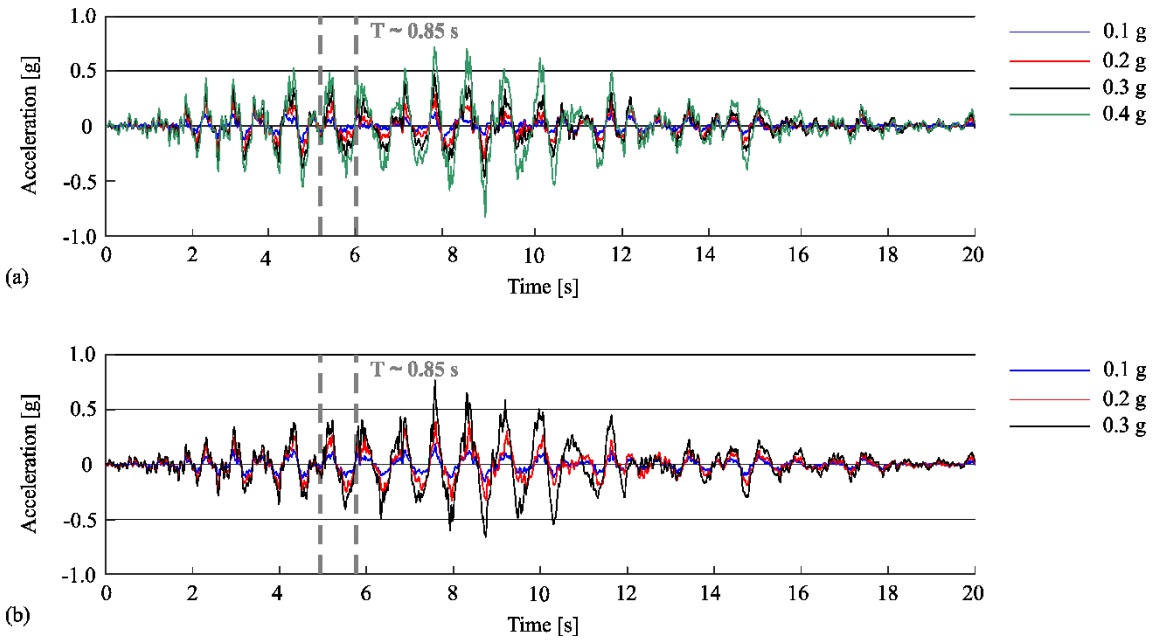

Figure 4.13: Acceleration response histories of the main structure, measured at the top of the slab: (a) symmetric and (b) asymmetric specimen

Slika 4.13: Pospeški glavne konstrukcije izmerjeni na vrhu plošče: (a) simetrični in (b) asimetrični preizkušanec

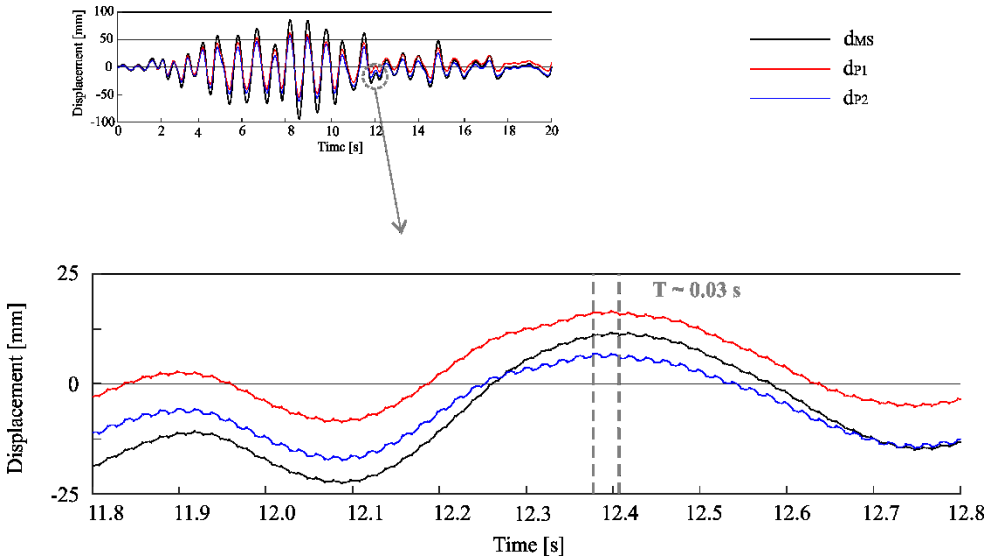

Figure 4.14: Period of vibration of the panels

Slika 4.14: Nihajni čas panelov

At low seismic intensities (0.1 g), the panel was pinned at the level of top connections and in this phase, it practically behaved like a hanging picture. After the friction in the top connections was activated, the panels slid at the level of top and bottom connections as a rigid body. At this phase, the panels' stiffness did not influence the response of the overall structure because they did not present any resistance and slid freely. The interaction between the panels and the main structure was relatively small.

Impacts in the connections occurred at higher seismic intensities. Because the gaps in the connections were depleted, there was some interaction between the panels and the main structure. Note that this occurred only for a very short moment (please see the discussion provided in Section 4.2.5), and the stiffness of the panels did not have a significant influence on the overall response of the main structure.

The small influence of the panels' stiffness on the response is demonstrated by a minor difference in the response of the structure with one and with two panels. The inclination of AD relationships is almost the same (see Figure 4.11), which shows no important difference in the stiffness of the two specimens.

Numerical analysis was performed to further demonstrate that the panel stiffness did not influence the response of the main structure. Force–displacement relationships (i.e. stiffness) of three different models are compared:

(1) a complete model of the specimen tested at shaking table with columns, panels, connections etc.

(2) model of the main structure without panels (only the mass of the panels was considered with no contribution of panel stiffness)

(3) model of the structure with panels and fixed top and bottom connections (complete interaction of the panels and main precast structure)

The numerical models shown in Chapter 5 were used to perform the analysis. Nonlinear dynamic analyses of the models were performed using the same ground motion as the shake table test.

Figures 4.15 and 4.16 show that the stiffness of the specimen tested on the shake table (1) was almost the same as the stiffness of the structure without panels (2). This indicates that the panel stiffness did not significantly influence the response of the overall structure. The main reason for that was the relative weakness of the connections between the panels and columns that isolate the panels from the main structure.

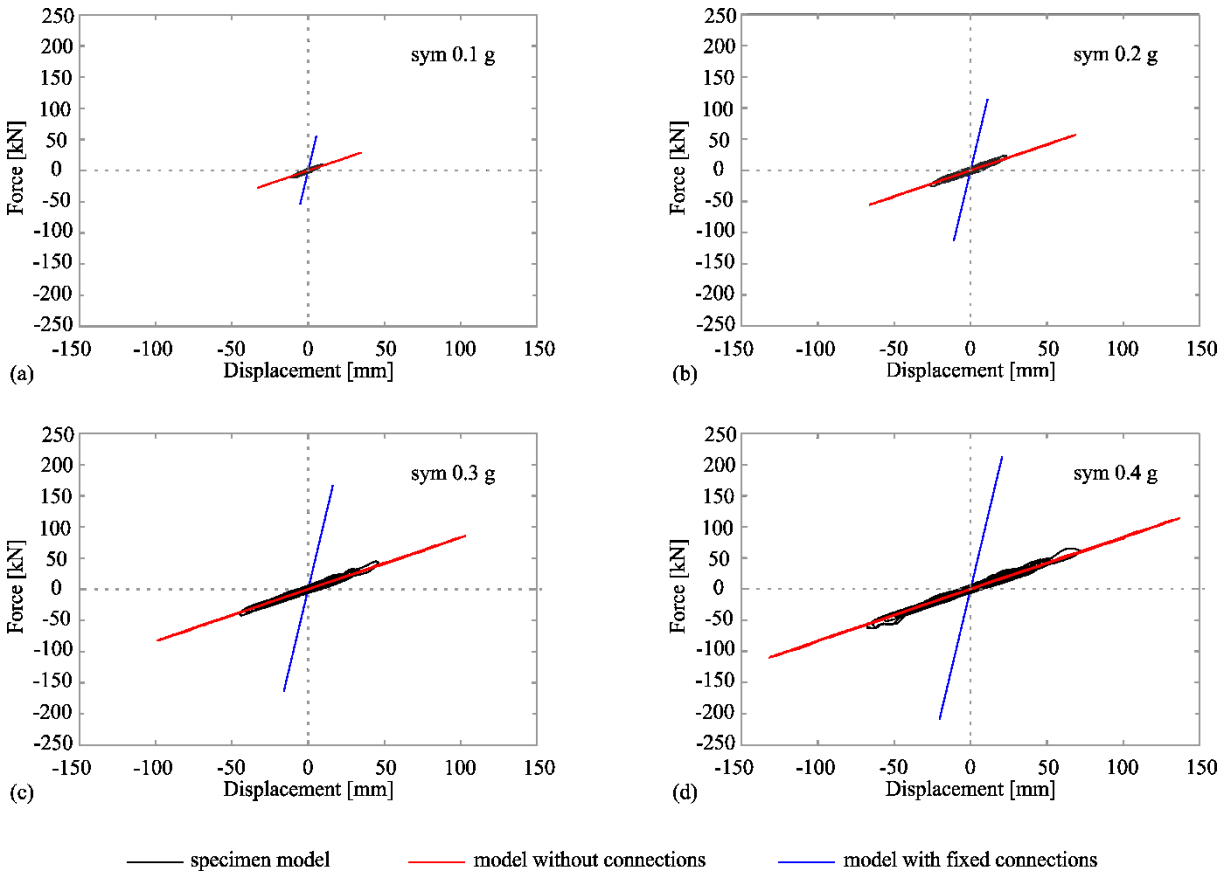

Figure 4.15: Comparison of the force–displacement relationships (i.e. the stiffness of the structure) of the model of the symmetric specimen tested at the shaking table (black), the structure model without panels (red) and the model with fixed cladding connections (blue): (a) PGA intensity 0.1 g, (b) PGA intensity 0.2 g, (c) PGA intensity 0.3 g and (d) PGA intensity 0.4 g

Slika 4.15: Primerjava odnosa sila-pomik (t.j. togost konstruckije) za model simetričnega preizkušanca (črna), model glavne konstrukcije brez panelov (rdeča) in model s fiksiranimi stiki (modra): (a) PGA intenziteta 0.1 g, (b) PGA intenziteta 0.2 g, (c) PGA intenziteta 0.3 g, (d) PGA intenziteta 0.4 g

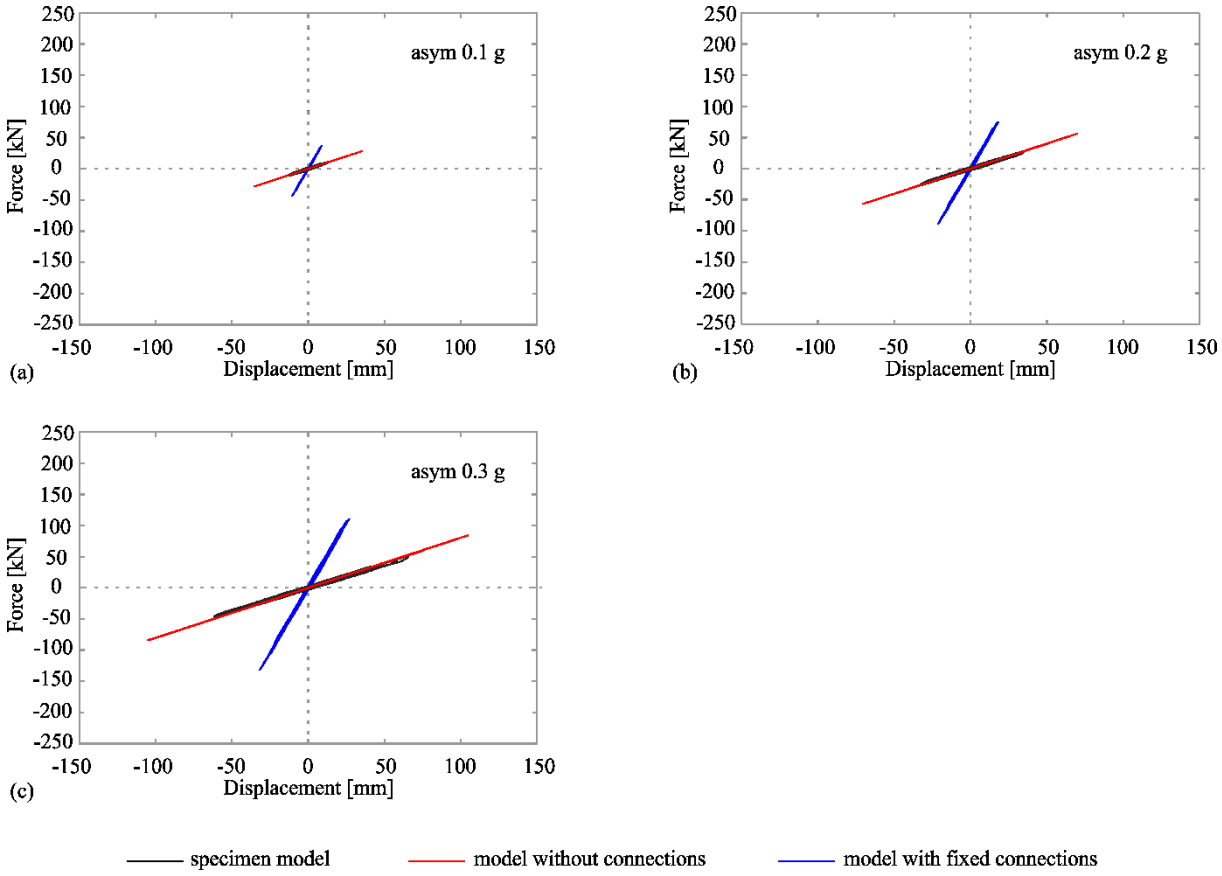

Figure 4.16: Comparison of the force–displacement relationships (i.e. the stiffness of the structure) of the model of the asymmetric specimen tested at the shaking table (black), the structure model without the panel (red) and the model with fixed cladding connections (blue): (a) PGA intensity 0.1 g, (b) PGA intensity 0.2 g, (c) PGA intensity 0.3 g and (d) PGA intensity 0.4 g

Slika 4.16: Primerjava odnosa sila-pomik (t.j. togost konstruckije) za model asimetričnega preizkušanca (črna), model glavne konstrukcije brez panela (rdeča) in model s fiksiranimi stiki (modra): (a) PGA intenziteta 0.1 g, (b) PGA intenziteta 0.2 g, (c) PGA intenziteta 0.3 g, (d) PGA intenziteta 0.4 g

The fundamental periods of the models are compared in Table 4.5. The periods of specimen model (1) and the structure without the panels (2) were also practically the same; 0.89 s for the symmetric specimen and 0.86 for the asymmetric specimen. The model with only one panel had a smaller period of vibration because of the smaller mass of the panels. The periods of models (1) and (2) were somewhat lower from the analytical estimated values in Table 4.4 because it was assumed for analytical estimation that the mass of the panels is concentrated at the top of the structure, whereas in the numerical models, the mass of the panels was concentrated at the actual position of the panels.

The third model (3) is intended to demonstrate the influence of the panels in the case of complete interaction of the panels and the main structure. The fundamental period of model (3) is considerably smaller because of the considerable influence of the panels' stiffness. Because the stiffness of the panels influenced the global response, the model with two panels had a smaller period of vibration that was not evident in shaking table tests.

Table 4.5: Period of vibration

Preglednica 4.5: Nihajni čas

Configuration	Model of the specimen	Model without connections + mass of the panels	Model with fixed connections	Shaking table test
Symmetric	0.89 s	0.89 s	0.25 s	0.76–0.85 s
Asymmetric	0.86 s	0.86 s	0.35 s	0.85–0.86 s

4.2.4 The response of cladding connections

The response of individual connections was similar to that observed during single component tests (Chapter 3). The response of the top connections during the shake table tests is illustrated in Figure 4.17, where the typical hysteretic response is also shown.

The response of the top connections consisted of the sliding and impact with the panel. In the first phase (Figure 4.17, phase 1), the bolt at the top slid along the steel box profile cast in the panel. At this stage, a limited friction force was activated. Its amount depends on the tightening torque applied to the bolt and the coefficient of friction between the steel elements.

The second phase starts when the bolt washer reaches the edge of the steel box, corresponding to the slip of the bolt d_{slip}. At this phase, the bolt is subjected to bending. Consequently, the lateral stiffness of the connection increases considerably (Figure 4.17, phase 2). Unlike the single-component tests, the cladding connections did not fail in any of the shaking table tests. Relative displacements between the panels and main structure at the top connections were smaller than the displacement capacity of the connection.

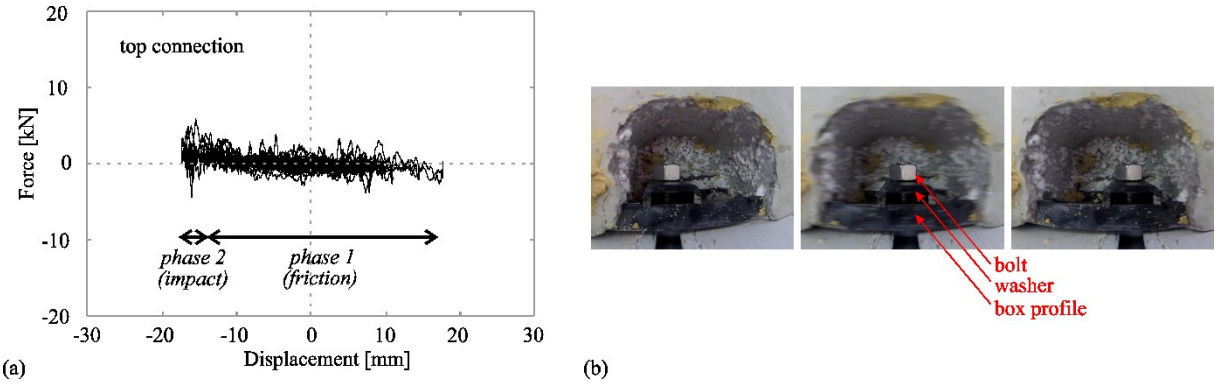

Figure 4.17: Response of the top connections during the shake table test: (a) typical hysteretic response and (b) response captured with GoPro camera

Slika 4.17: Odziv zgornjih stikov med testom na potresni mizi: (a) značilen histerezni odziv in (b) odziv zajet z GoPro kamero

The response of the bottom connection is illustrated in Figure 4.18. The response of the bottom connections was also similar to that observed during single component tests. Initially, the friction force was activated, followed by the sliding of the panel (phase 1 in Figure 4.18). When the available gap in the connection was depleted, there was an impact in the connection, and the stiffness of the connection increased considerably (phase 2 in Figure 4.18). Due to the large stiffness and strength of the cantilever bracket, the response was predominantly elastic.

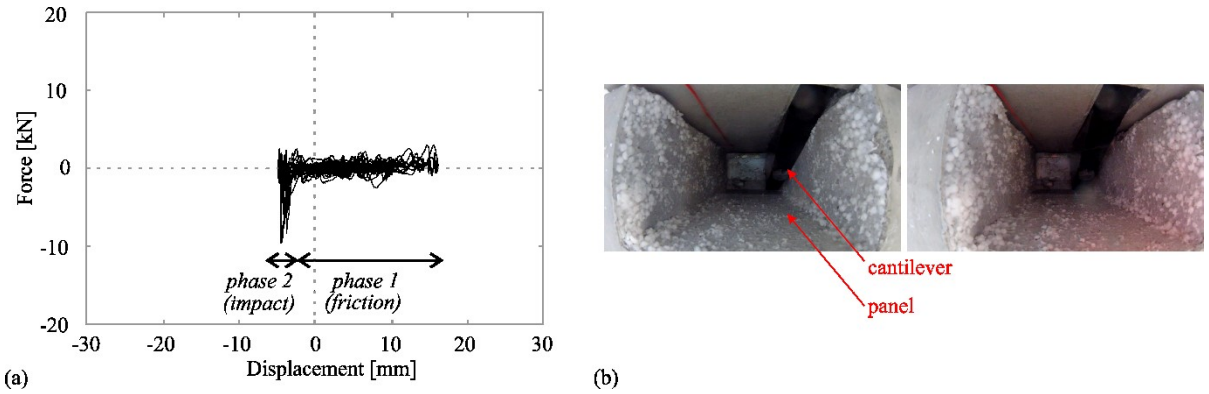

Figure 4.18: Response of the bottom connections during the shake table test: (a) typical hysteretic response and (b) response captured with GoPro camera

Slika 4.18: Odziv spodnjih stikov med testom na potresni mizi: (a) značilen histerezni odziv in (b) odziv zajet z GoPro kamero

The shake table tests were performed to analyse the system response of the horizontal panels. The panels were fastened to deformable columns (as in the real buildings) in the tests. Due to the columns' rotations and bending, the relative displacements between panels and columns (i.e. slips) at the level of top and bottom connections were different. This is the main difference between single component tests and shake table tests. Note, however, that this does not affect basic response mechanisms or type of failure of the connection because the movement of panels remains predominantly translational even when the columns are subjected to large rotations (bending). No significant rotations of the panel were observed, as shown in Figure 4.19, where the rotations of panel P2 during the shake table test at PGA intensity of 0.4 g are presented. Rotations were below 0.1%, even for the highest load intensity.

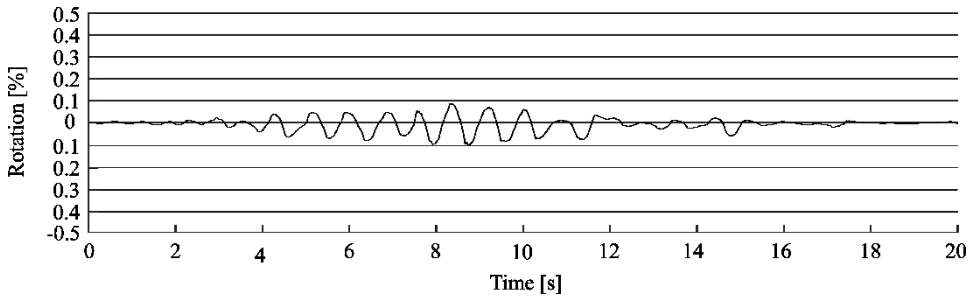

Figure 4.19: Rotations of the panel P2 during the shake table test at PGA intensity of 0.4 g

Slika 4.19: Rotacije panela P2 med testom na potresni mizi pri PGA intenziteti 0.4 g

In the top connections during shaking table tests, the relative rotation between column and panel occurred in the bolt, and the connection acted as pinned. The washer did not notably rotate and could slide over the box profile in a similar manner as in the tests of single components. Panels only lean on the steel stud of the bottom connection; thus, the rotations of columns and panels are independent of each other. Consequently, the panel response in the shaking table tests was predominantly translational despite the significant rotations (bending) of columns.

The velocities in the connections observed during the shake table tests were in the range of velocities applied to the connections in the component tests. The maximum velocities during single component tests were 0.04 m/s and 0.13 m/s for the slowest and the fastest test, respectively. Maximum velocities at bottom connections during the shake table test were 0.04 m/s and 0.16 m/s for the tests at the PGA of 0.1 g and 0.4 g, respectively.

4.2.5 The impacts between panels and connections

During the shake table tests, the impacts between panels and connections were observed for PGA intensities higher than 0.2 g. The impacts were mostly noticed at the bottom connections for both symmetric and asymmetric configurations of the specimen. The only case when there were also impacts at top connections was panel P2 at the test of PGA intensity 0.4 g.

Impacts occur when the gaps in the connections are depleted. The occurrence of impacts considerably depends on the initial size of the gaps in connections and the position of the panel relative to the columns. The gaps measured before each test run are listed in Table 4.6. Bold numbers present the slip (and position) at which the impacts occurred. The gaps (designed initially only to account for construction tolerances) are often very different in different connections (see Table 4.6). They are relatively small, even in ideal conditions when connections are centrally mounted. However, they can also be depleted even before an earthquake due to construction reasons.

An example is presented in Figure 4.20, where the initial gaps in the connections of panel P2 before the test at the PGA intensity of 0.4 g are presented. As shown, the position of the panel relative to the column is very asymmetric.

Because of the asymmetric position of the connections, the impacts occurred only at one side and at one connection at a time. In the case presented in Figure 4.20, the critical points were at the top and bottom connections of panel and column C3, where the gaps were very small on the right side of the connections.

Table 4.6: Available gaps in the connections measured before each test run (left/right in global coordinates)
Preglednica 4.6: Prosti pomik v stikih izmerjen pred vsakim testom (levo/desno v globalnih koordinatah)

Symmetric specimen	PGA 0.1 g gap [mm]	PGA 0.2 g gap [mm]	PGA 0.3 g gap [mm]	PGA 0.4 g gap [mm]
column C1: panel P1 top	30 / 50	30 / 50	25 / 55	20 / 60
column C1: panel P1 bottom	10 / 80	**10** / 80	**5** / 85	**5** / 85
column C2: panel P1 top	50 / 30	50 / 30	45 / 35	45 / 35
column C2: panel P1 bottom	35 / 55	35 / 55	40 / 50	35 / 55
column C3: panel P2 top	45 / 35	45 / 35	25 / 55	**15** / 65
column C3: panel P2 bottom	40 / 50	40 / 50	35 / 55	**15** / 75
column C4: panel P2 top	60 / 20	60 / 20	50 / 30	35 / 45
column C4: panel P2 bottom	45 / 45	45 / 45	50 / 40	35 / 55
Asymmetric specimen	PGA 0.1 g gap [mm]	PGA 0.2 g gap [mm]	PGA 0.3 g gap [mm]	
column C1: panel P1 top	30 / 50	30 / 50	25 / 55	
column C1: panel P1 bottom	**10** / 80	**10** / 80	**5** / 85	
column C2: panel P1 top	50 / 30	50 / 30	45 / 35	
column C2: panel P1 bottom	35 / 55	35 / 55	40 / 50	

Note: Numbers in bold present the slip and position at which the impacts occurred.

The position of the columns and panel at the moment of impact is illustrated in Figure 4.21. Due to the bending of columns, the sliding of the panel along the columns occurs in opposite directions at the level of top and bottom connections. For this reason and because of the eccentric position of the connections (shown in Figure 4.20), the impacts occurred at the top of the panel when columns deformed to the right and at the bottom when columns deformed to the left (see Figure 4.21).

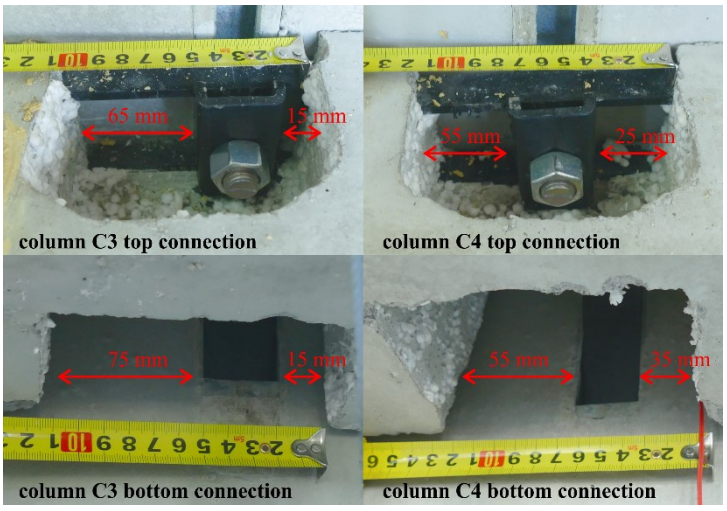

Figure 4.20: Positions of the panel P2 connections before the test at the PGA of 0.4 g
Slika 4.20: Pozicije stikov panela P2 pred testom z intenziteto 0.4 g

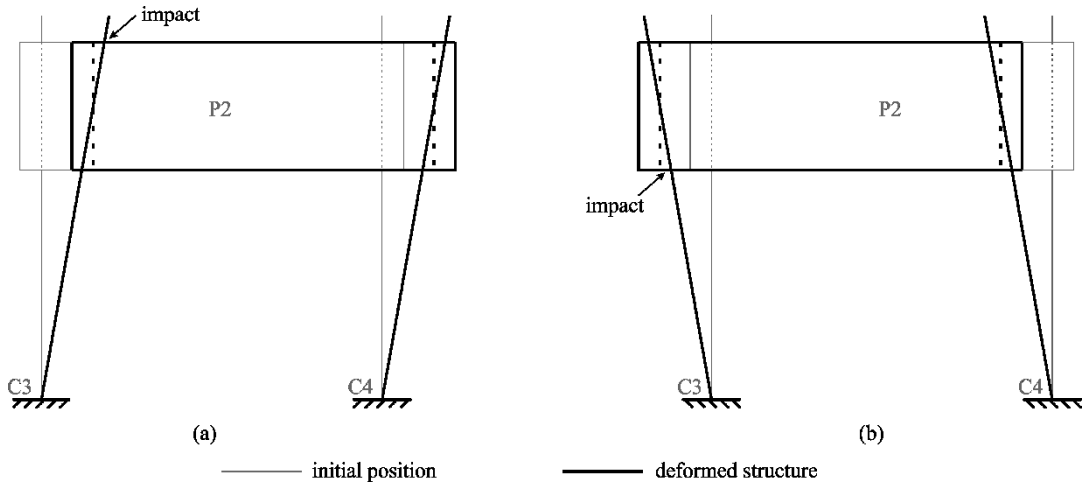

Figure 4.21: Positions of the columns and panel P2 at the moment of (a) impact at the top of the panel and (b) impact at the bottom of the panel

Slika 4.21: Pozicija stebrov in panela P2 v trenutku: (a) trka v zgornjem stiku in (b) trka v spodnjem stiku

Figure 4.22 plots the relative displacements between the panel and columns at the level of top and bottom connections (i.e. slips in the connections) together with the acceleration response histories of the panel. The impacts are shown as the limitation of relative displacements in the connections when the gap was depleted, and acceleration instantly increased.

Acceleration response histories of the main structure and both panels at PGA 0.4 g are compared in Figure 4.23. Impacts significantly affected only the acceleration of the panels. Their influence on the acceleration of the main structure was considerably smaller. As previously explained, instant increases of acceleration correspond to the impacts in the connections. Though obvious on the plot of panel acceleration, they cannot be seen in the plot of acceleration of the main structure (Figure 4.23, black line). This indicates that impacts did not significantly affect the response of the main precast structure.

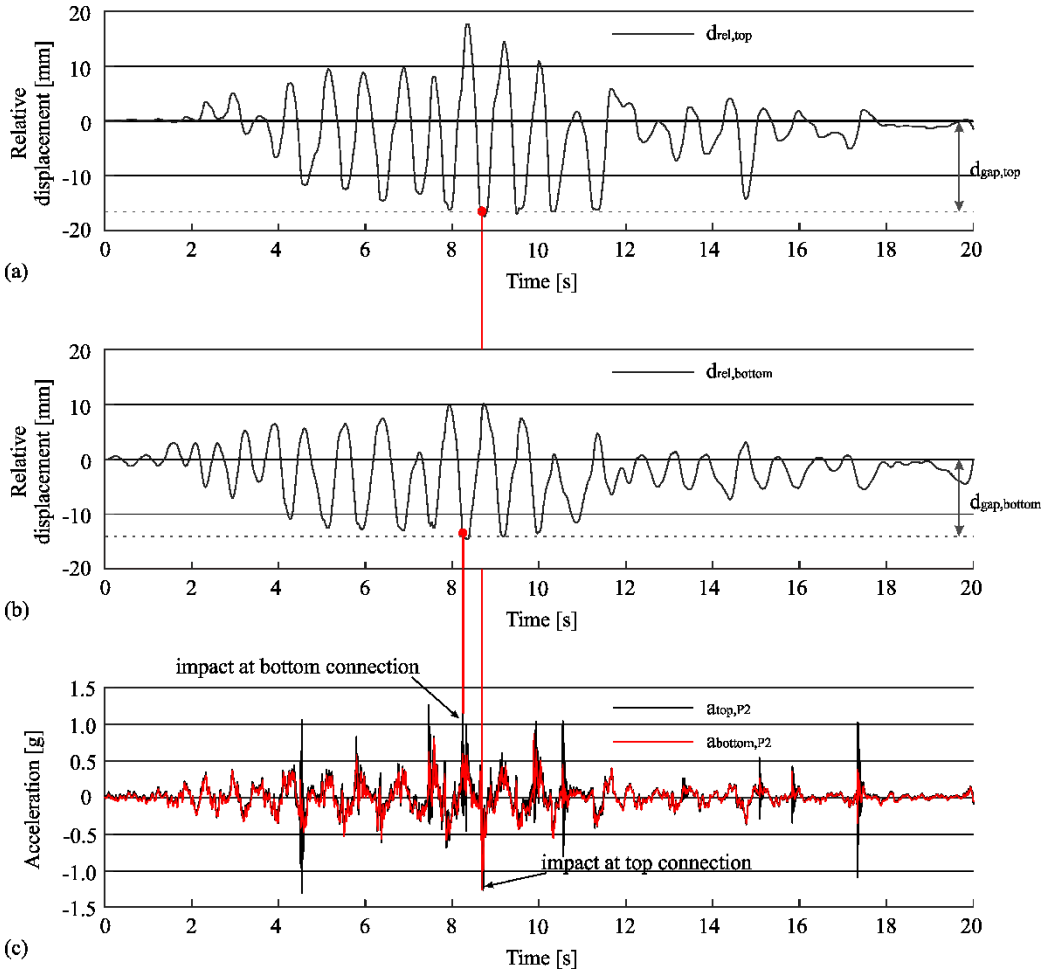

Figure 4.22: Impacts of the panel P2 at the PGA 0.4 g: (a) slip at the top connection, (b) slip at the bottom connection and (c) acceleration response histories of the panel (shaking table test)

Slika 4.22: Trki panela P2 pri PGA 0.4 g: (a) zdrs v zgornjem stiku, (b) zdrs v spodnjem stiku in (c) pospeški panela izmerjeni na zgornjem in spodnjem robu (test na potresni mizi)

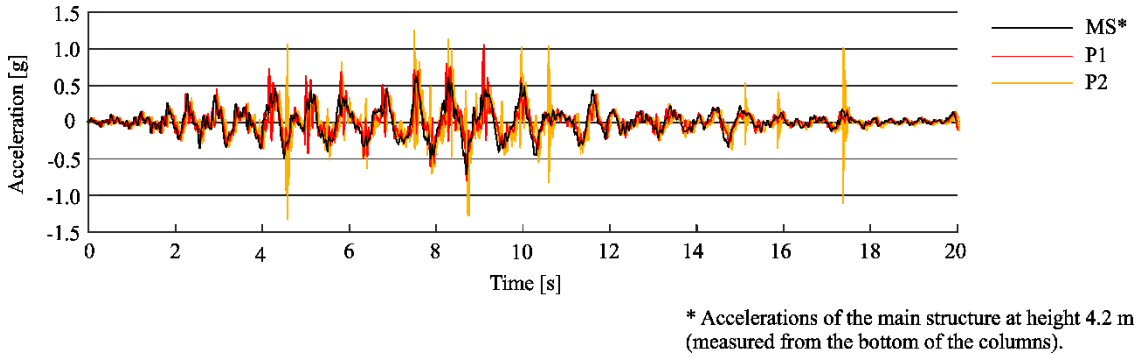

Figure 4.23: Acceleration response histories of the main structure, panel P1 and panel P2 for the symmetric specimen at the PGA 0.4 g (shaking table test)

Slika 4.23: Pospeški glavne konstrukcije, panela P1 in panela P2 simetričnega preizkušanca pri intenziteti PGA 0.4 g (test na potresni mizi)

To demonstrate the minor effect of impacts on the response of the main precast structure, the period of vibration was estimated at each time step of the analysis. The numerical model of the specimen (verified in Chapter 5) was used to perform such analysis.

Plots in Figure 4.24 present the period of vibration next to the time history of relative displacements and force in the bottom connection. At the moment of impact, the stiffness of the complete precast system increased due to the activated stiffness of the panel. There was a drop in the period of vibration (from 0.89 s to 0.34 s) due to the momentary higher stiffness of the structural system. However, this occurred for only a moment and did not have an important influence on the overall structure response. Displacements and accelerations of the main structure were not affected by impacts.

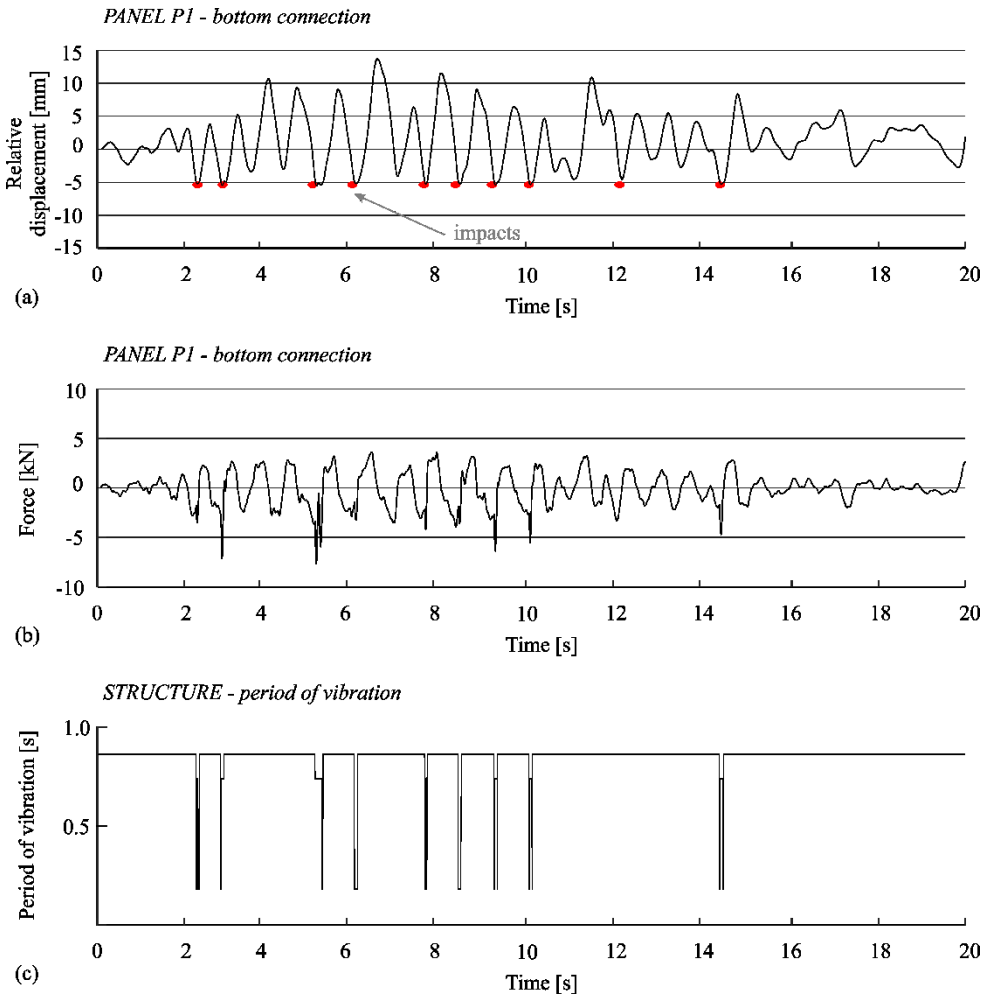

Figure 4.24: The period of vibration at the moments of impact for symmetric specimen at PGA intensity of 0.3 g: (a) displacements in bottom connection, (b) force in bottom connection and (c) the period of vibration evaluated at each time step of analysis (numerical model)

Slika 4.24: Nihajni čas v trenutku trkov simetričnega preizkušanca pri PGA intenziteti 0.3 g: (a) pomiki v spodnjem stiku, (b) sila v spodnjem stiku in (c) nihjani čas izvrednoten na vsakem koraku analize (numerični model)

The impacts were instantaneous and affected the stiffness of the main structure only for a moment. As observed, they did not have a significant influence on the global response of the structure. However, at the moment of impact, high lateral forces are activated in connections and locally, a large force can be induced into the column. Figure 4.25 shows the sum of the forces in all connections compared to the base shear column force. As shown, the force in connections is up to 30% of the base shear force.

During the tests, some spalling of the concrete was observed around the connections. Thus, high lateral forces that occur in the connections and are transferred into the columns may appreciably increase the shear demand in columns. This issue is further investigated within the parametric study in Chapter 6.

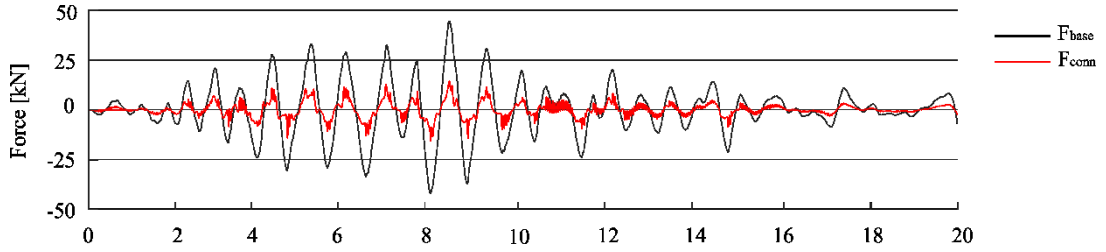

Figure 4.25: Force in the connections compared to the base shear force of the column at the tests of symmetric specimen at PGA intensity of 0.3 g (numerical model)

Slika 4.25: Sila v stikih v primerjavi s prečno silo ob vpetju stebra med testom simetričnega preizkušanca pri PGA intenziteti 0.3 g (numerični model)

4.2.6 Type of configuration

The influence of the specimen configuration (i.e. number of panels) on the seismic response is analysed in this section. As already demonstrated (see Section 4.2.3), the structure response was not significantly affected by the stiffness of the panels. There was also no significant difference between the stiffness of the symmetric and asymmetric specimen configurations (see Figure 4.11). However, the difference between the responses of the tested specimens with one and with two panels (i.e. asymmetric and symmetric configuration, respectively) was the amplitude of the main structure displacements.

Figure 4.26 compares displacements of the main structure for both specimen configurations and two intensities of seismic excitation. As shown, the maximum displacements of the asymmetric specimen were larger than the displacements of the symmetric specimen.

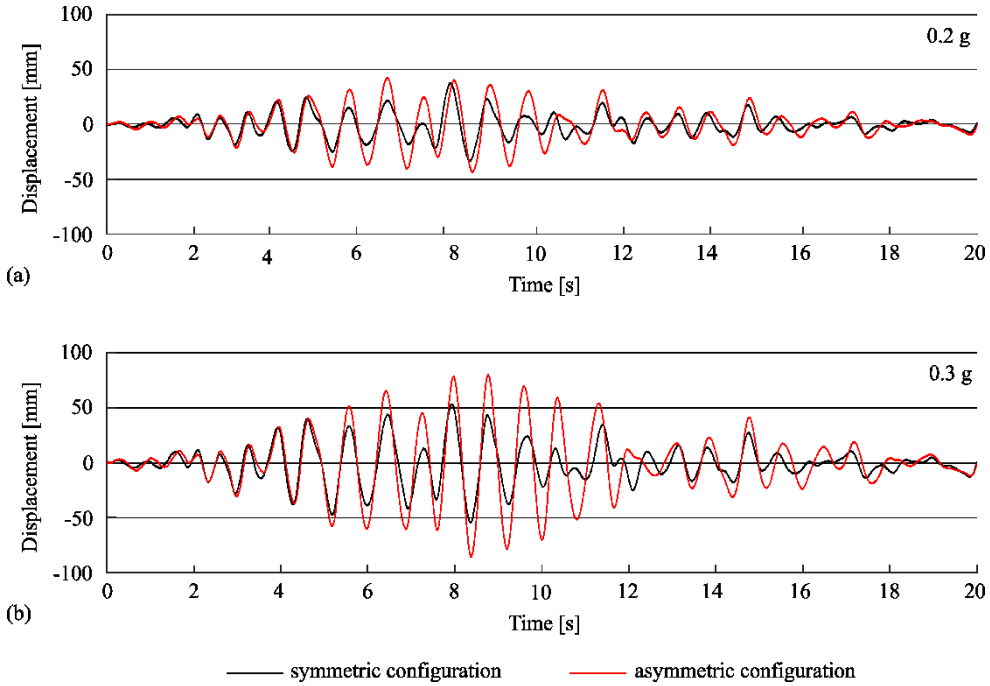

Figure 4.26: Displacements of the main structure for a symmetric and asymmetric specimen: (a) PGA 0.2 g and (b) PGA 0.3 g (shaking table test)

Slika 4.26: Pomiki glavne konstrukcije simetričnega in asimetričnega preizkušanca: (a) PGA 0.2 g in (b) PGA 0.3 g (test na potresni mizi)

During the shaking table test, the hysteretic damping within panel connections influenced the response of the main structure. There were twice as many cladding connections in the symmetric specimen as in the asymmetric one, and during seismic excitation, the panels acted as mass dampers. Figure 4.27 plots the energy dissipation in the connections against the cumulative displacement of the main structure for all the performed tests. There was an approximately twice as large dissipation of energy by the symmetric specimen.

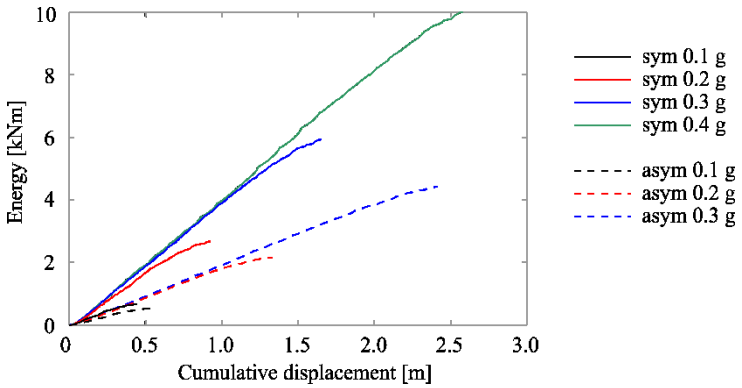

Figure 4.27: Dissipated energy in the connections (numerical model)

Slika 4.27: Disipirana energija v fasadnih stikih (numerični model)

The damping of the main structure during the test was estimated based on the amplitude reduction during free vibration of the structure (Fajfar, 1984) using the numerical models shown and verified

in Chapter 5. Estimated damping ratios were 8% and 5% for symmetric and asymmetric specimens, respectively (please note that usually, 2% Rayleigh damping is considered for the experiments).

To confirm the above observations, the displacement response spectra (scaled to the intensity of 1.0 g) at different damping levels are shown in Figure 4.28. From the comparison of maximum structure displacements given in Table 4.3 and the displacement spectra at period 0.85 s, it is possible to confirm a relatively good match. The maximum displacements of symmetric specimen at PGA intensities of 0.1 g to 0.3 g match the displacement response spectra at 8% damping, whereas the maximum displacements of asymmetric specimen at PGA intensities of 0.1 g and 0.2 g match well with the displacement response spectra at 5% damping. Some yielding was noted during the tests at the highest intensities, and thus the period of the structure was increased, which resulted in larger displacements during the tests.

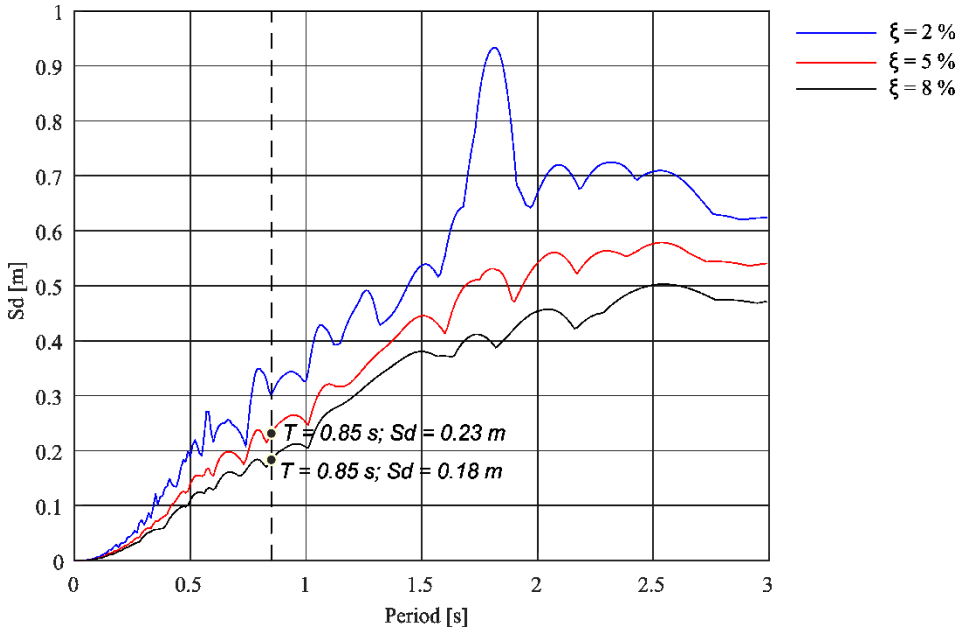

Figure 4.28: Displacement response spectra at 2%, 5% and 8% damping scaled to the intensity of 1.0 g
Slika 4.28: Spekter pomikov pri 2%, 5% in 8% dušenju skalirani na 1.0 g

To confirm this observation about damping, numerical analysis of the main structure without panels was performed. Only the mass of the panels was added to the main structure. To consider the damping provided by the fastening devices (not included in the model), the viscous damping was increased to 8% and 5%, considering the symmetric and asymmetric configuration of these devices, respectively.

The response of the structure model without connections is compared with the response of the tested specimen in Figures 4.29-4.32. The displacement and acceleration response histories of the structure without connections and the tested specimen match relatively well. The match is somewhat worse

for the results of symmetric specimen at PGA intensity of 0.4 g and asymmetric specimen at PGA intensity of 0.3 g. As already mentioned, this discrepancy is due to the yielding of the columns.

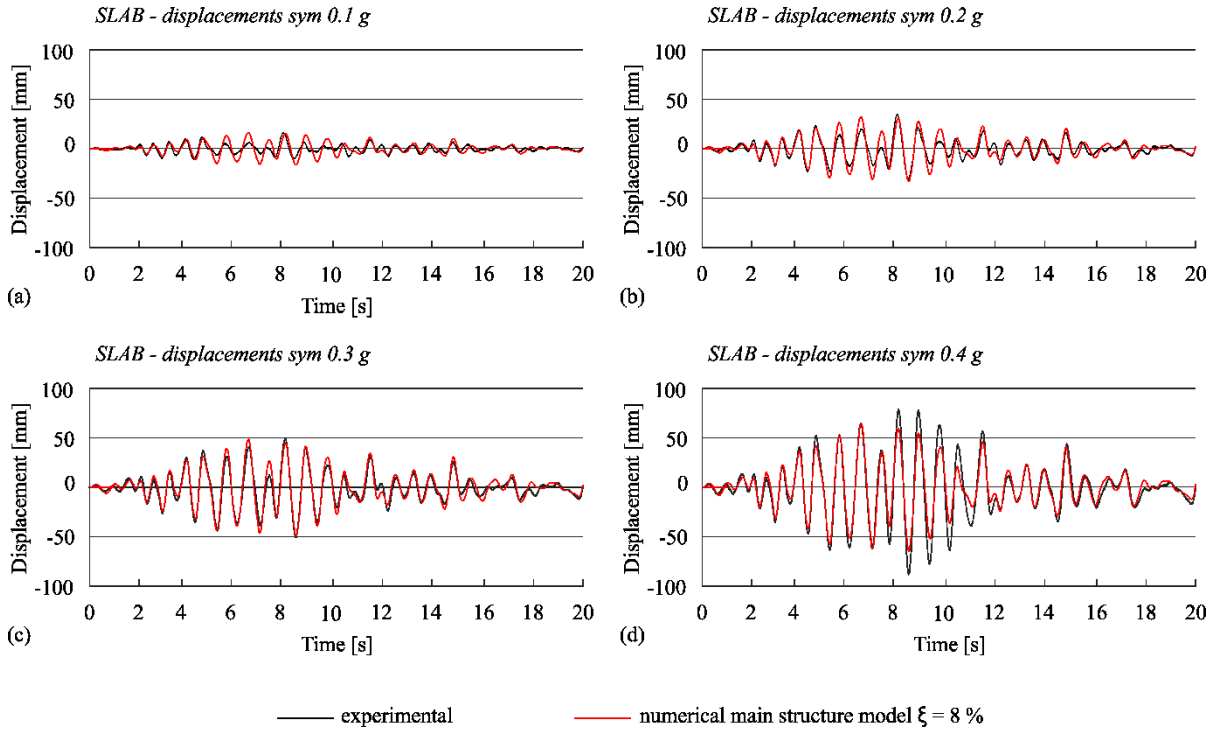

Figure 4.29: Comparison of experimental (black) and numerical (red) slab displacements of the main structure without panels and connections considering 8% damping ratio for symmetric structure: (a) 0.1 g PGA, (b) 0.2 g PGA, (c) 0.3 g PGA and (d) 0.4 g PGA

Slika 4.29: Primerjava ekperimentalnih (črna) in numeričnih (rdeča) pomikov simetrične konstrukcije brez panelov in stikov ob upoštevanju 8% koeficienta dušenja: (a) 0.1 g PGA, (b) 0.2 g PGA, (c) 0.3 g PGA, (d) 0.4 g PGA

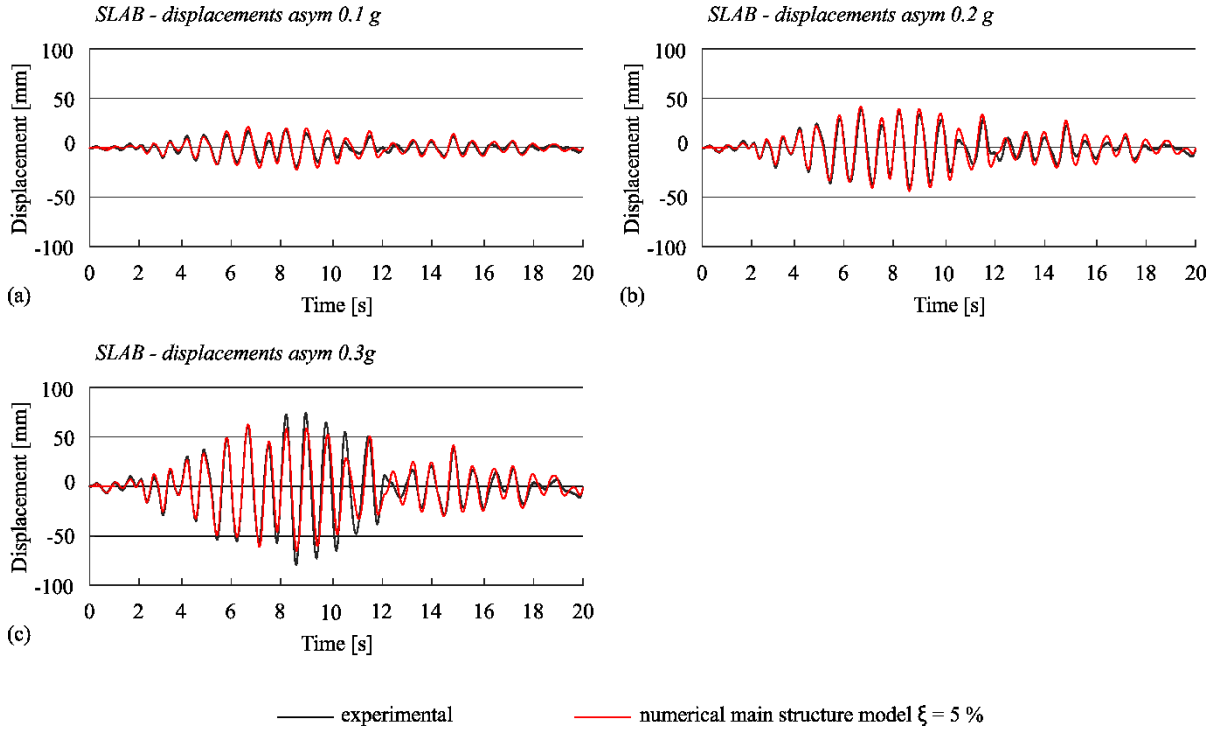

Figure 4.30: Comparison of experimental (black) and numerical (red) slab displacements of the main structure without panels and connections considering 5% damping ratio for asymmetric structure: (a) 0.1 g PGA, (b) 0.2 g PGA and (c) 0.3 g PGA

Slika 4.30: Primerjava ekperimentalnih (črna) in numeričnih (rdeča) pomikov asimetrične konstrukcije brez panelov in stikov ob upoštevanju 5% koeficienta dušenja: (a) 0.1 g PGA, (b) 0.2 g PGA, (c) 0.3 g PGA

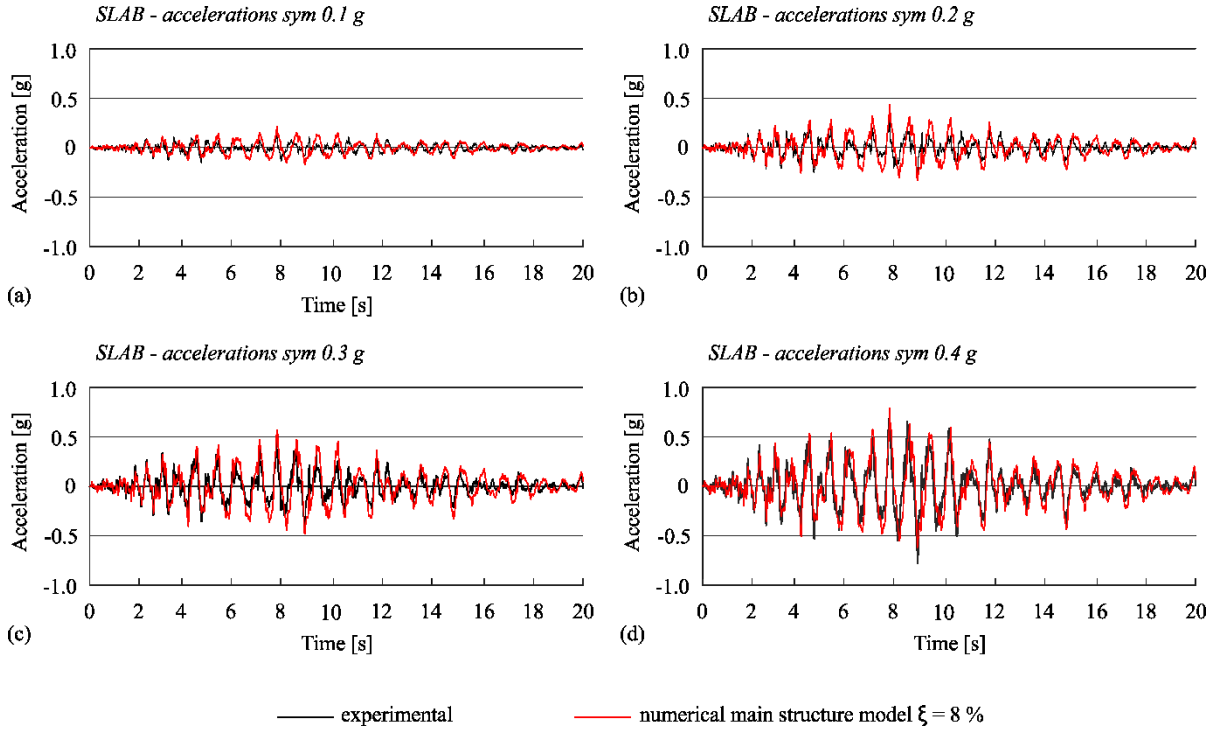

Figure 4.31: Comparison of experimental (black) and numerical (red) slab accelerations of the main structure without panels and connections considering 8% damping ratio for symmetric structure: (a) 0.1 g PGA, (b) 0.2 g PGA, (c) 0.3 g PGA and (d) 0.4 g PGA

Slika 4.31: Primerjava ekperimentalnih (črna) in numeričnih (rdeča) pospeškov simetrične konstrukcije brez panelov in stikov ob upoštevanju 8 % koeficienta dušenja: (a) 0.1 g PGA, (b) 0.2 g PGA, (c) 0.3 g PGA, (d) 0.4 g PGA

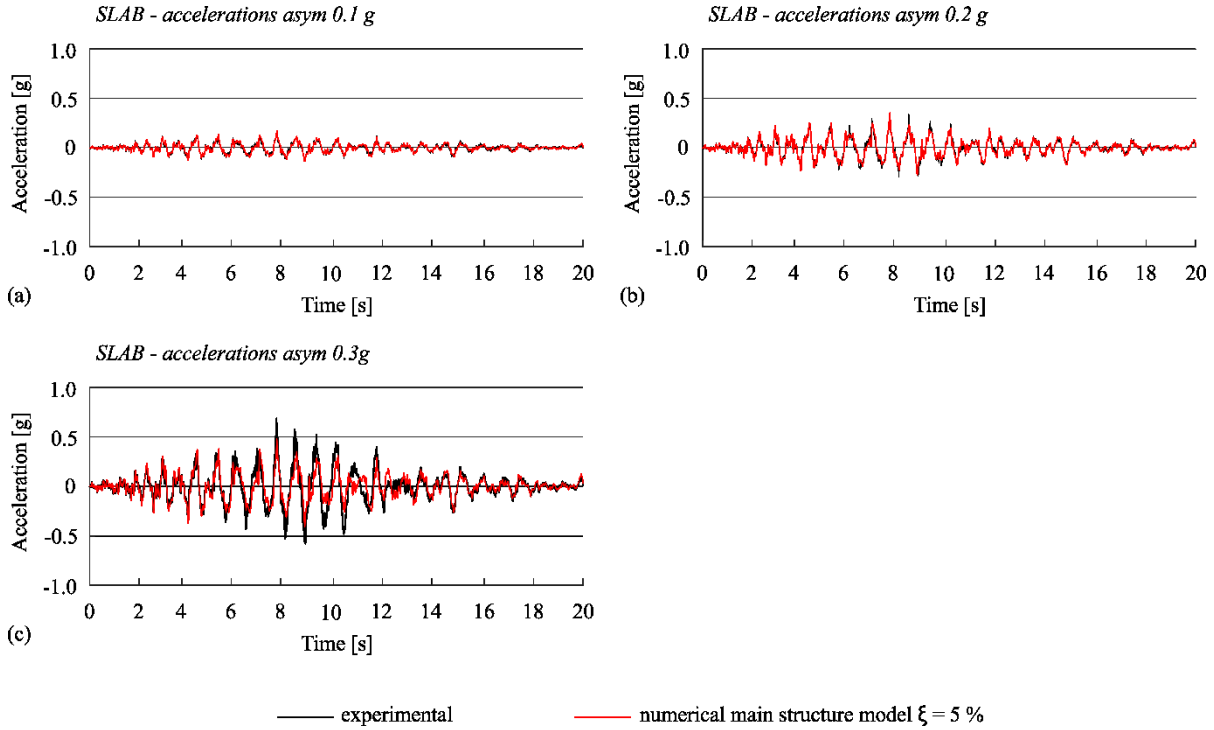

Figure 4.32: Comparison of experimental (black) and numerical (red) slab accelerations of the main structure without panels and connections considering 5% damping ratio for asymmetric structure: (a) 0.1 g PGA, (b) 0.2 g PGA and (c) 0.3 g PGA

Slika 4.32: Primerjava ekperimentalnih (črna) in numeričnih (rdeča) pospeškov asimetrične konstrukcije brez panelov in stikov ob upoštevanju 5 % koeficienta dušenja: (a) 0.1 g PGA, (b) 0.2 g PGA, (c) 0.3 g PGA

Damping in structures originates from different sources: the nonlinear behaviour of columns or the hysteretic response of cladding connections. The effect of hysteretic damping in the cladding connections was somewhat more pronounced during the experiment because the response of the columns was predominantly in the elastic range. Additionally, in real buildings, higher-than-experimental damping is expected (5%), and because of that, the influence of connections is also reduced.

4.2.7 The response in out-of-plane direction and torsion

Because the column cross-section properties are the same in both directions, as well as mass of the structure and panels, the period of the structure in the out-of-plane direction was similar to that in the in-plane direction. It is visible in the acceleration response histories in Figure 4.33.

The maximum slab accelerations in the out-of-plane direction are listed in Table 4.7. The accelerations in the out-of-plane direction amounted to around 30% of the accelerations in the in-plane direction. Thus, there was a load component also in out-of-plane directions, but the influence on the response of connections was not visible during the tests.

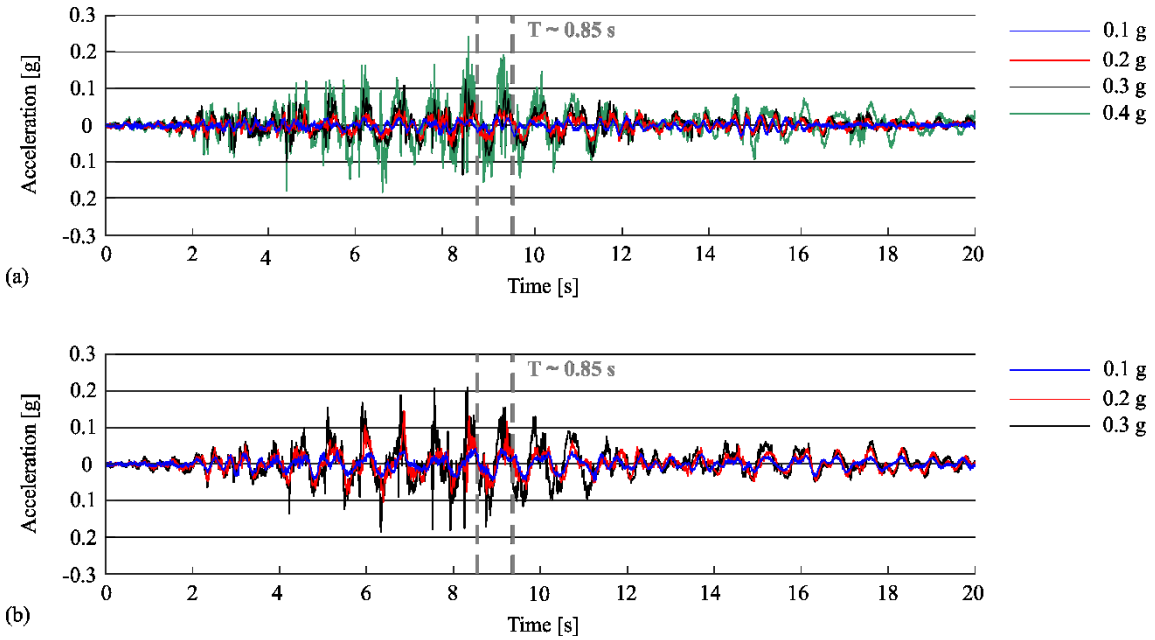

Figure 4.33: Acceleration response histories of the main structure in out-of-plane direction: (a) symmetric and (b) asymmetric specimen

Slika 4.33: Pospeški glavne konstrukcije v smeri izven ravnine: (a) simetrični in (b) asimetrični preizkušanec

Table 4.7: The maximum accelerations in the horizontal direction perpendicular to panel plane

Preglednica 4.7: Maksimalni pospeški v prečni smeri

Symmetric specimen	PGA 0.1 g	PGA 0.2 g	PGA 0.3 g	PGA 0.4 g
Acceleration of the slab [g]	0.03	0.06	0.14	0.24

Asymmetric specimen	PGA 0.1 g	PGA 0.2 g	PGA 0.3 g
Acceleration of the slab [g]	0.05	0.15	0.21

Figure 4.34 presents the rotations of the slab at the test of symmetric specimen at PGA intensity of 0.4 g and asymmetric specimen at PGA intensity of 0.3 g. The maximum slab rotation was below 0.5% for both tests. Thus, the torsion that occurred during the experiment was relatively small. It also did not appreciably affect the response of the specimen.

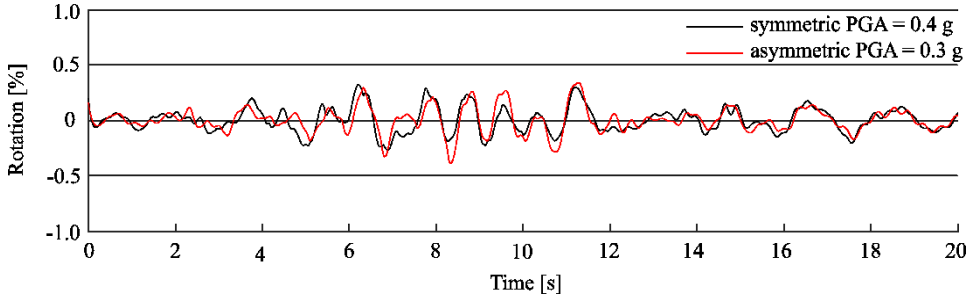

Figure 4.34: Rotation of the slab of symmetric specimen at the PGA intensity of 0.4 g (black) and asymmetric specimen at the PGA intensity of 0.3 g (red)

Slika 4.34: Rotacija plošče simetričnega preizkušanca pri PGA 0.4 g (črna) in asimetričnega preizkušanca pri PGA 0.3 g (rdeča)

4.3 Summary and conclusions of the chapter

In this chapter, the response observed within full-scale shaking table tests of horizontal cladding panels in a one-storey RC industrial building is analysed. The shaking table tests have been performed within the Slovenian research project in cooperation with the Institute of Earthquake Engineering and Engineering Seismology in Skopje, using their large shaking table (Zoubek et al., 2017). The tested fastening system used for attaching the horizontal cladding panels to the columns of the main structure is commonly used in Central Europe. It consists of top bolted connections that provide the out-of-plane stability of the panel and bottom cantilever connections that support the panels' weight.

One of the experimental study aims was to investigate the response of the panels during seismic excitation and their influence on the response of the main precast structure. Therefore, symmetric and asymmetric specimen configurations were tested up to a PGA seismic intensity of 0.4 g.

Although the failure of the connections was not reached, it was possible to define the complex behaviour mechanism of the panels. The response of cladding connections was similar to that observed during single component tests. Based on the test results, it was possible to define the numerical models (presented in Chapter 5) that were then used within the parametric study (Chapter 6) for detailed analysis of a wide array of industrial buildings with horizontal cladding panels.

The shake table tests gave an important insight into the behaviour of precast structures with horizontal concrete cladding panels. The important parameters that may influence the seismic response of such buildings were identified: different structural configuration, construction imperfections, interaction of the adjacent panels and the connection of the bottom panels to the foundation. The influence of these parameters on the seismic response of real structures is further

analysed with the parametric study (Chapter 6), where special attention was devoted to analysing the influence of the number of panels and their interaction, which was not possible to test because of limitations of the shake table.

The in-plane dynamic response of the complete precast cladding system with horizontal panels and fastening system typical for Central Europe was identified: the panels move predominantly translationally in their plane and mostly follow the movements of the main structure. For the whole duration of seismic excitation, the response of the panels is governed by the movement of the main structure that controls the vibration period.

At low column rotations, the panel was pinned at the level of top connections, and it practically behaved as a hung picture. After the friction in the top connections was activated, the panels slid translationally at the level of both connections as a rigid body. At this phase, the panel stiffness did not influence the response of the overall structure. The interaction between the panels and the main structure was relatively small.

Impacts in the connections occurred at higher seismic intensities. Because the gaps in the connections were depleted, there was some interaction between the panels and the main structure. Note that this occurred only for a very short moment, and the stiffness of the panels did not significantly influence the overall response of the main structure.

The response of the horizontal concrete façade systems highly depends on construction imperfections. The gaps in the connections are relatively small, even in ideal conditions when connections are centrally mounted. However, the gaps can also be depleted due to construction reasons, even before the earthquake. At the moment of impact, considerable forces activate in the connections and the failure that follows occurs in the top connections and is practically brittle. The influence of those forces on the response of precast structures is investigated within the parametric study in Chapter 6.

The effect of hysteretic damping in the cladding connections was quite pronounced during the experiment. In real buildings, the influence of the energy dissipation within connections is smaller; also, it presents a smaller share of total damping.

5 NUMERICAL MODELLING OF THE HORIZONTAL CONCRETE FAÇADE SYSTEMS IN RC PRECAST BUILDINGS

Hysteretic material models of the considered connections are presented in this chapter. The models are defined based on the experimental results and response analysis presented in Chapters 3 and 4. They are validated by simulating single components and full-scale shaking table experiments. Calibrated models are then used in Chapter 6 to analyse the seismic response of a wide array of RC precast buildings and develop complete insight into the influence of important parameters on the response of such buildings.

5.1 Numerical model of the fastening system

The response of the connections in the horizontal in-plane direction was modelled in the OpenSees software framework (McKenna & Fenves, 2010) by combining several standard, uniaxial material models. The numerical model was based on the results and observations of the single component tests and the full-scale shaking table tests presented in Chapters 3 and 4. The efficiency of the proposed numerical models is demonstrated in Section 5.2.

5.1.1 Numerical model of the top bolted connection

A typical response of the bolted top connections, presented in Figure 5.1, was simulated by combining three material models: *ElasticPP* (*EPP*), *ElasticPPGap* (*EPPGap*) and *Hysteretic*, as shown in Figure 5.2 (a). In the first phase of the response (Figure 5.1, phase 1), the friction between the steel elements was activated due to the tightening torque in the bolt. The *ElasticPP* (Figure 5.2 b) model was used to simulate this friction. The properties of the model were defined using the common Coulomb friction model described in detail in the following subsections.

In the second phase of the connection response, the bolt washer reached the edge of the steel box, and the gap in the connection was depleted. At this moment, the stiffness of the top connection almost instantly increased (Figure 5.1, phase 2), which was simulated by the series combination of the *ElasticPPGap* (Figure 5.2 c) and the *Hysteretic* (Figure 5.2 d) material models.

To define the complete model of the top connection, the impact model (series combination of the *ElasticPPGap* and *Hysteretic* material models) was added in parallel to the friction model (*ElasticPP*), as shown in Figure 5.2 (a).

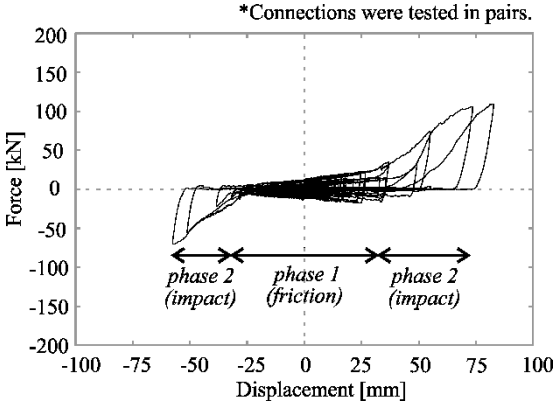

Figure 5.1: Typical hysteretic response of the top connection during the dynamic test on components
Slika 5.1: Značilen histerezni odziv zgornjega stika med dinamičnim testom zgornjih stikov

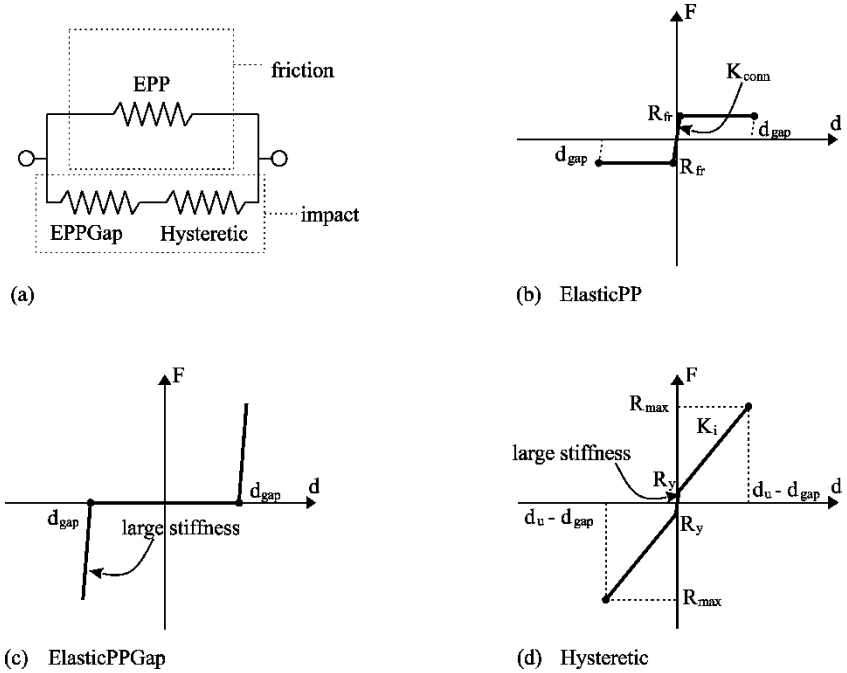

Figure 5.2: Schematic presentation of the macro model: (a) combination of different hysteretic material models used for the numerical simulation of top and bottom connections, (b) *ElasticPP*, (c) *ElasticPPGap* and (d) *Hysteretic* material models
Slika 5.2: Shematski prikaz makro numeričnega modela: (a) kombinacija različnih histrereznih materialnih modelov za numerično simulacijo zgornjih in spodnjih stikov, (b) *ElasticPP*, (c) *ElasticPPGap* in (d) *Hysteretic* materialni modeli

The force–displacement relationship of the numerical model used for the simulation of top connections response is schematically presented in Figure 5.3. The model parameters are the size of the gap ($d_{gap,top}$), the maximum displacement capacity (d_u), the friction force ($R_{fr,top}$), the

resistance of the top connection ($R_{max,top}$) and stiffness ($K_{conn,top}$, $K_{i,top}$) as presented in following paragraphs. The recommended values are summarised in Table 5.

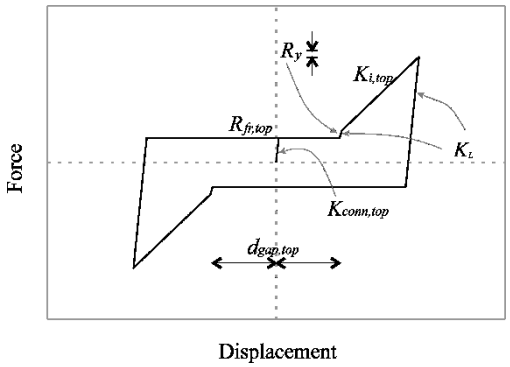

Figure 5.3: Schematic envelope of the numerical models of the top connection
Slika 5.3: Shematski prikaz ovojnice numeričnega modela zgornjega stika

Table 5.1: Recommended values of the model parameters of the top connection
Preglednica 5.1: Priporočene vrednosti modelnih parametrov zgornjega stika

Material characteristic	Value	Material characteristic	Value	Material characteristic	Value
$c_{fr,top}$	0.4	$K_{conn,top}$	$2 \cdot 10^4$ kN/m	K_L	$1 \cdot 10^4$ kN/m
$d_{gap,top}$*	±4.0 cm	$K_{i,top}$	$1.5 \cdot 10^3$ kN/m	R_y	0.01 kN
d_u*	±7.5 cm	$R_{max,top}$	58 kN	*px*, *py*, *d1*, *d2*, *b*	0, 0, 0, 0, 0

Legend: $c_{fr,top}$: friction coefficient between steel elements of the top connection, $d_{gap,top}$: gap in the top connection, d_u: displacement capacity of the top connection, $R_{max,top}$: resistance of the top connection, $K_{conn,top}$: initial stiffness of the top connection, $K_{i,top}$: bending stiffness of the top connection, K_L: large unloading stiffness after the gap is depleted, *px, py, d1, d2, b,* R_y: specific parameters *pinchx, pinchy, damage1, damage2, beta* and R_y of the hysteretic material model.
* The value corresponds to the centrally positioned connection.

Size of the gap

The initial position of the connections depends on the actual construction and the possible residual displacements after the earlier excitations. If the top connections are mounted centrally, then $d_{gap,top}$ is half the width of available space in the steel box (cast in the panel) reduced by half of the thickness of the bolt washer. The position of connections has an important influence on the response of the panel, as will be demonstrated later.

Displacement capacity

The displacement capacity of the top connection consists of the variable gap in the top connections $d_{gap,top}$, and the plastic deformation capacity of the bolt, which is about 3.5 cm. If the connections are installed in the middle of the gap, the total displacement capacity amounts to 7.5 cm.

Friction force

The friction force in the top connection was defined by using the common Coulomb friction model that assumes that the friction force is the product of the normal force on the surface and the constant coefficient of friction. Thus, the friction force in the top connection depends on the tightening torque in the bolt T_b and the coefficient of friction between the connection parts $c_{fr,top}$ (Zoubek, 2015):

$$R_{fr,top} = c_{fr,top}\, F_b \tag{5.1}$$

$$F_b = \frac{T_b}{c_0\, D_b} \tag{5.2}$$

The friction coefficient in the threaded bolt c_0 = 0.2 was considered. This is recommended friction coefficient for galvanised bolts without lubrication according to VDI 2230 standard (DIN VDI 2230 Part-1 cited by AmesWeb, 2020). The nominal diameter of the bolt D_b was 16 mm.

It is recommended to use a friction coefficient $c_{fr,top}$ of 0.4 for this type of connection. The value is estimated from the maximum friction force observed during the tests of top connections $R_{fr,top}$ = 8 kN and the tightening torque T_b = 65 Nm. The proposed value is in quite good agreement with the friction coefficients reported by Del Monte et al. (2019). They have evaluated the values of the static friction coefficient at about 0.45 and dynamic ones in the range 0.32–0.35, according to the tests on similar connection types.

It is not necessarily true that the tightening torque of the top connections in real precast structures will be 65 Nm, as prescribed by the producer. The tightening force also decreases during the seismic excitation due to loosening of the bolt. Generally, the friction forces activated in the connections are relatively small compared to the forces that occur in the main precast structure. The friction force observed during the shaking table tests was considerably smaller (Section 5.2.2). For the reasons listed above, using a friction force of 2 kN in the top connection is recommended. This force was also observed during the shake table tests.

Resistance of the top connection

According to the experimental results, the shear resistance of one top connection amounts to 58 kN for the connection with a stronger hot-rolled channel and around 34 kN if the cold-formed channel is used. Please see also the discussion provided in Section 3.3.5.

Stiffness

In general, the initial stiffness of the top connections ($K_{conn,top}$) is very large as long as the full friction force is not activated (see the recommended values in Table 5.1). After that, the stiffness is equal to zero as long as the gap is not depleted. Then the stiffness abruptly increases to K_i due to the activated bending stiffness of the bolt at the top.

The bending stiffness of the bolt at the top was estimated experimentally and analytically:

(1) Experimental estimation

The stiffness was experimentally estimated from the maximum force (58 kN) and displacement at the failure of the top connections. The calculation uses the displacement of the connection after the gap has been depleted (35 mm). The impact stiffness determined from experimental results is $1.7 \cdot 10^3$ kN/m.

(2) Analytical estimation

The impact stiffness was analytically estimated with formulas proposed by Belleri et al. (2016), who tested very similar top connections. According to the static scheme presented in Figure 5.4, the following formula was proposed:

$$K_{i,top} = \frac{12\,E\,I_b}{L_b^2} \frac{E\,I_b\,(k_{\theta,S1}+k_{\theta,S2})+k_{\theta,S1}\,k_{\theta,S2}L_b}{(12\,E^2\,I_b^2+4\,E\,I_b\,(k_{\theta,S1}+k_{\theta,S2})\,L_b+k_{\theta,S1}\,k_{\theta,S1}\,L_b^2)} \tag{5.3}$$

where EI_b is flexural stiffness of the bolt, L_b is the length of the bolt, and $k_{\theta,S1}$ and $k_{\theta,S2}$ are elastic rotational stiffness of springs *S1* and *S2*, respectively.

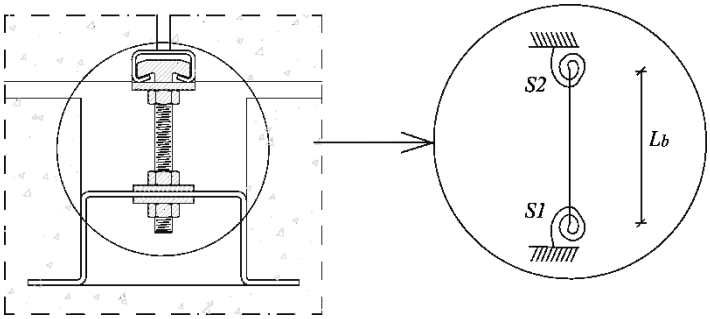

Figure 5.4: Static scheme of top connection (Belleri et al., 2016)

Slika 5.4: Shematski prikaz statičnega modela zgornjega stika (Belleri et al., 2016)

Calculated impact stiffness K_i is $1.4 \cdot 10^3$ kN/m. Bolt length L_b = 60 mm, bolt diameter D_b = 16 mm and the rotational stiffness $k_{\theta,S1} = 6 \cdot 10^3$ kN/m were used. Because the channel lip failure was relevant, the rotational stiffness $k_{\theta,S2}$ was equal to zero.

The experimentally estimated stiffness agrees quite well with those evaluated as proposed by Belleri et al. (2016). Use K_i stiffness of $1.5 \cdot 10^3$ kN/m in the numerical model is recommended.

The *Hysteretic* material model was used in series with *EPPGap* to model the response after the gap was closed. All the following specific parameters should be set to zero for this purpose: *pinchx*, *pinchy*, *damage1*, *damage2* and *beta*. A relatively small parameter R_y and large unloading stiffness K_L of the *Hysteretic* model behaviour (see the envelope in Figure 5.3) were used to define the steep unloading branch.

5.1.2 Numerical model of the bottom cantilever connection

The typical hysteretic response of the bottom connection is presented in Figure 5.5. Initially, the friction force was activated, followed by the sliding of the panel (Figure 5.5, phase 1). When the available gap in the connection was exhausted, the stiffness of the connection increased considerably due to the bending of the cantilever bracket (Figure 5.5, phase 2).

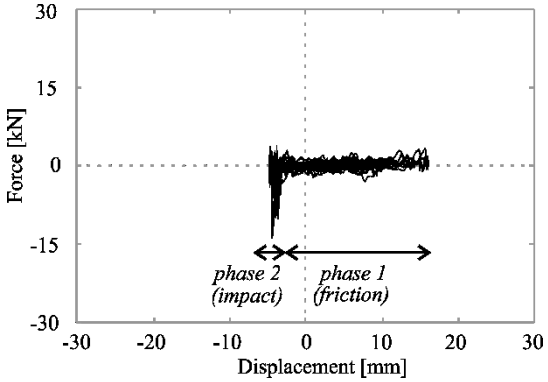

Figure 5.5: Typical hysteretic response of the bottom connection during the shake table test

Slika 5.5: Značilen histerezni odziv spodnjega stika med testom na potresni mizi

The analysis showed that the friction response of the bottom connection under the dynamic loading had somewhat different characteristics. Thus, the friction model of the bottom connection was different. In the presented tests (and the real buildings subjected to the seismic excitations), the panels were subjected to the dynamic load. The friction force in the bottom connection was considerably affected by the velocity of connections' excitations and damping, as observed in Section 3.3.5. Thus, the viscous friction model was used that assumes that the friction force is a linear function of the sliding speed (see Figure 5.6) to model friction in the bottom connection.

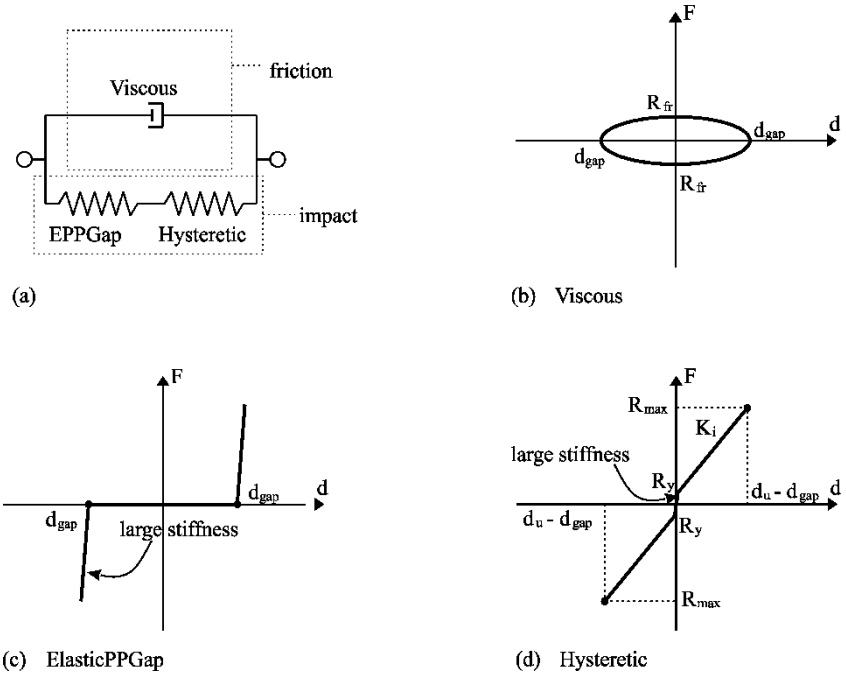

Figure 5.6: Schematic presentation of the macro model: (a) a combination of different hysteretic behaviours used for the numerical simulation of the bottom connections under dynamic loading, (b) *Viscous,* (c) *ElasticPPGap* and (d) *Hysteretic* material models

Slika 5.6: Shematski prikaz makro numeričnega modela: (a) kombinacija različnih histrereznih materialnih modelov za numerično simulacijo spodnjih stikov med dinamično obtežbo, (b) *Viscous,* (c) *ElasticPPGap* in (d) *Hysteretic* materialni modeli

Different friction models are available in the literature (Andersson et al., 2007; Liu et al., 2015). Commonly, the friction force is physically explained by the Coulomb friction behaviour as the product of normal force on the surface and the coefficient of friction that is generally acknowledged to be constant. However, the friction force may depend on the sliding speed, and the coefficient of friction between two objects may vary according to the relative speed of motion (Rabinowicz, 1956; Kragelskii, 1965).

The analysis of single component tests showed that the response of the bottom connections was rather viscoelastic, which implied that the parallel combination of the *Viscous* and *Elastic* models would be appropriate for simulating friction in the bottom connection. This model was used to simulate single component tests and was included in the original paper *Modelling in-plane dynamic response of a fastening system for horizontal concrete facade panels in RC precast buildings* (Starešinič et al., 2020).

However, it is difficult to explain the physical importance of the elastic spring in the bottom connections because there is no obvious source of stiffness during the sliding phase. Experimentally defined elastic stiffness was relatively small, and in principle, the viscous friction is usually modelled using only the *Viscous* material model. For this reason, the viscous friction model presented in Figure 5.6 (a, b) was used for the following numerical analyses.

As was the case for top connection, the significant increase of the connections' stiffness in the second phase of the response was simulated by the series combination of the *ElasticPPGap* (Figure 5.6 c) and the *Hysteretic* (Figure 5.6 d) material models. The complete model of the bottom connection was defined by the parallel combination of friction and impact models (Figure 5.6 a).

The common Coulomb model was used to model the friction in the bottom connection during the quasi-static cyclic tests because there were no dynamic effects. Thus, this model was similar to that used for modelling the top connections response (Figure 5.2).

The force–displacement relationship of the numerical models used to simulate bottom connection responses is schematically presented in Figure 5.7. The model parameters are the size of the gap ($d_{gap,bottom}$), the displacement capacity (d_u), friction force ($R_{fr,bottom}$), resistance of the cantilever ($R_{max,bottom}$), damping (c_{visc}) and stiffness ($K_{conn,bottom}$, $K_{i,bottom}$) as presented in following paragraphs. The recommended values are summarised in Table 5.2.

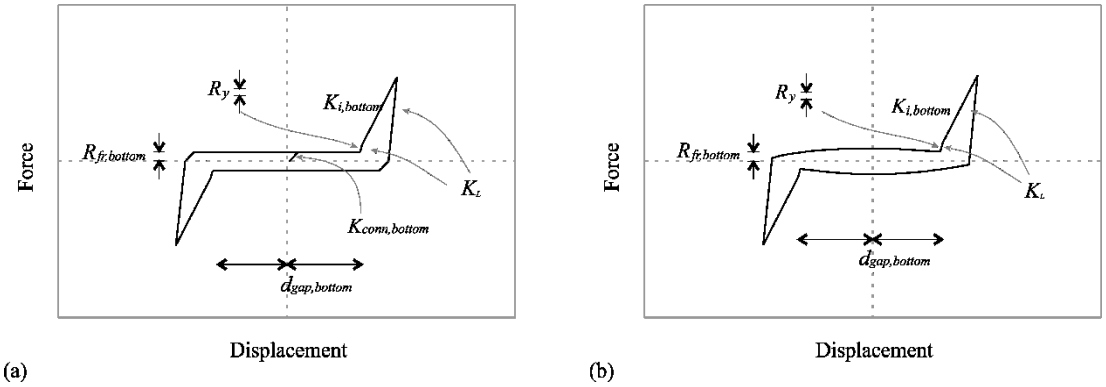

Figure 5.7: Schematic envelopes of numerical models of bottom connections: (a) during the cyclic test and (c) during the dynamic test

Slika 5.7: Shematski prikaz ovojnic numeričnega modela spodnjih stikov: (a) med ciklično obtežbo in (c) med dinamično obtežbo

Table 5.2: Recommended values of the model parameters of the bottom connection

Preglednica 5.2: Priporočene vrednosti modelnih parametrov spodnjega stika

Material characteristic	Value	Material characteristic	Value
$d_{gap,bottom}$*	±4.5 cm	$R_{fr,bottom}$	2 kN
$c_{visc,bottom}$	50 t/s	$K_{conn,bottom}$	$2 \cdot 10^3$ kN/m
$R_{max,bottom}$	176 kN	$K_{i,bottom}$	$1.5 \cdot 10^4$ kN/m
px, *py*, *d1*, *d2*, *b*	0, 0, 0, 0, 0	K_L	$1 \cdot 10^4$ kN/m
		R_y	0.01 kN

Legend: $d_{gap,bottom}$: gap in the bottom connection, $c_{visc,bottom}$: viscous damping coefficient, $R_{max,bottom}$: resistance of cantilever, $R_{fr,bottom}$: friction force in the bottom connection, $K_{conn,bottom}$: initial stiffness of the bottom connection, $K_{i,bottom}$: bending stiffness of the bottom connection, K_L: large unloading stiffness after the gap is depleted, *px, py, d1, d2, b,* R_y: specific parameters *pinchx, pinchy, damage1, damage2, beta* and R_y of the Hysteretic material model.

* Note that the value corresponds to the centrally positioned connection.

Size of the gap

The initial position of the connections depends on the actual construction and the possible residual displacements after the earlier excitations. If the bottom connections are mounted centrally, then $d_{gap,bottom}$ is half the width of the available space in the panel reduced by half of the thickness of the cantilever bracket. The position of connections has an important influence on the response of the panel, as will be demonstrated later.

Displacement capacity

The bottom connections did not fail during the tests. Thus it was not possible to define the displacement capacity of the bottom connection itself. However, the bottom connections always occur in pairs with the top connections, and top connections always fail before the bottom ones. Therefore, the displacement capacity of the top connection can be considered as the displacement capacity of the complete connection assembly (please see the discussion about the failure provided in Section 3.3.4).

Friction force and damping

The friction in the bottom connection was considerably smaller than in the top connections. It was estimated from the results of the single component tests. The friction force of the top connections was subtracted from friction of the complete fastening system. The friction force in the bottom connections was thus estimated to be 2 kN.

The recommended value of the damping coefficient $c_{visc,bottom}$ for the *Viscous* model was estimated based on the velocity and friction force measured in the tests. The value of 50 t/s was defined, which corresponds to a force of 2 kN at a velocity of 0.04 m/s.

Stiffness

The stiffness of the bottom connection was assumed to be zero during the sliding and until for as long as the gap is not depleted. Then the stiffness abruptly increases to K_i due to the activated bending stiffness of the steel cantilever.

The impact stiffness was experimentally estimated from the maximum force and displacement at the failure of the complete fastening system. The maximum force was estimated to 300 kN, which corresponds to two top and bottom connection pairs. Therefore, the force taken over by one bottom connection is 92 kN. The displacement of the connection after the gap has been depleted was 30 mm. The impact stiffness of the bottom connection determined from experimental results amounts to $3.1 \cdot 10^3$ kN/m. However, during the calibration of the dynamic test on the complete fastening system, the impact stiffness of the bottom connection was found to be much larger. To simulate the response of the connections accurately, the impact stiffness of the bottom connection was ten times larger than the impact stiffness of the top connections. Thus, a stiffness of $1.5 \cdot 10^4$ kN/m was used for the simulation of dynamic tests. It is also proposed for further numerical analyses.

As in the case of top connections, the *Hysteretic* material model was used in series with *EPPGap* to model the response after the gap was closed. All the following specific parameters should be set to zero for this purpose: *pinchx*, *pinchy*, *damage1*, *damage2* and *beta*. A relatively small parameter R_y and a large unloading stiffness K_L of the *Hysteretic* model behaviour (see the envelopes in Figure 5.7 and Table 5.2) were used to define the steep unloading branch.

The initial stiffness of the bottom connections ($K_{conn,bottom}$) used for modelling the common friction behaviour during the quasi-static cyclic tests is, in general, very large as long as the friction force is not activated (see the recommended value in Table 5.2). After that, the stiffness is equal to zero as long as the gap is not depleted.

Resistance of the cantilever

The resistance of the bearing cantilever was analytically estimated. The steel bracket is made out of steel grade S355J0, with mean yield and ultimate strength 414 N/mm^2 and 546 N/mm^2, respectively (Braconi et al., 2013). The failure in shear and bending is considered for estimating shear resistance, as presented in Figure 5.8 and the following equations.

Shear

$$A_v = 30 \cdot 150 = 4500\ mm \tag{5.1}$$

$$V_u = \frac{A_v \cdot f_u}{\sqrt{3}} = \frac{4500 \cdot 546}{\sqrt{3}} = 1419\ kN \tag{5.2}$$

Bending

$$W = \frac{b \cdot h^2}{6} = \frac{150 \cdot 30^2}{6} = 22500\ mm^4 \tag{5.3}$$

$$M_u = W \cdot f_u = 22500 \cdot 546 = 12285\ kNmm \tag{5.4}$$

$$V_u = \frac{M_u}{l} = \frac{W \cdot f_u}{l} = \frac{22500 \cdot 546}{70} = \mathbf{175.5\ kN} \tag{5.5}$$

The critical element is bending resistance with a corresponding shear force of 176 kN. It was not reached during the tests or numerical analysis, even with extremely eccentrically positioned connections (see the parametric analysis in Chapter 6).

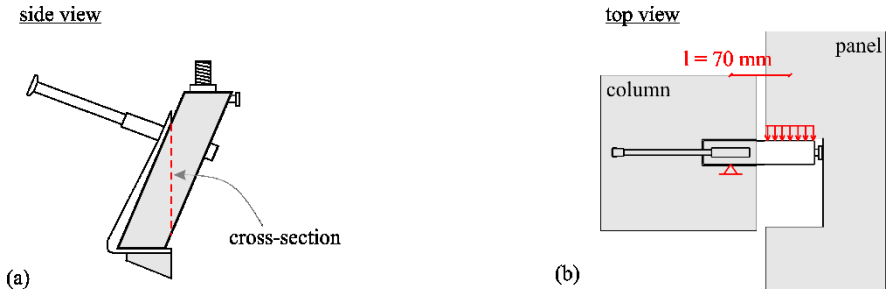

Figure 5.8: The scheme (a) of assumed critical cross sections and (b) scheme of a static model of bearing cantilever

Slika 5.8: Shematski prikaz (a) kritičnih prerezov in (b) statičnega modela jeklene konzole

5.2 Validation of the numerical models

5.2.1 Numerical modelling of single component tests

This section validates the numerical model of cladding connections for horizontal concrete panels by quasi-static cyclic and dynamic single component tests (presented in Chapter 3).

The scheme of a simple model is shown in Figure 5.9. Each connection is represented by a *zeroLength Element*, whose response in the horizontal direction is described with a combination of material models presented in Section 5.1. To model the vertical supports, two *ENT* (*Elastic-No Tension*) materials were added that ensure the stability of the model and are used to simulate lifting of the panel. Note that the lifting of the panel and the rotations are relatively small and not significant for the overall response because the cladding connections and panel response is predominantly translational (please see discussion in Sections 3.3.5 and 4.2.4). The rigid panel was modelled with *elasticBeamColumn* elements.

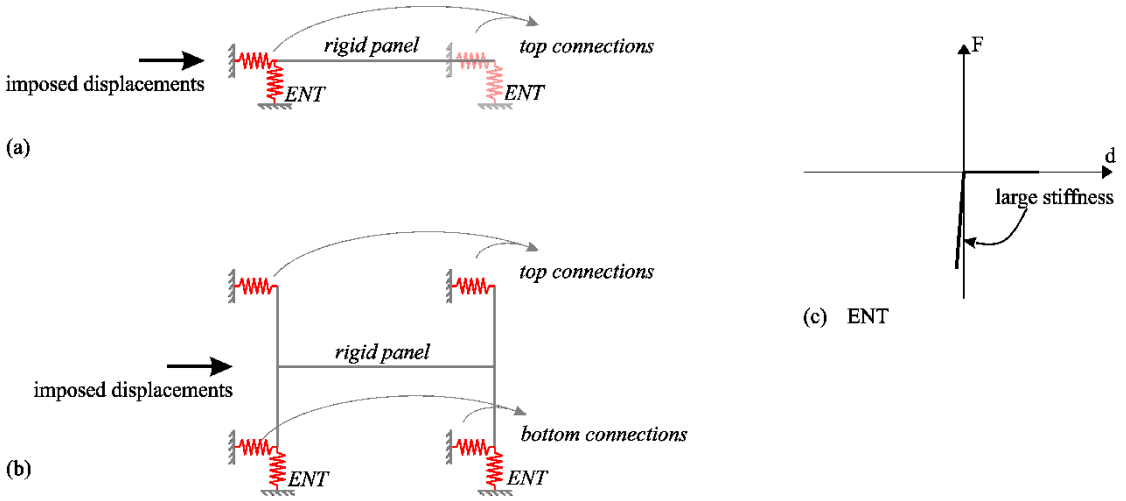

Figure 5.9: Schematic presentation of the numerical model for the single connection tests: (a) top connections, (b) complete fastening system and (c) *ENT* material model

Slika 5.9: Shematski prikaz numeričnega modela testov na fasadnih stikih: (a) zgornji stiki, (b) celoten sistem stikov, (c) *ENT* materialni model

The material parameters as recommended in Tables 5.1 and 5.2 were used for the simulation of the single component test. Because the position of the connections during single connection tests was almost ideal in the centre of the available space in the panel, the connection gaps were the same in both directions:

$$d_{gap,top} = \pm 4\ cm \tag{5.6}$$

$$d_{gap,bottom} = \pm 4.5\ cm \tag{5.7}$$

The friction force at the top connection was gradually reduced after each test due to the deformations and loosening of the bolt (see also Section 3.3.5). The values used for numerical modelling are provided in Table 5.3. The force–displacement relationships of the numerical models used for the simulation of the complete fastening system are schematically presented in Figure 5.10.

Table 5.3: Friction forces in the top connections

Preglednica 5.3: Sila trenja v zgornjih stikih

Test	$R_{fr,top}$ [kN]	Test	$R_{fr,top}$ [kN]
Tc1	5	*Cc1*	5
Tc2	5	*Cc2*	6
Td1	5 - 5 - 5 - 3 - 0	*Cd1*	8 - 6 - 4 - 3 - 2
Td2	8 - 6 - 0	*Cd2*	8 - 5 - 3 - 1 - 1
Td3	8 - 8 - 3		
Td4	8 - 5 - 2		

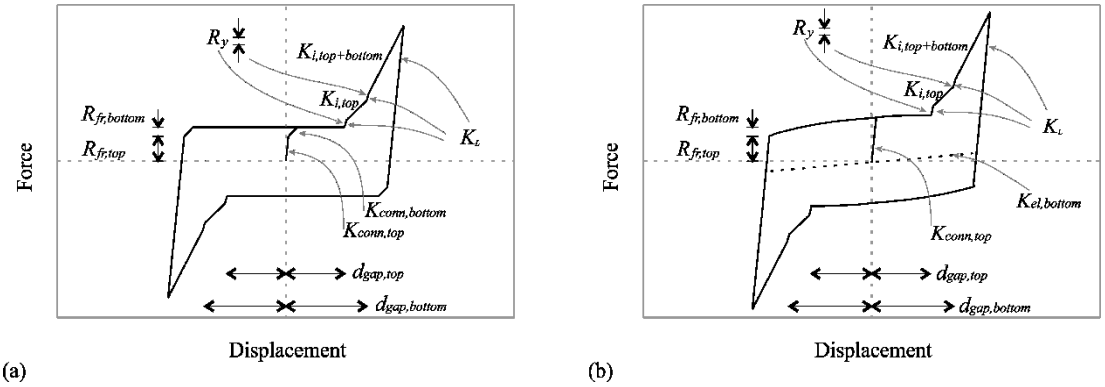

Figure 5.10: Schematic envelopes of numerical models: (a) only the top connections, (b) the complete fastening system during the cyclic test and (c) the complete fastening system during the dynamic test
Slika 5.10: Shematski prikaz ovojnic numeričnega modela: (a) samo zgornji stiki, (b) celoten sistem stikov med ciklično obtežbo in (c) celoten system stikov med dinamično obtežbo

The experimental and numerical hysteretic responses of the connections are compared in Figures 5.11–5.14. Figures 5.11 and 5.12 present the hysteretic responses of the top connections under the quasi-static cyclic (denoted with *'Tc'*) and dynamic loading (*'Td'*), respectively. Figures 5.13 and 5.14 present the response of the complete system under quasi-static cyclic (*'Cc'*) and dynamic loading (*'Cd'*), respectively. The hysteretic responses that correspond to all the test intensities are shown on each plot. A satisfying match between the experimental and numerical results was achieved with the proposed numerical models. To better evaluate the calibration, some graphs of the accumulated hysteretic energy during the dynamic tests are shown in Figure 5.15.

The numerical models describe the behaviour of the connections with quite high accuracy, although there are some differences in the experimental and numerical hysteretic responses. During the experiments, a small increase in the force during the sliding phase was observed, which was more obvious during the test of the top connections (Figures 5.11 and 5.12). However, this does not have an important influence on the overall response of the connections. As already mentioned, the friction forces activated in the analysed connections are relatively small compared to the forces in the main precast structure (i.e. columns) during the seismic excitation. Thus, this increase of the force was not simulated with the model, which assumes constant friction during the sliding phase.

In general, the match of experimental and numerical envelopes is quite good. The stiffness at the impacts of the top connection is, on average, well estimated. In some cases, it is overestimated for impacts in the positive direction and underestimated for impacts in the negative direction (see, for example, tests *Td2* and *Td4* in Figure 5.12).

For the simulation of cyclic tests, the impact stiffness of $3 \cdot 10^3$ kN/m was used for the bottom connection. This stiffness is somewhat underestimated, which is also shown with the response of connections in positive directions during the test *Cc2* (Figure 5.13 b). However, it is possible to

accurately describe the response with higher impact stiffness of $1.5 \cdot 10^4$ kN/m at the bottom connections (see the simulation of dynamic tests in Figure 5.14). Graphs in Figure 5.15 show a good match of the dissipated energy for the tests of top connections and the complete fastening system.

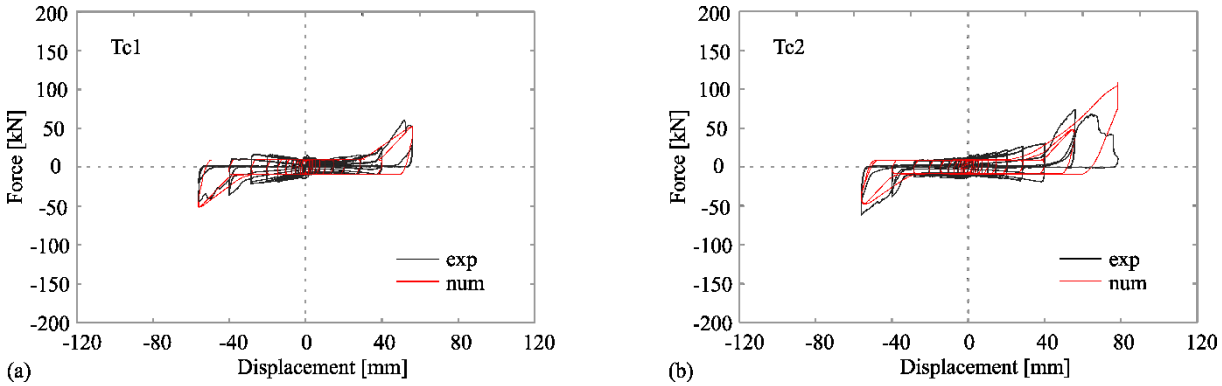

Figure 5.11: The experimental (black) and numerical (red) hysteretic responses of the top connections during the quasi-static cyclic tests: (a) test *Tc1* and (b) test *Tc2*

Slika 5.11: Ekperimentalni (črna) in numerični (rdeča) histerezni odziv zgornjih stikov med kvazi-statičnimi cikličnimi testi: (a) test *Tc1* and (b) test *Tc2*

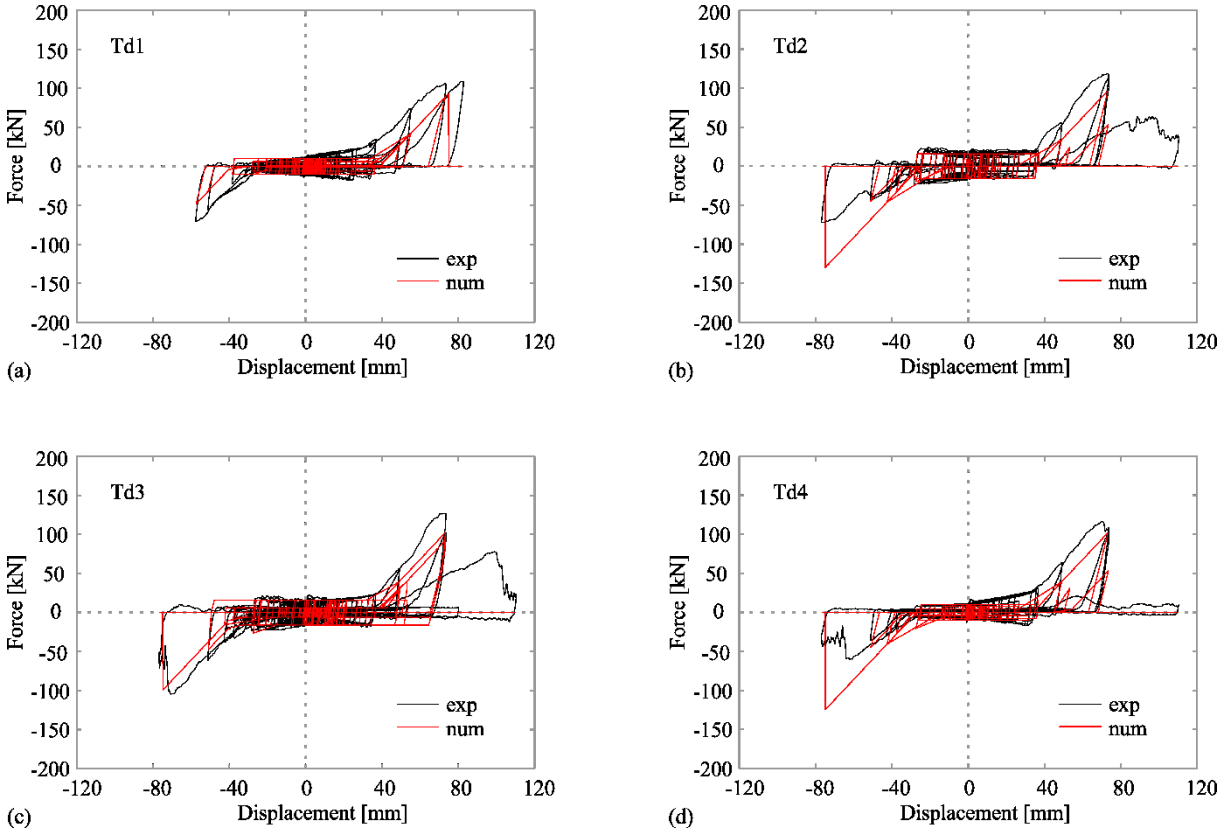

Figure 5.12: The experimental (black) and numerical (red) hysteretic responses of the top connections during the dynamic tests: (a) test *Td1*, (b) test *Td2*, (c) test *Td3* and (d) test *Td4*

Slika 5.12: Ekperimentalni (črna) in numerični (rdeča) histerezni odziv zgornjih stikov med dinamičnimi testi: (a) test *Td1*, (b) test *Td2*, (c) test *Td3* and (d) test *Td4*

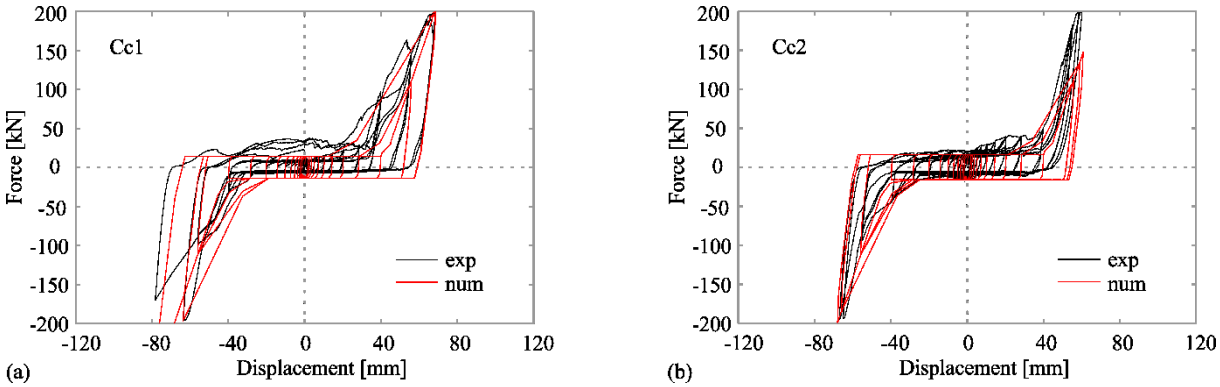

Figure 5.13: The experimental (black) and numerical (red) hysteretic responses of the complete fastening system during the quasi-static cyclic tests: (a) test *Cc1* and (b) test *Cc2*

Slika 5.13: Ekperimentalni (črna) in numerični (rdeča) histerezni odziv sistema stikov med kvazi-statičnimi cikličnimi testi: (a) test *Cc1* and (b) test *Cc2*

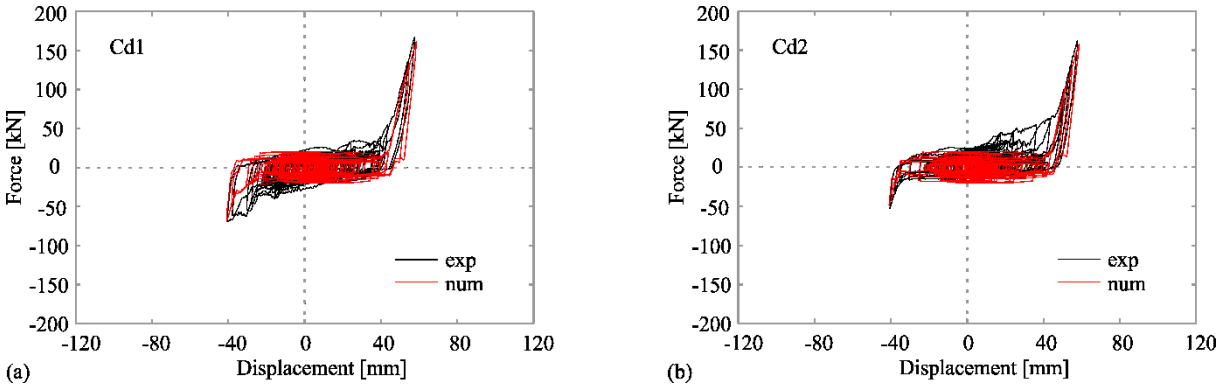

Figure 5.14: The experimental (black) and numerical (red) hysteretic responses of the complete fastening system connections during the dynamic tests: (a) test *Cd1* and (b) test *Cd2*

Slika 5.14: Ekperimentalni (črna) in numerični (rdeča) histerezni odziv sistema stikov med dinamičnimi testi: (a) test *Cd1* and (b) test *Cd2*

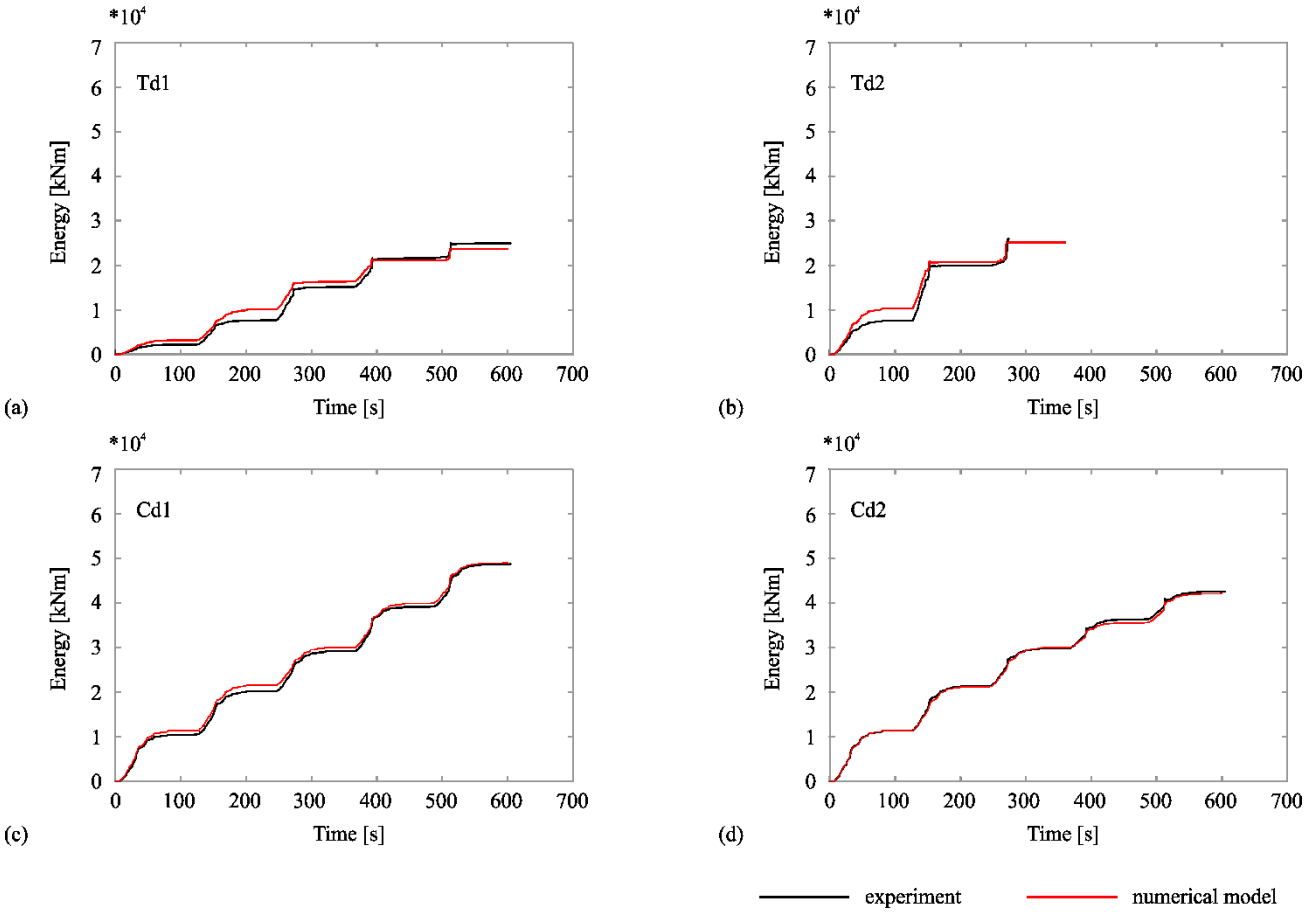

Figure 5.15: A comparison of the accumulated hysteretic energy during the experiments (black) and numerical (red) simulation of dynamic tests: (a) *Td1*, (b) *Td2* and (c) *Cd1* and (d) *Cd2*

Slika 5.15: Primerjava akumulirane histrezne energije med dinamičnimi testi (črna) in numerično simulacijo (rdeča): (a) *Td1*, (b) *Td2*, (c) *Cd1* in (d) *Cd2*

5.2.2 Numerical modelling of shaking table tests

Numerical models were also validated on shake table tests presented in Chapter 4. The numerical model used for simulation of the shake table tests was built in OpenSees software (McKenna & Fenves, 2010) and is schematically presented in Figure 5.16.

Because very limited yielding of the columns was observed during the shake table tests, the cantilever columns were modelled with simple *elasticBeamColumn* frame elements. Before the tests of structures with horizontal panels, the same main structure was used to test the response of vertical panels (19 tests with vertical panels were performed). Thus, during the analysis of the specimens with horizontal panels, the properties of the column cross section were reduced to 25% of the gross cross section to account for concrete cracking and the previous response history of the main structure. Note that the fundamental period of the main structure during the tests of vertical panels was around 0.7 s, which corresponds to 30% of the column gross section. Because many tests were

performed on the same main structure, the cross-section properties were further reduced for the tests of horizontal panels.

To achieve a better match of experimental and numerical response histories, the cross-section properties corresponding to 23% of the gross cross section were taken to analyse the asymmetric configuration of horizontal panels.

Rigid slab and panels were modelled using *elasticBeamColumn* elements because no damage was observed. The mass of the slab was concentrated in the centre of mass. Half the mass of the column was modelled at the top of each column, and the mass of the panel was concentrated at the centre of the panels' mass, as shown in Figure 5.16.

The cladding connections were modelled as presented in Section 5.1, and the model parameters are listed in Tables 5.1 and 5.2. During the shake table tests, the connections were not mounted centrally, and residual displacements in the connections were observed after each excitation. The gaps in connections were measured before every run (listed in Table 5.4) and used as input (d_{gap}) for numerical models.

Table 5.4: Initial gaps in the connections before each test run
Preglednica 5.4: Prosti pomik v stikih na začetku vsakega testa

Symmetric specimen	PGA 0.1 g gap [mm]	PGA 0.2 g gap [mm]	PGA 0.3 g gap [mm]	PGA 0.4 g gap [mm]
column C1: panel P1 top	−30 / +50	−30 / +50	−25 / +55	−20 / +60
column C1: panel P1 bottom	−10 / +80	−10 / +80	−5 / +85	−5 / +85
column C2: panel P1 top	−50 / +30	−50 / +30	−45 / +35	−45 / +35
column C2: panel P1 bottom	−35 / +55	−35 / +55	−40 / +50	−35 / +55
column C3: panel P2 top	−45 / +35	−45 / +35	−25 / +55	−15 / +65
column C3: panel P2 bottom	−40 / +50	−40 / +50	−35 / +55	−15 / +75
column C4: panel P2 top	−60 / +20	−60 / +20	−50 / +30	−35 / +45
column C4: panel P2 bottom	−45 / +45	−45 / +45	−50 / +40	−35 / +55
Asymmetric specimen	**PGA 0.1 g gap [mm]**	**PGA 0.2 g gap [mm]**	**PGA 0.3 g gap [mm]**	
column C1: panel P1 top	−30 / +50	−30 / +50	−25 / +55	
column C1: panel P1 bottom	−10 / +80	−10 / +80	−5 / +85	
column C2: panel P1 top	−50 / +30	−50 / +30	−45 / +35	
column C2: panel P1 bottom	−35 / +55	−35 / +55	−40 / +50	

The tightening torque in top connections was smaller than prescribed by the producer, which is often also the case in real structures (please see the discussion in Section 5.1.1). The friction force

in top connections was estimated to 2 kN, which corresponds to the tightening torque in the bolts of 16 Nm. The same value of friction force was used for the simulation of all shake table tests.

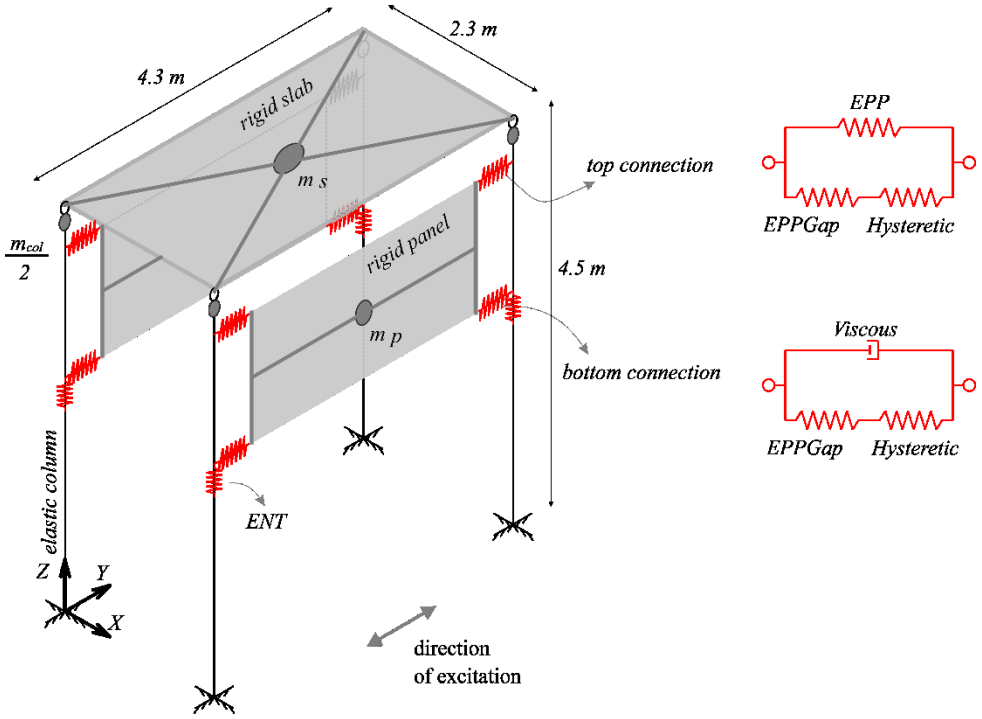

Figure 5.16: Schematic presentation of the numerical model for the shake table test

Slika 5.16: Shematski prikaz numeričnega modela testov na potresni mizi

The shake table tests presented in Chapter 4 were numerically simulated using the proposed models in a nonlinear response history analysis. These analyses used 2% viscous mass-proportional Rayleigh damping.

The experimental and numerical results are compared and show a reasonably good match between experimental and numerical results. This is illustrated in Figures 5.17–5.30, where the numerical results are compared to the results of shake table tests for symmetric and asymmetric configurations of the specimen and all test intensities.

The response of the main structure, that is, displacements and accelerations at the top of the structure and the top of the panels, is presented in Figures 5.17, 5.19, 5.21 and 5.23 for the symmetric specimen at PGA intensities from 0.1 g to 0.4 g and in Figures 5.25, 5.27 and 5.29 for asymmetric specimen at PGA intensities from 0.1 g to 0.3 g. The responses of the connections, that is, the relative displacements between the panels and the main structure at the level of top and bottom connections, are presented in Figures 5.18, 5.20, 5.22 and 5.24 for symmetric specimen configuration and in Figures 5.26, 5.28 and 5.30 for asymmetric specimen configuration.

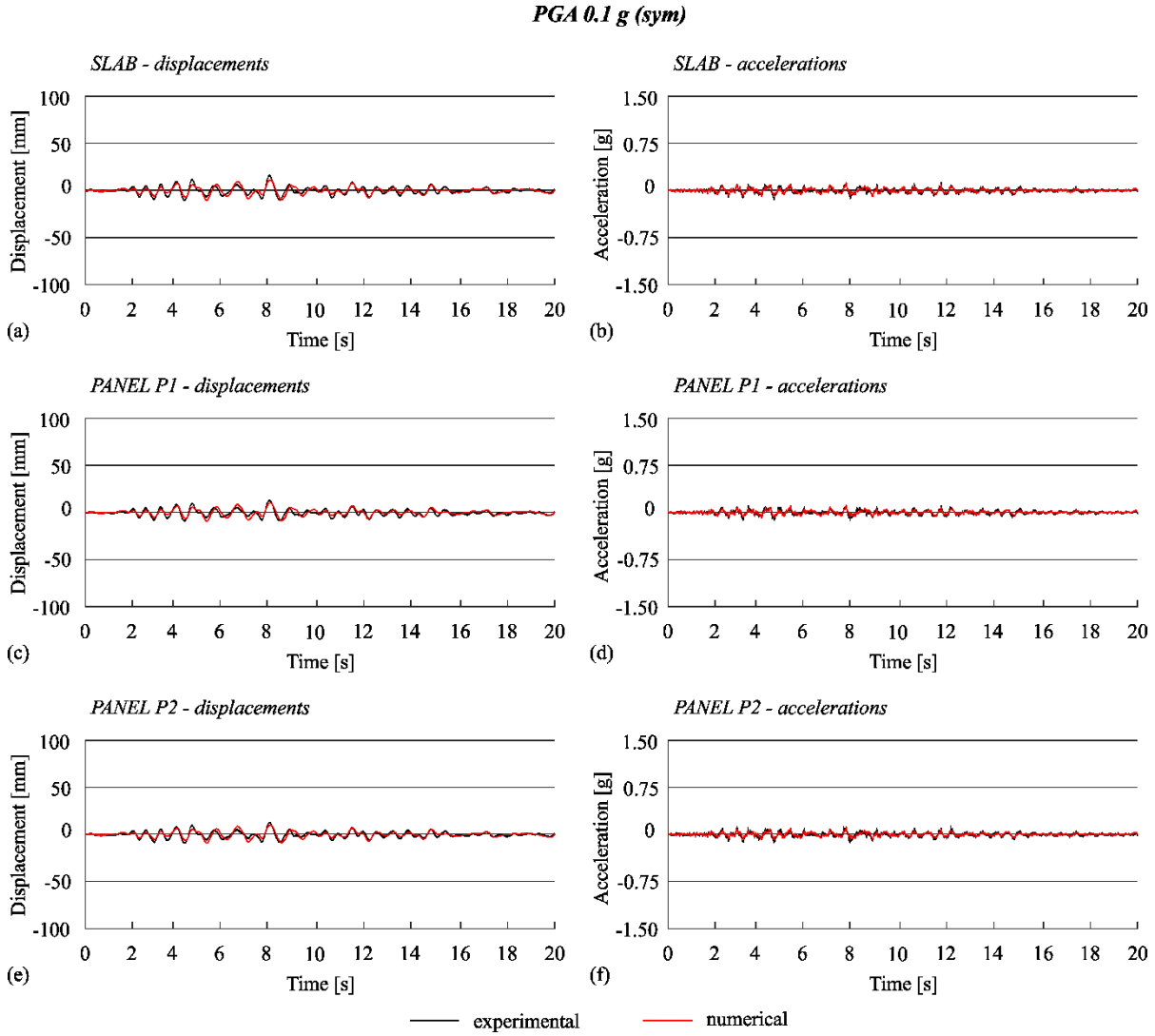

Figure 5.17: The experimental (black) and numerical (red) response histories of the symmetric specimen at 0.1 g: (a) displacements of the main structure, (b) accelerations of the main structure, (c) displacements of panel P1, (d) accelerations of panel P1, (e) displacements of panel P2 and (f) accelerations of panel P2

Slika 5.17: Eksperimentalni rezultati (črna) in numerična simulacija (rdeča) odziva simetričnega preizkušanca pri PGA intenziteti 0.1 g: (a) pomiki glavne konstrukcije, (b) pospeški glavne konstrukcije, (c) pomiki panela P1, (d) pospeški panela P1, (e) pomiki panela P2, (f) pospeški panela P2

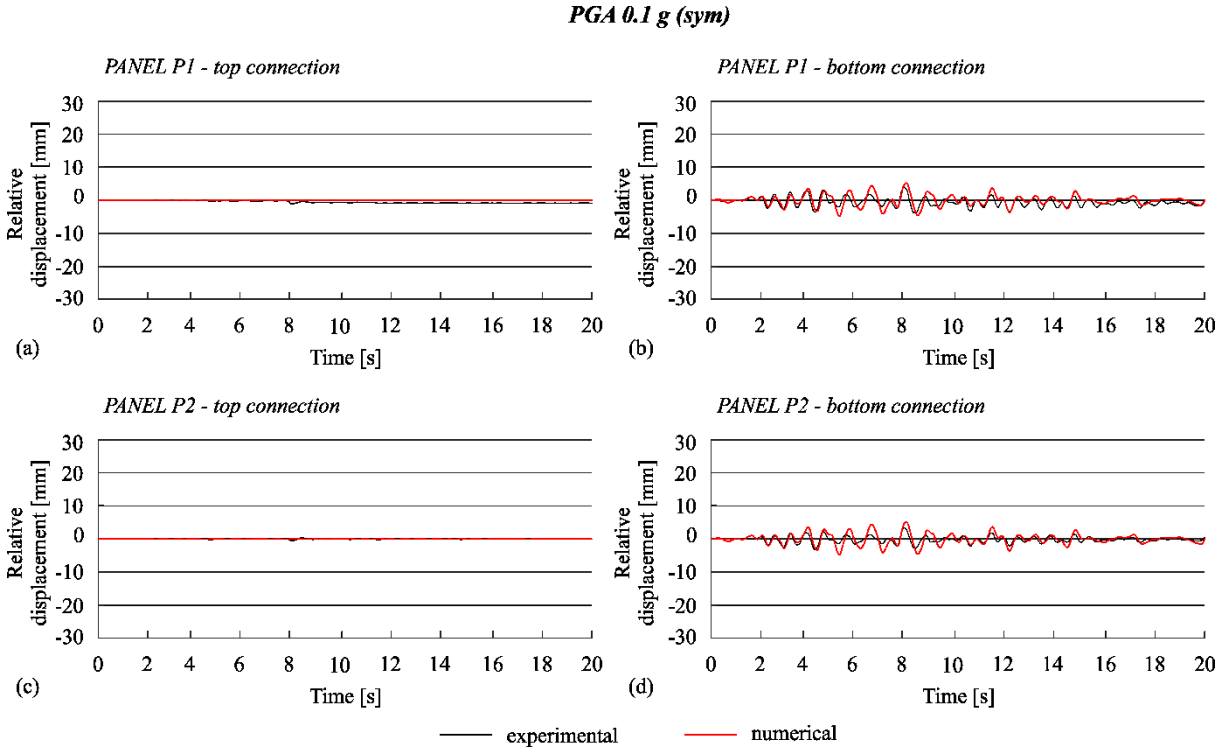

Figure 5.18: The experimental (black) and numerical (red) relative displacements between the panels and columns of the symmetric specimen at 0.1 g: (a) slips at the top connection of panel P1, (b) slips at the bottom connection of panel P1, (c) slips at the top connection of panel and (d) slips at the bottom connection of panel P2

Slika 5.18: Eksperimentalni rezultati (črna) in numerična simulacija (rdeča) relativnih pomikov med paneli in stebri simetričnega preizkušanca pri PGA intenziteti 0.1 g: (a) zdrs v zgornjem stiku panela P1, (b) zdrs v spodnjem stiku panela P1, (c) zdrs v zgornjem stiku panela P2, (d) zdrs v spodnjem stiku panela P2

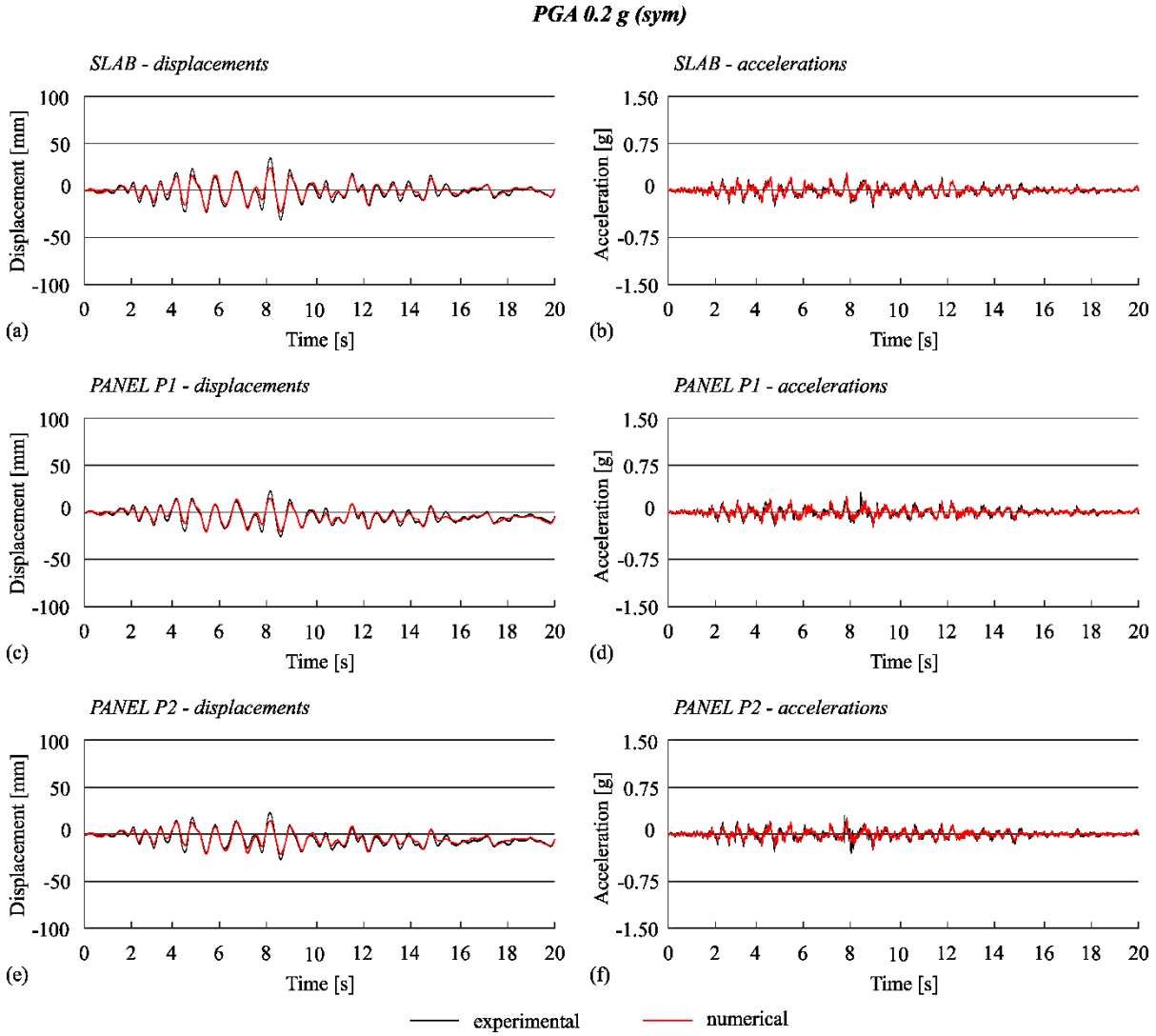

Figure 5.19: The experimental (black) and numerical (red) response histories of the symmetric specimen at 0.2 g: (a) displacements of the main structure, (b) accelerations of the main structure, (c) displacements of panel P1, (d) accelerations of panel P1, (e) displacements of panel P2 and (f) accelerations of panel P2

Slika 5.19: Eksperimentalni rezultati (črna) in numerična simulacija (rdeča) odziva simetričnega preizkušanca pri PGA intenziteti 0.2 g: (a) pomiki glavne konstrukcije, (b) pospeški glavne konstrukcije, (c) pomiki panela P1, (d) pospeški panela P1, (e) pomiki panela P2, (f) pospeški panela P2

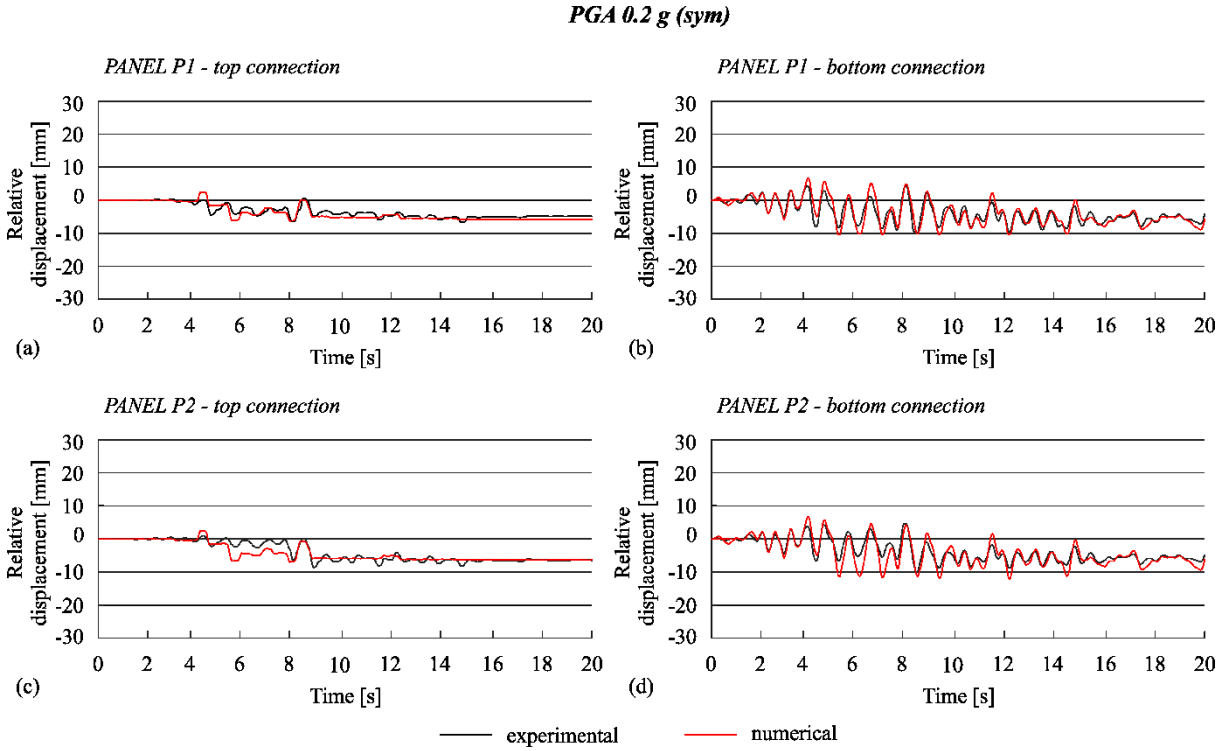

Figure 5.20: The experimental (black) and numerical (red) relative displacements between the panels and columns of the symmetric specimen at 0.2 g: (a) slips at the top connection of panel P1, (b) slips at the bottom connection of panel P1, (c) slips at the top connection of panel and (d) slips at the bottom connection of panel P2

Slika 5.20: Eksperimentalni rezultati (črna) in numerična simulacija (rdeča) relativnih pomikov med paneli in stebri simetričnega preizkušanca pri PGA intenziteti 0.2 g: (a) zdrs v zgornjem stiku panela P1, (b) zdrs v spodnjem stiku panela P1, (c) zdrs v zgornjem stiku panela P2, (d) zdrs v spodnjem stiku panela P2

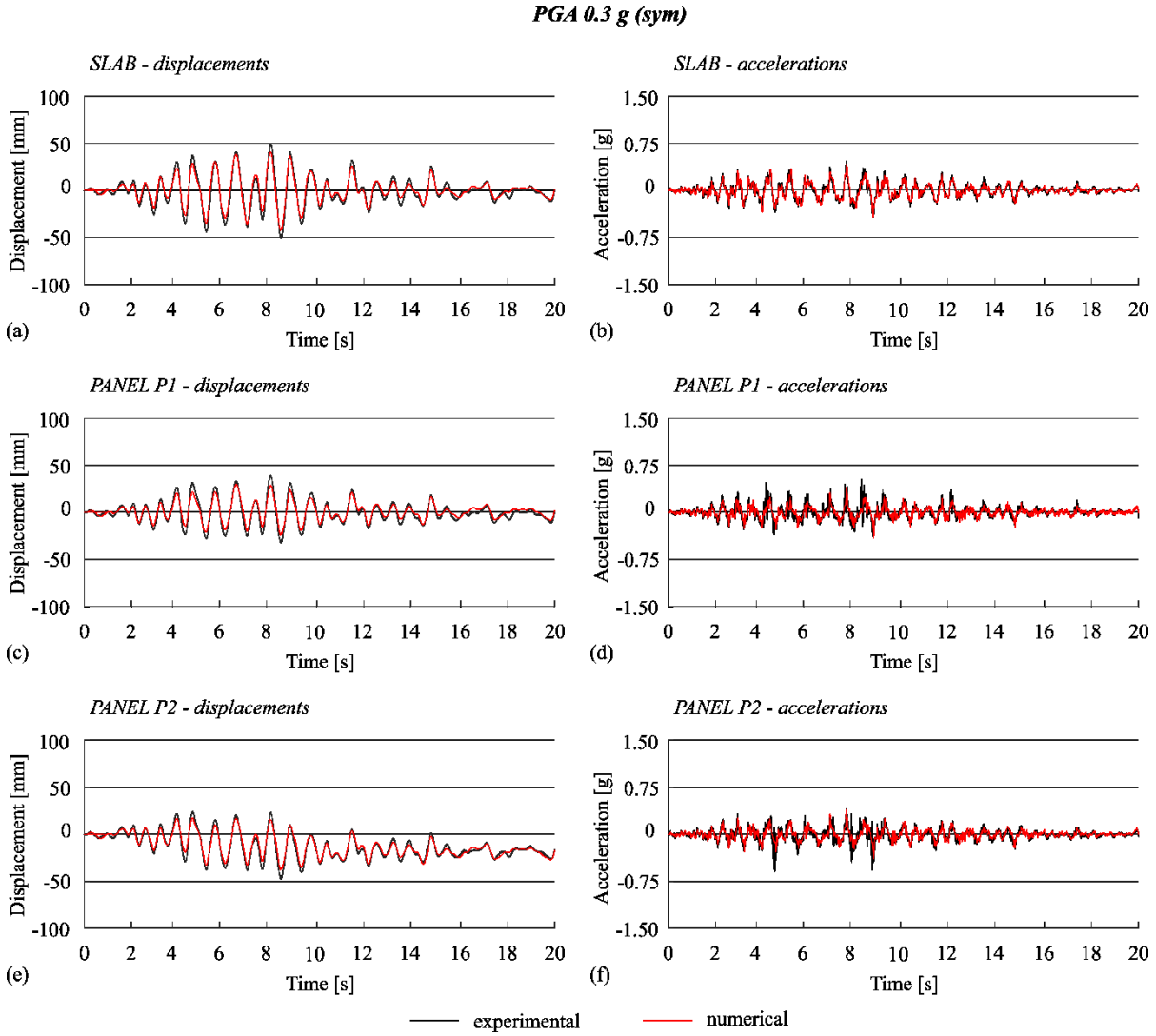

Figure 5.21: The experimental (black) and numerical (red) response histories of the symmetric specimen at 0.3 g: (a) displacements of the main structure, (b) accelerations of the main structure, (c) displacements of panel P1, (d) accelerations of panel P1, (e) displacements of panel P2 and (f) accelerations of panel P2

Slika 5.21: Eksperimentalni rezultati (črna) in numerična simulacija (rdeča) odziva simetričnega preizkušanca pri PGA intenziteti 0.3 g: (a) pomiki glavne konstrukcije, (b) pospeški glavne konstrukcije, (c) pomiki panela P1, (d) pospeški panela P1, (e) pomiki panela P2, (f) pospeški panela P2

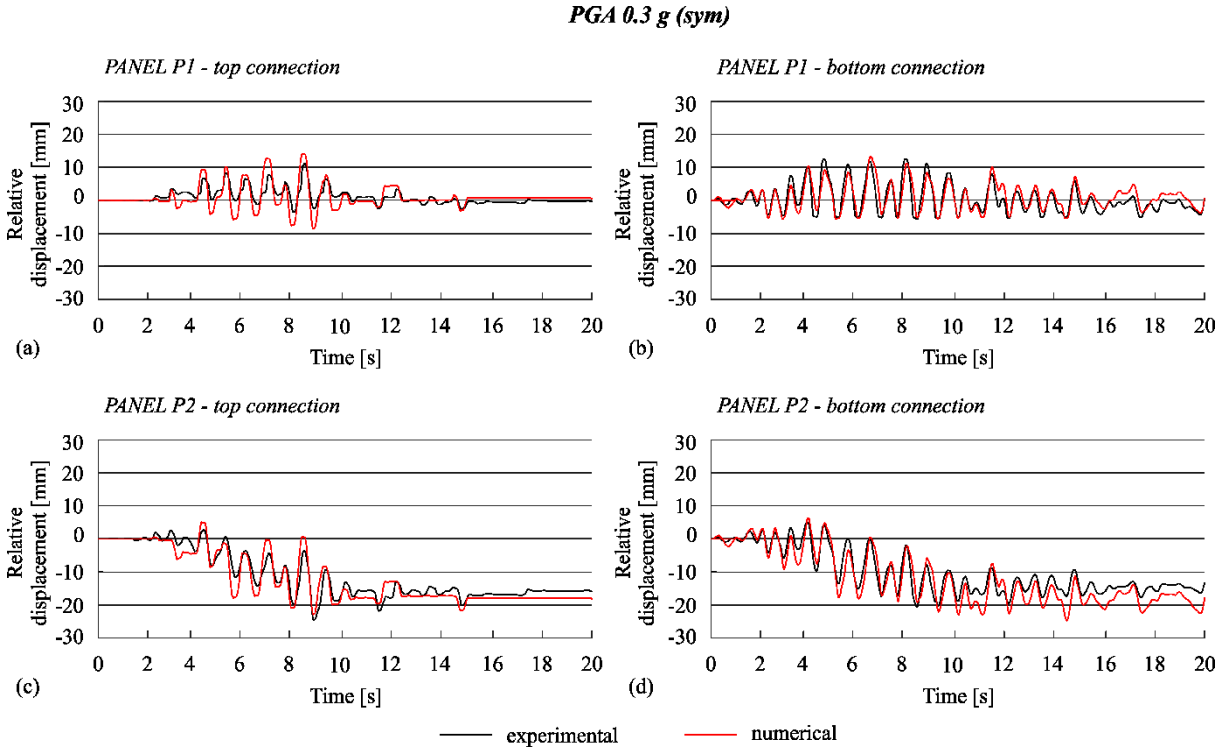

Figure 5.22: The experimental (black) and numerical (red) relative displacements between the panels and columns of the symmetric specimen at 0.3 g: (a) slips at the top connection of panel P1, (b) slips at the bottom connection of panel P1, (c) slips at the top connection of panel and (d) slips at the bottom connection of panel P2

Slika 5.22: Eksperimentalni rezultati (črna) in numerična simulacija (rdeča) relativnih pomikov med paneli in stebri simetričnega preizkušanca pri PGA intenziteti 0.3 g: (a) zdrs v zgornjem stiku panela P1, (b) zdrs v spodnjem stiku panela P1, (c) zdrs v zgornjem stiku panela P2, (d) zdrs v spodnjem stiku panela P2

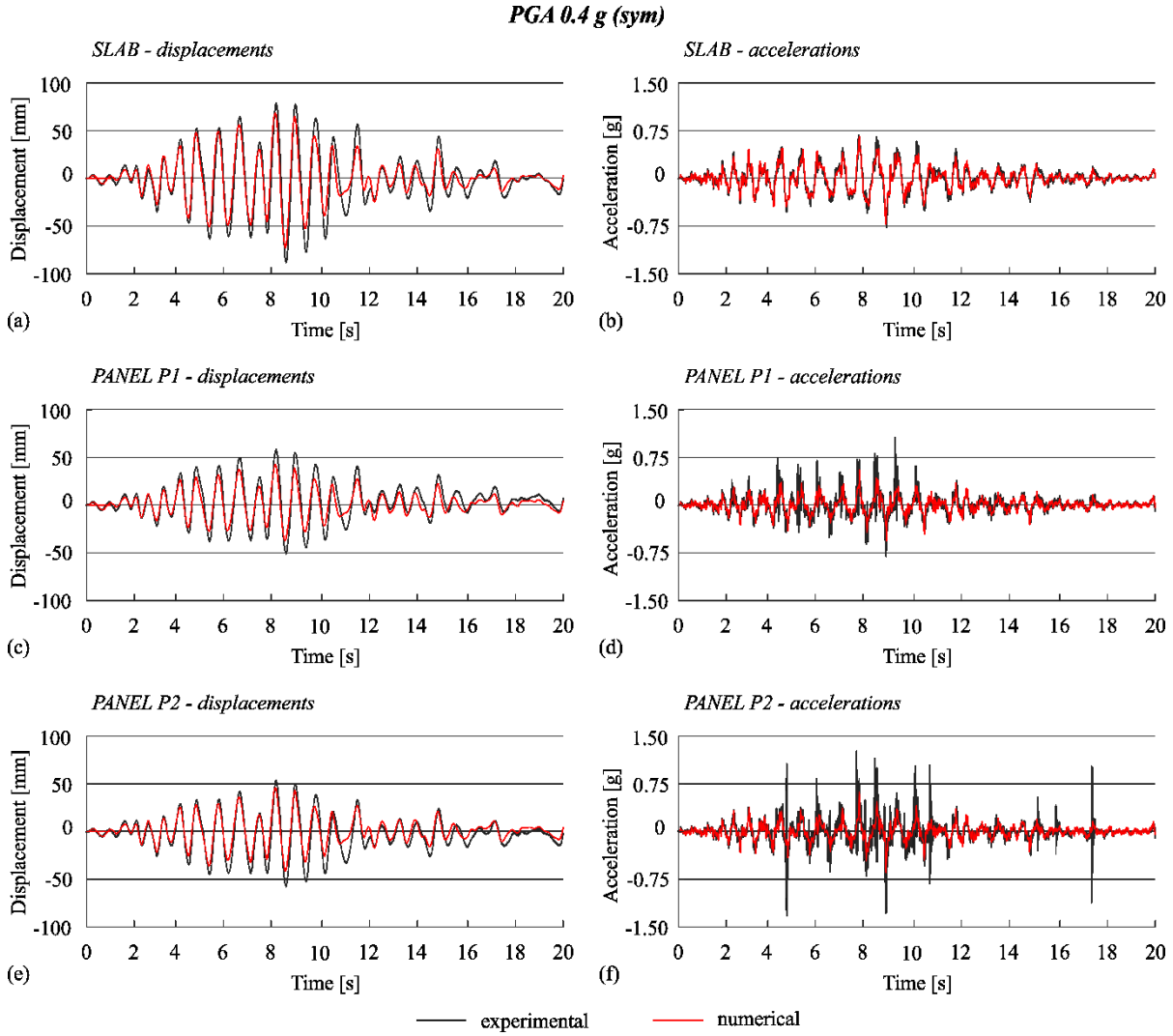

Figure 5.23: The experimental (black) and numerical (red) response histories of the symmetric specimen at 0.4 g: (a) displacements of the main structure, (b) accelerations of the main structure, (c) displacements of panel P1, (d) accelerations of panel P1, (e) displacements of panel P2 and (f) accelerations of panel P2

Slika 5.23: Eksperimentalni rezultati (črna) in numerična simulacija (rdeča) odziva simetričnega preizkušanca pri PGA intenziteti 0.4 g: (a) pomiki glavne konstrukcije, (b) pospeški glavne konstrukcije, (c) pomiki panela P1, (d) pospeški panela P1, (e) pomiki panela P2, (f) pospeški panela P2

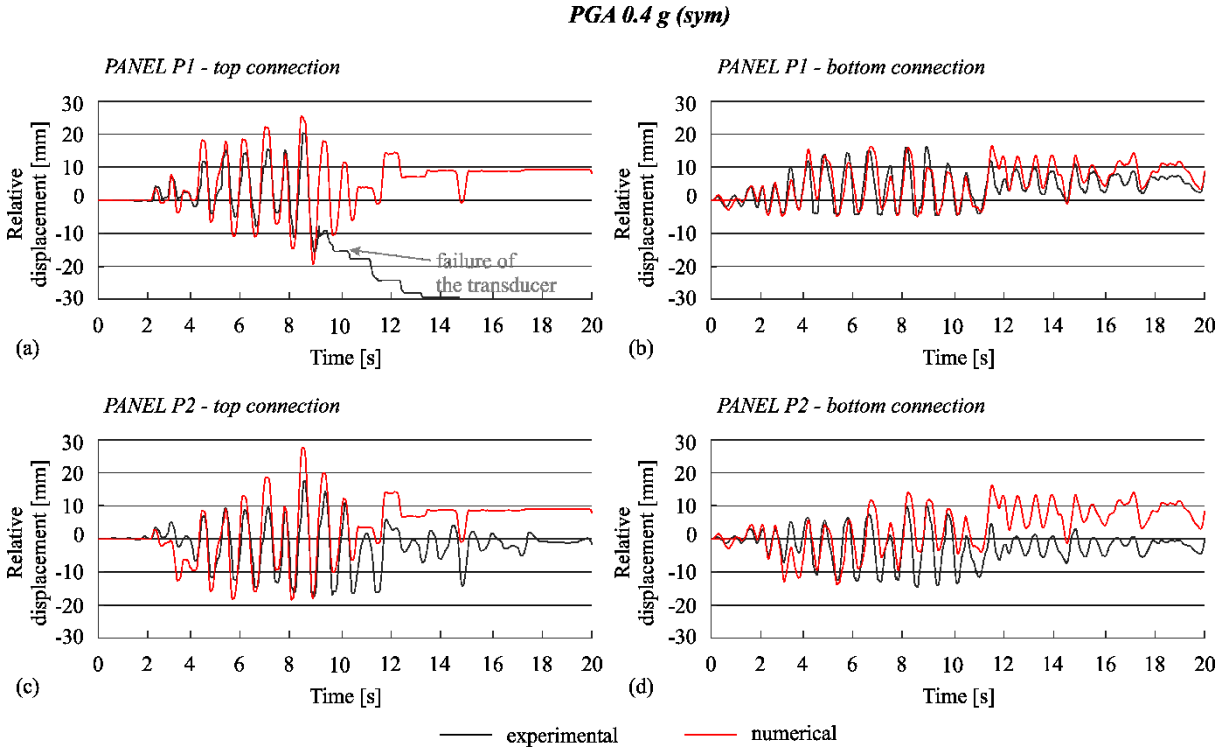

Figure 5.24: The experimental (black) and numerical (red) relative displacements between the panels and columns of the symmetric specimen at 0.4 g: (a) slips at the top connection of panel P1, (b) slips at the bottom connection of panel P1, (c) slips at the top connection of panel and (d) slips at the bottom connection of panel P2

Slika 5.24: Eksperimentalni rezultati (črna) in numerična simulacija (rdeča) relativnih pomikov med paneli in stebri simetričnega preizkušanca pri PGA intenziteti 0.4 g: (a) zdrs v zgornjem stiku panela P1, (b) zdrs v spodnjem stiku panela P1, (c) zdrs v zgornjem stiku panela P2, (d) zdrs v spodnjem stiku panela P2

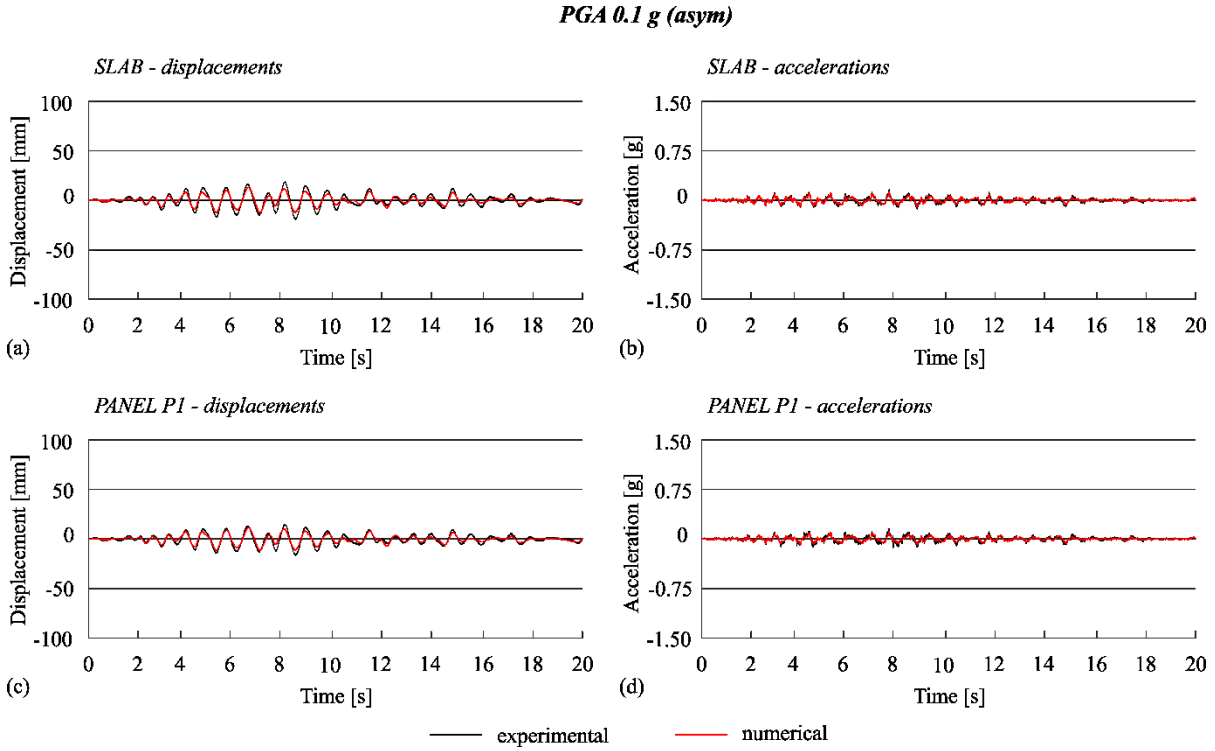

Figure 5.25: The experimental (black) and numerical (red) response histories of the asymmetric specimen at 0.1 g: (a) displacements of the main structure, (b) accelerations of the main structure, (c) displacements of panel P1 and (d) accelerations of panel P1

Slika 5.25: Eksperimentalni rezultati (črna) in numerična simulacija (rdeča) odziva asimetričnega preizkušanca pri PGA intenziteti 0.1 g: (a) pomiki glavne konstrukcije, (b) pospeški glavne konstrukcije, (c) pomiki panela P1, (d) pospeški panela P1

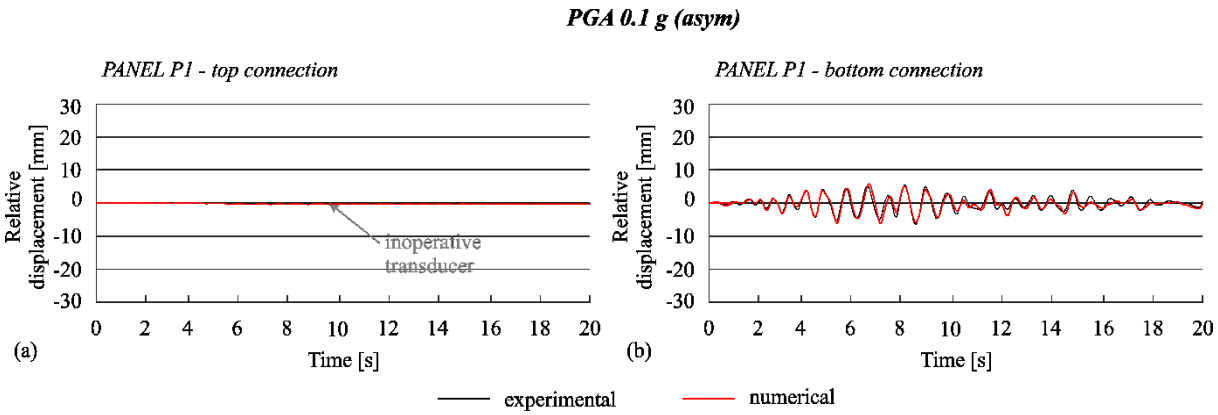

Figure 5.26: The experimental (black) and numerical (red) relative displacements between the panels and columns of the asymmetric specimen at 0.1 g: (a) slips at the top connection of panel P1, (b) slips at the bottom connection of panel P1

Slika 5.26: Eksperimentalni rezultati (črna) in numerična simulacija (rdeča) relativnih pomikov med paneli in stebri asimetričnega preizkušanca pri PGA intenziteti 0.1 g: (a) zdrs v zgornjem stiku panela P1, (b) zdrs v spodnjem stiku panela P1, (c) zdrs v zgornjem stiku panela P2

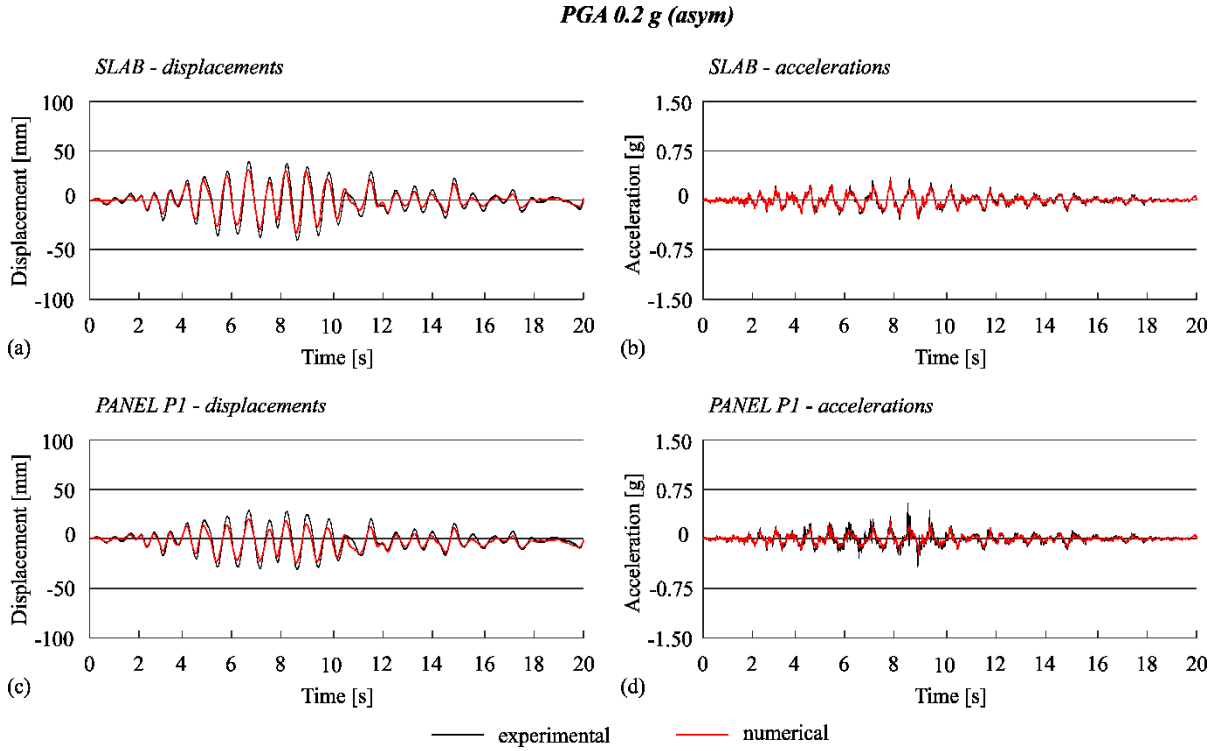

Figure 5.27: The experimental (black) and numerical (red) response histories of the asymmetric specimen at 0.2 g: (a) displacements of the main structure, (b) accelerations of the main structure, (c) displacements of panel P1 and (d) accelerations of panel P1

Slika 5.27: Eksperimentalni rezultati (črna) in numerična simulacija (rdeča) odziva asimetričnega preizkušanca pri PGA intenziteti 0.2 g: (a) pomiki glavne konstrukcije, (b) pospeški glavne konstrukcije, (c) pomiki panela P1, (d) pospeški panela P1

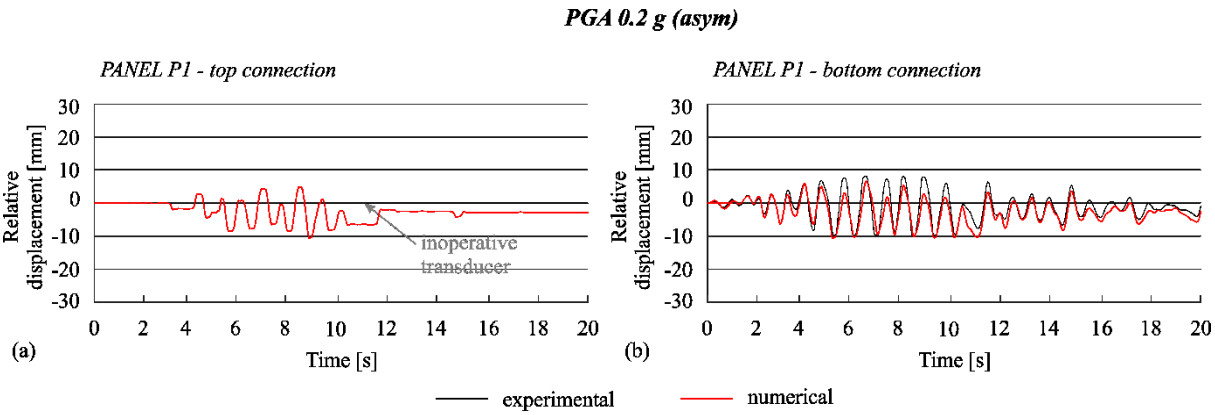

Figure 5.28: The experimental (black) and numerical (red) relative displacements between the panels and columns of the asymmetric specimen at 0.2 g: (a) slips at the top connection of panel P1, (b) slips at the bottom connection of panel P1

Slika 5.28: Eksperimentalni rezultati (črna) in numerična simulacija (rdeča) relativnih pomikov med paneli in stebri asimetričnega preizkušanca pri PGA intenziteti 0.2 g: (a) zdrs v zgornjem stiku panela P1, (b) zdrs v spodnjem stiku panela P1

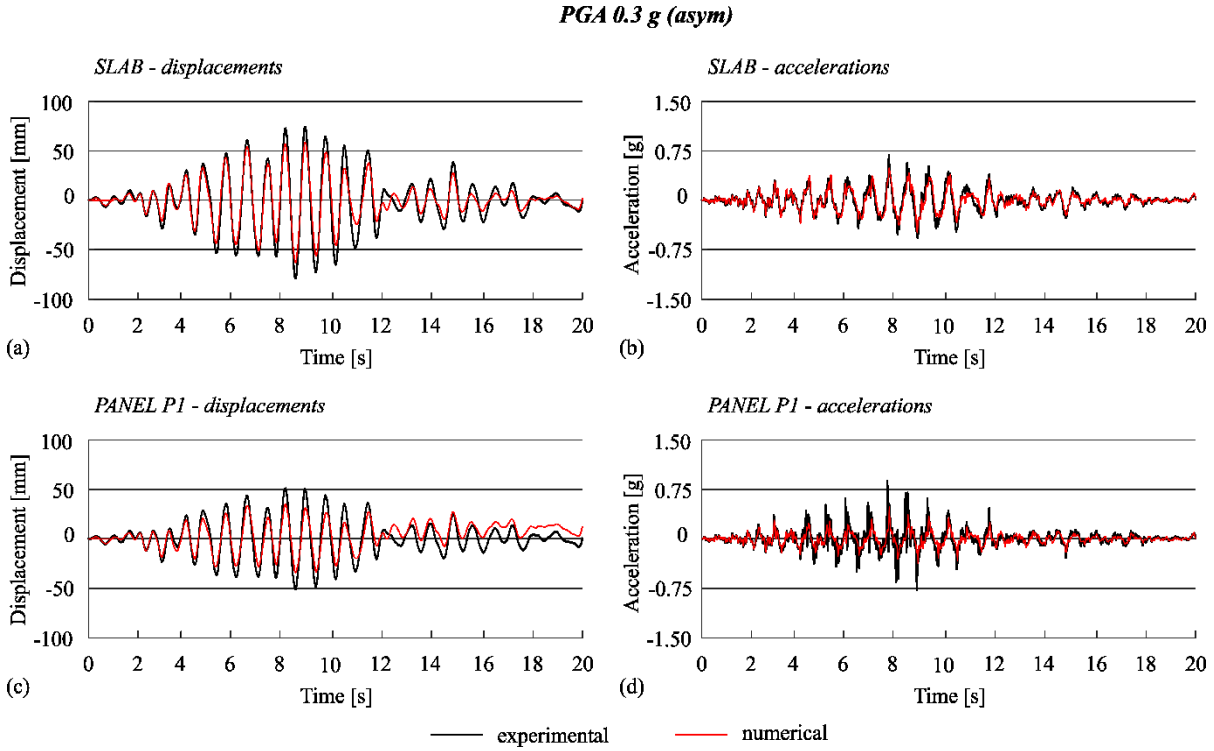

Figure 5.29: The experimental (black) and numerical (red) response histories of the asymmetric specimen at 0.3 g: (a) displacements of the main structure, (b) accelerations of the main structure, (c) displacements of panel P1 and (d) accelerations of panel P1

Slika 5.29: Eksperimentalni rezultati (črna) in numerična simulacija (rdeča) odziva asimetričnega preizkušanca pri PGA intenziteti 0.3 g: (a) pomiki glavne konstrukcije, (b) pospeški glavne konstrukcije, (c) pomiki panela P1, (d) pospeški panela P1

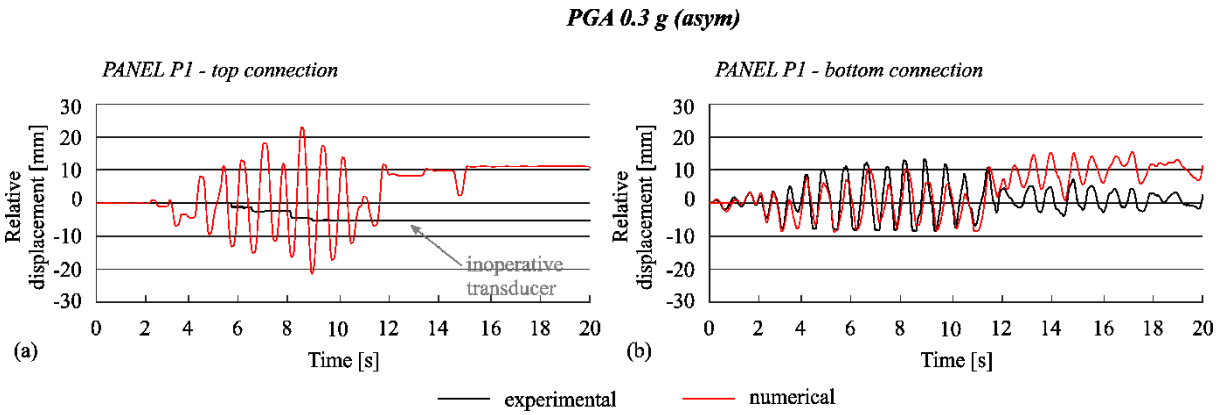

Figure 5.30: The experimental (black) and numerical (red) relative displacements between the panels and columns of the asymmetric specimen at 0.3 g: (a) slips at the top connection of panel P1, (b) slips at the bottom connection of panel P1

Slika 5.30: Eksperimentalni rezultati (črna) in numerična simulacija (rdeča) relativnih pomikov med paneli in stebri asimetričnega preizkušanca pri PGA intenziteti 0.3 g: (a) zdrs v zgornjem stiku panela P1, (b) zdrs v spodnjem stiku panela P1

The period of the structure

The fundamental periods of the main structure and the panels, and the period of the relative displacements were captured well, as shown in Figures 5.17–5.30.

The fundamental period of the numerical models is 0.89 s for the symmetric configuration and 0.86 s for the asymmetric configuration. The fundamental period of the specimen tested at the shaking table was estimated to 0.85 s for both specimen configurations (see Table 4.4 in Section 4.2.3).

Response of the cladding connections

The relative displacements in the top and bottom connections were simulated with high accuracy. The period and the amplitude of the relative displacements were very well described, which confirms the adequacy of the model and its parameters (initial stiffness of the connections, the friction force, and the damping ratio).

In most of the tests, it was also possible to simulate the residual displacements in the connections (see Figures 5.20 a-d, 5.22 c, d, 5.24 a, b). However, in two cases, the residual displacements are overestimated (Figure 5.24 c, d and Figure 5.30). The discrepancy in relative displacements of the asymmetric specimen (Figures 5.26 a, 5.28 a and 5.30 a) is due to an inoperative transducer that failed in one of the previous tests.

Note that impacts in the connections were captured well. This is demonstrated with the limitation of relative displacements in the negative direction of the connections shown in Figures 5.22 b, 5.24 b, 5.28 b and 5.30 b.

In general, the accelerations of the panels are well simulated. However, the accelerations at impacts are underestimated (Figures 5.23 d, f and 5.29 d). The experimental records were not filtered, and, therefore, the accelerations at impacts recorded during the experiments are also somewhat overestimated.

The numerical model includes a series combination of *ElasticPPGap* and *Hysteretic* material models to account for the impacts. The *ElasticPPGap* simulates the instant increase of the stiffness when the gap is closed, while the *Hysteretic* part of the model acts as an energy dissipater due to impacts. The model was originally developed to numerically model only connections, and this part was important to develop a good match for the component tests (see Figures 5.11-5.14).

To improve and simplify the numerical model, several different models, with and without the possibility for energy dissipation, were examined (e.g. *Kelvin-Voigt* or *Hertzdamp* models, see Muthukumar & DesRoches, 2006; Liu et al., 2014). They are schematically presented in Figure 5.31. In the OpenSees program, the *Kelvin-Voigt* (Figure 5.31 b) model was simulated with a combination of the *ElasticPPGap* material model and damping activated after the gap in the connection was depleted. The *ImpactMaterial* model (Figure 5.31 d) was used to model the *Hertzdamp* model (Figure 5.31 c).

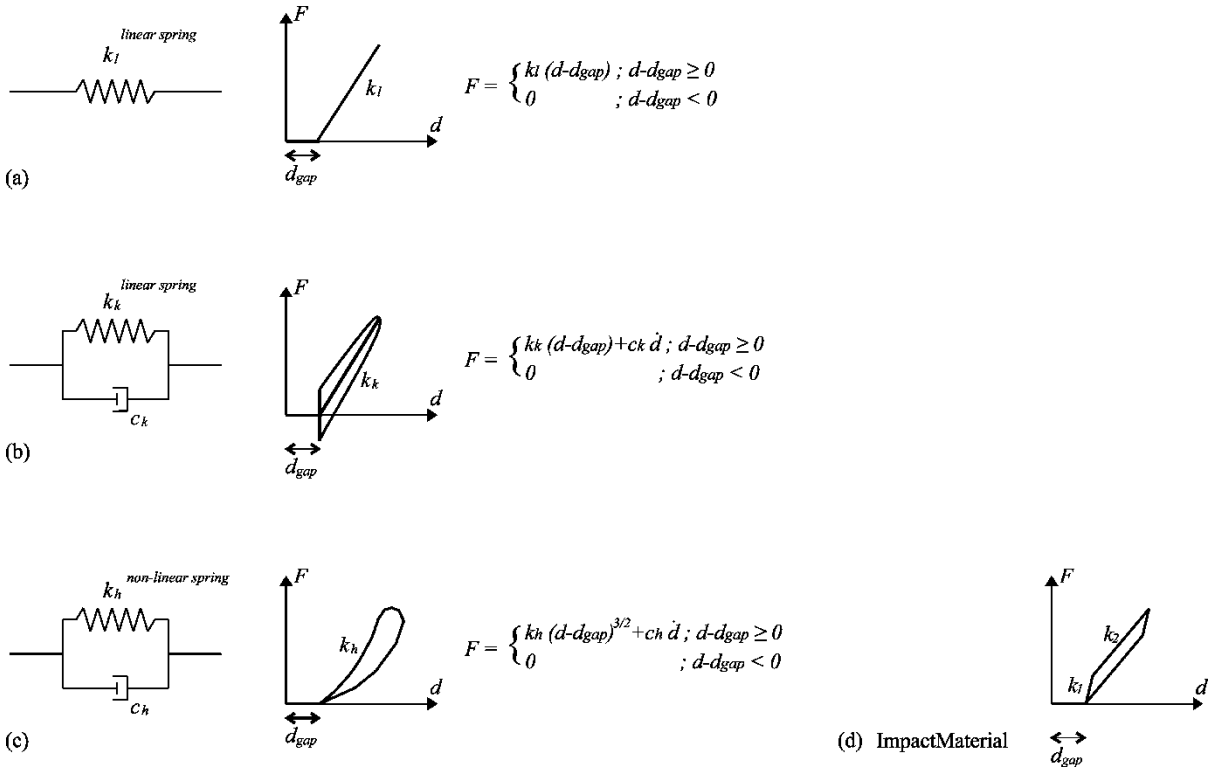

Figure 5.31: The impact models: (a) linear spring model, (b) *Kelvin-Voigt* model, (c) *Hertzdamp* model and (d) *ImpactMaterial* model

Slika 5.31: Modeli za simulacijo trkov: (a) linearna vzmet, (b) *Kelvin-Voigt* model, (c) *Hertzdamp* model, (d) *ImpactMaterial* model

However, the dissipation of energy during the impacts is very small compared to the dissipated energy due to friction in the connections. This is demonstrated in Figure 5.32, where the energy dissipated during the test of the complete fastening system is presented. As shown, the energy dissipation in the connections is predominantly due to friction. Thus, it was established that impacts could be sufficiently modelled using only a simple linear spring (i.e. ElasticPPGap material model) with sufficient stiffness Ki.

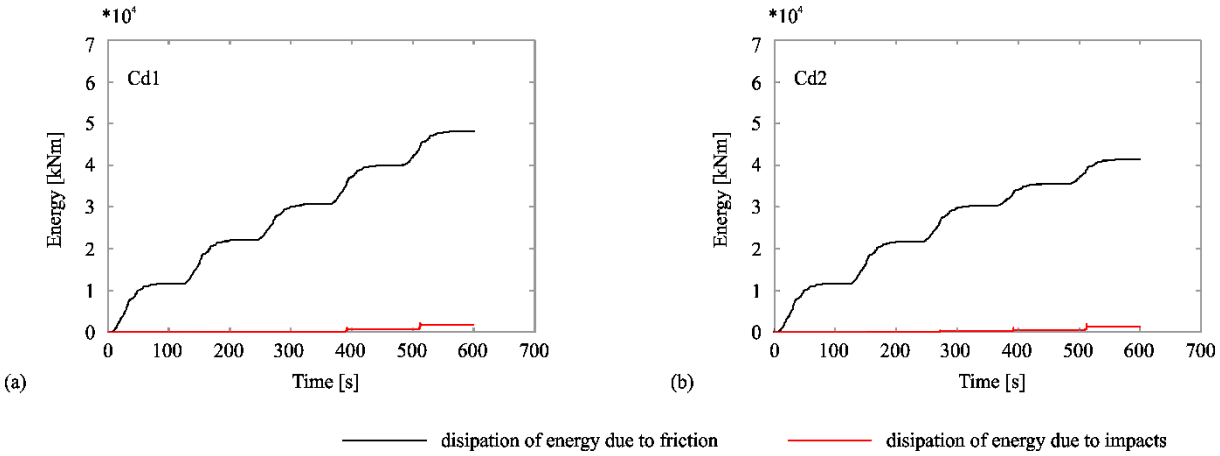

Figure 5.32: Dissipation of energy due to the friction and impacts in the connections: (a) test *Cd1*, (b) test *Cd2*

Slika 5.32: Disipacija energije zaradi trenja in trkov v stikih: (a) test *Cd1*, (b) test *Cd2*

Response of the main structure

In general, the match of the experimental and numerical response of the main structure is relatively good except for the highest intensities in Figure 5.23 (symmetric configuration at 0.4 g) and Figure 5.29 (asymmetric configuration at 0.3 g). For those cases, the maximum displacements and accelerations are somewhat underestimated. Because the columns were modelled with simple elastic elements, the yielding of the columns was not simulated properly. Note that during the tests at the highest intensities, the measured strain in the reinforcement was around the yield point (see Sections 4.2.2 and 4.2.6).

The other reason is that it was difficult to achieve the same level of accuracy for both the simulation of the main structure response and the connections response. It was practically impossible to simulate the response of the main structure and connections with the same accuracy at the same time. If the response of the main structure was captured well, then the relative displacements between the panels and columns were overestimated. The goal was set to simulate the response of the connections as accurately as possible by keeping the response of the main structure within reasonable accuracy. Thus, the response of the main structure is somewhat underestimated, which is most obvious at high seismic intensities. Note, however, that the period of vibration and response of the main structure at lower intensities are reproduced quite well.

The acceleration–displacement relationships are compared in Figures 5.33 and 5.34. The graphs show a good match of experimental and numerical AD relationships for the tests up to PGA intensity of 0.3 g for symmetric specimen and up to PGA intensities of 0.1 g and 0.2 g for the asymmetric specimen. As already discussed, the response of the main structure at the tests of higher intensities

is somewhat underestimated. As shown in Figure 5.33 (d), the yielding of the structure was not simulated with the numerical model.

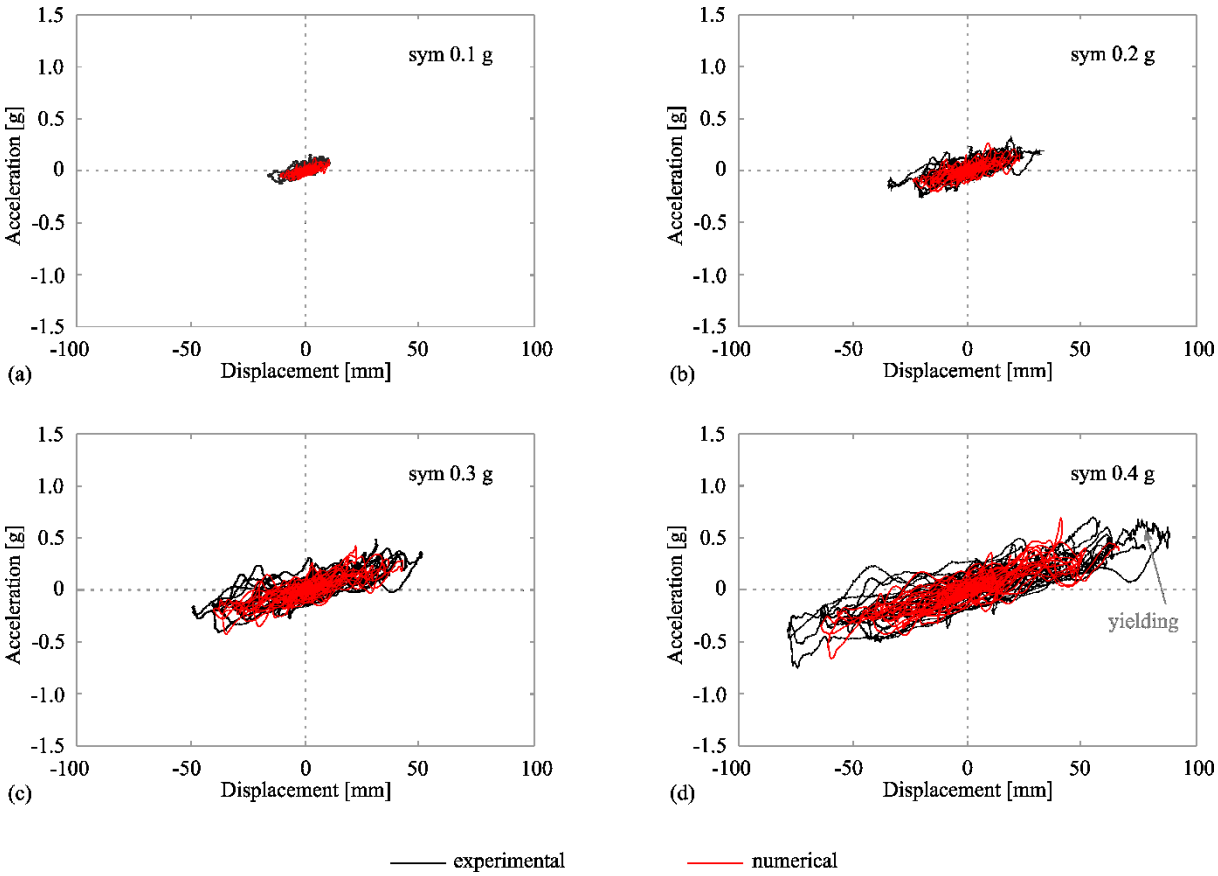

Figure 5.33: The experimental (black) and numerical (red) acceleration–displacement relationships at the top of the structure: (a) symmetric specimen at intensity 0.1 g, (b) symmetric specimen at intensity 0.2 g, (c) symmetric specimen at intensity 0.3 g and (d) symmetric specimen at intensity 0.4 g

Slika 5.33: Ekperimentalni (črna) in numerični (rdeča) odnos med pomiki in pospeški na vrhu konstrukcije: (a) simetrični preizkušanec pri intenziteti 0.1 g, (b) simetrični preizkušanec pri intenziteti 0.2 g, (c) simetrični preizkušanec pri intenziteti 0.3 g, (d) simetrični preizkušanec pri intenziteti 0.4 g

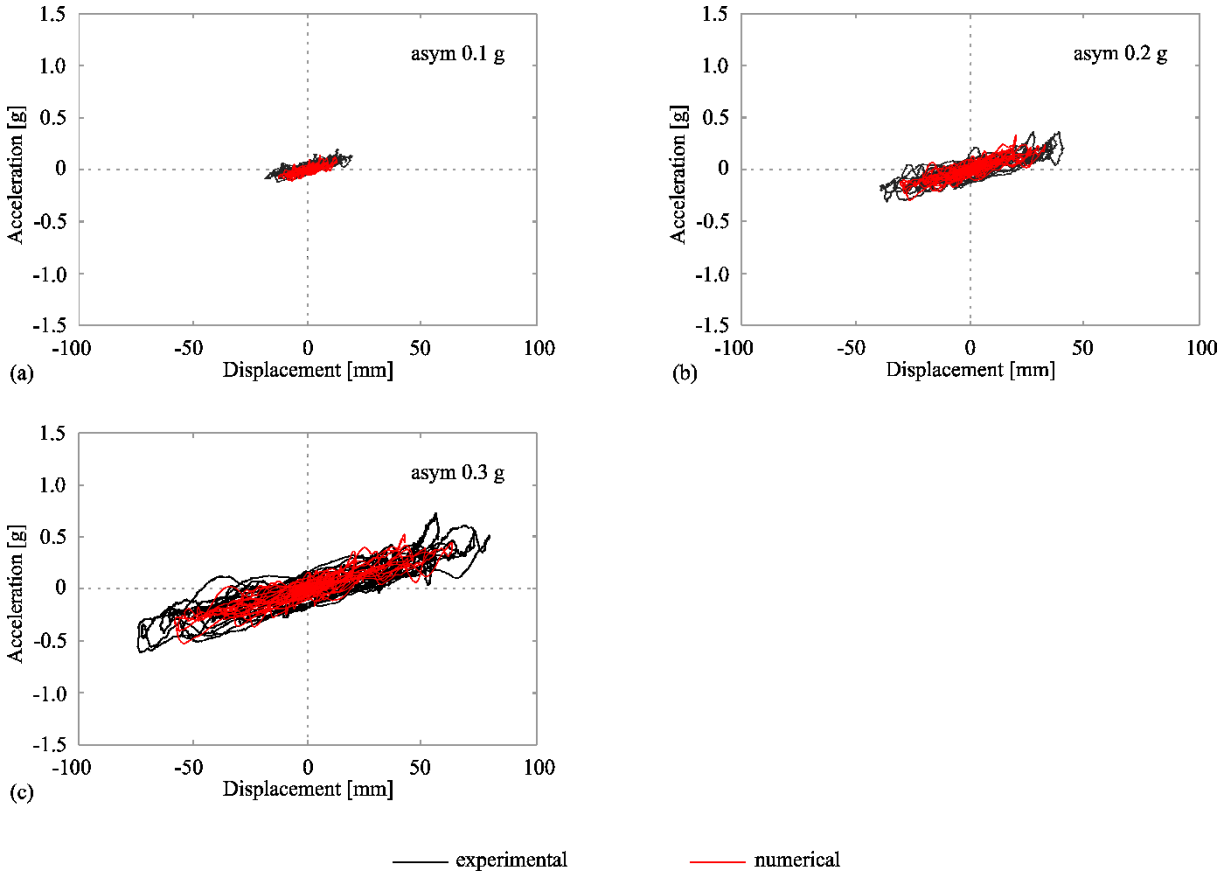

Figure 5.34: The experimental (black) and numerical (red) acceleration–displacement relationships at the top of the structure: (a) asymmetric specimen at intensity 0.1 g, (b) asymmetric specimen at intensity 0.2 g, and (c) asymmetric specimen at intensity 0.3 g

Slika 5.34: Ekperimentalni (črna) in numerični (rdeča) odnos med pomiki in pospeški na vrhu konstrukcije: (a) asimetrični preizkušanec pri intenziteti 0.1 g, (b) asimetrični preizkušanec pri intenziteti 0.2 g, (c) asimetrični preizkušanec pri intenziteti 0.3 g

The analysis of the seismic response of the tested precast structure was presented in Section 4.2. At the beginning of seismic excitation, the panel was pinned at the top connections and slid over the cantilever brackets at the bottom connections. At this phase, the panel practically behaved as an inverted pendulum (a picture). After the friction in the top connections was also activated, the panel slid at both top and bottom connections. The relative displacements between the panel and the main structure at the top and bottom side of the panel were in the opposite direction.

Note that this response is very well captured with the numerical model. There are no relative displacements at the level of top connections at the PGA seismic intensity of 0.1 g (Figures 5.17 a, c and 5.25 a), and the panels slid at the bottom connections (Figures 5.17 b, d and 5.25 b). At higher intensities, relative displacements at top and bottom connections occur in simulations and in shaking table tests.

At this phase, the panel did not resist the displacements and slid freely. The only forces that occurred in the connections were due to friction, which is relatively small compared to the forces that occur in the main structure. Therefore, at low seismic intensities, the interaction between the panels and the main structure was relatively small, and there was no influence of the panel stiffness on the overall response.

At higher seismic intensities, the impacts in the connections occurred. Because the gaps in the connections were depleted, there was some interaction between the panels and the main structure. Note that this influence of the panels' stiffness on the response of the structure is captured very well with the numerical model. This was demonstrated with an instant drop in the period of vibration at the moment of impacts (see Figure 4.24). Note that this occurred only for a very short moment (please see the discussion provided in Section 4.2.5), and the stiffness of the panels did not have a significant influence on the overall response of the main structure.

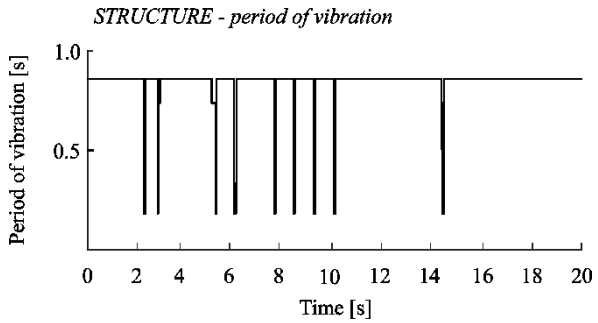

Figure 5.35: Decrease of the period of vibration at the moments of impact
Slika 5.35: Zmanjšanje nihajnega časa v trenutku trkov

However, at the moment of impact, relatively high lateral forces occur in the connections. High forces are transferred into the columns that may appreciably increase the demand on the columns (please see Section 4.2.5). A parametric study is performed in Chapter 6 to investigate this issue and the influence of important parameters on the response of RC precast buildings with horizontal panels.

5.3 Summary and conclusions of the chapter

The numerical models of cladding connections for horizontal concrete panels are presented in this chapter. Experimental force–displacement responses of the tested connections were used to define and calibrate numerical models that can describe the behaviour of the tested fastening system under cyclic and dynamic loading. The typical values of different parameters needed to define the models were proposed and calibrated by the experiments.

The numerical models are formulated by combining different material models available in the OpenSees program system. The numerical models of the tested cladding connections were validated by single component tests and full-scale shake table experiments. Results show a good match between the experiments and the numerical simulations.

Because the top and bottom cladding connections showed physically different response behaviours, they were modelled by different models. The typical Coulomb friction model was used to describe the friction in the top connection, whereas a viscous friction model better simulated the variable friction in the bottom connection.

The contacts (i.e. impacts) that occur when the gap for sliding of panels closes were simulated by an abrupt increase of the stiffness of the connection. Different models with and without the possibility of energy dissipation during the impacts were examined. However, most of the energy dissipation in the connections is due to the friction forces between the connection parts. Thus, it was concluded that impacts could be sufficiently modelled using only a simple linear spring (i.e. *ElasticPPGap* material model in OpenSees software).

6 PARAMETRIC STUDY OF ONE-STOREY PRECAST INDUSTRIAL BUILDINGS WITH HORIZONTAL CONCRETE FAÇADE SYSTEMS

This chapter presents an extensive parametric study of the seismic response of RC precast buildings with horizontal concrete façade systems and fastening devices typical for Central Europe. The main aim of the parametric study was to analyse the effect of various parameters on the response of RC precast buildings with horizontal concrete façade systems. One of the goals was to determine the influence of horizontal façade systems on the response of the overall system and analyse the interaction between the horizontal panels and the main precast structure.

The concrete cladding panels that are attached externally to the main precast structure are large and heavy. Failure of such large panels presents a danger to nearby objects and people's lives. The collapse of cladding panels might also interrupt industrial production, which causes considerable indirect economic losses. Thus, the panel response was analysed, and parameters that may influence panel failure were identified.

A wide array of one-storey RC precast buildings was included in this study. Various important parameters influencing their response were analysed: different structural configurations, construction imperfections (different initial positions of fastening devices), interaction of the adjacent panels (influence of the silicone sealant) and the connection of the bottom panels to the foundation. Numerical models of cladding connections defined and validated in Chapter 5 are used.

In the current design practice in Slovenia, the interaction between the panels and the main structural system of RC buildings and the interaction between adjacent panels are typically neglected. The influence of the panels on the overall seismic response is considered only by adding their mass to the mass of the main structure. This design approach is also thoroughly assessed within the study presented in this chapter. Finally, a proposal for improving analysed connections and a short overview of other systems used in Slovenia are provided.

Models for the numerical analysis were built in the OpenSees software framework (McKenna & Fenves, 2010). The MATLAB program was used to automate the analyses, vary the parameters, change the ground motions, and post-process the results.

6.1 Description of the parametric study

The parametric analysis was performed to identify the overall response of the analysed precast structural system and define the influence of different parameters. One of the interests was to define the influence, if any, of horizontal concrete panels on the system response and to analyse the interaction between the panels and the main precast structure.

6.1.1 Selection of precast structures

A set of 15 one-storey RC precast structures was used for the parametric analysis. The complete set of precast structures and their properties is listed in Table 6.1.

Table 6.1: Main properties of the analysed RC one-storey buildings
Preglednica 6.1: Glavne karakterisitke analiziranih AB enoetažnih stavb

Structure	m [t/column]	H [m]	b [m]	d_{bL} [mm]	s [m]	n_p	h_p [m]	m_p [t]	T [s]
m20H5	20	5	0.4	18	0.14	3	1.67	5.0	0.94
m20H7	20	7	0.4	18	0.14	4	1.75	5.3	1.56
m20H9	20	9	0.5	16	0.12	5	1.80	5.4	1.46
m40H5	40	5	0.5	20	0.16	3	1.67	5.0	0.85
m40H7	40	7	0.5	20	0.16	4	1.75	5.3	1.41
m40H9	40	9	0.6	20	0.12	5	1.80	5.4	1.43
m60H5	60	5	0.5	22	0.16	3	1.67	6.7	1.05
m60H7	60	7	0.6	22	0.12	4	1.75	7.0	1.20
m60H9	60	9	0.6	22	0.12	5	1.80	7.2	1.75
m80H5	80	5	0.6	25	0.12	3	1.67	6.7	0.84
m80H7	80	7	0.6	25	0.12	4	1.75	7.0	1.39
m80H9	80	9	0.7	20	0.16	5	1.80	7.2	1.49
m100H5	100	5	0.6	25	0.12	3	1.67	8.3	0.94
m100H7	100	7	0.6	28	0.12	4	1.75	8.8	1.55
m100H9	100	9	0.7	22	0.16	5	1.80	9.0	1.66

Legend: m: tributary mass of a structure, H: height of a structure, b: width of a column cross section, d_{bL}: longitudinal bar diameter, s: spacing of hoops, n_p: number of panels along the columns' height, h_p: height of one panel, m_p: mass of one panel, T: fundamental period of a structure.

The selection of precast structures was made considering typical dimensions, number of columns and number of panels found in Slovenian design practice. The span of the bays varied between 12 m and 30 m. The distance between columns along the buildings varied between 7.5 m and 12.5 m. Three different column heights H were considered (5, 7 and 9 m). The mass of the structure tributary to one column varied between 20 t and 100 t, including the 5 kN/m^2 uniformly distributed load on

the roof. All the structures were designed according to Eurocode 8 (CEN, 2004), considering a_g = 0.25 g and ground type C (see Zoubek, 2015). Forces were reduced with behaviour factor q = 3.0, which corresponds to the ductility class medium (DCM). Considering the mass and height of the structures, four different columns' cross-section types, presented in Figure 6.1, were taken into account. Concrete class C 40/50 and reinforcement B500C were considered in the design.

During the design of structures, the basic requirements of the Eurocode 8 have been met, except for the minimum cross-sectional dimension with respect to the height of the structure (clause 5.4.1.2.2 of EC8). The cross-sectional dimension of a column should not be smaller than one-tenth of the column height unless the drift sensitivity coefficient is smaller than 0.1 (which was not the case for the selected structures). However, this criterion is often disregarded during design, and the column cross sections found in practice are usually smaller.

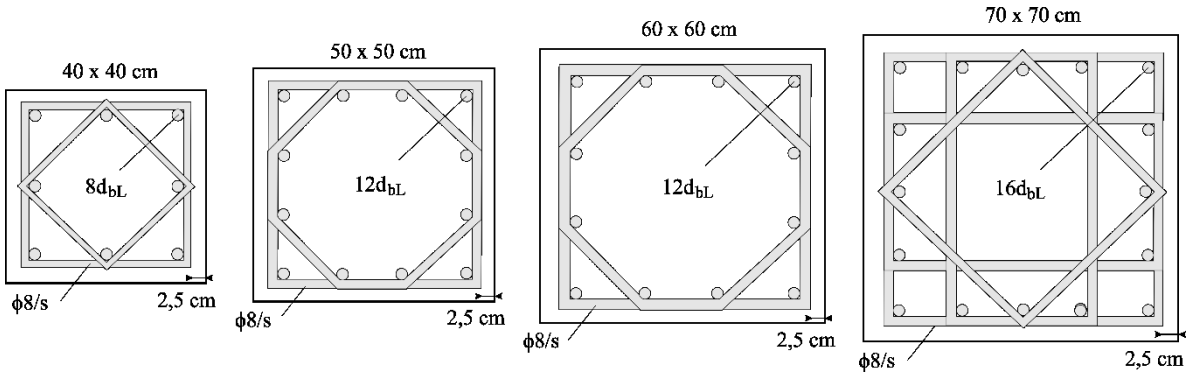

Figure 6.1: Column sections of the analysed RC one-storey buildings designed to EC8 (Zoubek, 2015)
Slika 6.1: Prerezi stebrov analiziranih AB enoetažnih stavb, ki so projektirane po EC8 (Zoubek, 2015)

Three to five horizontal panels were attached (n_p) to perimeter columns, depending on their height. The panels were modelled with equal height, although this may vary in practice. The composition of panels is described in Section 2.3. As shown in Figure 2.5 (a), the panel usually consists of two outer concrete layers and a thermal insulation layer in the middle. Panels with a total concrete thickness of 0.16 m were used in the parametric analysis. The mass of each panel m_p was calculated based on its thickness, height and length (i.e. span between the columns). A panel length of 7.5 m corresponds to a structure with a mass of 20 t/column and 40 t/column. A panel length of 10 m corresponds to a structure with a mass of 60 t/column and 80 t/column, and a panel length of 12.5 m corresponds to a mass of 100 t/column.

6.1.2 Selection of the ground motion records

Each building was subjected to a set of 30 accelerograms. Seismic records were selected from the Resorce database (Akkar et al., 2014) considering European earthquakes and are provided in

Appendix A. The ground motions were selected using a slightly modified procedure proposed by Jayaram et al. (2011). The EC8 elastic spectrum for Ljubljana, Slovenia (ground type C and a_g = 0.25 g for return period 475 years) was used as a target spectrum. The target dispersion was set to zero for all periods. Because the analysed precast structures have different fundamental periods, the T = 0 s was used as a conditional period (i.e. the spectra of ground motions were scaled to PGA in the process selecting the ground motions). Therefore, the dispersion of the spectra of selected ground motions was equal to zero only at period T = 0 s. Additionally, the source-to-site distance was limited to 5–55 km, the magnitude to 4–8, and the maximum scale factor was set to 3.5.

The effect of the individual earthquake on the response of the precast structure depends significantly on the shape of the response spectrum in the period range of the analysed buildings. Spectra of the selected ground motions are shown in Figure 6.2. The median spectrum matches the target Eurocode spectrum relatively well in the period range 0.9–1.8 s, which corresponds to the analysed precast structures (precast structures oscillate predominantly in the first mode).

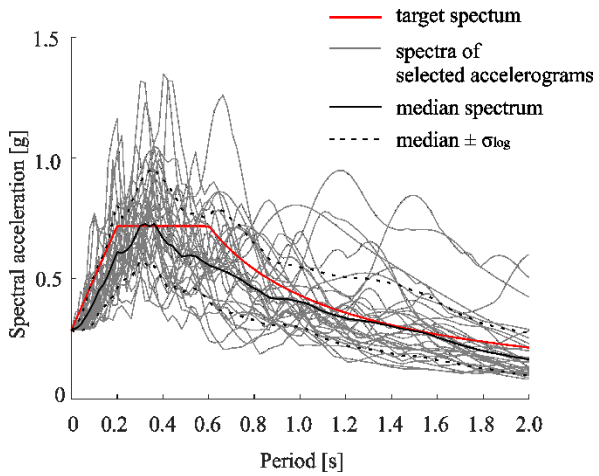

Figure 6.2: Spectra of the selected accelerograms and the target Eurocode 8 spectrum for the ground type C
Slika 6.2: Spektri pospeškov izbranih akcelerogramov in ciljni Evrokodov spekter za tip tal C

Nonlinear response history analyses were performed for three different intensity levels listed in Table 6.2. In addition to the intensity of a_g = 0.25 g, the records were also scaled to the intensities 0.425 g and 0.675 g that correspond to return periods of 2475 and 10,000 years, respectively. PGA values for the return periods other than 475 years were calculated using the importance factor γ_I (see Equations 6.1 and 6.2) that can be derived for different return periods according to Eurocode 8 (CEN, 2004).

$$\gamma_I = (T_{LR}/T_L)^{-1/e} \tag{6.1}$$

$$\gamma_I = (P_L/P_{LR})^{-1/e} \tag{6.2}$$

P_L is the value of the probability of exceedance in T_L years. Equation 6.1 is used to compute the value of the importance factor to achieve the same probability of exceedance in T_L years as in the T_{LR} years for which the reference seismic action is defined. Alternatively, Equation 6.2 can be used to achieve a probability of exceedance P_L in T_L years, other than the reference probability of exceedance P_{LR} over the same T_L years (CEN, 2004).

In Eurocode 8, the exponent *e* is denoted with *k.* The value of the exponent depends on the seismicity but is generally of the order of 3. This value was used and gives a relatively good estimation for the site location in Ljubljana. Values retrieved with the hazard analysis for site location in Ljubljana were somewhat smaller (Žižmond, 2019).

Table 6.2: Ground motion intensities used in parametric analysis
Preglednica 6.2: Intenzitete potresov uporabljenih v parametrični analizi

Return period T_R [years]	Probability of exceedance P_L in T_L years	Scale factor γ_I	a_g [g]
475	10% in 50 years	1.0	0.25
2475	2% in 50 years	1.7	0.425
10,000	0.5% in 50 years	2.7	0.675

6.1.3 Analysed parameters and summary of performed analyses

The selection of parameters for the analysis was made with regard to real precast structures that can be found in practice. The following parameters were varied and analysed:

- interaction between adjacent panels, that is, presence of the silicone sealant between panels,
- construction imperfections, that is, different initial positions of the connections,
- connection of bottom panels to the foundation,
- and different structural configurations, that is, different ratios between the number of all columns of the structure and the number of panels in the ground plan in the analysed direction.

Interaction of adjacent panels

Slots and ribs typically connect adjacent panels, and joints between the panels are afterwards filled with silicone strips. Usually, the silicone sealant is placed at both (external and internal) sides of the panels with a width-to-depth ratio of t_s:b_s = 2:1 (Figure 2.8 b).

The silicone connection causes a certain interaction between adjacent panels, so its influence on the response of panels and precast columns was analysed. The study considered silicone with a width of 30 mm and a depth of 15 mm, and a total length of silicone at both sides of the panel l_s was evaluated.

Construction imperfections

The connections present vital parts of precast structures and might have an important influence on the response of the overall structure. Because of imperfections during the casting and mounting of structures, different initial positions of the connections occur regularly in construction practice.

Initial positions of bolts at the top and cantilevers at the bottom connections are important. If the connections are centrally mounted, larger relative displacements between the column and panel are possible before activating significant forces. In this situation, the panel can slide almost freely (friction is very small) up to the relative displacements of 4 cm and 4.5 cm at the top and bottom connections, respectively. However, if the bolt and cantilever are shifted to the edge of the box at the top and opening at the bottom of the panel, relatively high forces activate in the connections even at small relative displacements between the column and panel in that direction. The resistance of the top and bottom connections is 55 kN and 179 kN, respectively. A top-connection displacement capacity of 3.5 cm after the gap in that connection is depleted was used in the analyses.

To account for different construction imperfections, different positions of the bolt (at the top connection) and cantilever (at the bottom connection) within the connection gap were considered: a centrally mounted bolt and cantilever equidistant from the opening edges in the panel (denoted with *M-middle*), and an extremely eccentrically positioned bolt and cantilever within the opening in the panel (*L-left* and *R-right*) with no gap available on one side.

The position of the top and bottom connections can be different for different panels in the structure. Within the parametric study, only three extreme position combinations (see Figure 6.3) were analysed:

- middle position of both top and bottom connections (*MM*),

- left position of both the top and bottom connections (*LL*),
- left position of top connection and right position of the bottom connection (*LR*).

It was assumed that all the top connections are mounted the same way and that all the bottom connections are mounted the same way, respectively.

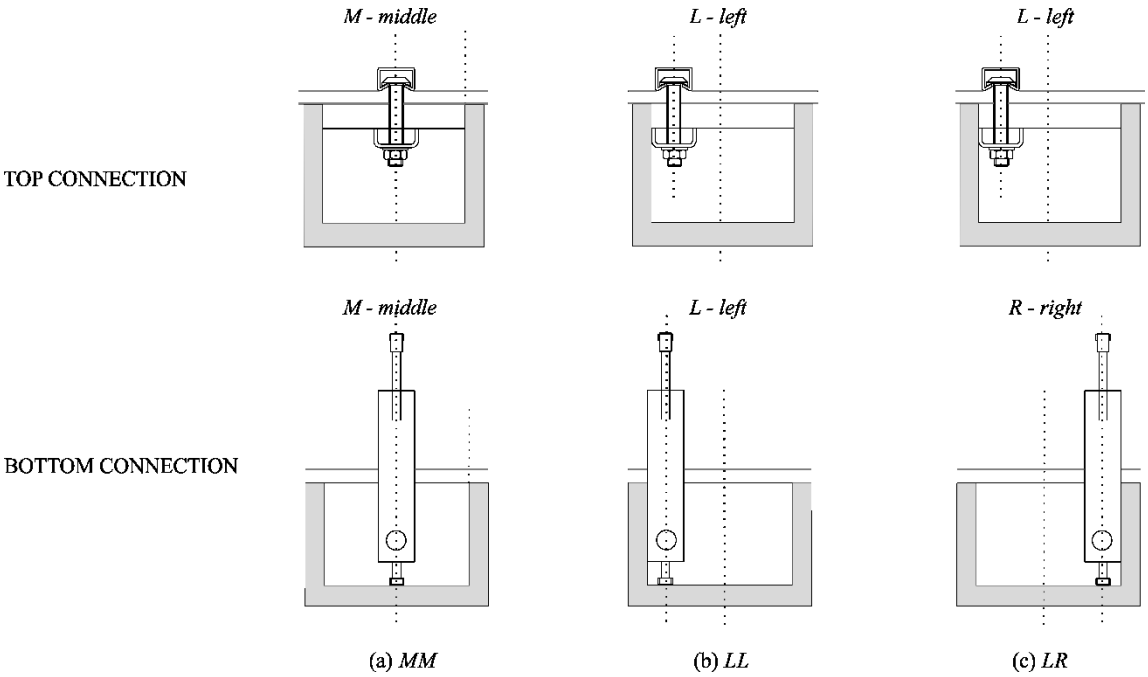

Figure 6.3: Different positions of (a) top and (b) bottom connections

Slika 6.3: Različne pozicije (a) zgornjih in (b) spodnjih stikov

Connection of bottom panels to the foundation

Different versions of the connection between the bottom panel and the foundation can be found in practice. The bottom panel is often attached to the foundation with steel anchors hammered into the façade panel and inserted into pre-drilled holes in the foundation (Figure 2.8 a). Afterwards, the connection is grouted by mortar. Under these conditions, the bottom panel is considered fixed to the foundation, which caused concern about the possible occurrence of the short-column effect.

For this reason, two possible connections of the bottom panel to the foundation were considered. The panel was either fully fixed to the foundation (*F-fixed*) or connected to the column as all the other panels (*C-connection*). In the latter case, the connection between the panel and foundation is provided only by the silicone sealant.

Ground plan configuration

Precast structures of different ground plan configurations can be found in practice. Floor plans of regular shape can be square or rectangular, with the same or a different number of columns in two orthogonal directions. The number of internal columns may also vary from structure to structure. Therefore, depending on the floor plan configurations, structures have different ratios between the number of columns and the number of cladding panels attached to the external columns, which can also be different in transversal and longitudinal directions. A higher number of panels compared to the number of columns might have a larger influence on the response of the precast system.

A k factor was introduced to account for different ground plan configurations of the structure and investigate the influence of the ratio between the number of columns and the number of panels/connections on the structures' seismic response. The coefficient presents the ratio between the number of all columns within the structure n_{col} and the number of panels in ground plan n_{pan} in the direction parallel to excitation (see Equation 6.3). Figure 6.4 presents an example for k factor equal to 2 (two columns per panel, as marked with the dotted line in Figure 6.4 a).

Equation 6.3 shows the calculation for one direction; however, both directions were examined in the parametric study, that is, all expected ratios in real structures.

$$k_x = \frac{n_{col}}{n_{pan}} = \frac{n_{col,x} \cdot n_{col,y}}{2 \cdot n_{span,x}} = \frac{n_{col,x} \cdot n_{col,y}}{2 \cdot (n_{col,x} - 1)} \tag{6.3}$$

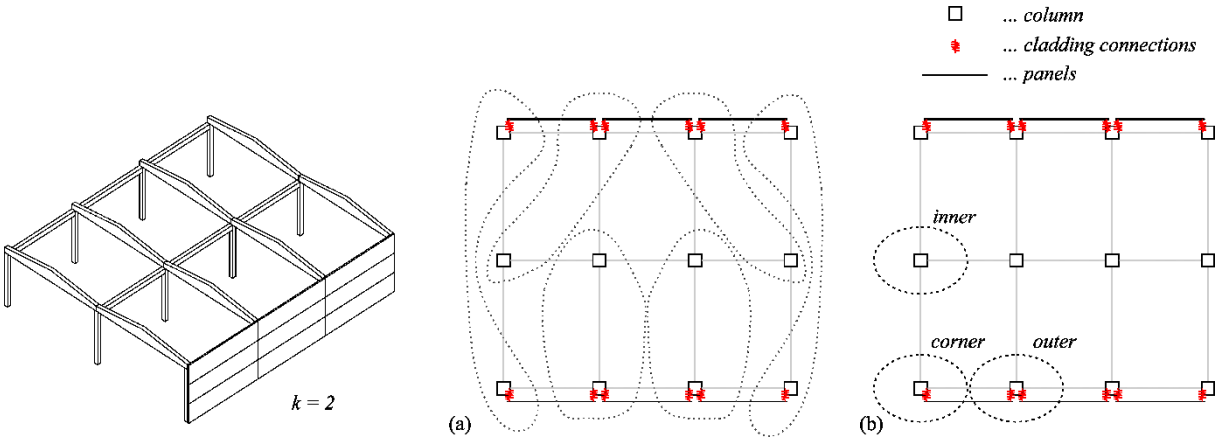

Figure 6.4: Typical example of a precast structure with ratio factor k = 2: (a) distribution of connections influence on the global response, (b) corner, inner and outer column of the structure
Slika 6.4: Krakteristični primer kontrukcije s faktorjem razmerja med stebri in paneli k = 2: (a) porazdelitev vpliva stikov na globalni odziv konstruckije, (b) vogalni, notranji in zunanji steber konstruckije

Some examples of different ground plan configurations and corresponding k factors are shown in Figure 6.5. Values of k are expected to be between 1 and 10 in real structures and implicitly take into account the ground plan configuration of the structure. A higher value of the k factor means a

larger number of columns compared to the number of panels/connections. For example, a structure wider in the direction perpendicular to excitation with many inner columns and fewer perimeter columns with panels has a larger *k* factor, whereas a structure longer in the direction of excitation has a lower *k* factor.

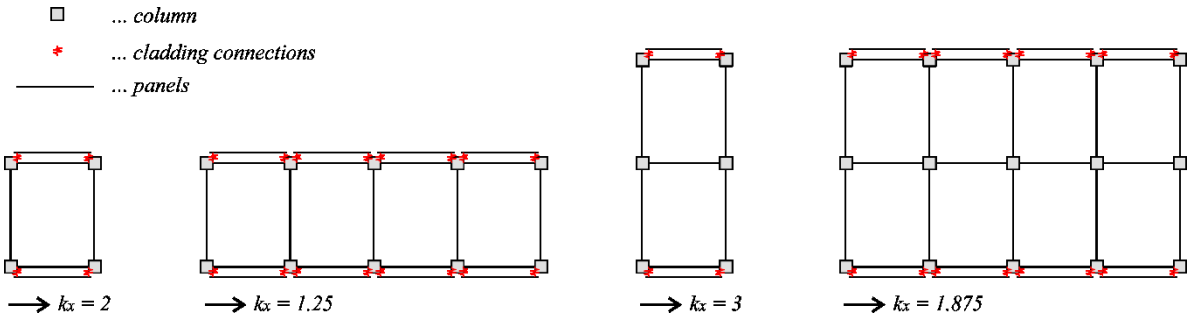

Figure 6.5: Different plans of the precast structures and corresponding *k* factors in the longitudinal direction

Slika 6.5: Različni tlorisi montažnih hal s pripadajočim faktorjem *k* v vzdolžni smeri

Summary of performed analyses

The parametric analyses were performed in several sets. Each set consisted of dynamic analyses of 15 one-storey RC precast structures subjected to 30 selected ground motions at three different intensities. Within each set of numerical analyses, the parameters were carefully selected and modified, as described in the following points. The test matrix is presented in Figure 6.6 and summarised in Table 3.3.

1. The first set of parametric analyses considered the following properties of precast structures: centrally positioned connections (*MM*), no silicone sealant (*N*), bottom panel fixed to the foundation (*F*) and ratio factor equal to 2.

2. Because the joints between adjacent panels are commonly filled with silicone, two sets of analyses were performed, taking into account the interaction between the panels. Both proposed models of silicone sealant were analysed and compared: *Pinching* (*P*) and *Elastic* (*E*). Other parameters were not changed.

The results of the first and second sets of analyses were compared to examine the influence of interaction between panels on the response.

3. Next, two sets of analyses were performed to investigate the influence of construction imperfections on the response. The presence of silicone sealant represents a realistic situation in practice. Therefore, the following parameters were selected: eccentrically

positioned connections (*LL* and *LR*), silicone-sealed joints (*P*), bottom panel fixed to the foundation (*F*) and ratio factor equal to 2.

To analyse the influence of construction imperfections on the response of panels and main precast structure, the results of the third set of analyses were compared (both 3.1 and 3.2 in Figure 6.6) with the results of the second set (2.1 in Figure 6.6). Therefore, in all analyses, joints were sealed with silicone (*P*), the bottom panel was fixed to the foundation (*F*), and the ratio factor was equal to 2, while the position of connections was varied (*MM*, *LL* and *LR*).

4. For the fourth set of analyses, the central position of connection was assumed (*MM*), silicone sealant was modelled (*P*), and a ratio factor of 2 was considered. However, the bottom panel was not fixed to the foundation but instead connected to the column as all the other panels (*C*). Results of these analyses were compared to the second set with a different connection of the bottom panel to the foundation.

5. The following analyses were performed to analyse the effect of geometry. Ten sets of analyses were performed to cover the complete range of ratio factors between the number of columns and the number of panels expected in real structures. The ratio factor k varied from 1 to 10 with a step of 1, while all the other parameters were fixed: the central position of the connections (*MM*), silicone-sealed joints (*P*) and bottom panel fixed to the foundation (*F*). Results were compared to investigate the influence of ground plan configuration on the structure's response.

VARIABLES: initial gap / silicone / bottom panel / ratio factor

MM	*N*	*F*	*1*
LL	*P*	*C*	*2*
LR	*E*		*3*
			...
			10

DYNAMIC ANALYSES: 15 structures
30 accelerograms
three intensities

initial gap: *MM - middle middle*
LL - left left
LR - left right

silicone: *N - no silicone*
P - Pinching
E - Elastic

bottom panel: *F - fixed*
C - connection

ratio factor: *from 1 to 10 with step 1*

TEST MATRIX:

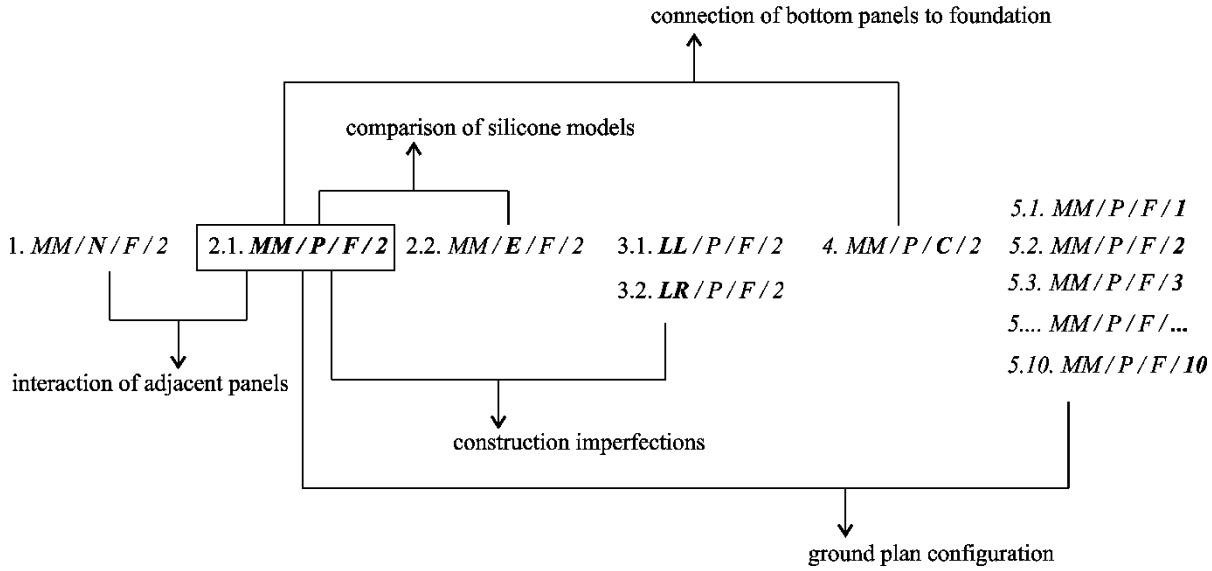

Figure 6.6: Test matrix of analyses performed within the parametric study

Slika 6.6: Matrika analiz izvedenih v okviru parametrične študije

Table 6.3: Matrix of performed analyses

Preglednica 6.3: MAtrika narejenih analiz

Parameter analysed	Position of the connections	Silicone model	Connection of bottom panel to foundation	Ratio factor	No. of structures	No. of accelerograms	No. of intensities	No. of analyses
Interaction of panels	*MM*	*N / P*	*F*	*2*	15	30	3	2700
Silicone models	*MM*	*P / E*	*F*	*2*	15	30	3	2700
Construction imperfections	*MM / LL / LR*	*P*	*F*	*2*	15	30	3	4050
Connection of bottom panel to foundation	*MM*	*P*	*F / C*	*2*	15	30	3	2700
Ground plan configuration	*MM*	*P*	*F*	*1 : 1 : 10*	15	30	3	13500

Legend: *MM*: central position of connection, *LL / LR*: eccentrically positioned connections, *N*: no silicone modelled, *P*: *Pinching* silicone model, *E*: *Elastic* silicone model, *F*: bottom panel fixed to foundation, *C*: bottom panel connected to column

6.2 Numerical model of RC precast structure

Each structure was modelled with an equivalent cantilever column with tributary mass at the top because it was supposed that the roof acts as a rigid diaphragm. This model has already been used within other research studies (Kramar, 2008; Zoubek, 2015). The model was extended to analyse the influence of the horizontal façade system and obtain global and local response parameters of the main structure and panels. A global response is described with displacements of the main structure, whereas locally, the influence of façade system on shear demand in columns is analysed. The model is presented in the following paragraphs and verified by analysing two typical structures (Section 6.2.4).

Figure 6.7 (a) shows the model of equivalent column and panels (from here on denoted as an *equivalent column-panels model*). As already mentioned, each main structure was modelled by an equivalent cantilever column with tributary mass at the top. All panels along the column height were modelled, each with a panel mass of m_p and connected to the equivalent column with two top and two bottom cladding connections per panel (see Figure 6.7 a). Therefore, two vertical axes of connections were considered as corresponding to the outer column.

A coefficient k was used to account for different ground plan configurations of the structure. The coefficient presents the ratio between the number of all columns of the structure n_{col} and the number of panels n_{pan} in the ground plan in the analysed direction (see Equation 6.3). Figure 6.4 (a) shows that the influence of the panels and cladding connections was distributed all over the structure. The factor k was used to modify (i.e. multiply) the tributary mass, stiffness and strength of the equivalent column (see Figure 6.7 a, c), whereas the properties of the connections were not varied.

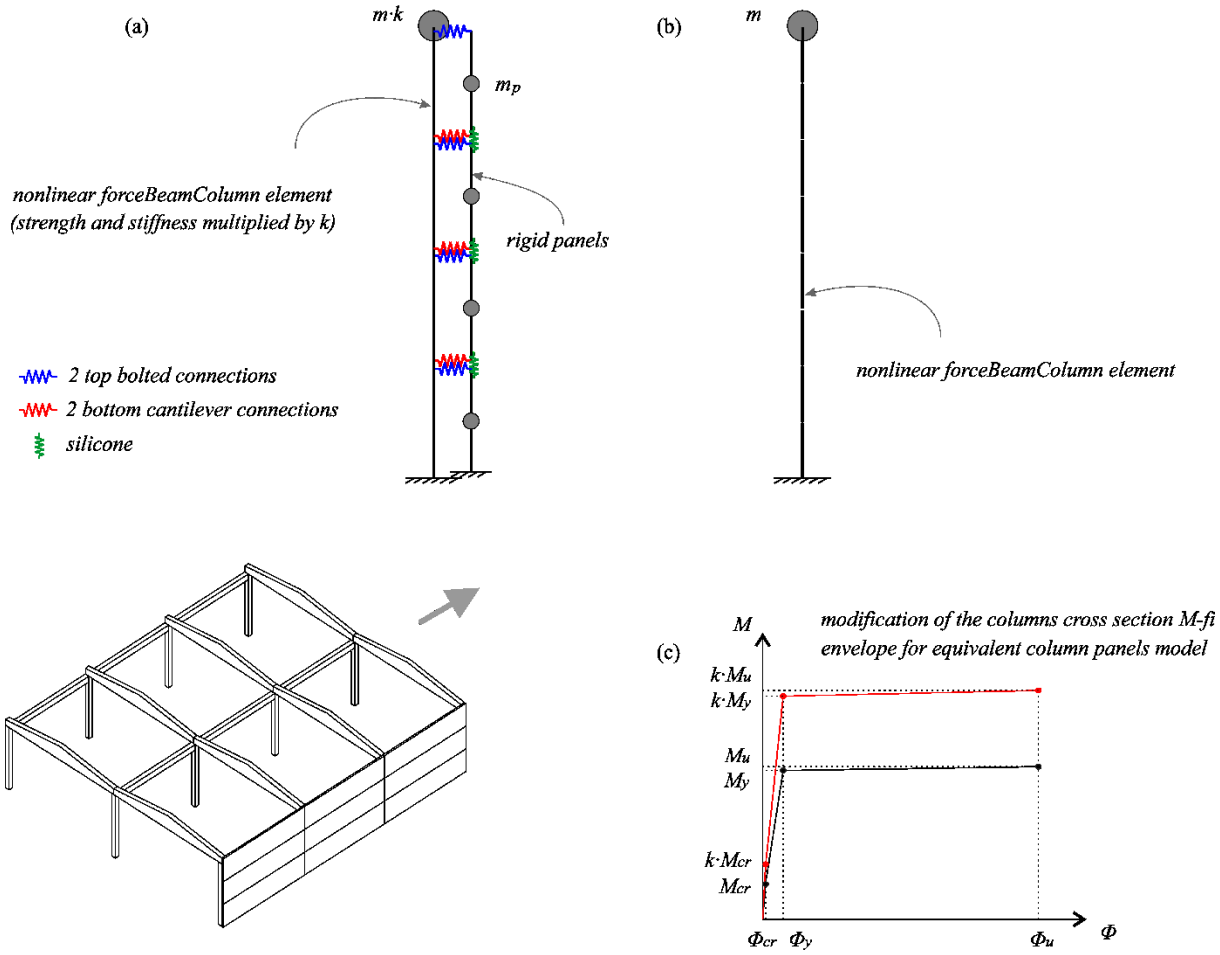

Figure 6.7: Equivalent models for the analysis of precast structure with horizontal façade system: (a) equivalent column-panels model, (b) column model and (c) modification of column cross-section moment–curvature envelopes

Slika 6.7: Model za analizo montažne konstrukcije z vodoravnim fasadnim sistemom: (a) model povprečnega stebra in panelov, (b) model stebra, (c) modifikacija moment–ukrivljenost ovojnice prereza stebra

This modelling approach (Figure 6.7 a) adequately simulated the influence of the horizontal façade system on the global response of the structure. Dynamic properties (e.g. fundamental period) of the equivalent model were the same as dynamic properties of the whole structure because the following properties were the same:

- the ratio between stiffness and mass of the main structure,
- the ratio between the stiffness of the main structure and stiffness of the panels,
- the ratio between the mass of the main structure and the mass of the panels.

The equivalent column-panels model gives complete information about the global response of the structural system, that is, displacements at the top of the columns and the response of panels and connections. However, the local influence of the façade system on the columns should be further

analysed because the columns were modified with factor *k* to preserve the dynamic properties of the structure. To account for the local effect of panels and connections, another set of analyses was performed on the *column model* without panels and with no modification of its properties (see Figure 6.7 b).

The procedure is as follows. First, a dynamic analysis of the equivalent column-panels model is performed to obtain the displacement response at the top of the column and response of the connections (displacements and forces). In this analysis, the tributary mass, stiffness, and strength of the column were modified with factor *k*, whereas the properties of the connections were not varied.

Then an analysis of the column model was performed, where the column properties were not modified. The displacement response at the top of the column and forces at the position of the connections were induced in this analysis. The analysis was performed for the outer column that is the most critical with two vertical axes of connections and the complete panel mass attached. Thus, the forces corresponding to two vertical axes of connections were considered.

The main characteristics were modelled quite well in the nonlinear range as well. As shown later (validation of the equivalent model is presented in Section 6.2.4), maximum response parameters were captured very well, as were the yielding and moment–curvature response of the columns.

The seismic response was investigated in the direction parallel to the panel plane. In parametric analyses, the influence of second-order theory (P-delta effect) was considered, as was the failure of the silicone sealant and the panels. When the failure occurred during calculation, the failed element (either silicone or panel) was removed from the model, and analysis proceeded until the end or until column failure. In all analyses, 5% mass-proportional Rayleigh damping was used.

6.2.1 Model of columns

Horizontal panels and connections along the height of analysed precast structures could influence the distribution of forces and deformations along the column height. It is theoretically possible that plastification of the column or larger lateral forces occur higher on the column and not at the base. To take this possibility into account, the response of the columns was modelled with the nonlinear beam-column elements with distributed plasticity. In such a manner, the influence of horizontal panels and cladding connections along the column height was taken into account. Such a model for cantilever columns has also been used to simulate the three-storey precast building tested within the SAFECAST project (Isaković et al., 2012b). The seismic response of a tested structure was well described by the model, which confirmed its adequacy.

Numerical models were built in OpenSees. The columns were modelled with nonlinear, force-based elements *forceBeamColumn* where the nonlinear response was defined by the moment–curvature relationship assigned to five integration points along each element, unlike the usual approach with a fibre section. The number of elements was adjusted to the number and configuration of connections (having a certain number of nodes for modelling connections between the column and panels was desired, and defined nodes correspond to the position of connections or assigned panel mass). For example, columns with a height of 5 m were modelled with six elements, whereas columns with a height of 7 and 9 m were modelled with eight and ten nonlinear beam-column elements, respectively.

Moment–curvature hysteretic behaviour was defined with the Takeda hysteretic rules (Takeda et al., 1970). To define a moment–curvature response envelope, it was necessary to perform a moment-curvature analysis of each column section, where the cross section was defined as an assemblage of different fibres with assigned stress–strain relationships. For this purpose, the confined concrete was modelled using Mander's model (Mander et al., 1988) as described in Eurocode 8-2, Appendix E (CEN, 2005). The Giuffré–Menegotto–Pinto model was used to model the stress–strain behaviour of reinforcement steel (material stress–strain curves are shown in Figure 6.8). In the OpenSees software framework, the *Concrete04* and *Steel02* material models were used with mean material properties (f_{cm} = 48 MPa, f_{ym} = 575 MPa, f_{tm} = 690 MPa).

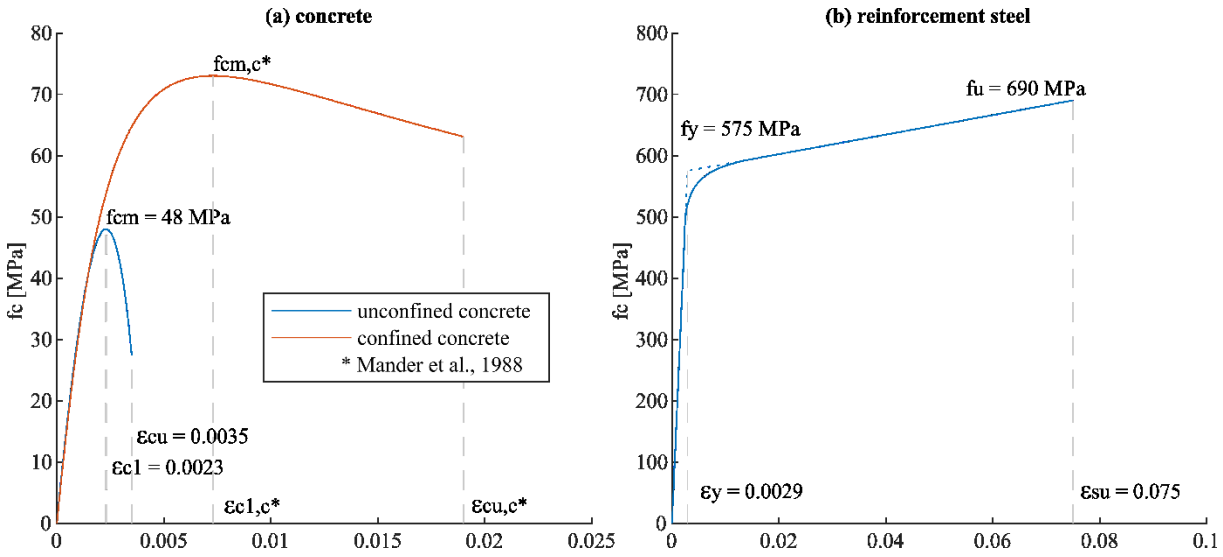

Figure 6.8: Stress–strain material envelopes for (a) concrete and (b) reinforcement steel

Slika 6.8: Odnos med napetostjo in deformacijo za (a) beton in (b) armaturo

Cracking moment and curvature were defined analytically. Moment M_{cr} was defined according to Equation 6.4, where W is the moment of resistance of the section, N is axial load, and A is the area of the cross section. Mean concrete tensile strength calculated by Equation 6.5 was used.

Corresponding curvature Φ_{cr} was calculated based on the initial stiffness of the cracked cross section (see Equation 6.6).

$$M_{cr} = W\left(\frac{N}{A} + f_{ctm}\right) \tag{6.4}$$

$$f_{ctm} = \frac{f_{cm}}{10} \tag{6.5}$$

$$\emptyset_{cr} = \frac{M_{cr}}{0.5EI} \tag{6.6}$$

The moment–curvature envelope then had to be appropriately idealised through the first yield point, as shown in Figure 6.9. The hardening slope was defined based on the equal energy principle of actual and idealised diagrams (see the hatched area in Figure 6.9). The failure of the cross section was defined at ultimate curvature corresponding to the strain of reinforcement at maximum load, which is 7.5% for the reinforcement ductility class C (Figure 6.9).

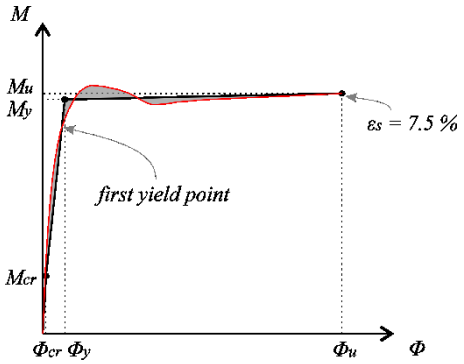

Figure 6.9: Idealisation of the moment–curvature diagram
Slika 6.9: Idealizacija diagrama moment–ukrivljenost

Input parameters for the nonlinear model of columns (see Section 6.2.1) are summarised in Table 6.4. To describe the hysteretic behaviour with the *Takeda* material model in Opensees, it is also necessary to define the factor α that defines unloading stiffness degradation. The value 0.5 is commonly used. An example of the column's hysteretic behaviour is shown in Figure 6.10 for structure *m60H7*.

In the last column of Table 6.4, the shear resistance of cross section V_R (Equation 6.7) is given (note that the capacity design was considered, and the shear resistance is much higher than M_u/H).

$$V_R = \frac{A_{sw}}{s} z f_{yw} cot\,\theta \tag{6.7}$$

A_{sw} is the cross-sectional area of the shear reinforcement, s is the spacing of the stirrups, z is the inner lever arm (approx. $0.9\,d$ or $0.8\,h$), f_{yw} is the yield strength of shear reinforcement, and θ is the angle between the concrete compression strut and the beam axis perpendicular to the shear force.

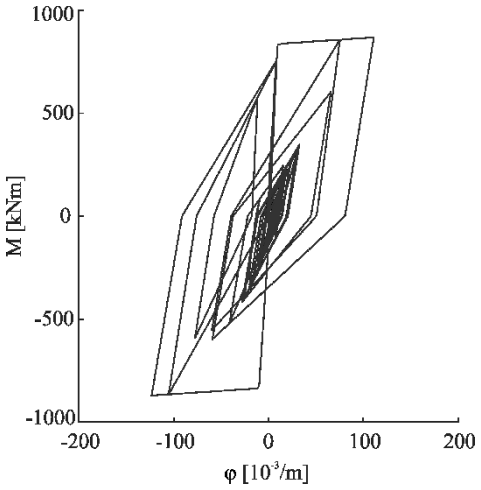

Figure 6.10: Hysteretic response behaviour of column *m60H7*

Slika 6.10: Histerezni odziv stebra *m60H7*

Table 6.4: Input parameters for the nonlinear model of the columns

Preglednica 6.4: Vhodni parametri za nelinerani model stebrov

Structure	Φ_{cr} [10^{-3}/m]	Φ_y [10^{-3}/m]	Φ_u [10^{-3}/m]	M_{cr} [kNm]	M_y [kNm]	M_u [kNm]	V_R [kN]
m20H5	1.7	13.1	257	64	223	244	227
m20H7	1.7	13.1	257	64	223	244	227
m20H9	1.3	9.7	190	116	338	378	359
m40H5	1.5	10.1	172	133	539	553	268
m40H7	1.5	10.1	172	133	539	553	268
m40H9	1.1	8.0	157	212	662	742	435
m60H5	1.7	10.5	152	149	658	664	267
m60H7	1.2	8.4	165	232	836	885	435
m60H9	1.2	8.4	165	232	836	885	435
m80H5	1.3	8.3	167	251	1036	1167	434
m80H7	1.3	8.6	146	251	1071	1085	434
m80H9	1.1	8.0	137	366	1165	1177	685
m100H5	1.4	8.3	168	271	1077	1210	434
m100H7	1.4	8.7	132	271	1305	1317	432
m100H9	1.1	8.0	117	389	1378	1399	684

Legend: Φ_{cr}*:* crack curvature, Φ_y*:* yield curvature, Φ_u*:* ultimate curvature, M_{cr}*:* crack moment, M_y*:* yield moment, M_u*:* ultimate moment, V_R*:* shear resistance

6.2.2 Model of connections

The cladding connections were modelled as described in Chapter 5. A friction force of 2 kN was considered in the sliding phase of the top connection. Failure of the fastening system was defined at the displacement of 3.5 cm after the top connection gap was depleted, which corresponds to the force of 55 kN in the top connection. The resistance of the bottom connection of 176 kN was used. When the connections failed, the panel and its connections were removed from the model. The analysis proceeded until the end or until the collapse of the column.

Two possible connections of the bottom panel to the foundation were analysed. They are presented in Figure 6.11. The panel was either fully fixed to the foundation (*F-fixed*) or connected to the column as all the other panels (*C-connection*).

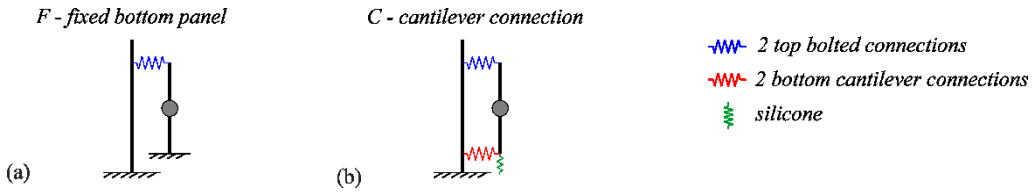

Figure 6.11: Connection of the bottom panel to the foundation: (a) panel fixed to the foundation, (b) panel attached to the column

Slika 6.11: Stik spodnjega panela s temeljem: (a) panel sidran v temelj, (b) panel pritrjen na steber

6.2.3 Silicone sealant model

Adjacent panels are typically connected by slots and ribs, and the joints are filled by narrow silicone strips. The response of silicone sealant under imposed shear strains was studied by Dal Lago et al. (Dal Lago, 2015; Dal Lago et al., 2017b; Negro & Lamperti Tornaghi, 2017), who performed several experiments on concrete blocks, sub-assemblies, and full-scale structures with cladding panels sealed with silicone.

The typical hysteretic response of the silicone sealant is presented in Figure 6.12 on a shear–stress versus shear–strain diagram. A relatively good agreement of the hysteretic response during the cyclic test on concrete blocks and subassembly structure was achieved. However, the experiments have shown a large scatter of the silicone properties because the material is usually not subjected to strict production control. Despite that, basic features of the silicone sealant have been identified. According to the results of Dal Lago et al. (2017), the silicone exhibits elastic behaviour up to about 100–150% shear strain, shear strength up to 0.25 MPa, and an ultimate deformation capacity of about 200% of strain. The cyclic response of the silicone sealant is characterised by significant

stiffness degradation and progressive damage. The mean shear elastic modulus was estimated to be 0.25 MPa.

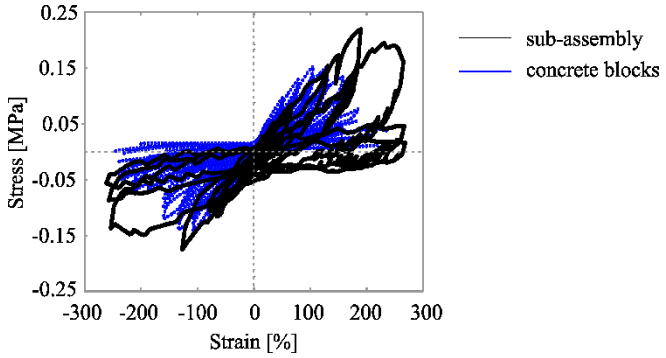

Figure 6.12: A comparison of the silicone sealant's hysteretic response during the cyclic tests performed on concrete blocks and subassembly structure

Slika 6.12: Primerjava histereznega odziva silikona med cikličnimi preizkusi na betonskih kockah in na sestavljenem preizkušancu z dvema paneloma

Different models can be used to simulate the response of silicone sealant. The *Pinching* model can describe the cyclic degradation of the stiffness and strength of silicone, whereas the *Elastic* model assumes the completely elastic behaviour of the silicone joints.

The properties of the *Pinching* model were calibrated by Menichini (2019) based on experimental results from Dal Lago et al. (2017b) and are presented in Figure 6.13. The model is evaluated in Figure 6.14 by comparing the analysis with the experiment on a subassembly specimen published by Dal Lago et al. (2017b).

Dal Lago et al. (2017b) proposed that the silicone response can also be simulated with a relatively simple *Elastic* material model with assumed average stiffness of the silicone sealant. The stiffness of the elastic link should be evaluated by Equation 6.8, using the estimated mean initial shear modulus of silicone G_s = 0.25 MPa, width t_s, depth b_s and length l_s of silicone strips. The equivalent stiffness of the *Elastic* model is plotted with the blue line in Figure 6.14 for the example of the subassembly test (Dal Lago et al., 2017b). As can be observed, the stiffness of the elastic link is somewhat larger than the initial stiffness of the silicone sealant.

$$k_{eq} = \frac{G_s \cdot b_s \cdot l_s}{t_s} \tag{6.8}$$

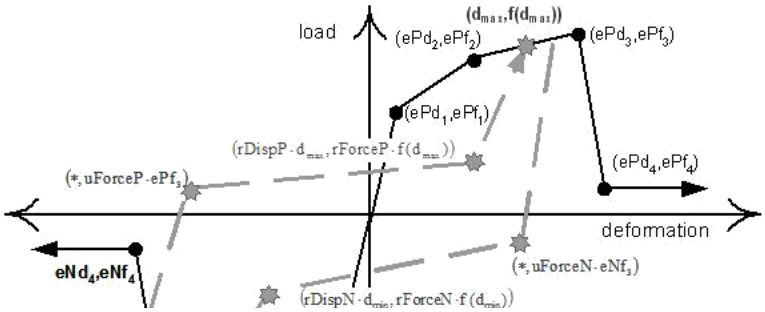

Pinching4 model parameters:

ts ... width of silicone strips [mm]
bs ... depth of silicone strips [mm]
ls ... total length of silicone strips [m]

[ePf1 ePf2 ePf3 ePf4], [eNf1 eNf2 eNf3 eNf4] ... force points on the response envelope
[ePd1 ePd2 ePd3 ePd4], [eNd1 eNd2 eNd3 eNd4] ... deformation points on the response envelope

rDispP, rDispN ... ratio of the deformation at which reloading occurs to the max/min historic deformation demand
rForceP, rForceN ... ratio of the force at which reloading begins to force corresponding to the max/min historic deformation demand
uForceP, uForceN ... ratio of strength developed upon unloading from negative load to the max/min strength developed under monotonic loading

[gK1 gK2 gK3 gK4 gKLim], [0.0 0.0 0.3 0.2 100] ... values controlling cyclic degradation model for unloading stiffness degradation
[gD1 gD2 gD3 gD4 gDLim], [0.15 0.0 1.0 1.0 100] ... values controlling cyclic degradation model for reloading stiffness degradation
[gF1 gF2 gF3 gF4 gFLim], [0.0 4.0 1.0 1.0 100] ... values controlling cyclic degradation model for strength degradation

gE ... value used to define maximum energy dissipation under cyclic loading
dmgType ... type of damage ("cycle"/"energy")

Figure 6.13: *Pinching4* model parameters (McKenna & Fenves, 2010)

Slika 6.13: Parametri materialnega modela *Pinching4* (McKenna & Fenves, 2010)

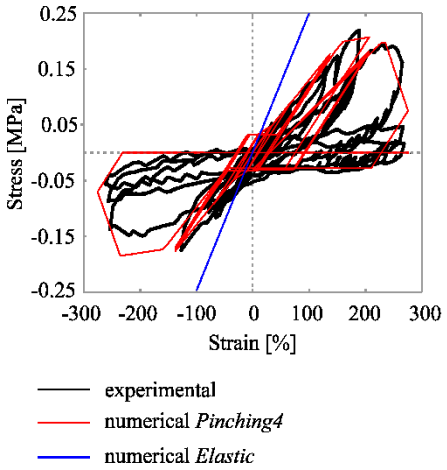

Pinching4 model parameters:

ts = 15 mm
bs = 15 mm
ls = 4.66 m

[ePf1 ePf2 ePf3 ePf4] = [eNf1 eNf2 eNf3 eNf4] = [0.023 0.21 0.224 0.0]*ls*bs
[ePd1 ePd2 ePd3 ePd4] = [eNd1 eNd2 eNd3 eNd4] = [0.146 1.6 2.35 3.0]*ts*10^{-3}
rDispP = rDispN = 0.3
rForceP = rForceN = 0.04
uForceP = uForceN = 0.15
[gK1 gK2 gK3 gK4 gKLim] = [0.0 0.0 0.3 0.2 100]
[gD1 gD2 gD3 gD4 gDLim] = [0.15 0.0 1.0 1.0 100]
[gF1 gF2 gF3 gF4 gFLim] = [0.0 4.0 1.0 1.0 100]
gE = 43
dmgType = "energy"

Figure 6.14: A comparison of the experimental and numerical results of the silicone sealant's hysteretic response during the subassembly test

Slika 6.14: Primerjava eksperimentalnih rezulatov in numeričnega histereznega odziva silikonskega tesnila

Within the study, both models of the silicone sealant (*P-Pinching* and *E-Elastic*) were tested on the set of 15 different structures subjected to 30 accelerograms at three intensities (the selection of structures and ground motions for parametric study are presented in Section 6.1). Failure of the *Pinching* silicone model was defined at a shear strain of 200%. However, because the silicone

exhibits elastic behaviour up to about 100–150%, failure of the elastic link silicone model was defined at a shear strain of 150%.

Because of the higher initial stiffness and no degradation of the *Elastic* silicone model, the effect on the response of precast structure was larger than when using the *Pinching* model. The influence of the *Elastic* silicone model on the displacements and shear demand in the column was larger, and more failures of silicone sealant and panels were recorded. It would be more appropriate to consider the lower initial or average stiffness of the silicone sealant.

Because a relatively large scatter of silicone sealant's mechanical properties was observed during the tests, and because the properties of silicone severely deteriorate due to climatic and ageing effects, the stiffening contribution of the silicone is not reliable and relatively limited. Because the characteristics of the silicone sealant may significantly alter due to the degradation of material (Chew, 2000), the *Elastic* silicone model may give too-conservative results (it overestimates the displacement and force demand at cladding connections and, consequently, also the shear demand in columns).

The silicone model *P-Pinching* was used in the parametric study to account for the effect of silicone sealant and to analyse the interaction of adjacent panels. The analyses considered that the silicone sealant fails during the excitation, and failure was defined at a shear strain of 200%. After the deformation capacity was exceeded, the silicone was removed from the model, and the analysis proceeded. To analyse the effect that silicone sealant has on the seismic response of the precast structure, models without the silicone sealant, *N-no silicone* were also included in the parametric analyses.

However, maximum displacements of structures were also relatively well estimated with the *Elastic* model (because of the earlier failure of silicone joints compared to the *Pinching* model). For those reasons and due to its simplicity, the *Elastic* model of silicone sealant could be suitable for use in the design.

6.2.4 Validation of the equivalent model of the structure and the calculation scheme

This section validates the numerical model and procedure used to analyse precast structures with horizontal panels with two typical examples. A structure with a tributary mass of 60 t at the top of the column and a height of 9 m (denoted with *m60H9*) was analysed. Results are compared with the three-dimensional models of the complete structure. Two ground plan configurations were evaluated, corresponding to the ratio factors $k = 2$ and $k = 1.3$ (see Figure 6.15).

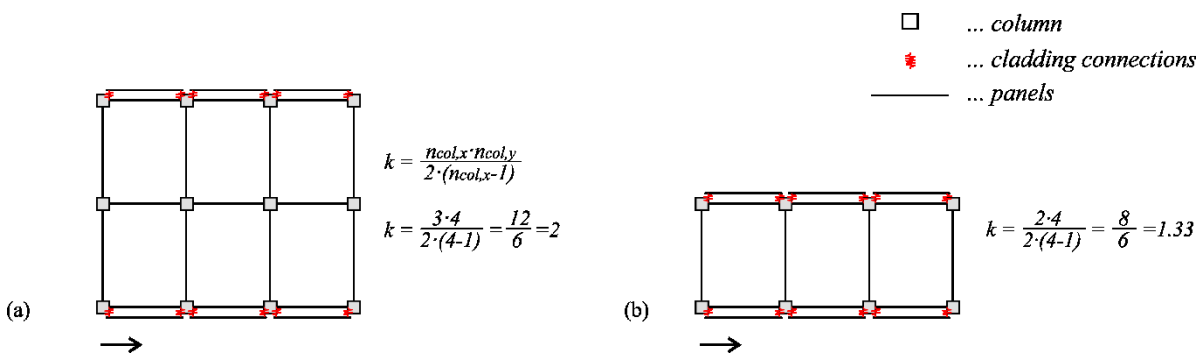

Figure 6.15: Precast structure *m60H9* with: (a) ratio factor $k = 2$ and (b) ratio factor $k = 1.3$

Slika 6.15: Montažna stavba *m60H9*: (a) s faktorjem $k = 2$ in (b) s faktorjem $k = 1.3$

The nonlinear model of columns was defined as presented in Section 6.2.1, with the following parameters: $\Phi_{cr} = 1.2 \cdot 10^{-3}$/m, $\Phi_y = 8.4 \cdot 10^{-3}$/m, $\Phi_u = 165 \cdot 10^{-3}$/m, $M_{cr} = 232$ kNm, $M_y = 836$ kNm and $M_u = 885$ kNm. Cladding connections were modelled as described in Section 6.2.2. All the panels were connected to columns by centrally positioned connections (gaps in the connections were the same at both sides of the connection). The *Elastic* model was used to simulate the response of silicone sealant because of its simplicity. Structures were subjected to ground motion record number 14 (see Appendix A) at $a_g = 0.675$ g.

The results of equivalent and complete structure models are compared in the following sections. As presented, internal forces and deformations obtained with the equivalent model are a good match with the full three-dimensional model.

Structure m60H9 with ratio k = 2

This section presents the results of the numerical analysis of structure *m60H9* with the ratio factor $k = 2$ (Figure 6.16). The structure has 12 columns; four columns in the analysed direction and three columns in the transverse direction. Altogether, 30 panels (six in the ground plan and five along the column height) are mounted at the two external sides of the structure.

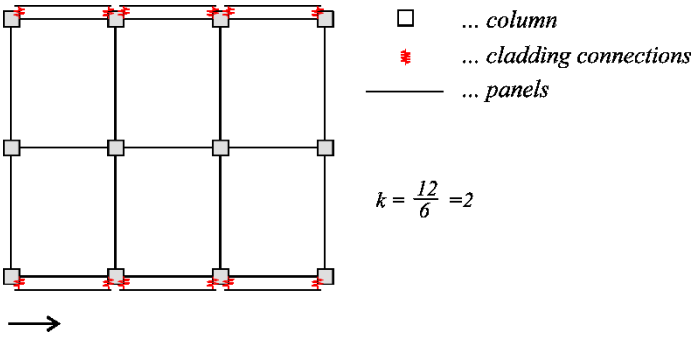

Figure 6.16: Precast structure *m60H9* with ratio factor $k = 2$

Slika 6.16: Montažna stavba *m60H9* s faktorjem $k = 2$

Figures 6.17-6.22 compare the internal forces and deformations obtained by different models. As presented, results obtained with equivalent models are in relatively good agreement with the results of the full three-dimensional model.

Figure 6.17 presents the maximum displacements of the column along its height and displacement response history at the top of the column. As shown, the maximum displacements at the top of the column are practically the same.

Figure 6.18 presents the maximum slips and forces that occur in connections along the structure's height. Figures 6.19 and 6.20 compare the displacement and force response histories for cladding connections of the panel at the top of the structure. The match of the results is very good.

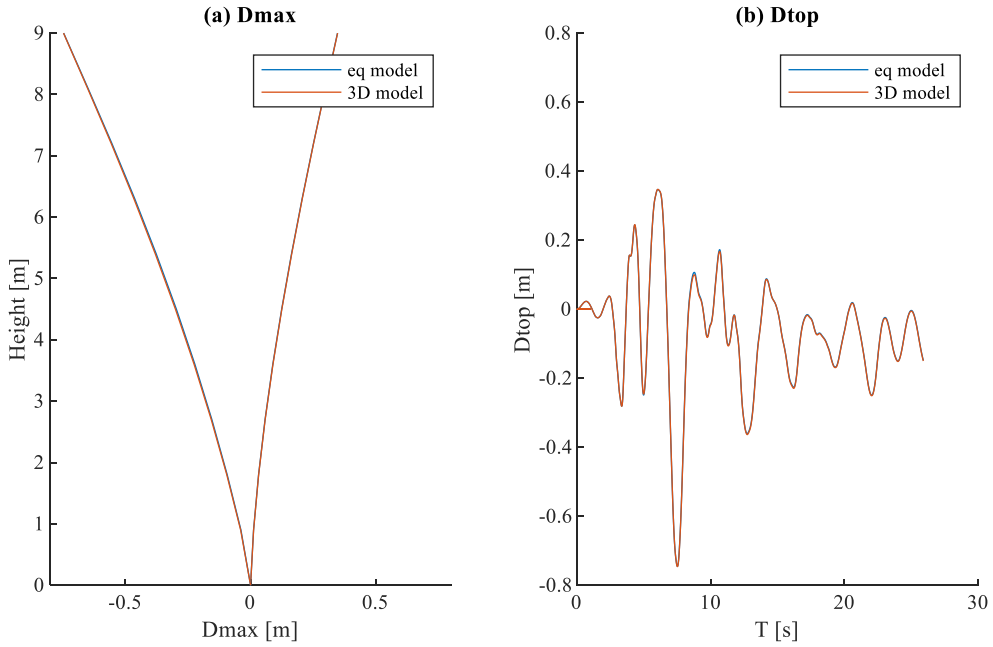

Figure 6.17: Displacements of the column (*m60H9*, $k = 2$): (a) displacement envelope along the column height and (b) displacement response history at the top of the column

Slika 6.17: Pomiki stebra (*m60H9*, $k = 2$): (a) ovojnica pomikov po višini stebra in (b) časovni potek pomikov na vrhu stebra

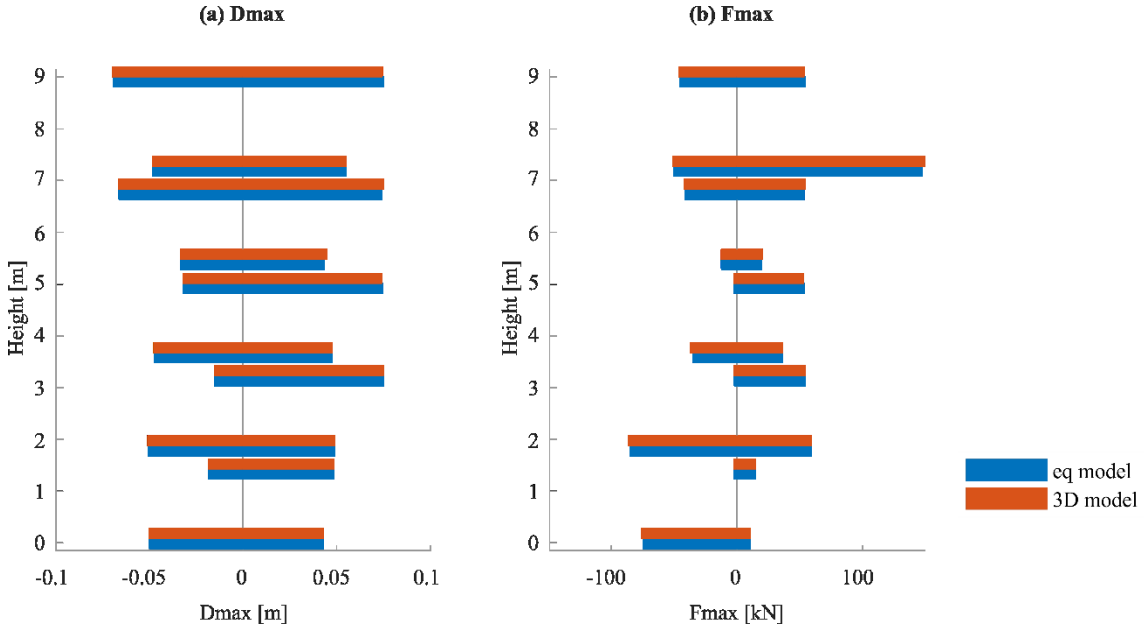

Figure 6.18: Maximum response of the connections (*m60H9*, k = 2): (a) slips and (b) forces in connections

Slika 6.18: Maksimalni odziv stikov (*m60H9*, k = 2): (a) zdrsi in (b) sile v stikih

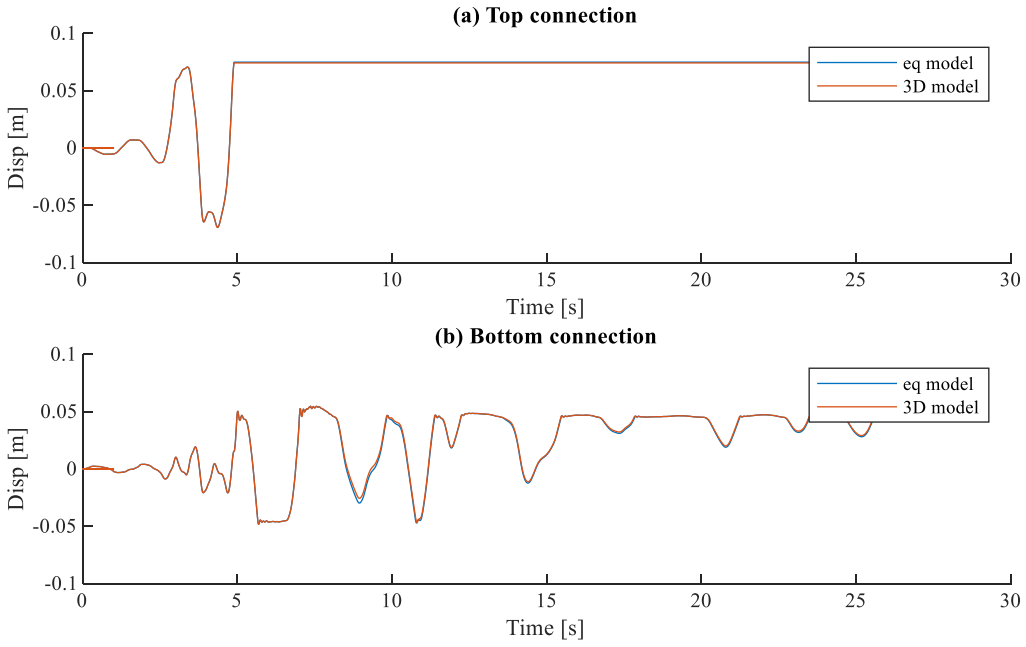

Figure 6.19: Displacement response histories at top and bottom connections of the top panel (*m60H9*, k = 2)

Slika 6.19: Časovni potek zdrsov v zgornjem in spodnjem stiku vrhnjega panela (*m60H9*, k = 2)

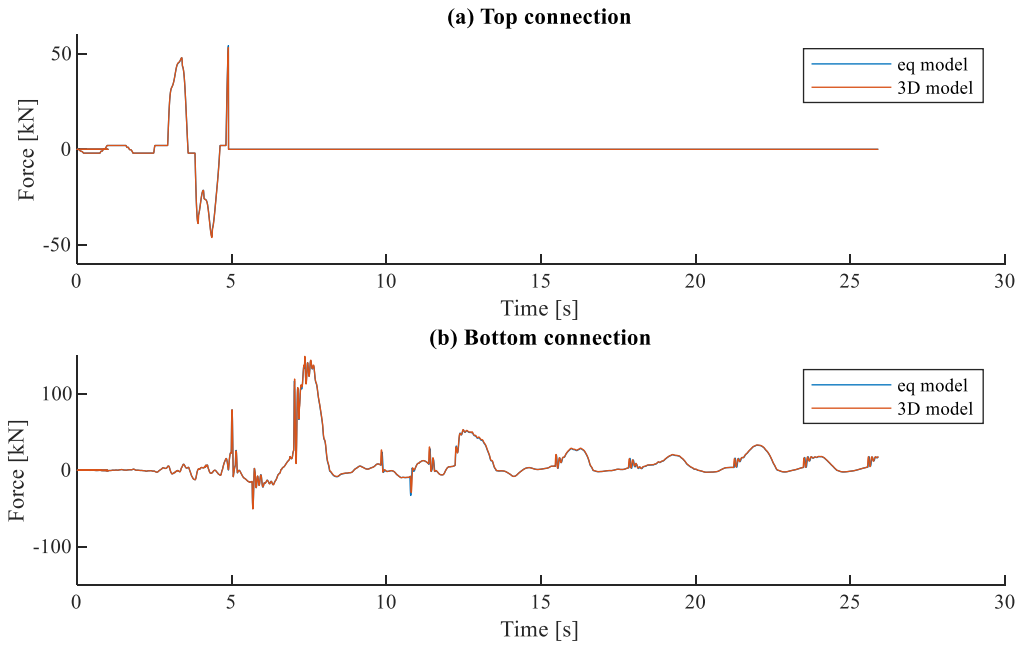

Figure 6.20: Force response histories at top and bottom connections of the top panel (*m60H9*, $k = 2$)

Slika 6.20: Časovni potek sil v zgornjem in spodnjem stiku vrhnjega panela (*m60H9*, $k = 2$)

Figure 6.21 presents the maximum shear force, moment and curvature along the column height. The response of the column at its base is compared in Figure 6.22, where the moment–curvature hysteretic response and response histories are presented. There is only a small discrepancy in the results, which is acceptable given the simplification of the model.

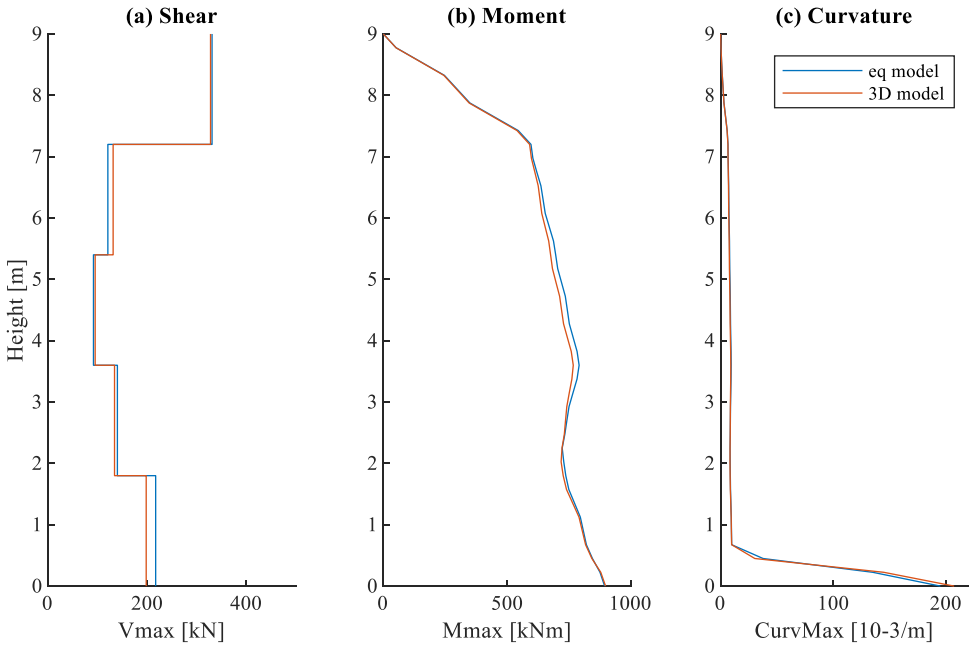

Figure 6.21: Maximum (a) shear forces, (b) moments and (c) curvature along the column height (*m60H9*, $k = 2$)

Slika 6.21: Maksimalna (a) strižna sila, (b) momenti in (c) ukrivljenost po višini stebra (*m60H9*, $k = 2$)

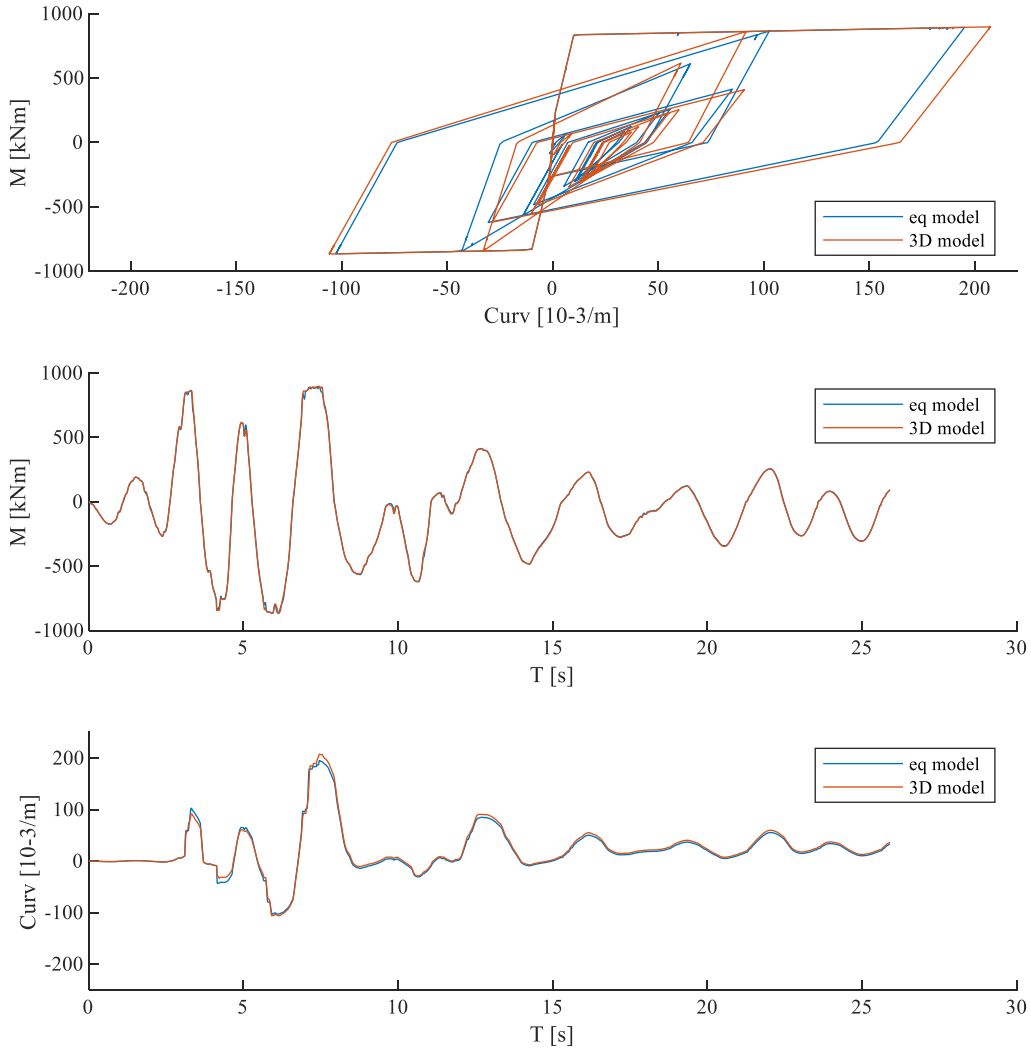

Figure 6.22: Response of the column at its base (*m60H9*, k = 2): (a) moment–curvature hysteretic response, (b) moment response history and (c) curvature response history

Slika 6.22: Odziv stebra ob vpetju (*m60H9*, k = 2): (a) histerezni odziv moment–ukrivljenost, (b) časovni potek momentov in (c) časovni potek ukrivljenosti

Structure m60H9 with ratio k = 1.3

The results of numerical analyses of structure *m60H9* with the ratio factor k = 1.3 (Figure 6.23) are presented in this section. The structure has eight columns; four columns in the analysed direction and two columns in the transverse direction. As for the previous case, 30 panels (six in the ground plan and five along the column height) are mounted at two external sides of the structure.

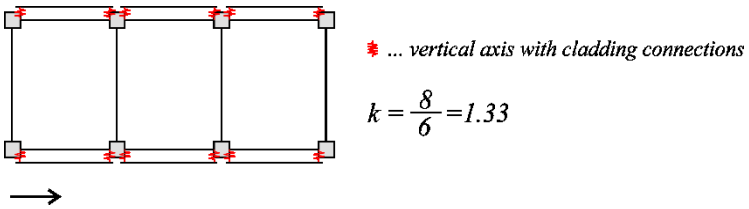

Figure 6.23: Precast structure *m60H9* with ratio factor k = 1.3

Slika 6.23: Montažna stavba *m60H9* s faktorjem k = 1.3

Figure 6.24 presents the maximum displacements of the column along its height and displacement response history at the top of the column. Results obtained with the equivalent model are in good agreement with the results of the full three-dimensional model.

Figure 6.25-6.27 compare the response of the connections. Maximum slips and forces along the structure's height and response histories for the connections of the panel at the top are shown. The match of these results is also very good.

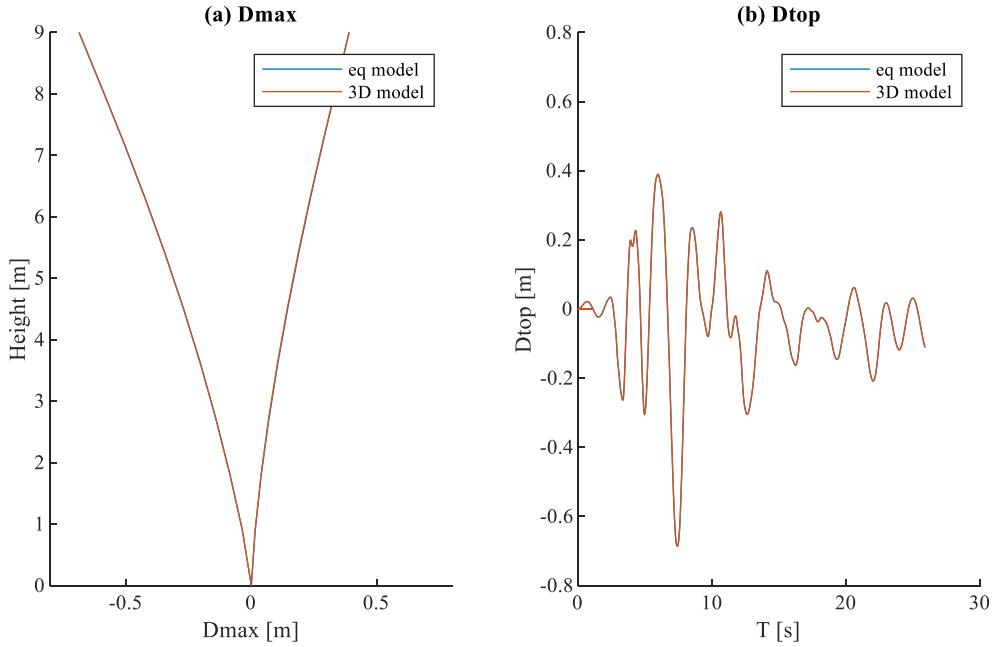

Figure 6.24: Displacements of the column (*m60H9*, k = 1.3): (a) displacement envelope along the column height and (b) displacement response history at the top of the column

Slika 6.24: Pomiki stebra (*m60H9*, k = 1.3): (a) ovojnica pomikov po višini stebra in (b) časovni potek pomikov na vrhu stebra

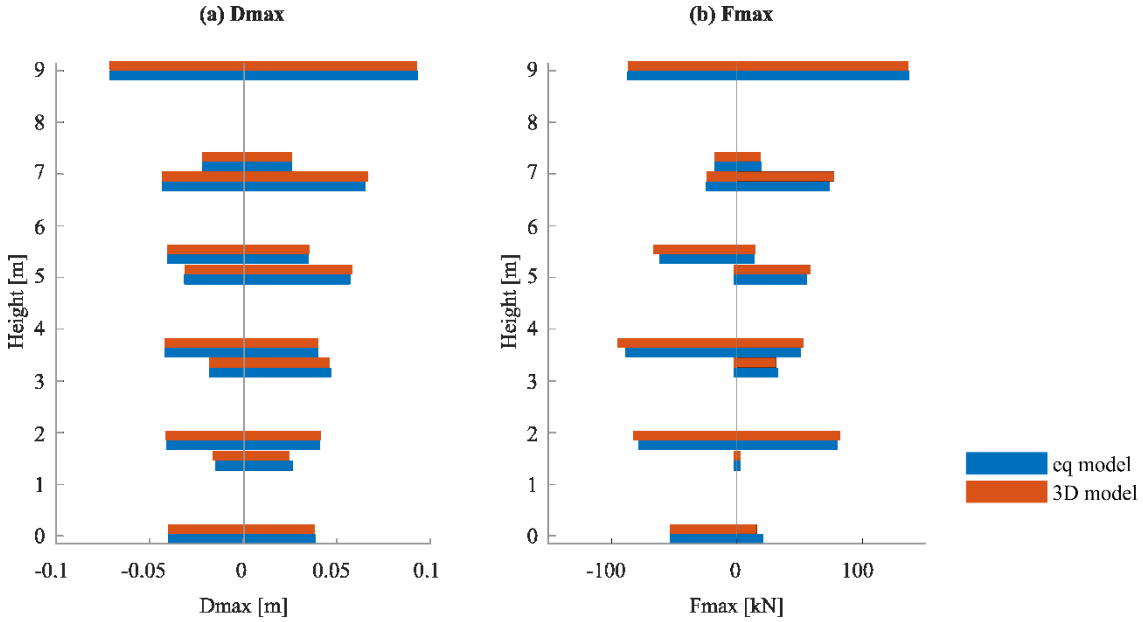

Figure 6.25: Maximum response of the connections (*m60H9*, k = 1.3): (a) slips and (b) forces in connections

Slika 6.25: Maksimalni odziv stikov (*m60H9*, k = 1.3): (a) zdrsi in (b) sile v stikih

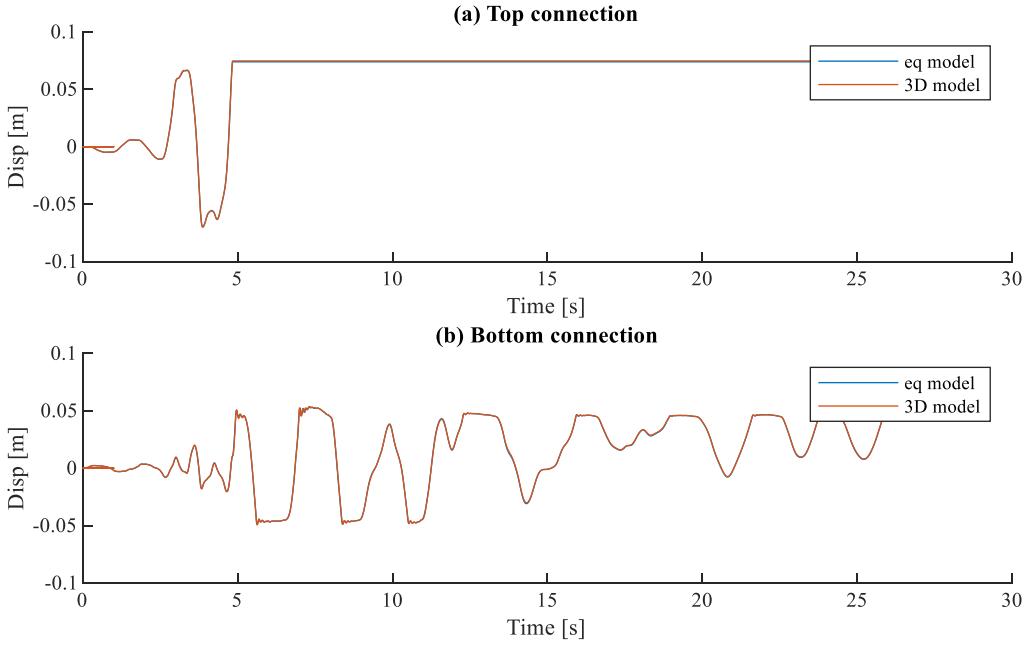

Figure 6.26: Displacement response histories at top and bottom connections of the top panel (*m60H9*, k = 1.3)

Slika 6.26: Časovni potek zdrsov v zgornjem in spodnjem stiku vrhnjega panela (*m60H9*, k = 1.3)

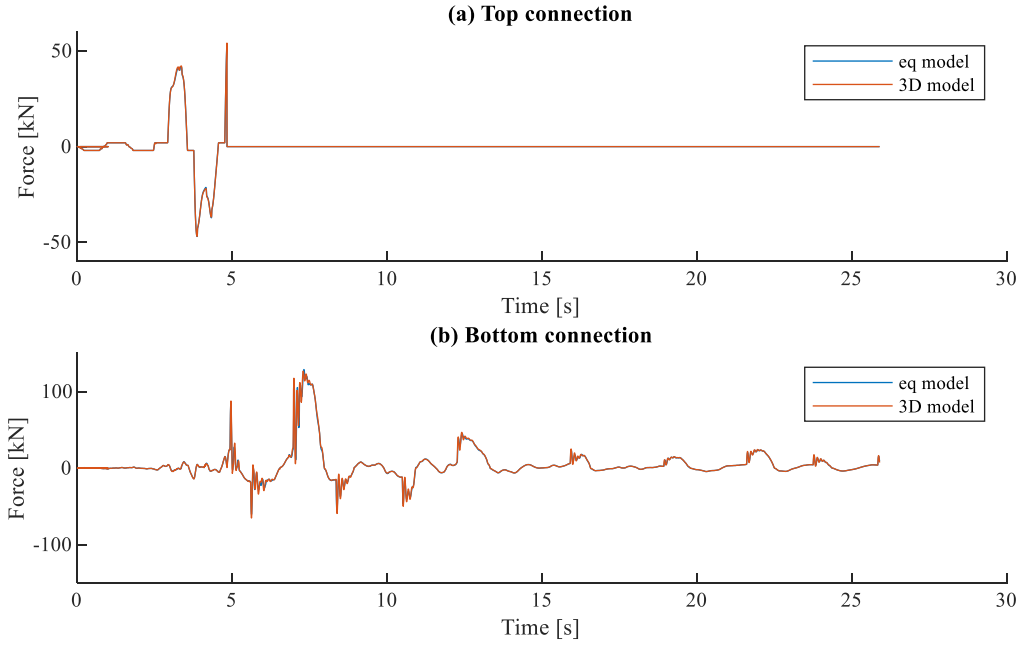

Figure 6.27: Force response histories at top and bottom connections of the top panel (*m60H9*, k = 1.3)

Slika 6.27: Časovni potek sil v zgornjem in spodnjem stiku vrhnjega panela (*m60H9*, k = 1.3)

Figure 6.28 presents the maximum shear force, moment and curvature along the column height, respectively. The response of the column at its base is compared in Figure 6.29, where the moment–curvature hysteretic response and response histories are presented. In general, the match of all the results is very good.

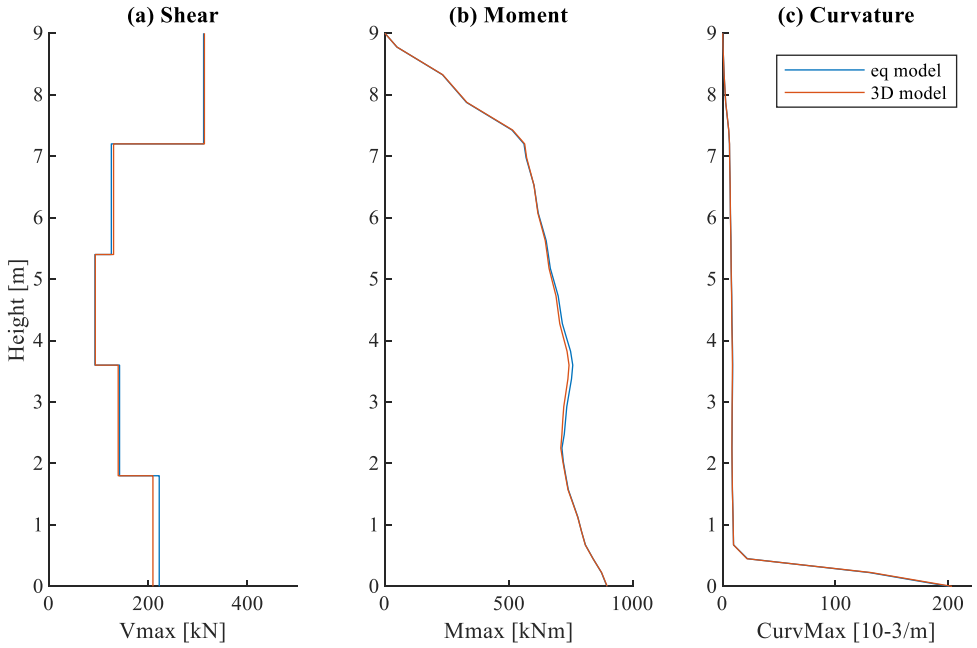

Figure 6.28: Maximum (a) shear forces, (b) moments and (c) curvatures along the column height (*m60H9*, k = 1.3)

Slika 6.28: Maksimalna (a) strižna sila, (b) momenti in (c) ukrivljenost po višini stebra (*m60H9*, k = 1.3)

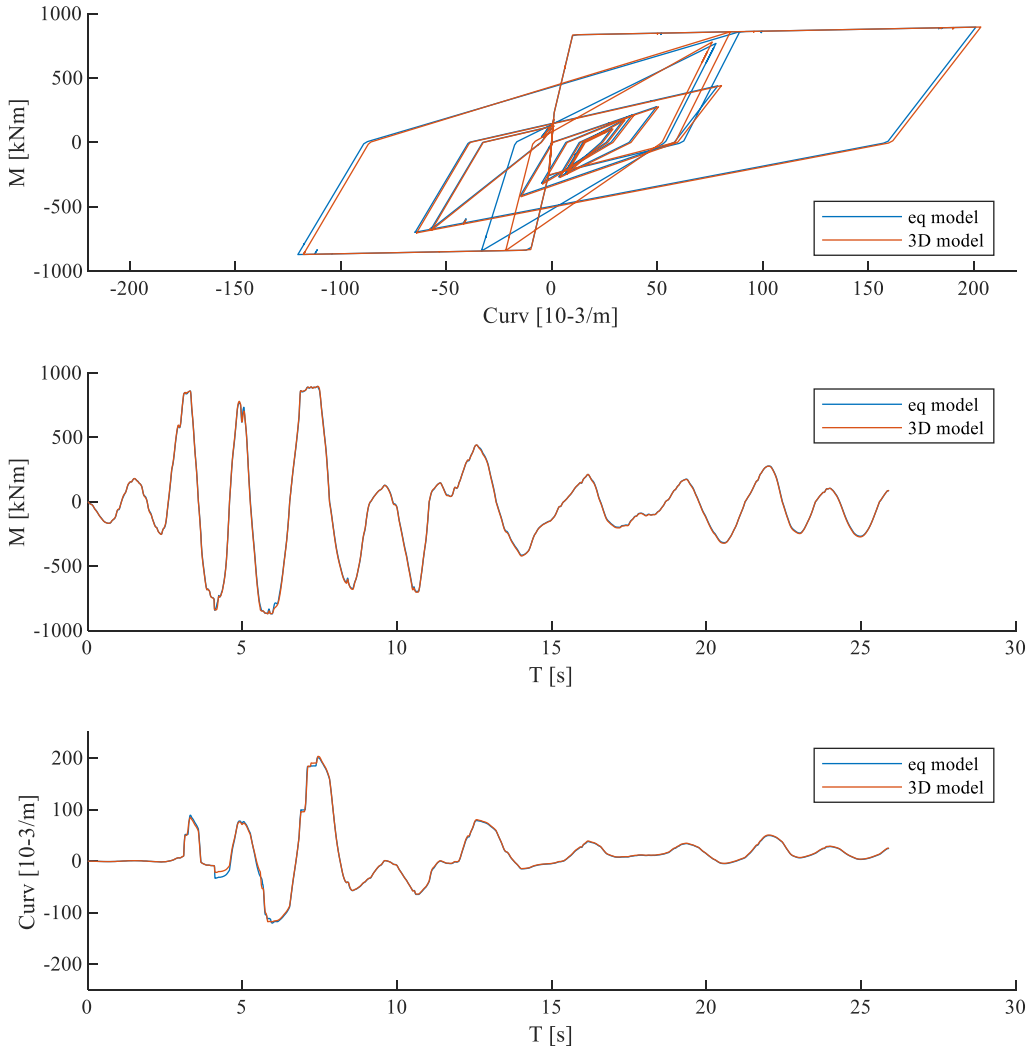

Figure 6.29: Response of the column at its base (*m60H9*, k = 1.3): (a) moment–curvature hysteretic response, (b) moment response history and (c) curvature response history

Slika 6.29: Odziv stebra ob vpetju (*m60H9*, k = 1.3): (a) histerezni odziv moment–ukrivljenost, (b) časovni potek momentov in (c) časovni potek ukrivljenosti

6.3 The response of precast structure and panels

This section describes the typical response of a precast structure in detail, and parameters essential for analysing demand and capacity on the fastening system are defined. Because the silicone sealant could, in certain cases, appreciably influence the response of panels, the typical response of the precast structure is presented for both cases, without and with silicone. In the following sections, the typical response mechanism is explained, and the most significant observations are shown for

three characteristic examples (structures *m60H5*, *m60H7* and *m60H9*) for the case of one accelerogram (ground motion record number 14, see Appendix A).

Here, the parameter *column drift along the single panel* is explained. As will be demonstrated later, it gives information about the response of the fastening system and is used to define the fastening system's demand and capacity.

In literature, the term drift is used to describe both the displacement and rotation of the element. Because of this inconsistency in the use and definition of the term, the terminology used in the dissertation must be clarified. Therefore, *drift* is the lateral displacement of one level relative to the level above or below, whereas *drift ratio* is the drift divided by the height between the considered levels.

As shown in Figure 6.30 and Equation 6.9, the drift of the column along the single panel (Δd_{col}) is defined as the difference in absolute column displacements at the top and bottom levels of the panel ($|d_{col,top} - d_{col,bottom}|$). Because the movement of the panels and connections is predominantly translational, this is the same as the absolute value of the difference in slips at the top and bottom connections ($|d_{slip,top} - d_{slip,bottom}|$).

$$\Delta d_{col,p} = \left|d_{col,top} - d_{col,bottom}\right| = \left|d_{slip,top} - d_{slip,bottom}\right| \tag{6.9}$$

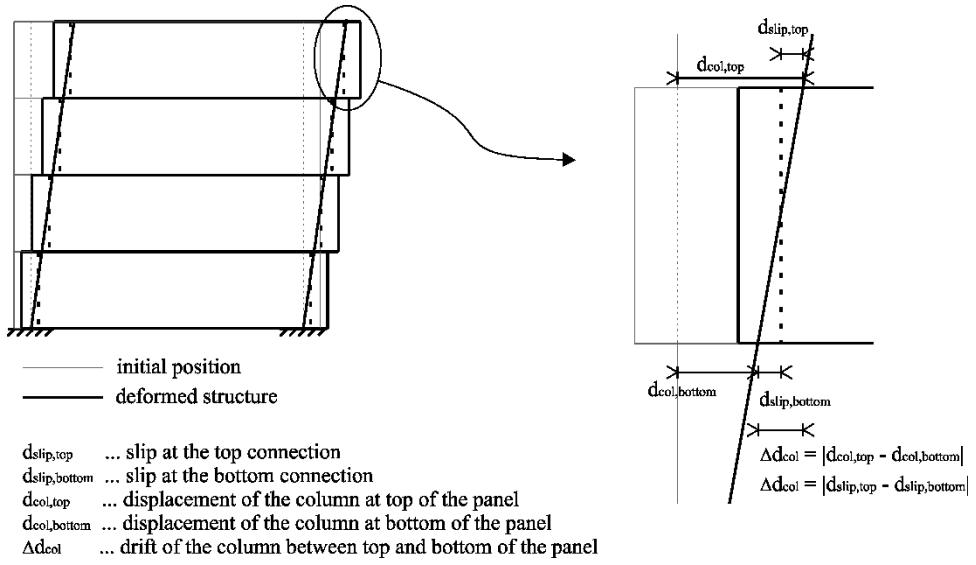

Figure 6.30: Column drift along the single panel
Slika 6.30: Pomik stebra na nivoju panela

In parametric study, maximum drifts were monitored (an example is shown in Figure 6.31). The connections failed at a certain column drift along a single panel. This drift at failure is the maximum

difference in slips at the top and bottom connections of the panel and presents the capacity of the complete fastening system (see also Sections 6.3.1 and 6.3.2).

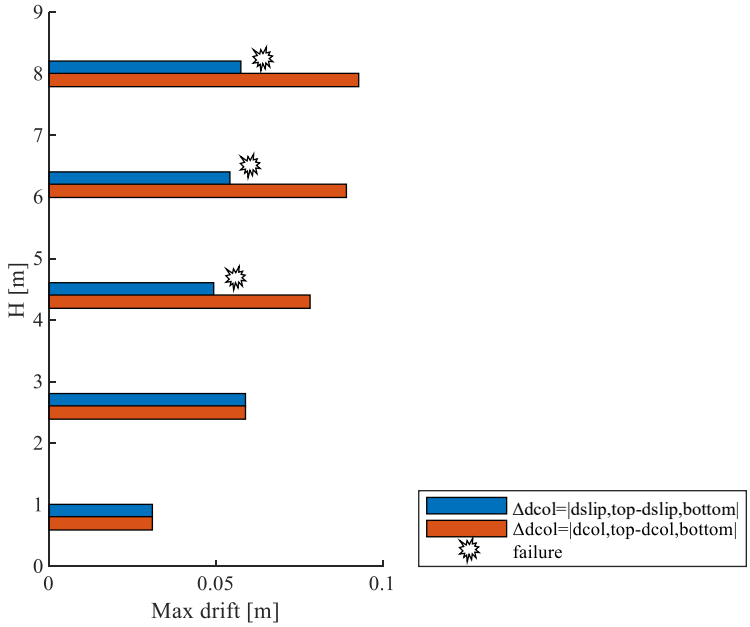

Figure 6.31: Maximum column drift along a single panel
Slika 6.31: Največji pomik stebra na nivoju panela

6.3.1 Interaction of the connections and demand on the fastening system

The parametric study results show that the top and bottom connections interact with each other and should be treated together as a complete fastening system. The demand on the complete fastening system can be expressed in terms of the column drift along the single panel. As observed during experiments, the top connection is the weakest component of the fastening system. After contact, its strength and stiffness are lower, and thus panel failure always occurs at the top connection.

A summary of the response is given in the following:

- At low seismic excitations, the panel behaves as if it was pinned at the top and sliding occurs only at the bottom connection.
- With increasing demand, sliding also occurs at the top connection. From that point on, the drift demand is taken over by both connections that move simultaneously.
- When the gap in one of the connections is depleted (either at the top or bottom connection), the stiffness of that connection increases and high lateral forces occur (demand on the connection).

- When the column and panel are in contact at one of the connections, the slip increases in the other connection until the gaps in both connections are depleted. There is a strong tendency of the fastening system to slide until the gaps in both connections are closed.

- After the gaps are depleted in both connections, the slips increase faster at the top connections because of their smaller stiffness compared to the bottom connections.

- Failure of the fastening system and panel occurs when the resistance of the top connection is reached.

Because column drift increases along column height, the panel at the top of the structure was most exposed to failure. However, if the bottom panel was fixed to the foundation, all the demand on bottom fastenings was taken only by the top connection. In that case, the first failure of the fastening system often occurred at the bottom panel. This will be further explained within the parametric study in Section 6.4.3.

6.3.2 Capacity of the fastening system

Because the demand on the fastening system is expressed with column drift along a single panel, the capacity of the fastenings should also be expressed this way. At this point, it is necessary to differentiate the capacity of the top connections in terms of connection slips and the capacity of the complete fastening system in terms of column drift along a single panel. In this section, they are denoted as *displacement capacity* of the top connection and *drift capacity* of the fastening system. The first is the capacity of the top connection that is always the same and is known from experiment; it is the sliding capacity of the connections plus approximately 3.5 cm after the gap in the connection is depleted. At this slip, the resistance of the top connection is reached (approx. 55 kN).

As explained earlier, the column drift along the single panel is the same as the difference in slips at the top and bottom connection. Thus, the drift capacity of the fastening system is the column drift along the single panel at which the connections fail.

The most important parameter that affects the drift capacity of the analysed system is construction imperfections. When connections are positioned eccentrically, there was no available sliding capacity, and failure of the fastening system occurred earlier. The influence of different eccentrical positions (*LL* and *LR*) is discussed in Section 6.4.2.

The drift capacity of the fastening system is the highest if connections are positioned centrally with no interaction between adjoining panels. When silicone sealant is applied, the drift capacity of the

fastening system somewhat reduces because the slips at top and bottom connections do not always occur in the opposite directions (Section 6.4.1).

If the bottom panel is fixed to the foundation, its response differs from the higher panel responses. The drift demand is taken over only by the top connection. For that reason, the drift capacity of the lowest fastening system (at the bottom panel) is much smaller than the drift capacity of fastening systems above (see Section 6.4.3). For that reason, the first failure of the fastening system sometimes occurred also at the bottom panel (Figure 6.33).

Figures 6.32 and 6.33 show column drift along the single panel at the failure of fastening systems for different parameter combinations. Results are presented as median values and standard deviations. The values within one standard deviation account for about 68% of the data. Figure 6.32 considers all failures of the fastening systems, whereas Figure 6.33 only examines column drifts along a single panel at the failure of the first fastening system. Parametric analyses performed at a_g = 0.675 g were considered. Note that failure of the panels was mostly observed for the accelerograms with response spectra above the EC8 elastic spectrum.

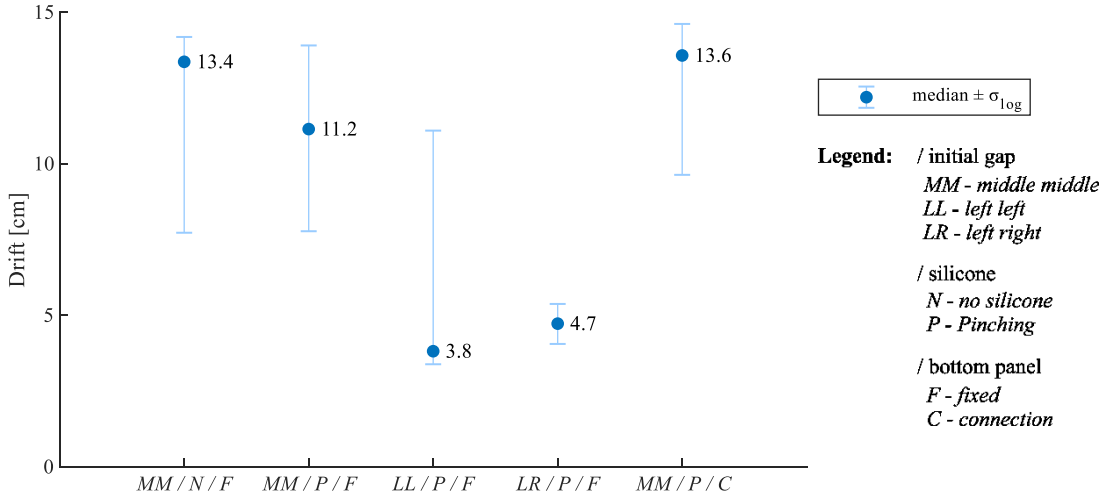

Figure 6.32: Column drift along the single panel at the failure of fastening system
Slika 6.32: Drifta stebra na nivoju panela pri porušitvi stikov

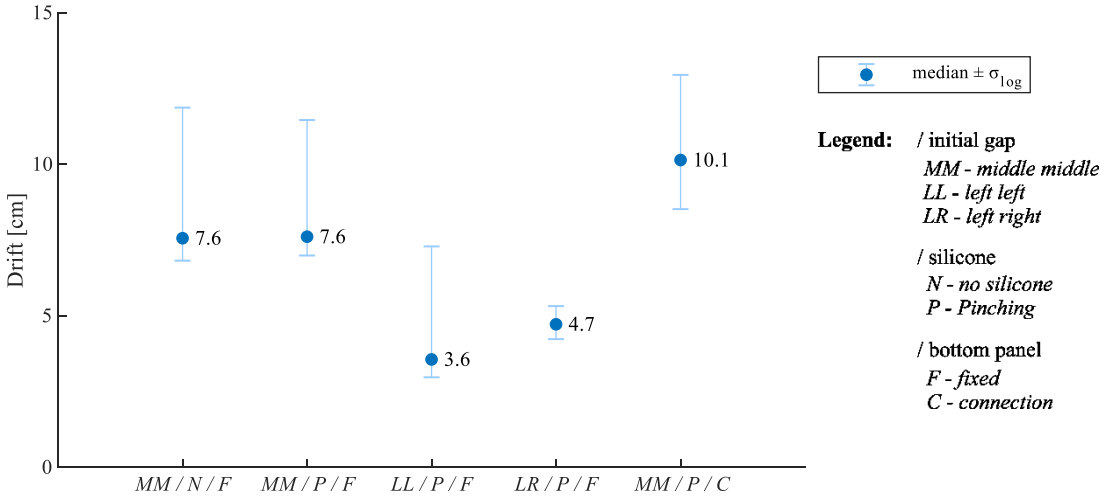

Figure 6.33: Column drift along the single panel at the failure of the first fastening system
Slika 6.33: Drifta stebra na nivoju panela pri porušitvi prvih stikov

The capacity of the fastening system is affected by different parameters, of which the most important are gaps in connections. After the connection gap closes, brittle failure of the top connection follows. To protect fastenings from failure, it is recommended to consider only the sliding capacity of the connections. Thus, the drift capacity could be expressed as a sum of the smallest gaps at the top and bottom connections.

The presence of silicone sealant and connection of the bottom panel to the foundation also influenced the drift capacity of the fastening system. If an interaction between the panels is present, displacements at top and bottom connections can occur in the same direction with respect to the column. If the bottom panel is fixed, the drift capacity of its fastening system is the same as the displacement capacity of only the top connections.

Thus, if we want a conservative estimation of capacity, the drift capacity could be defined as the sliding capacity of top connections that are the critical component. No safety factors are directly defined, but this is still a conservative estimation. After the contact of column and panel is reached, the displacement can increase for approximately another 3.5 cm, which is not taken into account. This displacement could be considered a safety measure. This conservative estimation means that a structure with gaps that are already completely closed in its initial position is unsafe and will be likely to sustain substantial damage to the connections in the event of an earthquake.

6.3.3 Typical response of the structure and panels without silicone sealant

The response of connections and panels depended on the intensity of seismic excitation and the deformations of columns, as shown in Figure 6.34. Because there was no silicone sealant in between panels, each panel slid individually.

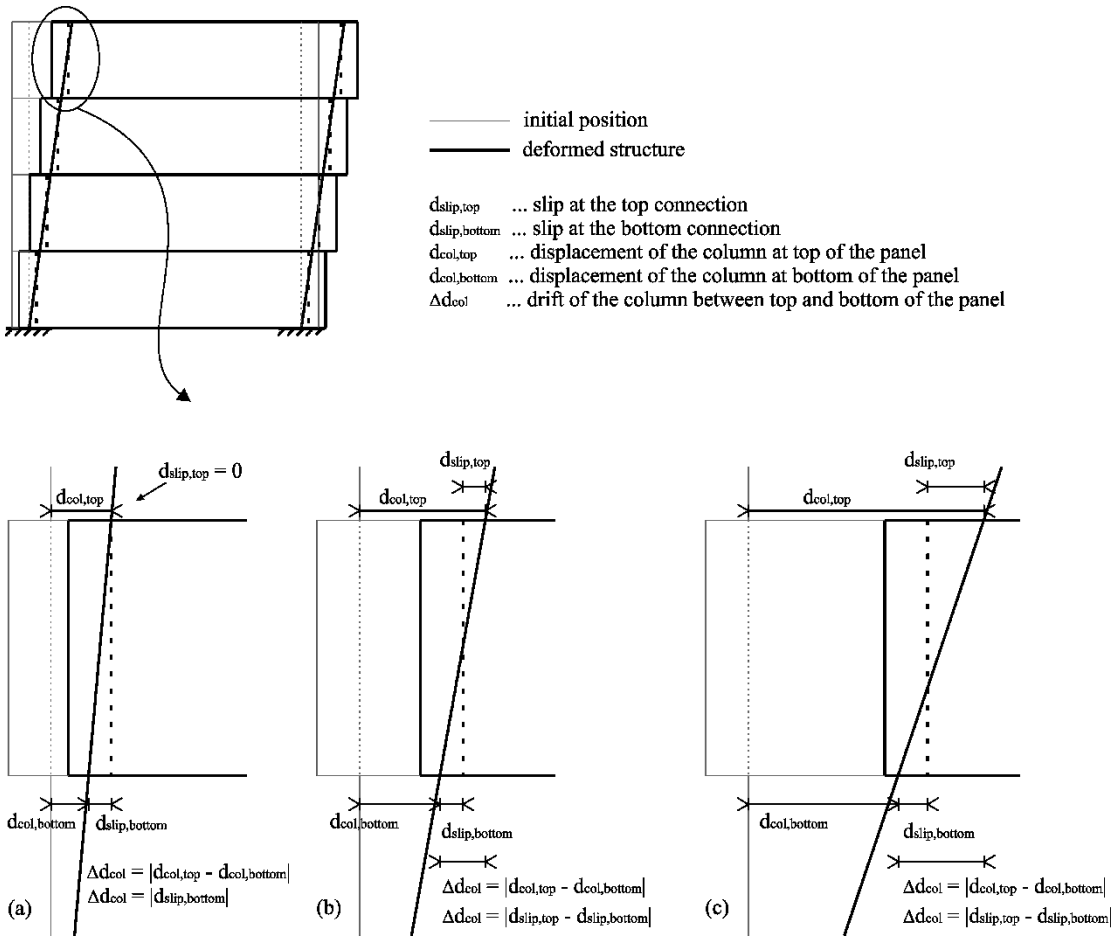

Figure 6.34: Typical response of the structure with horizontal cladding panels: (a) small column rotations, (b) medium column rotations and (c) large column rotations

Slika 6.34: Značilen odziv konstrukcije s horizontalnimi paneli: (a) majhne rotacije stebra, (b) srednje rotacije stebra in (c) velike rotacije stebra

(1) At lower seismic intensities, there were no relative displacements between the top of the panel and the column (Figure 6.34 a). Panels followed the movement of the main precast structure as pinned to the columns at the level of top connections and slid over the bottom fastening device.

(2) When the structure was subjected to stronger seismic excitations, deformations of columns become considerable, and sliding also occurred at the top connections. Slips at top and bottom connections typically occurred in the opposite directions (Figure 6.34 b). The movement of the panels was predominantly translational.

Slips at the top and bottom connections were usually larger at panels higher along the column (see Figures 6.35-6.37 a). Forces that occurred in the connections were relatively small and only due to the friction (Figures 6.35-6.37 b). They were somewhat larger at bottom connections.

Column drift along the single panel, that is, the difference in slips at top and bottom connections ($\Delta d_{col} = |d_{slip,top} - d_{slip,bottom}|$), increases along the column height (Figure 6.38). No failures of the connections were observed in the analysed structures.

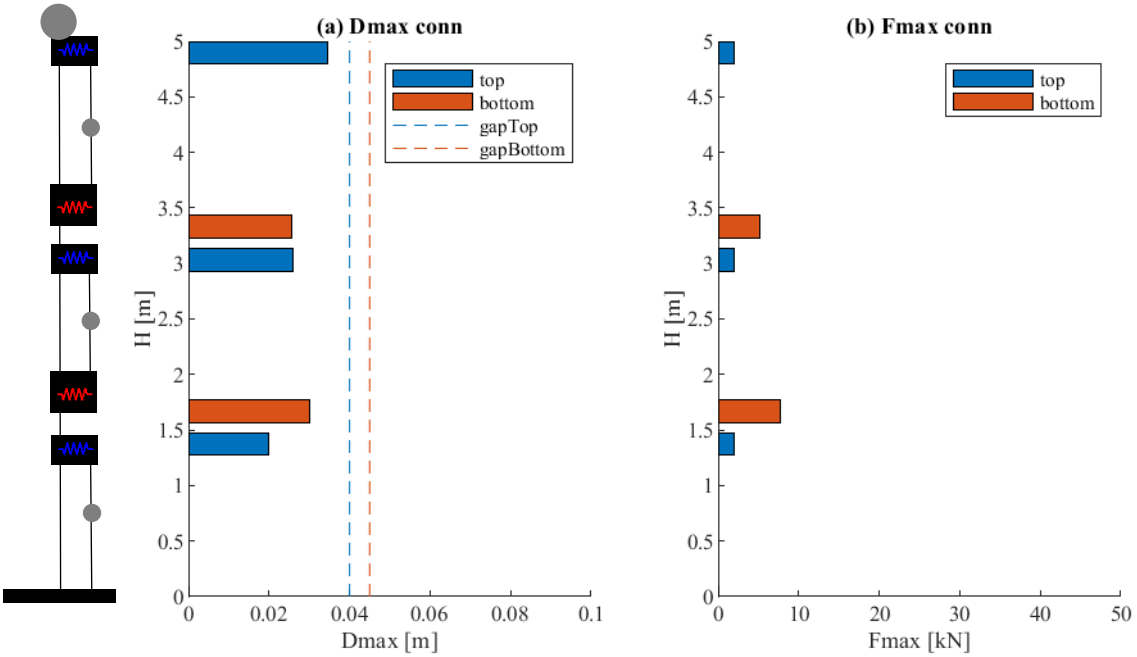

Figure 6.35: Structure *m60H5* without silicone sealant at a_g = 0.25 g: (a) maximum slips in cladding connections, (b) maximum forces in cladding connections

Slika 6.35: Montažna hala *m60H5* brez silikonskega tesnila pri a_g = 0.25 g: (a) največji zdrsi fasadnih stikov, (b) največje sile v fasadnih stikih

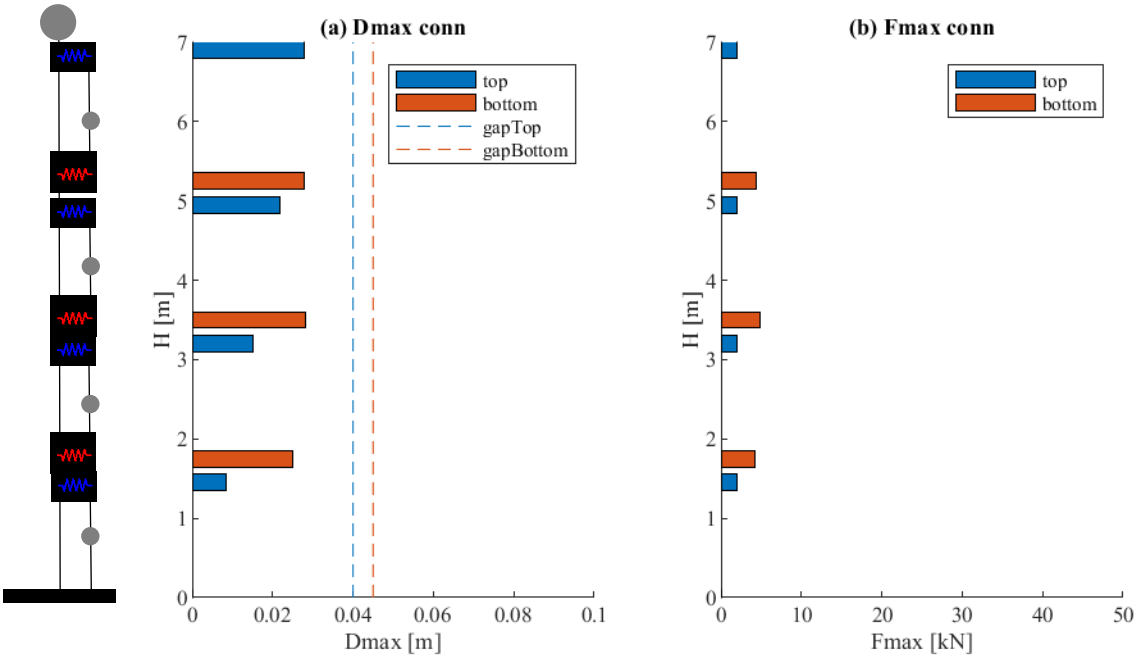

Figure 6.36: Structure *m60H7* without silicone sealant at a_g = 0.25 g: (a) maximum slips in cladding connections, (b) maximum forces in cladding connections

Slika 6.36: Montažna hala *m60H7* brez silikonskega tesnila pri a_g = 0.25g: (a) največji zdrsi fasadnih stikov, (b) največje sile v fasadnih stikih

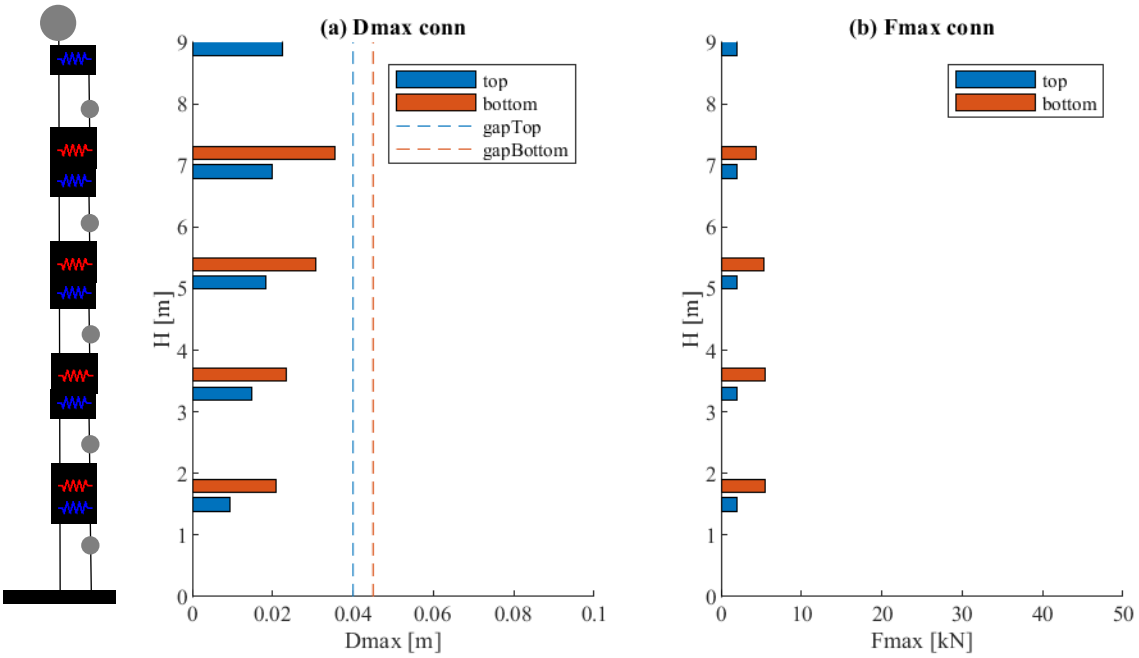

Figure 6.37: Structure *m60H9* without silicone sealant at a_g = 0.25 g: (a) maximum slips in cladding connections, (b) maximum forces in cladding connections

Slika 6.37: Montažna hala *m60H9* brez silikonskega tesnila pri a_g = 0.25g: (a) največji zdrsi fasadnih stikov, (b) največje sile v fasadnih stikih

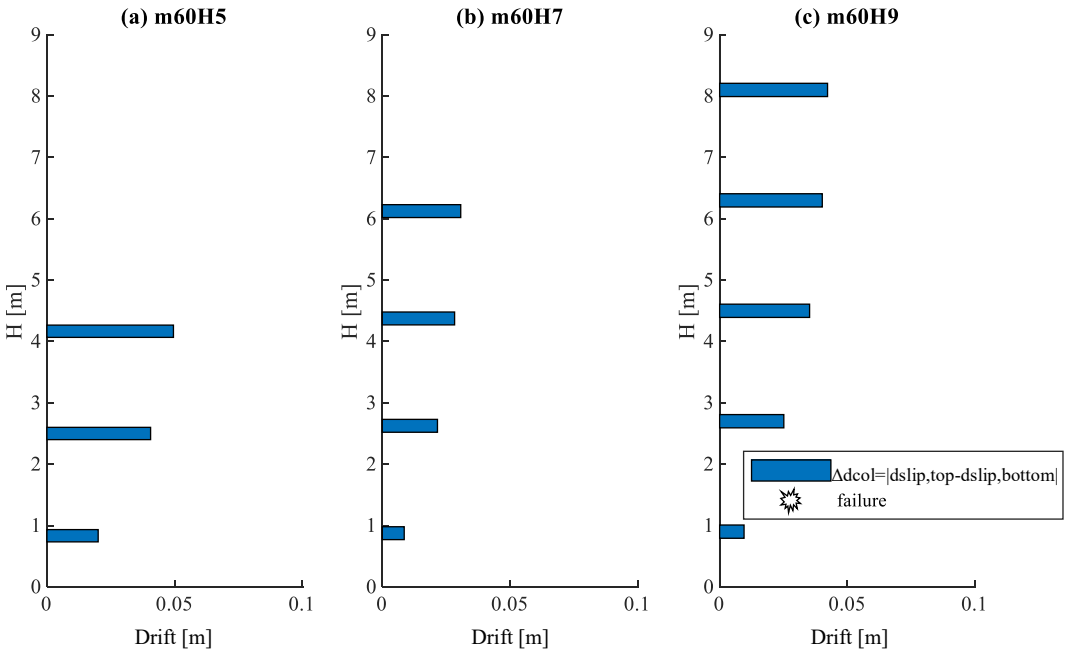

Figure 6.38: Maximum difference in slips at top and bottom connections (i.e. column drift along each panel) in structures without silicone sealant at a_g = 0.25 g: (a) *m60H5*, (b) *m60H7* and (c) *m60H9*

Slika 6.38: Največja razlika v pomikih v zgornjem in spodnjem stiku (t.j. drift stebra na nivoju panela) pri halah brez silikonskega tesnila in a_g = 0.25 g: (a) *m60H5*, (b) *m60H7*, (c) *m60H9*

(3) When the deformations of columns increase (Figure 6.34 c), the column comes into contact with the panel (i.e. gaps at the top and bottom connections are depleted). Maximum slips in connections are shown in Figures 6.39-6.41 (a) for three examples at a_g = 0.675 g. Note that structure *m60H5* failed in bending before most of the gaps were closed. At structures *m60H7* and *m60H9,* yielding of the column was observed. As observed earlier, the max column drift along the single panel increases along the column height (Figure 6.42). No failure of the connections was observed for the presented characteristic cases.

Due to the impacts between panels and columns, forces in the connections were substantially increased. The maximum impact forces at single connections were typically in the range of 10 to 20 kN at a_g = 0.675 g (see Figures 6.39-6.41 b) and also 45 kN for other structures analysed within the parametric study. Forces in the connections were different along the column height and different at top and bottom connections. Because of the response of connections in opposite directions (see Figure 6.34), forces at top and bottom connections partially cancelled each other out. The total contribution of impact forces on the response of columns is analysed in the following sections (see Section 6.4).

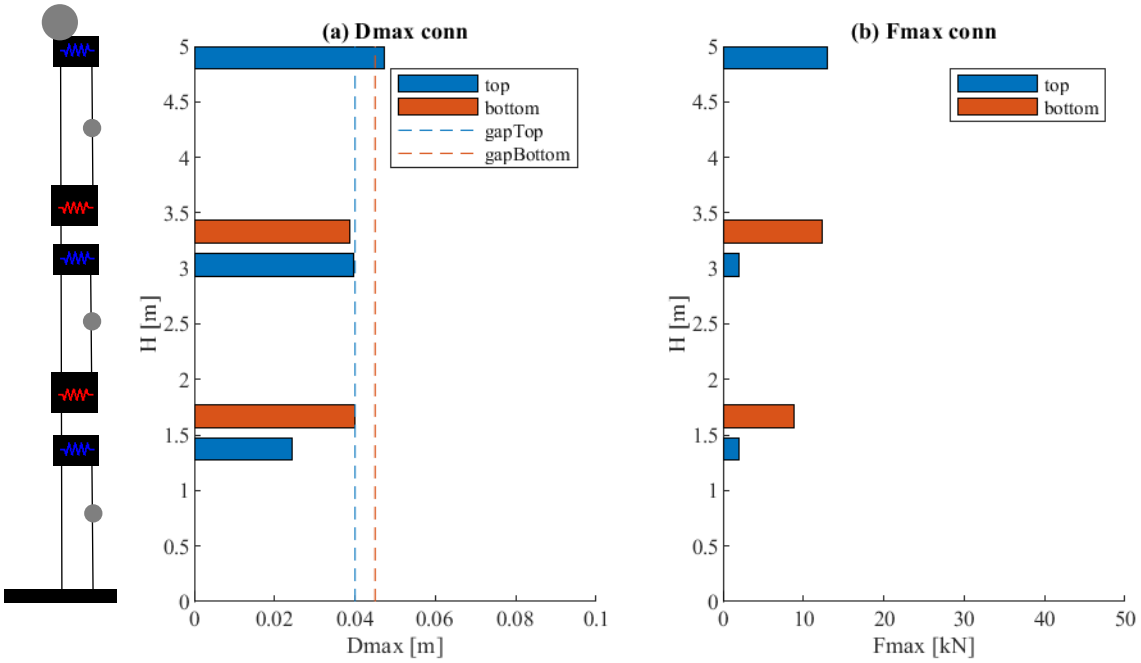

Figure 6.39: Structure *m60H5* without silicone sealant at a_g = 0.675 g: (a) maximum slips in cladding connections, (b) maximum forces in cladding connections

Slika 6.39: Montažna hala *m60H5* brez silikonskega tesnila pri a_g = 0.675 g: (a) največji relativni pomiki fasadnih stikov, (b) največje sile v fasadnih stikih

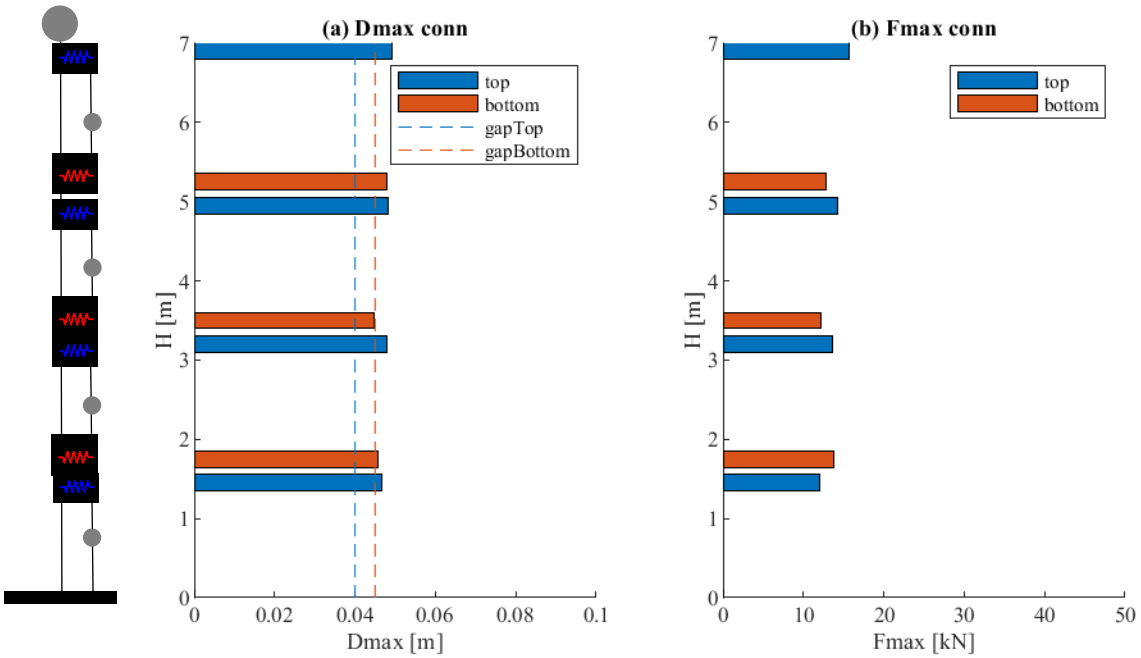

Figure 6.40: Structure *m60H7* without silicone sealant at a_g = 0.675 g: (a) maximum slips in cladding connections, (b) maximum forces in cladding connections

Slika 6.40: Montažna hala *m60H7* brez silikonskega tesnila pri a_g = 0.675g: (a) največji zdrsi fasadnih stikov, (b) največje sile v fasadnih stikih

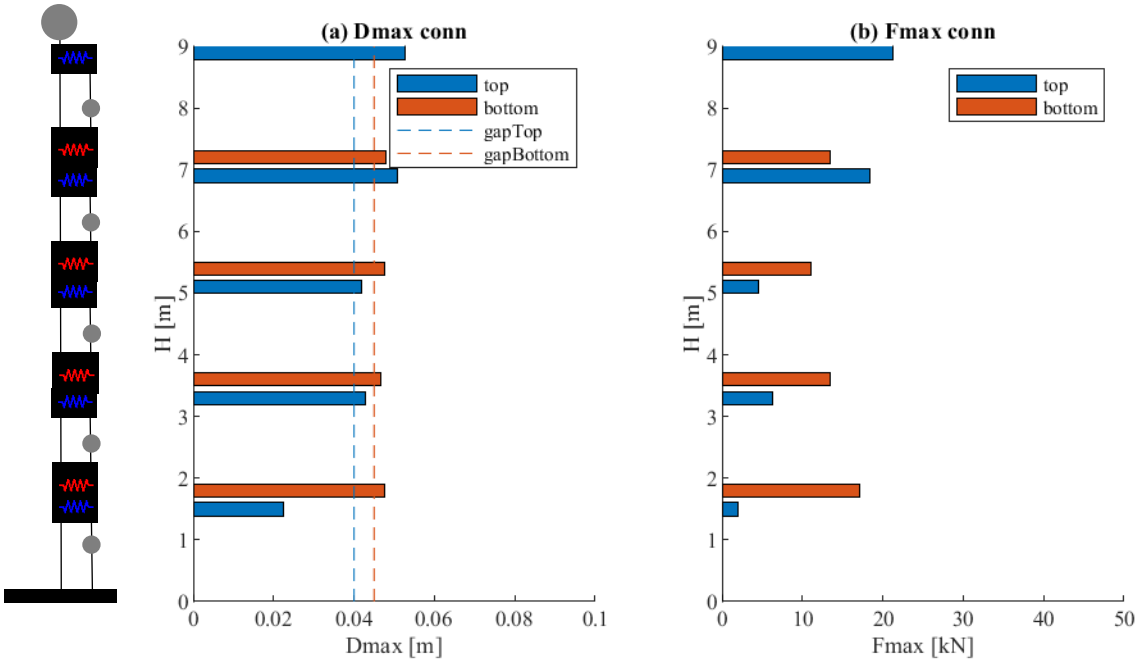

Figure 6.41: Structure *m60H9* without silicone sealant at a_g = 0.675 g: (a) maximum slips in cladding connections, (b) maximum forces in cladding connections

Slika 6.41: Montažna hala *m60H9* brez silikonskega tesnila pri a_g = 0.675g: (a) največji zdrsi fasadnih stikov, (b) največje sile v fasadnih stikih

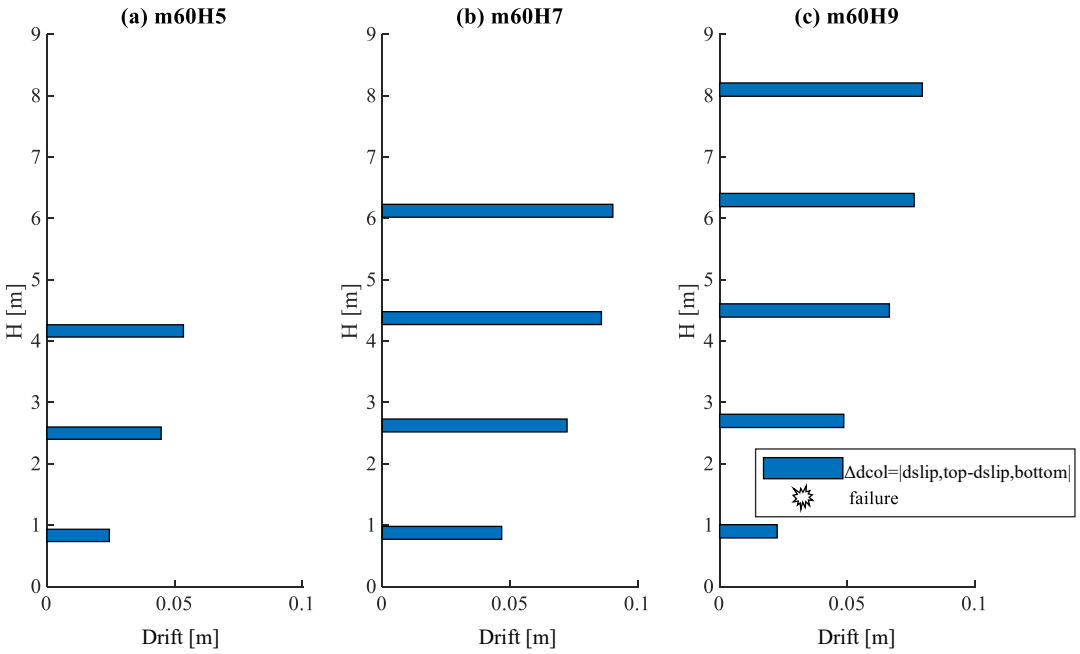

Figure 6.42: Maximum difference in slips at top and bottom connections (i.e. column's drift along each panel) in structures without silicone sealant at a_g = 0.675 g: (a) *m60H5*, (b) *m60H7* and (c) *m60H9*

Slika 6.42: Največja razlika v pomikih v zgornjem in spodnjem stiku (t.j. drift stebra na nivoju panela) pri halah brez silikonskega tesnila in a_g = 0.675 g: (a) *m60H5*, (b) *m60H7*, (c) *m60H9*

Figures 6.43 and 6.44 show displacement and force response histories for the connections of structure *m60H9* at a_g = 0.675 g. As shown, gaps might be depleted only at some connections (either top or bottom, and not for all panels), and impacts do not necessarily occur at all connections at the same time. As already mentioned, forces at top and bottom connections typically act in opposite directions.

The largest influence on the response is expected at the outer column, where there are two vertical axes of the connections on the column. Results are presented in Figure 6.45 for three characteristic examples at the highest intensity (a_g = 0.675 g). Results for a_g = 0.25 g can be found in Appendix B.

Figure 6.45 shows the maximum shear demand in the column compared to M_u/H. Results are shown for a_g = 0.675 g because, at design intensity (a_g = 0.25 g), there were no impacts between panels and columns, and thus no important influence of connections on shear demand in columns. As shown in Figure 6.45, the shear demand might exceed the shear force M_u/H because of the lateral forces induced from the connections during the impacts. At impacts between the column and panels, the higher modes of vibration are activated that lower the position of the resultant force closer to the column base. An increase of the relative contribution of the higher modes during the inelastic response was observed for RC walls and multi-storey precast structures (UL, POLIMI, 2012). Although the shear demand has exceeded the force M_u/H, no shear failure was recorded because the shear resistance V_R of the columns was much higher.

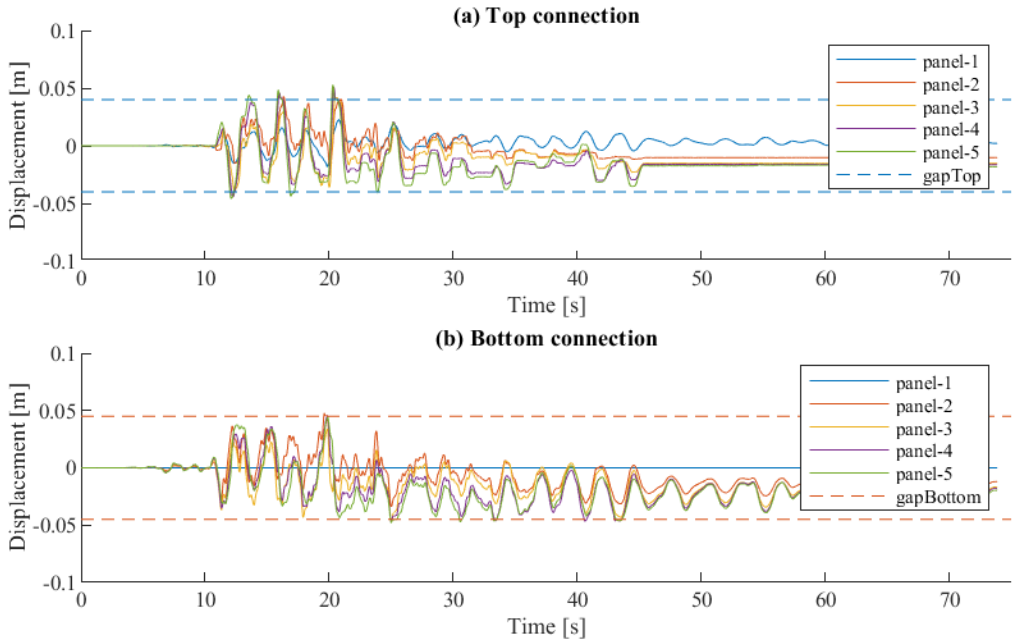

Figure 6.43: Structure *m60H9* without silicone sealant at a_g = 0.675 g: (a) displacement response history for the top connections, (b) displacement response history for the bottom connections

Slika 6.43: Montažna hala *m60H9* brez silikonskega tesnila pri a_g = 0.675 g: (a) časovni potek pomikov v zgornjih stikih, (b) časovni potek pomikov v spodnjih stikih

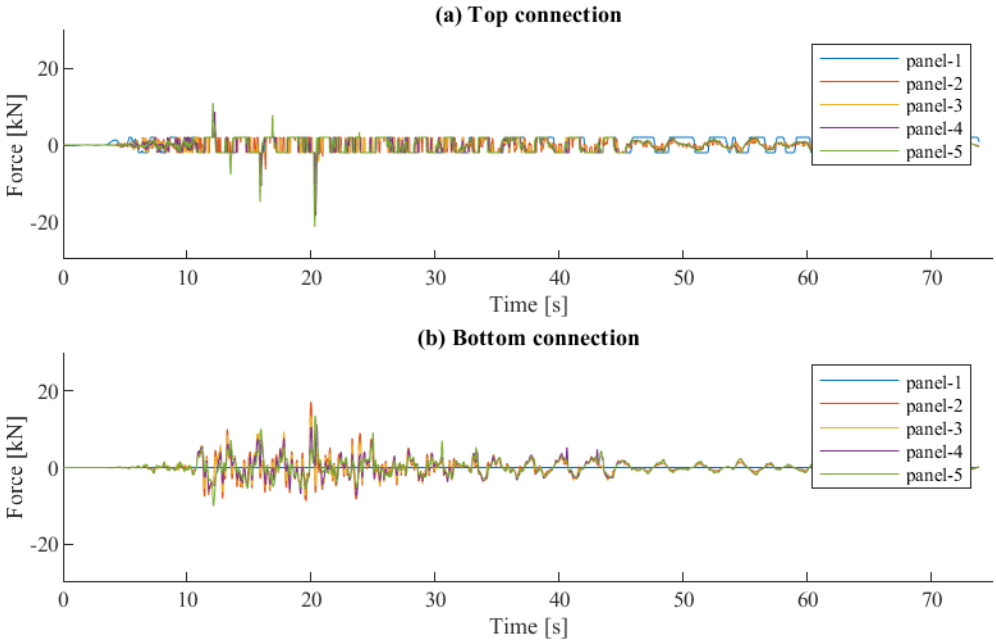

Figure 6.44: Structure *m60H9* without silicone sealant at a_g = 0.675 g: (a) force response history for the top connections, (b) force response history for the bottom connections

Slika 6.44: Montažna hala *m60H9* brez silikonskega tesnila pri a_g = 0.675 g: (a) časovni potek sil v zgornjih stikih, (b) časovni potek sil v spodnjih stikih

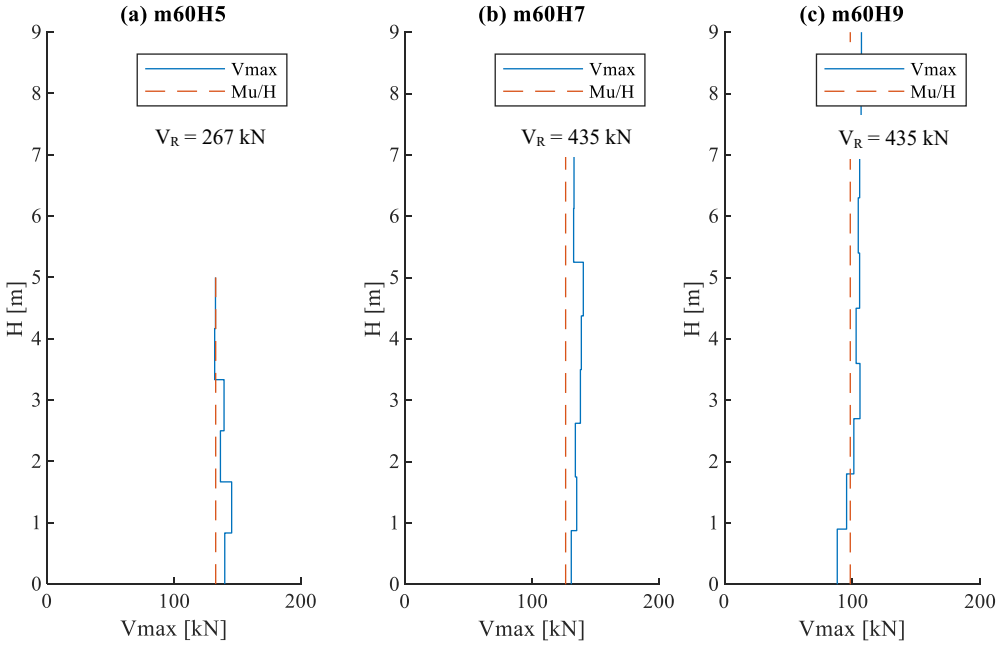

Figure 6.45: Maximum shear force along the column height for structures without silicone sealant at a_g = 0.675 g: (a) *m60H5*, (b) *m60H7* and (c) *m60H9*

Slika 6.45: Maksimalna strižna sila po višini stebra pri halah brez silikonskega tesnila in a_g = 0.675 g: (a) *m60H5*, (b) *m60H7*, (c) *m60H9*

6.3.4 Typical response of the structure and panels with silicone sealant

If the joints between the panels are sealed with silicone, the response of the panels is somewhat different. As stated previously, relevant response parameters are shown for three characteristic examples here, and more results are provided in Appendix C.

The influence of silicone sealant on the response of panels and slips at the connections is noticeable. When there was no silicone, the relative displacements between the panel and main structure at the top and bottom connection occurred in opposite directions. With silicone sealant and increased interaction between the panels, responses of top and bottom connections were not necessarily in opposite directions.

Different panel responses are shown in Figure 6.46. At larger column displacements and due to the interaction between the panels, one or more panels at the top of the structure shifted completely to one side of the column. Relative displacements between the column and panel at the top of the structure were in the same direction at the level of top and bottom connections (Figure 6.46 b). Regardless of the panel position, the column drift along the single panel was equal to the absolute value of the difference in slips at top and bottom connections (Figure 6.46 a and b).

Because of the interaction between panels, they lagged behind deformations of the column. Relative displacements were the largest at top connections of the top panel, where gaps closed earlier compared to the structure without silicone sealant (Figures 6.47 a-6.49 a). The maximum displacements at bottom connections were almost the same for all panels along the column height.

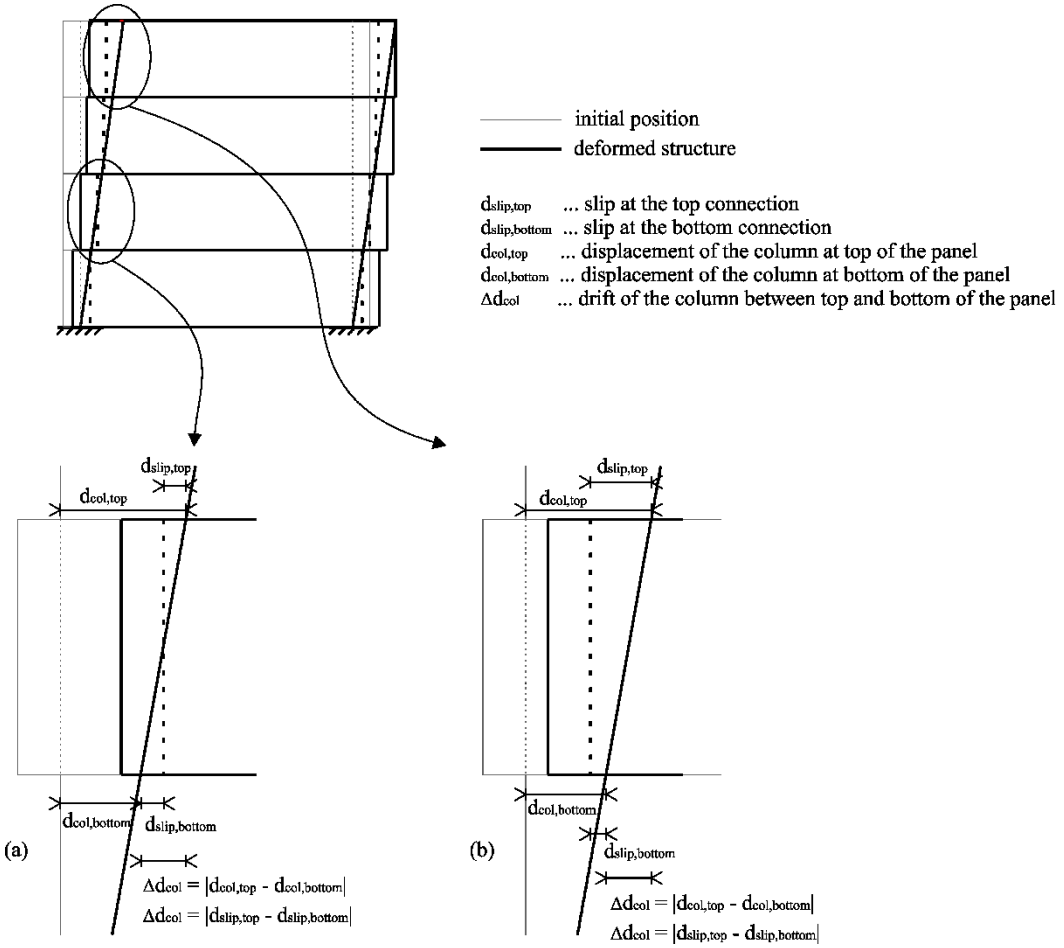

Figure 6.46: Response of the structure with silicone sealant between the horizontal panels: (a) response of top and bottom connections in opposite directions and (b) response of top and bottom connections in the same direction with respect to the column

Slika 6.46: Odziv konstrukcije s silikonskim tesnilom med horizontalnimi paneli: (a) relativni pomiki v zgornjem in spodnjem stiku v nasprotnih smereh, (b) relativni pomiki v zgornjem in spodnjem stiku v isti smeri glede na steber

Figures 6.47 (b)-6.49 (b) show the maximum forces at cladding connections. The highest forces (10-15 kN) occurred at the top connection of the top panel because the gap was closed. Otherwise, forces in other connections were relatively small and only because of friction during sliding.

The column drift along the single panel increased along the column height (Figure 6.50 and Figure 6.54). No failure of connections was observed for the presented characteristic cases. However, in general, the failure of the connections occurs earlier if silicone sealant is used (i.e. at smaller column drifts). This is discussed in the following sections.

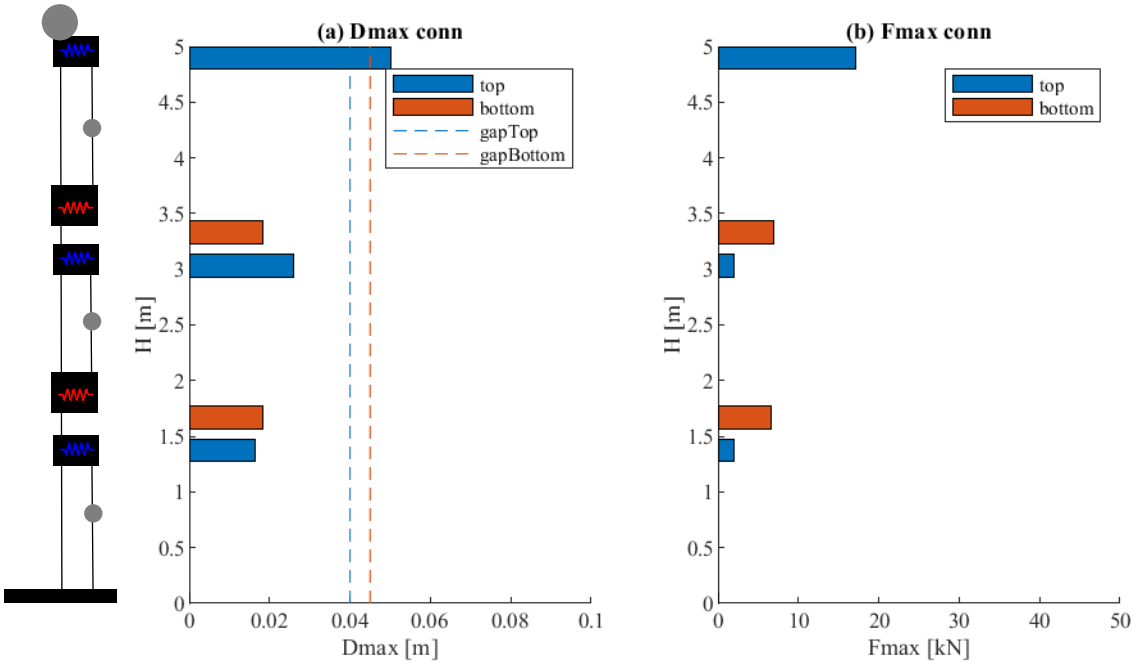

Figure 6.47: Structure *m60H5* with silicone sealant at a_g = 0.25 g: (a) maximum slips in cladding connections, (b) maximum forces in cladding connections

Slika 6.47: Montažna hala *m60H5* s silikonskim tesnilom pri a_g = 0.25g: (a) največji zdrsi fasadnih stikov, (b) največje sile v fasadnih stikih

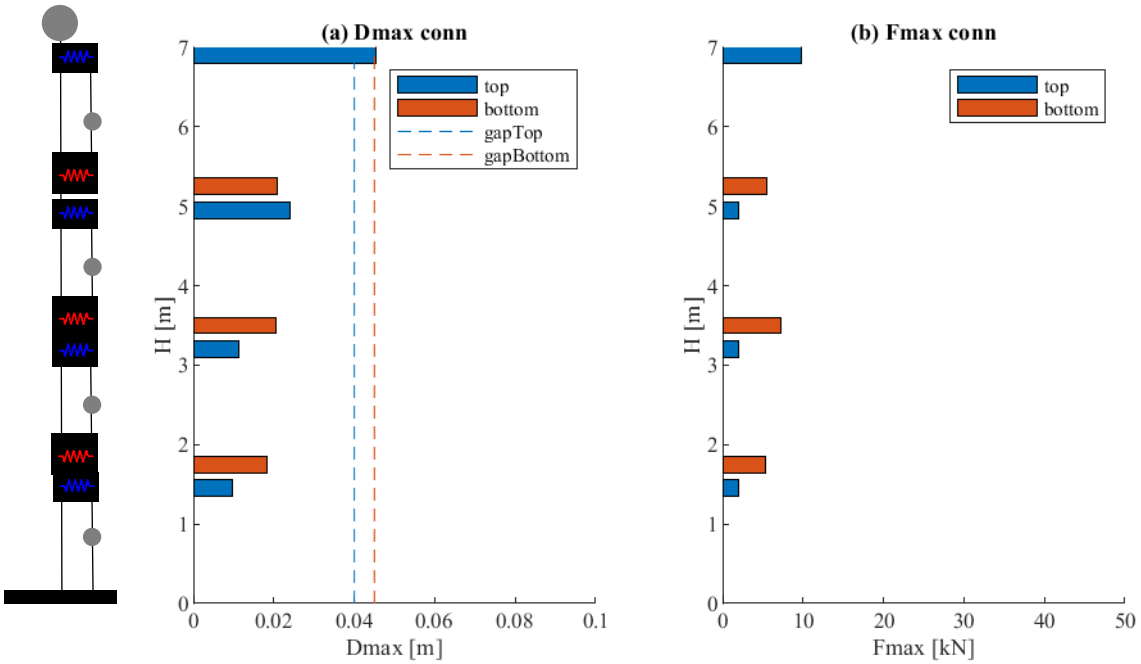

Figure 6.48: Structure *m60H7* with silicone sealant at a_g = 0.25 g: (a) maximum slips in cladding connections, (b) maximum forces in cladding connections

Slika 6.48: Montažna hala *m60H7* s silikonskim tesnilom pri a_g = 0.25g: (a) največji zdrsi fasadnih stikov, (b) največje sile v fasadnih stikih

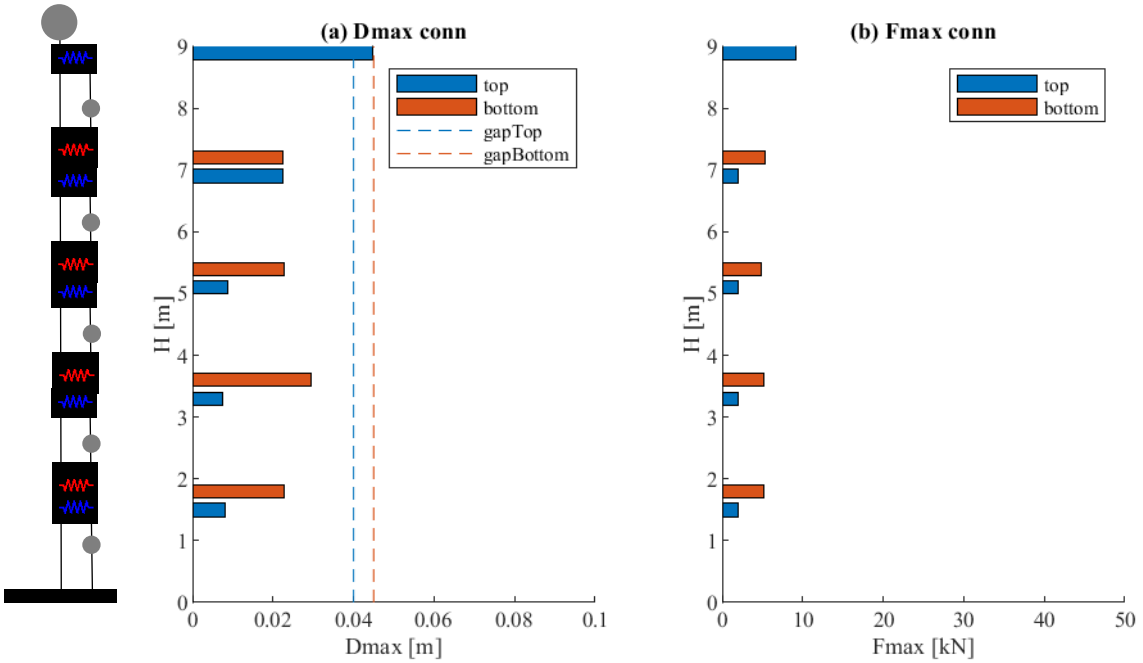

Figure 6.49: Structure *m60H9* with silicone sealant at a_g = 0.25 g: (a) maximum slips in cladding connections, (b) maximum forces in cladding connections

Slika 6.49: Montažna hala *m60H9* s silikonskim tesnilom pri a_g = 0.25g: (a) največji zdrsi fasadnih stikov, (b) največje sile v fasadnih stikih

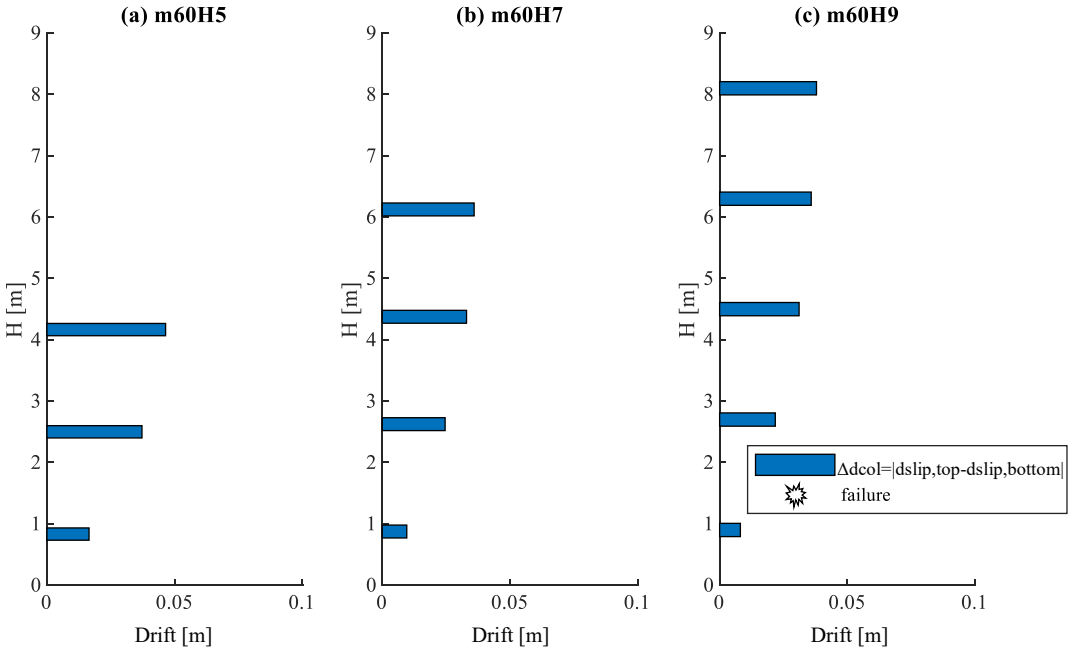

Figure 6.50: Maximum difference in slips at top and bottom connections (i.e. column drift along each panel) in structures with silicone sealant at a_g = 0.25 g: (a) *m60H5*, (b) *m60H7* and (c) *m60H9*

Slika 6.50: Največja razlika v pomikih v zgornjem in spodnjem stiku (t.j. drift stebra na nivoju panela) pri halah s silikonskim tesnilom in a_g = 0.25 g: (a) *m60H5*, (b) *m60H7*, (c) *m60H9*

With increasing intensity, the forces that occurred in the top connection of the top panels were larger because of stronger impacts (30-35 kN). At very strong intensity (e. g. a_g = 0.675 g), gaps also closed at lower panels and bottom connections (see Figures 6.52 and 6.53). Forces that occurred in the connections were considerably higher (up to 50 kN). The highest forces at top connections occurred at the top panel, whereas the highest forces at the bottom connection were observed at lower panels. Structure *m60H5* failed due to exceeded bending capacity of columns before impact at lower panels occurred.

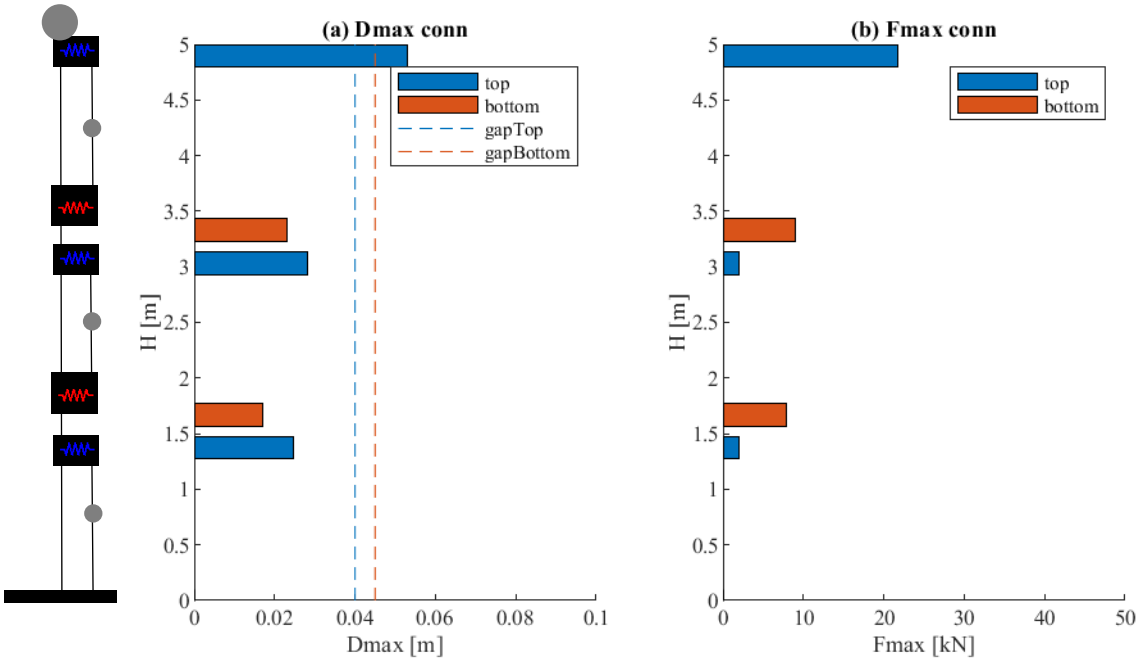

Figure 6.51: Structure *m60H5* with silicone sealant at a_g = 0.675 g: (a) maximum slips in cladding connections, (b) maximum forces in cladding connections

Slika 6.51: Montažna hala *m60H5* s silikonskim tesnilom pri a_g = 0.675g: (a) največji zdrsi fasadnih stikov, (b) največje sile v fasadnih stikih

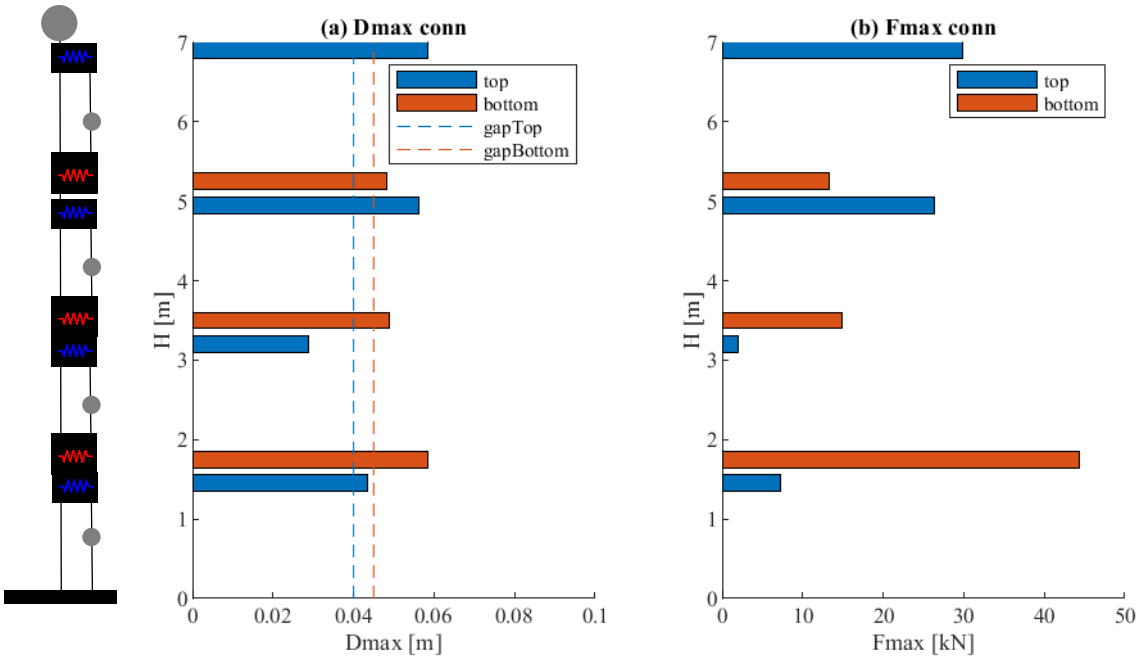

Figure 6.52: Structure *m60H7* with silicone sealant at a_g = 0.675 g: (a) maximum slips in cladding connections, (b) maximum forces in cladding connections

Slika 6.52: Montažna hala *m60H7* s silikonskim tesnilom pri a_g = 0.675g: (a) največji zdrsi fasadnih stikov, (b) največje sile v fasadnih stikih

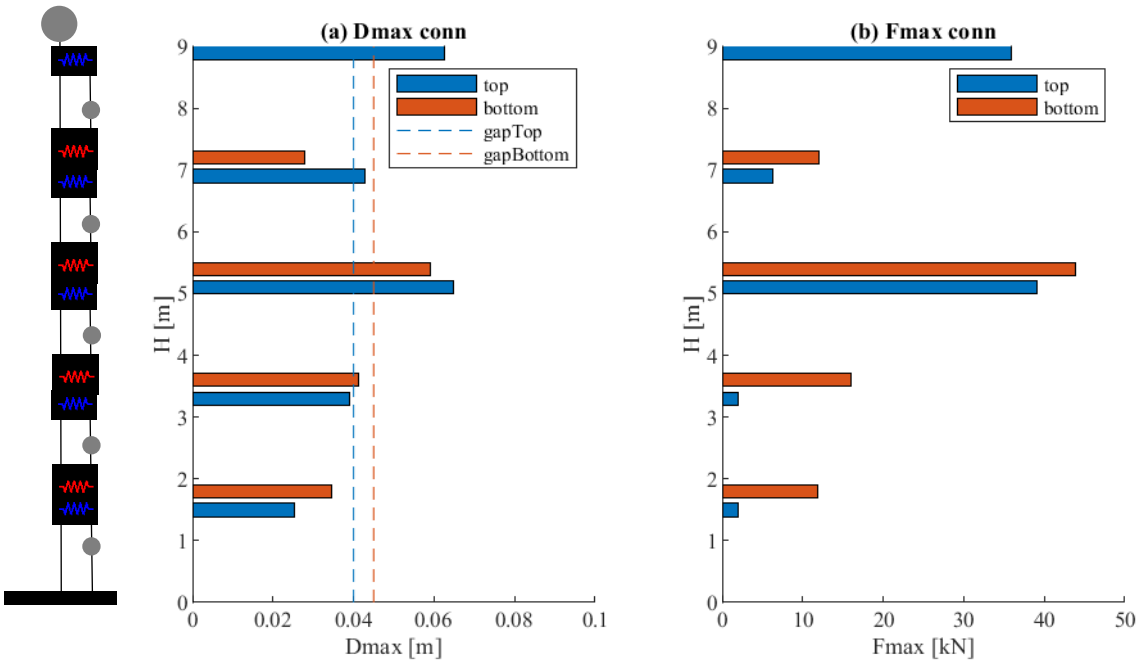

Figure 6.53: Structure *m60H9* with silicone sealant at a_g = 0.675 g: (a) maximum slips in cladding connections, (b) maximum forces in cladding connections

Slika 6.53: Montažna hala *m60H9* s silikonskim tesnilom pri a_g = 0.675g: (a) največji zdrsi fasadnih stikov, (b) največje sile v fasadnih stikih

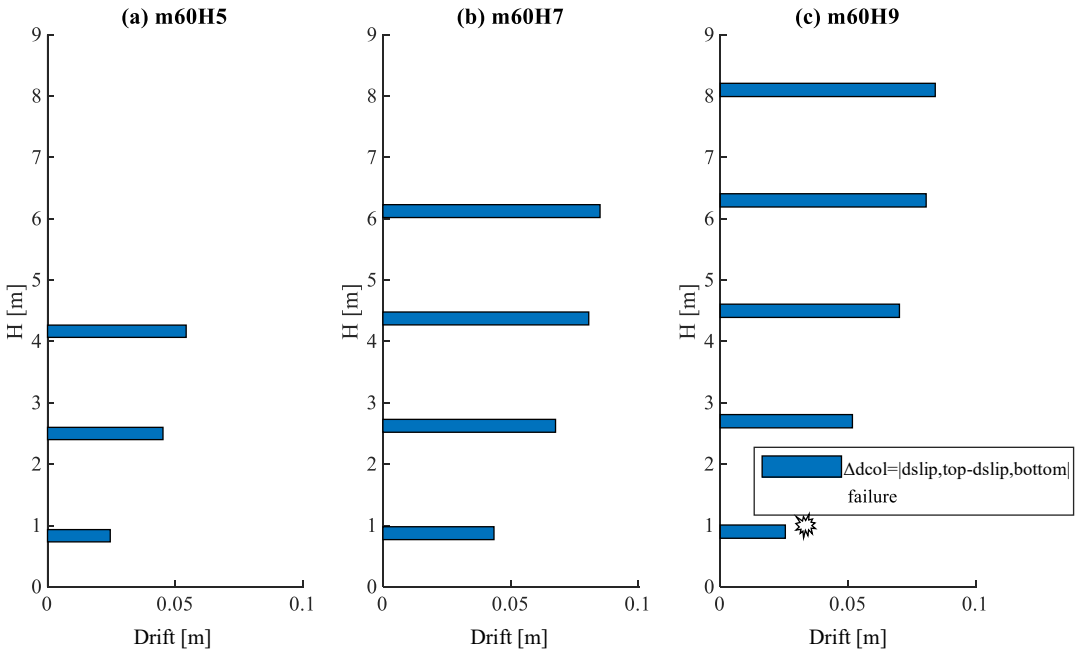

Figure 6.54: Maximum difference in slips at top and bottom connections (i.e. column's drift along each panel) in structures with silicone sealant at a_g = 0.675 g: (a) *m60H5*, (b) *m60H7* and (c) *m60H9*
Slika 6.54: Največja razlika v pomikih v zgornjem in spodnjem stiku (t.j. drift stebra na nivoju panela) pri halah s silikonskim tesnilom in a_g = 0.675 g: (a) *m60H5*, (b) *m60H7*, (c) *m60H9*

From the drifts presented in Figures 6.50 and 6.54, it can be observed that although silicone has influenced the response of panels, it did not have an important influence on the response of columns. The panels that are connected by silicone sealant did not significantly change the response of columns. The influence of the panel stiffness on the response of the main structure was limited due to the strong degradation of the stiffness of the silicone. Responses of structures with and without silicone-sealed panels are compared more in detail in Section 6.4.1.

Figures 6.55 and 6.56 present the displacement and force response histories of the connections for structure *m60H9*. Compared to the typical response of the same structure without silicone sealant, more impacts in the connections occurred if the silicone sealant was used. The lateral forces in the connections were larger.

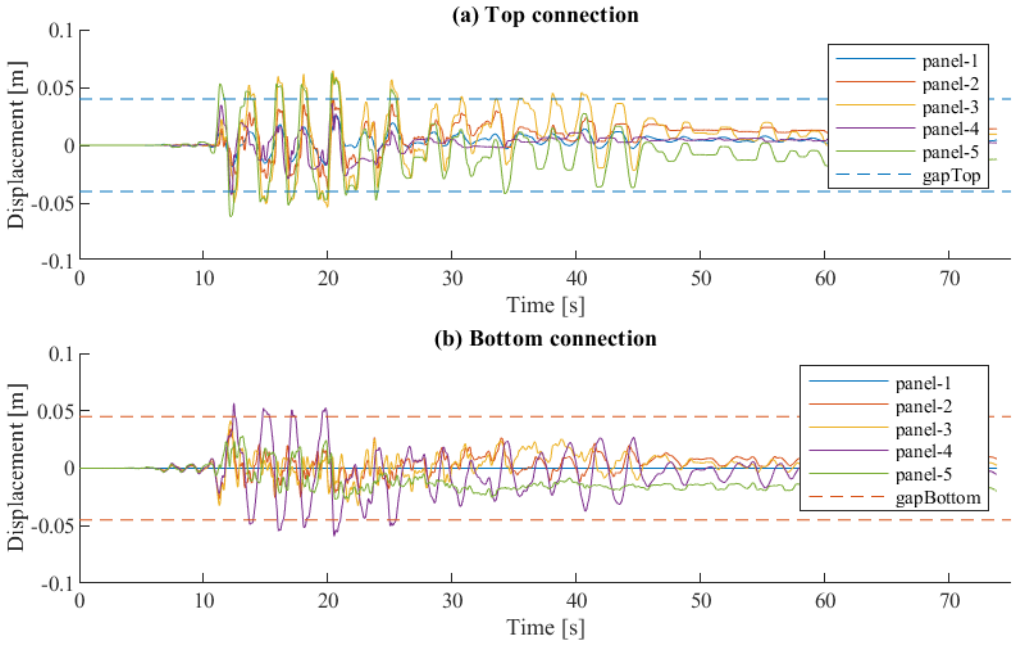

Figure 6.55: Structure *m60H9* with silicone sealant at a_g = 0.675 g: (a) displacement response history for the top connections, (b) displacement response history for the bottom connections

Slika 6.55: Montažna hala *m60H9* s silikonskim tesnilom pri a_g = 0.675 g: (a) časovni potek pomikov v zgornjih stikih, (b) časovni potek pomikov v spodnjih stikih

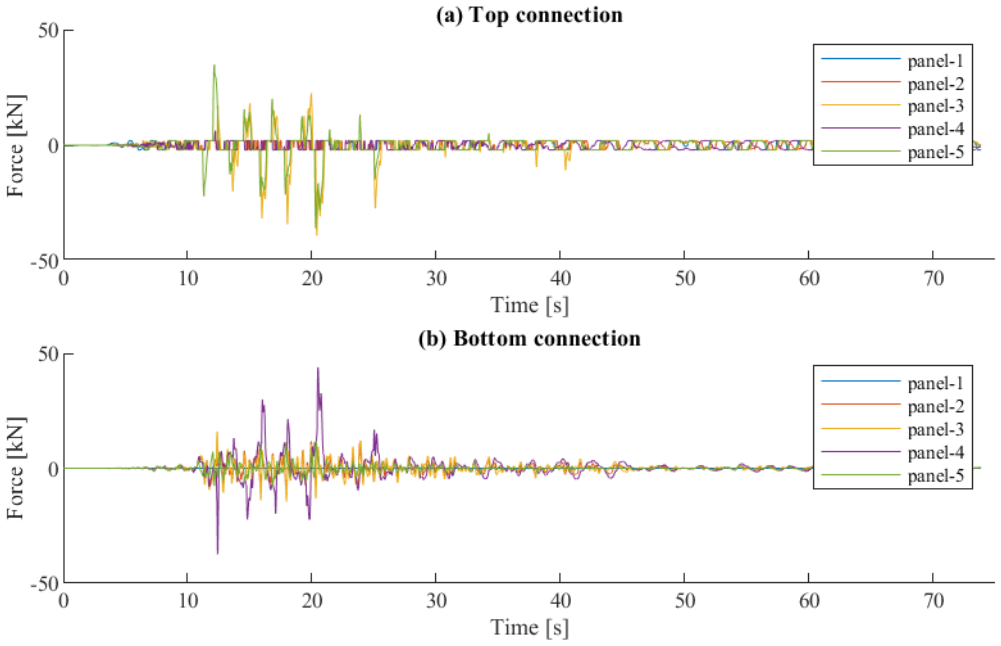

Figure 6.56: Structure *m60H9* with silicone sealant at a_g = 0.675 g: (a) force response history for the top connections, (b) force response history for the bottom connections

Slika 6.56: Montažna hala *m60H9* s silikonskim tesnilom pri a_g = 0.675 g: (a) časovni potek sil v zgornjih stikih, (b) časovni potek sil v spodnjih stikih

Figure 6.57 presents the shear force along the column height for a_g = 0.675 g and compared to M_u/H. Because of more impacts and higher forces in the connections, the influence of higher modes was larger. The shear demand in columns was increased. Formulation of a short-column effect can be noticed for structure *m60H7*. However, no failure occurred because the shear resistance was much higher than the demand.

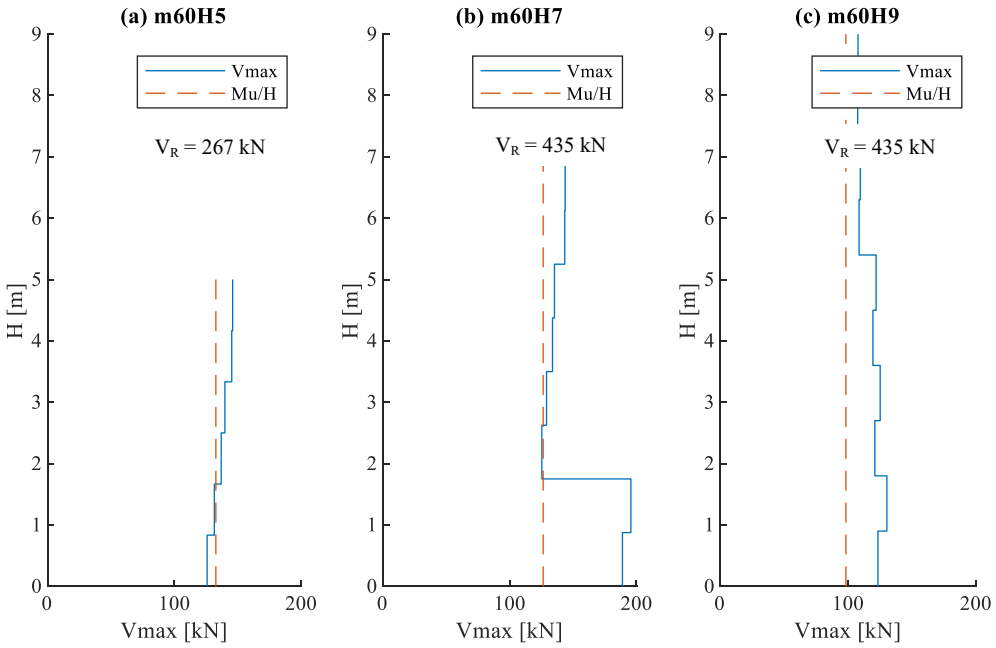

Figure 6.57: Maximum shear force along the column height for structures with silicone sealant at a_g = 0.675 g: (a) *m60H5*, (b) *m60H7* and (c) *m60H9*

Slika 6.57: Maksimalna strižna sila po višini stebra pri halah s silikonskim tesnilom in a_g = 0.675 g: (a) *m60H5*, (b) *m60H7*, (c) *m60H9*

6.4 Results of the parametric study

The influence of different parameters (silicone sealant, construction imperfections, connection of bottom panels to foundation and ratio between columns and connections) was analysed in the following subsections. The response of the panels was compared for structures with different parameters. The maximum displacements and forces at top and bottom connections were evaluated for the complete range of structures. Also, the drift capacity of the fastening system was analysed considering different parameters.

The influence of different parameters and panels on the overall structure response was analysed by comparing column displacements and force–displacement responses. The shear demand in columns is also shown to evaluate the effect of high forces that occurred during the impacts.

The assumption of lognormal distribution of seismic response parameters is often used in literature (FEMA P-58-1, 2012; Snoj, 2014). Common parameters that describe this distribution are median value and standard deviation of natural logarithms. These two parameters are also used in the following to present the parametric study results. Values within one standard deviation account for about 68% of the data. Medians and standard deviations were estimated from the results of nonlinear dynamic analyses of structures (thirty ground motion records per each structure, intensity and combination of parameters).

6.4.1 Influence of the silicone sealant between adjacent panels on the response

Responses of structures with and without silicone sealant are compared to analyse the influence of silicone sealant on the response of precast structure and panels. The central position of connections was taken into account (*MM*), the bottom panel was fixed to the foundation (*F*), and the ratio *k* was equal to 2. Within the first set of analyses, no interaction between the panels was used (*N*), whereas, in the other set, the silicone sealant was modelled (*P*).

Influence of silicone sealant on the response of panels

Responses of structures without and with silicone sealant are compared in Figure 6.58. Here, only the response of structure *m60H9* is presented. Similar results for the other two structure heights can be found in Appendix C. When silicone sealant was used, there was some interaction between the adjacent panels. Panels did not respond independently from each other, as was the case when there was no silicone, but they were connected. The sealant restricted and reduced the movement of panels to a considerable degree.

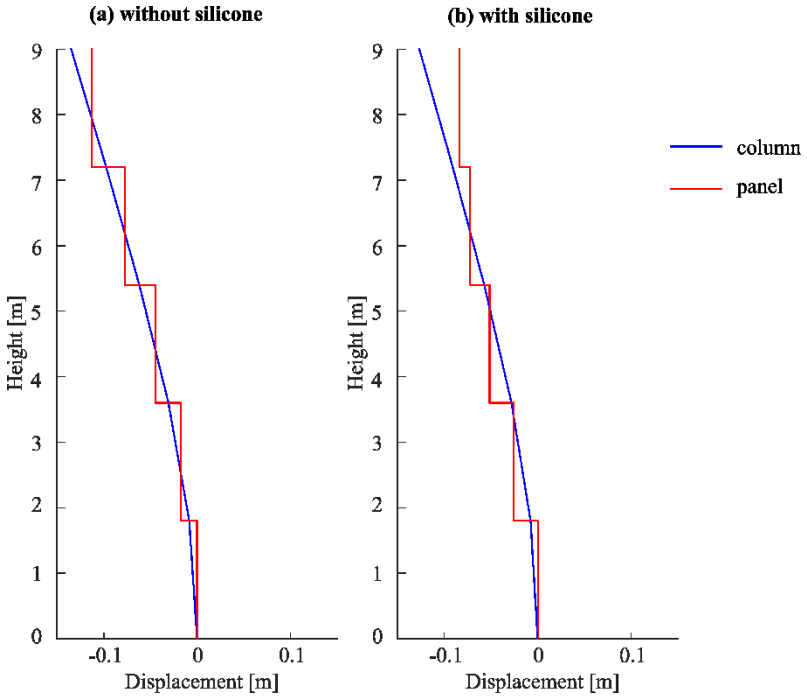

Figure 6.58: Response of precast structure *m60H9*: (a) without silicone-sealed joints and (b) with silicone sealant

Slika 6.58: Odziv konstrukcije *m60H9*: (a) brez silikona in (b) s silikonom

The maximum slips in the connections are compared for structures with and without silicone sealant in Figure 6.59 for a_g = 0.25 g. The presence of silicone sealant increased displacement demand at top cladding connections because, at higher panels, the maximum response of connections was in the same direction with respect to the column. This might lead to an earlier failure of the panels because top connections are the weakest component. The most exposed was the panel at the top of the structure (see Figure 6.58 b).

The maximum column drift along the single panel is shown in Figure 6.60. This drift presents the demand on the fastening system and was almost the same for structures with and without silicone. The influence of silicone sealant on the column's displacement response is not significant. That response is analysed in the following subsection. However, the top and bottom connections are in interaction, and drift demand is distributed between them. Because of the silicone sealant, the slips were larger at top connections that are the critical component. Some impacts between the column and panels occurred earlier when silicone was used. Because of larger slips at top connections, they were, in general, somewhat smaller at bottom connections.

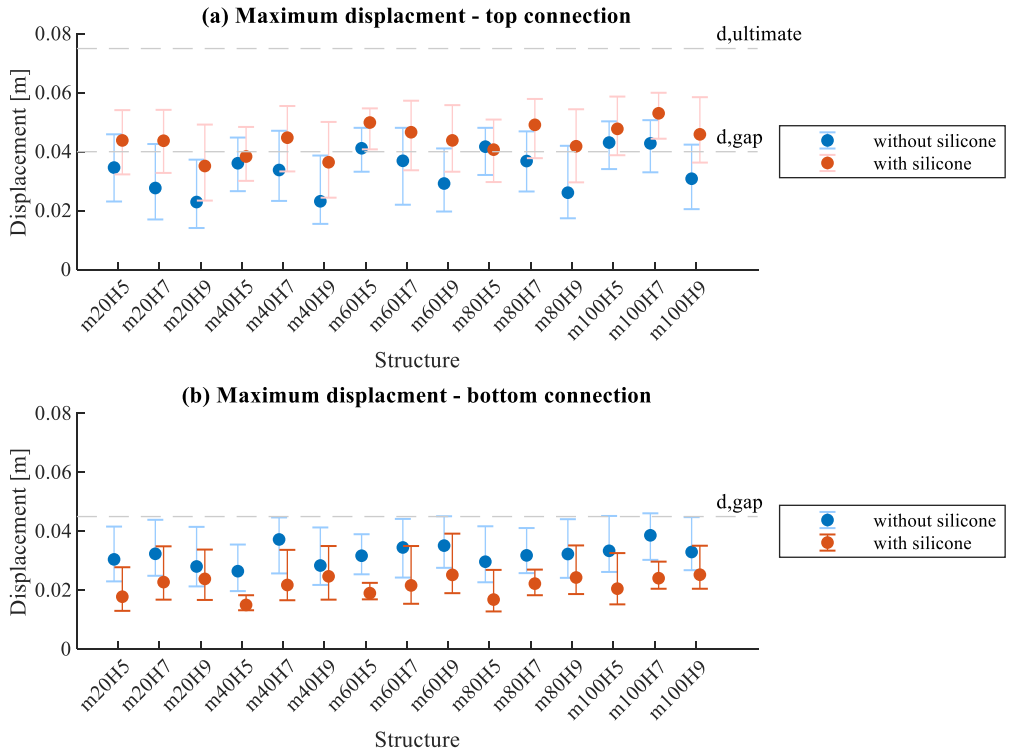

Figure 6.59: Maximum slips at (a) top connections and (b) bottom connections at a_g = 0.25 g

Slika 6.59: Maksimalni zdrsi v (a) zgornjih in (b) spodnjih stikih pri a_g = 0.25 g

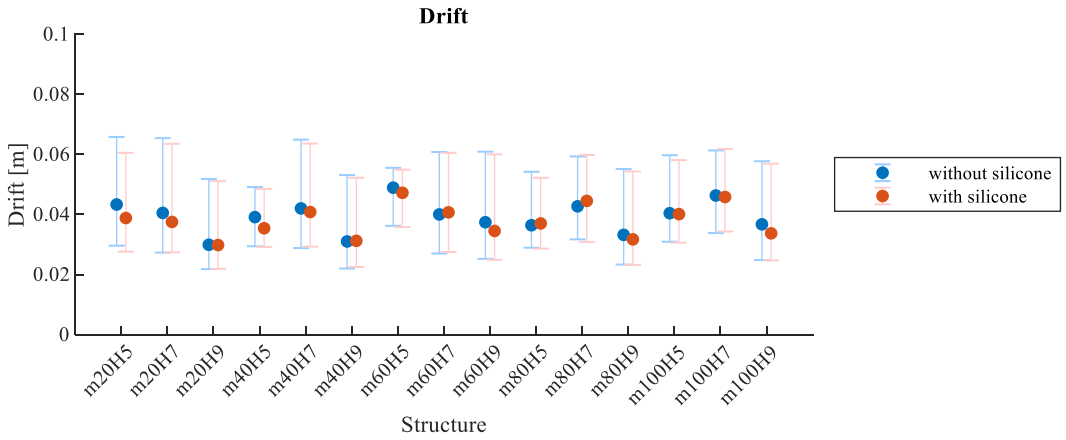

Figure 6.60: Maximum column drift along the single panel for structures with and without silicone sealant at a_g = 0.25 g

Slika 6.60: Maximalni drift stebra na nivoju panela za hale s silikonom in brez silikona pri a_g = 0.25 g

Because of larger slips at top connections, the fastening system failed at smaller drifts in structures with silicone. In other words, the drift capacity of the fastening system was reduced if the silicone sealant was applied. If no interaction between panels and the central position of the connections were taken into account (*MM / N / F / 1*), the fastening system failed at 13.4 cm median column drift along the single panel (Figure 6.32). When silicone sealant was considered (*MM / P / F / 1*), the demand on the top connections was larger for the same drift, and the fastening system failed

earlier. Thus, the median drift capacity of the complete fastening system decreased to 11.2 cm (Figure 6.32). Several failures of the connections were observed at smaller drifts for the panel position at one side of the column, as presented in Figure 6.46 (b).

For both cases, with and without silicone sealant, the first failure of fastenings often occurred at the bottom panel (see the median drift capacity of 7.6 cm in Figure 6.33). The bottom panel's drift capacity was the same as the displacement capacity of the top connections (approx. 7.5 cm, i.e. 4 cm sliding capacity + 3.5 cm after the gap is depleted) because the panel at the bottom was fixed to the foundation, and the top connections presented the only part of the fastening system. The influence of the connection of bottom panels to the foundation on the response is discussed later in Section 6.4.3.

Figure 6.61 compares the maximum forces in connections for structures with and without silicone sealant at a_g = 0.675 g. At both top and bottom connections, forces were higher when silicone sealant was applied. Because of the panels connected with silicone, higher forces were induced at top connections of higher panels and at bottom connections of lower panels (see the response behaviour in Figure 6.58 b). Structures *m40H5*, *m60H5*, *m80H7* and *m100H7* have failed for most of the applied accelerograms at a_g = 0.675 g, and thus, there is a smaller difference in the response of connections.

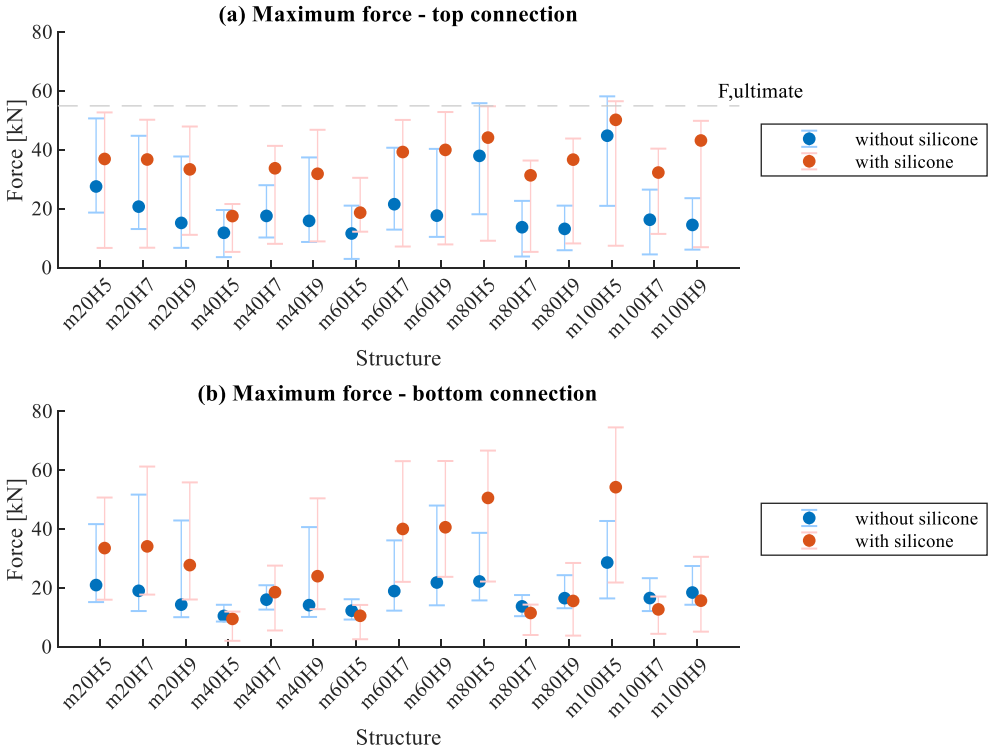

Figure 6.61: Maximum force at (a) top connections and (b) bottom connections at a_g = 0.675 g
Slika 6.61: Maksimalna sila v (a) zgornjih in (b) spodnjih stikih pri a_g = 0.675 g

Influence of silicone sealant on the global response of the structure

To analyse the influence of panels on the global response of structures, the maximum displacements recorded at the top of columns are compared for structures with and without silicone-sealed joints in Figure 6.62. Despite the influence that silicone had on the response of panels, the maximum displacements of structures were not affected as much (Figure 6.62).

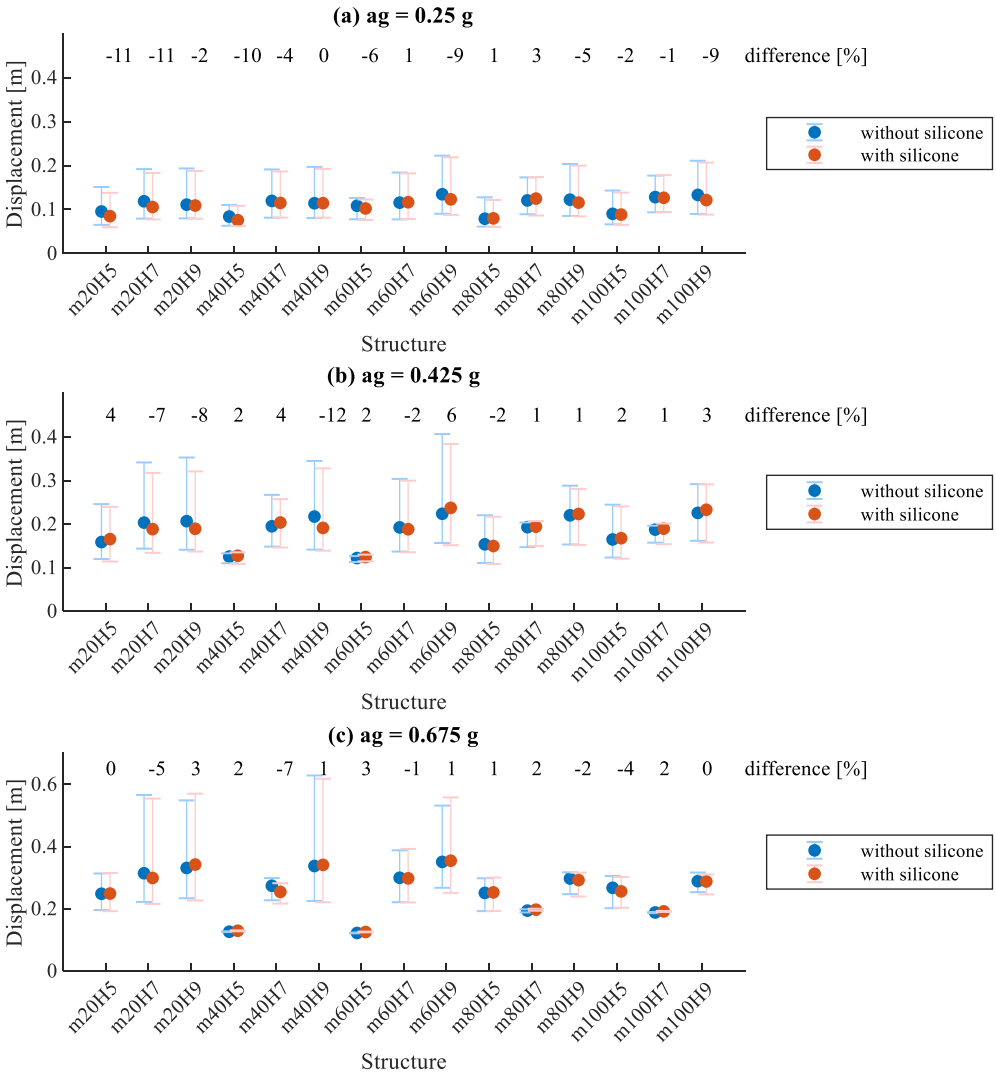

Figure 6.62: Maximum displacement at the top of the structure with and without silicone joints between the panels: (a) a_g = 0.25 g, (b) a_g = 0.425 g and (c) a_g = 0.675 g

Slika 6.62: Maksimalni pomik na vrhu konstrukcij s silikonom in brez silikona med paneli: (a) a_g = 0.25 g, (b) a_g = 0.425 g in (c) a_g = 0.675 g

The relatively small difference in structure displacements is a consequence of the significant deterioration of silicone sealant. For higher intensities (Figure 6.62 c), the difference in maximum

structure displacements was even smaller. The interaction between panels and structure because of impacts was not significant. Due to their short duration, impacts did not have an important influence on the structure's displacements.

Figure 6.63 shows the column force–displacement hysteretic responses for the three characteristic examples (structures *m60H5*, *m60H7* and *m60H9*) with and without silicone sealant. As shown, the responses of structures with and without silicone sealant are similar. The stiffness of the structure was not affected by the presence of silicone.

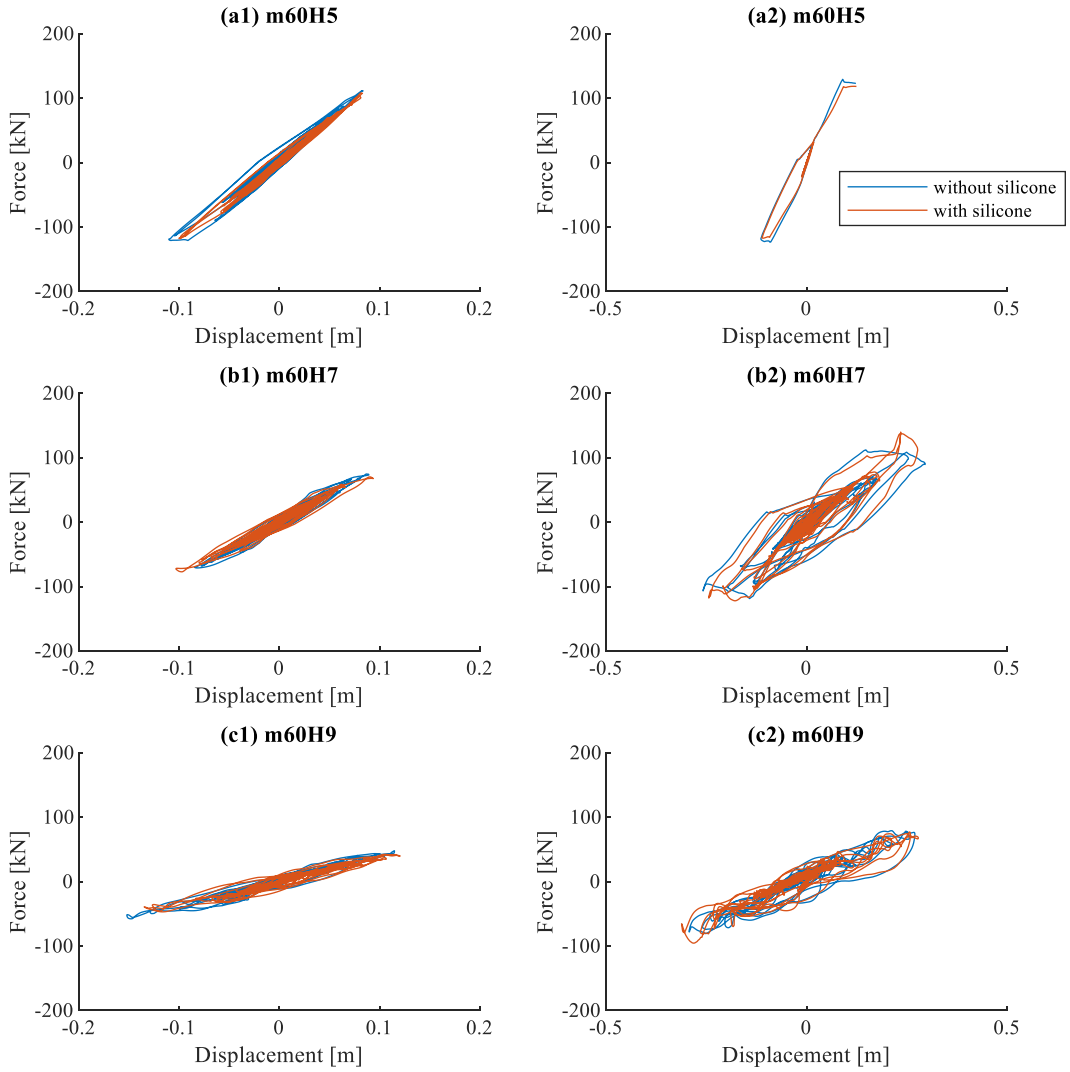

Figure 6.63: Column's force–displacement response for structures with and without silicone at (1) a_g = 0.25 g and (2) a_g = 0.675 g: (a) structure *m60H5*, (b) structure *m60H7* and (c) structure *m60H9*

Slika 6.63: Odziv sila - pomik za steber v konstrukcijah s silikonom in brez silikona pri (1) a_g = 0.25 g in (2) a_g = 0.675 g: (a) hala *m60H5*, (b) hala *m60H7*, (c) hala *m60H9*

To further demonstrate the small influence of silicone sealant on the response of columns, the displacement response histories recorded at the top of the columns are compared in Figures 6.64 and 6.65 for three characteristic examples with and without silicone sealant at different intensities. As can be seen, the influence of panels on the column response is not significant, despite the silicone-sealed panels.

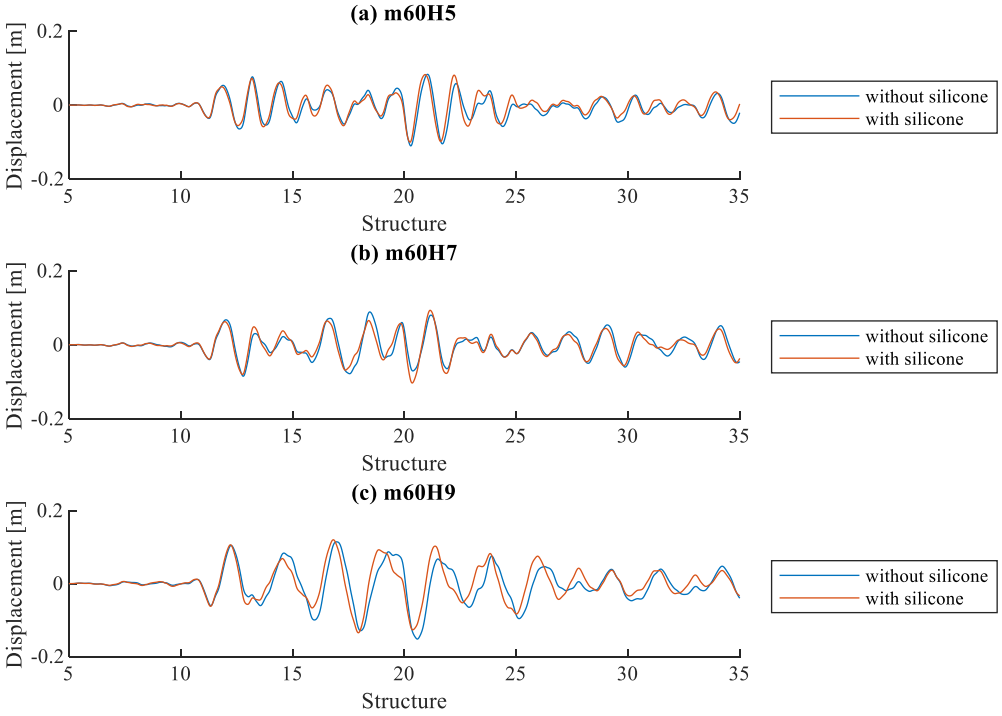

Figure 6.64: Displacement response history at the top of the column for structures with and without silicone at a_g = 0.25 g: (a) structure *m20H7*, (b) structure *m60H7* and (c) structure *m60H9*

Slika 6.64: Časovni potek pomikov na vrhu stebra konstrukcij s silikonom in brez silikona pri a_g = 0.25 g: (a) hala *m20H7*, (b) hala *m60H7*, (c) hala *m60H9*

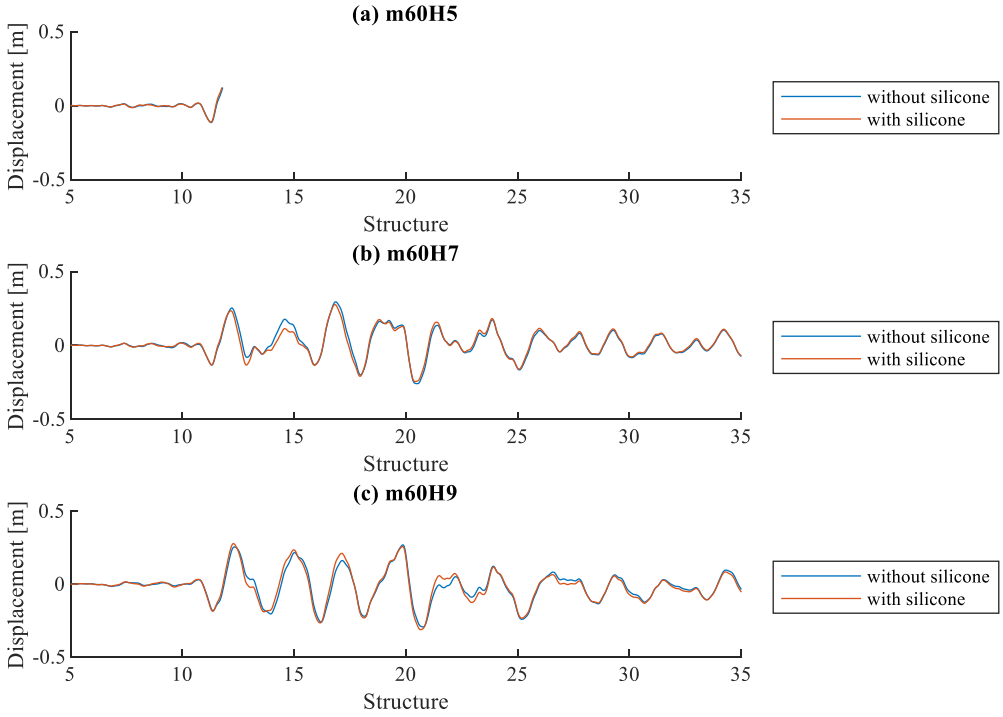

Figure 6.65: Displacement response history at the top of the column for structures with and without silicone at a_g = 0.675 g: (a) structure *m20H7*, (b) structure *m60H7* and (c) structure *m60H9*

Slika 6.65: Časovni potek pomikov na vrhu stebra konstrukcij s silikonom in brez silikona pri a_g = 0.675 g: (a) hala *m20H7*, (b) hala *m60H7*, (c) hala *m60H9*

Influence of silicone sealant on the shear demand in column

The influence of silicone sealant on lateral forces in the connections was analysed by comparing maximum shear forces in columns for structures with and without silicone sealant (Figure 6.66). The increase of the force due to the presence of silicone is expressed as a percentage above the results for each structure. The influence of silicone on shear forces in columns was somewhat larger for structures with silicone sealant, but in general, this effect was small.

Because of the silicone, there were more impacts between the column and panels, and higher forces were activated in the connections (see also Figure 6.61). In certain cases, the influence of higher vibration modes that activate during the impacts was noticeable for structures with silicone. The shear force in columns was higher for slender structures with small tributary mass (*m20H7*, *m20H9*).

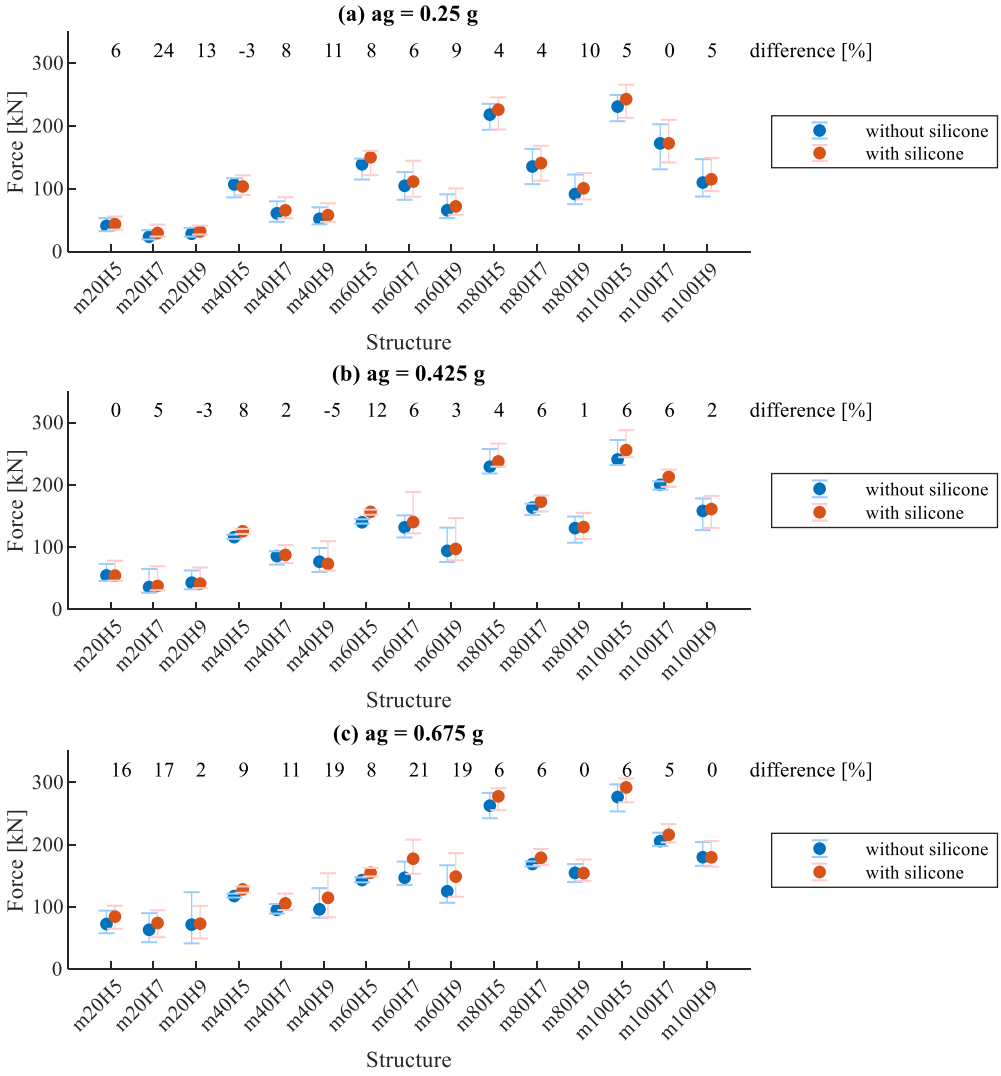

Figure 6.66: Maximum shear force in column for structures with and without silicone sealant: (a) a_g = 0.25 g, (b) a_g = 0.425 g and (c) a_g = 0.675 g

Slika 6.66: Maksimalna strižna sila v stebru za hale s silikonom in brez silikona med paneli: (a) a_g = 0.25 g, (b) a_g = 0.425 g in (c) a_g = 0.675 g

Figures 6.67 and 6.68 compare the maximum shear force in columns for the three examples with and without silicone. For the design intensity (a_g = 0.25 g), the influence of silicone sealant on the shear demand in the column is negligible. Formulation of the short-column effect for structure *m60H7* is because of a fixed bottom panel (see Section 6.4.3) and occurred at an intensity much higher than demand. However, the maximum forces were still below the column's shear resistance.

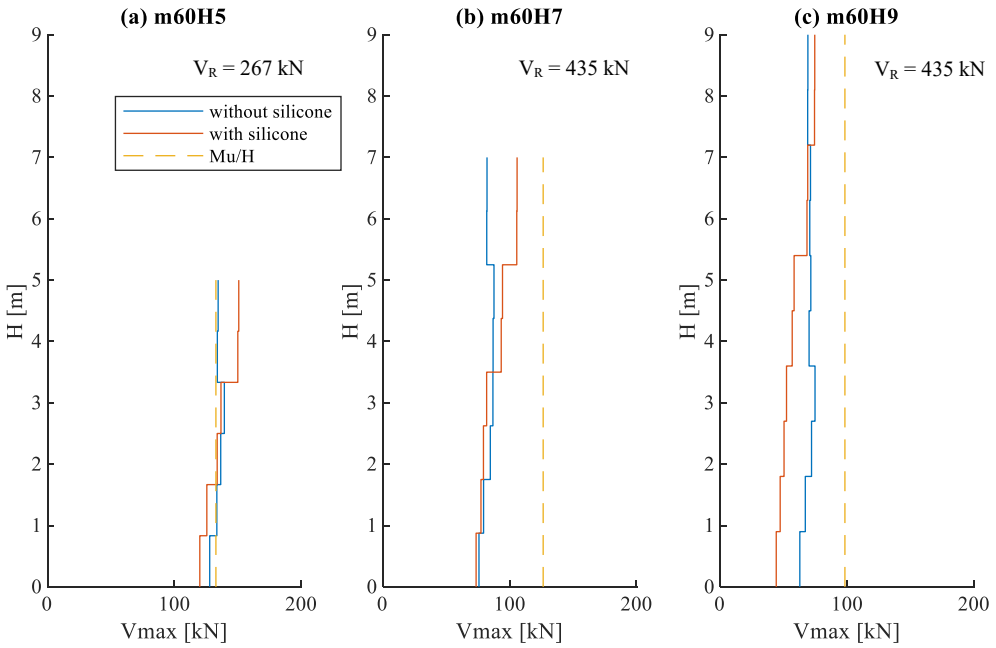

Figure 6.67: Maximum shear force along the column height for structures with and without silicone sealant at a_g = 0.25 g: (a) *m60H5*, (b) *m60H7* and (c) *m60H9*

Slika 6.67: Maksimalna strižna sila po višini stebra pri halah s silikonom in brez silikona pri a_g = 0.25 g: (a) *m60H5*, (b) *m60H7*, (c) *m60H9*

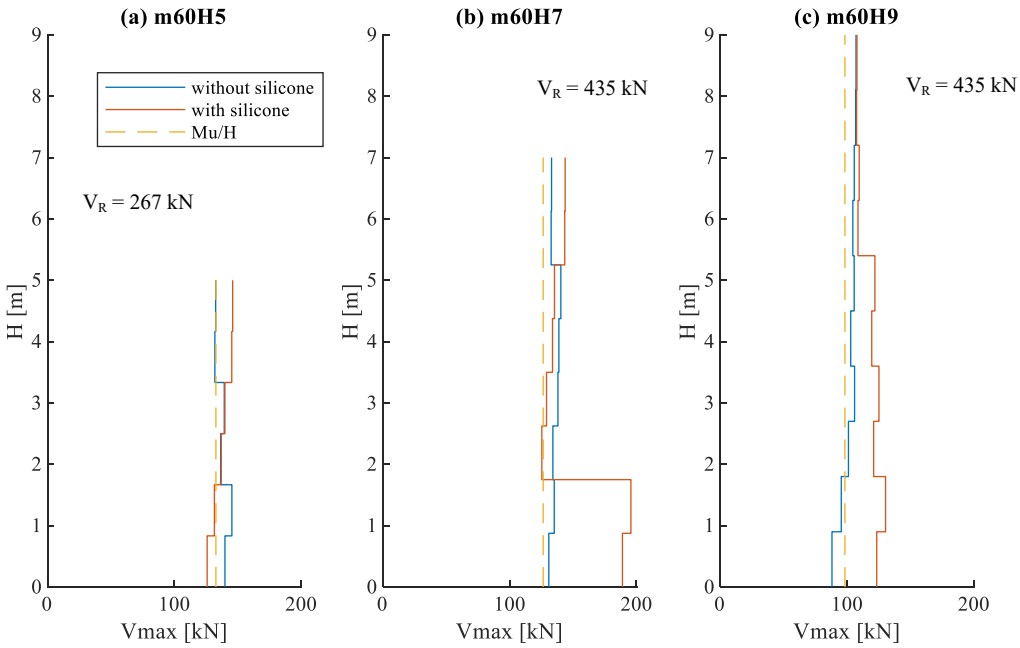

Figure 6.68: Maximum shear force along the column height for structures with and without silicone sealant at a_g = 0.675 g: (a) *m60H5*, (b) *m60H7* and (c) *m60H9*

Slika 6.68: Maksimalna strižna sila po višini stebra pri halah s silikonom in brez silikona pri a_g = 0.675 g: (a) *m60H5*, (b) *m60H7*, (c) *m60H9*

6.4.2 Influence of construction imperfections on the response

Gaps in cladding connections intended only for construction purposes enable the cladding connections to slide during the seismic excitation. The initial position of connections and the size of the gaps at the top and bottom connections appreciably influenced the response. The size of gaps depends on construction tolerances and can vary within the structure. If connections are eccentrically mounted, and gaps are small, relatively high lateral forces in cladding connections activate even at small relative displacements between the column and panel.

This section analyses the influence of eccentrically mounted connections on the response of panels and the main structure. Two extreme eccentric positions of the connections were considered (see Figure 6.3):

- left position of both top and bottom connections (*LL*),
- left position of top connection and right position of the bottom connection (*LR*).

It was assumed that all top connections within the structure are mounted in the same way and that all bottom connections within the structure are mounted in the same way, respectively (the number of analyses performed within the parametric study was large already with this assumption). In the analyses, it was supposed that joints are sealed with silicone, as is usual in real structures. The silicone was modelled with the *Pinching* material model (*P*) that considers the stiffness degradation of the sealant. The ratio of columns to connections *k* was set to 2, and the bottom panel was fixed to the foundation (*F*).

Influence of construction imperfections on the response of panels

In the sliding phase of connections, the response of connections is limited by the available gap. However, after the gap is closed, there is a high increase in the force demand for a relatively small displacement increment. In the most unfavourable case, gaps are already closed in the initial position. Thus, connection sliding is prevented in one direction, whereas larger slips are possible in the other direction. The forces at connections were observed to analyse the response, and the column drift along the panels is used as the critical demand parameter.

First, it should be clarified that slips typically also occur in opposite directions for structures with silicone sealant at the beginning of excitation. The response of the top and bottom connections in the same direction was observed at larger column displacements in structures with silicone sealant.

The response of the façade panel for the *LL* and *LR* position of the connections is shown in Figure 6.69 (a) and (b), respectively. Because of different displacements at top and bottom connections and different initial gaps, impacts occurred at different relative column and panel positions for *LL* and *LR* position of the connection (see Figure 6.69):

- When the gaps were depleted at the same side of the top and bottom connections (*LL*), the force initially increased only at one connection (either top or bottom). At the other connection, relatively large slips were allowed before depletion of the gap. This happened because of the typical response of the connections in opposite directions.

- When the gaps were closed diagonally (*LR*), impacts at the connections occurred at both the top and bottom edges of the panel at the same time. This occurred at the beginning of the excitation.

- There is a strong tendency in the connections to slide until the gaps in both connections are closed. This would be an additional reason for a much larger increase in the forces if the connections were positioned diagonally (*LR*).

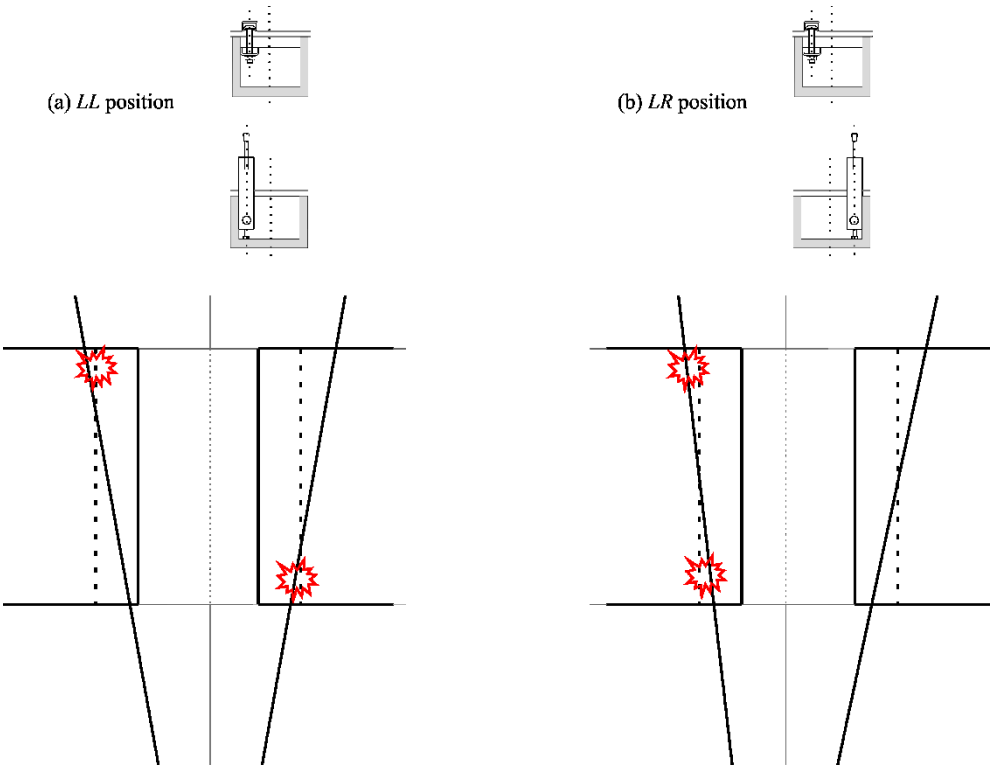

Figure 6.69: Response of the structure with an eccentric position of the connections with marked points of impacts: (a) *LL* position of connections and (b) *LR* position of connections,
Slika 6.69: Odziv konstrukcije z ekscentričnimi stiki in označenimi mesti udarcev: (a) *LL* pozicija stikov in (b) *LR* pozicija stikov

Responses of panels for centrally and eccentrically positioned connections are also presented in Figure 6.70 for an example of a structure that is 9 m tall. Similar results for the other two heights can be found in Appendices D and E, where the results of characteristic precast structures with eccentrically positioned connections are summarised.

As shown in Figure 6.70, for the *LL* position of the connections, impacts between column and panels occurred at top connections when the column leaned to one side, and impacts occurred at bottom connections when the column leaned to the other side. Note that this did not happen at all connections within the structure.

In contrast, for the *LR* connection position, the impacts between the column and panels occurred at all connections (top and bottom connections and at all panels) when the column deformed at one side. However, when the column moved to the other side, relatively large slips in the connections were allowed, and no impacts were observed.

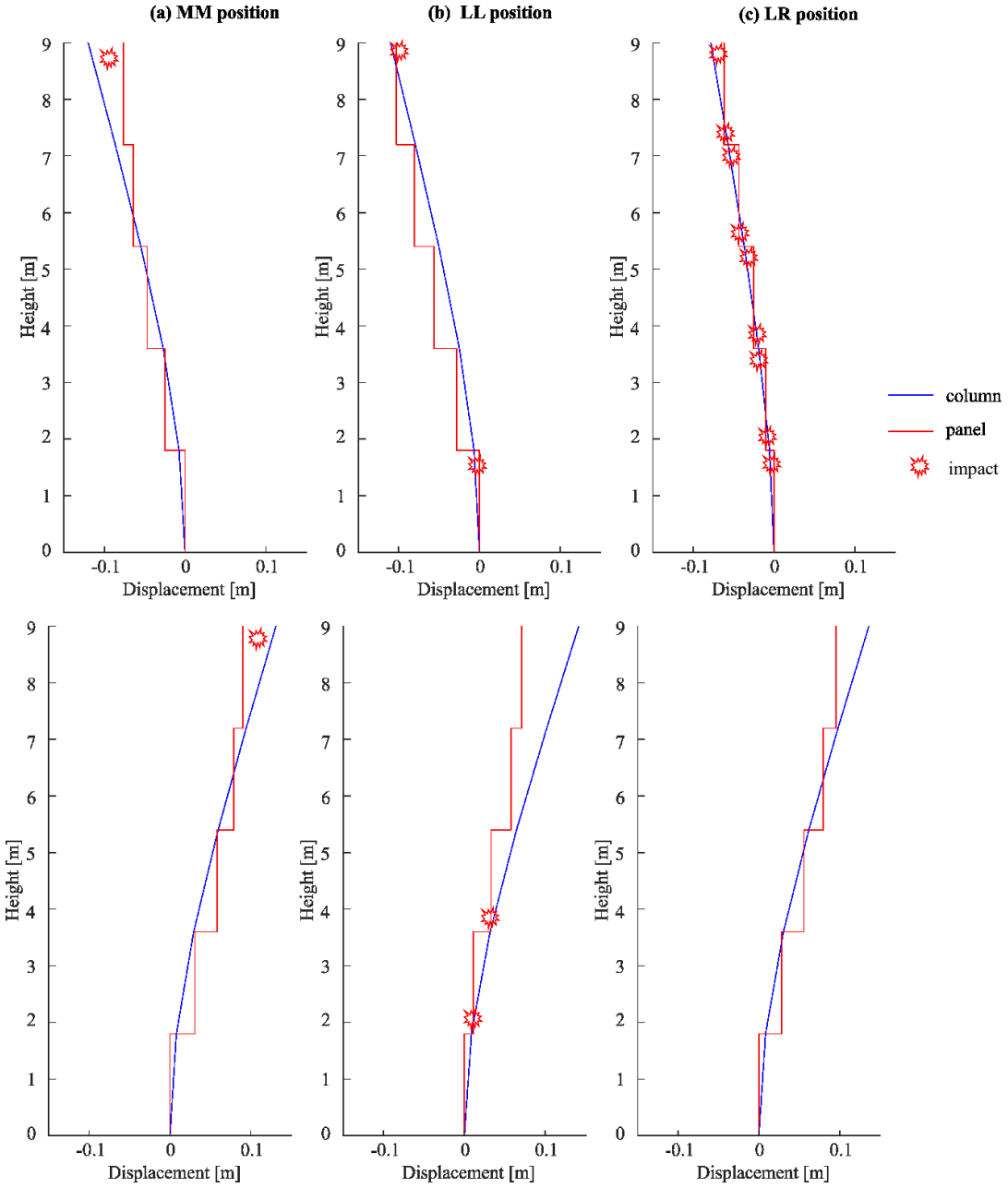

Figure 6.70: Response of precast structure *m60H9*: (a) centrally positioned connections *MM*, (b) eccentric position of connections *LL* and (c) eccentric position of connections *LR*

Slika 6.70: Odziv konstrukcije *m60H9*: (a) sredinska pozicija stikov *MM*, (b) ekscentrična pozicija stikov *LL* in (c) ekscentrična pozicija stikov *LR*

Figures 6.71-6.73 compare the maximum forces that occurred in the connections of three characteristic examples (*m60H5*, *m60H7* and *m60H9*) at a_g = 0.25 g for extreme positions of the connections: (a) *MM*, (b) *LL* and (c) *LR*. Results have shown that the *LR* position of gaps is the most unfavourable.

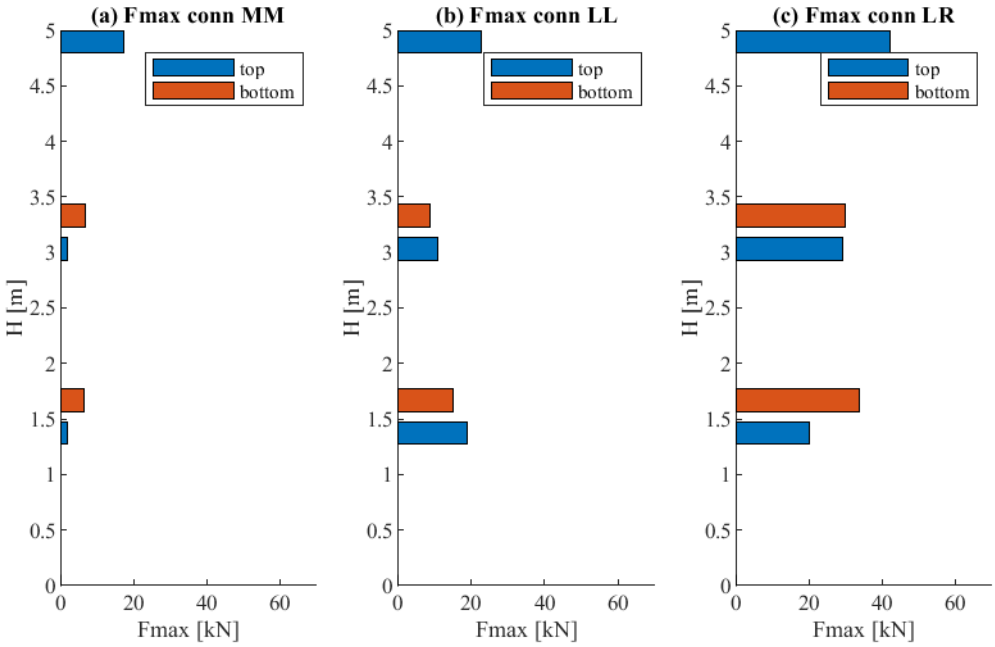

Figure 6.71: Maximum forces in cladding connections for structure *m60H5* at a_g = 0.25 g: (a) centrally positioned connections *MM*, (b) eccentrically positioned connections *LL* and (c) eccentrically positioned connections *LR*

Slika 6.71: Največje sile v fasadnih stikih montažne hale *m60H5* pri a_g = 0.25g: (a) sredinska pozicija stikov *MM*, (b) ekscentrična pozicija stikov *LL*, (c) ekscentrična pozicija stikov *LR*

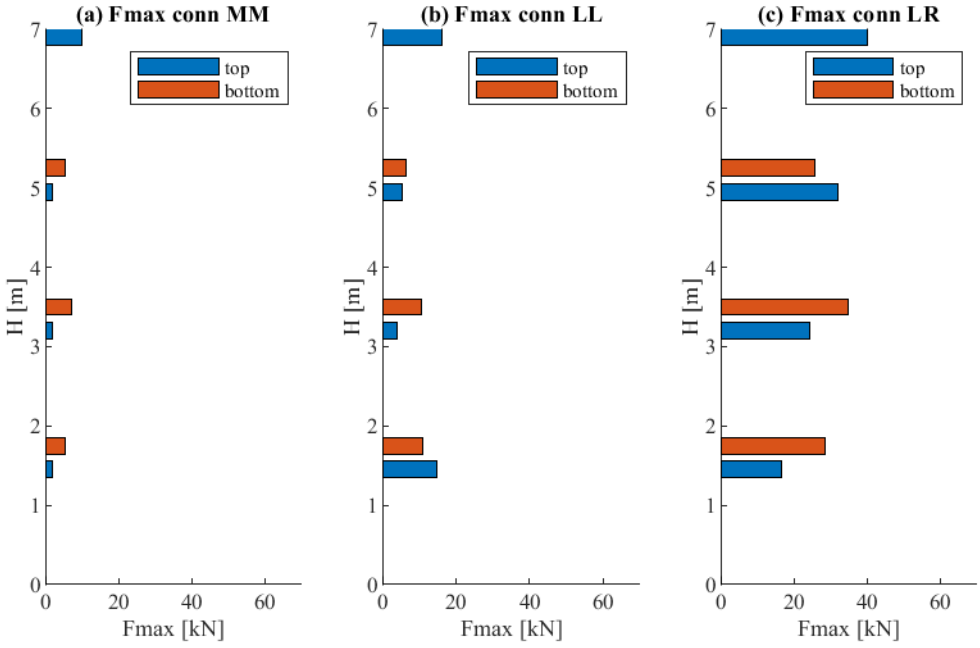

Figure 6.72: Maximum forces in cladding connections for structure *m60H7* at a_g = 0.25 g: (a) centrally positioned connections *MM*, (b) eccentrically positioned connections *LL* and (c) eccentrically positioned connections *LR*

Slika 6.72: Največje sile v fasadnih stikih montažne hale *m60H7* pri a_g = 0.25g: (a) sredinska pozicija stikov *MM*, (b) ekscentrična pozicija stikov *LL*, (c) ekscentrična pozicija stikov *LR*

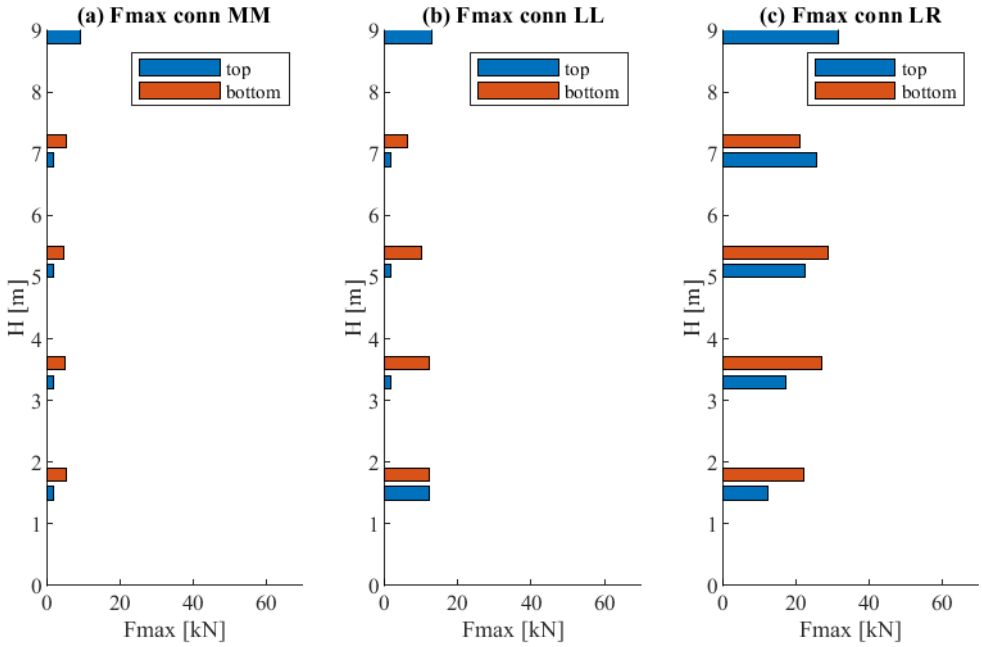

Figure 6.73: Maximum forces in cladding connections for structure *m60H9* at a_g = 0.25 g: (a) centrally positioned connections *MM*, (b) eccentrically positioned connections *LL* and (c) eccentrically positioned connections *LR*

Slika 6.73: Največje sile v fasadnih stikih montažne hale *m60H9* pri a_g = 0.25g: (a) sredinska pozicija stikov *MM*, (b) ekscentrična pozicija stikov *LL*, (c) ekscentrična pozicija stikov *LR*

Maximum forces at top and bottom connections are shown in Figures 6.74 and 6.75 for the complete set of structures for connections' centric and eccentric positions. As already observed for characteristic examples, forces in the connections were much larger for the eccentric *LR* position of the connections.

Although the connections were positioned eccentrically, the median maximum force at top connections was below its resistance of 55 kN at a_g = 0.25 g. However, at higher intensities, the resistance of the top connection was exceeded many times when the connections were in the initial *LR* position, and many panel failures were recorded.

Although the forces in one of the connections for the *LL* position are already activated at the beginning of the excitation, a relatively small number of failures were recorded. The reason is that larger slips are allowed at the other connections in the fastening system that take over the drift demand.

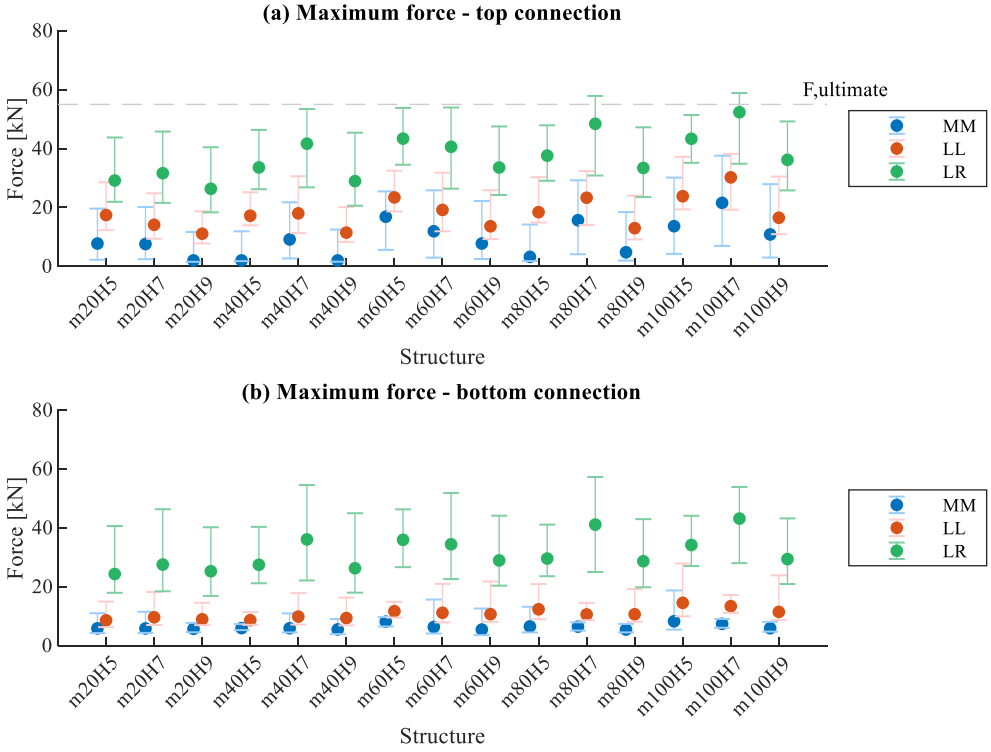

Figure 6.74: Maximum force connections for different initial positions of the connections at a_g = 0.25 g

Slika 6.74: Maksimalne sile v stikih za različne začetne pozicije stikov pri a_g = 0.25 g

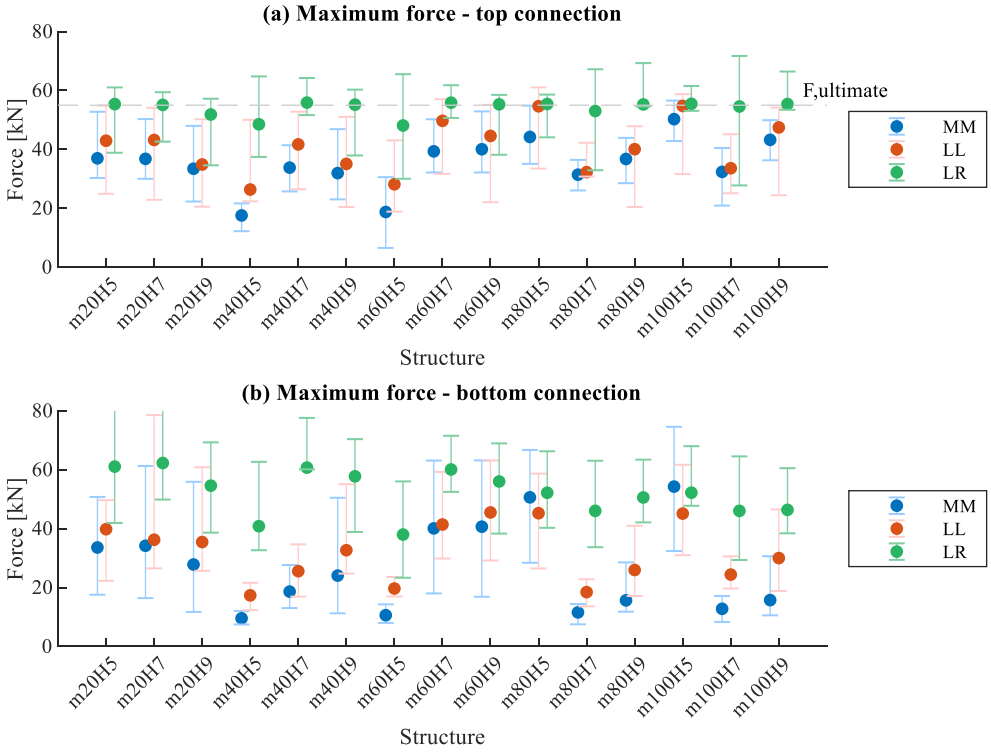

Figure 6.75: Maximum force at connections for different initial positions of the connections at a_g = 0.675 g

Slika 6.75: Maksimalne sile v stikih za različne začetne pozicije stikov pri a_g = 0.675 g

Figures 6.76 and 6.77 show the difference in slips at top and bottom connections (i.e. column drift along the single panel) for the three characteristic examples with the eccentric position of connections at a_g = 0.675 g. The fastenings that usually failed first were at the panel at the top of the structure because the demand on the fastening system, that is, column drift along the single panel, was the largest at the top of the column (Figures 6.76 and 6.77). Then, the failure of the lower panels followed.

In some cases, failure of the connections at the bottom panel occurred first (usually for the *LL* position of the connections). Because the bottom panel was fixed to the foundation, all the demand was taken over only by the top connection that consequently failed first (for example, Figure 6.76 b). This response can be explained in Figure 6.70 b (top). Impacts occurred at top connections in both the top and bottom panels of the structure. Although the demand at the top of the column is greater (drift increases along with the column height), there is some sliding capacity available at the bottom connection of the top panel because the connections are in interaction. However, there is no more sliding capacity available at the bottom panel, which consequently fails first.

The eccentric position of the connections significantly reduced the fastening system's drift capacity. Because the bottom panel was fixed to the foundation, its drift capacity was the same as the top connections' displacement capacity. This was 7.5 cm and 3.5 cm for the case of centrally and eccentrically positioned connections, respectively. Panels higher along the column had a larger drift capacity due to the contribution of their bottom connections.

In the *LL* connection position, the fastening system failed at the median column drift along a single panel of 3.8 cm. In the *LR* connection position, the fastenings failed at a median drift of 4.7 cm (Figure 6.32). When connections were positioned diagonally eccentrically (*LR*), there was no available sliding capacity of the connections on the higher panels. Thus, failure of the connections occurred even at small drifts, and the first failure typically occurred at the top of the structure. The dispersion of the results was appropriately smaller. The drift capacity of the complete fastening system was somewhat larger than the top connections' displacement capacity (approx. 3.5 cm after the gap is depleted) because there was some contribution from the bottom connections.

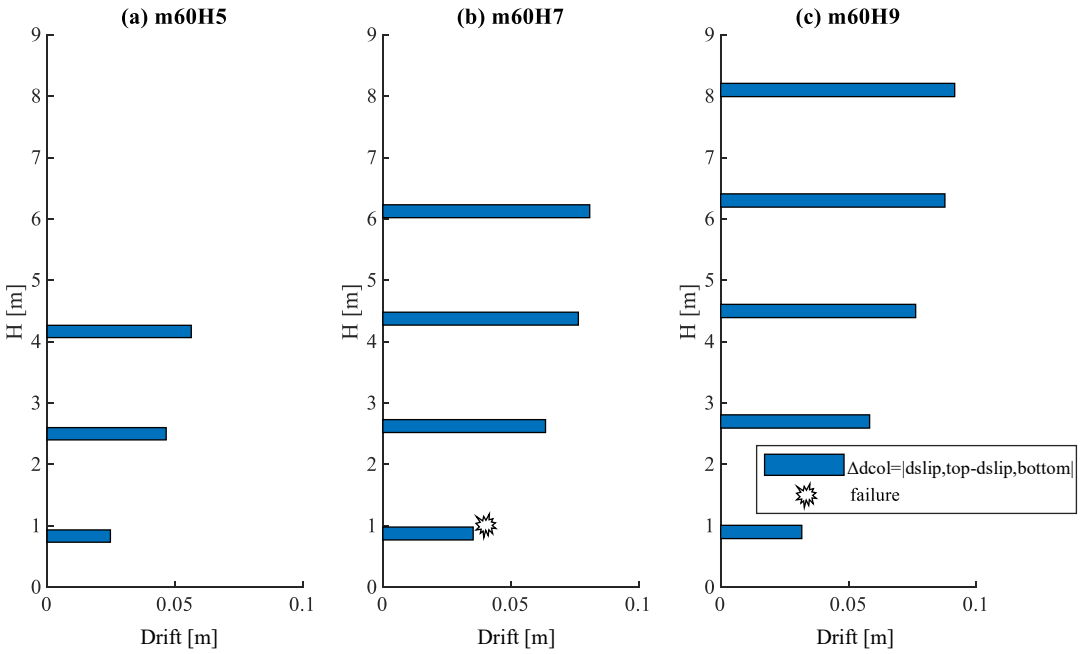

Figure 6.76: Maximum difference in slips at top and bottom connections for the *LL* connection position at a_g = 0.675 g: (a) structure *m60H5*, (b) structure *m60H7* and (c) structure *m60H9*

Slika 6.76: Največja razlika v pomikih v zgornjem in spodnjem stiku za ekscentrično *LL* pozicijo stikov pri a_g = 0.675 g: (a) *m60H5*, (b) *m60H7*, (c) *m60H9*

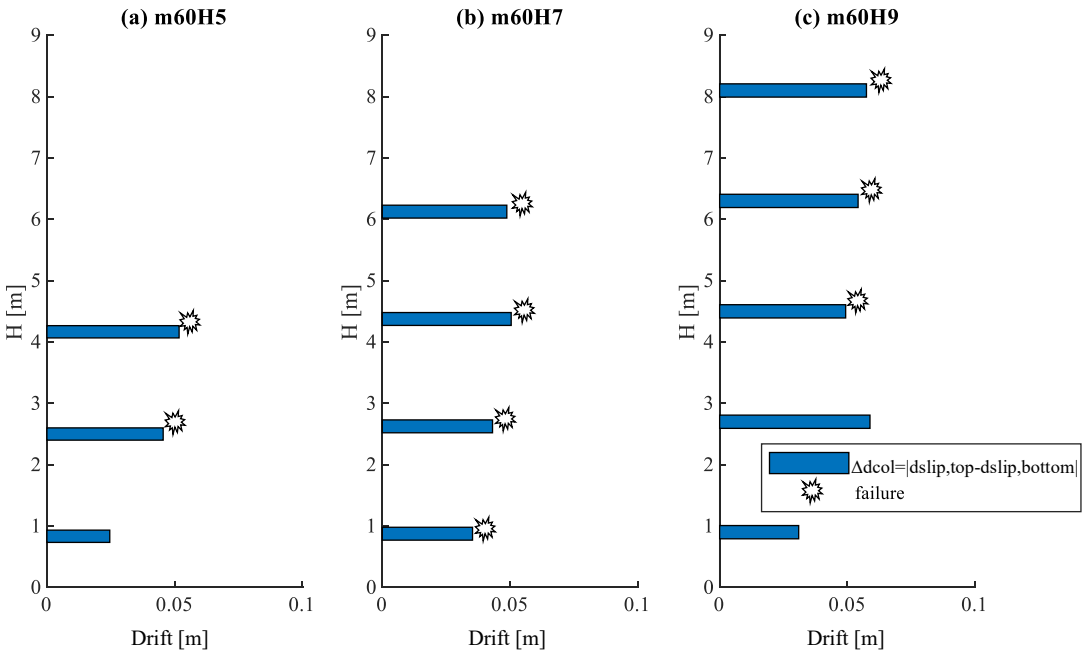

Figure 6.77: Maximum difference in slips at top and bottom connections for *LR* connection position at a_g = 0.675 g: (a) structure *m60H5*, (b) structure *m60H7*, (c) structure *m60H9*

Slika 6.77: Največja razlika v pomikih v zgornjem in spodnjem stiku za ekscentrično *LR* pozicijo stikov pri a_g = 0.675 g: (a) *m60H5*, (b) *m60H7*, (c) *m60H9*

Influence of construction imperfections on the global response of the structure

To analyse the influence of construction imperfections on the global response of the structure, displacements of the main structure were compared for different initial positions of the connections. Figure 6.78 compares the maximum displacements at the top of the column for centrally (*MM*) and eccentrically positioned connections (*LL* and *LR*).

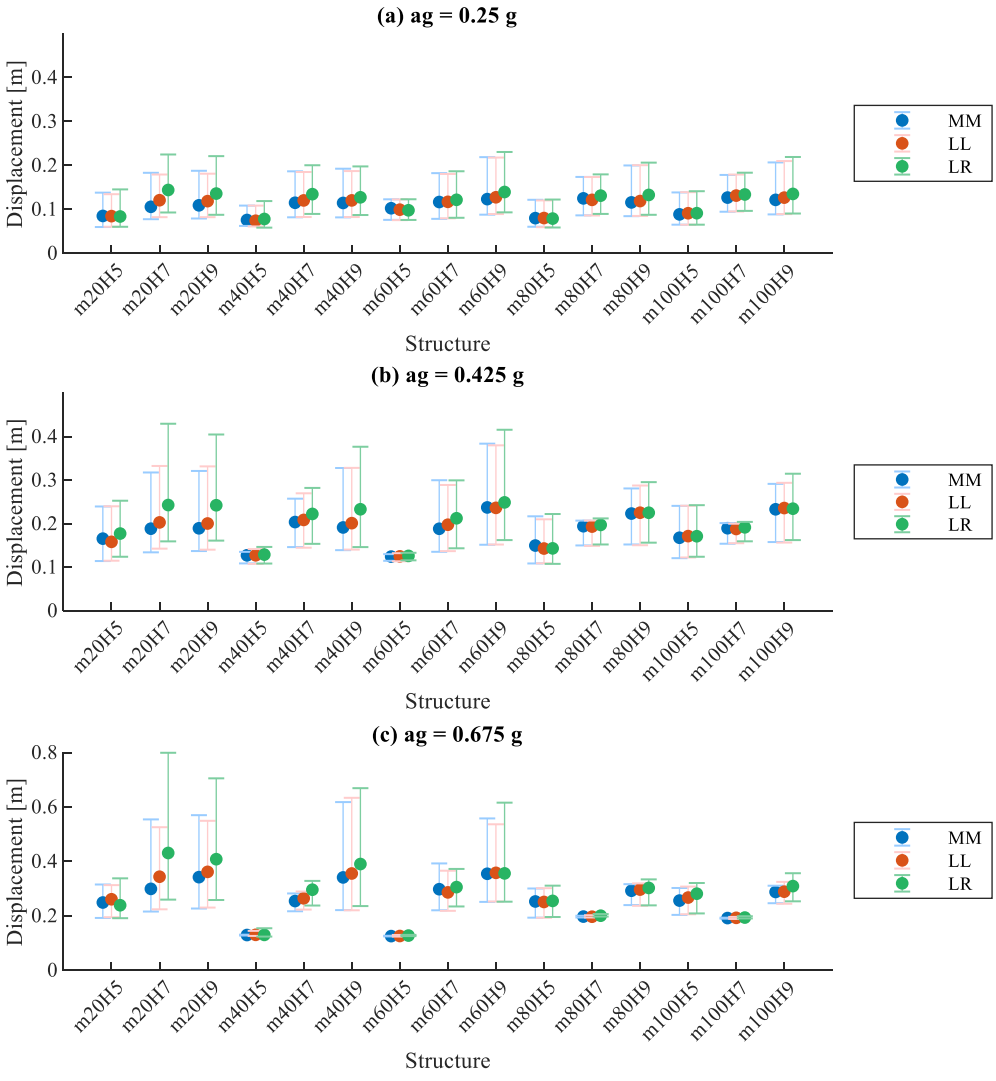

Figure 6.78: Maximum displacement at the top of the structure at (a) a_g = 0.25 g, (b) a_g = 0.425 g and (c) a_g = 0.675 g

Slika 6.78: Maksimalni pomik na vrhu konstrukcij pri (a) a_g = 0.25 g, (b) a_g = 0.425 g in (c) a_g = 0.675 g

The influence of construction imperfections on the main structure's displacements was limited. Construction imperfections influenced the global response of structures in slender structures with small tributary mass and stiffness of the columns (*m20H7*, *m20H9*, *m40H7* and *m40H9*), but even

in those cases, the effect was small. Figure 6.79 shows the difference in median maximum displacements at the top of structures with centrally and eccentrically (*LR*) positioned connections for different tributary masses, stiffness and column slenderness.

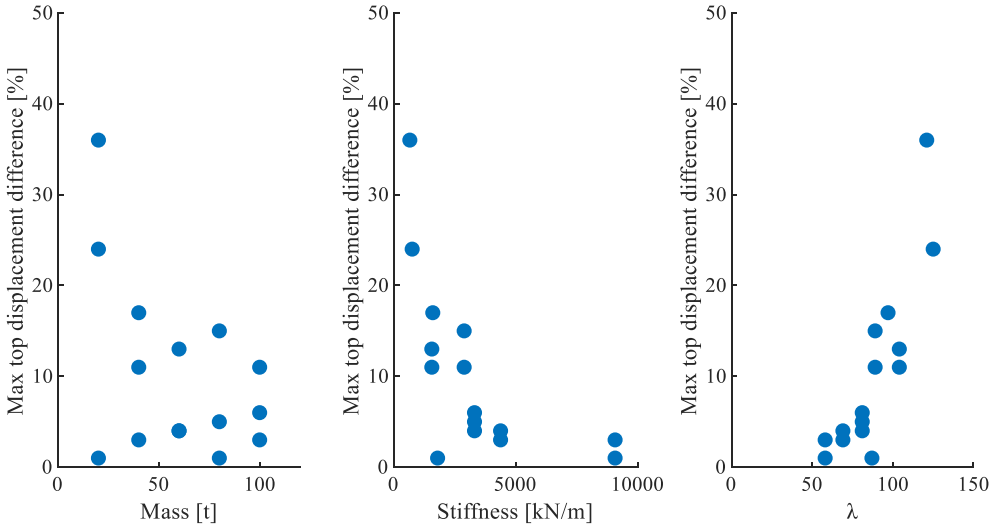

Figure 6.79: Difference in median values of maximum top displacements at a_g = 0.25 g for structures with centrally (*MM*) and eccentrically (*LR*) positioned connections with respect to (a) tributary mass per column, (b) stiffness of the column and (c) slenderness of the column

Slika 6.79: Razlika med maksimalnim pomikom na vrhu konstrukcije pri a_g = 0.25 g za konstrukcije s centrično (*MM*) in ekscentrično (*LR*) pozicioniranimi stiki v odvisnosti od: (a) mase povprečnega stebra, (b) togosti stebra in (c) vitkosti stebra

The response of structures affected by the presence of panels and the eccentric position of the connections was further analysed. Interestingly, the main structure's displacements were typically somewhat larger in the case of the eccentrically positioned connections. One of the reasons could be damping in connections that occurred during the sliding and affected displacements of the structure, as were observed during the shake table tests. When connections were positioned eccentrically, there was less sliding compared to their central position.

Otherwise, the influence of construction imperfections and panels on the response of the main structure was negligible. As already mentioned, impacts in the connections occur only for a moment and do not affect the main structure's global response. To confirm these observations, the force–displacement hysteretic responses of columns *m20H7*, *m60H7* and *m60H9* are shown in Figure 6.80 for ground motion no. 4 at a_g equal to 0.25 g and 0.675 g, respectively. Structure *m20H7* was chosen because the construction imperfections had the most influence on the displacements (see Figure 6.78). In general, the stiffness of the column was not much affected by the position of the connections.

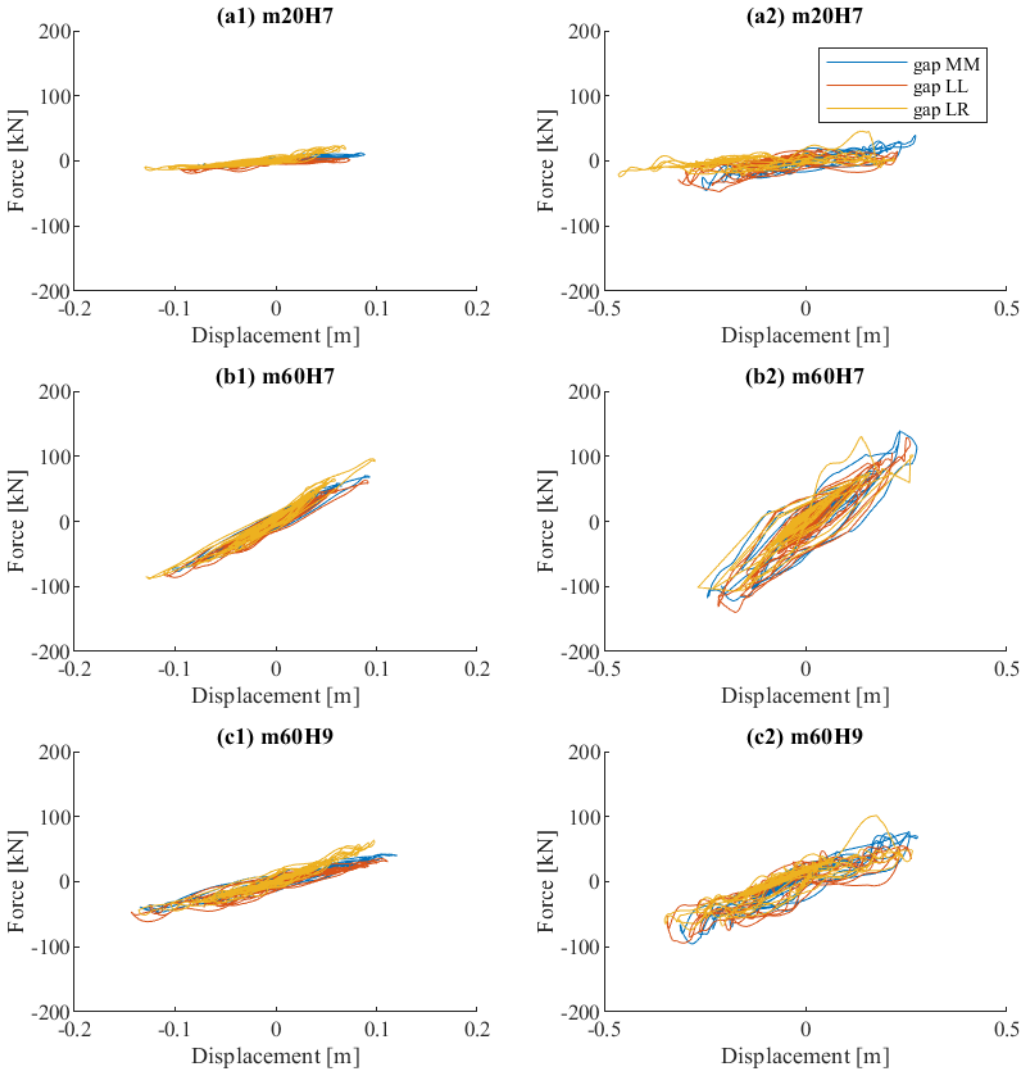

Figure 6.80: Column force–displacement response for structures with different initial positions of the connections at (1) a_g = 0.25 g and (2) a_g = 0.675 g: (a) structure *m20H7*, (b) structure *m60H7*, (c) structure *m60H9*

Slika 6.80: Odziv sila - pomik stebra v konstrukcijah z različno začetno pozicijo stikov pri (1) a_g = 0.25 g in (2) a_g = 0.675 g: (a) hala *m20H7*, (b) hala *m60H7*, (c) hala *m60H9*

Figures 6.81 and 6.82 present displacement responses for the same three structures for different positions of the connections. As shown, the period of vibration was almost the same regardless of the connection position, which indicates that the façade system does not have an important influence on the stiffness of the main precast structure. There was only a minor effect of impacts on the overall displacement response history. This effect can be seen in the displacement response of structure *m60H9*. At higher intensities, when there were stronger impacts (e.g. a_g = 0.675 g), the panels have failed before their influence on the response would be more substantial.

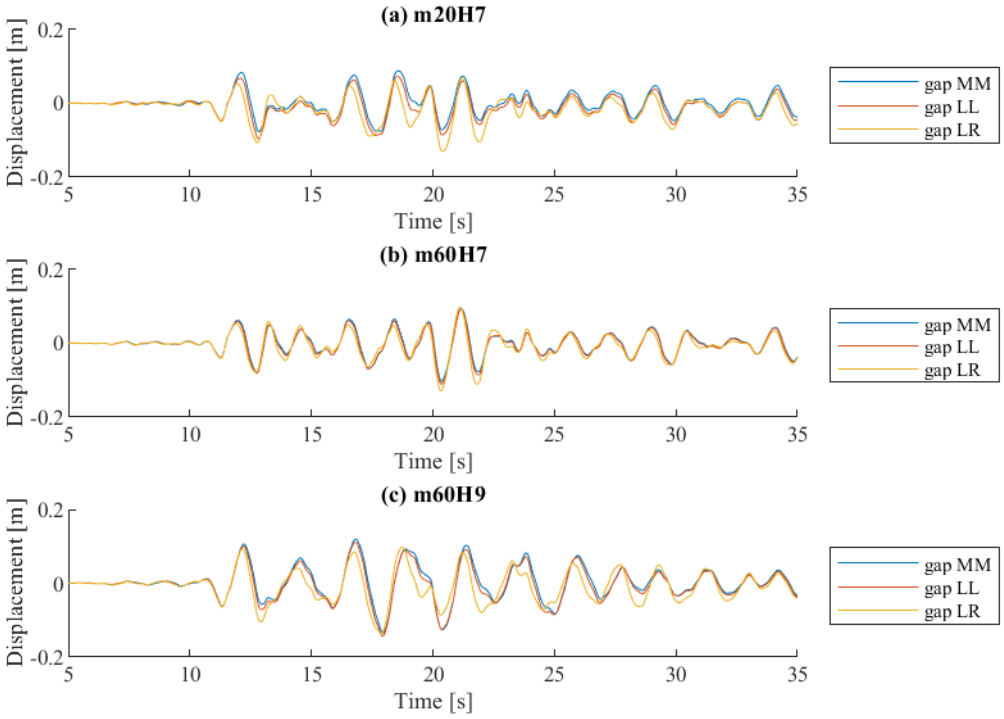

Figure 6.81: Displacement response history at the top of the column at a_g = 0.25 g: (a) structure *m20H7*, (b) structure *m60H7*, (c) structure *m60H9*

Slika 6.81: Časovni potek pomikov na vrhu stebra pri a_g = 0.25 g: (a) hala *m20H7*, (b) hala *m60H7*, (c) hala *m60H9*

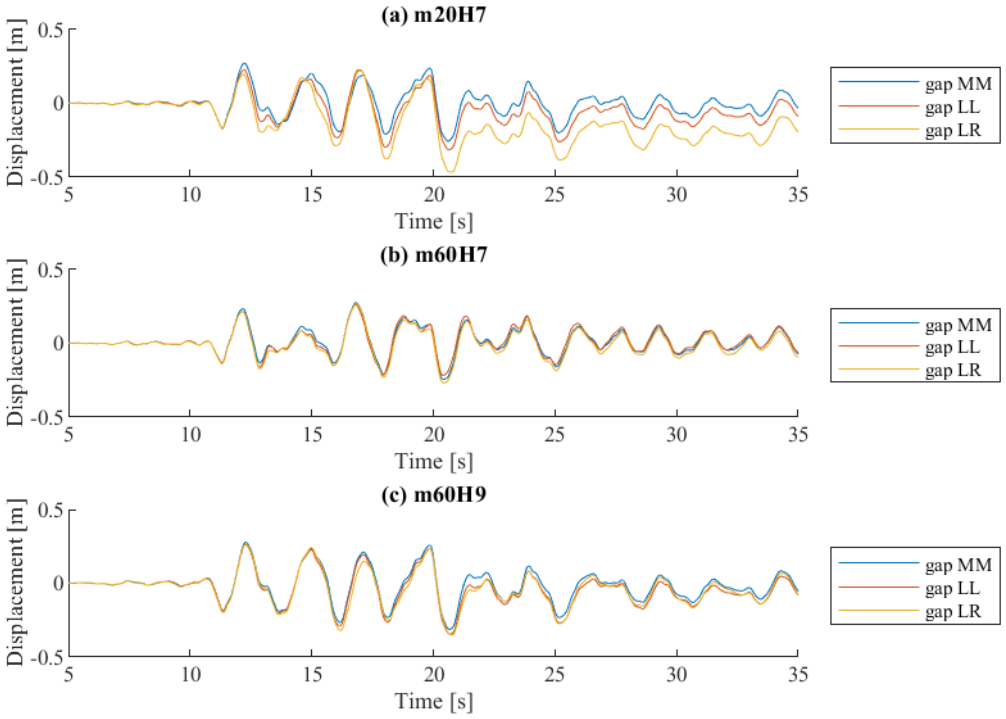

Figure 6.82: Displacement response history at the top of the column at a_g = 0.675 g: (a) structure *m20H7*, (b) structure *m60H7*, (c) structure *m60H9*

Slika 6.82: Časovni potek pomikov na vrhu stebra pri a_g = 0.675 g: (a) hala *m20H7*, (b) hala *m60H7*, (c) hala *m60H9*

Influence of construction imperfections on the shear demand in the column

The maximum shear in the column is compared in Figure 6.83 for centric (*MM*) and both eccentric positions (*LL* and *LR*) of the connections. Somewhat higher shear forces were noticed in the case of the eccentric *LR* position of the connections.

During the impacts in the *LR* position, high lateral forces occurred in opposite directions at the top and bottom of the panel and partially cancelled each other. From that point of view, the *LL* position of the connections might have a worse effect on shear in the column. However, there were more impacts in the *LR* position, and forces in connections were considerably larger. For that reason, the influence on columns was also somewhat greater.

However, this influence was, in general, small, and because of capacity design and minimum reinforcement requirements, the shear resistance was not exceeded. Figures 6.84 and 6.85 show the maximum shear force in the column for different connection positions for three characteristic

structures. As shown, the position of the connections could influence the shear force distribution along the column. However, the influence on the maximum force in a column is negligible.

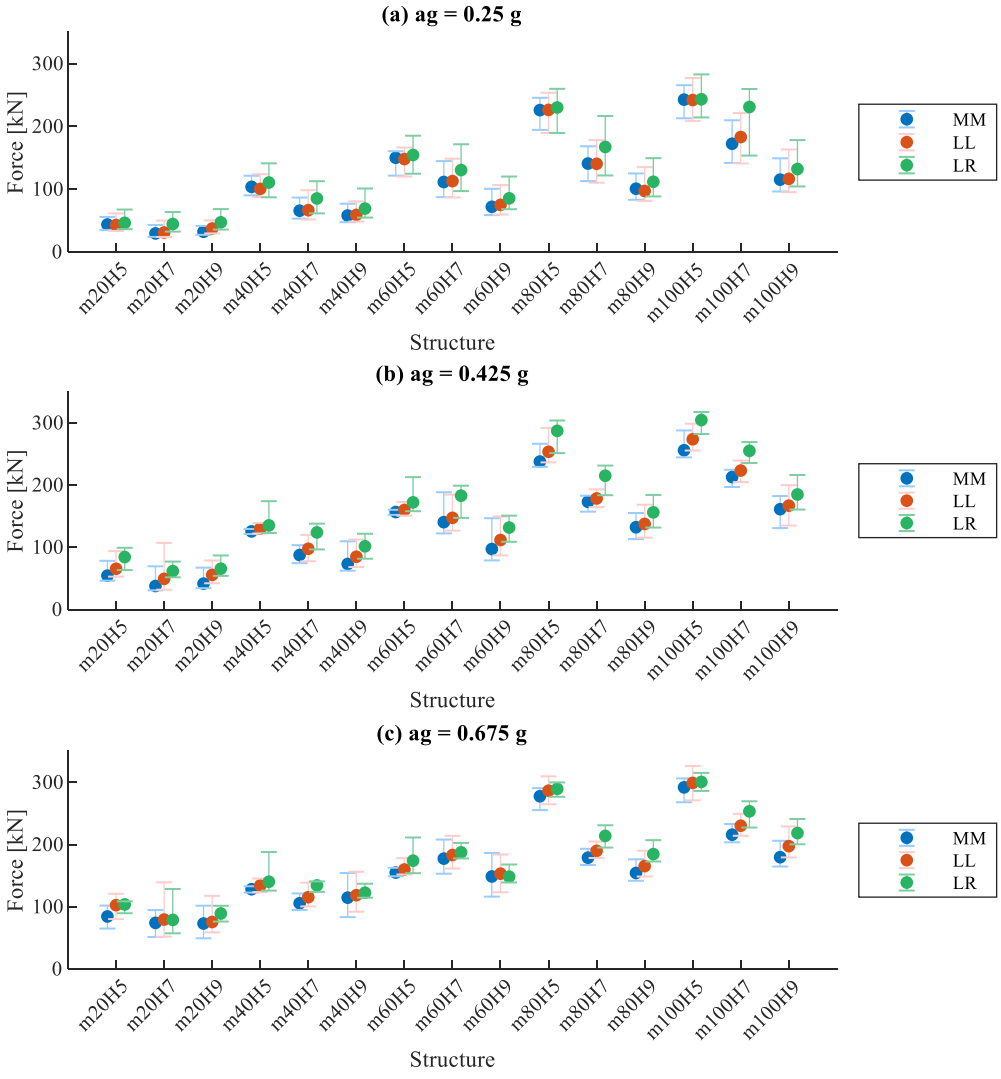

Figure 6.83: Maximum shear force in the column at (a) a_g = 0.25 g, (b) a_g = 0.425 g and (c) a_g = 0.675 g

Slika 6.83: Maksimalne strižne sile v stebru pri (a) a_g = 0.25 g, (b) a_g = 0.425 g in (c) a_g = 0.675 g

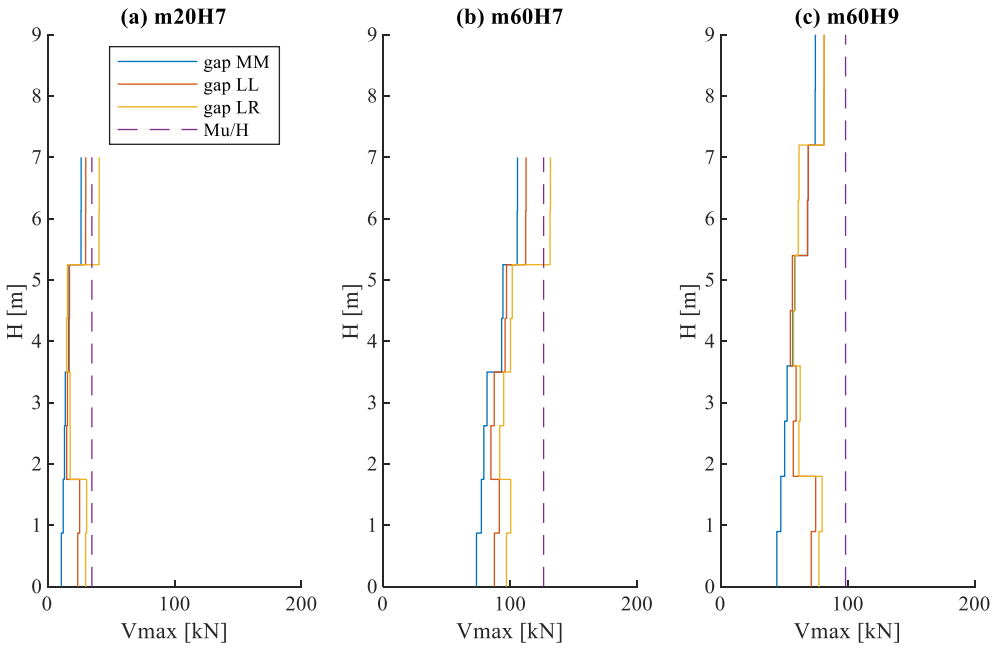

Figure 6.84: Maximum shear force along the column height for different initial positions of connections at a_g = 0.25 g: (a) *m60H5*, (b) *m60H7* and (c) *m60H9*

Slika 6.84: Maksimalna strižna sila po višini stebra pri halah z različnimi začetnimi pozicijami stikov pri a_g = 0.25 g: (a) *m60H5*, (b) *m60H7*, (c) *m60H9*

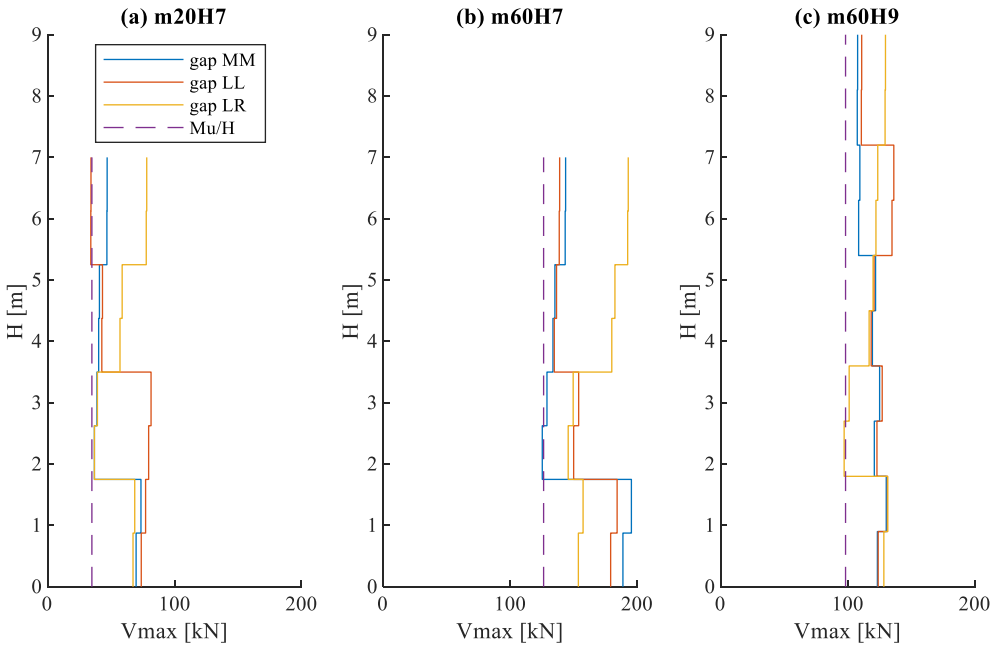

Figure 6.85: Maximum shear force along the column height for different initial positions of connections at a_g = 0.675 g: (a) *m60H5*, (b) *m60H7* and (c) *m60H9*

Slika 6.85: Maksimalna strižna sila po višini stebra pri halah z različnimi začetnimi pozicijami stikov pri a_g = 0.675 g: (a) *m60H5*, (b) *m60H7*, (c) *m60H9*

6.4.3 Influence of the connection of bottom panels to the foundation on the response

The lowest panels that are often fixed to the foundation caused concern about the possible occurrence of the short-column effect. For that reason, two possible connections of bottom panels to the foundation were considered, and their influence on the shear distribution was analysed. The panel was either fixed to the foundation (*F-fixed*) or connected to the column as all other panels (*C-connection*). In the latter case, the connection between panel and foundation was provided only by silicone sealant. In numerical analyses, silicone-sealed joints (*P*) were taken into account between all the panels, as is usual in real structures. It was supposed that all the connections were positioned centrally (*MM*), and the ratio factor *k* was set to 2.

Influence of the connection of bottom panel to the foundation on the response of panels

The bottom panel's connection to the foundation had an important influence on the response of the bottom panel and only a minor influence on the response of other panels. The difference in the bottom panel's response for two different connections is depicted in Figure 6.86.

When the bottom panel was connected to the column as all the other panels (Figure 6.86 a), relative displacements between the column and panel occurred at both the top and bottom edges of the panel. Responses of top and bottom connections were typically in opposite directions. However, if the bottom panel was fixed to the foundation, relative displacements occurred only at the bottom panel's top connection (Figure 6.86 b). Because the bottom panel was fixed to the foundation, relative displacements at the top connection were larger, leading to an earlier failure of the fastening system. Although such failure would not necessarily cause a collapse of the panel because it was fixed at the bottom edge, repairing the damage would be difficult. All the higher panels would have to be removed to repair the bottom panel.

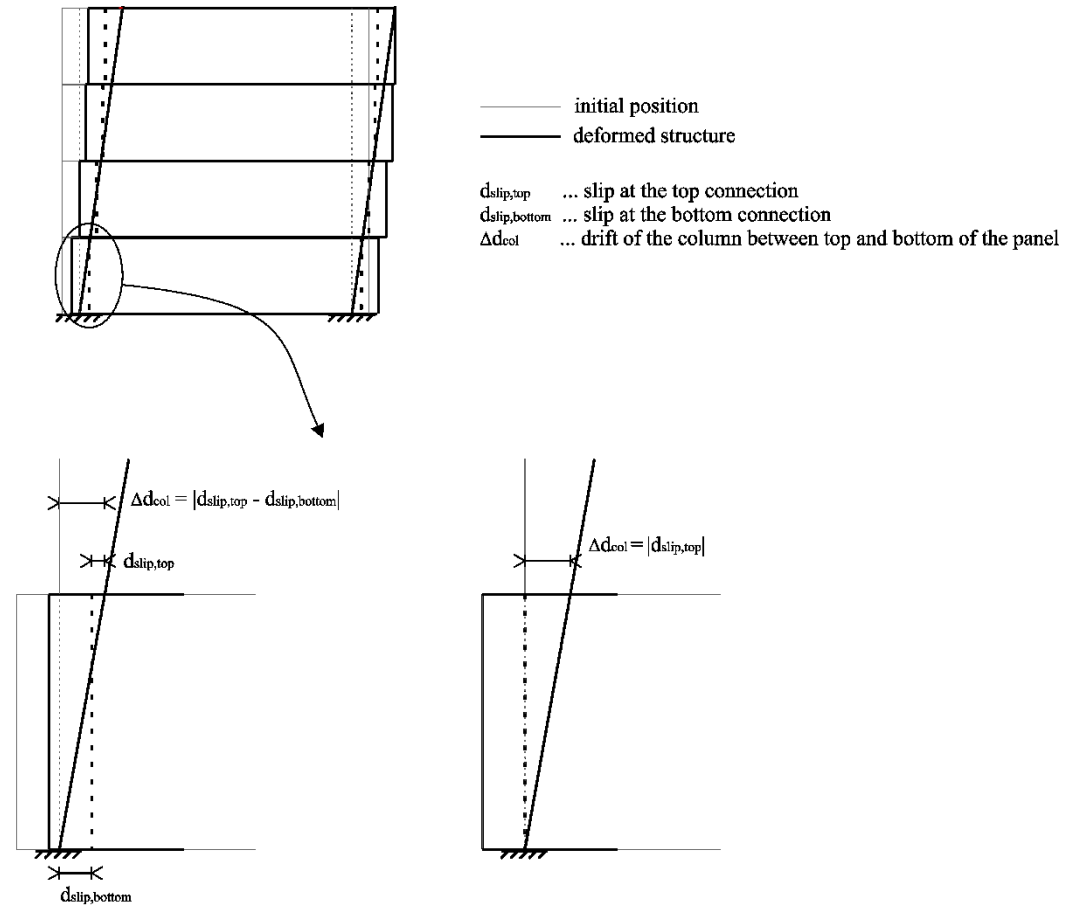

Figure 6.86: Response of the structure with horizontal cladding panels: (a) bottom panel connected to the column with cantilever connection and sealed with silicone to the foundation, (b) bottom panel fixed to the foundation

Slika 6.86: Odziv konstrukcije s horizontalnimi paneli: (a) spodnji panel pritrjen na steber, (b) spodnji panel fiksiran v temelj

There were more failures if the bottom panel was fixed to the foundation because of the many failures of the top connections of the bottom panels. If the bottom panel was fixed to the foundation, the column drift along the single panel at the point of fastening failure was, in general, smaller (11.2 cm if all failed fastenings were considered and 7.6 cm if only the first failure was taken into account) than if the bottom panel was connected to the column as all the higher panels were (13.6 cm and 10.1 cm for all failed fastenings and only first failures, respectively). Please see Figures 6.32 and 6.33.

If the bottom panel was fixed to the foundation, the drift capacity of the fastening system was the same as the displacement capacity of the top connections (7.5 cm and 3.5 cm in the case of centrally and eccentrically positioned connections, respectively). However, if the bottom panel was connected to the column, the drift capacity of the complete fastening system was larger due to the

contribution of the bottom connections. It was the same as the capacity of fastening systems of the higher panels. Thus, for the panel response, it is better not to fix the bottom panel to the foundation.

Figures 6.87 and 6.88 present the maximum slips at top and bottom connections for two different connections of the bottom panel to the foundation, respectively. As shown, at the bottom panel, there were slips only at top connections if the panel was fixed to the foundation. The difference in maximum displacements at other panels was minor and not important for the response of panels. This is shown in Figure 6.89, where maximum displacements at connections are compared for all the structures at a_g = 0.25 g.

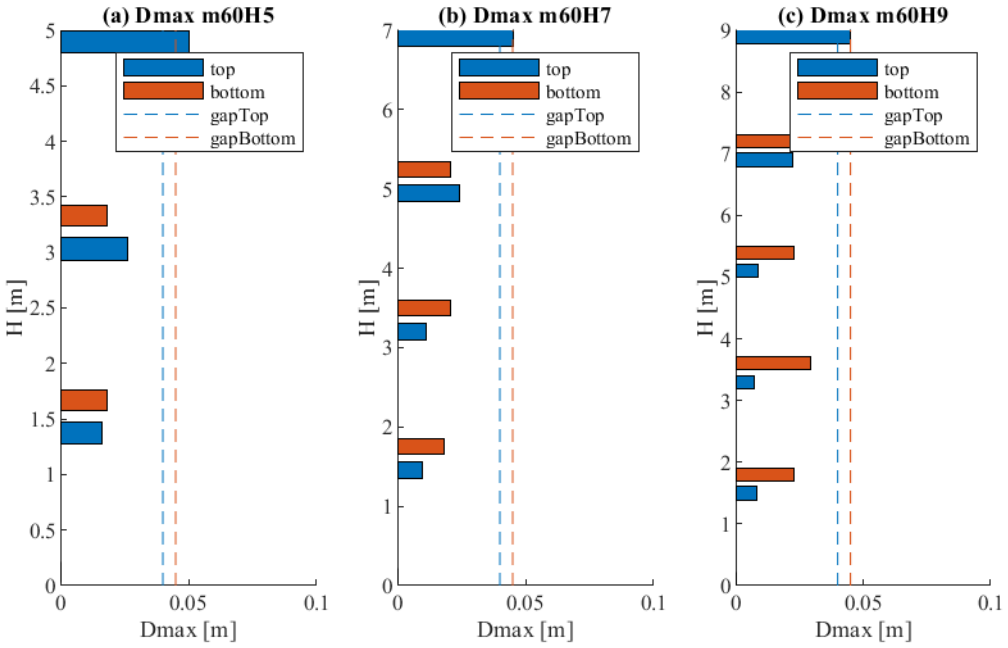

Figure 6.87: Maximum slips at cladding connections for structure with fixed bottom panel (*F*) at a_g = 0.25 g: (a) structure *m60H5*, (b) structure *m60H7* and (c) structure *m60H9*

Slika 6.87: Največji zdrsi fasadnih stikov pri a_g = 0.25 g v primeru, ko je spodnji panel fiksiran v temelj (*F*): (a) konstrukcija *m60H5*, (b) konstrukcija *m60H7*, (c) konstrukcija *m60H9*

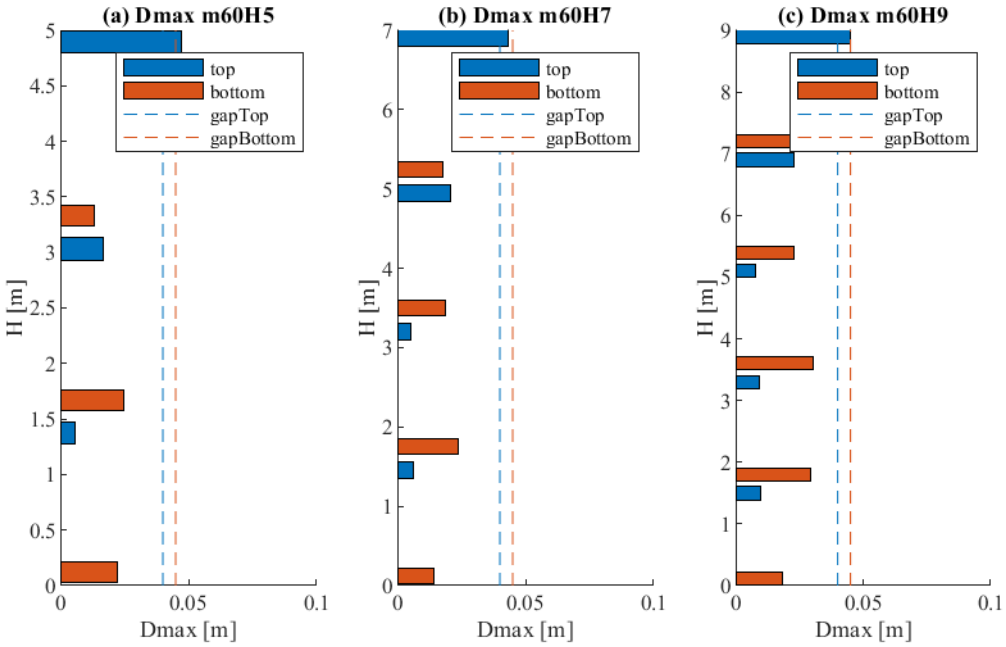

Figure 6.88: Maximum slips at cladding connections for structure with bottom panel connected to the column (*C*) and sealed to the foundation at a_g = 0.25 g: (a) structure *m60H5*, (b) structure *m60H7* and (c) structure *m60H9*

Slika 6.88: Največji zdrsi fasadnih stikov pri a_g = 0.25 g v primeru, ko je spodnji panel pritjen na steber (*C*): (a) konstrukcija *m60H5*, (b) konstrukcija *m60H7*, (c) konstrukcija *m60H9*

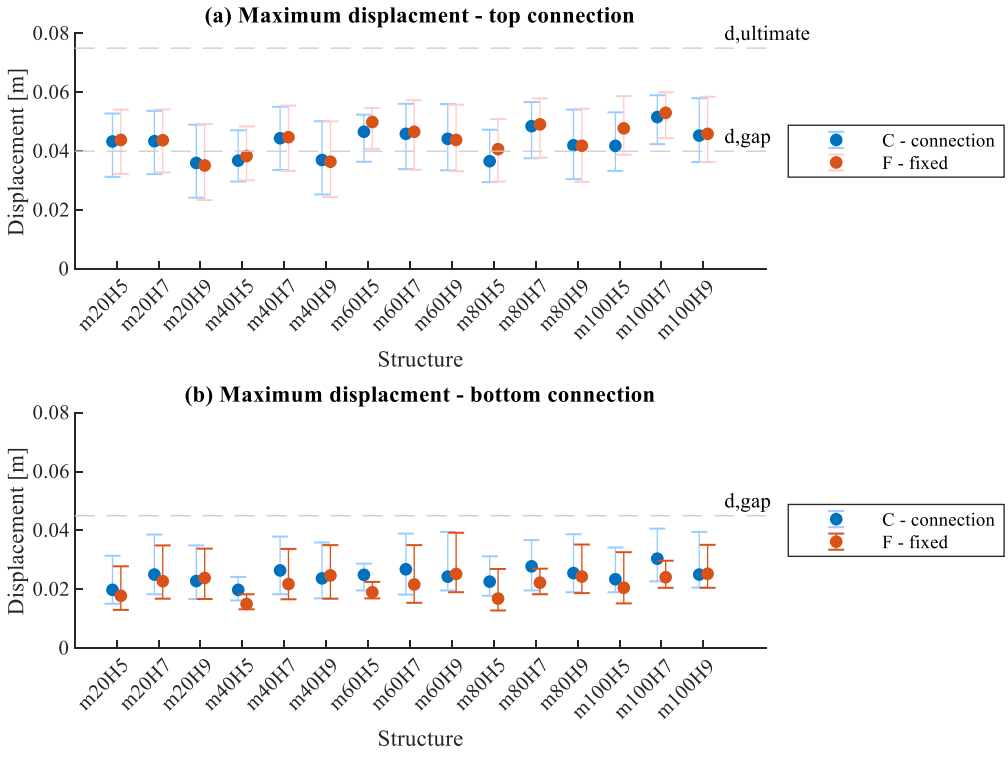

Figure 6.89: Maximum slips at (a) top connections and (b) bottom connections at a_g = 0.25 g

Slika 6.89: Maksimalni zdrsi v (a) zgornjih in (b) spodnjih stikih pri a_g = 0.25 g

When the bottom panel was fixed to the foundation, in general, higher forces at bottom connections occurred. The comparison is shown in Figure 6.90 for a_g = 0.675 g when strong impacts have occurred. The influence of those forces on the shear demand was analysed and is discussed in the following paragraphs. All the results of characteristic structures with fixed and connected bottom panels are gathered in Appendices C and F.

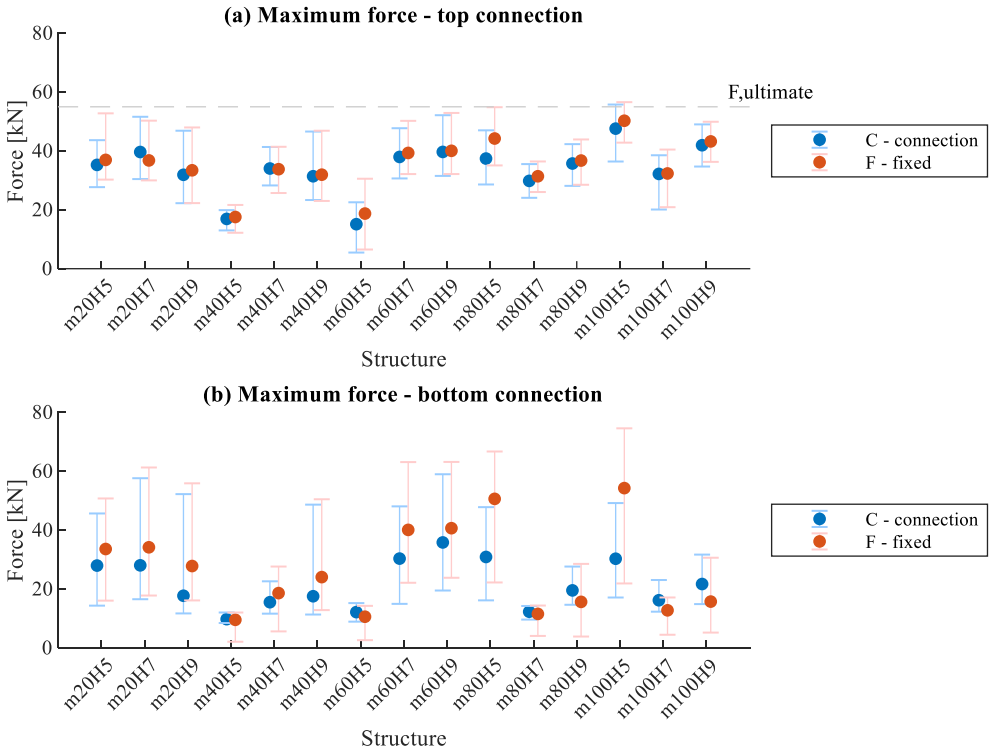

Figure 6.90: Maximum force at (a) top connections and (b) bottom connections at a_g = 0.675 g
Slika 6.90: Maksimalna sila v (a) zgornjih in (b) spodnjih stikih pri a_g = 0.675 g

Influence of the connection of bottom panel to the foundation on the global response of the structure

The maximum displacements of structures with different connections of the bottom panel to the foundation are shown in Figure 6.91. As expected, the influence of the connection of bottom panels to the foundation on the structure's global response is very small. The difference in the maximum displacements of the columns was negligible.

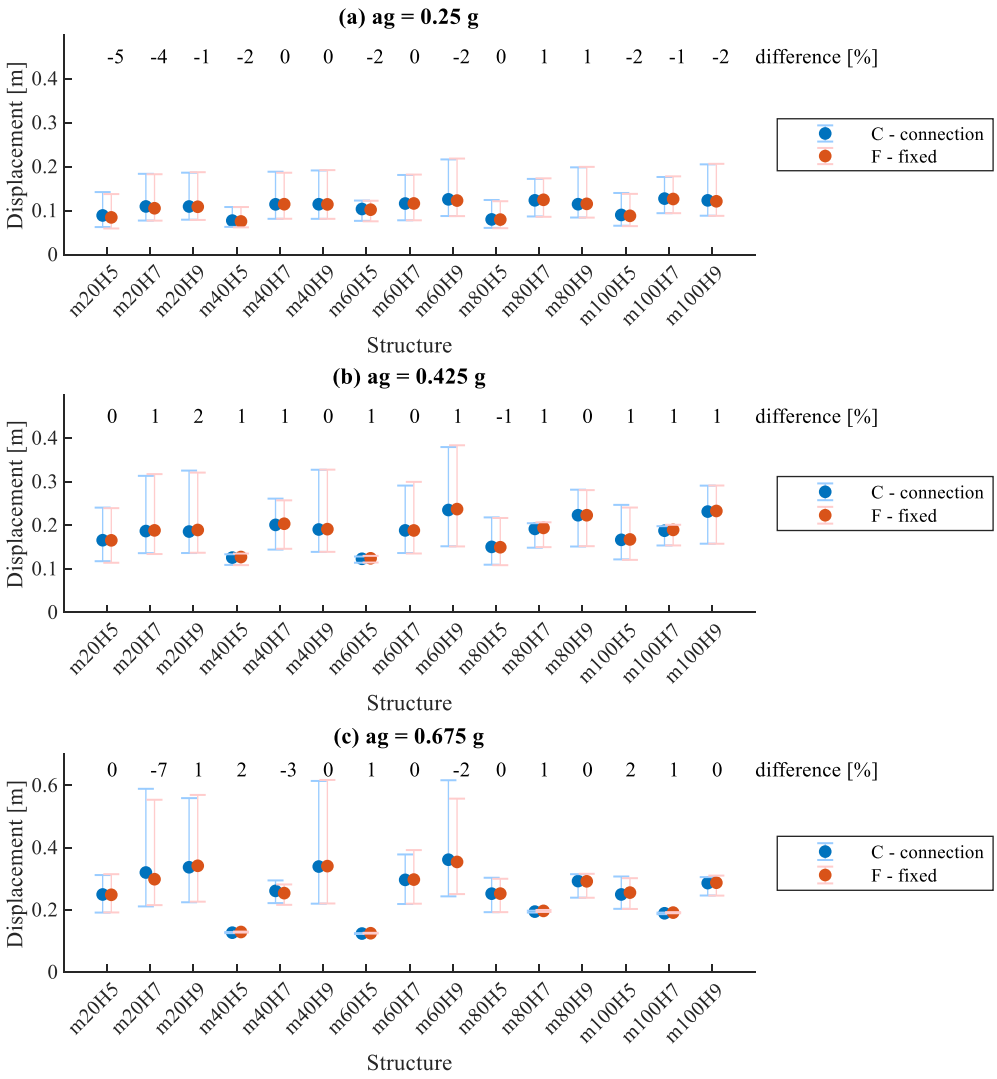

Figure 6.91: Maximum displacement at the top of the structure with bottom panel fixed to the foundation and bottom panel connected to the column as all other panels: (a) $a_g = 0.25$ g, (b) $a_g = 0.425$ g and (c) $a_g = 0.675$ g
Slika 6.91: Maksimalni pomik na vrhu konstrukcij s fiksiranim spodnjim panelom in spodnjim panelom, ki je obešen na steber: (a) $a_g = 0.25$ g, (b) $a_g = 0.425$ g in (c) $a_g = 0.675$ g

Influence of the connection of bottom panel to the foundation on the shear demand in column

As shown in Figure 6.90, the maximum force at a single bottom connection was higher in the case of the fixed bottom panel to the foundation. The overall maximum shear demand in the column was not affected so much. Figure 6.92 compares the maximum shear force for the two types of connections of the bottom panel. As shown, the maximum force is only slightly higher in the case of a fixed bottom panel.

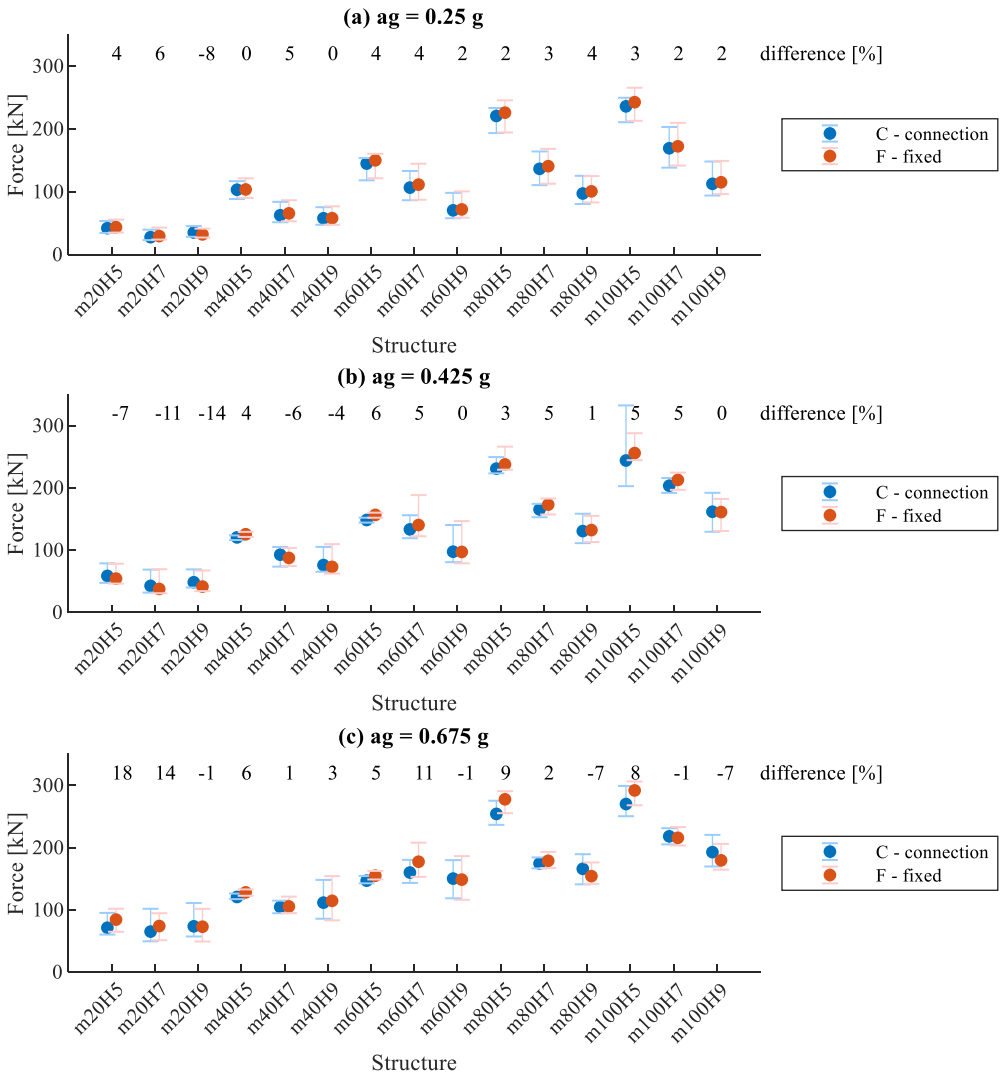

Figure 6.92: Maximum shear force in the column for structures with bottom panel fixed to the foundation and bottom panel connected to the column as all other panels: (a) a_g = 0.25 g, (b) a_g = 0.425 g and (c) a_g = 0.675 g

Slika 6.92: Maksimalna strižna sile v stebru za hale s fiksiranim spodnjim panelom in spodnjim panelom, ki je obešen na steber: (a) a_g = 0.25 g, (b) a_g = 0.425 g in (c) a_g = 0.675 g

The distribution of maximum shear forces along the column is shown in Figures 6.93 and 6.94 for three characteristic cases. For the design intensity a_g = 0.25 g, there was practically no influence of connection of the bottom panel on the shear force along the column. As shown, the distribution of force changes only in some cases at a higher intensity (e.g. structure *m60H7* in Figure 6.94). However, the maximum force that occurred in the column was not so different. Reasons for the change in the distribution of forces can be various and difficult to predict, for example, selection of structure, the influence of higher modes, the mass and height of the panels, or ground motion.

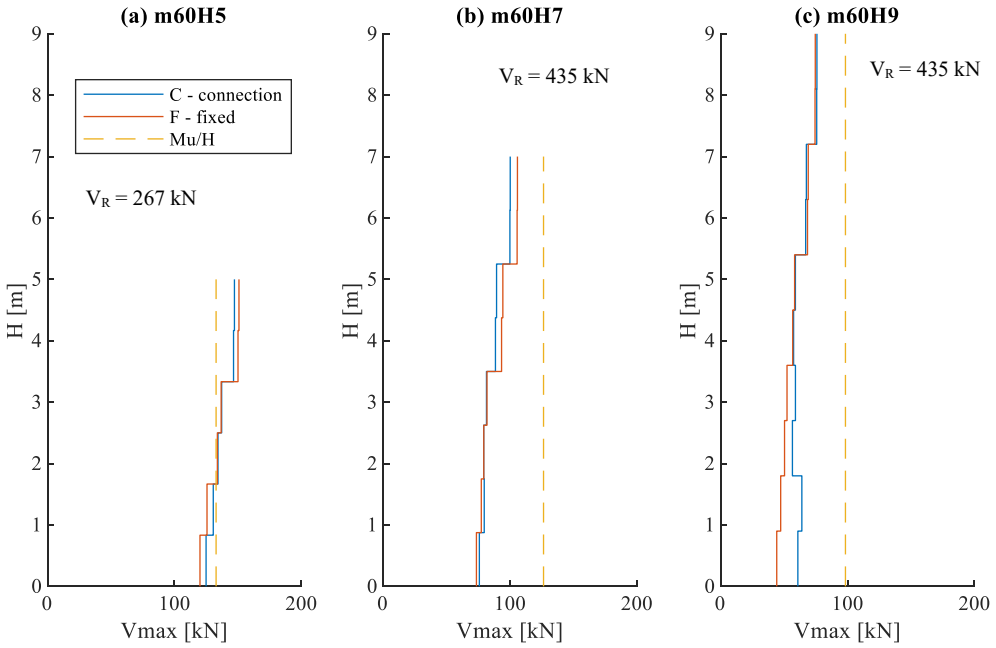

Figure 6.93: Maximum shear force in the column at a_g = 0.25 g: (a) structure *m60H5*, (b) structure *m60H7* and (c) structure *m60H9*

Slika 6.93: Največja strižna sila v stebru pri a_g = 0.25 g: (a) hala *m60H5*, (b) hala *m60H7*, (c) hala *m60H9*

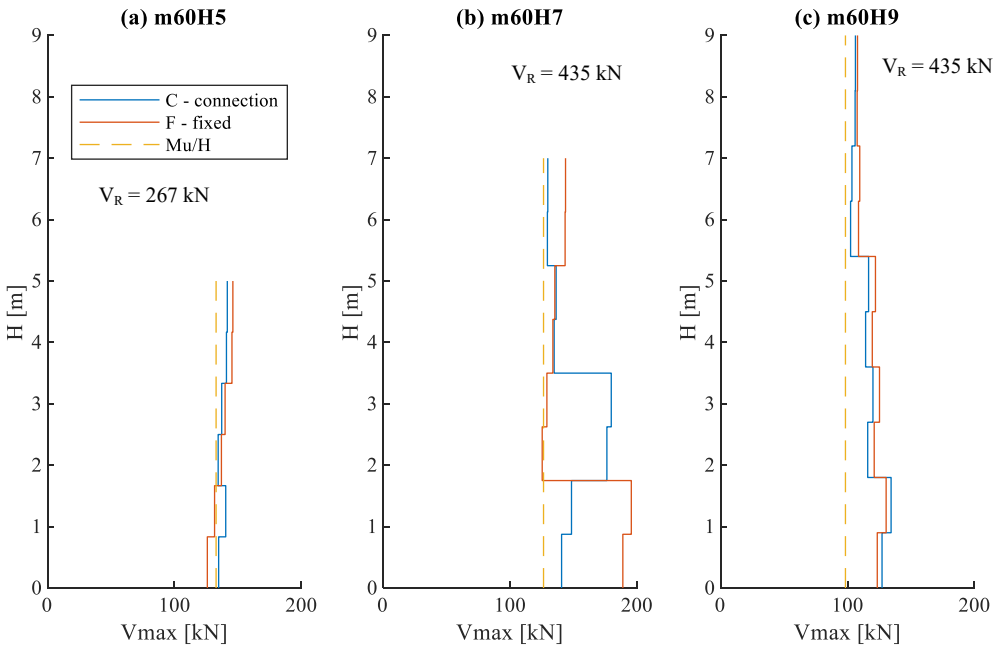

Figure 6.94: Maximum shear force in the column at a_g = 0.675 g: (a) structure *m60H5*, (b) structure *m60H7* and (c) structure *m60H9*

Slika 6.94: Največja strižna sila v stebru pri a_g = 0.675 g: (a) hala *m60H5*, (b) hala *m60H7*, (c) hala *m60H9*

6.4.4 Influence of the ratio k = columns/panels on the response

This section investigates the effect of the structure's ground plan configuration on the overall seismic response by changing the *k* ratio. As described in Section 6.1.3, the ratio *k* presents the ratio between the number of all columns of the structure n_{col} and the number of panels in ground plan n_{pan} in the considered direction.

The entire range of masses and heights (presented in Table 6.1) was considered in the study. It was supposed that the connections were positioned centrally (*MM*), and the bottom panels were fixed to the foundation (*F*). Interaction between adjacent panels was taken into account as is usual in real structures; the silicone was modelled with a *Pinching* material model (*P*).

Values of *k* were varied from 1 to 10, which is an expected range of *k* factors in real structures. A higher value of the *k* factor means a larger number of columns compared to the number of panels. Results of the parametric study and the influence of ratio *k* on the response parameters are discussed in the following paragraphs. Results are shown for *k* factors 1, 2, 4 and 10 because there was no important difference in responses of structures with a ratio of *k* between 4 and 10.

Influence of ratio k on the response of panels

In general, the response of the connections was not much affected by changing the *k* factor. Displacements at connections are shown for a_g = 0.25 g (see Figure 6.95), for which most connections were in the sliding phase, and the gaps were often closed only at the top panel's top connection (see Section 6.4.1). The forces are shown for a_g = 0.675 g when many impacts have occurred.

As shown in Figures 6.95 and 6.96, displacements and forces in connections were not much affected by the size of *k*. Some influence on the connection forces was observed only for structures *m40H5*, *m60H5*, *m80H7* and *m100H7,* where the maximum force at the top connection was somewhat larger for $k = 1$. For $k = 1$, the maximum forces at the bottom connections were also slightly smaller for some structures. However, these discrepancies are negligible. Because the influence of the *k* factor on the response of the connections was not significant, it also did not have an important effect on the drift capacity of the fastening system, either the failure of silicone sealant or the failure of fastenings.

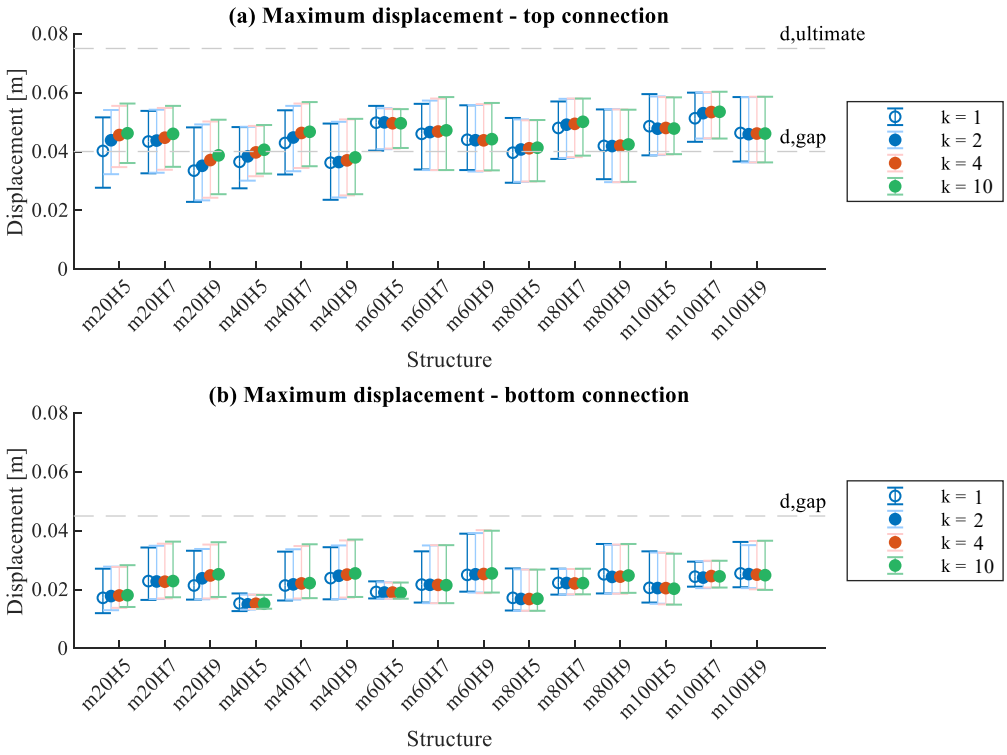

Figure 6.95: Maximum slips at (a) top connections and (b) bottom connections at a_g = 0.25 g

Slika 6.95: Maksimalni zdrsi v (a) zgornjih in (b) spodnjih stikih pri a_g = 0.25 g

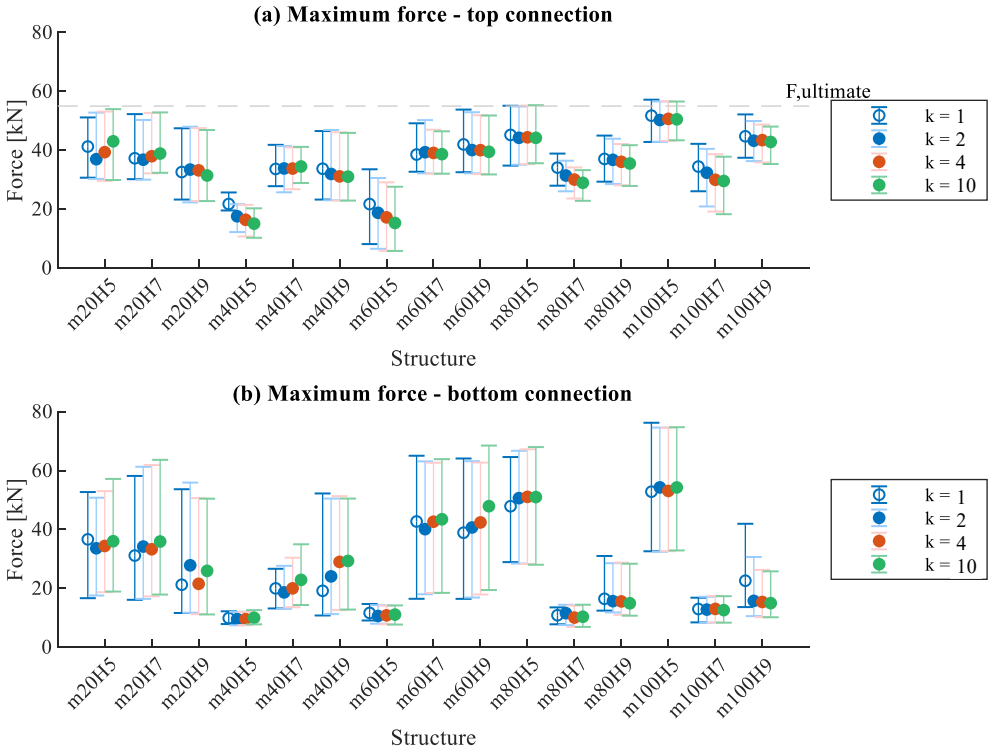

Figure 6.96: Maximum force at (a) top connections and (b) bottom connections at a_g = 0.675 g

Slika 6.96: Maksimalna sila v (a) zgornjih in (b) spodnjih stikih pri a_g = 0.675 g

Influence of ratio k on the global response of the structure

Figure 6.97 presents the maximum displacements at the top of the structure. There was some influence of the ratio between the number of columns and the number of connections on the global response of precast structures. However, no important difference in the responses of structures with a ratio of *k* from 4 to 10 was observed.

The displacement response of the columns was noticeably different only for the smallest *k* ratio of 1.0 (the smallest number of columns compared to the number of panels) in the case of slender structures with small tributary mass and small column stiffness (e.g. *m20H7*, *m20H9*, *m40H7*). This is presented in Figure 6.98, where the difference in median values of maximum displacements for structures with ratio *k* equal to 1 and 10 is shown.

Therefore, the panels influenced the response of slender structures with very small stiffness of the main structure compared to the façade system (smaller *k* ratio). As already observed in previous sections, the response of those structures was also affected by silicone sealant and the position of connections.

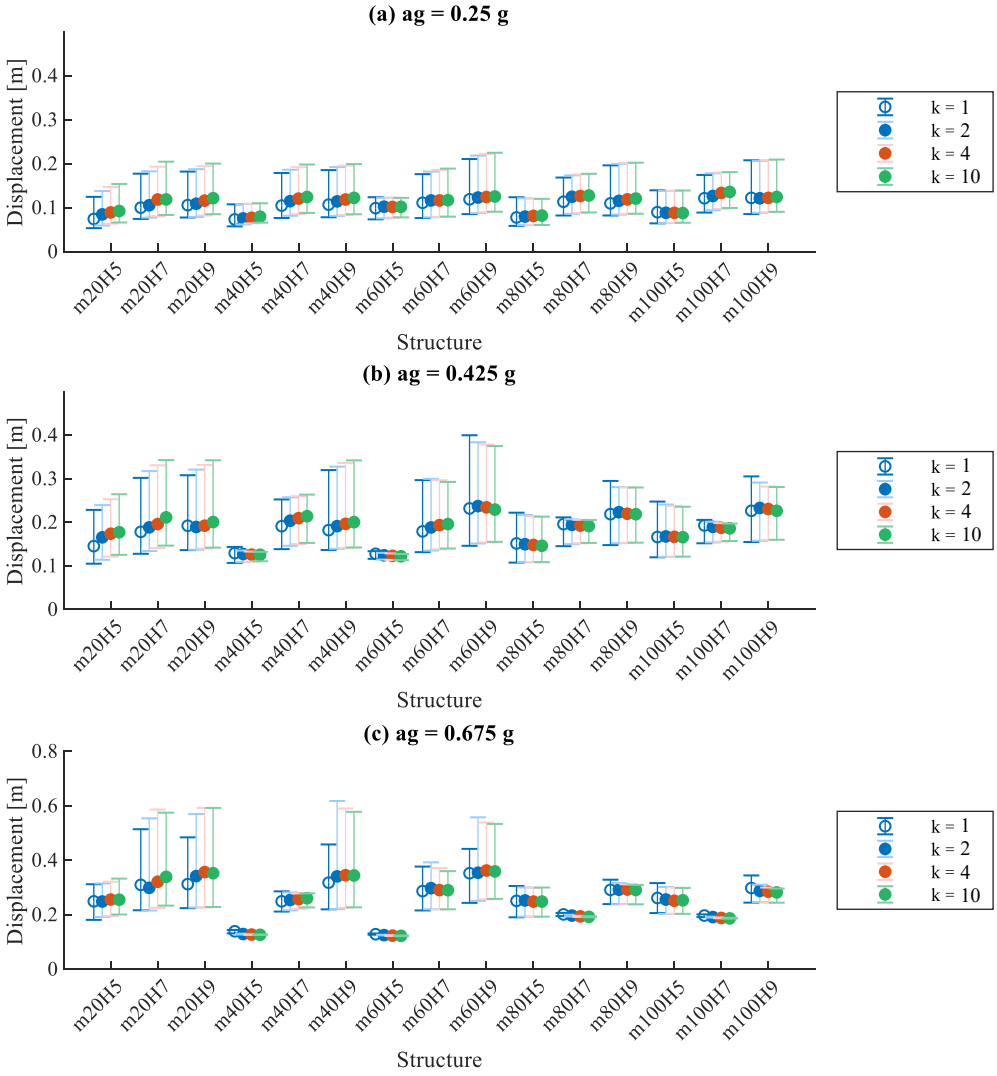

Figure 6.97: Maximum displacement at the top of the structure at (a) a_g = 0.25 g, (b) a_g = 0.425 g and (c) a_g = 0.675 g

Slika 6.97: Maksimalni pomik na vrhu konstrukcij pri (a) a_g = 0.25 g, (b) a_g = 0.425 g in (c) a_g = 0.675 g

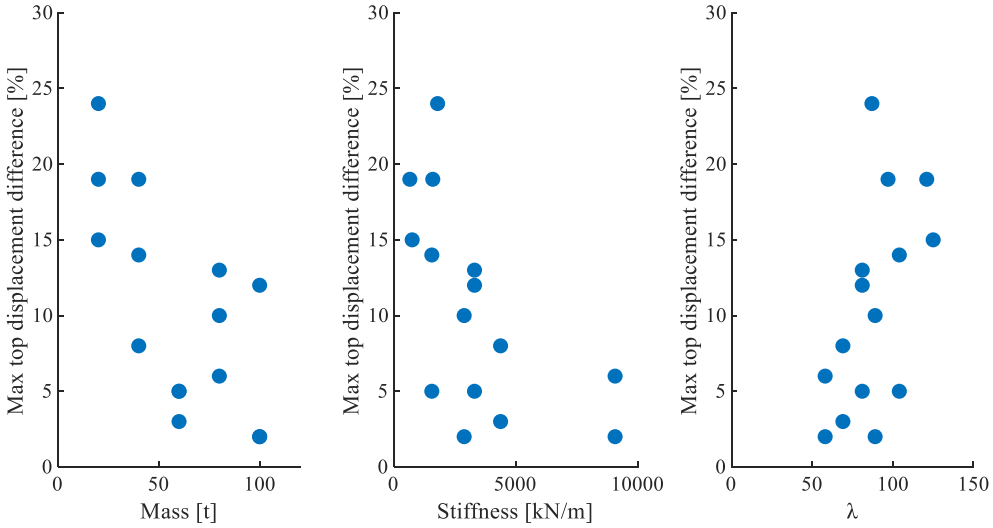

Figure 6.98: Difference in median values of maximum top displacements at a_g = 0.25 g for structures with k ratio equal to 1 and 10 with respect to (a) tributary mass per column, (b) stiffness of the column and (c) slenderness of the column

Slika 6.98: Razlika med maksimalnim pomikom na vrhu konstrukcije pri a_g = 0.25 g za konstrukcije s faktorjem razmerja 1 in 10 v odvisnosti od (a) mase povprečnega stebra, (b) togosti stebra in (c) vitkosti stebra

The force–displacement response of columns is presented considering different values of k in Figure 6.99. As shown, the influence of panels on the stiffness of the main structure is negligible. Some magnification of shear forces can be observed in Figure 6.99 (c2) that occurred due to the contribution of higher modes of vibration. This effect was noticed at higher intensities for relatively slender structures.

Figures 6.100 and 6.101 compare the displacement response histories for structures with different values of k. The period of compared structures is almost the same, which shows that the influence of k and panels on the structure response is small.

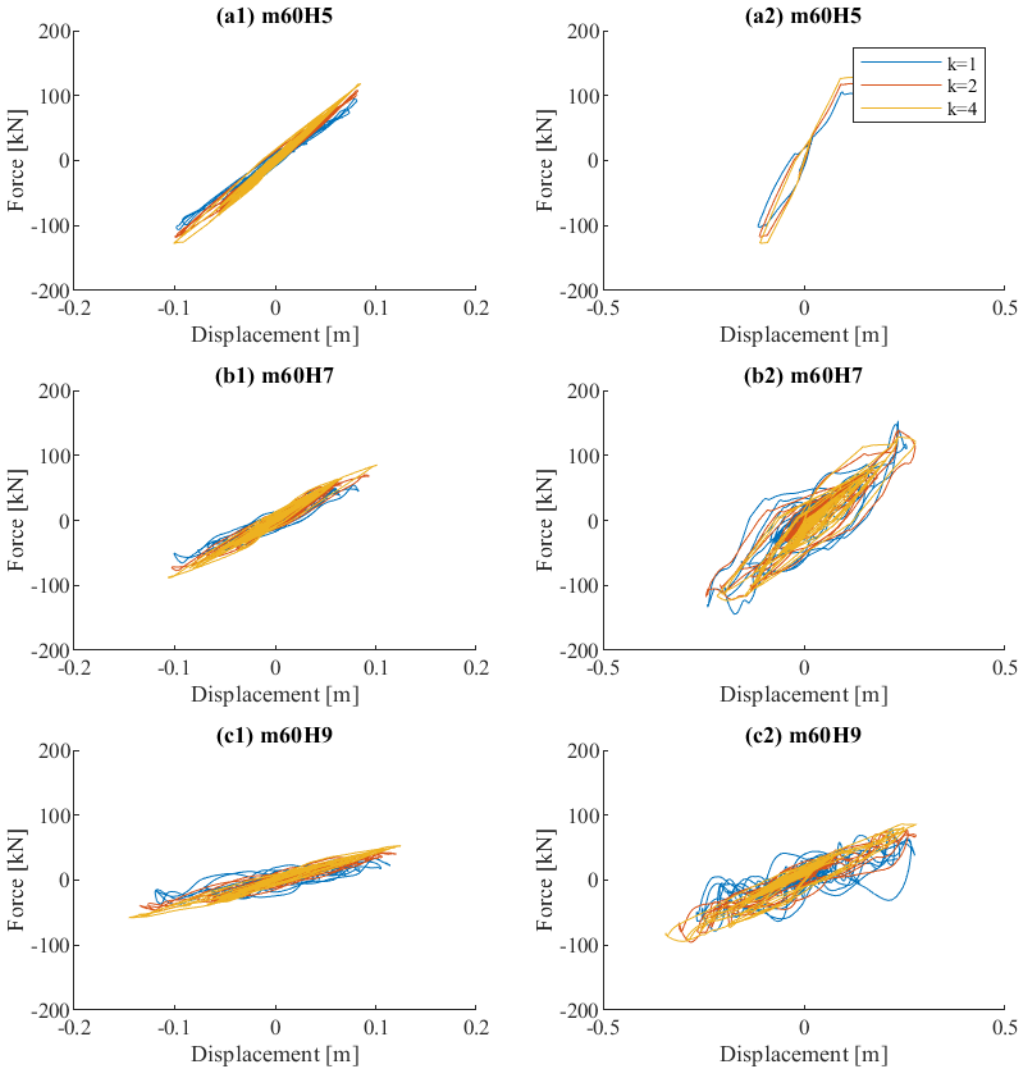

Figure 6.99: Column force–displacement response for structures with different k ratios at (1) a_g = 0.25 g and (2) a_g = 0.675 g: (a) structure *m60H5*, (b) structure *m60H7* and (c) structure *m60H9*

Slika 6.99: Odziv sila - pomik za steber v konstrukcijah z različnim razmerjem k pri (1) a_g = 0.25 g in (2) a_g = 0.675 g: (a) hala *m60H5*, (b) hala *m60H7*, (c) hala *m60H9*

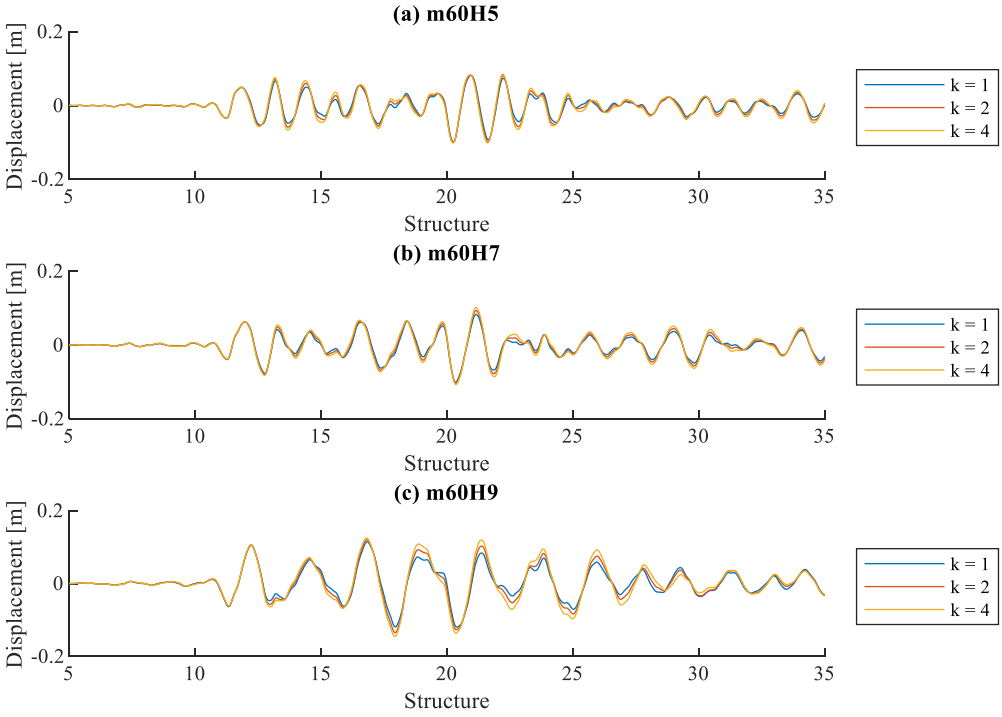

Figure 6.100: Displacement response history at the top of the column for structures with different k ratios at a_g = 0.25 g: (a) structure *m20H7*, (b) structure *m60H7* and (c) structure *m60H9*

Slika 6.100: Časovni potek pomikov na vrhu stebra konstrukcij z različnim razmerjem k pri a_g = 0.25 g: (a) hala *m20H7*, (b) hala *m60H7*, (c) hala *m60H9*

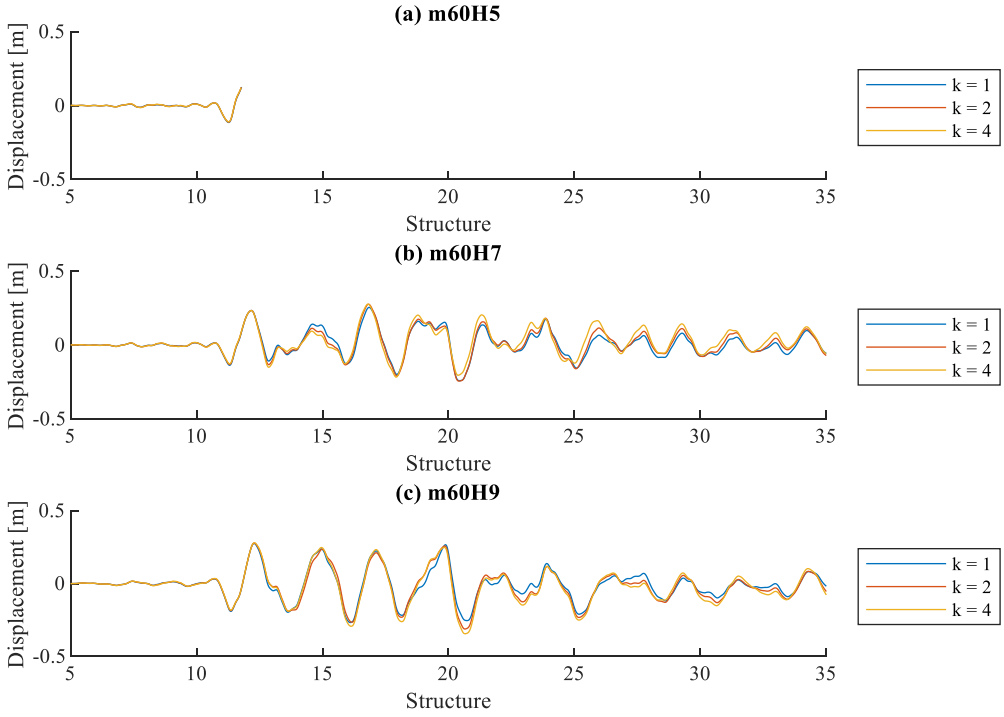

Figure 6.101: Displacement response history at the top of the column for structures with different k ratios at a_g = 0.675 g: (a) structure *m20H7*, (b) structure *m60H7* and (c) structure *m60H9*

Slika 6.101: Časovni potek pomikov na vrhu stebra konstrukcij z različnim razmerjem k pri a_g = 0.675 g: (a) hala *m20H7*, (b) hala *m60H7*, (c) hala *m60H9*

Influence of k ratio on the shear demand in columns

Figure 6.102 presents the maximum shear forces recorded in columns. Because the ratio factor did not significantly influence forces in connections, the influence on maximum forces in columns was negligible.

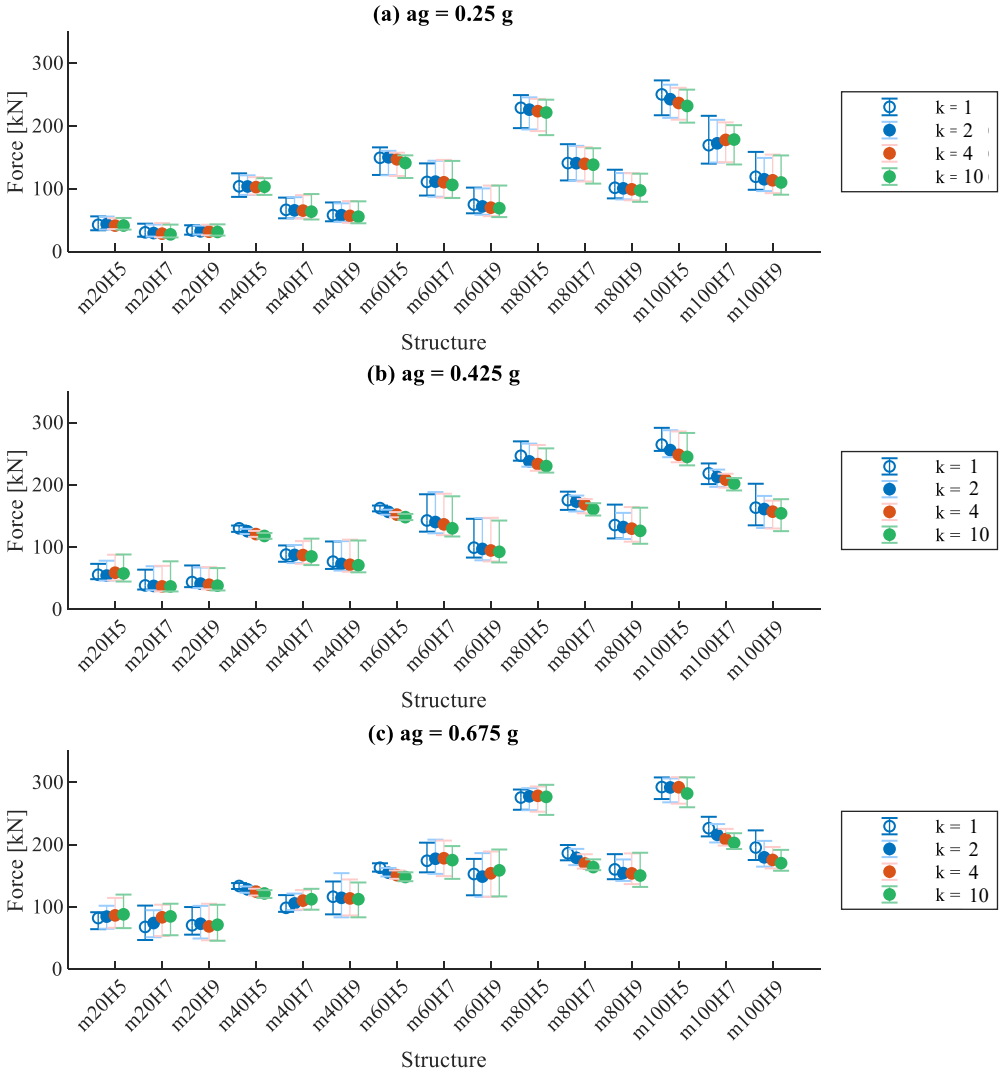

Figure 6.102: Maximum shear force in the column at (a) a_g = 0.25 g, (b) a_g = 0.425 g and (c) a_g = 0.675 g
Slika 6.102: Maksimalna strižna sila v stebru pri (a) a_g = 0.25 g, (b) a_g = 0.425 g in (c) a_g = 0.675 g

6.5 Assessment of the design approach used in practice

In the design practice of precast industrial buildings with concrete façade systems, cladding panels are often considered only as masses added to the main structure. To evaluate this design approach, it was necessary to assess the influence of the panels on the response of the main structure by evaluating the interaction between the panels and the main structure.

The parametric study results established that the influence of panels on the overall response of structures was limited. The comparison of column force-displacement responses showed that the interaction of panels and main structure in terms of stiffness was minimal for most analysed

structures. During sliding of connections without contact, the stiffness of the connections was negligible. After the gaps were closed, there was some interaction of panels with the column. However, the duration of impacts was very short and did not influence the displacement response of the structure. The influence of silicone sealant on the main structure's displacements was also only minor because the stiffness of silicone sealant severely deteriorates during seismic excitation.

Higher forces in the connections were activated during impacts, and the contribution of higher vibration modes was increased. For that reason, the distribution of shear forces along the column changed at higher intensities in some cases. For the design intensity (a_g = 0.25 g), the influence of panels was not important. The structures that were noticeably affected by the presence of panels were typically slender structures with a relatively small mass (e.g. structures *m20H7*, *m20H9*, *m40H9* and *m60H9*), especially if the number of columns was very small compared to the number of vertical axes of connections (*k* factor less than one).

Maximum shear demand in the column is compared to M_u/H and shear resistance V_R in Figures 6.103 and 6.104 for two intensities (a_g = 0.25 g and a_g = 0.675 g). Because of the lateral forces induced from the connections and contribution of higher vibration modes during the impacts at higher intensities, the shear demand mostly exceeded the shear force M_u/H. As mentioned, at design intensity (a_g = 0.25 g), this effect was negligible.

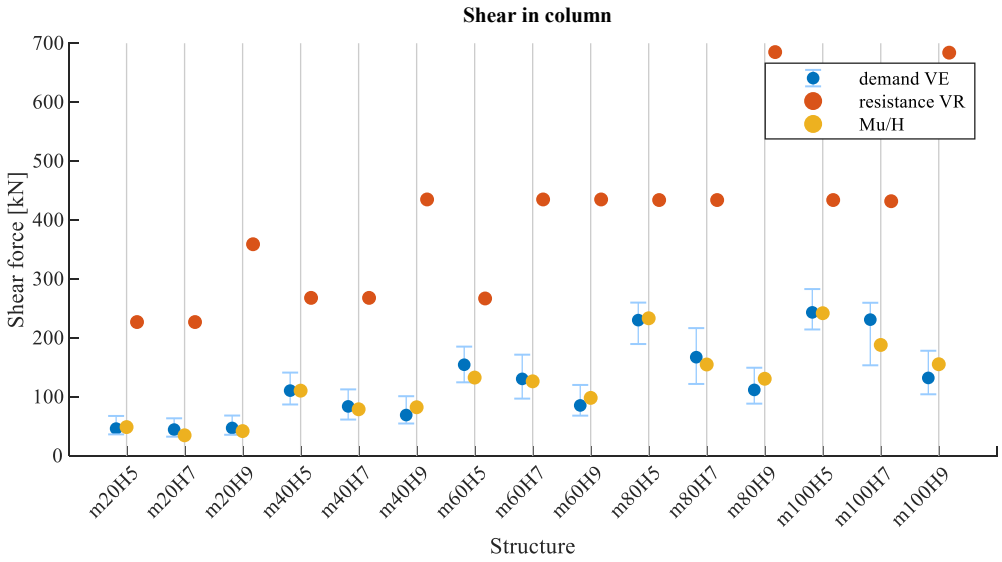

Figure 6.103: Maximum shear force in the column compared to shear resistance and moment resistance divided by the height of the structure at a_g = 0.25 g

Slika 6.103: Maksimalne strižna sila v stebru v primerjavi s strižno nosilnostjo in upogibno nosilnostjo deljeno z višino hale pri a_g = 0.25 g

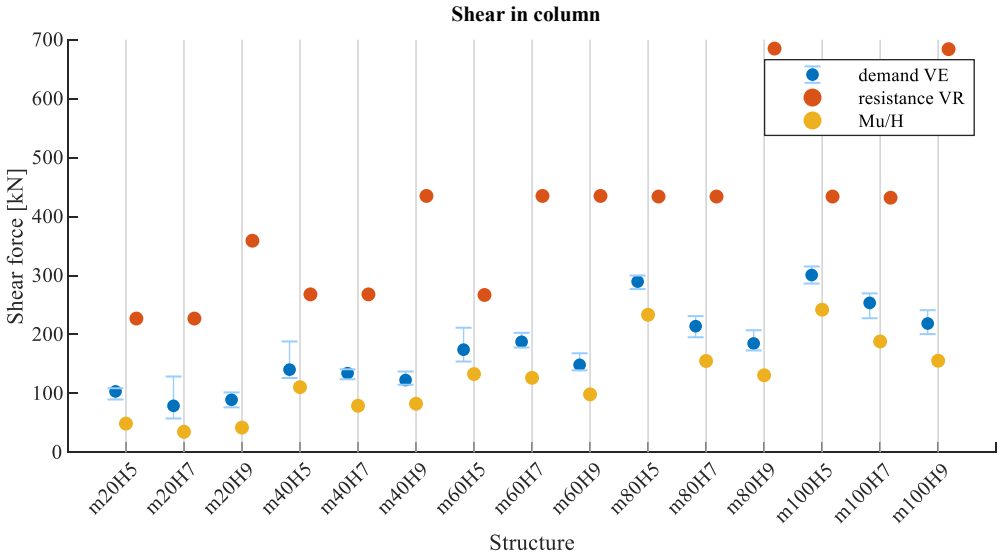

Figure 6.104: Maximum shear force in the column compared to shear resistance and moment resistance divided by the height of the structure at a_g = 0.675 g

Slika 6.104: Maksimalna strižna sila v stebru v primerjavi s strižno nosilnostjo in upogibno nosilnostjo deljeno z višino hale pri a_g = 0.675 g

Usually, the shear force is limited with the bending resistance. Therefore, the maximum shear that can occur in cantilever columns amounts to the bending resistance divided by the column height (M_u/H). When the capacity design is taken into account, a shear resistance higher than this shear force should be provided. However, the contribution of higher modes of vibration increases during the inelastic response of columns and impacts between the column and panels. This lowers the resultant force closer to the column base, and the force M_u/H might be exceeded. For most of the structures, the minimum criterion for the reinforcement was relevant (Kramar, 2008; Zoubek, 2015), and because of that, the shear resistance was much higher than the demand. No shear column failure was observed in any of the analyses.

The response of the columns can be reasonably well estimated with the current design approach for most of the structures. Structures that require more thorough calculation are slender structures with a relatively small tributary mass (e.g. tributary mass 20 t per column). For those structures, a somewhat greater influence of panels and contribution of higher modes of vibration in the inelastic range was observed.

6.5.1 Estimation of demand on the fastening system

Because the current design approach does not give any direct information about the response of panels, an attempt was made to correlate the response of the main structure to the demand on the fastening system.

Demand on the fastening system is the column drift along a single panel. Therefore, displacement demand for the structure was correlated to the column drift along the panel. A relatively good estimation of column drift can be made with the relationship shown in Equation 6.10, where d_{top} is the displacement at the top of the structure, H is the height of the structure, $\Delta d_{col,p}$ is column drift along the single panel, and h_p is the height of the panel.

$$\frac{d_{top}}{H} = \frac{\Delta d_{col,p}}{h_p} \quad \rightarrow \quad \Delta d_{col,p} = \frac{d_{top}}{H} \cdot h_p \tag{6.10}$$

Note that the drift of the column along a single panel estimated according to Equation 6.10 is an average drift. The column drift increases along with the column height (see, for example, Figures 6.50 and 6.54) and thus, drift at the top of the structure is somewhat higher than the estimated average drift.

Because the average drift (Equation 6.10) underestimates the demand, the ratio between the average and maximum drifts at the panel level was evaluated using nonlinear analyses of precast structures. Calculations included silicone-sealed joints, bottom panel fixed to the foundation, central position of the connections, and ratio k equal to 2. The results are shown in Figure 6.105. As follows, the estimation of the maximum column drift along the single panel is on the safe side if the right hand of Equation 6.10 is multiplied by 1.45 (see Equation 6.11).

$$\Delta d_{col,p} = \frac{d_{top}}{H} \cdot h_p \cdot 1.45 \tag{6.11}$$

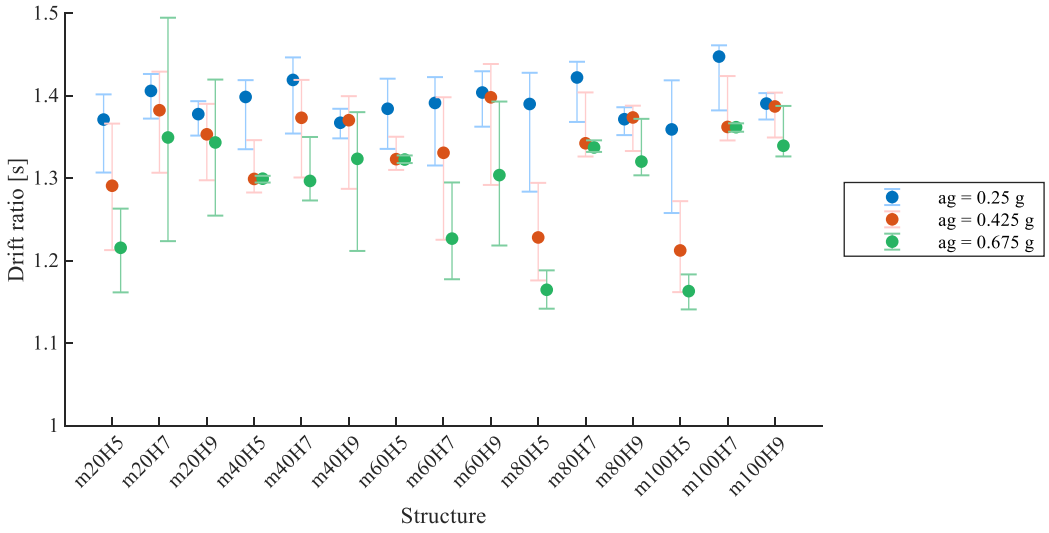

Figure 6.105: Ratio between the maximum and average column drifts along the single panel
Slika 6.105: Razmerje med maksimalnim in povprečnim driftom stebra na nivoju panela

The ratio between the column drift along the panel at the top and the average column drift along a single panel can also be expressed analytically for different structures. As shown in Figure 6.106,

displacement at the top of the structure d_{top} can be expressed as the sum of the plastic part $d_{top,pl}$ and the elastic part $d_{top,el}$. It is approximately the sum of the displacement due to rotation of the plastic hinge and displacement due to the elastic deformations of the column.

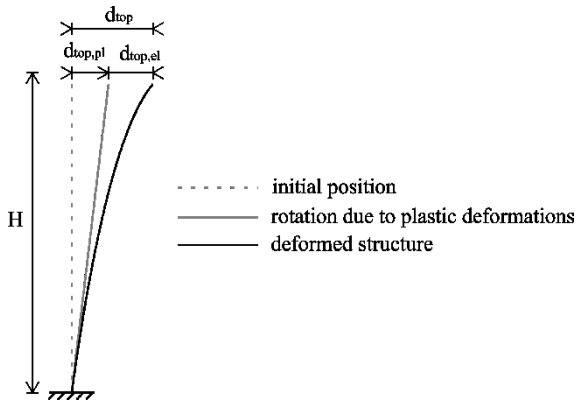

Figure 6.106: Deflection of a cantilever column
Slika 6.106: Deformacijska linija konzolnega stebra

The ratio between the maximum and average column drifts along the single panel can be estimated with Equations 6.12 and 6.13. Here, the expressions are shown in their final form. Their derivation is presented in Appendix G. The ratio depends on the height of the column (H), the height of the panel (h_p) and the share of plastic displacement (r_d).

$$\frac{\Delta d_{col,p,top}}{\Delta d_{col,p,avg}} = r_d + A \cdot (1 - r_d) \tag{6.12}$$

$$A = \frac{2H^3 - (H - h_p)^2(2H + h_p)}{2H^2 \cdot h_p} \tag{6.13}$$

A is the ratio between the maximum and average column drifts along the single panel due to the elastic part of deformations. It is derived from the formula of cantilever deflection under concentrated load at the free end (see Appendix G). The share of plastic displacement r_d is, however, not known in advance (see also Equations 6.14 and 6.15). For that reason, the ratio of maximum to average column drifts along the single panel is evaluated for three types of structures and different shares of plastic and elastic deformations in Table 6.5.

$$d_{top,pl} = r_d \cdot d_{top} \tag{6.14}$$

$$d_{top,el} = (1 - r_d) \cdot d_{top} \tag{6.15}$$

Table 6.5: The ratio of maximum to average column drifts along the single panel
Preglednica 6.5: Razmerje med največjim in povprečnim driftom stebra na nivoju panela

Column height H [m]	Panel height h_p [m]	Share of plastic displacement r_d	$\Delta d_{col,p,top}$ / $\Delta d_{col,p,avg}$
5	1.67	0	1.44
		0.2	1.36
		0.4	1.27
		0.6	1.18
		…	…
7	1.75	0	1.47
		0.2	1.38
		0.4	1.28
		0.6	1.19
		…	…
9	1.80	0	1.48
		0.2	1.38
		0.4	1.29
		0.6	1.19
		…	…

The parametric study results show that the displacements critical for the failure of fastenings occur after the yielding of structures. Table 6.5 shows that the ratio between the maximum and average drifts decreases with increasing plastic part of deformations. This can also be seen in Figure 6.105, where the median ratio decreases with increasing excitation intensity. Thus, the estimation of 1.45 taken from the parametric study is appropriate.

Maximum displacement at the top of the structure can be calculated from EC8 elastic response spectra (for $T_C \leq T \leq 2$ s):

$$S_d = \frac{a_g S \eta 2{,}5 T_C}{T} \left(\frac{T}{2\pi}\right)^2 \tag{6.16}$$

Note that Equation 6.16 is approximately valid also for the nonlinear response because of the equal-displacement rule. This is, however, an approximate estimate because the exact value of the period of vibration is not known.

An average drift of the column along the single panel, that is, drift demand on the fastening system, can be estimated as:

$$\Delta d_{col,p} = \frac{a_g S \eta 2{,}5 T_C T}{4\pi^2} \frac{h_p}{H} \cdot 1.45 \tag{6.17}$$

From Equation 6.17, it follows that drift demand on the fastening system increases with the increasing period of the structure, decreases with increasing height of the structure, and increases with increasing height of the panel.

Expressing a_g from Equation 6.17 gives a formula to estimate max a_g [m/s^2] based on the known drift capacity of the fastening system:

$$a_g = \frac{4\pi^2}{S\eta 2{,}5 T_C T} \frac{\Delta d_{col,p} H}{h_p \cdot 1.45} \tag{6.18}$$

For the first use of Equation 6.18, it was supposed that structures are located in Ljubljana on ground type C, with a damping ratio of 5% and a common panel height of 2 m. The drift capacity of the fastening system was assumed to be 4 cm. This is the sliding capacity of the top connections if they are positioned centrally. Thus at maximum ground accelerations estimated as follows, the connections are expected to only slide in the case of the central position of connection. For estimation of connections drift capacity, please see also Section 6.3.2.

Equation 6.18 simplifies to Equation 6.19 for the given location (Ljubljana, ground type C) and the height of the panel (2 m). In Equation 6.19, a_g is expressed in acceleration of gravity [g], the structure's height in meters [m] and period of vibration in seconds [s]. Ground acceleration critical for the failure of fastenings was estimated, and results are presented in Table 6.6 for three different heights (5, 7 and 9 m) and three fundamental periods of vibration (1.0, 1.5 and 2 s).

$$a_g = 0.032 \frac{H}{T} \tag{6.19}$$

For example, in Ljubljana, where a_g = 0.25 g, the capacity of the connections is expected to be exceeded for most of the selected structures, except for 9-m-high structures with a period of vibration T = 1.0 s. Like the location in Ljubljana, the drift demand on the fastening system can be roughly estimated for any structure at any location. All that must be known are the period of vibration, the height of the structure, and specific characteristics of the response spectra. It is interesting to note that shorter structures with a high period of vibration are more critical, but typically, shorter structures also have lower periods of vibration (see the set of structures for parametric analysis in Section 6.1.1).

Table 6.6: Estimated ground acceleration at the drift capacity of the fastening system
Preglednica 6.6: Ocenjen maksimalni pospešek tal pri katerem je dosežena kapaciteta fasadnega sistema

Height of the structure H [m]	Fundamental period T [s]	Estimated a_g [g]
5	1.0	0.16
7	1.0	0.23
9	1.0	0.29
5	1.5	0.11
7	1.5	0.15
9	1.5	0.19
5	2.0	0.08
7	2.0	0.11
9	2.0	0.14

6.6 Proposal for better connections

As shown in previous sections, the response of columns, that is, the main structural system, was not significantly affected by different parameters of the horizontal façade system. The panels, on the other hand, were affected. If there were extreme construction imperfections and panels were mounted diagonally eccentrically (*LR*), the drift capacity of the system was significantly reduced, and demand on connections increased. This section gives a proposal for the improvement of the existing horizontal concrete façade systems.

As already explained, space (gaps) in connections provides tolerances during construction. If tolerances are exhausted, the sliding capacity of the connections is reduced to zero. There is, therefore, a possibility for improving connections by enlarging the available gap. This improvement presents an analogy to centrally positioned cladding connections that have shown better seismic response (see Section 6.4.2). However, because of construction and mounting imperfections that regularly occur in practice, it is relatively difficult to ensure that all connections will be mounted perfectly in the centre.

The position of connections completely depends on the accuracy of casting and mounting. However, it is obviously possible to ensure that they will be mounted within the gap space of existing connections. Prescribing the mounting area of connections would guarantee that. Therefore, if the mounting area were limited and gaps were larger, there would always be some sliding capacity of the connections provided.

Equation 6.20 can be used to estimate the sliding capacity required to satisfy the drift demand for a structure with a specific height and period of vibration at a specific location. The estimated drift

demands for structures with three different heights (5, 7 and 9 m), three periods of vibration (1.0, 1.5 and 2.0 s) and height of the panel equal to 2 m at a site location in Ljubljana (a_g = 0.25 g) on ground type C are calculated using Equation 6.21. Results are collected in Table 6.7.

$$\Delta d_{col,p} = \frac{a_g S \mu 2{,}5 T_C T}{4\pi^2} \frac{h_p}{H} \cdot 1.45 \tag{6.20}$$

$$\Delta d_{col,p} = 0.214 \frac{T}{H} \tag{6.21}$$

Table 6.7: Estimated drift demand on the fastening system

Preglednica 6.7: Ocenjen potrebni drift sistema fasadnih stikov

Height of the structure H [m]	Fundamental period T [s]	Estimated drift demand [m]
5	1.0	0.06
7	1.0	0.04
9	1.0	0.03
5	1.5	0.09
7	1.5	0.07
9	1.5	0.05
5	2.0	0.12
7	2.0	0.09
9	2.0	0.07

For example, the sliding capacity of the top connections of a 9-m-high structure with a period of vibration of 1.5 s should be 5 cm. An example of proposed improvement is shown in Figure 6.107 (b). The available gap distance of the connections is enlarged by 5 cm, whereas the space intended for mounting is kept the same as existing connections (Figure 6.107 a). In this way, the required sliding capacity can be estimated for any structure at any location, and the connections could be appropriately modified. Note that this is an approximate estimate.

Structural limitations should also be considered. Namely, if the connections should be mounted centrally, the dimensions of the column's cross section should be relatively large, but columns cannot be increased indefinitely. For the situation presented in previous paragraphs and Figure 6.107 (b), each connection is 28 cm wide. There are two connections per column, and each channel demands a certain layer of concrete at each side (min 10 cm, for the channels used in this study). Some space should also be provided between the adjacent panels (approximately 5 cm). As follows, the total column cross-section width should be at least 67 cm (Figure 6.108).

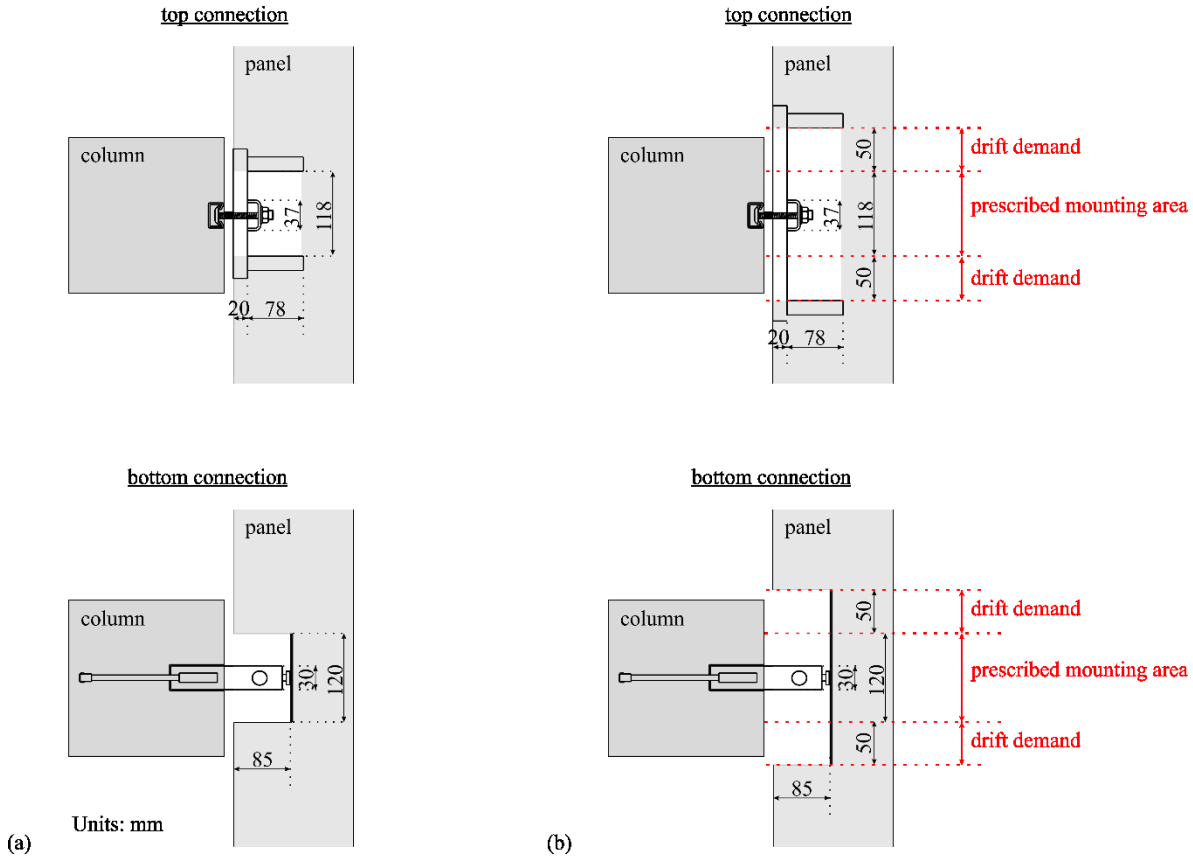

Figure 6.107: Cladding connections for horizontal concrete panels: (a) existing and (b) improved

Slika 6.107: Fasadni stiki za pritrjevanje vodoravnih betonskih panelov: (a) obstoječi in (b) izboljšani

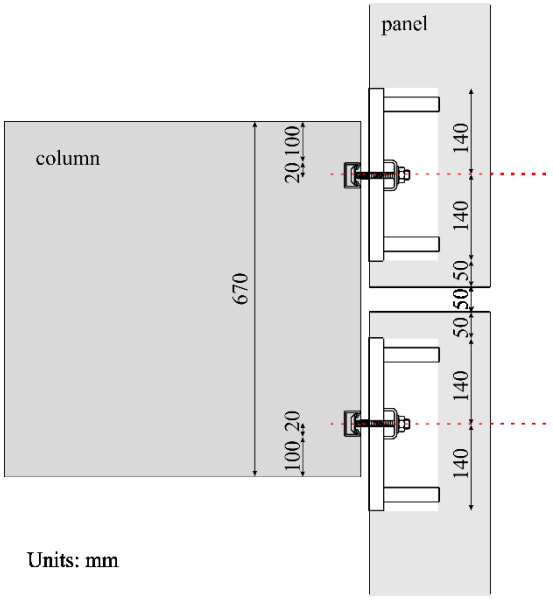

Figure 6.108: Example of minimum column cross-section dimensions

Slika 6.108: Pimer minimalnih dimenzij stebra

The cantilever connections could also be modified like the connections at the top of panels to avoid impacts at bottom connections. Similar modification of cladding connections to improve their displacement capacity has been studied by Del Monte et al. (2019).

6.7 Short overview of other systems used in Slovenia

Other horizontal façade systems, like the one studied within this dissertation, are used in Slovenian construction practice. This section gives a brief overview of these systems and outlines the differences compared to the fastening system investigated within the dissertation. Some suggestions for further research are given.

Usually, the same system is used for top connections, but it is finished differently. After the connection is mounted, the concrete is poured into the connection box (Figure 6.109). Such treatment is primarily intended for protection against corrosion.

Because of the concrete, the sliding of connections is prevented, and thus it is supposed that pouring of the top connections provides pinned connections. Such a measure could result in promising behaviour of the connections also at higher drift demands. However, several concerns have been raised and should be further investigated:

- Some doubts have been raised about pinned boundary conditions. Because of the concrete, displacements and rotations of the connection might be prevented. In that case, lateral forces in connections may arise even at small seismic excitations. Thus, this connection type should be tested to define the correct support behaviour at the top connection.

- The demand and capacity of the concrete and bolt at the top should be defined. The concrete cracks at some point during the loading. After cracking, the system behaves as has been analysed and explained in previous sections.

- In the case of poured top connections, all the drift demand is taken over only by the bottom connections until the concrete at the top cracks. Thus, impacts at the bottom connection could occur earlier than for the fastening system analysed within the dissertation.

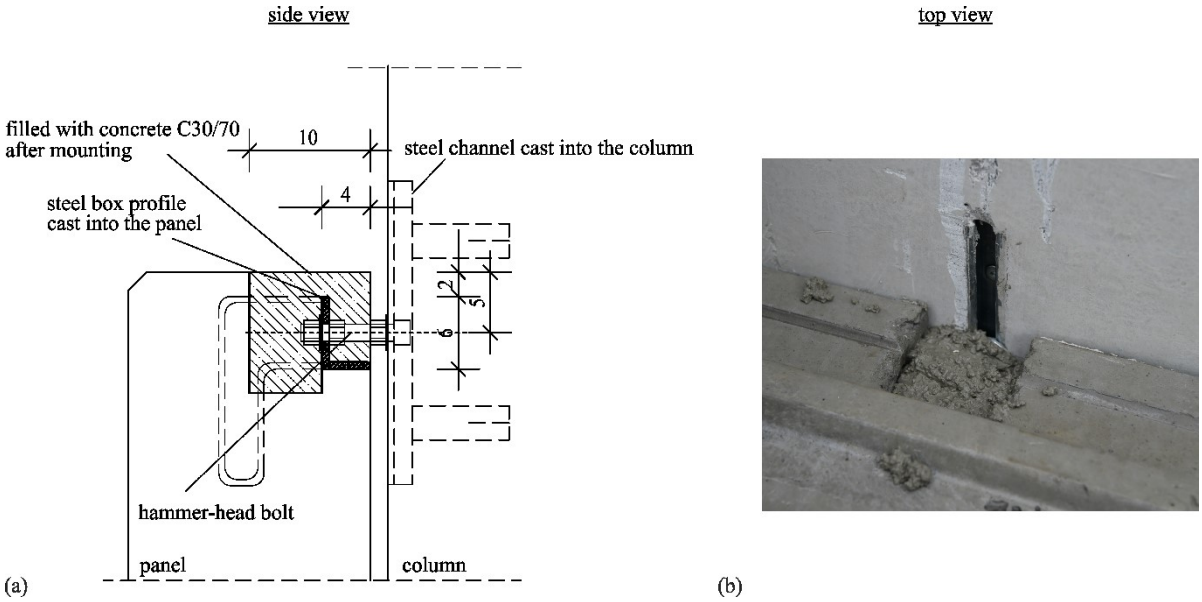

Figure 6.109: Top cladding connection filled with concrete: (a) sketch of a side view (Bužinel, 2019) and (b) photo of the connection taken at the construction site

Slika 6.109: Zgornji stik zalit z betonom: (a) skica pogleda od strani (Bužinel, 2019) in (b) fotografija stika posneta na gradbišču

In practice, some of the façade systems are built without the bottom cantilever connections. Instead of the connections, the panels are often simply placed on top of each other and connected by slots and ribs. In some areas, rubber strips are placed between the panels.

During an earthquake, panels follow the movement of the columns in the direction parallel to the panel plane. There are no impacts between column and panel at the level of connections, which is considered an advantage. However, at corners of the structure, impacts between the panels in two perpendicular directions may occur. These impacts were not analysed within the dissertation. Some authors (e.g. Scotta et al., 2015) also warn that the friction coefficient between the adjacent panels is the critical factor that influences the system's response and may lead to a dual wall-frame behaviour of precast structures. Therefore, the influence of friction on the system's overall response should be analysed in more detail. For now, it is possible to claim that the seismic response of a system is reliable if there is low friction between the panels. According to Scotta et al. (2015), the optimal range of friction coefficient is between 0.1 and 0.2. One of their proposals to maintain the friction within this range are sliders made of coupled PTFE (also known as Teflon™) and steel plates slotted between panel interfaces.

At some construction sites, adjacent panels are connected using steel anchors (Figure 6.110). This measure is often taken with the belief that the anchors will provide additional panel stability. However, anchors make the connections between panels practically fixed, and there is a strong interaction between the panels. This solution changes the structural behaviour and was not discussed

in the dissertation. Dual wall-frame behaviour of the structure may result in much higher force demand on cladding panels because, until the failure of reinforcement bars, the panels are considered as structural elements Additional studies are required to analyse the behaviour of such precast systems and to define design requirements for columns and panels.

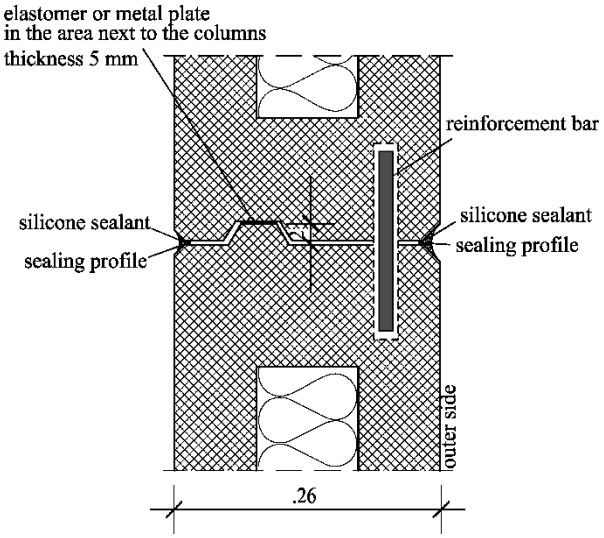

Figure 6.110: An example of the connection between the adjacent panels
Slika 6.110: Primer stika dveh panelov

Seemingly small alternations of fastenings could result in a significant difference in the response, but they are not necessarily always critical because it depends on the capacity of connecting elements. There is a possibility that higher levels of interaction between adjacent panels and between the structure and panels would be activated. Further studies should analyse the fastening system with poured top connections and no connections at the bottom edge of the panel that is relatively common in Slovenian construction practice.

6.8 Summary and conclusions of the chapter

The chapter presents an extensive parametric study of the seismic response of RC precast buildings with horizontal concrete façade systems using fastening devices typical in Central Europe. A wide array of one-storey RC precast buildings was included in this study. Various important parameters influencing their response were analysed: different structural configuration, construction imperfections (different initial positions of fastening devices), the effect of silicone sealant, and the connection of bottom panels to the foundation.

Influence of analysed parameters on the response of panels

The displacement and drift capacity of the system is significantly affected by construction imperfections. If panels are not mounted centrally, relatively large lateral forces are activated earlier, leading to earlier connection failure.

Within the dissertation, the interaction between the panels along the column's height was analysed, that is, silicone sealant placed horizontally between panels. The possible interaction of panels in adjacent spans (sealed with vertical stripes of silicone) was not considered in the study. For the structural type considered in the dissertation, there is no interaction between the panels in structures without silicone sealant. Slips at top and bottom connections are typically in the opposite direction with respect to columns. The response of panels is somewhat different when silicone sealant is used. Slips at top and bottom connections tend to occur in the same direction, which reduces the fastening system's drift capacity. Thus, if silicone sealant is used, failure of the connections occurs at a somewhat smaller column drift along the single panel.

The connection of bottom panels to the foundation also has some influence, but only on the response of the bottom panel. If the bottom panel is fixed to the foundation, all the displacement demand is taken over only by top connection, which results in earlier failures of the bottom panel fastenings. There was no important influence of the ratio between the number of columns and the number of connections on the panel response.

Influence of façade system on the response of the main structure

The parametric study showed that the interaction of panels and the main structure caused by sliding in connections and impacts between column and panels is minor. During sliding of connections without contact, the stiffness of connections is negligible, and the panel had practically no influence on the response of the main precast structure. After the gaps were closed, there was some interaction of panels with the main structure. However, the duration of impacts was very short, and the interaction was activated only for a short time. The influence of panels on the global response of structures was negligible.

The distribution of shear forces along the column changed in some cases at higher intensities. These effects have only limited influence on the response of the structure and occur only in some structures. The structures that were noticeably affected by the presence of panels were typically slender structures with a relatively small mass (e.g. structures *m20H7*, *m20H9*, *m40H9* and *m60H9*), especially if the number of columns was very small compared to the number of panels (very small k factor).

For those structures, the contribution of higher vibration modes during the impacts was increased. For that reason, the position of the resultant force was closer to the base of the column, and in certain cases, the shear demand exceeded the shear force M_u/H. This effect was relatively small for the design intensity a_g = 0.25 g. However, the columns' shear resistance was also sufficient at higher intensities because the minimum reinforcement criteria and capacity design were considered.

Capacity and demand of the fastening system

The capacity and demand of the fastening system could be expressed as column drift along a single panel. Because the drift increases along the column's height, the panel that fails first is typically the panel at the top of the structure. However, if the bottom panel is fixed, the capacity of its fastening system is significantly reduced. In this case, the first failure may occur at the bottom panel.

The capacity of the fastening system is most affected by the initial position of the connections and gaps provided for sliding. After the connection gap closes, brittle failure of the top connection follows. Using only the sliding capacity of the top connections, which are the critical part of the fastening system, is recommended for conservative estimates and to protect fastenings from failure.

The parametric study showed that the influence of panels on the overall structure's response was limited. The interaction of panels and structure is minimal, and in general, does not affect the response of the main precast structure. In design practice, panels' influence on the overall seismic response is taken into account only by adding their mass to the mass of the main structural system. The response of the columns can be reasonably well estimated with the current design approach for most structures. Structures that require more detailed calculation are slender structures with a relatively small tributary mass (e.g. a tributary mass of 20 t per column).

A procedure for a rough estimation of the demand on connections and a relatively fast assessment of different structures at different locations is also proposed in this chapter. It provides an approximate calculation of drifts in connections from design spectra. A proposal for the improvement of the connection's drift capacity and guides for required gaps are presented.

Note that all observations and conclusions apply only to the considered type of fastening system.

7 NUMERICAL ANALYSIS OF SEISMIC RESTRAINERS INTENDED FOR THE SEISMIC PROTECTION OF CLADDING PANELS

A proposal for improving cladding connections, presented in Chapter 6, is suitable for implementing new precast buildings. However, thousands of buildings in Europe are already built. Panel failure should be prevented in those old buildings where damage to the connections is expected. A second-line backup system, that is, *restrainers,* can be used for this purpose.

Restrainers were initially developed in the framework of the SAFECLADDING project and would be used to protect the cladding panels from falling when the capacity of cladding connections is exceeded. They are designed in a way that enables installation in existing buildings. More than 100 tensile tests were performed within the SAFECLADDING project, and a simple design formula and numerical model were developed (Isaković et al., 2014a; Zoubek, 2015; Zoubek et al., 2016). The proposed design formula and model have already been tested for use in precast buildings with vertical cladding panels (Zoubek, 2015; Blaž Zoubek et al., 2016).

In this chapter, this procedure was modified for use with horizontal panels. Maximum impact force in restrainers was estimated for critical structures with horizontal panels. Results of numerical response history analyses were used to evaluate the analytical procedure for estimating the demand on restrainers proposed in Zoubek et al. (2016).

7.1 Design concept

The design concept of the restrainers as the second-line backup system for protecting (strengthening) the cladding panels is presented in this section. The idea is already well established in bridge construction, where restrainer devices are used to limit relative displacements and prevent loss of support (Randall et al., 1999). Restrainers proved to be very efficient even when strong earthquakes occurred, as the Northridge earthquake in the USA, 1994.

Restrainers are devices used to connect two components of the structure and prevent their detachment (e.g. main precast structure and cladding panel in prefabricated industrial buildings), as shown in Figure 7.1. In the case of the failure of primary cladding connections, the panel fails in the direction perpendicular to its plane. At that moment, the restrainer rope is activated, and the tension force is transmitted through specially designed rope terminations into the steel elements and

then into the panel and column. A detailed description of restrainers can be found in Zoubek (2015) and Zoubek et al. (2016).

The space intended for mounting the restrainer system is limited. For this reason, the design concept of the restrainer system in precast buildings is different from that typically used in bridges, and short ropes with a length up to 70 cm are used. The rope is loose and, despite limited space, long enough not to be activated before the failure of primary cladding connections. Therefore, the restrainers do not fix the panels to the precast structure but only provide a second line of protection upon panel failure.

Restrainers are typically made of steel and thus susceptible to corrosion and other aggressive environmental conditions. To avoid such problems, they can be made of modern materials, such as plastic wires or fibre ropes, also used in marine engineering and mountain climbing. Those materials also have other advantages compared to steel: higher strength and lower weight (see Zoubek, 2015).

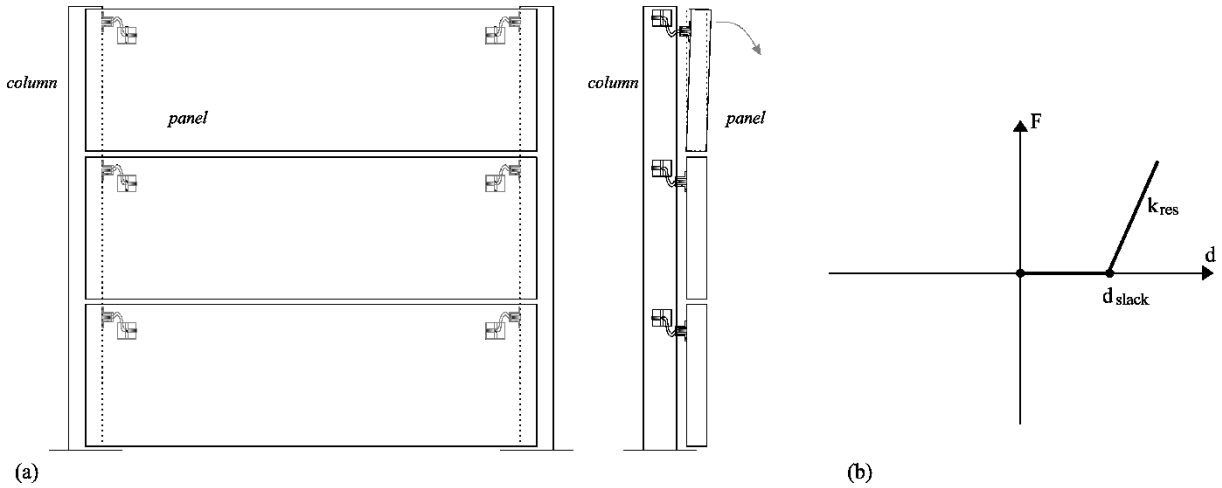

Figure 7.1: The restrainer system: (a) design concept, (b) force–displacement response of restrainer
Slika 7.1: Pridrževalni system: (a) idejna zasnova, (b) odziv pridrževalca sila–pomik

The response of the restrainer is presented in Figure 7.1 (b). Relative displacement at which the restrainer is tightened is denoted as the restrainer's effective length d_{slack}. Until this displacement, the restrainer is loose and inactive so that there is no force in it. The rope is long enough to allow relative displacements between the column and panel and not be activated until the primary cladding connections fail. After activation, the tension force in the restrainer increases linearly and is proportional to the stiffness k_{res}. The response of the restrainer is elastic.

When the in-plane capacity of cladding connections is exceeded, the panel fails in the out-of-plane direction. The problem is actually three dimensional, and the restrainer is activated at an angle. Thus, the displacement at which the restrainer is activated is not the same as relative in-plane displacement that is critical for the cladding connections. Due to limited space, the ropes should be

short but long enough to enable relative displacements between the column and panel without activation of the restrainer. An effective restrainer length of 30 cm should be appropriate for attaching horizontal panels. This length was defined based on the expected relative displacements in the connections and the geometry of anchoring devices.

The stiffness k_{res} may vary from 1 MN/m to 5 MN/m and depends mainly on the rope material and type of loading. Several experiments have been performed to define the strength and initial stiffness of the restrainer system (Isaković et al., 2014a; Zoubek, 2015), and synthetic ropes were identified as the most suitable for the protection of cladding panels (Zoubek, 2015). According to recently performed experiments, the Φ10 synthetic restrainers subjected to dynamic loading had initial stiffness around 3000 N/m. This value was used for k_{res} in the following analytical and numerical analyses.

7.2 Analytical estimation of the maximum force in the restrainers

7.2.1 Design formulas

Impact forces that could occur in a short restrainer should be defined to adequately design the restrainer ropes. Formulas proposed by Zoubek et al. (2016) were used for analytical estimation of maximum impact force. For the complete derivation of the formula, please refer to that paper. Here only the closed-form expression for estimation of maximum impact force in the restrainer (Equation 7.1) and the equations (7.2–7.6) required for evaluation of the parameters are presented.

$$F_{res,max} = f_0\left(1 - \frac{f_0}{\sqrt{{f_0}^2+{f_v}^2}}\right) + f_v\sqrt{1 - \frac{{f_0}^2}{{f_0}^2+{f_v}^2}} \tag{7.1}$$

$$f_v = v_{r0}\sqrt{k_{res}m_{pr}} \tag{7.2}$$

$$f_0 = m_{pr}a_s \tag{7.3}$$

Parameter k_{res} is the stiffness of the restrainer system, m_{pr} is the mass of the panel attributed to each restrainer, v_{r0} is the initial relative velocity of the panel in the out-of-plane direction and a_s is the acceleration of the main precast structure.

Therefore, the main parameters that determine the size of forces are stiffness of the restrainer system, the attributed mass of the panel, the relative velocity between the panel and the main structure and acceleration of the primary structure at the moment of activation. The attributed panels' mass is defined considering the number of installed restrainers per panel, the structure's

geometry and failure type. Two restrainers per horizontal panel could be used to connect each panel with two columns at sides, as shown in Figure 7.1 (a). Because the restrainers are short, it was assumed that at the moment of activation, the horizontal panel is detached from the structure only at the top, while at the bottom, it is still supported by the bottom cladding connections. Using this assumption, the mass attributed to each restrainer m_{pr} corresponds to ¼ of the whole panel mass m_p. However, if the panel also slides in the out-of-plane direction at the bottom edge, the whole panel hangs on two restrainers. Then the mass attributed to each restrainer is $m_p/2$.

When the panel fails, there is also some vertical amplification of force due to the gravity loads that could be very important, especially if the panel is completely detached at the bottom edge. It is necessary to be aware that this vertical amplification of forces is not taken into account within the design formula and should be further investigated.

The stiffness of the system is known from experiments, whereas the estimation of the relative velocity between the panel and the structure at the moment of activation v_{r0} and acceleration of the structure a_s is not so trivial. According to Zoubek et al. (2016), good results can be achieved using Equations 7.4-7.6.

It is difficult to estimate the relative velocity at the time of activation of the restrainer. For this reason, Zoubek et al. (2016) proposed to use the maximum relative velocity, which is a more conservative approach. In such a way, the maximum relative velocity between the panel and the main structure can be easily estimated with Equation 7.4, where $v_{r,max}$ is maximum relative velocity and $v_{s,max}$ is the maximum velocity of the structure.

$$v_{r0} = \frac{v_{r,max}}{v_{s,max}} S_v(T_s) \tag{7.4}$$

$$S_v(T_s) = S_a(T_s) \frac{T_s}{2\pi} \tag{7.5}$$

$$a_s = S_a(T_s) \tag{7.6}$$

The velocity ratio $v_{r,max}/v_{s,max}$ for horizontal panels was defined with the numerical analysis. Using a value of 1.5 is proposed for horizontal cladding panels (see Section 7.3.2). The spectral acceleration $S_a(T_s)$ and spectral velocity $S_v(T_s)$ should be calculated using the EC8 elastic acceleration spectrum (Equation 7.5). T_s is the fundamental period of the main precast structure.

This estimate is conservative because the maximum relative velocity and maximum velocity of the structure do not occur simultaneously and not necessary at the same time as the activation of the restrainer.

7.2.2 Estimation of maximum restrainer demand

Maximum impact forces that could act in restrainers were calculated with the above design formula for the same set of 15 structures analysed within the parametric study (see Section 6.1.1). Formulas were evaluated for the attributed panel masses $m_p/4$ and $m_p/2$. The EC8 elastic acceleration spectrum was used to calculate the spectral acceleration and velocity. Ground type C was considered, and a a_g = 0.25 g was used.

Results are presented in Figure 7.2 for the attributed panel masses $m_p/4$ and $m_p/2$. Median maximum forces $F_{res,max}$ are presented for (a) different structures, (b) for different panel masses and (c) different fundamental periods of the main structure.

The trend of the attributed panel masses is obvious. However, there is almost no effect of the period of vibration. The reason for that can be found in the design formulas presented in Equations 7.7 and 7.8. In general, Equation 7.1 for estimation of maximum impact force in the restrainer consists of two parts, f_v and f_0.

$$f_v = v_{r0}\sqrt{k_{res}m_{pr}} = \frac{v_{r,max}}{v_{s,max}}\frac{a_g S \mu 2{,}5 T_C}{2\pi}\sqrt{k_{res}m_{pr}} \tag{7.7}$$

$$f_0 = m_{pr}a_s = m_{pr}\frac{2\pi}{a_g S \mu 2{,}5 T_C T} \tag{7.8}$$

From Equations 7.7 and 7.8, it follows that maximum forces in restrainers are in general higher for structures with higher panel masses and lower for structures with a higher period. However, the contribution of part f_v is much higher than f_0. As it was evaluated and is shown in Figure 7.3, the force f_v presents 90–95% of the total force demand. This shows that force in the restrainer mainly depends on the relative velocity between the panel and the main structure, the stiffness of the restrainer and the attributed mass of the panel. Thus, the influence of the attributed panel's mass is much stronger than the period of vibration, and for that reason, no evident trend can be observed in Figure 7.2 (c).

Due to the much higher contribution of force f_v, the maximum restrainer demand increases approximately with the square root of the attributed panel's mass. The ratio between median forces for attributed masses $m_p/4$ and $m_p/2$ was about 1.44, which is approximately the square root of 2.

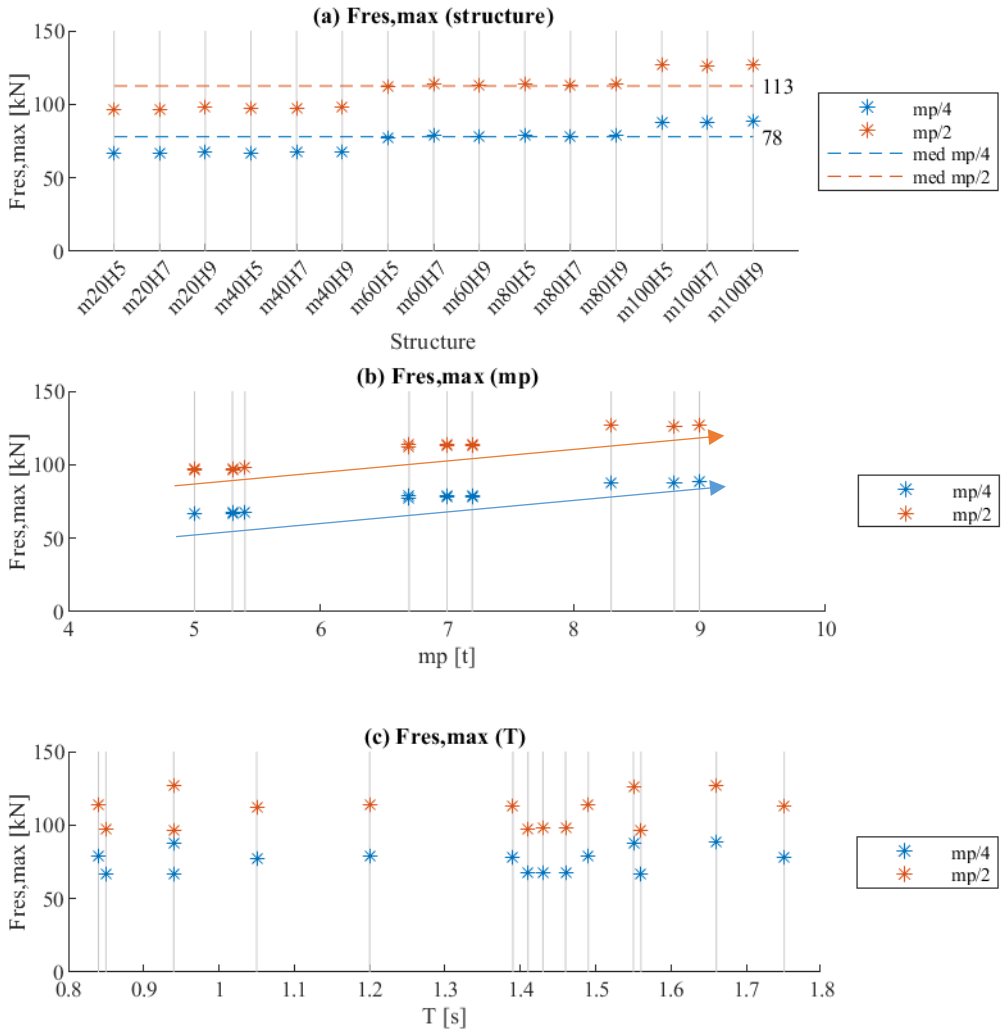

Figure 7.2: Maximum impact force in the restrainer estimated by design formula for attributed panel mass $m_p/4$ and $m_p/2$ per each restrainer: (a) $F_{res,max}$ for different structures, (b) $F_{res,max}$ for different panel masses and (c) $F_{res,max}$ for different fundamental periods

Slika 7.2: Maksimalna sila v pridrževalcu ocenjena s predlagano forumlo za pridrževalce s pripadajočo maso $m_p/4$ in $m_p/2$: (a) $F_{res,max}$ za različne konstrukcije, (b) $F_{res,max}$ glede na maso panela in (c) $F_{res,max}$ glede na nihajni čas konstrukcije

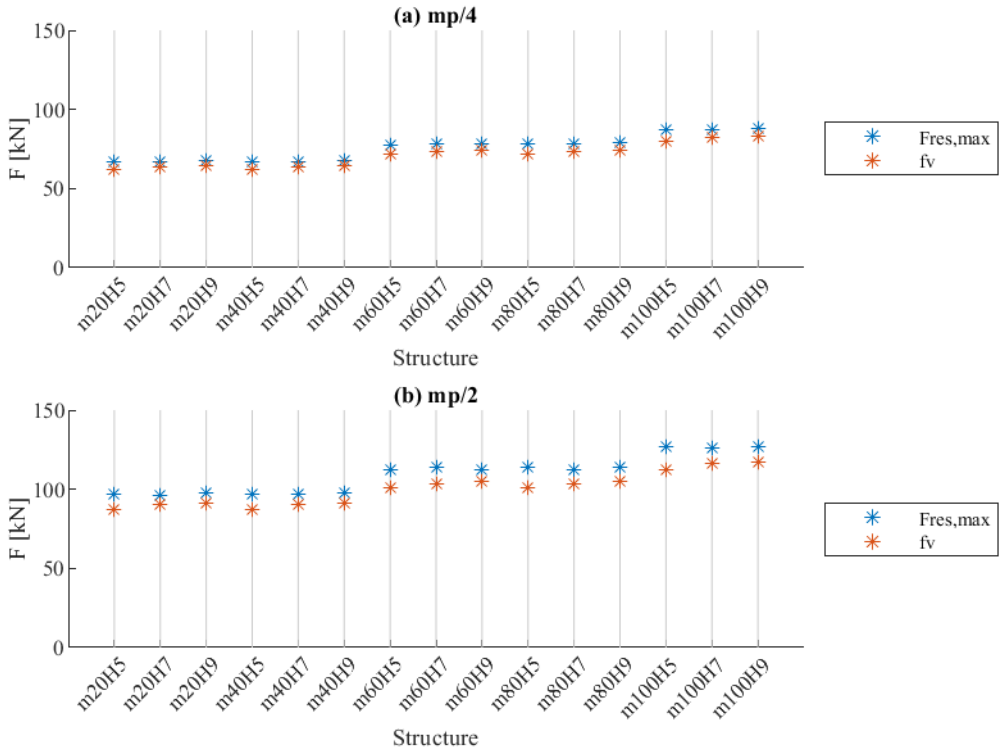

Figure 7.3: Maximum impact force in the restrainer $F_{res,max}$ compared to force f_v for attributed panel mass: (a) $m_p/4$ and (b) $m_p/2$

Slika 7.3: Primerjava maksimalne sile v pridrževalcu $F_{res,max}$ in sile f_v za pridrževalce s pripadajočo maso: (a) $m_p/4$ in (b) $m_p/2$

7.3 Numerical estimation of the maximum forces in restrainers

The maximum impact forces that could act in the restrainers were evaluated using response history analysis. Results of numerical analyses were compared with the maximum forces in restrainers evaluated by the proposed design formula (Equations 7.1–7.8). The analytical procedure was evaluated for the case of horizontal panels. The velocity ratio $v_{r,max}/v_{s,max}$ used in the design procedure was defined using response history analyses.

7.3.1 Numerical model and analysis

All models were built in the Opensees software framework (McKenna & Fenves, 2010). To simulate the response of the restrainer shown in Figure 7.1 (b), the *ElasticPPGap* material model was used. The material properties were defined based on data from experiments and literature (Isaković et al., 2014a; Zoubek, 2015; Zoubek et al., 2016). The stiffness of restrainers k_{res} = 3000 kN/m was taken

into account. It corresponds to synthetic restrainers of diameter Φ10 subjected to dynamic loading. The effective length of restrainers d_{slack} = 30 cm was used.

The structures were modelled as it is shown in Figure 7.4 (a). The model consisted of an average structure's column with the tributary mass at the top (it was already shown in Chapter 6 that panels do not contribute significantly to the response of the main structure). At the top of the structure, one restrainer with the mass of the tributary panels was added.

The panel attached at the top of the structure is expected to fail first. Also, the largest relative velocity between the panel and the structure is expected at the top of the structure. The relative velocity between the panel and the structure is one of the main parameters determining the impact force in the restrainer (see also Section 7.2.1).

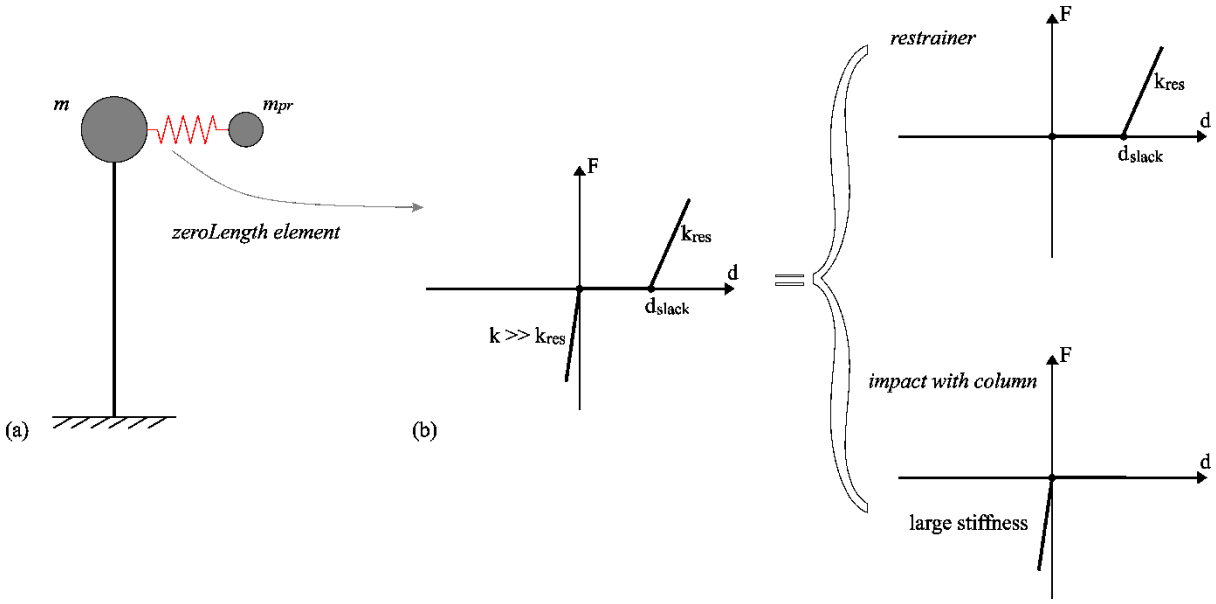

Figure 7.4: Numerical model for the analysis of the restrainers: (a) numerical model of the main structure, restrainer and attributed panel mass and (b) combined material model of the restrainer and material model of impacts between panel and column

Slika 7.4: Numerični model za analizo pridrževalcev: (a) numerični model glavne konstrukcije, pridrževalca in pripadajoče mase ter (b) kombinirana materialni model za odnos sila-pomik v pridrževalcu ter materialni model za trke med panelom in kontrukcijo

The attributed panel mass depends on the number of attached restrainers and the geometry of the structure, as discussed in Section 7.2.1. The response history analyses were used to examine the potential failure modes for $m_p/2$ and $m_p/4$.

Response history analyses were performed in the direction perpendicular to the plane of panels to estimate the maximum forces that could appear in the restrainer. In principle, the analysis should be three-dimensional, as an in-plane response is critical for cladding panels, and an out-of-plane

response is critical for restrainers. However, the idea was to estimate the maximum forces that could act in the restrainer, which does not necessarily correspond to the moment of failure of the primary cladding connections (parallel to panel plane). This approach is thus rather conservative. Please note that maximum response parameters are also considered within the analytical procedure because it is difficult to estimate the relative velocity at the time of restrainer activation (Section 7.2.1).

Impacts of the panel with the main structure were modelled with another *ElasticPPGap* material model (Figure 7.4 b). It was assumed that the response of the element in the compression is elastic with relatively high stiffness. As shown in Figure 7.4 (b), the material model of restrainer (in the positive direction) and the material model of impacts (in the negative direction) were combined and simulated with the same *zeroLength* element.

For the analysis, the same 15 structures and 30 accelerograms were used as within the parametric study in the previous chapter (see Sections 6.1.1 and 6.1.2). Structures with k factor 2, eccentric position of connections (*LR*), silicone-sealed joints (*P*), and the bottom panel fixed to the foundation (*F*) were used. However, only the critical cases when the failure of connections occurred were considered.

In the response history analyses, 5% viscous mass-proportional Rayleigh damping was taken into account. The damping ratio does not significantly affect the level of forces in the restrainer because only a small amount of mechanical energy can be converted through damping in a very short time when the restrainers are activated (Fajfar, 1984; Blaž Zoubek et al., 2016).

7.3.2 Results of numerical analyses and evaluation of the analytical procedure

Maximum impact force in the restrainer $F_{res,max}$

Results of response history analyses are compared to the analytical result in Figures 7.5 and 7.6. Median maximum forces from numerical analyses were 54 kN and 75 kN for attributed panel masses $m_p/4$ and $m_p/2$, respectively. Values are below the median forces estimated with the design formula (78 kN and 113 kN for attributed panel masses $m_p/4$ and $m_p/2$, respectively). As shown, quite a good match between the results was achieved, although analytical estimation gives more conservative results in general.

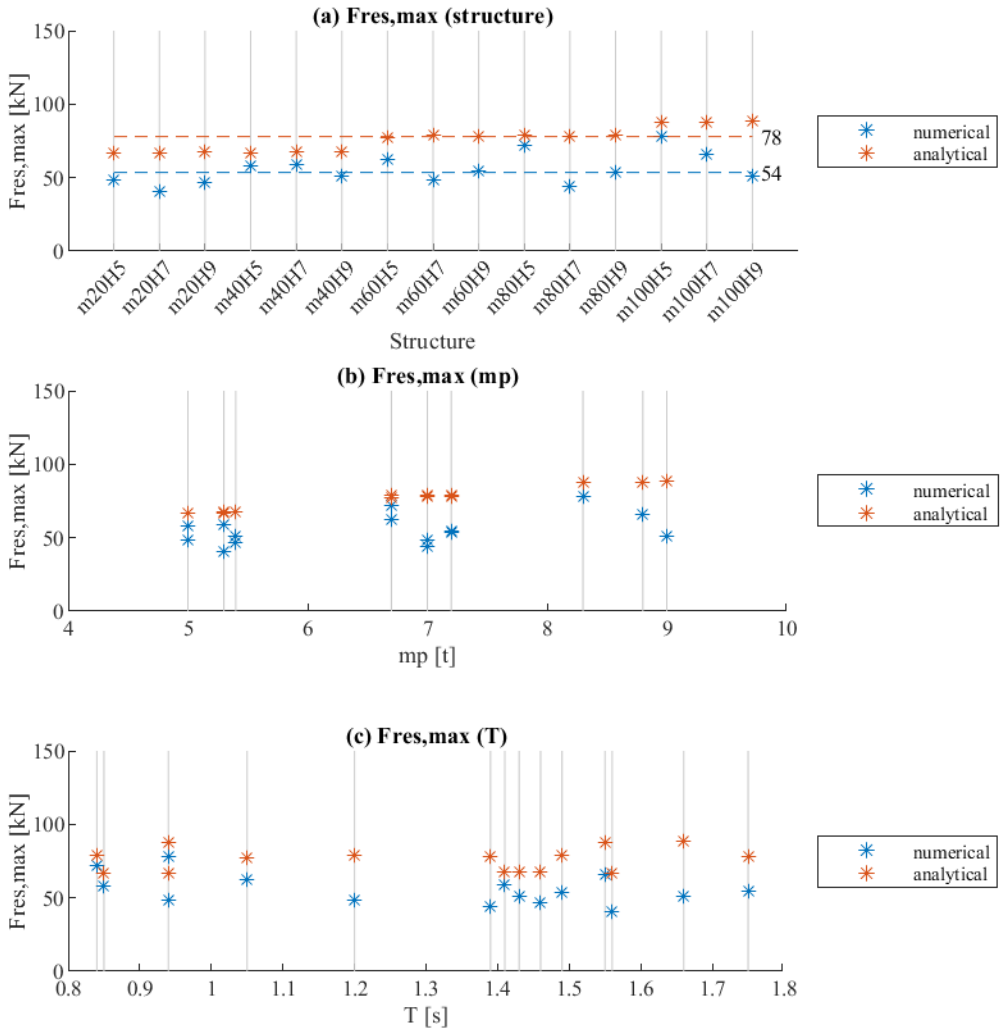

Figure 7.5: Comparison of analytical estimation and numerical results for attributed panel mass $m_p/4$: (a) $F_{res,max}$ for different structures, (b) $F_{res,max}$ for different panel masses and (c) $F_{res,max}$ for different fundamental periods

Slika 7.5: Primerjava analitične ocene in numeričnih rezultatov za pridrževalce s pripadajočo maso $m_p/4$: (a) $F_{res,max}$ za različne konstrukcije, (b) $F_{res,max}$ glede na maso panela in (c) $F_{res,max}$ glede na nihajni čas konstrukcije

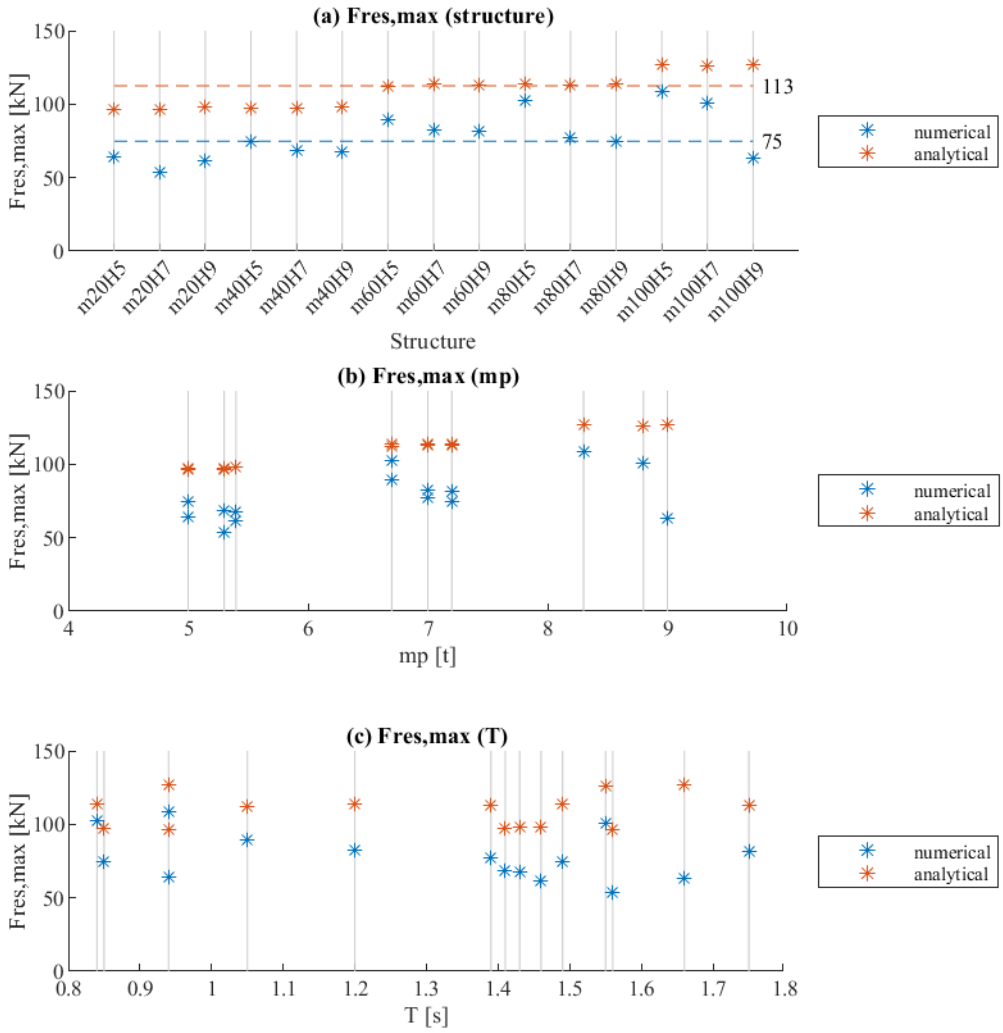

Figure 7.6: Comparison of analytical estimation and numerical results for attributed panel mass $m_p/2$: (a) $F_{res,max}$ for different structures, (b) $F_{res,max}$ for different panel masses and (c) $F_{res,max}$ for different fundamental periods

Slika 7.6: Primerjava analitične ocene in numeričnih rezultatov za pridrževalce s pripadajočo maso $m_p/2$: (a) $F_{res,max}$ za različne konstrukcije, (b) $F_{res,max}$ glede na maso panela in (c) $F_{res,max}$ glede na nihajni čas konstrukcije

Velocity ratio $v_{r,max}/v_{s,max}$

Based on the results of response history analyses, a ratio of the maximum relative velocity between panels and the main structure $v_{r,max}$ to the maximum velocity of the main structure $v_{s,max}$ was proposed. Velocity ratios estimated using response history analyses for two attributed panel masses are presented in Figure 7.7.

There is no obvious difference in velocity rations for different panel masses. If structures with similar masses were considered, only a small decrease in velocity ratio for higher periods was observed (see arrows in Figure 7.7 a). This trend matches the observations of Zoubek et al. (2016) for vertical panels. However, the trend was not so obvious, and thus a conservative value of 1.5 is proposed for use in the design formula for all precast structures with horizontal panels.

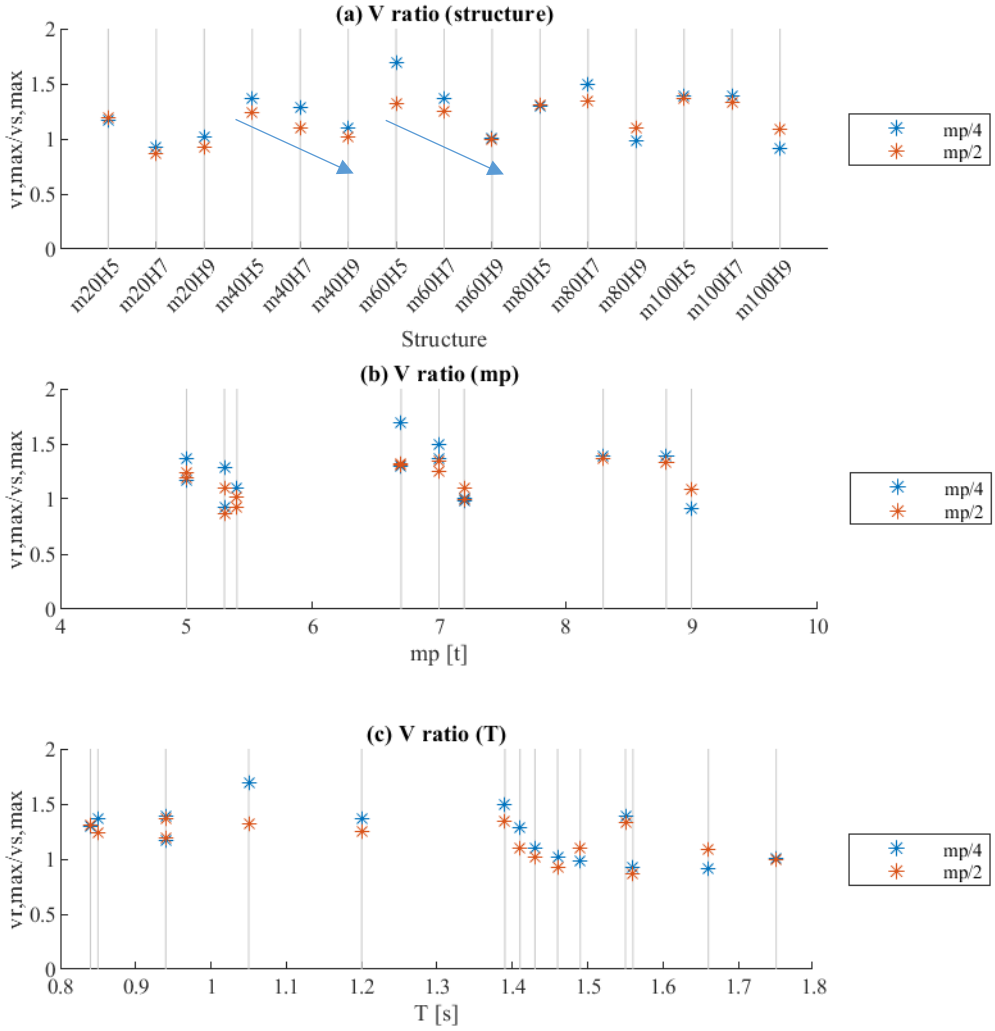

Figure 7.7: Velocity ratio $v_{r,max}$ / $v_{s,max}$ estimated using nonlinear dynamic analyses: (a) for different structures, (b) for different panel masses and (c) for different fundamental periods

Slika 7.7: Razmerje hitrosti $v_{r,max}$ / $v_{s,max}$ določeno z nelinearno dinamično analizo odziva: (a) za različne konstrukcije, (b) glede na maso panela in (c) glede na nihajni čas konstrukcije

7.4 Summary and conclusions of the chapter

Restrainers are second-line backup devices used to prevent the failure of the panels in the case of failure of primary cladding connections. They are used to protect the cladding panels from falling when the capacity of the cladding connections is exceeded. Restrainers do not affect the properties of the primary connection devices nor the response of the main precast structure. They are designed so they can be installed on existing buildings. This chapter presents an analytical and numerical analysis of the seismic demand on restrainers used to protect horizontal cladding panels.

The evaluation of the seismic demand at the time of activation of the restrainer is a relatively complex task. The restrainers are activated at the moment when the primary cladding connections fail and in a very short time. For the maximum response of the restrainers, three parameters that increase the demand are significant: the stiffness of the restrainer, the initial relative velocity of the panel and the panel mass attributed to the single restrainer.

A relatively simple analytical procedure could be used to design restrainers. The parameter that most affected the maximum force that could act on restrainers is the mass of the panel. The force demand increases approximately by the square root of the attributed panel's mass.

When the panel fails, some vertical amplification of force due to the gravity loads could be very important, especially if the panel is completely detached at the bottom edge. It should be emphasised that this is not taken into account within the design formula and should be further investigated.

Response history analyses were performed on a set of structures identified as critical for the failure of connections during the parametric analysis (Chapter 6). The ratio between the maximum relative velocity and the maximum velocity of the structure was evaluated for horizontal panels. Based on the results of response history analyses, the proposed velocity ratio $v_{r,max} / v_{s,max}$ is 1.5. This ratio was used in the analytical procedure for the estimation of maximum impact forces in the restrainers. The match of numerical and analytical results was reasonable, although the analytical procedure gives, in general, a more conservative estimation of the maximum force. Results have confirmed the usefulness of the analytical procedure for calculating maximum impact forces that could occur on the restrainers.

8 CONCLUSIONS

This dissertation investigates the seismic performance of prefabricated RC structures with horizontal concrete façade systems. The type of structure and connections considered are typically used in prefabricated buildings across Central Europe. Several failures of cladding panels were observed during the recent strong earthquakes in Northern Italy, and reasons for their failure are one of the questions addressed in the dissertation.

Most analytical research presented in the dissertation was supported by extensive experimental results. Experimental research from static and dynamic tests on single cladding connections and complete fastening system up to full-scale tests on the shaking table was considered. Shaking table tests were not performed as part of the dissertation, but the test results were used to define and analyse response mechanisms and verify models. Many tests were numerically simulated by the newly developed numerical models, and the simulations were quite successful.

The main goals of the dissertation were to investigate the seismic response of prefabricated RC structures with horizontal panels, define appropriate numerical models, analyse the influence of various parameters on the seismic response of the structural system, analyse the interaction between the panels and the main precast structure, and determine the influence of horizontal façade system on the overall response of the structure. The goals were successfully accomplished. Work can be briefly summarised as:

- Results of the dynamic experiments on the cladding connections for horizontal panels were analysed in detail. A typical seismic response mechanism of the complete fastening system was identified. The failure criteria and capacity of the fastening system were determined.

- Full-scale shaking table tests on the RC precast structure with non-structural horizontal RC cladding panels were used to define and analyse the seismic response of the complete structural system.

- New numerical models of cladding connections were formulated and validated on single component tests and full-scale shake table experiments.

- An extensive parametric study of one-storey precast industrial buildings with horizontal panels was performed. Various important parameters were analysed: structural configuration, construction imperfections (different initial positions of fastening devices),

the interaction of adjacent panels (influence of the silicone sealant), and the connection of bottom panels to the foundation.

- Parameters that influence the response and capacity of the façade system were identified. The initial position of cladding connections has the most significant influence on the response of panels because it defines how much the panels can slide before the impacts in the connections occur.

- The influence of the horizontal façade system on the response of the main precast structure was analysed. It was shown that panels do not significantly affect the response of the main structure. The influence of panels was slightly more noticeable only at higher intensities and in slender structures with a relatively small mass.

- The design approach commonly used in practice was thoroughly assessed. A simple procedure for a rough estimation of demand on the façade system was presented.

- A proposal for improving the investigated façade system was based on providing more space for the sliding of connections. A procedure for calculating the required space was developed.

- Numerical analysis of restrainer systems in precast structures with horizontal panels was performed, and an analytical procedure for estimating restrainer demand was evaluated.

The most important findings and conclusions are presented in more detail in the following paragraphs.

The response of cladding connections for horizontal panels

The investigated fastening system consists of two parts: a pair of top bolted connections that provide the horizontal stability of the panels and a pair of bottom cantilever connections that support the weight of the cladding panel. Cyclic and dynamic tests of single connections were performed in two sets: (a) tests on the top connections and (b) tests on the complete fastening system, consisting of top bolted and bottom cantilever connections.

A typical response mechanism of the fastening system was identified based on the experimental results and observations. It consists of three distinct stages: sliding with small friction, contact with the panel causing an increase in stiffness of the connection, and brittle failure. In the sliding phase, the fastening system enables relative displacements between the panel and the structure.

The experimental analysis showed that the top connection is the weakest component of the fastening system. Thus, the capacity of the complete fastening system is limited by the capacity of top connections. That capacity strongly depends on the initial size of gaps, which depends on the accuracy of construction. Failure of the connections occurs at a displacement about 3.5 cm larger than the initial gap size of the top connection. A resistance of approximately 55 kN was measured at failure.

Numerical modelling of the fastening system

Numerical models for connections were based on force–displacement relationships. The models were formulated in the OpenSees software framework by combining different existing material model behaviours.

The analysis of the experimental results showed that the responses of the top and bottom connections under dynamic loading have somewhat different characteristics. The top connection appears to exhibit typical Coulomb friction behaviour, whereas the response of the bottom connection is viscoelastic. This was considered in the numerical models.

The impacts that occur when the gap for sliding of panels closes were simulated by a sudden increase in connection stiffness. It was shown that the dissipation of energy during the impacts is negligible, and therefore, the impacts could be sufficiently modelled with a simple linear spring.

In the dissertation, typical values of different model parameters are proposed and calibrated by experiments. The proposed numerical models can describe the response of the fastening system under cyclic and dynamic loading. A reasonably good match of the experimental and numerical results was achieved for single components and for the full-scale building on the shaking table.

The response of horizontal concrete façade system

The shaking table tests gave valuable information about the earthquake performance of the complete precast system with horizontal concrete cladding panels. The cladding panels moved predominantly translationally in their plane and, in general, followed the movements of the main structure, but there were slips in the connections.

Experimental observations were augmented by a comprehensive parametric study considering a wide array of one-storey RC precast buildings. Based on the experimental observations and

numerical analyses, a typical response of the investigated horizontal concrete façade system was identified and can be described as follows.

At low intensities, rigid panels move as if they are pinned at the top connections and slide at the bottom connections. After the friction at top connections is activated at higher intensities, panels slide at both top and bottom connections. The response of panels is predominantly translational, and relative displacements between the panel and the main structure are typically in opposite directions at the top and bottom edges of the panel. The study showed that the top and bottom connections interact with each other and should be treated together. The column drift along the single panel presents a measure of demand on the fastening system.

With increasing drift demand, gaps in the connections are depleted, and impacts between columns and panels occur. At that point, the stiffness of the connections significantly increases, and high lateral forces occur. Failure of the fastening system follows when the resistance of the top connection is reached.

Parameters that influence the response of the analysed façade system

The influence of various parameters on the response of the façade system was analysed. The panel response is most affected by construction imperfections. Gaps in cladding connections are intended only for construction purposes but also enable sliding of the connections. Thus, if gaps in the connections are already closed at the initial stage, the displacement capacity of the system is significantly reduced. The force in the top connection increases even at small relative displacements, which leads to an earlier failure of fastenings. The most unfavourable position of connections is diagonally eccentric at the top and bottom connections of a panel.

Silicone-sealed joints cause noticeable interaction between adjacent panels. For that reason, the demand for top connections is somewhat greater, and the failure could occur earlier. Because the stiffness of silicone sealant severely deteriorates, its influence on the response is not as large as the influence of the construction imperfections.

If the bottom panel was fixed to the foundation, all the drift demand was taken only by the top connections of that panel. Thus, in the case of a fixed bottom panel, the first failure of the fastening system often occurred at the bottom panel and not at the top of the structure.

The capacity of the fastening system

Extensive research showed that failure of the fastening system occurs when the capacity of top connections is reached. This happens at a certain amount of column drift along a single panel. The dissertation evaluates the correlation between the column drift along the panel height and the demand and capacity of the fastening system.

The drift capacity of the fastenings depends on several parameters that influence the panel response. From all analysed parameters, the available gaps in the connections had the most important influence on the capacity of the fastening system. Because of construction imperfections, the sliding capacity of connections can be considerably reduced, which leads to fastening failure at relatively small drift demand (i.e. column drift along the single panel). Other parameters that noticeably influenced the drift capacity of the fastening system were silicone sealant between adjacent panels and the connection of bottom panels to the foundation.

Because of the silicone-sealed joints, there was some interaction between panels. It was shown that in that case, displacements at top and bottom connections were not necessarily in opposite directions. The capacity of the top connection was reached at smaller drift demand, which means that the drift capacity of the fastening system was reduced.

When the bottom panel was fixed to the foundation, the complete drift capacity of that panel was provided only by the top connections, and for that reason, it was smaller. This applies only to the bottom panels, whereas the connection of the bottom panel to the foundation did not influence the capacity of the higher panels.

To adequately protect panels from falling and avoid activation of high forces, impacts in the connections should be prevented. For conservative estimation of the fastening system's capacity (for design purpose), the capacity could be expressed only as the sliding capacity of the top connections. In that case, all negative effects of analysed parameters are taken into account, activation of high forces in connections is prevented, and the panels are adequately protected against failure. Under these conditions, any structure with gaps that are already completely closed in its initial position is considered as unsafe as far as the panels are concerned.

Influence of the façade system on the main precast structure's response

The influence of the panels on the overall response of the structure was limited. For most analysed structures, the interaction of panels and the main structure in terms of stiffness was minimal. During sliding of connections without contact, the stiffness of connections is negligible, and the panel had

almost no influence on the response of the main precast structure. After the gaps were closed, there was some interaction of panels with the main structure. However, the duration of impacts was very short, and the interaction was activated only for a short time. For that reason, the displacement response of majority structures was also not significantly affected by impacts.

There was some interaction between adjacent panels because of the silicone sealant. However, the silicone sealant is subjected to severe stiffness deterioration during the seismic excitation, which reduces its effect on the structure. For that reason, the influence on the main structure's stiffness and displacements was only minor.

High lateral forces were activated during the impacts, and their influence on shear demand in the column was analysed. At higher intensities, the contribution of high vibration modes was increased in some structures, which lowered the resultant force closer to the base of the column. Structures that were somewhat more affected by the presence of panels were typically slender structures with a relatively small mass (e.g. structures *m20H7*, *m20H9*, *m40H9* and *m60H9*), especially if the number of columns was very small compared to the number of panels (*k* factor 1). However, because the minimum reinforcement criteria and capacity design according to EC8 were considered in the design, the shear resistance of the columns (analysed within the parametric study) was not exceeded.

The connection of bottom panels did not significantly affect the maximum shear force but affected the distribution of forces along the height of the column. If the bottom panel was fixed to the foundation, maximum shear force typically occurred at the base of the column. Otherwise, the maximum shear force could occur higher along the column's height.

Design procedure used in practice

In the current design practice in Slovenia, the interaction between panels and the main structural system of RC buildings is neglected. The influence of the panels on the overall seismic response is taken into account only by adding the mass of the panels to the main structural system. It has been found that such an approach can estimate the response of the main structural system reasonably well for most of the structures. Structures that require more detailed calculation are very slender structures with small tributary mass.

To assess the response of horizontal panels, the demand on connections (i.e. required capacity) can be relatively simply estimated from an average column drift along a single panel. The procedure presented in the dissertation gives a rough estimation. The fundamental period of the main precast

structure, height of the structure, height of the panel and specific characteristics of the response spectra are all that are needed.

Proposal for the improvement of investigated connections

It was observed that the initial position of cladding connections appreciably influenced the response and capacity of horizontal concrete façade systems. For that reason, a relatively simple proposal for improvement of the connections by increasing the available gap was presented. The required gap sizes could be designed according to the expected drift demand depending on the panel's height, the structure's period and height and the seismic displacement demand. Structural limitations should also be considered because the column's cross section cannot be increased indefinitely.

Restrainers for seismic protection of cladding panels

In the last part of the dissertation, seismic restrainers intended to protect horizontal panels were numerically analysed. An existing analytical procedure for estimating the demand on restrainers for vertical panels was modified for horizontal panels.

The ratio between the maximum relative velocity and the maximum velocity of the structure, an essential parameter in the analysis, was defined for horizontal panels. The value proposed for use in the analytical procedure is 1.5. Compared to the numerical results, the analytical procedure gave generally more conservative estimates of the maximum impact force in the restrainer.

Different failure modes were discussed, and the problem of vertical amplification of forces, which is not considered in the procedure, was highlighted. This problem remains open for further research.

8.1 Major contributions of the thesis

The analysis of experimental results, the verified numerical models and the following parametric study on real RC precast structures contribute to the understanding of the behaviour of the façade system that is typically used in the European practice. Extensive experiments provided a fundamental basis for analytical and numerical studies performed within the framework of this dissertation. The analysis of the façade system response during the shaking table tests gave important information about the dynamic response of the complete structural system.

The defined macro numerical models of connections based on the force–displacement relationships were formulated and validated by single-component experiments and shake table tests. The models can be easily implemented in the numerical models and used in further numerical analyses.

The main contribution of the dissertation is an extensive numerical parametric study. Parameters that influence the seismic response of horizontal concrete façade systems in prefabricated buildings are discussed and analysed. The behaviour and capacity of the commonly used façade system are most susceptible to the initial position of connections.

The influence of the façade system on the main precast structure was thoroughly analysed. It was shown that the influence of horizontal panels on the main structure's global response is mostly limited and that the current design approach is suitable for use in practice. A relatively simple procedure for assessing horizontal façade systems performance that can be used with the current design procedure was presented.

8.2 Recommendations for future work

During the work performed within the scopes of the dissertation, the following possibilities for further research were recognised.

- Numerical models proposed and validated within the dissertation could be used in additional studies of the fragility and seismic risk of precast industrial buildings with horizontal façade systems.

- All the findings and conclusions presented within the thesis apply only to the analysed type of fastening systems for horizontal cladding panels. A short overview of other systems used in practice is given, highlighting differences from the analysed system. In Slovenian construction practice, the top connections are often poured with the concrete after the mounting. The seismic performance of such connections should be analysed. Further studies to evaluate the effect of friction between the adjacent panels are also recommended.

The application of restrainers in precast buildings is a relatively new field of research. Performing additional tests to define appropriate failure mode and account for the vertical amplification of forces is recommended. The analytical procedure should be appropriately modified.

9 RAZŠIRJENI SLOVENSKI POVZETEK (Extended abstract in Slovene)

9.1 Uvod

Armiranobetonske industrijske montažne hale predstavljajo enega najpogostejših konstrukcijskih sistemov v Evropi. Med preteklimi potresi je bilo mogoče opaziti zelo raznoliko obnašanje AB-montažnih hal – od sorazmerno dobrega obnašanja pa vse do katastrofalnih porušitev. Razumevanje odziva tega sistema med potresno obtežbo je bilo precej slabo, kar je vodilo v precej konservativne omejitve v predpisih. Rigorozni predpisi, konservativen pristop in nizki faktorji obnašanja so montažne hale postavili v podrejen položaj v primerjavi z monolitno armiranobetonsko gradnjo.

Zaradi zgoraj navedenih razlogov so bile v zadnjih dveh desetletjih in pol v več raziskovalnih središčih po Evropi izvedene obsežne in sistematične študije obnašanja AB-montažnih hal. Pridobljeno je bilo veliko pomembnih podatkov o potresnem odzivu tega konstrukcijskega sistema. Kljub obsežnosti raziskav pa sorazmerno kompleksen potresni odziv betonskih fasadnih sistemov še ni bil dovolj raziskan. Potrebna je bila kompleksnejša analiza potresnega odziva celotnega konstrukcijskega sistema. Zato so se obsežne raziskave nadaljevale v okviru slovenskega nacionalnega projekta *Potresna žilavost in utrjevanje montažnih industrijskih stavb z betonskimi fasadami*, ki ga je financirala Javna agencija za raziskovalno dejavnost Republike Slovenije (ARRS). Eden glavnih delov projekta je bil posvečen testom na potresni mizi in študijam obnašanja tipičnih fasadnih sistemov za AB-montažne hale v srednji Evropi. Rezultati teh eksperimentov so bili uporabljeni za študijo mehanizmov obnašanja in verifikacijo modelov, predstavljenih v tej nalogi.

9.1.1 Obravnavana problematika in vsebina doktorske disertacije

Montažne industrijske stavbe postajajo vse bolj priljubljen konstrukcijski sistem, saj omogočajo velike odprte prostore in sorazmerno hitro gradnjo ob nizkih stroških. Na veliko razširjenost konstrukcijskega sistema kaže tudi podatek, da se na letni ravni v Evropi zgradi približno 50 milijonov kvadratnih metrov montažnih stavb (Fischinger et al., 2014). Te se uporablja predvsem za industrijske namene pa tudi za gradnjo velikih nakupovalnih središč.

Pretekli potresi v Italiji so pokazali, da neustrezno načrtovanje montažnih stavb med močnimi potresi lahko povzroči katastrofalne posledice. Poleg ogrožanja človeških življenj je zaradi

neposredne škode na objektih in prekinitve proizvodnih procesov nastala ogromna gospodarska izguba (Bournas et al., 2013; Magliulo et al., 2014; Savoia et al., 2017).

Da bi se izognili katastrofalnim posledicam, je bilo izvedenih več evropskih raziskovalnih projektov, ki so zajemali obsežne eksperimentalne študije in numerične analize AB-montažnih zgradb. Eden izmed zadnjih projektov, ki je združeval moči akademskih strokovnjakov in partnerjev iz industrije, je bil projekt SAFECLADDING (2015), v okviru katerega so bili raziskani stiki med fasadnimi paneli in glavno montažno konstrukcijo. Pred projektom SAFECLADDING in nekaterimi vzporednimi študijami (Belleri et al., 2016; Belleri et al., 2018; Del Monte et al., 2019) je bil potresni odziv fasadnih panelov popolnoma neznan. Niso bili poznani temeljni mehanizmi odziva in projektantska praksa ni bila primerna. Upoštevan je bil le odziv panelov v smeri zunaj ravnine (CEN, 2004), medtem ko je za fasadne stike bolj kritičen vodoravni odziv v smeri ravnine panelov (Toniolo & Colombo, 2012; Bournas et al., 2013; Fischinger et al., 2014; Magliulo et al., 2014; Belleri et al., 2016). Visok delež poškodb na montažnih halah so po italijanskih potresih pripisali ravno padcu panelov zaradi porušitve fasadnih stikov.

Obsežne eksperimentalne in analitične študije (Negro & Lamperti Tornaghi, 2017; Toniolo & Dal Lago, 2017), izvedene v okviru projekta SAFECLADDING, so znatno izboljšale razumevanje potresnega odziva fasadnih stikov. Del raziskav, ki je bil opravljen na Fakulteti za gradbeništvo in geodezijo Univerze v Ljubljani, je bil namenjen analizi fasadnih stikov, ki se pogosto uporabljajo za pritrjevanje navpičnih (Zoubek et al., 2016) in vodoravnih fasadnih panelov v srednji Evropi. Čeprav je bilo pridobljenih veliko pomembnih informacij o potresnem odzivu obravnavanih fasadnih sistemov, s preteklimi raziskavami ni bilo mogoče v celoti razložiti kompleksnega sistemskega odziva.

Številne analitične in numerične študije različnih tipov fasadnih stikov so bile po večini omejene na monotone in ciklične teste posameznih komponent (Belleri et al., 2016; Zoubek et al., 2016; Psycharis et al., 2018; Yüksel et al., 2018; Del Monte et al., 2019) in nekaj psevdodinamičnih testov na konstrukcijah v velikem merilu (Negro & Lamperti Tornaghi, 2017; Toniolo & Dal Lago, 2017). Tako so bile študije osredinjene predvsem na analizo potresnega odziva posameznih komponent, medtem ko so ostali nepojasnjeni številni vidiki zapletenega obnašanja montažnega sistema v celoti.

Sledili so testi na potresni mizi v naravnem merilu, ki so omogočili celovit vpogled v obnašanje montažnega sistema z betonskimi fasadnimi paneli. Eksperimentalna raziskava je bila narejena v okviru projekta *Potresna žilavost in utrjevanje montažnih industrijskih stavb z betonskimi fasadami* v sodelovanju z inštitutom IZIIS (Inštitut za potresno inženirstvo in inženirsko seizmologijo) iz Skopja. Glavni cilj testov na potresni mizi je bil analiza potresnega odziva celotnega konstrukcijskega sistema z armiranobetonskimi fasadnimi paneli ob upoštevanju realnih robnih

pogojev. V okviru testov so bili variirani različni parametri, kot so: orientacija panelov, tip fasadnih stikov in konfiguracija preizkušanca (simetrična in asimetrična). V doktorski disertaciji so predstavljeni in analizirani rezultati testov na potresni mizi, ki obravnavajo vodoravno orientirane fasadne panele.

Testi na potresni mizi ter nadaljnje numerične in analitične študije so bili izvedeni z namenom, da bi preučili obnašanje montažnega sistema med dinamično potresno obtežbo ter ovrednotili morebitno interakcijo med fasadnimi paneli in glavno montažno konstrukcijo.

Predhodno so bili izvedeni testi posameznih komponent, tj. fasadnih stikov, katerih namen je bil pridobiti čim več podatkov o osnovnih mehanizmih obnašanja in kapaciteti obravnavanega sistema. Ti so omogočili načrtovanje testa na potresni mizi in so prav tako predstavljeni v okviru doktorske naloge.

Eksperimentom so sledile analitične študije in formulacija ustreznih makronumeričnih modelov, ki lahko opišejo obnašanje fasadnega sistema med ciklično in dinamično obtežbo. V okviru disertacije so bile raziskane različne možnosti modeliranja potresnega odziva vodoravnih fasadnih sistemov. Veljavnost in uporabnost numeričnega modela sta bili potrjeni s simulacijo testov posameznih stikov in simulacijo testa celotnega sistema na potresni mizi.

Numerični model je bil uporabljen za analizo realnih armiranobetonskih montažnih stavb v okviru parametrične študije, ki predstavlja osrednji del disertacije. Eden izmed glavnih ciljev parametrične študije je bila identifikacija parametrov, ki vplivajo na potresni odziv vodoravnih fasadnih sistemov v AB-montažnih halah. Poleg tega sta bila namena študije tudi analiza vpliva vodoravnih panelov na odziv glavne montažne konstrukcije ter analiza interakcije med paneli in glavno konstrukcijo. Obravnavani so bili naslednji parametri: različna konfiguracija oziroma geometrija stavbe, konstrukcijske nepravilnosti (različne začetne pozicije stikov kot posledica neprecizne montaže panelov), interakcija med sosednjimi paneli (vpliv silikonskega tesnila) in različni stiki spodnjih panelov s temeljem.

V projektantski praksi so fasadni paneli običajno obravnavani kot nekonstrukcijski elementi, pri čemer se upošteva samo njihovo maso, vpliv togosti panelov in stikov na odziv montažne stavbe pa se zanemari. Po zadnjih močnih potresih v Italiji je veliko padcev panelov pritegnilo pozornost, kar je postavilo pod vprašaj tudi dozdajšnji projektantski pristop. Zato je v okviru disertacije ta pristop podrobneje ovrednoten. Kot eden izmed rezultatov študije je podan tudi predlog za izboljšavo analiziranih stikov.

Padec fasadnih panelov bi lahko preprečili s tako imenovanimi pridrževalci, ki bi varovali panele ob odpovedi primarnih fasadnih stikov (Zoubek, 2015; Zoubek et al., 2016). Zato smo ovrednotili

obstoječi postopek za analitično oceno obremenitev v pridrževalcih za varovanje vodoravnih panelov.

9.2 Fasadni stiki za pritrjevanje vodoravnih betonskih fasadnih panelov

9.2.1 Opis fasadnih stikov

Sistem obravnavanih fasadnih stikov sestavljata par zgornjih stikov, ki zagotavlja stabilnost panela v vodoravni smeri, in par spodnjih stikov, ki podpira težo panela (slika 9.1). Kot je prikazano na sliki 9.2, je zgornji stik sestavljen iz navpičnega jeklenega kanala, zabetoniranega v steber, in posebnega škatlastega elementa, ki je vgrajen na zgornjem robu panela. Elementa sta povezana z vijakom s kladivasto glavo, ki se ga med montažo vstavi v kanal (betoniran v steber), zavrti in na strani panela privije na škatlast element.

Spodnji stik predstavlja jeklena konzola, sestavljena iz treh elementov (slika 9.3): posebne škatle, ki je vgrajena v steber, jeklenega nosilca in jeklene ploščice, ki je vgrajena na vrhu odprtine v panelu. Med montažo se jekleni nosilec vstavi v škatlo in privije. Nato se panel preprosto položi na konzolo in pričvrsti na vrhu s posebnimi vijaki s kladivasto glavo.

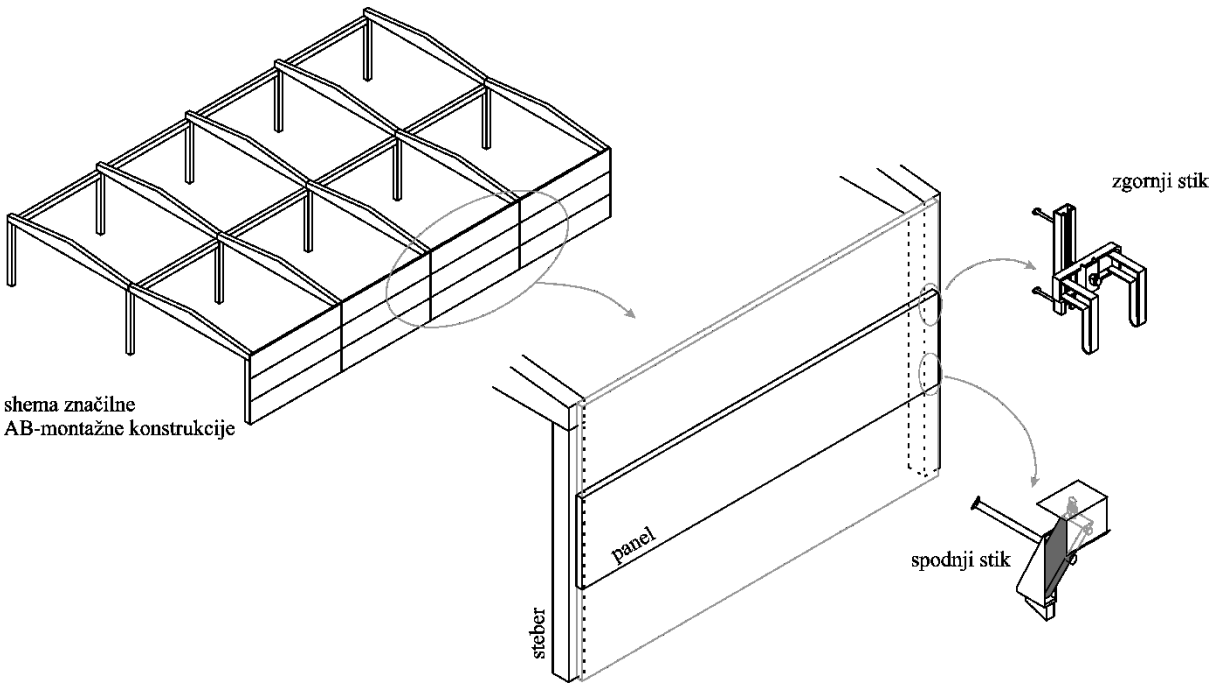

Slika 9.1: Shematski prikaz značilne armiranobetonske montažne hale z vodoravnimi paneli
Figure 9.1: Scheme of a typical RC precast structure with horizontal panels

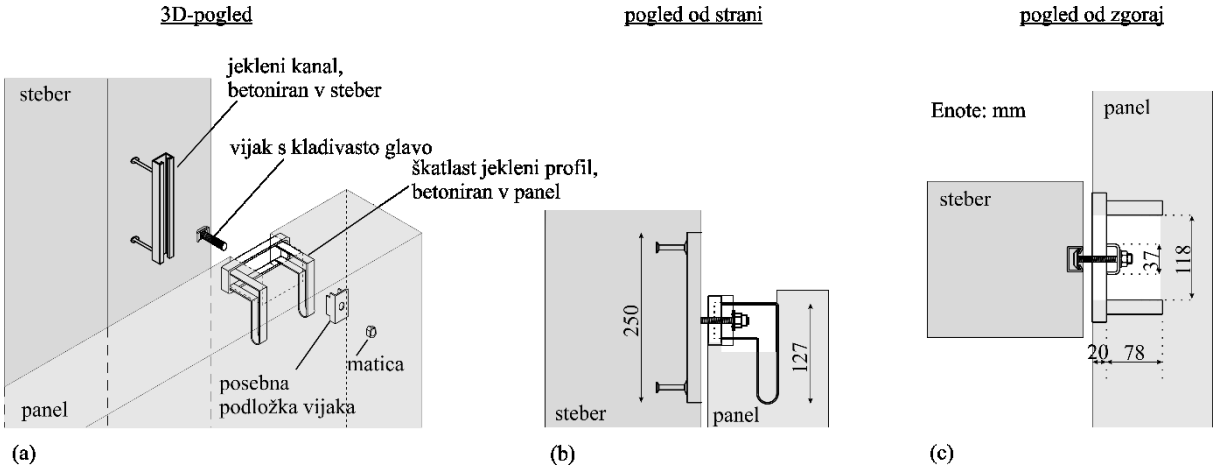

Slika 9.2: Sestava zgornjega vijačenega stika: a) 3D-pogled, b) stranski pogled, c) pogled od zgoraj

Figure 9.2: The assembly of the top bolted connection: a) 3D view, b) side view, c) top view

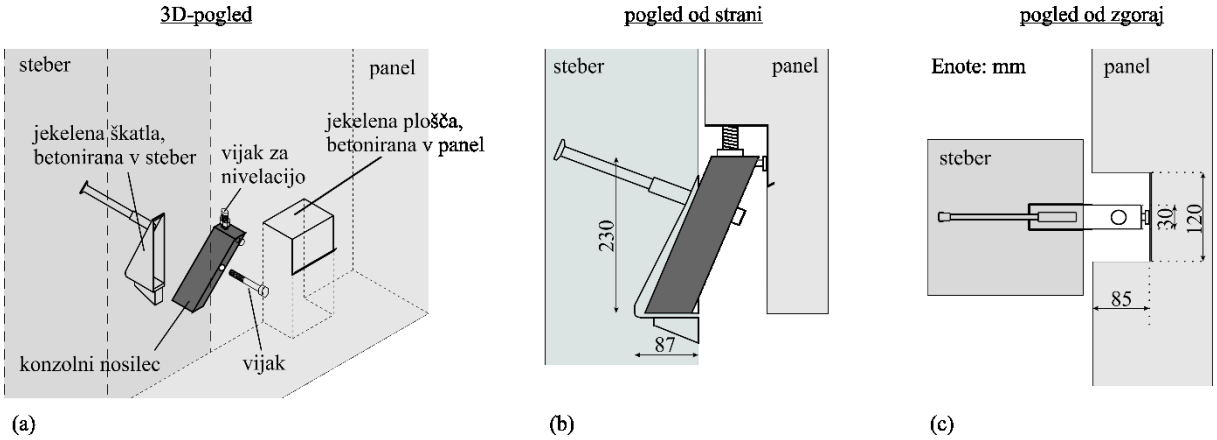

Slika 9.3: Sestava spodnjega konzolnega stika: a) 3D-pogled, b) stranski pogled, c) pogled od zgoraj

Figure 9.3: The assembly of the bottom cantilever connection: a) 3D view, b) side view, c) top view

9.2.2 Mehanizem odziva fasadnih stikov

Za analizo obnašanja fasadnih stikov med potresno obtežbo sta bila izvedena dva sklopa cikličnih in dinamičnih preizkusov. Fasadni stiki so bili preizkušeni v vodoravni smeri vzporedno z ravnino panelov, pri čemer je bil glavni namen preizkusov določitev mehanizma odziva obravnavanih stikov in njihove kapacitete.

V prvem sklopu preizkusov so bili testirani samo zgornji stiki, medtem ko je bil drugi sklop preizkusov narejen na celotnem sistemu stikov, ki vključuje zgornje in spodnje stike. Skupno so bili izvedeni štirje ciklični preizkusi in šest dinamičnih preizkusov.

Mehanizem odziva zgornjih fasadnih stikov lahko opišemo s tremi fazami, prikazanimi na sliki 9.4:

(1) V prvi fazi (med 1 in 2) vijak drsi ob jeklenem škatlastem profilu (glejte sliko 9.4). Aktivirana je sorazmerno majhna sila trenja, katere velikost je odvisna od momenta privitja vijaka in koeficienta trenja med jeklenimi elementi (posebno oblikovana podložka vijaka drsi ob jeklenem škatlastem profilu).

(2) Začetek druge faze nastopi, ko podložka jeklenega vijaka zadane ob rob odprtine profila, vgrajenega v panel (glejte sliko 9.4 b), kar sovpada s pomikom d_{gap} = 3–4 cm. V tej fazi je vijak podvržen upogibnim obremenitvam, kar povzroči izrazit skok v togosti. Opažene so bile plastične deformacije vijaka in kanala, vgrajenega v steber.

(3) V zadnji fazi je dosežena porušitev stika, ki običajno nastopi zaradi znatnih plastičnih deformacij kanala in izpuljenja vijaka (slika 9.4, faza 3).

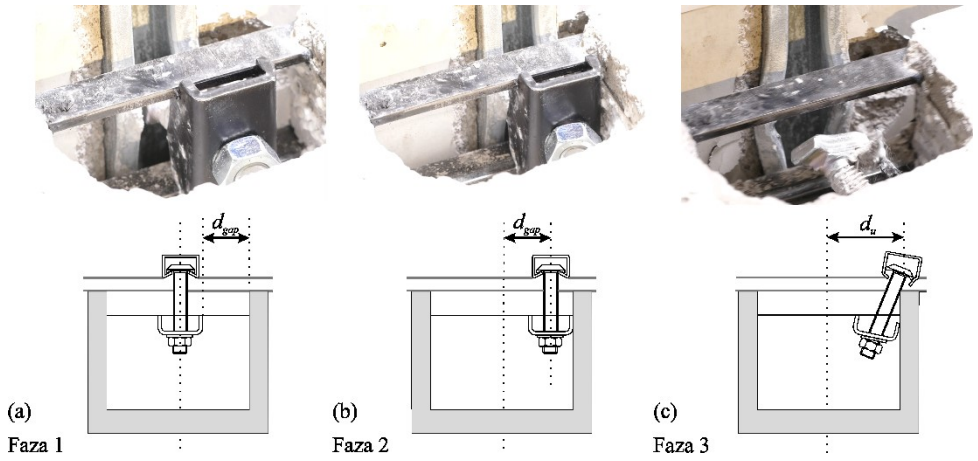

Slika 9.4: Porušni mehanizem zgornjega vijačenega stika: a) začetna lega, b) podložka vijaka doseže rob jeklenega profila v panelu, c) porušitev stika zaradi plastičnih deformacij kanala in izpuljenja vijaka

Figure 9.4: The failure mechanism of the top bolted connections: a) initial position, b) the special bolt washer reaches the edge of the steel box profile cast in the panel, c) failure due to the plastic deformations of the channel and the bolt being pulled out

Mehanizem odziva spodnjih stikov prav tako lahko opišemo s tremi fazami, ki so predstavljene na sliki 9.5:

(1) Po aktivaciji sile trenja sledi faza drsenja panela (slika 9.5 a). Trenje v spodnjih stikih je bilo bistveno manjše od trenja v zgornjih stikih.

(2) Potem ko je prostor v stiku izkoriščen (slika 9.5 b), togost stika ob upogibnih obremenitvah konzole znatno naraste.

(3) Zaradi velike togosti in nosilnosti konzol je bil njihov odziv med preizkusi pretežno elastičen. Na koncu testov, ki so bili po večini prekinjeni zaradi presežene kapacitete bata, so bile opazne le minimalne deformacije konzol (glejte sliko 9.5 c).

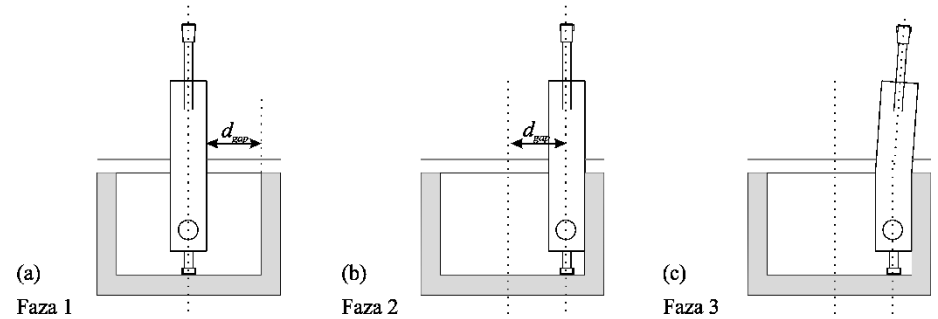

Slika 9.5: Mehanizem odziva spodnjega konzolnega stika: a) začetna lega, b) jeklena konzola doseže rob odprtine v panelu, c) na koncu testa je konzola le minimalno deformirana

Figure 9.5: The behaviour mechanism of the bottom bearing cantilever connection: a) initial position, b) the cantilever bracket reaches the edge of the opening, c) there were minor deformations in the connection at the end of the test

Preizkusi fasadnih stikov so bili narejeni na preizkušancu z zgornjimi stiki in preizkušancu s celotnim sistemov stikov (par zgornjih in par spodnjih stikov). Na sliki 9.6 sta prestavljeni tipični ovojnici sila – pomik histereznih odzivov z označenimi posameznimi fazami odziva zgornjih stikov in celotnega sistema stikov.

V prikazanem primeru in med testi na splošno je bil prosti pomik v zgornjih in spodnjih stikih izkoriščen skoraj hkrati. Velja opomniti, da v realnih konstrukcijah navadno ni tako in da je velikost prostega pomika odvisna od izkoriščenosti konstrukcijskih toleranc, tj. začetne pozicije vijaka in konzole glede na odprtino v panelu.

Pri testu celotnega sistema (slika 9.6 b) lahko porast v togosti opazimo dvakrat. Ko je bil dosežen pomik $d_{\text{gap, top}}$, je prišlo v zgornjem stiku do prvega stika s panelom. Ob tem je togost sistema stikov skokovito narastla zaradi povečanja togosti v zgornjih stikih. Sledilo je povečanje pomikov do $d_{\text{gap, bottom}}$, ko je togost sistema stikov ponovno narastla zaradi aktivacije togosti v spodnjih stikih. Vsi stiki, oba zgornja in oba spodnja, so bili v stiku s panelom.

Zaradi izkoriščene kapacitete bata so bili testi sistema stikov prekinjeni, preden je bila dosežena porušitev, vendar pa so bili ob koncu preizkusa zgornji stiki precej poškodovani, pri čemer so jekleni kanali in vijaki utrpeli znatne nepovratne deformacije. Pričakovati je bilo porušitev zgornjih stikov ob sorazmerno majhnem povečanju pomikov. Ker so bile poškodbe spodnjih stikov ob koncu testa le minimalne, lahko sklenemo, da bi prišlo do porušitve celotnega sistema zaradi porušitve zgornjih stikov. Upoštevajoč deformacijsko kapaciteto zgornjih stikov d_u in skoraj elastični odziv

spodnjih stikov, je kapaciteta celotnega sistema stikov ocenjena, kot je prikazano s črtkano linijo na sliki 9.6 b.

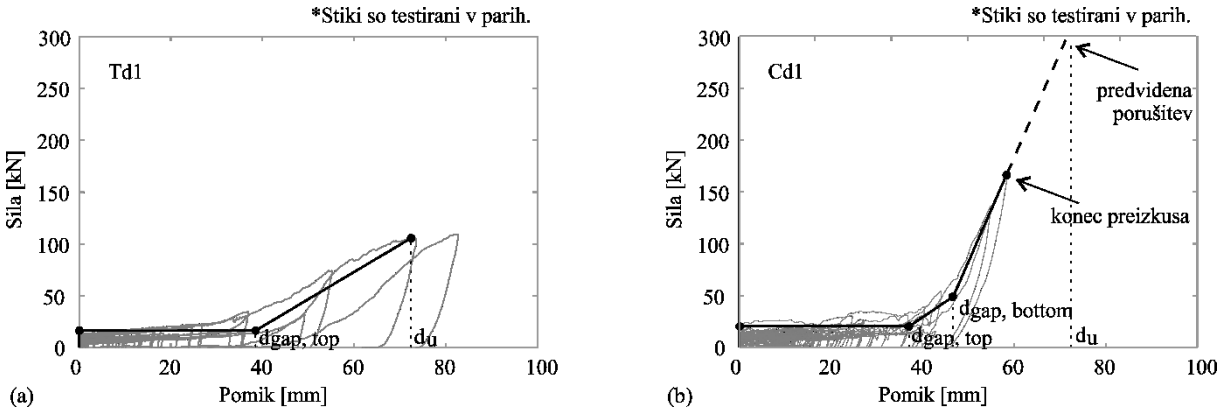

Slika 9.6: Ovojnice odziva stikov: a) zgornji stik in b) celoten sistem stikov

Figure 9.6: Response envelopes of the connections: a) top connections and b) the complete fastening system

9.3 Montažni sistem z vodoravnimi betonskimi fasadnimi paneli

9.3.1 Eksperimentalne preiskave na potresni mizi

Montažna enoetažna konstrukcija, ki je bila testirana na potresni mizi, je prikazana na slikah 9.7. Preizkušanca sestavljajo štirje stebri (vsak z maso 1 t), strešna plošča (9.1 t) in vodoravna betonska panela (vsak 2.6 t). Stebri kvadratnega prereza 0,3 m x 0,3 m (slika 9.7 b) so bili visoki 4,5 m in armirani z 8 vzdolžnimi palicami Φ16 ter stremeni Φ8 na razdalji 5 cm in 10 cm. Razdalja med stremeni je bila krajša ob vpetju stebra in na območju montaže panela. Stebri in grede so bili povezani z mozničnimi stiki.

Vodoravni paneli so bili na glavno konstrukcijo pritrjeni s fasadnimi stiki, predstavljenimi v poglavju 9.2.1 (sliki 9.7 c in d). Preizkušeni sta bili dve konfiguraciji, simetrična z dvema paneloma, kot je prikazano na sliki 9.7 a), in asimetrična s samo enim panelom. Zaradi omejitve prevrnitvenega momenta, ki ga lahko prenese potresna miza, je bilo mogoče testirati le po en panel na vsaki strani konstrukcije.

Preizkušanec je bil obremenjen v vodoravni smeri vzporedno z ravnino panelov. Za definicijo obtežbe je bil uporabljen akcelerogram Petrovac N-S, ki je bil zabeležen med potresom v Črni gori leta 1979. Izbrani akcelerogram je bil modificiran, tako da se ujema z Evrokodovim spektrom za tip tal B. Najprej so bili narejeni štirje preizkusi simetrične konstrukcije (po en panel na vsaki strani konstrukcije) s postopnim povečevanjem PGA intenzitete od 0,1 g do 0,4 g. Nato je bil en panel odstranjen in sledili so trije testi asimetrične konstrukcije pri PGA-intenzitetah 0,1 g, 0,2 g in 0,3 g.

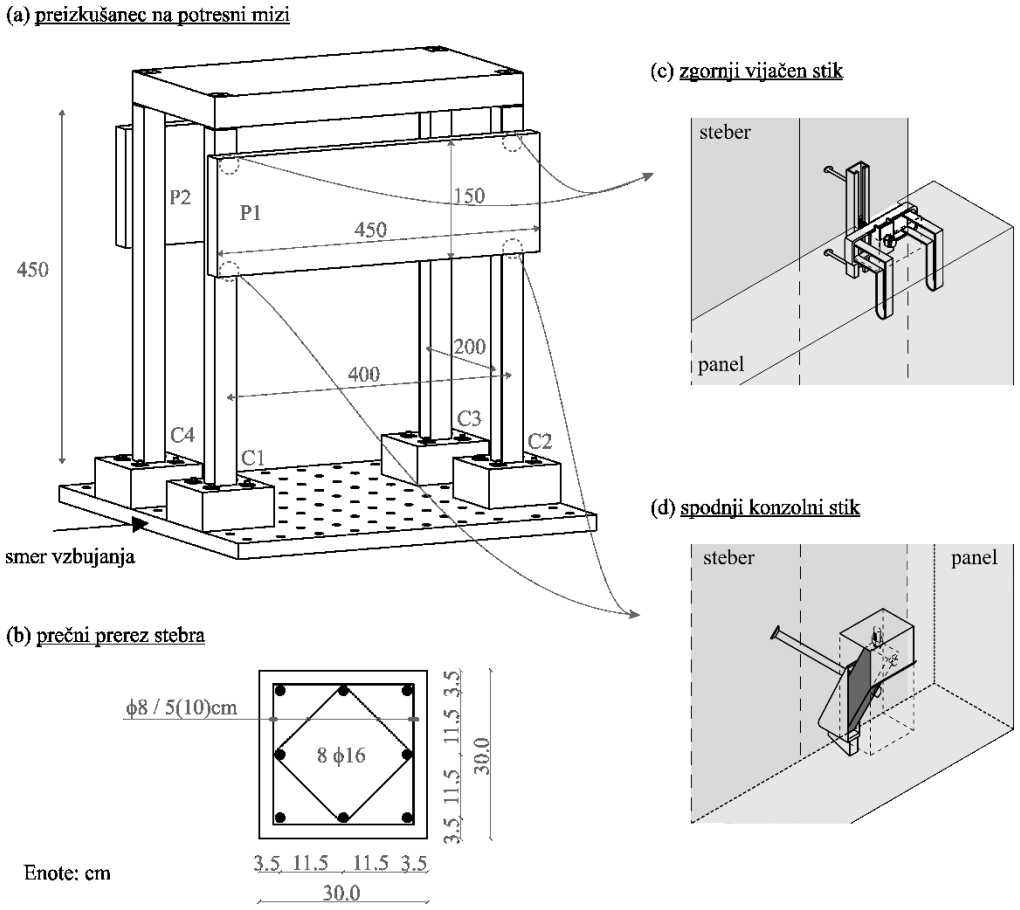

Slika 9.7: Preizkušanec na potresni mizi: a) geometrija v 3D-pogledu, b) prečni prerez stebra, c) zgornji fasadni stik in d) spodnji fasadni stik

Figure 9.7: Tested specimen at shake table: a) geometry in 3D view, b) columns' cross-section, c) top cladding connection and d) bottom cladding connection

9.3.2 Odziv panelov in glavne konstrukcije

Mehanizem odziva preizkušanca med testom na potresni mizi je prikazan na sliki 9.8. V splošnem panel sledi pomikom stebra. Pri nizkih intenzitetah obtežbe (slika 9.8 a) ni bilo nobenih zdrsov v zgornjih stikih. Relativni pomiki med konstrukcijo in paneli so bili zabeleženi le na spodnjem robu panelov. Zdrs v spodnjem stiku je bil enak pomiku stebra na ravni panela.

Pri večjih intenzitetah (slika 9.8 b) so bili zdrsi zabeleženi v zgornjih in spodnjih fasadnih stikih, in sicer v nasprotnih smereh. Vsota absolutnih zdrsov v zgornjem in spodnjem stiku je enaka pomiku stebra na ravni panela, ki ga izračunamo iz absolutnih pomikov stebra.

Osnovni nihajni čas konstrukcije je bil okoli 0,85 s. Nihajni čas panelov je bil enak, kar potrjuje ugotovitev, da se paneli gibljejo skupaj s konstrukcijo. Majhna razlika v amplitudi pomikov stebra in panela je bila enaka zdrsu panela v zgornjem stiku.

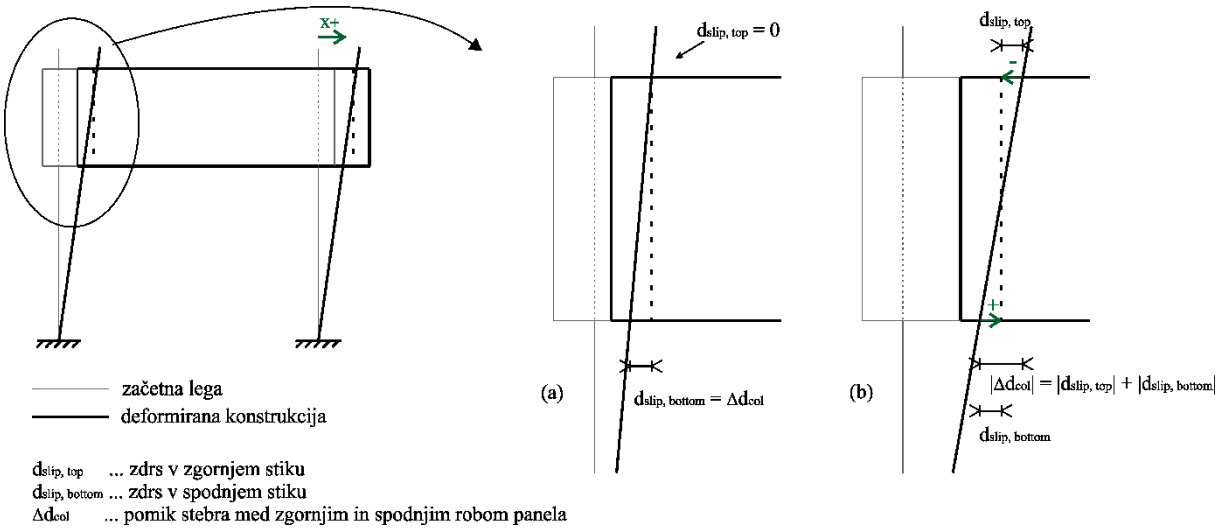

Slika 9.8: Mehanizem obnašanja vodoravnih fasadnih panelov pri a) nizki intenziteti obtežbe in b) visoki intenziteti obtežbe

Figure 9.8: Behaviour mechanism of the horizontal cladding panel at a) low load intensity and b) high load intensity

Mehanizem odziva posameznih fasadnih stikov med testi na potresni mizi je bil dejansko enak odzivu stikov med testi posameznih komponent, le da med testi na potresni mizi ni bila dosežena porušitev. Bistvena razlika je bila v smeri drsenja, in sicer je bilo med testom na potresni mizi drsenje v zgornjih in spodnjih stikih v nasprotnih smereh, kot je tudi pričakovati v realnih stavbah, vendar pa smer drsenja nima bistvenega vpliva na mehanizem odziva stikov ali definirani tip porušitve, ker je gibanje panela translacijsko. Rotacije panelov so bile zanemarljive.

Odziv stebrov med preizkusom na potresni mizi je bil pretežno elastičen. Manjše tečenje armature je bilo opaženo le pri dveh testih z najvišjo intenziteto. Ker so bile lastnosti prečnega prereza stebrov ter masa konstrukcije in panelov enaki v obeh smereh, sta bila tudi nihajna časa v obeh pravokotnih smereh dejansko enaka.

Velja omeniti, da so pospeški konstrukcije pravokotno na smer vzbujanja znašali približno 30 % pospeškov v smeri vzporedno z ravnino panelov (smer potresne obtežbe), s čimer je bila upoštevana tudi prečna komponenta vzbujanja, vendar pa med preizkusom ni bilo vidnega vpliva na odziv fasadnih stikov v smeri prečno na ravnino panelov. Torzija plošče je bila razmeroma majhna (tudi med testi asimetričnega preizkušanca) in ni imela pomembnega vpliva na odziv konstrukcije.

V začetnih fazah odziva, ko se panel obnaša kot slika, pritrjena v zgornjih stikih in v fazi drsenja panela na zgornjem in spodnjem robu, paneli s svojo togostjo niso vplivali na globalni odziv glavne montažne konstrukcije. V tej fazi se aktivira le majhno trenje in paneli skoraj prosto drsijo, zato je bila interakcija med paneli in konstrukcijo zelo majhna. Pri višjih intenzitetah je bilo mogoče opaziti več trkov med paneli in stiki; v teh trenutkih se pojavi določena interakcija med paneli in glavno

konstrukcijo, vendar je bilo to sodelovanje prisotno tako kratek čas, da ni imelo bistvenega vpliva na globalni odziv preizkušanca (tj. na pomike in pospeške glavne konstrukcije). Z numerično analizo je bilo pozneje ugotovljeno, da se med trki aktivira sorazmerno visoka sila. Med testi na potresni mizi so prečne sile v stikih tudi do 30 % celotne prečne sile ob vpetju. Ta vpliv je detajlno raziskan pozneje v okviru parametrične študije.

V okviru disertacije je bila narejena numerična analiza treh različnih modelov preizkušanca, s katero smo potrdili majhen vpliv togosti panelov na odziv glavne montažne konstrukcije. V analizi smo primerjali odziv celotnega modela preizkušanca s stebri, paneli in s stiki (model stikov je opisan v razdelku 9.4) z odzivom modela glavne konstrukcije brez stikov, pri čemer je upoštevana le masa panelov (v tem modelu ni bilo nobene interakcije v togosti panelov in glavne konstrukcije), in z odzivom modela glavne konstrukcije s paneli, ki so popolnoma fiksirani v zgornjih in spodnjih stikih (s tem modelom smo simulirali popolno interakcijo togosti panelov in glavne konstrukcije). Pokazali smo, da sta bila togost in nihajni čas preizkušanca skoraj enaka togosti in nihajnemu času konstrukcije, pri kateri je upoštevana le masa panelov, kar potrjuje, da stiki niso imeli bistvenega vpliva na odziv montažnega sistema.

9.4 Numerično modeliranje fasadnih stikov

Numerični model, ki opisuje histerezni odziv fasadnih stikov, je bil definiran v programskem okolju OpenSees (McKenna & Fenves, 2010) s kombinacijo različnih materialnih modelov. Uporabljeni modeli in način kombiniranja so prikazani na sliki 9.9. Odziv vsakega stika je bil opisan z vzporedno vezavo dveh delov, pri čemer prvi opisuje trenje v stiku, drugi pa simulira trke med panelom in stikom.

Analiza testov posameznih komponent je pokazala, da je obnašanje zgornjega in spodnjega stika ob dinamični obtežbi nekoliko drugačno. Medtem ko trenje v zgornjem stiku lahko opišemo s splošno poznanim Columbovim trenjem, je bil odziv spodnjega stika med drsenjem pretežno viskozen. Zato smo konstantno trenje v zgornjem stiku simulirali z materialnim modelom *Elastic-Perfectly Plastic (EPP)* (slika 9.9 a), spremenljivo trenje v spodnjem stiku pa z materialnim modelom *Viscous* (slika 9.9 b). Za simulacijo spodnjih stikov med ciklično obtežbo se lahko uporabi enak model kot za zgornje stike (ni dinamičnih vplivov).

V okviru disertacije smo preučevali različne možnosti za simulacijo trkov, pri čemer smo raziskali tudi možnost disipacije energije med trki. Ugotovili smo, da disipacija energije v stikih primarno izhaja iz trenja in da je med trki minimalna. Zato je bil za simulacijo trkov izbran preprost model elastične vzmeti z veliko togostjo (tj. model *ElasticPPGap* na sliki 9.9 e).

V nadaljevanju so predstavljeni in zbrani modelni parametri za zgornje in spodnje stike: velikost prostega pomika v stiku (d_{gap}), kapaciteta pomika stikov (d_u), sila trenja (R_{fr}), največja sila v stiku (R_{max}), dušenje (c_{visc}) in togost (K_{conn}, K_i). Priporočene vrednosti parametrov so zbrane v preglednici 9.1. Veljavnost in uporabnost numeričnega modela sta bili potrjeni s simulacijo testov posameznih stikov in simulacijo testa celotne konstrukcije na potresni mizi.

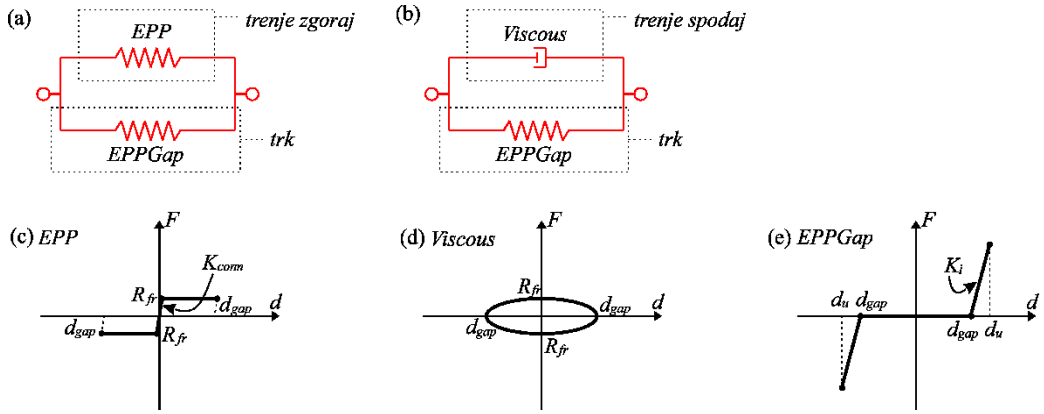

Slika 9.9: Shematski prikaz numeričnega modela: a) kombinacija histrereznih materialnih modelov za numerično simulacijo zgornjega stika, b) kombinacija histrereznih materialnih modelov za numerično simulacijo spodnjega stika, c) materialni model *ElasticPP*, d) materialni model *Viscous*, e) materialni model *ElasticPPGap*

Figure 9.9: Schematic presentation of the model: a) combination of hysteretic material models used for the numerical simulation of top connection, b) combination of hysteretic material models used for the numerical simulation of bottom connection, c) *ElasticPP*, d) *Viscous* in e) *ElasticPPGap* material models

Preglednica 9.1: Priporočene vrednosti modelnih parametrov

Table 9.1: Recommended values of the model parameters

Parameter	Vrednost	Parameter	Vrednost
$d_{gap,\ top}$*	±4,0 cm	d_u	±7,5 cm
$d_{gap,\ bottom}$*	±4,5 cm	$K_{conn,\ top}$	$2 \cdot 10^4$ kN/m
$c_{fr,\ top}$	0,4	$K_{conn,\ bottom}$	$2 \cdot 10^3$ kN/m
$R_{fr,\ bottom}$	2 kN	$K_{i,\ top}$	$1{,}5 \cdot 10^3$ kN/m
$c_{visc,\ bottom}$	50 t/s	$K_{i,\ bottom}$	$1{,}5 \cdot 10^4$ kN/m

Legenda: $d_{gap,\ top}$ … prosti pomik v spodnjem stiku, $d_{gap,\ top}$ … prosti pomik v spodnjem stiku, d_u … kapaciteta pomika, $c_{fr,\ top}$ … koeficient trenja v zgornjem stiku, $R_{fr,\ bottom}$ … sila trenja v spodnjem stiku (ciklična obtežba), $c_{visc,\ bottom}$ … koeficient dušenja (dinamična obtežba), $K_{conn,\ top}$ … začetna togost zgornjega stika, $K_{conn,\ bottom}$ … začetna togost spodnjega stika, $K_{i,\ top}$ … upogibna togost zgornjega stika, $K_{i,\ bottom}$ … upogibna togost spodnjega stika

* Vrednost pripada stikom, montiranim na sredi odprtine v panelu.

Prosti pomik v stiku

Začetna pozicija stika je odvisna od izkoriščenosti konstrukcijskih toleranc pri gradnji in morebitnih zaostalih pomikov po predhodnih vzbujanjih konstrukcije. Pri večini testov posameznih komponent so bili stiki v idealni poziciji na sredini odprtin v panelu. V tem primeru je bila velikost prostega pomika enaka polovici odprtine v panelu, zmanjšana za polovico debeline konzole ($d_{gap,\ bottom}$) ali podložke vijaka ($d_{gap,\ top}$).

Pri testih na potresni mizi je bil proces betoniranja in gradnje nekoliko zahtevnejši, kar je posledično pomenilo manj natančno montažo stikov. Poleg tega so bili po posameznih vzbujanjih preizkušanca zabeleženi zaostali pomiki. Zato smo pred vsakim testom izmerili velikosti prostih pomikov v stikih in te vrednosti nato uporabili pri simulaciji naslednje faze eksperimenta.

Kapaciteta pomika

Mejni pomik fasadnega sistema je definiran s kapaciteto pomika v zgornjem stiku oziroma bolj točno z deformacijsko kapaciteto stika po tem, ko je prosti pomik v zgornjem stiku izkoriščen. Torej je mejni pomik vsota variabilnega prostega pomika in deformacijske kapacitete vijaka v zgornjem stiku. Ta znaša 3,5 cm. Če so stiki modelirani idealno na sredini odprtine v panelu, znaša mejni pomik 7,5 cm.

Sila trenja

Trenje v zgornjem stiku je odvisno od momenta privitja vijaka in koeficienta trenja med posameznimi elementi stika. Priporočena vrednost koeficienta trenja za obravnavani stik je 0,4. Med testi posameznih komponent je največja zabeležena sila trenja 8 kN, kar sovpada s predpisanim momentom privitja 65 Nm. Ni pa nujno, da bodo v realnih konstrukcijah vijaki pritrjeni, kot je predpisano. Sila trenja se med potresno obtežbo postopoma zmanjšuje tudi zaradi rahljanja vijaka in je sorazmerno majhna v primerjavi s silami v glavni konstrukciji. Zato je priporočena sila trenja v zgornjih stikih 2 kN. Takšna je bila uporabljena tudi za simulacijo testov na potresni mizi.

Dušenje

Silo trenja v spodnjem stiku smo ocenili iz testov posameznih komponent, tako da smo od sile v vseh stikih odšteli silo trenja v zgornjih stikih. Maksimalna sila trenja v spodnjem stiku znaša približno 2 kN.

Vrednost koeficienta dušenja v spodnjem stiku je bila določena na podlagi izmerjenih hitrosti in ocenjenih sil med testi posameznih komponent ter pozneje kalibrirana z numeričnimi simulacijami. Priporočena vrednost koeficienta dušenja je 50 t/s, kar ustreza sili 2 kN pri hitrosti 0,04 m/s.

Togost

Začetna togost stikov je sorazmerno velika, vendar pa to velja, dokler ne pride do drsenja v stikih. V fazi drsenja je togost stikov dejansko nič. Ob kontaktu stika s panelom pa togost stika sunkovito naraste zaradi aktivacije sorazmerno velike upogibne togosti vijaka (zgoraj) in konzole (spodaj). Vrednosti v preglednici 9. so bile določene eksperimentalno in analitično. Ocenjena togost ob udarcu v spodnjih stikih je približno desetkrat večja od togosti ob udarcu v zgornjih stikih.

9.5 Parametrična študija enoetažnih montažnih stavb z vodoravnimi betonskimi fasadnimi paneli

Osrednji del disertacije predstavlja parametrična študija, v okviru katere je bil analiziran vpliv različnih parametrov na odziv enoetažnih montažnih stavb z vodoravnimi betonskimi fasadnimi sistemi. Eden izmed namenov študije je bila tudi analiza vpliva vodoravnih panelov na odziv glavne montažne konstrukcije ter analiza interakcije med paneli in glavno konstrukcijo.

Za modeliranje montažnih hal smo uporabili t. i. ekvivalentni model povprečnega stebra, ki je že uveljavljen v praksi. Da bi lahko pridobili popolno informacijo o odzivu montažnega sistema in vplivu panelov na odziv glavne konstrukcije (globalni vpliv na pomike konstrukcije pa tudi lokalni vpliv na sile v stebru), smo v okviru parametrične študije uporabili t. i. *ekvivalentni model stebra in panelov* ter *model povprečnega stebra*. S kombinacijo nelinearne dinamične analize ekvivalentnega modela stebra s paneli in analize modela stebra dobimo kompletno informacijo o odzivu montažne hale (o glavni konstrukciji in stikih oz. panelih).

Da bi lahko upoštevali vpliv različne konfiguracije tlorisov stavb, smo vpeljali faktor razmerja k, ki predstavlja razmerje med številom stebrov v konstrukciji in številom panelov v tlorisu v obravnavani smeri. Tega smo v računskem postopku uporabili za modifikacijo karakteristik stebra,

medtem ko lastnosti stikov nismo spreminjali. Veljavnost postopka za numerično analizo montažnih hal z vodoravnimi paneli je bila potrjena z analizo 3D-modelov dveh tipičnih montažnih stavb.

9.5.1 Izbor konstrukcij in parametrov za analizo

V parametrični študiji je bil uporabljen nabor 15 AB-montažnih hal z vodoravnimi paneli. Pri izbiri konstrukcij so bile upoštevane tipične montažne hale, ki jih lahko najdemo v slovenski praksi. Povprečna pripadajoča masa enega stebra je od 20 t do 100 t s korakom 20 t. Upoštevali smo tri različne višine konstrukcij (5, 7 in 9 m), število panelov pa je bilo določeno glede na višino konstrukcije. Tako so bili na halo z višino 5 m pritrjeni trije paneli ter na hale z višinami 7 m in 9 m po štirje oziroma pet panelov. Upoštevali smo predpostavko, da so višine panelov znotraj ene konstrukcije enake. Maso panelov smo izračunali iz pripadajoče višine panela, debeline betonskega dela panelov 0,16 m in iz dolžine panelov, ki je enaka razponu med stebri. Pri tem smo za konstrukcije z masami 20 t/steber in 40 t/steber privzeli dolžino panelov 7,5 m, za konstrukcije z masami 60 t/steber in 80 t/steber dolžino 10 m ter za konstrukcije z maso 100 t/steber dolžino panelov 12,5 m.

Vsi stebri so bili dimenzionirani po Evrokodu 8 (CEN, 2004) za tip tal C in maksimalni pospešek tal a_g = 0,25 g (Zoubek, 2015). Pri tem je bila upoštevana večina zahtev standarda, razen zahteve glede minimalne dimenzije prereza stebra, ki naj ne bi bila manjša od 1/10 višine stebra, vendar se tega merila pogosto ne upošteva niti v praksi in tako izbor konstrukcij odraža realno stanje.

Za numerične analize konstrukcij smo uporabili nabor 30 akcelerogramov pri treh intenzitetah. Pri tem smo variirali in analizirali vpliv naslednjih parametrov: interakcija med sosednjimi paneli (vpliv silikonskega tesnila), konstrukcijske nepravilnosti (začetna pozicija stikov), stik spodnjih panelov s temeljem in konfiguracija stavbe.

Interakcija med sosednjimi paneli

V praksi se običajno reže med paneli na obeh straneh zapolni s silikonskim tesnilom, ki povzroči določeno raven interakcije med sosednjimi paneli. V okviru naloge smo testirali elastični model in »pinching« model silikona. Zadnji upošteva degradacijo materiala in je bil ocenjen kot primernejši in zato uporabljen v parametričnih analizah.

V analizah je bila upoštevana porušitev tesnila pri mejni deformaciji. Ob porušitvi je bil element odstranjen iz modela in se je numerična analiza nadaljevala do konca oziroma morebitne porušitve stebrov. V okviru parametrične študije smo analizirali konstrukcije s silikonom in brez njega.

Konstrukcijske nepravilnosti

V montažnih konstrukcijah imajo stiki bistveno vlogo in posledično ima lahko njihov odziv velik vpliv na odziv fasadnega sistema. Zaradi neprecizne izdelave in montaže AB-elementov se v praksi redno pojavljajo konstrukcije nepravilnosti. Pri obravnavanih montažnih halah so zato začetne pozicije stikov lahko zelo različne.

Pri idealnocentrično montiranih stikih so med panelom in stebrom mogoči večji relativni pomiki. V tem primeru lahko panel skoraj prosto drsi (trenje je zelo majhno) do velikosti pomikov 4 cm v zgornjem stiku in 4,5 cm v spodnjem stiku. Če sta vijak zgoraj ali konzola spodaj premaknjena na rob odprtine v panelu, pa se znatne sile v stikih aktivirajo že pri majhnem relativnem pomiku med stebrom in panelom.

Da bi analizirali vpliv konstrukcijskih nepravilnosti na odziv sistema, smo v študiji upoštevali različne začetne pozicije stikov, in sicer stike, montirane idealnocentrično, ter dve ekstremno ekscentrični poziciji stikov. Tako so bili pri ekscentrični poziciji prvič vsi stiki montirani na eni strani odprtine in je bil prosti pomik izkoriščen na isti strani zgornjih in spodnjih stikih. V drugem primeru pa so bili zgornji in spodnji stiki montirani diagonalno ekscentrično (prosti pomik je bil izkoriščen v nasprotnih smereh na zgornjem in spodnjem robu panela). Pri tem smo privzeli, da so vsi zgornji stiki v konstrukciji montirani na enak način in vsi spodnji stiki na enak način.

Ob porušitvi stikov je bil porušen panel odstranjen iz modela in numerična analiza se je nadaljevala do konca oziroma do porušitve stebra.

Stik spodnjih panelov s temeljem

V praksi se pojavljajo različne izvedbe stikov spodnjih panelov s temeljem. Spodnji panel je lahko podprt s fasadnimi stiki, preprosto položen ali pa sidran v temelj. Sidranje je sorazmerno pogost način izvedbe v praksi. Pri tem se jeklena sidra predhodno zabije v panele, izvrta se luknje v temelj in na koncu stik zalije s cementno malto. Tako je spodnji panel na dnu dejansko fiksiran, kar vzbuja skrb o morebitnem pojavu učinka kratkega stebra. Zato smo v parametričnih analizah obravnavali dve možnosti: spodnji panel, fiksiran v temelj, in spodnji panel, pritrjen na steber s fasadnimi stiki (na enak način kot vsi zgornji paneli). V drugem primeru je bil stik med panelom in temeljem zapolnjen s silikonskim tesnilom.

Konfiguracija stavbe

Montažne hale imajo lahko različne konfiguracije tlorisov – kvadratne ali pravokotne oblike, ki so lahko ožje ali širše, z enakim ali različnim številom stebrov v pravokotnih smereh. Stavbe z različno tlorisno konfiguracijo imajo različna razmerja med številom stebrov in številom panelov, pritrjenih na zunanje stebre; to razmerje je lahko različno v vzdolžni in prečni smeri konstrukcije.

Za analizo vpliva konfiguracije stavbe na odziv montažnega sistema je bil uporabljen faktor *k*, ki predstavlja razmerje med številom stebrov in številom panelov v tlorisu v obravnavani smeri. Višja vrednost faktorja predstavlja večje število stebrov v primerjavi s številom panelov, kar velja npr. za širšo konstrukcijo, ki ima v obravnavani smeri večje število notranjih stebrov v primerjavi s sorazmerno majhnim številom robnih stebrov s paneli. Medtem ima taka konstrukcija v drugi pravokotni (daljši) smeri manjši faktor *k*. V parametrični študiji smo upoštevali celotni razpon pričakovanih faktorjev v realnih konstrukcijah, in sicer od 1 do 10.

9.5.2 Odziv montažne hale z vodoravnimi paneli

Odziv vodoravnih panelov in stikov je odvisen od intenzitete obtežbe in deformacije stebrov. Če med paneli ni silikona, vsak panel drsi posebej (slika 9.10). Pri manjši intenziteti se togi paneli obnašajo kot slika, pritrjena v zgornjih stikih, ki drsi na spodnjem robu (slika 9.10 a). Pri tem paneli sledijo gibanju glavne konstrukcije.

Pri višjih intenzitetah in večjih deformacijah stebrov se aktivira trenje tudi v zgornjih stikih – paneli drsijo zgoraj in spodaj. Odziv panelov je translacijski in relativni pomiki med glavno konstrukcijo in paneli so običajno v nasprotnih smereh na zgornjem in spodnjem robu panela (slika 9.10 b). Študija je pokazala, da sta odziva zgornjih in spodnjih stikov povezana in da je treba stike posameznega panela obravnavati skupaj.

Ker je odziv panela translacijski, lahko obremenitev fasadnega sistema izrazimo v obliki pomika stebra na ravni panela (Δd_{col}). Kot prikazujeta slika 9.10 in enačba 9.1, je pomik stebra na ravni panela, ki ga izračunamo iz razlike absolutnih pomikov stebra na zgornjem in spodnjem robu panela ($|d_{col,\ top} - d_{col,\ bottom}|$), enak absolutni vrednosti razlike med zdrsi v zgornjem in spodnjem stiku ($|d_{slip,\ top} - d_{slip,\ bottom}|$).

$$\Delta d_{col,\,p} = \left|d_{col,\,top} - d_{col,\,bottom}\right| = \left|d_{slip,\,top} - d_{slip,\,bottom}\right| \qquad (9.1)$$

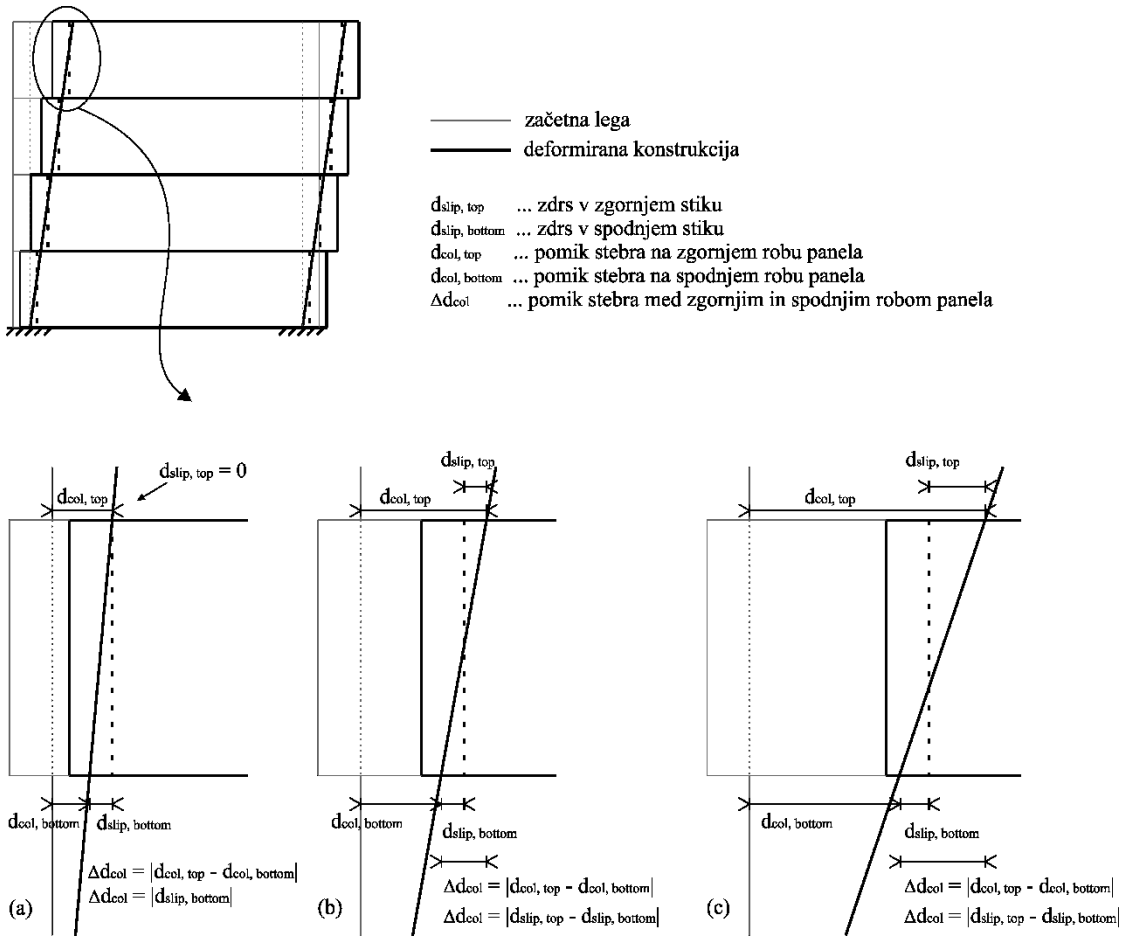

Slika 9.10: Značilen odziv konstrukcije s horizontalnimi paneli: a) majhne rotacije stebra, b) srednje rotacije stebra, c) velike rotacije stebra

Figure 9.10: Typical response of the structure with horizontal cladding panels: a) small column rotations, b) medium column rotations, c) large column rotations

Z naraščanjem obremenitev (slika 9.10 c) pride do udarcev med stebrom in panelom. V tem trenutku togost stika skokovito naraste, pri čemer se v stikih aktivirajo sorazmerno visoke sile. Do porušitve fasadnega sistema pride v trenutku, ko je presežena odpornost zgornjega stika.

V konstrukcijah s silikonom se pojavi interakcija med sosednjimi paneli in se zato odziv panelov nekoliko spremeni, kot je prikazano na sliki 9.11. Zaradi interakcije med paneli lahko pri večjih deformacijah stebra panel zdrsne zgoraj in spodaj v isti smeri glede na steber (slika 9.11 b). Ne glede na pozicijo panela še vedno velja enačba 9.1.

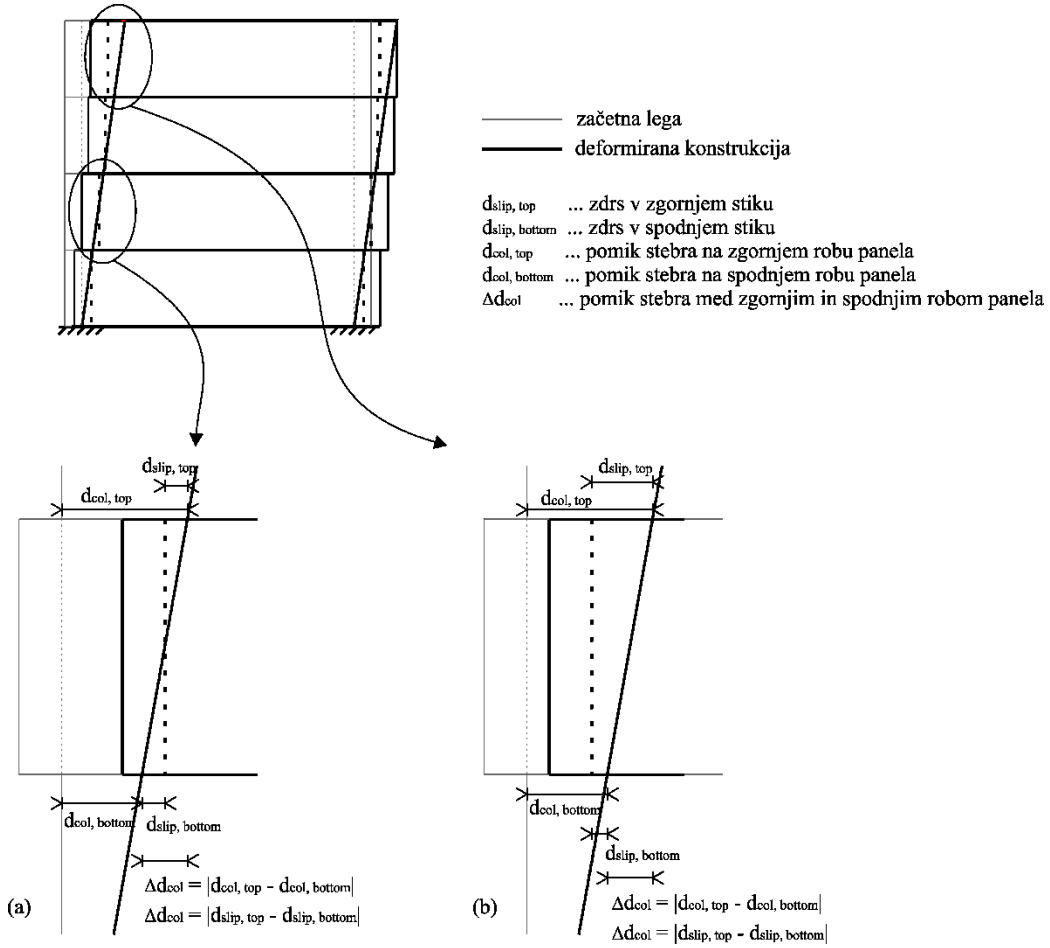

Slika 9.11: Odziv konstrukcije s silikonskim tesnilom med horizontalnimi paneli: a) relativni pomiki v zgornjem in spodnjem stiku v nasprotnih smereh, b) relativni pomiki v zgornjem in spodnjem stiku v isti smeri glede na steber

Figure 9.11: Response of the structure with silicone sealant between the horizontal panels: a) response of top and bottom connections in opposite directions, b) response of top and bottom connections in the same direction with respect to column

9.5.3 Vpliv analiziranih parametrov na odziv fasadnega sistema

S parametrično analizo smo pokazali, da ima na odziv fasadnega sistema največji vpliv začetna pozicija stikov. Prosti pomik v stiku, ki je v osnovi namenjen tolerancam pri montaži, omogoča določeno drsenje fasadnih stikov. Če so tolerance izkoriščene že pri montaži, je drsenje v eni smeri popolnoma preprečeno in bistveno zmanjša kapaciteto pomika stika (drsna kapaciteta je v tem primeru v eni smeri enaka nič). Sile v stikih se aktivirajo že pri zelo majhnih obremenitvah, kar pripelje do zgodnejšega padca panela. Najbolj neugodna je diagonalno ekscentrična pozicija stikov.

Uporaba silikona v stikih med paneli povzroči določeno interakcijo med paneli. Zaradi spremenjenega odziva se poveča pomik v zgornjem stiku, kar prav tako lahko vodi v zgodnejši padec panela, a vpliv silikona ni tako znaten kot vpliv začetne pozicije stikov.

Stik spodnjega panela s temeljem ima precejšen vpliv na odziv spodnjega panela, a dejansko nima vpliva na odziv fasadnega sistema višje po konstrukciji. Če je spodnji panel fiksiran, se ves relativni pomik tega panela zgodi le v zgornjih stikih. To pripelje do več porušitev spodnjega panela. Razmerje med številom stebrov in stikov v konstrukciji (faktor k) nima pomembnega vpliva na odziv panelov in fasadnih stikov.

9.5.4 Kapaciteta fasadnega sistema

Panel pade v trenutku, ko je presežena odpornost zgornjega stika, to je *kapaciteta zgornjega stika* (3,5 cm po tem, ko je izkoriščen prosti pomik v stiku, pri pribl. 55 kN). Ta vrednost je absolutna lastnost samega stika in je presežena pri določenem pomiku stebra na ravni panela. V nalogi smo zato pokazali, da obstaja korelacija med pomikom stebra na ravni panela in obremenitvijo ter *kapaciteto fasadnega sistema*, torej lahko kapaciteto celotnega fasadnega sistema izrazimo s pomikom stebra na ravni panela.

Med vsemi analiziranimi parametri ima največji vpliv na kapaciteto fasadnega sistema začetni položaj stikov. Ko je drsna kapaciteta stikov izkoriščena že v začetni fazi, pride do porušitve panela pri manjšem pomiku stebra na ravni panela, torej je kapaciteta fasadnega sistema v tem primeru manjša.

Drug parameter, ki ima sicer precej manjši, a opazen vpliv na kapaciteto fasadnega sistema, je interakcija med sosednjimi paneli. Zaradi silikona, ki povzroči določeno interakcijo med paneli, odziv zgornjih in spodnjih stikov pri večjih pomikih stebra ni nujno v nasprotnih smereh. Ta sprememba mehanizma odziva panela nekoliko zmanjša kapaciteto fasadnega sistema, ker je kapaciteta zgornjega stika dosežena pri manjšem pomiku stebra na ravni panela.

Ker pomik stebra na ravni panela navadno narašča po višini stebra, običajno prvi pade panel na vrhu konstrukcije. To pa ne drži, če je spodnji panel vpet v temelj. Takrat se pogosto prvi porušijo stiki na dnu konstrukcije. V tem primeru je kapaciteta fasadnega stika spodnjega panela manjša, ker se celoten pomik zgodi le v zgornjem stiku. To velja le za spodnji panel, medtem ko stik spodnjega panela s temeljem ni imel vpliva na kapaciteto višje ležečih panelov.

Za konservativno oceno kapacitete stikov (npr. za namen projektiranja konstrukcij) bi lahko kapaciteto stikov izrazili le z drsno kapaciteto zgornjega stika. Tako hkrati upoštevamo vse

negativne vplive analiziranih parametrov, preprečimo aktivacijo sorazmerno visokih sil v stikih in ustrezno zavarujemo panel pred porušitvijo. Velja omeniti, da je v tem primeru konstrukcija, ki ima v začetni legi popolnoma izkoriščeno drsno kapaciteto stikov, opredeljena kot neustrezna. Kapaciteta je takrat namreč nič.

9.5.5 Vpliv fasadnega sistema na odziv glavne konstrukcije

Interakcija med paneli in glavno konstrukcijo se lahko pojavi kot posledica drsenja in udarcev v stikih. Pokazali smo, da imajo ti učinki zelo omejen vpliv na odziv glavne montažne konstrukcije. Med drsenjem stikov je njihova togost zanemarljivo majhna in enako velja za aktivirano trenje. V tej fazi paneli niso imeli skoraj nobenega vpliva na odziv glavne konstrukcije. Po tem, ko je drsna kapaciteta stikov izkoriščena, pride zaradi udarcev v stikih do določenega sodelovanja med fasadnim sistemom in glavno montažno konstrukcijo, vendar je čas trajanja udarcev zelo kratek in se interakcija zgodi le za trenutek, kar po večini nima znatnega vpliva na pomike niti na togost glavne konstrukcije.

Zaradi silikona med paneli je bilo njihovo obnašanje podobno šibko povezani steni, vendar pa je silikon med dinamično obtežbo podvržen znatni degradaciji materiala in zmanjšanju togosti, kar zmanjša njegov vpliv na konstrukcijo. Zaradi teh razlogov je vpliv silikona na pomike glavne konstrukcije nepomemben.

Pri projektni intenziteti (a_g = 0,25 g) je bil vpliv panelov na sile v stebru zanemarljiv. Pri višjih intenzitetah pa je bilo mogoče v nekaterih primerih opaziti večji vpliv udarcev, med katerimi se poveča vpliv višjih nihajnih oblik. Posledično je bila rezultanta sil pomaknjena nižje po stebru in je bila strižna obremenitev ponekod večja od sile, ki naj bi bila omejena z upogibnim momentom (M_u/H). Vpliv fasadnega sistema na odziv glavne konstrukcije je bil opazen predvsem pri vitkih stebrih s sorazmerno majhno pripadajočo maso stebra. Kljub temu strižna odpornost stebrov ni bila presežena, ker so bili v procesu projektiranja upoštevani minimalna merila in princip načrtovanja nosilnosti po EC8 (posledično je bila strižna nosilnost veliko večja od M_u/H in tudi strižnih obremenitev). Stik spodnjega panela s temeljem ni imel bistvenega vpliva na velikost strižnih sil, je pa v nekaterih primerih vplival na njihovo porazdelitev po višini stebra.

9.5.6 Projektantska praksa in ocena obremenitev fasadnega sistema

V projektantski praksi so fasadni paneli običajno obravnavani kot nekonstrukcijski elementi, pri čemer se upošteva samo njihovo maso, vpliv togosti panelov in stikov na odziv montažne stavbe pa

se zanemari. Na osnovi rezultatov parametrične študije lahko ugotovimo, da je projektantska praksa po večini ustrezna. Le zelo vitke konstrukcije z majhno maso povprečnega stebra zahtevajo nekoliko natančnejšo analizo.

V nalogi je podan sorazmerno preprost postopek za približno oceno obremenitev in potrebne kapacitete fasadnega sistema. To lahko precej preprosto ocenimo neposredno iz projektnega spektra pomikov, pri čemer potrebujemo le podatke o nihajnem času, višini konstrukcije in o višini panela.

Postopek temelji na definiciji obremenitev in kapacitete fasadnega sistema v obliki pomika stebra na ravni panela. Povprečni pomik stebra na ravni panela lahko ocenimo z enačbo 9.2:

$$\frac{d_{top}}{H} = \frac{\Delta d_{col,p}}{h_p} \quad \rightarrow \quad \Delta d_{col,p} = \frac{d_{top}}{H} \cdot h_p \tag{9.2}$$

Največji pomik na vrhu konstrukcije (d_{col}) določimo iz projektnega spektra pomikov (9.3), medtem ko sta višina konstrukcije (H) in višina panela poznana (h_p). Enačba 9.3 velja za območje nihajnih časov $T_C \leq T \leq 2$ s.

$$S_d = \frac{a_g S \mu 2{,}5 T_C}{T} \left(\frac{T}{2\pi}\right)^2 \tag{9.3}$$

Ker pomik stebra na ravni panela navadno narašča po višini stebra, enačba 9.2 ne poda najbolj neugodne ocene obremenitev. Zato smo vpeljali faktor 1.45, ki je bil določen s parametrično študijo in analitično ter prestavlja konservativno oceno razmerja med največjim in povprečnim pomikom stebra na ravni panela. Tako lahko obremenitev in potrebno kapaciteto fasadnega sistema izrazimo v obliki pomika s formulo 9.4.

$$\Delta d_{col,p} = \frac{a_g S \mu 2{,}5 T_C T}{4\pi^2} \frac{h_p}{H} \cdot 1.45 \tag{9.4}$$

Če enačbo 9.4 izrazimo v obliki enačbe 9.5, lahko ob znani višini panela in kapaciteti fasadnega sistema določimo največji pospešek tal, ki ga lahko prenese fasadni sistem montažne konstrukcije z višino H in nihajnim časom T.

$$a_g = \frac{4\pi^2}{S \mu 2{,}5 T_C T} \frac{\Delta d_{col,p} H}{h_p \cdot 1.45} \tag{9.5}$$

9.6 Pridrževalci za varovanje vodoravnih panelov

V zadnjem delu naloge sta bili narejeni numerična analiza in presoja pridrževalcev. Obstoječi analitični postopek za oceno obremenitev pridrževalcev za navpične panele je bil modificiran za uporabo ob vodoravnih panelih.

V analitičnem postopku se kot eden izmed bistvenih parametrov pojavi razmerje med največjo relativno hitrostjo (med panelom in konstrukcijo) in največjo hitrostjo glavne konstrukcije. Z numerično analizo je bila določena priporočena vrednost tega razmerja, ki za primer vodoravnih panelov znaša 1.5.

V primerjavi z numeričnimi rezultati smo z analitičnim postopkom dobili na splošno bolj konservativne ocene udarne sile v pridrževalnem sistemu. Izpostavljen je bil problem različnih načinov porušitve in vertikalne amplifikacije sil, ki ni upoštevana v postopku. Zadnje ostaja odprto vprašanje za nadaljnje raziskave.

9.7 Zaključki

V nalogi smo raziskali potresni odziv AB-montažnih hal z vodoravnimi fasadnimi sistemi. Konstrukcijski tip obravnavanih stavb in fasadnih stikov je značilen za armiranobetonske industrijske stavbe v srednji Evropi. Med preteklimi potresi v Italiji je bil opažen sorazmerno slab odziv fasadnih panelov, kar je bil vzrok za študijo, predstavljeno v okviru disertacije.

Pretežno analitična študija je podprta z obsežnimi eksperimentalnimi raziskavami, ki vključujejo statične in dinamične preizkuse posameznih stikov in celotnega sistema stikov pa tudi preizkuse celotnega konstrukcijskega sistema v naravnem merilu na potresni mizi. Testi na potresni mizi sicer niso bili narejeni v okviru naloge, so pa bili rezultati testov uporabljeni za študijo mehanizmov obnašanja in validacijo numeričnih modelov. Številni testi so bili uspešno simulirani z na novo definiranimi numeričnimi modeli.

Glavni cilji disertacije so bili: analiza potresnega odziva montažnih AB-konstrukcij z vodoravnimi betonskimi fasadnimi paneli, izboljšanje obstoječih in formulacija boljših numeričnih modelov, določitev parametrov, ki imajo pomemben vpliv na obnašanje analiziranega sistema, ter ovrednotenje interakcije med paneli in glavno montažno konstrukcijo ter vplivom horizontalnega fasadnega sistema na celoten odziv konstrukcije. Cilji so bili uspešno doseženi in jih povzemamo v naslednjih točkah (vsa opažanja in zaključki se nanašajo samo na obravnavani tip fasadnega sistema):

- Rezultati dinamičnih preizkusov fasadnih stikov so bili podrobno analizirani. Prepoznan je bil značilen mehanizem odziva celotnega sistema stikov med potresno obtežbo. Ugotovljeno je bilo merilo porušitve in določena je bila kapaciteta stikov.

- Potresni odziv celotnega montažnega sistema je bil preučen in analiziran na testih na potresni mizi v naravnem merilu.

- Veljavnost in uporabnost razvitih numeričnih modelov sta bili potrjeni s simulacijo testov posameznih stikov in simulacijo testa celotnega montažnega sistema na potresni mizi.

- Narejena je bila obsežna parametrična študija enoetažnih montažnih industrijskih stavb z vodoravnimi paneli. Analizirani so bili različni parametri: konfiguracija stavbe, konstrukcijske nepravilnosti (različne začetne pozicije stikov), interakcija med sosednjimi paneli (vpliv silikonskega tesnila) in stik spodnjega panela s temeljem.

- Določeni so bili parametri, ki vplivajo na odziv in kapaciteto fasadnega sistema. Najpomembnejši vpliv na odziv panelov ima začetna pozicija fasadnih stikov, ker ta določa, kolikšni so lahko relativni pomiki med paneli in glavno konstrukcijo, preden pride do udarcev v stikih.

- Analiziran je bil vpliv vodoravnih fasadnih sistemov na odziv glavne montažne konstrukcije. Pokazalo se je, da paneli nimajo bistvenega vpliva na odziv glavne konstrukcije. Ta je bil nekoliko opaznejši le pri višjih intenzitetah in vitkih stavbah z majhno maso.

- Ovrednoten in potrjen je bil projektantski pristop, ki se pogosto uporablja v praksi. Razvit in predstavljen je sorazmerno preprost postopek za približno oceno obremenitev fasadnega sistema, ki bi ga lahko uporabili v fazi projektiranja montažne konstrukcije.

- Podan je predlog za izboljšanje fasadnih stikov, ki temelji na zagotavljanju več drsnega pomika.

- Narejena je bila numerična analiza pridrževalcev za varovanje vodoravnih panelov, s katero smo ovrednotili postopek za analitično oceno obremenitev v pridrževalcih.

BIBLIOGRAPHY

Akkar, S., Sandikkaya, M. a., Şenyurt, M., Azari Sisi, A., Ay, B.O., Traversa, P., Douglas, J., Cotton, F., Luzi, L., Hernandez, B., Godey, S. 2014. Reference database for seismic ground-motion in Europe (RESORCE). Bulletin Of Earthquake Engineering 12, 1: 311–339. doi:10.1007/s10518-013-9506-8.

AmesWeb. 2020. AmesWeb - Advanced Mechanical Engineering Solutions. Bolt screw friction coefficient table. https://amesweb.info/Screws/bolt-screw-friction-coefficient-table.aspx. Accessed July 2020.

Andersson, S., Söderberg, A., Björklund, S. 2007. Friction models for sliding dry, boundary and mixed lubricated contacts. Tribology International 40, 4: 580–587. doi:10.1016/j.triboint.2005.11.014.

Arslan, M.H., Korkmaz, H.H., Gulay, F.G. 2006. Damage and failure pattern of prefabricated structures after major earthquakes in Turkey and shortfalls of the Turkish Earthquake code. Engineering Failure Analysis 13, 4: 537–557. doi:10.1016/j.engfailanal.2005.02.006.

ATC. Applied Technology Council 2007. Interim Testing Protocols for Determining the Seismic Performance Characteristics of Structural and Non-structural components - FEMA461. Washington DC, Federal Emergency Management Agency.

Babič, A., Dolšek, M. 2016. Seismic fragility functions of industrial precast building classes. Engineering Structures 118: 357–370. doi:10.1016/j.engstruct.2016.03.069.

Belleri, A., Brunesi, E., Nascimbene, R., Pagani, M., Riva, P. 2015. Seismic performance of precast industrial facilities following major earthquakes in the Italian territory. Journal Of Performance Of Constructed Facilities 29, 5. doi:10.1061/(ASCE)CF.1943-5509.0000617.

Belleri, A., Cornali, F., Passoni, C., Marini, A., Riva, P. 2018. Evaluation of out-of-plane seismic performance of column-to-column precast concrete cladding panels in one-storey industrial buildings. Earthquake Engineering & Structural Dynamics 47, 2: 397–417. doi:10.1002/eqe.2956.

Belleri, A., Torquati, M., Marini, A., Riva, P. 2016. Horizontal cladding panels: in-plane seismic performance in precast concrete buildings. Bulletin Of Earthquake Engineering 14, 4: 1103–1129. doi:10.1007/s10518-015-9861-8.

Biondini, F., Toniolo, G. 2009. Probabilistic calibration and experimental validation of the seismic design criteria for one-story concrete frames. Journal Of Earthquake Engineering 13: 426–462. doi:10.1080/13632460802598610.

Biondini, F., Toniolo, G. 2004. Validation of seismic design criteria for concrete frames based on Monte Carlo simulation and full-scale pseudodynamic tests. In: 13th World Conference on Earthquake Engineering.

Biondini, F., Toniolo, G., Zhao, B. 2008. Pseudodynamic tests on full scale prototypes of precast structures. In: 14th World Conference on Earthquake Engineering.

Bournas, D.A., Negro, P., Taucer, F.F. 2013. Performance of industrial buildings during the Emilia earthquakes in Northern Italy and recommendations for their strengthening. Bulletin Of Earthquake Engineering 12, 5: 2383–2404. doi:10.1007/s10518-013-9466-z.

Braconi, A., Finetto, M., Degee, H., Hausoul, N., Hoffmeister, B., Gündel, M., Karmanos, S., Pappa, P., Varelis, G., Rinaldi, V., Obiala, R., Hjaij, M., Somja, H., Badalassi, M., Caprili, S., Salvatore, W. 2013. Optimising the seismic performance of steel and steel-concrete structures by standardising material quality control (OPUS).

BTC. 2014. BTC Company portrait. https://www.btc.si/en/about-us. Accessed 20 February 2019.

Bužinel, I. 2019. RC precast structures in Slovenia. Practice of Kolektor CPG, d.o.o. Personal communication. (5th December 2019)

CEN. 1998–1:2004. Eurocode 8: Design of structures for earthquake resistance - Part 1: General rules, seismic actions and rules for buildings. Brussels, European Committee for Standardisation.

CEN. 1998–2:2005. Eurocode 8: Design of structures for earthquake resistance - Part 2: Bridges. Brussels, European Committee for Standardisation.

Chew, M.Y.L. 2000. Joint sealant for wall cladding. Polymer Testing 19, 6: 643–651. doi:10.1016/S0142-9418(99)00038-0.

CLADDINGS. 2016. Seismic resilience and strengthening of precast industrial buildings with concrete

claddings.
http://claddings.fgg.uni-lj.si/

Colombo, A., Lamperti, M., Negro, P., Toniolo, G. 2016a. Design Guidelines for Wall Panel Connections.
doi:10.2788/546845.

Colombo, A., Negro, P., Toniolo, G., Lamperti, M. 2016b. Design Guidelines for Precast Structures with Cladding Panels.
doi:10.2788/956612.

Dal Lago, B.A. 2015. Seismic performance of precast structures with dissipative cladding panel connections. PhD thesis. Politechnico di Milano, Italy.

Dal Lago, B., Biondini, F., Toniolo, G. 2018. Experimental Investigation on Steel W-Shaped Folded Plate Dissipative Connectors for Horizontal Precast Concrete Cladding Panels. Journal Of Earthquake Engineering 22, 5: 778–800.
doi:10.1080/13632469.2016.1264333.

Dal Lago, B., Biondini, F., Toniolo, G. 2017a. Friction-based dissipative devices for precast concrete panels. Engineering Structures 147: 356–371.
doi:10.1016/j.engstruct.2017.05.050.

Dal Lago, B., Biondini, F., Toniolo, G., Lamperti Tornaghi, M. 2017b. Experimental investigation on the influence of silicone sealant on the seismic behaviour of precast facades. Bulletin Of Earthquake Engineering 15: 1771–1787.
doi:10.1007/s10518-016-0045-y.

Dal Lago, B., Lamperti Tornaghi, M. 2018. Sliding channel cladding connections for precast structures subjected to earthquake action. Bulletin Of Earthquake Engineering 16: 5621–5646.
doi:10.1007/s10518-018-0410-0.

Daniell, J., Vervaeck, A. 2012. Damaging earthquakes database. 2012 – the year in review. CEDIM Research Report 2013-01. Karlsruhe, Centre for Disaster Management and Risk Reduction Technology: 47 f.

Dogan, M., Özbaşaran, H., Günaydin, A. 2010. Effect of seismic loading to prefabricated connections. Applied Sciences And Engineering 11, 1: 47–58.

EEFIT, D'Ayala, D. (ed.), Free, M. (ed). 2003. The Kocaeli, Turkey Earthquake of 17 August 1999. A field report by EEFIT. London, Institution of Structural Engineers, Earthquake Engineering Field

investigation Team: 195 p.

EERI, Stratta, J. L., Wyllie, L. A. Jr. 1976. Preliminary Reconnaissance Report on Italian Earthquake of May 6, 1976. Earthquake Engineering Research Institute: 9 p.

EERI. 1989. Performance of industrial facilities. In: Armenian earthquake reconnaissance report. Earthquake Spectra 5, S1: 101–113.
doi:10.1193/1.1585238.

Ercolino, M., Magliulo, G., Manfredi, G. 2016. Failure of a precast RC building due to Emilia-Romagna earthquakes. Engineering Structures 118: 262–273.
doi:10.1016/j.engstruct.2016.03.054.

Esposito, S., Stojadinovic, B., Babič, A., Dolšek, M., Iqbal, S., Selva, J., Broccardo, M., Mignan, A., Giardini, D. 2020. Risk-Based Multilevel Methodology to Stress Test Critical Infrastructure Systems. Journal Of Infrastructure Systems 26, 1: 04019035.
doi:10.1061/(ASCE)IS.1943-555X.0000520.

Fajfar, P. 1984. Dinamika gradbenih konstrukcij. Ljubljana, Slovenija, University of Ljubljana, FAGG: 519 p.

Fajfar, P., Banovec, J., Saje, F. 1978. Behaviour of prefabricated industrial building in Breginj during the Friuli earthquake. In: 6th European Conference on Earthquake Engineering. Dubrovnik, Yugoslav Association for Earthquake Engineering, Ljubljana: 493–500 pp.

Fajfar, P., Duhovnik, J., Reflak, J., Fischinger, M., Breška, Z. 1981. The behavior of buildings and other structures during the earthquakes of 1979 in Montenegro. IKPIR publication, Ljubljana, Slovenia: University of Ljubljana, Department of civil engineering, Institute of structural and earthquake engineering.

FEMA. P-58-1 / September 2012. Seismic performance assessment of buildings: Volume 1 - Methodology. Washington D.C., Federal Emergency Managemenet Agency.

Ferrara, L., Colombo, A., Negro, P., Toniolo, G. 2004. Precast vs. cast-in-situ reinforced concrete industrial buildings under earthquake loading: an assessment via pseudodynamic tests. In: 13th World Conference on Earthquake Engineering.

Fischinger, M., Kramar, M., Isaković, T. 2008. Cyclic response of slender RC columns typical of precast industrial buildings. Bulletin Of Earthquake Engineering 6, 3: 519–534.
doi:10.1007/s10518-008-9064-7.

Fischinger, M., Zoubek, B., Isaković, T. 2014. Seismic response of precast industrial buildings. In: Ansal, A. (ed.), Perspectives on European earthquake engineering and seismology, Volume 1. Berlin, Springer: 131–177.

Halfen. 2010. Design of anchor channels. VBBF Verein zur Förderung und Entwicklung der Befestigungs-, Bewehrungs- und Fassadentechnik e.V. (ed.), Dusseldorf, Druckstudio GmbH: 70 p.

HALFEN. 2016. HALFEN International GmbH.
https://www.halfen.com. Accessed 11th February 2016.

Isaković, T., Fischinger, M., Karadogan, F., Kremmyda, G.D., Dal Lago, B., Pegan, A., Psycharis, I.N., Trost M., Tsoukantas, S.G., Yüksel, E. 2012a. Catalogue on the existing cladding panel systems and connections in precast buildings with the identification of their possible seismic deficiencies. SAFECLADDING, Deliverable 1.1. Ljubljana, Slovenia: University of Ljubljana.

Isaković, T., Kramar, M., Zoubek, B., Fischinger, M. 2012b. Calibrated programs for structural analysis. SAFECAST, Deliverable 5.1. Ljubljana.

Isaković, T., Zoubek, B., Fischinger, M. 2012c. Previous projects' findings. SAFECLADDING, Deliverable 1.4. Ljubljana, Slovenia: University of Ljubljana.

Isaković, T., Zoubek, B., Fischinger, M. 2014a. Report and card files on the tests preformed on existing connections - update. SAFECLADDING, Deliverable 1.3. Ljubljana.

Isaković, T., Zoubek, B., Fischinger, M. 2018. Full-scale shake table tests of cladding panels. In: 16th European Conference on Earthquake Engineering. Thessaloniki, Greece.

Isaković, T., Zoubek, B., Lopatič, J., Fischinger, M. 2014b. Experimental research of typical cladding panel. In: Second European conference on earthquake engineering and seismology. Istanbul, Turkey, 25-29 August 2014: 1–10 pp.

Isaković, T., Zoubek, B., Lopatič, J., Urbas, M., Fischinger, M. 2013. Report and card files on the tests performed on existing connections. SAFECLADDING, Deliverable 1.2. Ljubljana, Slovenia: University of Ljubljana.

IUPAC. 1997. Compendium of Chemical Terminology, 2nd ed. (the "Gold Book"). Compiled by A. D. McNaught and A. Wilkinson. Blackwell Scientific Publications, Oxford (1997). XML on-line corrected version: http://goldbook.iupac.org (2006-) created by M. Nic, J. Jirat, B. Kosata; updates compiled by A. Jenkins. ISBN 0-9678550-9-8.
https://doi.org/10.1351/goldbook. Accessed 20th August 2018.

IZIIS. 2016. DYNLAB - Seismic Shaking Table. http://www.iziis.edu.mk/?page_id=170. Accessed June 2016.

Jayaram, N., Lin, T., Baker, J.W. 2011. A computationally efficient ground-motion selection algorithm for matching a target response spectrum mean and variance. Earthquake Spectra 27, 3: 797–815. http://dx.doi.org/10.1193/1.3608002.

Kragelskii, I.V. 1965. Friction and Wear. London, Butterworths.

Kramar, M. 2008. Seismic vulnerability of the precast reinforced concrete structures. PhD thesis. University of Ljubljana, Slovenia.

Kramar, M., Isaković, T., Fischinger, M. 2010. Seismic collapse risk of precast industrial buildings with strong connections. Earthquake Engineering & Structural Dynamics 39: 847–868. doi:10.1002/eqe.970.

Liberatore, L., Sorrentino, L., Liberatore, D., Decanini, L.D. 2013. Failure of industrial structures induced by the Emilia (Italy) 2012 earthquakes. Engineering Failure Analysis 34: 629–647. doi:10.1016/j.engfailanal.2013.02.009.

Liu, Y., Liu, W.-G., Wang, X., He, W.-F., Yang, Q.-R. 2014. New Equivalent Linear Impact Model for Simulation of Seismic Isolated Structure Pounding against Moat Wall. Shock And Vibration 2014: 1–10. doi: 10.1155/2014/151237.

Liu, Y.F., Li, J., Zhang, Z.M., Hu, X.H., Zhang, W.J. 2015. Experimental comparison of five friction models on the same test-bed of the micro stick-slip motion system. Mechanical Sciences 6, 1: 15–28. doi:10.5194/ms-6-15-2015.

Magliulo, G., Ercolino, M., Petrone, C., Coppola, O., Manfredi, G. 2014. The Emilia earthquake: Seismic performance of precast reinforced concrete buildings. Earthquake Spectra 30, 2: 891–912. doi:10.1193/091012EQS285M.

Mander, J.B., Priestley, M.J.N., Park, R. 1988. Theoretical Stress-Strain Model for Confined Concrete. Journal Of Structural Engineering 114, 8: 1804–1826. http://dx.doi.org/10.1061/(ASCE)0733-9445(1988)114:8(1804).

McKenna, F., Fenves, G.L. 2010. Open System for Earthquake Engineering Simulation (OpenSees). Pacific Earthquake Engineering Research Center.

http://opensees.berkeley.edu.

Menichini, G., Isaković, T. 2018. Modeling the seismic response of vertical concrete cladding panels. V: Italian concrete days 2018 - Giornate aicap 2018 Congresso CTE.

Muthukumar, S., DesRoches, R. 2006. A Hertz contact model with non-linear damping for pounding simulation. Earthquake Engineering & Structural Dynamics 35, 7: 811–828. doi:10.1002/eqe.557.

Del Monte, E., Falsini, C., Boschi, S., Menichini, G., Orlando, M. 2019. An innovative cladding panel connection for RC precast buildings. Bulletin Of Earthquake Engineering 17, 2: 845–865. doi:10.1007/s10518-018-0470-1.

Negro, P., Bournas, D.A., Molina, F.J. 2013. Pseudodynamic tests on a full-scale 3-storey precast concrete building: Global response. Engineering Structures 57: 594–608. doi:10.1016/j.engstruct.2013.05.047.

Negro, P., Lamperti Tornaghi, M. 2017. Seismic response of precast structures with vertical cladding panels: The SAFECLADDING experimental campaign. Engineering Structures 132: 205–228. doi:10.1016/j.engstruct.2016.11.020.

Negro, P., Toniolo, G. 2012. Design Guidelines for Connections of Precast Structures under Seismic Actions. doi:10.2777/37605.

Psycharis, I.N., Kalyviotis, I.M., Mouzakis, H.P. 2018. Experimental investigation of the response of precast concrete cladding panels with integrated connections under monotonic and cyclic loading. Engineering Structures 159: 75–88. doi:10.1016/j.engstruct.2017.12.036.

Rabinowicz, E. 1956. Stick and Slip. Scientific American 194, 5: 109–118.

Randall, M.J., Saiidi, M.S., Maragakis, E.M., Isaković, T. 1999. Restrainer design procedures for multi-span simply-supported bridges. Technical Report MCEER, 99-0011. Buffalo.

Saatcioglu, M., Mitchell, D., Tinawi, R., Gardner, N.J., Gillies, A.G., Ghobarah, A., Anderson, D.L., Lau, D. 2001. The August 17, 1999, Kocaeli (Turkey) earthquake — damage to structures. Canadian Journal Of Civil Engineering 28, 4: 715–737. doi:10.1139/cjce-28-4-715.

SAFECLADDING. 2015. SAFECLADDING project – Improved Fastening Systems of Cladding Wall

Panels of Precast Buildings in Seismic Zones.
http://www.safecladding.eu. Accessed 18th January 2019.

Saisi, A., Toniolo, G. 1998. Precast RC columns under cyclic loading: an experimental programme oriented to EC8. Studi e ricerche, Scuola di specializzazione. Politecnico di Milano 19: 373–414.

Savoia, M., Buratti, N., Vincenzi, L. 2017. Damage and collapses in industrial precast buildings after the 2012 Emilia earthquake. Engineering Structures 137: 162–180.
doi:10.1016/j.engstruct.2017.01.059.

Scotta, R., De Stefani, L., Vitaliani, R. 2015. Passive control of precast building response using cladding panels as dissipative shear walls. Bulletin Of Earthquake Engineering 13: 3527–3552.
doi:10.1007/s10518-015-9763-9.

Snoj, J. 2014. Ocena potresnega tveganja zidanih stavb. Doctoral dissertation. Ljubljana, University of Ljubljana, Faculty of Civil and Geodetic Engineering.

Starešinič, G., Zoubek, B., Gams, M., Isaković, T., Fischinger, M. 2020. Modelling in-plane dynamic response of a fastening system for horizontal concrete facade panels in RC precast buildings. Engineering Structures 224, 111210.
doi:10.1016/j.engstruct.2020.111210.

Takeda, T., Sozen, M.A., Nielsen, N.N. 1970. Reinforced concrete response to simulated earthquakes. Journal Of The Structural Division 96, 12: 2557–2573.

Toniolo, G. 2012a. European research on seismic behaviour of precast structures. In: 2012 NZSEE Conference. Christchurch, New Zealand.

Toniolo, G. 2012b. SAFECAST Project: European research on seismic behaviour of the connections of precast structures. In: 15th World Conference on Earthquake Engineering. Lisboa, Portugal.

Toniolo, G., Colombo, A. 2012. Precast concrete structures: the lessons learned from the L'Aquila earthquake. Structural Concrete 13, 2: 73–83.
doi:10.1002/suco.201100052.

Toniolo, G., Dal Lago, B. 2017. Conceptual design and full-scale experimentation of cladding panel connection systems of precast buildings. Earthquake Engineering & Structural Dynamics 46, 14: 2565–2586.
doi:10.1002/eqe.2918.

Tzenov, L., Sotirov, L., Boncheva, P. 1978. Study of some damaged industrial buildings due to Vrancea

earthquake. In: 6th European Conference on Earthquake Engineering.

UL, POLIMI. 2012. Generalization of results to different structures. SAFECAST, Deliverable 5.2.

Yüksel, E., Karadoğan, F., Özkaynak, H., Khajehdehi, A., Güllü, A., Smyrou, E., Bal, İ.E. 2018. Behaviour of steel cushions subjected to combined actions. Bulletin Of Earthquake Engineering 16, 2: 707–729.
doi:10.1007/s10518-017-0217-4.

ZAG. 2019. Equipment overview.
http://www.zag.si/en/equipment. Accessed March 2019.

Zoubek, B. 2015. Influence of the connections on the seismic response of precast reinforced concrete structures. PhD thesis. University of Ljubljana, Slovenia.

Zoubek, B., Fahjan, Y., Fischinger, M., Isakovic, T. 2014. Nonlinear finite element modelling of centric dowel connections in precast buildings. Computers and Concrete 14: 463–477. doi:10.12989/cac.2014.14.4.463.

Zoubek, B., Fischinger, M., Isaković, T. 2016a. Cyclic response of hammer-head strap cladding-to-structure connections used in RC precast building. Engineering Structures 119: 135–148.
doi:10.1016/j.engstruct.2016.04.002.

Zoubek, B., Fischinger, M., Isaković, T. 2016b. Seismic response of short restrainers used to protect cladding panels in RC precast buildings. Journal Of Vibration And Control 24, 4: 645–658.
doi:10.1177/1077546316659780.

Zoubek, B., Fischinger, M., Isaković, T. 2015. Estimation of the cyclic capacity of beam-to-column dowel connections in precast industrial buildings. Bulletin Of Earthquake Engineering 13, 7: 2145–2168.
doi:10.1007/s10518-014-9711-0.

Zoubek, B., Isakovic, T., Fahjan, Y., Fischinger, M. 2013. Cyclic failure analysis of the beam-to-column dowel connections in precast industrial buildings. Engineering Structures 52: 179–191.
doi:10.1016/j.engstruct.2013.02.028.

Zoubek, B., Isaković, T., Jankovič, G., Fischinger, M. 2017. Intermediate report 3.1: Shaking table tests on a full-scale model. Ljubljana.

Žižmond, J. 2019. Hazard analysis for site location in Ljubljana. Personal communication. (22nd August 2019)

APPENDICES